USGS
science for a changing world

The Cerrillos Uplift, the La Bajada Constriction, and Hydrogeologic Framework of the Santo Domingo Basin, Rio Grande Rift, New Mexico

Professional Paper 1720

U.S. Department of the Interior
U.S. Geological Survey

Cover. High-oblique scene looking northeast up the Rio Grande valley showing the La Bajada constriction area, which is the focus of this report, and the region beyond. The broad multicolored area in the foreground is the geologic map of the Cochiti Pueblo area (see pl. 2) that is draped over a 30-m-hillshade of the region rendered with a color-ramped transparent hypsometric tint. The scene, which was generated with ESRI ArcGlobe software version 9.1 by T.R. Brandt, is illuminated from the northwest; vertical exaggeration is 3. The La Bajada fault escarpment and White Rock Canyon are clearly visible in the right and central parts of image, respectively. Lowlands of the Española Basin are apparent just northeast of the geologic map area, and the bordering high peaks of the Jemez and Sangre de Cristo Mountains are rendered in light shades of gray in the upper left and upper right parts of the image, respectively.

The Cerrillos Uplift, the La Bajada Constriction, and Hydrogeologic Framework of the Santo Domingo Basin, Rio Grande Rift, New Mexico

Edited by Scott A. Minor

Contributions by David A. Sawyer, Scott A. Minor, V.J.S. Grauch, Brian D. Rodriguez, Ren A. Thompson, David P. Dethier[1], Mark R. Hudson, Maria Deszcz-Pan, William C. McIntosh[2], Ralph R. Shroba, Gary A. Smith[3], and Theodore R. Brandt

[1] Williams College
[2] New Mexico Bureau of Geology and Mineral Resources
[3] University of New Mexico

Volume comprises Chapters A, B, C, D, E, F, and G

Professional Paper 1720

U.S. Department of the Interior
U.S. Geological Survey

U.S. Department of the Interior
DIRK KEMPTHORNE, Secretary

U.S. Geological Survey
Mark D. Myers, Director

U.S. Geological Survey, Reston, Virginia: 2006

For sale by U.S. Geological Survey Information Services
Box 25286, Denver Federal Center
Denver, CO 80225

For more information on the USGS—the Federal source for science about the Earth, its natural and living resources, natural hazards, and the environment:
World Wide Web: http://www.usgs.gov
Telephone: 1-888-ASK-USGS

Any use of trade, product, or firm names is for descriptive purposes only and does not imply endorsement by the U.S. Government.

Although this report is in the public domain, permission must be secured from the individual copyright owners to reproduce any copyrighted materials contained within this report.

Suggested citation:
Minor, S.A., ed., 2006, The Cerrillos uplift, the La Bajada constriction, and hydrogeologic framework of the Santo Domingo Basin, Rio Grande rift, New Mexico: U.S. Geological Survey Professional Paper 1720, 189 p.

Volume Contents

A. Geologic Setting of the La Bajada Constriction and Cochiti Pueblo Area, New Mexico 3
By David A. Sawyer and Scott A. Minor

B. Stratigraphy of Upper Cenozoic Fluvial Deposits of the La Bajada Constriction Area, New Mexico....27
By David P. Dethier and David A. Sawyer

C. Cenozoic Volcanism of the La Bajada Constriction Area, New Mexico 43
By Ren A. Thompson, David A. Sawyer, Mark R. Hudson, V.J.S. Grauch, and W.C. McIntosh

D. Gravity and Aeromagnetic Studies of the Santo Domingo Basin Area, New Mexico 63
By V.J.S. Grauch, David A. Sawyer, Scott A. Minor, Mark R. Hudson, and Ren A. Thompson

E. Structure of the Santo Domingo Basin and La Bajada Constriction Area, New Mexico 91
By Scott A. Minor, Mark R. Hudson, V.J.S. Grauch, and David A. Sawyer

F. Electromagnetic Studies and Subsurface Mapping of Electrical Resistivity in the La Bajada Constriction Area, New Mexico....121
By Brian D. Rodriguez, Maria Deszcz-Pan, and David A. Sawyer

G. Hydrogeologic Framework of the La Bajada Constriction Area, New Mexico—Integration of Subsurface and Surface Geology....167
By David A. Sawyer and Scott A. Minor

Plates

[On CD-ROM]

1. Map Showing Physiographic and Cultural Features of the Santo Domingo Basin and Adjoining Areas, New Mexico
2. Geologic Map of the Cochiti Pueblo Area, New Mexico
By David A. Sawyer, Scott A. Minor, Ren A. Thompson, Ralph R. Shroba, Gary A. Smith, David P. Dethier, V.J.S. Grauch, and Theodore R. Brandt
3. Isostatic Residual Gravity Map of the Santo Domingo Basin Area, New Mexico
By V.J.S. Grauch, Scott A. Minor, and David A. Sawyer
4. Reduced-to-Pole Aeromagnetic Map of the Santo Domingo Basin Area, New Mexico
By V.J.S. Grauch and David A. Sawyer
5. Map Showing Reduced-to-Pole Aeromagnetic Data, Geology, and Topography for the Cochiti Pueblo Area, New Mexico
By V.J.S. Grauch, Mark R. Hudson, Ren A. Thompson, Scott A. Minor, and David A. Sawyer
6. Geologic Cross Sections Spanning the La Bajada Constriction and Northern Cerrillos Uplift, New Mexico
By David A. Sawyer, Scott A. Minor, V.J.S. Grauch, Brian D. Rodriguez, and Ren A. Thompson

Conversion Factors and Abbreviations

Multiply	By	To obtain
foot (ft)	0.3048	meter (m)
inch (in.)	25.4	millimeter (mm)
mile (mi)	1.609	kilometer (km)

AAR	amino-acid racemization
AMT	audio-magnetotelluric
DEM	digital elevation model
elev.	elevation
EM	electromagnetic
FFT	fast Fourier transform
ft	foot, feet
GR API	gamma-ray API units
g/cc	grams per cubic centimeter
Hz	hertz
in.	inch, inches
ka	kiloannum; thousands of years ago
kg/m^3	kilograms per cubic meter
km	kilometer(s)
k.y.	thousand years
m	meter(s)
ms	millisecond
m.y.	million years
Ma	megaannum; millions of years ago
mgal	milligal
ms	milliseconds
MT	magnetotelluric
mV	millivolts
nT	nanoTesla
ohm-m	ohm-metre(s) per meter
RDI	resistivity depth-image
RTP	reduced-to-pole
SI	système international; international system of units of measure
SWL	static water level
TDEM	time-domain electromagnetic
TE	transverse electric
TM	transverse magnetic
USGS	United States Geological Survey

Geologic Setting of the La Bajada Constriction and Cochiti Pueblo Area, New Mexico

By David A. Sawyer and Scott A. Minor

Chapter A of

The Cerrillos Uplift, the La Bajada Constriction, and Hydrogeologic Framework of the Santo Domingo Basin, Rio Grande Rift, New Mexico

Edited by Scott A. Minor

Professional Paper 1720–A

U.S. Department of the Interior
U.S. Geological Survey

Contents

Abstract 3
Introduction and Setting 3
Context 3
Purpose of Study 4
Geographic Setting 4
Land Use and Ownership 6
Population Growth and Demands on Water 6
Previous Geologic Mapping 6
Geologic Setting of the La Bajada Constriction Area 9
Rio Grande Rift 9
Basin Architecture and Terminology 9
Original Definitions of the La Bajada Constriction and Cerrillos Uplift 9
Geologic Definition of the La Bajada Constriction and Surrounding Basins 11
Cerros Del Rio Volcanic Field and Cerrillos Uplift 13
Santo Domingo Valley 14
Saint Peters Dome Block 14
Stratigraphy of Pre-Rift Rocks 14
Precambrian and Paleozoic Rocks 15
Mesozoic Sedimentary Rocks 15
Pre-Rift Tertiary Rocks 17
Hydrostratigraphic Properties of Pre-Rift Sedimentary and Igneous Rocks 18
References Cited 19

Figures

A1. Index map of the Rio Grande rift in northern New Mexico showing principal geologic and geographic features, cities, and towns mentioned in text 5
A2. Tectonic map of a segment of the middle Rio Grande rift showing the Santo Domingo, northern Albuquerque, and Española Basins and the La Bajada constriction 8
A3. Isostatic residual gravity model of the Santo Domingo Basin area showing gravity stations and major faults 10
A4. Digital elevation model image of the Cochiti Pueblo area showing the La Bajada constriction between bounding Cerrillos uplift and Saint Peters Dome block 12

Table

A1. Thicknesses of basal Cretaceous, Jurassic, Triassic, and Paleozoic stratigraphic units 16

Geologic Setting of the La Bajada Constriction and Cochiti Pueblo Area, New Mexico

By David A. Sawyer and Scott A. Minor

Abstract

The geologic, geophysical, and hydrogeologic studies of the La Bajada constriction area and adjacent Santo Domingo Basin presented in this chapter and following chapters of this report are largely an outgrowth of regional hydrogeologic investigations in the Albuquerque Basin, greater Santa Fe area, Los Alamos National Laboratory, and Native American pueblos, especially the Pueblo de Cochiti. The La Bajada constriction area contains a complex mosaic of federal (National Forest, National Park, and Bureau of Land Management), State of New Mexico, Native American, and private lands. The scientific results summarized in this report are intended to provide critical information for the citizens of New Mexico and for the governmental officials who represent them in order to better manage the various land surface environments and groundwater resources of this complex and vital region.

The geologic, geophysical, and hydrogeologic properties of the Santo Domingo Basin and La Bajada constriction are the result of tectonic and volcanic processes related to the late Tertiary and Quaternary Rio Grande rift. The La Bajada constriction is herein defined as the relatively narrow structural trough, containing >200 m of basin-fill sediments and bounded by rift-flank uplifts, that links the southern part of the Española Basin and the northeast part of the Santo Domingo Basin. The La Bajada constriction area can be subdivided into three terranes based on topographic expression, structural configuration, and dominant stratigraphy: (1) an elevated Cerros del Rio volcanic field–Cerrillos uplift eastern-border terrane; (2) the central Santo Domingo valley; and (3) an elevated Saint Peters Dome block western-border terrane. The southeastern boundary of the La Bajada constriction and the western border of the Cerrillos uplift are well defined by the La Bajada fault-zone escarpment south of the Cañada de Santa Fe, but to the north the boundary steps eastward to the geophysically expressed Tetilla fault zone buried beneath Pliocene basalts and andesites of the Cerros del Rio volcanic field. The Cerrillos uplift consists of upwarped Mesozoic marine and continental sedimentary rocks unconformably overlain by Eocene and Oligocene sedimentary and volcanic rocks and intruded by Eocene and Oligocene stocks. The western boundary of the La Bajada constriction is sharply defined by the Pajarito fault zone and the footwall Saint Peters Dome block. To the southwest the Pajarito fault zone dies out at the surface, but an older, aligned, buried structure continues to the southwest as a geophysically expressed basin-bounding fault. Rocks underlying the Saint Peters Dome block consist mainly of Miocene volcanic rocks of the Jemez volcanic field. Between the Saint Peters Dome block and the Cerrillos uplift, the La Bajada constriction is filled by Miocene to Pleistocene Santa Fe Group basin-fill sediments that interfinger with and are overlain by volcanic rocks of the Cerros del Rio volcanic field and early Pleistocene Bandelier Tuff erupted from nearby Valles caldera.

The stratigraphy and lithology of the pre-rift (Proterozoic through early Miocene) basement and sedimentary rocks underlying the region and their effects on the hydrogeology of the La Bajada constriction area are summarized in this chapter. Cretaceous marine sedimentary rocks in the Cerrillos uplift form a regional groundwater barrier that retards or prevents flow from the southern Espanola Basin into the Santo Domingo Basin. Overlying Eocene and Oligocene sedimentary and volcanic rocks (the Galisteo and Espinaso Formations, respectively), which may be variably hydraulically conductive, thicken eastward away from the La Bajada constriction and Santo Domingo Basin.

Introduction and Setting

Context

Studies by the U.S. Geological Survey were begun in 1996 to improve understanding of the geologic framework of the Albuquerque composite basin and adjoining areas, in order that more accurate hydrogeologic parameters could be applied to new hydrologic models. The ultimate goal of this multidisciplinary effort has been to better quantify estimates of future water supplies for northern New Mexico's growing urban centers, which largely subsist on aquifers in the Rio Grande rift basins (Bartolino and Cole, 2002). From preexisting hydrologic models it became evident that hydrogeologic uncertainties were large in the Santo Domingo Basin area, immediately upgradient from the greater Albuquerque metropolitan area, and particularly in the northeast part of the basin. Accordingly, a priority for the new geologic and geophysical investigations was to better determine the hydrogeologic framework of the Santo Domingo Basin, especially geologic controls of underflow in the northeasternmost part of the basin known as the La Bajada constriction (defined subsequently in this chapter—see Basin

Architecture and Terminology section). In addition, because subsurface information from deep wells and geophysical logs was almost completely lacking for the Santo Domingo Basin, our hydrogeologic studies in this area depended almost entirely on new surface geologic mapping and on geophysical imaging of the subsurface, calibrated by a small amount of water-well information. The current report presents the results of the U.S. Geological Survey's recent geologic and geophysical investigations of the hydrogeologic framework of the northeast part of the Santo Domingo Basin and flanking uplands, including the La Bajada constriction area that was the focus of our study.

In this chapter we provide some background on the societal issues that were most important in defining the scope and purpose of these multidisciplinary studies of the basin aquifer system in this part of the Rio Grande rift. We define the intrabasin and basin-bounding geologic features, review relevant previous investigations, and introduce and describe stratigraphic and structural features that affect the ground-water flow system. Finally, in this chapter we summarize geology and hydrostratigraphy of the older pre-rift rocks beneath and flanking the Santo Domingo and Española Basins.

Purpose of Study

The overall purpose of this study is to improve knowledge of the hydrogeology of the Rio Grande aquifer within the Santo Domingo Basin and adjoining parts of the Albuquerque and Española Basins. The Rio Grande aquifer can be viewed as that portion of the Rio Grande rift basin fill that is hydraulically connected to the Rio Grande. The Rio Grande aquifer has been undergoing recharge since the last glacial maximum (22,000–19,000 years ago) and the peak of pluvial rainfall (Sanford and Plummer, 2000; Sanford and others, 2004a,b; Plummer and others, 2004a,b). Nevertheless, large portions of northern New Mexico adjoining, and locally within, the Albuquerque and Santo Domingo Basins have very old ground water (>25,000 years old), indicating that they have not recently been recharged (Sanford and others, 2000). Considerable potential exists for contamination of the Rio Grande aquifer, particularly by radionuclides released during nuclear weapons research and production at the Los Alamos National Laboratory just north of the study area. Geologic controls on fast migration pathways and travel times within the aquifer need to be better determined. Both the rate of recharge by the Rio Grande and the potential for fast migration of contaminants are functions of the hydraulic conductivity of the basin-fill sediments and faults of the Rio Grande rift. Spatial variability of hydraulic conductivity in the rift basins is largely a consequence of the tectonic and volcanic history of the rift. Describing this history and, particularly, the resulting geologic framework in the La Bajada constriction area, where ground water flows from the Española Basin into the Santo Domingo Basin, is a primary objective of this report. Better understanding of the subsurface geology affecting the ground-water resources of the region will improve hydrologic models of the age, movement, and recharge of ground water, and better models will improve the basis for managing the finite ground-water resources of northern New Mexico. Synthesis of multidisciplinary investigations involving geologic mapping, high-resolution airborne magnetic surveys, lithologic and geophysical logging of wells, surface-based electrical and magnetic surveys, enhanced satellite imagery, and hydrologic data will refine our understanding of the aquifer systems in the Santo Domingo Basin and the La Bajada constriction.

Geographic Setting

A prominent and important physiographic element of the study area is the chain of valleys and canyons occupied by the Rio Grande (Bryan and McCann, 1937) that result from geologic rift processes. The lowlands surrounding the Rio Grande between Pilar (fig. A1) on the north and its confluence with Cañada (Spanish for canyon) Ancha just south of Otowi Bridge and Buckman Mesa (La Mesita) (pl. 1) compose the Española Valley (fig. A2). Historically, this area was known as the Upper Rio Grande Valley during early Hispanic settlement that began in 1598, particularly in the areas of Española (then called Santa Cruz) and Santa Fe (fig. A1). South of Cañada Ancha the Rio Grande flows through White Rock Canyon, which separates Pajarito Plateau on the northwest from Caja del Rio Plateau on the southeast. White Rock Canyon is formed where the Rio Grande dissects the volcanic highland that separates the Española Valley from the Santo Domingo Valley (SDV, pl. 1, fig. A2). The Rio Grande exits the steep gorge of White Rock Canyon at Cochiti Pueblo and flows south through the broad lowlands of Santo Domingo Valley towards Bernalillo and Albuquerque (pl. 1). The La Bajada escarpment east of Cochiti Pueblo (pl. 1) forms the traditional northeastern boundary of the Lower Rio Grande Valley and also represents part of the eastern boundary of the Santo Domingo structural basin (see discussion below). The southern end of the Santo Domingo Valley is located north of Bernalillo where the Rio Grande lowlands become narrow between Santa Ana Mesa and the north end of the Sandia Mountains before widening again into the northern Albuquerque Basin (pl. 1, figs. A1, A2). The Cerrillos Hills, north of the Galisteo River, and the Caja del Rio Plateau form uplands separating the Santo Domingo Basin from the Española Basin to the northeast. The Santa Fe River cuts through this higher terrain in Cañada de Santa Fe before merging to the west with the Rio Grande in Santo Domingo Basin. Saint Peters Dome, northwest of Santo Domingo Basin, is a small massif of local peaks on the southeastern flank of the Jemez Mountains (pl. 1).

Figure A1 (facing page). Rio Grande rift region in northern New Mexico showing principal geologic and geographic features, cities, and towns mentioned in the text. BB, Bearhead Basin; CC, Cañada de Cochiti fault; CDRVF, Cerros del Rio volcanic field; EB, Embudo fault zone; HEB, Hagan embayment; JZ, Jemez fault; LB, La Bajada fault zone; PJ, Pajarito fault zone; RC, Rincon fault; SAMVF, Santa Ana Mesa volcanic field; SF, San Francisco fault; SY, San Ysidro fault; TJ, Tijeras fault zone; VV, Valley View fault. Modified from Smith, McIntosh, and Kuhle (2001).

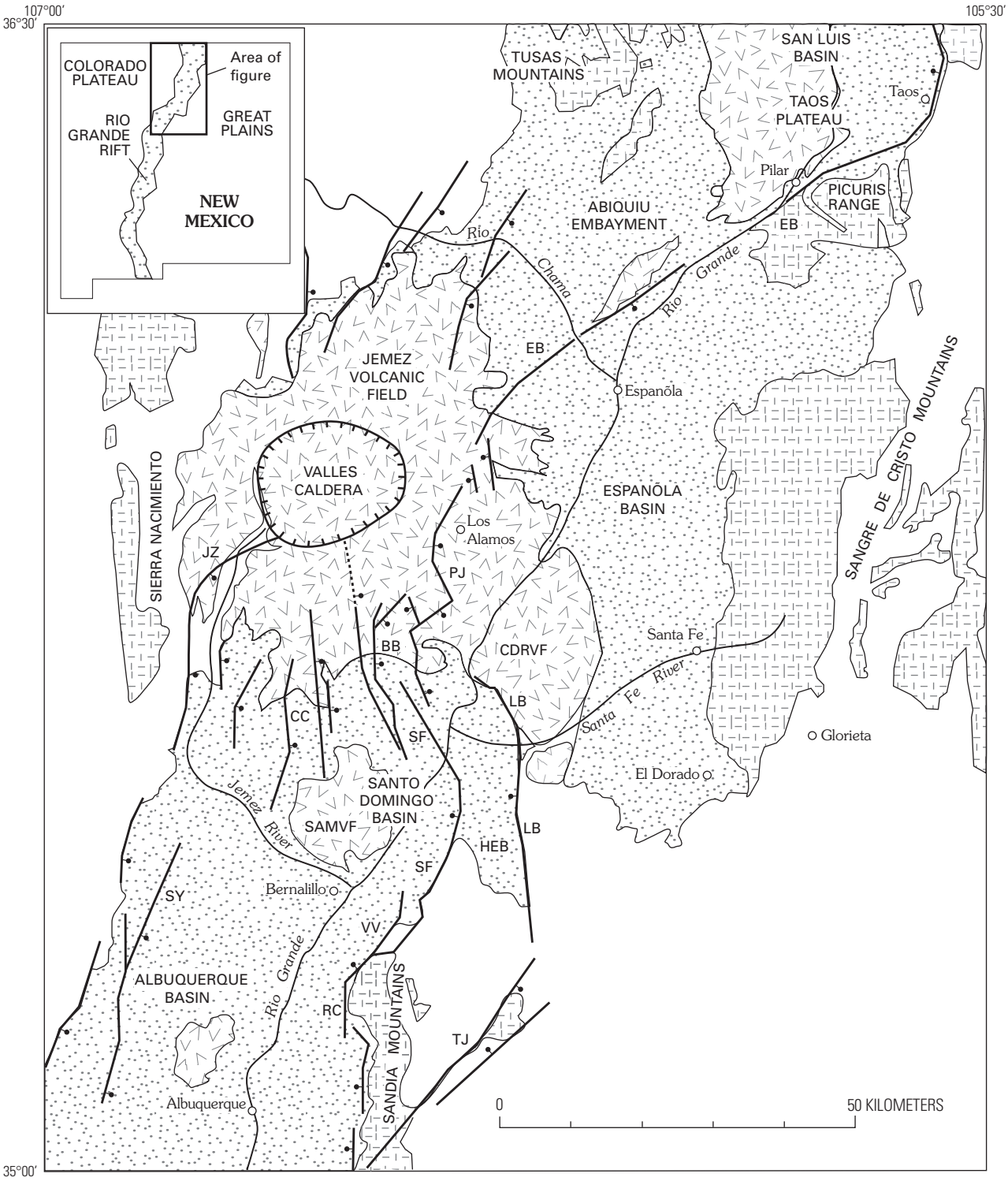

EXPLANATION

- **Pleistocene–Miocene volcanic rocks**
- **Pleistocene–Oligocene basin-fill sediment**
- **Lower Oligocene–Paleozoic rocks**
- **Precambrian rocks**
- **Major fault**—Bar and ball on downthrown block; dotted where concealed
- **Boundary of caldera**

It is important to note that the La Bajada constriction is a geologic feature that is largely covered by younger plateau-forming volcanic rocks of the Cerros del Rio volcanic field (CDRVF, fig. A2). Therefore, apart from the narrowing of Santo Domingo Valley at its northern end in White Rock Canyon, the constriction has little physiographic expression.

Land Use and Ownership

Land ownership and use in the Española and Santo Domingo Valleys is a complex mosaic of Native American lands, U.S. Government lands, Spanish land grants, and other minor state and private jurisdictions. Adjoining White Rock Canyon on the west are the federal lands of Bandelier National Monument on the southern Pajarito Plateau and on the east the Caja del Rio Plateau, administered by Santa Fe National Forest (SFNF) (pl. 1). Los Alamos National Laboratory, which occupies land of the Ramon Vigil Grant on the Pajarito Plateau, is administered by the U.S. Department of Energy. National Park Service and U.S. Forest Service public lands lie between the area of Los Alamos National Laboratory and Los Alamos County, in the central Pajarito Plateau, and the Pueblo lands of the northern Santo Domingo Valley. The Pueblo lands within Santo Domingo Valley (Cochiti, Santo Domingo, San Felipe, and Santa Ana Pueblos) are located largely in Sandoval County. Most of the Caja del Rio Plateau and the southern Española Valley are in Santa Fe County. San Ildefonso, Pojoaque, and Tesuque Pueblos border the study area on the north and east. Spanish land grants within the area that are now private include the centrally located Cañada de Cochiti Grant, between Bandelier National Monument and Cochiti Pueblo, and the Mesita de Juana Lopez, Ortiz Mine, and the Tejon Grants, along the east side of Santo Domingo Valley. To the west, most of the higher Jemez Mountains are federal land within the jurisdiction of Santa Fe National Forest, including the Valles Caldera National Preserve (enacted by Congress in 2000), which occupies the land of the former Baca Grant. Tribal lands of the Zia and Jemez Pueblos occupy large parts of the southern and western Jemez Mountains on the west side of the Santo Domingo Basin. The U.S. Bureau of Land Management (BLM) oversees a relatively small amount of federal land in the Santo Domingo and Española Basins—several tracts east of the Caja del Rio Plateau, west of Cochiti Pueblo, and east and south of San Felipe Pueblo. Kasha-Katuwe Tent Rocks National Monument (pl. 1) was established in January 2001 on BLM federal land west of Cochiti Pueblo.

The small Hispanic communities of Peña Blanca and Algodones and the towns of Bernalillo and Placitas are the only relatively large settlements outside of Pueblo lands in the Santo Domingo Valley (pl. 1). In the southern Española Basin east of Caja del Rio Plateau, metropolitan Santa Fe is the most rapidly growing population center in northern New Mexico.

In this report the term “Cochiti Pueblo area” informally refers to the six-quadrangle area shown on the geologic map in plate 2 (see pl. 1 for regional location) that is the focus of this study. Public access to most of the study area and surrounding region is restricted, owing to the almost complete (>80 percent) ownership of Santo Domingo Basin lands by the sovereign Indian Pueblos of Cochiti, Santo Domingo, San Felipe, Santa Ana, Zia, and Jemez.

Population Growth and Demands on Water

The Rio Grande aquifer underlying the Rio Grande from Cochiti Dam (pl. 1) downstream to just north of Socorro (to San Acacia, about 21 km north of Socorro) is the principal source of municipal water for the rapidly growing Albuquerque and Santa Fe metropolitan areas (Kernodle, McAda, and Thorn, 1995). This critical resource is more limited in geographic area, vertical extent, and water storage capacity than previously thought (Thorn, McAda, and Kernodle, 1993; Kernodle, McAda, and Thorn, 1995). Water shortfalls in northern New Mexico could have serious consequences for the state, because approximately 900,000 people (nearly 50 percent of the population of New Mexico, according to the U.S. Census Bureau, *http://factfinder.census.gov*; September 2005) live in the region (Bartolino, 1999). Future growth and sustainable land management depend on accurate assessment and protection of the region’s ground-water resources. In order to better understand the ground-water resources, we need a better understanding of the hydrogeology of the Santa Fe Group sedimentary deposits that fill the Rio Grande Basins and contain the principal ground-water aquifers.

Santa Fe County has grown substantially, from approximately 75,000 in 1980 to more than 125,000 in 2000, and averaged about 30 percent growth in both the 1980s and 1990s (U.S. Census Bureau, *http://factfinder.census.gov*; September 2005). This rate of growth is the second most rapid in New Mexico, after that of the Las Cruces and Doña Ana County area, and it is similar to the rate of growth of the Rio Rancho area northwest of Albuquerque (pl. 1). Most growth in Santa Fe County has been in the City of Santa Fe and in unincorporated areas adjoining the city. Growth is also evident to the south adjoining Highway 14 toward the town of Cerrillos and in the older Hispanic land grants and villages of Cieneguilla, Cañon, and La Cienega closer to Santa Fe (pl. 1). Since 1950 Santa Fe has kept up with increased demands for water by pumping the basin-fill aquifer at the Buckman well field in Cañada Ancha (pl. 1) and by increasingly exploiting the shallow Ancha aquifer south of the city. The rapid population growth in metropolitan Santa Fe and similar growth in the Rio Rancho area north of Albuquerque will increase the demand for ground water for the foreseeable future.

Previous Geologic Mapping

Previous geologic mapping in the La Bajada constriction area is briefly outlined below to summarize the state of geologic knowledge at the beginning of this study. As described in a subsequent section of this chapter, early studies

by Kirk Bryan (1938) and V.C. Kelley (1952, 1977) provided the foundation for the definition and basic geometry of the La Bajada constriction and Cerrillos uplift. Stearns (1953a,b,c) published the results of his Ph.D. dissertation under Kirk Bryan on the Galisteo area, including a 1:120,000-scale geologic map (Stearns, 1953b) of the area from Placitas to Santa Fe (pl. 1), largely east of the Santo Domingo Basin. Stearns (1953a) described the stratigraphic units and structure of this vast area, including the Espinaso Ridge, Hagan embayment, Galisteo monocline, Cerrillos Hills, and Cerros del Rio volcanic field (pl. 1, fig. A2), and he provided a sound geologic framework for subsequent work. Disbrow and Stoll (1957) studied the Cerrillos area and produced a 1:31,680-scale geologic map of the Cerrillos Hills and southernmost Cerros del Rio volcanic field. Stoll's U.S. Geological Survey (USGS) field work and mapping (1945–46) combined with Disbrow's graduate work at the University of New Mexico (1950–51) provided the first detailed study of Oligocene intrusive activity and related mineralization in the Cerrillos Hills. As part of their study, Disbrow and Stoll (1957) delineated the causes and timing of local and regional deformation in the Cerrillos Hills area.

Sun and Baldwin's (1958) study of the La Cienega area (pl. 1), which included a detailed (1:15,840-scale) geologic map, was an outgrowth of Baldwin's regional geologic mapping from 1951 to 1954 as part of USGS water resource investigations in the Santa Fe area (Spiegel and Baldwin, 1963). Spiegel and Baldwin (1963) published a comprehensive report on the geology and water resources of the Santa Fe area that summarized field research conducted mainly in 1951–52. This work, which included four 1:24,000-scale geologic quadrangle maps east and northeast of the La Bajada constriction and Cochiti Pueblo area, is also described in this report. Geophysical surveys and interpretations were a substantial contribution of Spiegel and Baldwin's report, which offered new structural interpretations of the Santa Fe embayment (fig. A2) and the edge of the Cerros del Rio volcanic field and improved understanding of the hydrogeology of the rift's basin-fill sequence.

Subsequent geologic mapping of the La Bajada constriction area was conducted as part of regional studies of the Rio Grande rift and Jemez volcanic field. Smith, Bailey, and Ross (1970) published a 1:125,000-scale map of the volcanic geology of the Jemez Mountains. This synthesis represented more than two decades of geologic investigations in the Jemez Mountains by R.L. Smith, who during this time developed the volcanologic concepts of ash-flow tuffs, zoning, cooling units, and resurgent calderas. Roy A. Bailey integrated more than 15 years of his own field work into the Jemez geologic map when he compiled it in 1967; he included work by Clarence S. Ross dating back to the 1920s. Although the map was compiled at a small scale to allow for generalization of geologic relations, the overall framework of volcanic and sedimentary units and faults that they portray for the La Bajada constriction area has held up remarkably well. Smith, Bailey, and Ross (1970) first recognized Pleistocene volcanism (younger than 1.61 million years ago (Ma)) in the western Cerros del Rio volcanic field east of the Rio Grande. The only aspect of their mapping that has required appreciable revision was their simplified treatment of the Santa Fe Group basin-fill sediments and younger surficial sedimentary deposits.

In the early 1950s Kelley (1952) identified most major geologic features within the area of the La Bajada constriction. More than two decades later Kelley (1977) published a memoir on the geology of the Albuquerque Basin that included a geologic map at a scale of 1:190,000. The following year he published a companion geologic map at 1:125,000-scale of the Española Basin (Kelley, 1978), which incorporated the volcanic geology of Smith, Bailey, and Ross (1970) "with very little modification." In these two works he summarized at reconnaissance scale what was then known about Rio Grande rift structure, tectonics, basin-filling sedimentary and volcanic rocks and, in a more generalized manner, bordering pre-rift rocks. Kelley's tectonic interpretations included defining major border and internal faults of the Santo Domingo Basin and recognizing the extent and configuration of basin-flanking uplift blocks and embayments. Kelley (1979) defined the Hagan "bench" (HB on fig. D1) as an elevated structural block in the northeast part of the Santo Domingo Basin, which he compared with the better studied Hubbell bench farther south in the Albuquerque Basin (fig. A1). Most details of the fault pattern in the Santo Domingo Basin have been modified by more recent detailed geologic mapping (described below) and differ somewhat from Kelley's interpretations (see Dethier, 1999; Smith, McIntosh, and Kuhle, 2001; Minor and Hudson, 2006). Collectively, Smith, Bailey, and Ross (1970) and Kelley (1977, 1978) established the fundamental geologic framework of the Jemez volcanic field and the adjoining Española, Santo Domingo, and Albuquerque Basins.

Building on the foundation work of Kelley and other workers, subsequent investigators have pursued more detailed and local geologic, geochemical, and geophysical studies. Several works that encompassed parts of the area of the La Bajada constriction and included geologic maps were published in the 1990s. The geology of the Saint Peters Dome area (pl. 1) was mapped at a scale of 1:24,000 by Goff, Gardner, and Valentine (1990) to delineate the Pajarito (PJ) fault zone (figs. A2–A4) for seismic hazard evaluation and to characterize the contact relations and ages of older eruptive units of the Jemez volcanic field that are exposed in the area. Cather (1992) provided a more detailed geologic map and stratigraphic description of older sedimentary rocks (Eocene Galisteo Formation) exposed at Saint Peters Dome and interpreted them in the context of Eocene (late Laramide) tectonic deformation.

Grant (1997, 1999) reviewed the subsurface geology and hydrogeology of the Santa Fe embayment (fig. A2) for the New Mexico Office of State Engineer. These reports contain a comprehensive synthesis of published data on the geology, geophysics, and hydrology of the area from the Sangre de Cristo Mountains west to the Cerros del Rio volcanic field and emphasize the area from Galisteo River north to Tesuque Pueblo (pl. 1). He presented important new information on petroleum test wells in the Santa Fe embayment region and made inferences about the structural controls of the regional

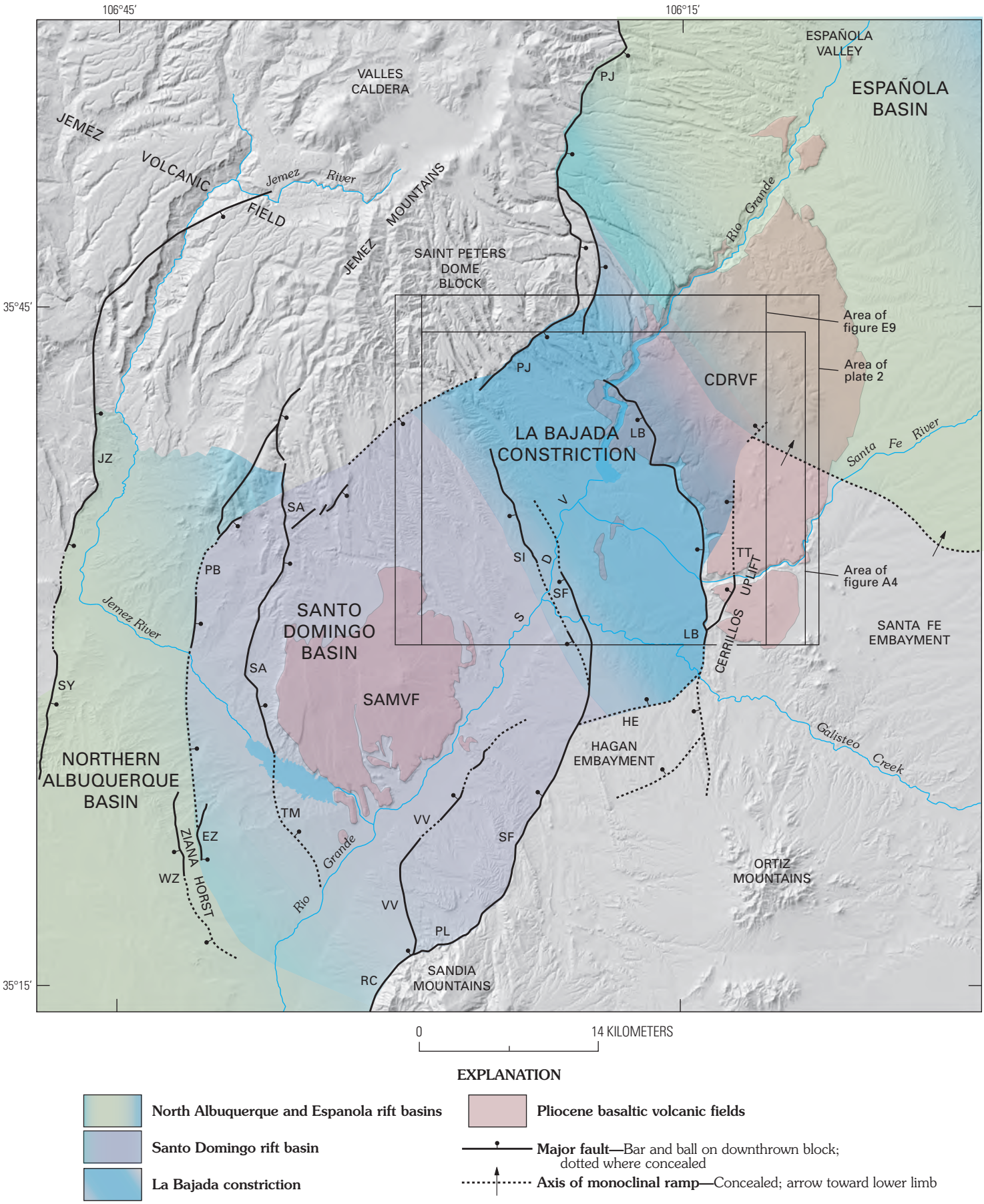
106°45′
106°15′
35°45′
35°15′
ESPAÑOLA VALLEY
ESPAÑOLA BASIN
VALLES CALDERA
JEMEZ VOLCANIC FIELD
JEMEZ MOUNTAINS
Jemez River
Rio Grande
SAINT PETERS DOME BLOCK
Area of figure E9
Area of plate 2
Area of figure A4
CDRVF
LA BAJADA CONSTRICTION
Santa Fe River
SANTO DOMINGO BASIN
SAMVF
SANTA FE EMBAYMENT
HAGAN EMBAYMENT
Galisteo Creek
NORTHERN ALBUQUERQUE BASIN
ZIANA HORST
ORTIZ MOUNTAINS
SANDIA MOUNTAINS
CERRILLOS UPLIFT
PJ
LB
JZ
SA
PB
SI
D
V
S
SF
TT
SY
HE
TM
EZ
WZ
VV
PL
RC
0
14 KILOMETERS
EXPLANATION
North Albuquerque and Espanola rift basins
Santo Domingo rift basin
La Bajada constriction
Pliocene basaltic volcanic fields
Major fault—Bar and ball on downthrown block; dotted where concealed
Axis of monoclinal ramp—Concealed; arrow toward lower limb

Figure A2 (facing page). Segment of the middle Rio Grande rift showing the extent, topographic expression (gray background shading), and principal structural borders of the contiguous Santo Domingo, northern Albuquerque, and Española Basins and the La Bajada constriction. La Bajada constriction overlaps northeast part of Santo Domingo Basin and southwest part of Española Basin. Areas of three other figures or plates of this report are outlined. Background topographic shading based on 30-m digital elevation model. SDV, Santo Domingo Valley. Pliocene basaltic volcanic fields: Cerros del Rio (CDRVF) and Santa Ana Mesa (SAMVF). Fault and fault zones: EZ, East Ziana; HE, Hagan Embayment; JZ, Jemez; LB, La Bajada; PB, Pico Butte; PJ, Pajarito; PL, Placitas; RC, Rincon; SA, Santa Ana; SF, San Francisco; SI, Sile; SY, San Ysidro; TM, Tamaya; TT, Tetilla; VV, Valley View; WZ, West Ziana.

hydrogeology of the basin-fill aquifer system. Grant recognized that intrusions in the Cerrillos Hills (pl. 1) cause large perturbations of the regional ground-water flow system. In these reports brief but important mention was made of a continuation of the Santo Domingo structural basin north beneath the Cerros del Rio volcanic field. Grant (1997, 1999) argued for substantial ground-water underflow in the Rio Grande basin-fill aquifer beneath rocks of the volcanic field from the Española Basin into the Santo Domingo Basin owing to an absence of prominent structural or stratigraphic barriers between them.

During the past 10 years, geology was mapped at 1:24,000 scale by the USGS and the University of New Mexico in the La Bajada constriction study area in the following 7.5′ quadrangles (fig. A4): Tetilla Peak (Sawyer and others, 2002); Santo Domingo Pueblo (Smith and Kuhle, 1998a); and Santo Domingo Pueblo SW (Smith and Kuhle, 1998b). Building on this mapping, three reports have been published on the hydrogeology, structure, and tectonics of Santo Domingo Basin (Smith and Kuhle, 1998c; Smith, McIntosh, and Kuhle, 2001; Minor and Hudson, 2006) and on the Quaternary geology of the lower White Rock Canyon area (Dethier, 1999). These results and other topical syntheses generated from recent USGS and New Mexico Bureau of Geology and Mineral Resources geologic joint investigations are reviewed and summarized in subsequent chapters of this report. Recent geologic maps of areas adjoining the study area that have been published by the New Mexico Bureau of Geology and Mineral Resources (Madrid quadrangle to the south by Maynard, Sawyer, and Rogers, 2001; the San Felipe Pueblo NE quadrangle to the southwest by Cather, Connell, and Black, 2000; and Turquoise Hill quadrangle to the east by Koning and Hallett, 2000) provide additional surface geologic constraints on structures and deposits of the region.

Geologic Setting of the La Bajada Constriction Area

Rio Grande Rift

The geologic, geophysical, and hydrogeologic properties of the Santo Domingo Basin and La Bajada constriction result from processes related to evolution of the Rio Grande rift. The Rio Grande rift is a major continental rift system (fig. A1 inset) that separates the Colorado Plateau microplate on the west from the stable North American craton underlying the Great Plains to the east (Kelley, 1977; Chapin and Cather, 1994). From New Mexico northward, the Rio Grande rift continues as a major tectonic feature through the San Luis Valley of Colorado and then narrows into the Upper Arkansas River valley. The rift becomes poorly defined in northern Colorado and south-central Wyoming, where it is expressed by a series of discontinuous normal faults and isolated Tertiary volcanic features. South from approximately the latitude of Socorro, New Mexico, the Rio Grande rift widens into a series of basins and ranges that merge with the eastern part of the Basin and Range province of southern Arizona, southern New Mexico, west Texas, and northern Mexico (principally in the states of Sonora and Chihuahua). In southern Colorado and northern New Mexico, the Rio Grande rift is a distinct regional physiographic feature that forms a chain of broad valleys (San Luis, Española, Santo Domingo, and Albuquerque Valleys) through which the Rio Grande flows southward. These valleys are underlain by, and are more or less coincident with, structural basins (San Luis, Española, Santo Domingo, and Albuquerque Basins) that compose this part of the Rio Grande rift. The Rio Grande rift basins are arranged in a right-stepping en echelon pattern from the northern New Mexico border to Socorro (Kelley, 1982). The landforms characterizing these basins result from the combined effects, during the last 30 million years, of extensional tectonism, intrabasinal sedimentary deposition, and volcanism associated with rifting (Chapin, 1971; Tweto, 1978, 1979; Baldridge, Bartov, and Kron, 1983; Smith, McIntosh, and Kuhle, 2001; Smith, 2004). Large mountain ranges east of the Rio Grande rift (such as the Sangre de Cristo, Sandia, and Manzano Mountains) were strongly uplifted during the rifting. The volcanic San Juan Mountains (36–26 Ma), the dominantly nonvolcanic Tusas Mountains, and the volcanic Jemez Mountains (12 Ma–50 thousand years ago (ka)) that form the western border of the Rio Grande rift were generally uplifted less.

Basin Architecture and Terminology

Original Definitions of the La Bajada Constriction and Cerrillos Uplift

In the two quotations below, text in brackets is added to identify to geographic localities implied by the text:

“The La Bajada constriction, which bounds the [Española] basin on the south, is formed by the La Bajada fault zone which

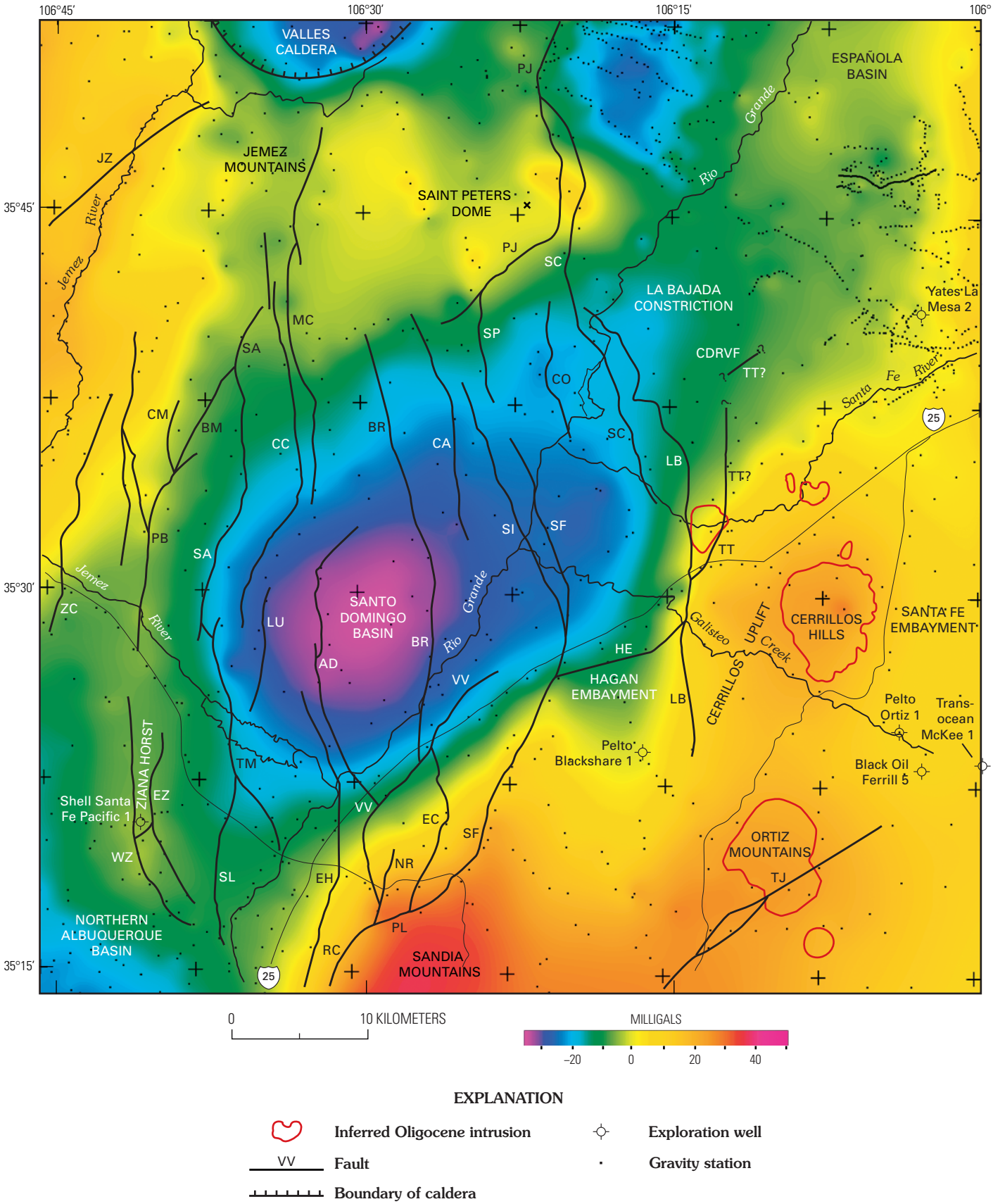

EXPLANATION

Inferred Oligocene intrusion

Fault (VV)

Boundary of caldera

Exploration well

Gravity station

Figure A3 (facing page). Isostatic residual gravity model of the Santo Domingo Basin area showing gravity stations and major faults in the Santo Domingo Basin and adjoining areas. Locations of the Santo Domingo and Española Basins, Sandia Mountains, Cerrillos uplift, Saint Peters Dome block, and Ziana horst shown in the figure are based on the gravity model. Outlines of Oligocene monzonite intrusions inferred from aeromagnetic data (see chapter D, this volume). Fault and fault zone abbreviations: AD, Algodones; BM, Borrego Mesa; BR, Borrego; CA, Camada; CC, Cañada de Cochiti; CM, Chamisa Mesa; CO, Cochiti; EC, Escala; EH, East Heights; EZ, East Ziana; HE, Hagan Embayment; JZ, Jemez; LB, La Bajada; LU, Luce; MC, Mesita Cocida; NR, North Rincon; PB, Pico Butte; PJ, Pajarito; PL, Placitas; RC, Rincon; SA, Santa Ana; SC, Sanchez; SF, San Francisco; SI, Sile; SL, South Luce; SP, South Pajarito; TJ, Tijeras; TM, Tamaya; TT, Tetilla; VV, Valley View; WZ, West Ziana; ZC, Zia County Dump

separates the Santo Domingo basin from the Cerrillos uplift and the White Rock channel. The Cerrillos uplift consists of Mesozoic and early Tertiary sediments and middle Tertiary volcanic rocks intruded by several porphyry masses. The connecting structure between the Española and Santo Domingo Basins is the White Rock channel. This linkage between the two basins lies between the buried northern edge of the Cerrillos uplift and a small salient [Saint Peters Dome] at the southeastern edge of the Jemez uplift." (Kelley, 1952, p. 93)

Thus, Kelley (1952) outlined the basic geologic elements defining the boundary between the Española and Santo Domingo Basins of the Rio Grande rift (or depression, as it was known at that time). The northern boundary of the Santo Domingo Basin was identified by Kelley as the La Bajada constriction, where the Rio Grande rift narrows and then widens again into the adjoining Española Basin (fig. A2). The northwest boundary of the La Bajada constriction was defined where pre-rift rocks are exposed in the footwall of the down-to-east Pajarito fault zone at Saint Peters Dome which, in turn, becomes the western boundary of the Española Basin (fig. A2). The southeast boundary of the La Bajada constriction was recognized as the northern edge of the Cerrillos uplift, which was known to be largely hidden beneath mafic lavas of the Cerros del Rio volcanic field (CDRVF, fig. A2). Kelley's work amplified an earlier description of the Cerrillos uplift by Kirk Bryan (1938, p. 213):

"Separating the subbasin west of Santa Fe from the Santo Domingo Valley is a prong of older rocks projecting northwest from the Ortiz Mountains. The Cerrillos Hills, composed of andesite intrusions and other crystalline rocks, form the southern portion of this prong. The northern portion is blanketed by Quaternary basalt, so that there is no distinction on the surface between this prong and the basalts of Santa Fe age that form the Cerros del Rio. The west side is marked by a strong north-south fault [La Bajada fault zone] which passes through Rosario siding. The east side is covered by Quaternary gravel, but doubtless detailed study will show the presence of faults."

The locations of the features described above were first depicted by Kelley in a map displaying major tectonic features of the La Bajada constriction area (Kelley, 1952, p. 92). The term "White Rock channel" has found little further acceptance or usage, but most of the other tectonic features described and mapped by Kelley in the La Bajada constriction area have been tacitly adopted in all subsequent geologic work in the region. Kelley did not provide a more precise definition or explain the hydrogeologic significance of the La Bajada constriction, and he did not specifically address the role that the La Bajada fault zone and buried faults farther east play in controlling the distribution and continuity of the basin-fill aquifer in the subsurface.

Geologic Definition of the La Bajada Constriction and Surrounding Basins

The salient geologic features of the La Bajada constriction, as presently defined, and the overlapping Santo Domingo Basin are introduced in this section. Detailed descriptions of the constriction, and new geologic and geophysical observations upon which they are based, are presented in subsequent chapters of this report.

We adopt the definition of the Santo Domingo Basin provided by Smith, McIntosh, and Kuhle (2001). The Santo Domingo Basin is situated between the Albuquerque Basin to the south and the Española Basin to the north (fig. A1). The large Albuquerque Basin is a composite structural feature that can be divided into several smaller subbasins, including the northern Albuquerque (or Calabacillas) Basin (fig. A2) that is adjacent to the Santo Domingo Basin (Ferguson and others, 1995; Hawley and Whitworth, 1996; Grauch, Gillespie, and Keller, 1999). The northern Albuquerque Basin is a dominantly east-tilted half graben bounded on its east side along the base of the Sandia Mountains by the large-displacement Rincon (RC) normal fault zone (fig. A2). The Española Basin is a west-tilted half graben bounded on its west side by the large-displacement Pajarito (PJ) normal fault zone. The intervening Santo Domingo Basin is an antiformal symmetric graben bounded by the east-dipping East Ziana (EZ), Pico Butte (PB), Santa Ana (SA), and Tamaya (TM) faults on the west and the west-dipping La Bajada (LB) and San Francisco (SF) faults on the east (fig. A2; chapter E, this volume) (Smith, McIntosh, and Kuhle, 2001).

Interpretation of gravity data (fig. A3) indicates a marked thickening of Santa Fe Group sediments in the Santo Domingo Basin southwest of the San Francisco fault (chapter D, this volume; Grauch, Gillespie, and Keller, 1999). On the basis of this change in basin-fill thickness, the Santo Domingo Basin can be divided into two structural subbasins. The surface trace and projection of the San Francisco fault (SF) approximates the boundary between a shallower (<2.5-km-thick basin fill) in the northeast part of the Santo Domingo Basin in the footwall block of the San Francisco fault and a deeper (2.5- to >4-km-thick basin fill) main part of the Santo Domingo Basin in the hanging-wall block of the fault (figs. A2, A3).

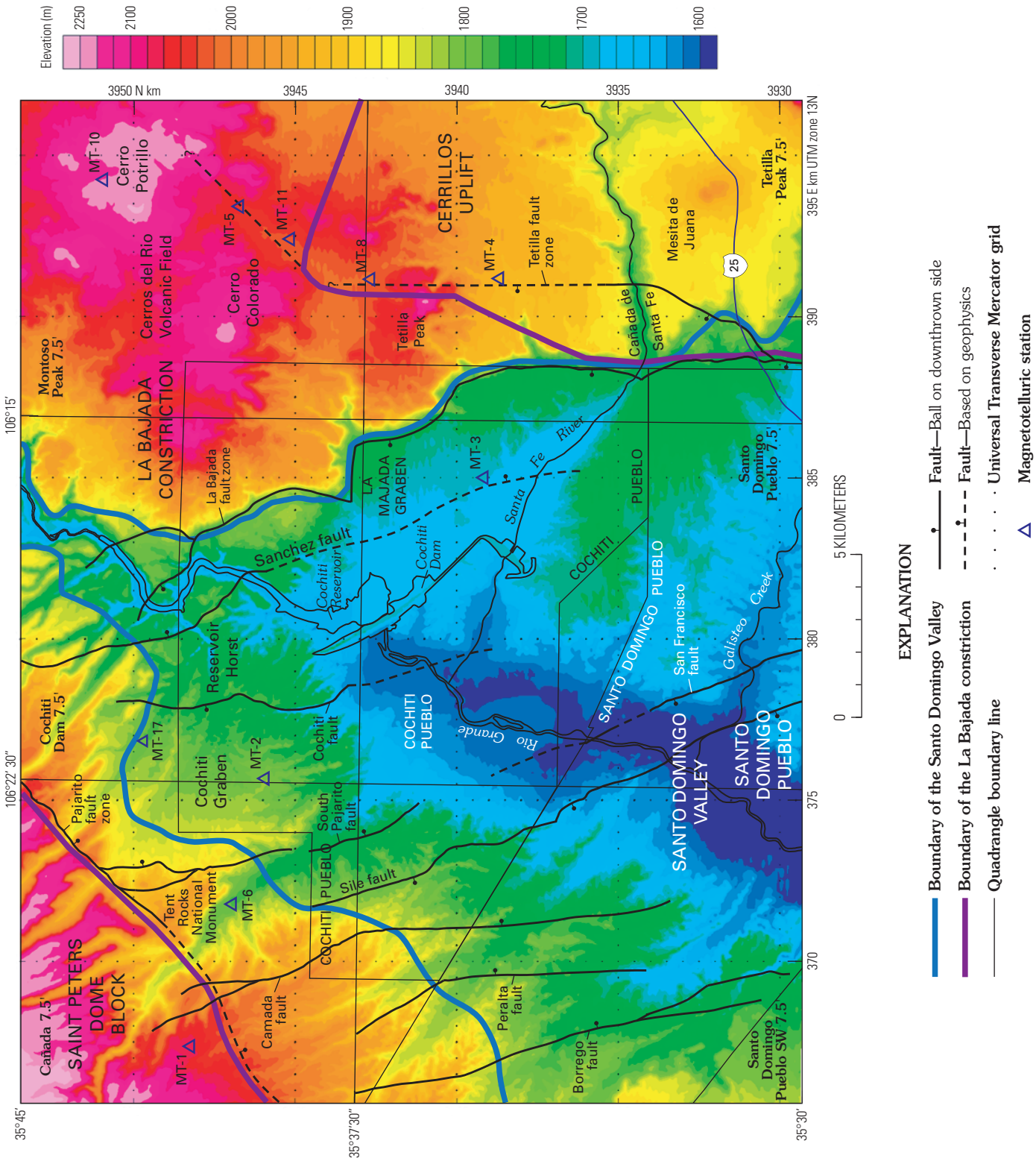
Elevation (m)
2250
2100
2000
1900
1800
1700
1600
3950 N km
3945
3940
3935
3930
395 E km UTM zone 13N
390
385
380
375
370
106°15'
106°22' 30"
35°45'
35°37'30"
35°30'
0
5 KILOMETERS
MT-10
Cerro Potrillo
MT-5
MT-11
Montoso Peak 7.5'
Cerros del Rio Volcanic Field
Cerro Colorado
LA BAJADA CONSTRICTION
La Bajada fault zone
MT-8
Tetilla Peak
CERRILLOS UPLIFT
MT-4
Tetilla fault zone
Mesita de Juana
Tetilla Peak 7.5'
Cañada de Santa Fe
25
Cochiti Dam 7.5'
MT-17
Reservoir Horst
Sanchez fault
Cochiti Reservoir
Cochiti Dam
LA MAJADA GRABEN
MT-3
Santa Fe River
COCHITI PUEBLO
Santo Domingo Pueblo 7.5'
Pajarito fault zone
Cochiti Graben
MT-2
Cochiti fault
COCHITI PUEBLO
Rio Grande
SANTO DOMINGO PUEBLO
San Francisco fault
Galisteo Creek
Tent Rocks National Monument
MT-6
South Pajarito fault
Sile fault
COCHITI PUEBLO
SANTO DOMINGO VALLEY
SANTO DOMINGO PUEBLO
Cañada 7.5'
SAINT PETERS DOME BLOCK
MT-1
Camada fault
Peralta fault
Borrego fault
Santo Domingo Pueblo SW 7.5'
EXPLANATION
Boundary of the Santo Domingo Valley
Boundary of the La Bajada constriction
Quadrangle boundary line
Fault—Ball on downthrown side
Fault—Based on geophysics
Universal Transverse Mercator grid
Magnetotelluric station

Figure A4 (facing page). Cochiti Pueblo area, showing La Bajada constriction between bounding Cerrillos uplift and Saint Peters Dome block. Lowlands of the Santo Domingo Valley in the northeast part of the Santo Domingo Basin separate the western border terrane, which consists of the Saint Peters Dome block and adjacent uplands southeast of the Pajarito fault zone, from the eastern border terrane, which consists of the Cerrillos uplift and onlapping Cerros del Rio volcanic field. The northern Santo Domingo Valley, underlain by basin-fill deposits, is subdivided into the Cochiti graben, Reservoir horst, and La Majada graben; see text for descriptions. UTM, universal transverse mercator.

The La Bajada constriction is the relatively narrow structural trough linking the southern part of the Española Basin and the northeastern part of the Santo Domingo Basin (fig. A2). It is bounded by rift-flank uplifts and is occupied by basin-fill sediments of the Santa Fe Group. In the present study we restrict the La Bajada constriction to those parts of the structural trough containing large (≥200 m) preserved thicknesses of basin-fill sediments, because such deposits most likely provide hydrologic connectivity for ground water flowing between the Española and Santo Domingo Basins. Large faults that form the principal structural borders of the constriction are various branches and segments of the Pajarito (PJ), La Bajada (LB), and Tetilla (TT) fault zones (fig. A2). The Pajarito fault zone, which is the western principal structure bounding the present-day Española Basin, branches south of Saint Peters Dome into several splays (figs. A3, A4). Near Saint Peters Dome, one such splay of the Pajarito (herein named the Sanchez (SC) fault) bends southeastward from the southwest-striking, gravity-defined (chapters D and E, this volume), main Pajarito fault strand toward the center of the La Bajada constriction (figs. A3, A4). Splays of the La Bajada fault zone curve northwestward into the center of the constriction and overlap the Sanchez fault from the opposite, eastern border of the Santo Domingo Basin (figs. A3, A4). The Sanchez, La Bajada, and other faults offset Pliocene-Pleistocene volcanic rocks of the Cerros del Rio and Jemez volcanic fields in the central part of the La Bajada constriction, whereas these same young volcanic rocks overlie buried, gravity-defined, basement structural highs on the flanks of the constriction.

The La Bajada constriction area can be subdivided into three terranes on the basis of topographic expression, structural configuration, and dominant stratigraphy: the elevated Cerros del Rio volcanic field–Cerrillos uplift eastern border terrane; the central Santo Domingo Valley; and the elevated Saint Peters Dome block western border terrane (figs. A2, A4). Each of these terranes is described separately below.

Cerros Del Rio Volcanic Field and Cerrillos Uplift

The eastern border terrane consists primarily of two geologic elements: the Pliocene Cerros del Rio volcanic field (CDRVF) and the Cerrillos uplift composed of Miocene and older basement rocks (figs. A2, A4). The La Bajada fault zone bounds the west side of this eastern border terrane. The coincident, west-facing, La Bajada escarpment is the physiographic boundary between the Santo Domingo Valley and the elevated Caja del Rio Plateau (pl. 1). Young (≤2.7 Ma) basalts and andesites of Cerros del Rio exposed east of the escarpment are relatively unfaulted and form a geomorphically well-expressed volcanic plateau made up of many eruptive vents and surrounding lava-capped mesas (pl. 2; chapter C, this volume). Nearly all of the Cerros del Rio volcanic rocks in the eastern border terrane lie at elevations above 1,800 m (fig. A4), and constructional volcanic landforms in the central and northern Cerros del Rio rise to elevations greater than 2,200 m. The late Pliocene age (2.7–2.2 Ma) and little-deformed character of this volcanic plateau indicate that for about the last 3 m.y. the footwall block of the La Bajada fault zone has remained tectonically stable. A gentle (<2°) eastward tilt of basal basalt flows at the south end of the Cerros del Rio volcanic plateau suggest only mild uplift in the footwall of the La Bajada fault zone.

The Cerrillos uplift, which forms the southeastern border of the La Bajada constriction, is a structural high that is mostly buried beneath lava of the Cerros del Rio volcanic field (CDRVF) (figs. A2, A4). North of the Santa Fe River (Cañada de Santa Fe), where it is completely concealed, the Cerrillos uplift is largely delineated by gravity data (fig. A3; chapter D, this volume). In the region extending from Cañada de Santa Fe southward around the margins of the Mesita de Juana volcano (fig. A4), exposed pre-rift rocks of the Cerrillos uplift consist of Mesozoic sedimentary rocks unconformably overlain by Eocene Galisteo Formation and upper Eocene–Oligocene Espinaso Formation (pl. 2), all dipping moderately (11°–15°) east-northeastward. This homoclinal sequence of rocks, the Galisteo monocline (pl. 1) of Stearns (1953a), is a surface expression of rift-flank uplift in the footwall block of the southern La Bajada fault zone. The Cerrillos uplift (figs. A2, A3) has weak topographic expression other than at the Cerrillos Hills and Ortiz Mountains (pl. 1) in its central and southern parts, which are underlain by resistant upper Eocene–Oligocene intrusive rocks.

North of Cañada de Santa Fe the gravity-expressed western border of the Cerrillos uplift projects northward, away from the northwest-striking La Bajada fault zone, and merges with a buried northern projection of the Tetilla fault zone (figs. A2, A3, A4). Where exposed to the south in the La Bajada escarpment near U.S. Interstate 25 (pl. 1, 2; fig. A4), the Tetilla fault zone strikes northeastward and juxtaposes Eocene–Oligocene rocks and overlying Miocene(?) rift basin-fill sediments against Mesozoic sedimentary rocks (pl. 2). North of Cañada de Santa Fe the fault zone is buried by Pliocene Cerros del Rio basalts, and it is projected northward for several kilometers on the basis of subsurface electromagnetic evidence (chapters E and F, this volume; figs. A2, A4). On the basis of several lines of geologic and geophysical evidence, the Cerrillos uplift also continues northward on the upthrown side of the Tetilla fault zone beneath cap rock of the

Cerros del Rio volcanic field. The buried north end of the Cerrillos uplift and coincident northeast "corner" of the La Bajada constriction (that is, where it opens up into the Española Basin) (fig. A2) are delineated from subsurface geologic and geophysical interpretations presented in subsequent chapters of this report (chapters D, E, F, and G, this volume).

Santo Domingo Valley

The northeast part of the Santo Domingo Valley overlaps the southwest part of the La Bajada constriction (figs. A2, A4). This area contains a complex interfingering of rift basin-fill sedimentary deposits and volcanic rocks of the Jemez and Cerros del Rio volcanic fields that are cut by regularly spaced, mainly north-northwest-striking normal faults. The thickness of basin-fill deposits differs in different fault blocks because of the variable tectonic and growth-fault histories of individual blocks. Three main structural domains identified within the Santo Domingo Valley in the Cochiti Pueblo area are, from west to east, the Cochiti graben, Reservoir horst, and La Majada graben (fig. A4). These domains are briefly described below. Fuller descriptions and interpretations of the domains are provided in subsequent chapters of this report, and their significance with respect to the hydrogeologic framework of the La Bajada constriction is addressed in chapter G (this volume).

South of Saint Peters Dome, the north-trending Cochiti graben is bounded by the east-dipping South Pajarito fault and the west-dipping Cochiti fault (fig. A4). Several additional, smaller displacement north-striking faults lie within the graben (pl. 2). The Cochiti graben contains extensive exposures of the Otowi Member (unit Qbo, lower member) of the Bandelier Tuff (chapter B, this volume) that have been downdropped between the two bounding faults (pl. 2). The southeastern margin of exposed rocks of the Jemez volcanic field extends farther south within the graben than on its flanks, because the Bandelier Tuff is better preserved within the graben. Southwest of the graben, between the South Pajarito and Sile faults (fig. A4), a narrow yet stratigraphically distinct horst locally forms the boundary between the northeast part of the Santo Domingo Basin and the deeper central part of the basin to the southwest.

The centrally located Reservoir horst, which borders the east side of the Cochiti graben, is located between the Cochiti fault and the southern part of the newly identified, down-to-east Sanchez fault (chapter E, this volume; fig. A4). The southern part of the Sanchez fault is delineated on the basis of aeromagnetic and electromagnetic constraints presented in chapters D and F of this volume. Cerros del Rio basalts and interfingering Santa Fe Group ancestral Rio Grande axial river gravels are exposed within the Reservoir horst (pl. 2). The basaltic rocks and associated near-vent basaltic hydromagmatic deposits form the foundation for Cochiti Dam and underlie Cochiti Reservoir (fig. A4) (Smith and Kuhle, 1998a; Smith, McIntosh, and Kuhle, 2001).

The La Majada graben is located directly east of the Reservoir horst between the down-to-east Sanchez fault and the down-to-west La Bajada fault zone (fig. A4). Cerros del Rio basalt in this graben is downdropped at least 500 m relative to exposures in the footwall of the La Bajada fault (Smith, McIntosh, and Kuhle, 2001; chapter G, this volume). Scalloped fault splays of the La Bajada fault zone locally cut across the La Majada graben (chapter E, this volume). Santa Fe Group axial river and eastern piedmont sediments underlie most of the La Majada graben (pl. 2) (Smith, McIntosh, and Kuhle, 2001).

Saint Peters Dome Block

The northwestern border of the La Bajada constriction is formed by a northeast-striking segment of the Pajarito fault zone and its upthrown Saint Peters Dome footwall block directly to the west (figs. A2, A3). The western border terrane extends from the footwall block of the Pajarito fault zone towards the constriction axis as far east as the simplified 1,800-m-elevation contour (wide blue line, fig. A4). At Saint Peters Dome proper, just west of the La Bajada constriction, pre-rift Eocene Galisteo Formation sedimentary rocks (unit Tg, pl. 2) are exposed underneath rocks of the Jemez volcanic field. Southwest of Saint Peters Dome is a prominent topographic bench where the northeast-trending main trace of the Pajarito fault offsets the 1.22-Ma cliff-forming Tshirege Member (unit Qbt, upper member) of the Bandelier Tuff and where the South Pajarito fault branches from the main trace and heads southward towards Tent Rocks National Monument (pl. 2, fig. A4). Gravity data (chapter D, this volume) suggest that the northeast-striking segment of the Pajarito fault zone may continue to the southwest as a buried large-displacement fault and, thus, may form the northwest border of the main Santo Domingo structural basin (figs. A2, A3). Upper Tshirege (unit Qbt) and lower Otowi (unit Qbo) Members of the Bandelier Tuff are well preserved in the tablelands between the main northeast-striking Pajarito fault zone and the Rio Grande north of Cochiti Reservoir (pl. 2). Within and south of Peralta Canyon (pl. 1), the western border terrane is underlain by locally faulted Miocene to Pliocene Cochiti Formation (unit QTc) sedimentary deposits (pl. 2) representing western piedmont fill of the Santo Domingo Basin (Smith, McIntosh, and Kuhle, 2001).

Stratigraphy of Pre-Rift Rocks

The stratigraphy of Precambrian crystalline basement rocks and overlying Paleozoic, Mesozoic, and lower Tertiary pre-rift sedimentary rocks is briefly described here to provide geologic context for the younger rift-fill deposits, volcanic rocks, and associated structures that are the main focus of this report. The reader is referred to chapters B and C of this volume for descriptions of Miocene and younger rift basin-fill sediments and volcanic rocks, respectively.

Precambrian and Paleozoic Rocks

Precambrian rocks are not exposed in the La Bajada constriction nor in the flanking Saint Peters Dome and Cerrillos uplifts, so the characteristics of basement rocks underlying the area at depth are inferred from exposures in other parts of the region. South of the Cochiti Pueblo area in the Hagan embayment and Sandia Mountains, exposed basement rocks consist of Middle Proterozoic 1.4-Ga Sandia Granite (Kelley and Northrop, 1975); in the Sangre de Cristo Mountains east of the Española Basin (fig. A1) they are largely Early Proterozoic (1.7–1.6 Ga) granite and gneiss (Karlstrom and others, 1999, 2004). Basement rocks underlying the La Bajada constriction area and Española Basin probably resemble the granites and gneisses in the Sangre de Cristo Mountains and Hagan embayment but not the supracrustal metapelitic rocks exposed in the Picuris Range and Tusas Mountains to the north (fig. A1) (Karlstrom and others, 1999, 2004). The aeromagnetic signature beneath the Española Basin closely resembles the patterns typically observed for Proterozoic granites (chapter D, this volume). The controversial Yates La Mesa 2 (sec. 24, T. 17 N., R. 8 E.) drill hole (pl. 1, fig. A3) provides the only direct evidence of the nature of geologic basement beneath the Española Basin. G.A. Smith (University of New Mexico, oral commun., 2000) and S.M. Cather and R.F. Broadhead (New Mexico Bureau of Geology and Mineral Resources; oral commun., 2000) considered “granite wash” at the bottom of this hole (7,534–7,710 ft depth) to represent Proterozoic granite, consistent with borehole geophysical log data. Alternatively, Grant (1997, 1999) interpreted the material in the bottom of the hole as arkosic sedimentary rocks of the Eocene Galisteo Formation.

No Paleozoic rocks are exposed in the La Bajada constriction area, but Pennsylvanian and Permian beds are exposed elsewhere in north-central New Mexico (table A1) (Lucas, Rowland, and others, 1999). Pennsylvanian marine carbonate strata have been observed in the Transocean McKee 1 drill hole in the nearby Santa Fe embayment (pl. 1, fig. A3) and consist of limestone of the Madera Group and probably the underlying more clastic Sandia Formation (table A1) (Black, 1979, 1999; Myers, 1982; Broadhead, 1997). Overlying Permian sedimentary rocks in the drill hole include the marine San Andres Limestone and the predominantly continental and clastic Glorieta Sandstone, Yeso Formation (including the distinct eolian Meseta Blanca Sandstone Member), and Abo Formation (Lucas, Rowland, and others, 1999). East of the Santa Fe embayment, Pennsylvanian, Permian, and Triassic sedimentary rocks are widely exposed in the Glorieta area and southeastern Sangre de Cristo Mountains (Baltz and Myers, 1999). Gross thickness of the Pennsylvanian-Jurassic section in the region ranges from a minimum of 1,272 m in the Shell Santa Fe Pacific 1 well (see fig. A3 for location) to a maximum of about 1,800 m in the Hagan Basin surface section (Lucas and others, 1999; Cather and others, 2002) and the Transocean McKee 1 well (table A1). Black and Hiss (1974) interpreted the Shell Santa Fe Pacific 1 stratigraphic section to have been thinned by recurrent local uplift and erosion in Pennsylvanian, Cretaceous, and Oligocene-Miocene time. A more representative minimum Pennsylvanian-Jurassic thickness in this well is probably closer to 1,350–1,375 m.

Mesozoic Sedimentary Rocks

In the La Bajada constriction area, Mesozoic sedimentary rocks are exposed only in the footwall block of the La Bajada fault zone within the Galisteo monocline and in Cañada de Santa Fe (pls. 1, 2). The oldest Mesozoic rocks exposed are Upper Triassic Chinle Formation (unit Ꞧc) that crops out in the footwall of the La Bajada fault zone; it is more widely exposed immediately to the south of the area shown in plate 2 (Bachman, 1975; Lucas and Heckert, 1995; Maynard, Sawyer, and Rogers, 2001). The Chinle Formation consists of red-brown mudstone and siltstone. Bachman (1975) estimated a stratigraphic thickness of at least 150 m for Chinle exposed in the Galisteo monocline, but a more thorough examination of regional data from wells and measured sections (table A1) suggests a thickness as much as 500 m or more. The thick upper clay-rich part of the Chinle exposed in the Galisteo monocline probably correlates with the Petrified Forest Member (Lucas, Heckert, and Estep, 1999). The unconformably overlying Middle Jurassic Entrada Sandstone (unit Je, pl. 2), which is also exposed in the La Bajada footwall block in the Galisteo monocline, is characteristically a medium- to fine-grained, reddish-brown to yellowish-gray, quartzose sandstone. The 30–60-m-thick Entrada (table A1) is a resistant ledge former and is massive to planar and cross bedded. Where exposed in the region the unit is divisible into two parts of subequal thickness: a reddish-brown lower section and a dominantly yellowish-gray upper section (Lucas, Anderson, and Pigman, 1995).

The Todilto Formation (unit Jt, pl. 2), which overlies the Entrada, is a conspicuous ledge-forming unit consisting of a lower thin limestone member and an upper thicker gypsum member (Kirkland, Denison, and Evans, 1995; Lucas, Anderson, and Pigman, 1995). Condon and Huffman (1988) referred to this unit in the San Juan Basin as the Todilto Limestone Member of the Wanakah Formation, but a consensus of more recent geologic mapping in New Mexico has consistently been to use the formation-rank term Todilto Formation. The lower limestone is medium gray to yellow, thinly laminated to massive, and about 5 m thick. The gypsum member is white, massive, and pervasively brecciated where exposed at the surface. Thickness of the Todilto is quite variable, and it commonly ranges from 20 to 70 m regionally (table A1). The Todilto crops out as leached gypsiferous residuum intermixed with clay in weathered exposures, and scattered coarse gypsum crystals (as long as 5–10 cm) commonly coat surface exposures. Todilto gypsum has been mined at the Rosario quarry along the La Bajada escarpment about 3 km south of the area shown in plate 2.

Stratigraphically above the Todilto is a heterogeneous ~100-m-thick set of beds (table A1) that includes a basal, red to red-brown siltstone overlain by a grayish-red, ~30-m-thick sequence of gypsiferous siltstones and sandstones that were

Table A1. Thicknesses of basal Cretaceous, Jurassic, Triassic, and Paleozoic stratigraphic units.

[Thicknesses in meters; indented thickness values in parentheses are for members included in the total thickness values of formation listed above. Thickness values measured in drill holes are the first author's original picks from borehole geophysical logs in the southeast San Juan Basin, building upon the work of Huffman and Condon (1994). Data from measured sections exposed at the surface in San Ysidro, Placitas, and Hagan areas are composited from Lucas and others (1999a,b,c), Bernalillo-Placitas (Connell and others, 1999), and Hagan (Cather and others, 2002) geologic maps, and from University of New Mexico theses by Menne (1989) and Picha (1982). Locations of drill holes in the Santo Domingo Basin region indicated in table as section, township, and range. Southeast San Juan Basin wells are as follows: Sun El Paso Federal 1 (sec. 10, T. 22 N., R. 6 W.), Union Caldwell Ranch 1–M–13 (sec. 13, T. 21 N., R. 5 W.), Pan American Petroleum USA C–1 (sec. 17, T. 20 N., R. 3 W.), Magnolia Petroleum Hutchinson 1 (sec. 14, T. 19 N., R. 3 W.), El Paso Natural Gas Elliott State 1 (sec. 36, T. 19 N., R. 2 W.), Sun Sandoval Federal 1 (sec. 24, T. 18 N., R. 3 W.), Shell Wright 41–26 (sec. 26, T. 17 N., R. 3 W.), Texaco Howard Major 1 (sec. 10, T. 13 N., R. 3W.), Caprock L–Bar Ranch 1 (sec. 2, T. 13 N., R. 4 W.), Austra–Tex Exxon Mineral Federal 1 (sec. 23, T. 12 N., R. 4 W.), Austra–Tex Rio Puerco Federal 1 (sec. 7, T. 12 N., R. 2 W.), and Shell Laguna Wilson Trust 1 (sec. 8, T. 9 N., R. 1 W.). N. pe., not penetated; N. pr., not present; italics or queries, tentative picks]

Stratigraphic units (age)	Thicknesses of units in drill holes and measured sections											
	Southeast San Juan Basin wells n=12		Mobil Jemez Pueblo 1 sec. 28, T. 18 N., R. 1 W.	Enexco Shirl 2 sec. 9, T. 16 N., R. 2 W.	Houston Booth Drought 2 sec. 1, T. 15 N., R. 4 W.	Avila Odlum 1 sec. 15, T. 15 N., R. 1 E.	Humble SFP B 1 sec. 20, T. 14 N., R. 1 W.	San Ysidro (Lucas)	Shell SFP 1 (Lucas) sec. 18, T. 13 N., R. 3 E.	Placitas (Menne; Connell and others)	Hagan (Lucas and others; (Cather; Picha)	Trans-ocean McKee 1 sec. 1, T. 13 N., R. 9 E.
	Median	Range										
Dakota Sandstone (K)	78	31–120	119	82	79	N.pr.	>127		85			67
Morrison Formation (J)	264	192–297	236	262	275	266	263	256	191	259	323	*252?*
Jackpile Sandstone Member	(29)	(8–67)		(22)	(21)	(15)	(21)	(60)	(27)	(21)	(63)	(38)
Brushy Basin Member	(75)	(34–95)	(98)	(93)	(85)	(106)	(75)	(80)	(80)	(73)	(128)	*(112?)*
Westwater Canyon Member	(64)	(47–149)	(66)	(52)	(84)	(39)	(44)	(36)	(26)	(66)	(75)	*(47?)*
Recapture/Bluff Ss Members and "Summerville/ Wanakah"(?) unit.	(89)	(54–141)	(72)	(95)	(84)	(106)	(123)	(80)	(59)	(99)	(57)	(72)
Todilto Formation (J)	22	4–35	31	39	25	38	29	53	24	20	73	25
Entrada Sandstone (J)	50	33–65	60	43	49	43	52	30	61	37	49	63
Chinle Formation (Ꞧ)	360	269–535	322	408	421	397	402	478	308	503	524	520
Agua Zarca Member	(18)	(0–34)		(13)	(28)	(20)	(27)	(61)	(31)	(67)		(13)
San Andres Limestone (P)	14	6–44	9	19	18	10	39	24	8	24	5	15
Glorieta Sandstone (P)	32	23–58	22	35	40	42	45	31	24	15	12	53
Yeso Formation–upper (P)	33	22–280	88	66	91	185	198	160	118	115		210
Meseta Blanca Member (P)	69	30–76	68	83	81	65	71		46	60		52
Abo Formation (P)	364	287–494	304	337	337	327	318	174	267	326	112	*168*
Madera Group (ℙ)	290	178–506	134	239	240	250	287	232	168	384	384	*>209 (>365?)*
Sandia Formation (ℙ)	43	27–157	30	42	43	19	26	90	N. pr.	59	58	N. pe.
Mississippian rocks	25	28–79	N. pr.	20?	N. pr.	N. pr.	N. pr.	9	N. pr.	22	22	N. pe.
Elevation of Precambrian			290	–261	–221	216	41		–1,586			*–668*
Total thickness												
Jurassic-Triassic	715	627–882	649	751	769	744	774	816	585	818	940	860
Permian-Pennsylvanian	916	488–1,431	655	841	850	898	958	711	631	984	571	*>705*
Jurassic-Triassic-Paleozoic	1,680	1,214–2,180	1,304	1,592	1,619	1,642	1,732	1,527	1,216	1,802	1,511	*>1,565*

correlated with the Wanakah Formation by Stearns (1953a), Condon and Huffman (1988), and Condon (1989). Condon and Huffman (1988) named these beds the Beclabito Member of the Wanakah Formation. Alternatively, Lucas, Anderson, and Pigman (1995) and Lucas and Anderson (1997) have assigned this sequence of beds to the Beclabito Member of the Summerville Formation in the Hagan embayment and in extensive areas west of the Rio Grande rift. Owing to persistent disagreement among several workers regarding the stratigraphic relations of these various formations and members, we informally refer to this unit as "Summerville/Wanakah" (table A1; unit Jwb, pl. 2).

The Upper Jurassic Morrison Formation is widely exposed in the Galisteo Creek watershed within the Cerrillos uplift. It has commonly been divided into four members in northern New Mexico. They are, from the base upwards, the Westwater Canyon Member (unit Jmw, pl. 2), Brushy Basin Member (unit Jmb), and Jackpile Sandstone Member (unit Jmj). These subdivisions of the Morrison Formation, which have long been used in the San Juan Basin and adjoining areas (Santos, 1975), have been used locally with some modification in the Hagan embayment (Lucas, Anderson, and Pigman, 1995) and San Ysidro areas (Anderson and Lucas, 1996, 1997; Lucas, Estep, and Anderson, 1999). Lateral variability in rock types and the lack of well-recognized unconformities between members of the Morrison has led to uncertainty and disagreement about stratigraphic assignments within the formation (Condon and Peterson, 1986; Lucas, Anderson, and Pigman, 1995; Anderson and Lucas, 1996, 1997; Lucas and others, 1999a). USGS geologists and most other workers investigating the Gallup-Grants-Laguna uranium belt of the southern San Juan Basin and Sierra Nacimiento (Woodward, 1987) have generally used the names Recapture and Westwater Canyon Members instead of the Salt Wash Member for the lower and central part of the Morrison (Condon and Peterson, 1986; Condon and Huffman, 1994, Huffman and Condon, 1994). We generally adopt this stratigraphic usage in the La Bajada constriction area. However, because it is difficult to distinguish in the subsurface, the Recapture Member (and the intertonguing Bluff Sandstone in the southeast San Juan Basin (Santos, 1975)) is combined with the "Summerville/Wanakah" unit in thickness measurements shown in table A1. In this report we follow the general consensus of other workers in New Mexico on nomenclature and characteristics of the Brushy Basin and Jackpile Members of the Morrison. The braided-stream fluvial depositional environment represented by most of the Morrison contrasts with the eolian and marginal marine saline deposits of the underlying the Entrada and Todilto Formations. On the basis of surface exposures and drill-hole penetrations flanking the Rio Grande rift (table A1), the total thickness of the Morrison Formation in the La Bajada footwall block ranges from 191 to 323 m.

In the La Bajada constriction area, the Cretaceous Dakota Sandstone unconformably overlies the Morrison Formation in the footwall block of the La Bajada fault zone (pl. 2). Stratigraphic usage for the Dakota Sandstone in north-central New Mexico is complex and at present only partially resolved, particularly east of the Rio Grande rift. Our general usage is after Landis, Dane, and Cobban (1973), who subdivided the intertonguing Dakota Sandstone and Mancos Shale in west-central New Mexico into, from bottom to top, the basal Oak Canyon Member of the Dakota Sandstone, the Cubero Tongue of the Dakota Sandstone, the Clay Mesa Tongue of the Mancos Shale, the Paguate Tongue of the Dakota Sandstone, the Whitewater Arroyo Tongue of the Mancos Shale, and the Twowells Tongue of the Dakota Sandstone. Sandstone exposed in the Galisteo monocline (pl. 1) has been mapped by Maynard, Sawyer, and Rogers (2001) and Sawyer and others (2002) as the Cubero Tongue (unit Kdc, pl. 2) of the Dakota Sandstone, and underlying shale as the Oak Canyon Member (unit Kdo).

The Mancos Shale, which overlies the Dakota Sandstone where it is exposed in the La Bajada escarpment (pl. 2), consists of thick marine shale, calcareous shale, and sandy shale, with minor beds of limestone and bentonite. The Mancos regionally intertongues with coal-bearing continental deposits of the Crevasse Canyon Formation and the overlying Mesaverde Group; these units are not exposed in the study area but may exist nearby in the subsurface. Locally, sandy uppermost Mancos exposures are laterally equivalent to what Bachman (1975) termed Niobrara Member in the Madrid quadrangle south of the Cochiti Pueblo map area (pl. 2). Members of the Mancos Shale in the La Bajada constriction region (Sawyer and others, 2002) are subdivided in part on the basis of a proposed Mancos principal reference section (Leckie, Kirkland, and Elder, 1997) in the San Juan Basin north of Mesa Verde National Park in Colorado. These members, from the base upward, are thin shale partly equivalent to the Graneros Shale Member and the overlying Bridge Creek Limestone Member, undivided (unit Kmb, pl. 2); the Blue Hill and Fairport Members of the Carlile Shale and the overlying Juana Lopez Member, all undivided (unit Kmj); and the upper part of the Niobrara Member (unit Kmn) (Leckie, Kirkland, and Elder, 1997; Sawyer and others, 2002). These members correlate with formal stratigraphic units assigned to the Cretaceous Western Interior seaway deposits of Colorado and western New Mexico (Molenaar, 1983; Leckie, Kirkland, and Elder, 1997). Mancos Shale in the area of the Galisteo Creek watershed just south of the map area (pl. 2) is approximately 600–700 m thick (Stearns, 1953c; Bachman, 1975; Cobban, W.A., and Sawyer, D.A., unpub. data, 2005)

Pre-Rift Tertiary Rocks

The Eocene Galisteo Formation (unit Tg) is exposed on both flanks of the La Bajada constriction in the footwall block of the La Bajada fault zone and in the Saint Peters Dome area (pl. 2). In the La Bajada footwall it consists of red to brownish-yellow sandstone, red mudstone, and conglomerate. The sandstones range from well-sorted, fine-grained sandstone to more poorly sorted, coarse-grained, silty sandstone. Conglomerate clasts include white, gray, and black chert pebbles and gray

limestone cobbles. Galisteo Formation deposits crop out in three distinct areas on the east side of the constriction: southwest-dipping beds in the vicinity of La Cienega; northeast-dipping beds disconformably overlying the Mancos Shale in Cañada de Santa Fe midway between the villages of La Cienega and La Bajada; and in a number of variously tilted fault blocks underlying the Pliocene Cerros del Rio basalt flows near U.S. Interstate 25 at the base of the La Bajada escarpment (pl. 2). Galisteo sedimentary rocks exposed at these locations correspond with the upper part of the formation and are not underlain by any deposits of the Paleocene(?)–lower Eocene Diamond Tail Formation (Lucas and others, 1997; S.M. Cather, New Mexico Bureau of Mines and Mineral Resources, oral commun., 1998). It is possible, however, that the Diamond Tail is present in the subsurface of the La Bajada constriction area. The Galisteo Formation in this part of New Mexico is interpreted to have been deposited during the late part of the Laramide orogeny (Cather, 1992), resulting in great regional variations in thickness of the formation. Although the Galisteo Formation has a maximum thickness of 1,060 m near the villages of Cerrillos and Galisteo (pl. 1) (Bachman, 1975) southeast of the La Bajada constriction area (fig. A2), the unit is only 340–400 m thick in the La Cienega–Cañada de Santa Fe area on the southern Caja del Rio Plateau (pl. 1, 2) (Sun and Baldwin, 1958).

In the Saint Peters Dome area, steeply west-dipping beds of the Galisteo Formation are exposed in the uplifted footwall block of the Pajarito (PJ) fault zone (pl. 2, figs. A2, A3) (Cather, 1992). The Galisteo there consists of tan to pink to brick red beds of well-indurated sandstone, siltstone, arkose, and conglomerate. The conglomerate contains pebbles and boulders of limestone, chert, and granitic rock derived from Precambrian and Paleozoic source terranes. The base of the Galisteo at Saint Peters Dome is not exposed, and the unit is unconformably overlain by sediments of the Santa Fe Group; the unit at the Saint Peters Dome exposure has a minimum thickness of about 200 m (Cather, 1992).

The Eocene and Oligocene Espinaso Formation (unit Te) conformably overlies Galisteo sedimentary rocks in exposures in the Cerrillos uplift area (pl. 2). Along the La Bajada escarpment, near its intersection with U.S. Interstate 25, the Espinaso consists mainly of clast-supported volcanic and sedimentary breccia containing andesite or latite clasts (or both), and it also includes subordinate interbedded volcaniclastic sedimentary rocks. The Espinaso Formation is described in more detail in chapter C (this volume). Eocene and Oligocene monzonite and monzonite porphyry intrusive rocks (unit Tmi) similar in age and composition to rocks of the Espinaso Formation are exposed in the Cerrillos uplift area (including the Cerrillos Hills) on the southeast flank of the La Bajada constriction (pl. 2, fig. A3). These rocks, which intrude and deform rocks of the Galisteo (unit Tg) and Espinaso (unit Te) Formations, are also discussed in more detail in chapter C (this volume).

The Cieneguilla Basanite (unit Tc, pl. 2) (Sawyer and others, 2002), which overlies intrusive rocks (unit Tmi) and rocks of the Espinaso Formation (unit Te), consists of basanite, nephelinite, minor basalt flows, and interbedded volcaniclastic and epiclastic sediments. The unit was mapped as the Cieneguilla Limburgite by Stearns (1953b). The Cieneguilla Basanite is further described in chapter C (this volume).

The youngest pre-rift rocks exposed in the La Bajada constriction area are a sequence of light-gray ash-rich silty sandstone and siltstone beds (unit Tab) that unconformably overlie Espinaso deposits at the west mouth of Cañada de Santa Fe near the village of La Bajada (pl. 2). These sedimentary rocks form prominent low cliffs and contain ash-fall beds (0.2–0.5 m thick) that are commonly admixed with detrital silt and minor arkosic sand. The lower part of this unit locally contains thin limestone beds interbedded with gray, green, and red siltstone and claystone that were interpreted by Stearns (1953b) to be lacustrine in origin. The unit is tentatively correlated with the volcaniclastic Abiquiu Formation (Stearns, 1953b) present in the Abiquiu embayment about 70 km north of the study area (fig. A1). Stearns (1953b) also suggested possible correlation with the Zia Sand exposed in the Jemez River area about 45 km west of the Cochiti Pueblo area.

Hydrostratigraphic Properties of Pre-Rift Sedimentary and Igneous Rocks

Hydrostratigraphic properties of pre-rift rocks in the La Bajada constriction region differ greatly (Lewis and West, 1995). In general, none of the Oligocene and older sedimentary rocks approach the high permeability and yield of the mid-Miocene and younger poorly consolidated Santa Fe Group basin-fill deposits. Hydrologic properties of the pre-rift Tertiary rocks are transitional between those of the overlying poorly consolidated rift-basin aquifer units and underlying Cretaceous confining units. Pre-rift Tertiary strata of the Galisteo Formation and overlying Espinaso and Abiquiu(?) Formations are probably hydrologically connected with basin-aquifer units of the Santa Fe Group. Spiegel and Baldwin (1963) considered the Galisteo Formation so poor a water source even for domestic and stock wells that it should be drilled only as a last resort. In the proposed La Bajada Ranch subdivision south of Cañada de Santa Fe, Peery and Pearson (1994) concluded that even if the Galisteo is not a good aquifer, it is at least considerably better than the other confining units in the area. In the La Cienega area (pl. 1) some domestic wells yield water from the Galisteo Formation (Spiegel and Baldwin, 1963), whereas in other wells Galisteo has such low permeability that it and subjacent Mesozoic sedimentary formations act as a single confining unit (Lewis and West, 1995). More work is needed to characterize vertical and lateral variations in permeability and hydraulic conductivity within the Galisteo and associated Diamond Tail Formations, which are as much as 1 km thick in the Galisteo Creek watershed (Abbott, Cather, and Goodwin, 1995). Post-Galisteo pre-rift volcaniclastic and igneous rocks such as the Espinaso Formation, monzonites associated with the Cerrillos Hills intrusive center, and the Cieneguilla

Basanite may locally provide adequate supply for domestic or small stock wells owing to fracture-induced permeability (Shomaker, 1995).

The stratigraphically highest regional confining unit is generally Upper Cretaceous marine shale. In the exposed footwall block of the La Bajada fault zone, this unit is the very low permeability Mancos Shale. In the area underlain by the Cerrillos uplift, the 600–700-m-thick Mancos Shale functions as a local hydrologic "confining basement" for the Cenozoic aquifer system, and it affects the configuration of the regional ground-water flow system and the connectivity of conductive Tertiary sedimentary and volcanic rocks. Such Cretaceous marine shales have extremely low hydraulic conductivity, from 10–16 to 10–19 m/s (Bredehoeft, Neuzil, and Milly, 1983; Belitz and Bredehoft, 1988; Neuzil, 1994). Although some wells in the Cerrillos uplift area may locally intersect fractures or fractured igneous dikes in Mancos Shale that yield small amounts of water (Peery and Pearson, 1994), the shales generally have very low potential as aquifers.

Subregionally, the thick Mancos Shale prevents hydrologic connection of the overlying Rio Grande aquifer system (sediments of the Santa Fe Group and immediately subjacent Tertiary rocks) with deeper potential aquifers in Jurassic, Permian, and especially Pennsylvanian carbonate sedimentary rocks. Triassic Chinle Formation continental clay-rich sedimentary rocks, although thick (>300 m; Lucas, Heckert, and Estep, 1999), probably have very low transmissivity. The Chinle and Mancos confining units have a profound effect not just on water availability but also on water quality. Brackish to saline waters are typical of these formations in much of southern Santa Fe County (Lewis and West, 1995). Low hydraulic conductivity hydrostratigraphic units (the Mancos Shale and other underlying confining units) are present within the upper kilometer of section within the Cerrillos uplift area and probably the Saint Peters Dome block. Equivalent confining units are buried 1.5–4 km beneath more permeable rift basin-fill sediments and volcanic rocks in the Santo Domingo Basin and La Bajada constriction.

In the San Juan Basin to the west, more productive aquifer sandstones exist in the middle and lower parts of the Morrison Formation and beneath the Chinle Formation in the Permian Glorieta Sandstone and San Andres Limestone. A critical condition in Santa Fe County is whether these moderately good aquifers have been exposed at the surface to late Pleistocene recharge, which can then travel laterally in somewhat well-connected fracture networks or in porous sandstones. Greater than 300 m of low permeability rocks of the Chinle separate these two moderately productive intervals. Wherever these rocks have been structurally uplifted and tilted, as along the margin of the Hagan embayment or possibly in the buried Cerrillos uplift, potential pathways exist for late Pleistocene recharge of the Morrison and Glorieta–San Andres aquifers.

Little is known of the aquifer properties of deeply buried carbonates of the Pennsylvanian Madera Group in the Cerrillos uplift area. On the basis of a more thorough study of correlative rocks in the Sandia and Manzano Mountains (Titus, 1980), they may form good aquifers where recharged by Pleistocene water. This potential is particularly likely where Pennsylvanian carbonates are exposed in the foothills adjoining the Sangre de Cristo Range near eastern Santa Fe and the town of El Dorado (fig. A1). The structural configuration of the northeast-dipping northeastern flank of the Cerrillos uplift (fig. A2) is unfavorable for recharge from the Sangre de Cristo Mountains (Grauch and Bankey, 2003; discussed in more detail in subsequent chapters of this report). Buried Precambrian granite and granitic gneiss basement rocks that presumably underlie Paleozoic rocks in the La Bajada constriction area generally provide poor quantities of water elsewhere in the region, suitable only for local domestic supply or stock.

References Cited

Abbott, J.C., Cather, S.M., and Goodwin, L.B., 1995, Paleogene synorogenic sedimentation in the Galisteo Basin related to the Tijeras-Cañoncito fault system: New Mexico Geological Society 46th field conference, Geology of the Santa Fe Region, Guidebook, p. 271–278.

Anderson, O.J., and Lucas, S.G., 1996, Stratigraphy and depositional environments of middle and upper Jurassic rocks, southeastern San Juan Basin, New Mexico: New Mexico Geological Society 47th field conference, Jemez Mountains Region, Guidebook, p. 205–210.

Anderson, O.J., and Lucas, S.G., 1997, The Upper Jurassic Morrison Formation in the Four Corners region: New Mexico Geological Society 48th field conference, Mesozoic Geology and Paleontology of the Four Corners Area, Guidebook, p. 139–155.

Bachman, G.O., 1975, Geologic map of the Madrid quadrangle, Santa Fe and Sandoval Counties: U.S. Geological Survey Geologic Quadrangle Map GQ–1268, scale 1:62,500.

Baldridge, W.S., Bartov, Yuval, and Kron, Andrea, 1983, Geologic map of the Rio Grande rift and southeastern Colorado Plateau, New Mexico and Arizona, *supplement to* Riecker, R.E., ed., Rio Grande rift—Tectonics and magmatism (book and map), 2d printing, American Geophysical Union, scale 1:500,000.

Baltz, E.H., and Myers, D.A., 1999, Stratigraphic framework of upper Paleozoic rocks, southeast Sangre de Cristo Mountains, New Mexico, *with a section on* Speculations and implications for regional interpretation of Ancestral Rocky Mountain paleotectonics: New Mexico Bureau of Geology and Mineral Resources Memoir 48, 269 p.

Bartolino, J.R., 1999, Introduction: U.S. Geological Survey Middle Rio Grande Basin Study—3d Annual Workshop: Albuquerque, New Mexico, February 24–25, 1999, Proceedings: U.S. Geological Survey Open-File Report 99–203, p. 2.

Bartolino, J.R., and Cole, J.C., 2002, Ground-water resources of the Middle Rio Grande Basin, New Mexico: U.S. Geological Survey Circular 1222, 132 p.

Belitz, K.R., and Bredehoeft, J.D., 1988, Hydrodynamics of Denver Basin—Explanation of subnormal fluid pressures: American Association of Petroleum Geologists Bulletin, v. 72, no. 11, p. 1334–1359.

Black, B.A., 1979, Structure and stratigraphy of the Hagan embayment—A new look: New Mexico Geological Society 30th field conference, Santa Fe Country, Guidebook, p. 101–105.

Black, B.A., 1999, Oil and gas exploration in the Hagan embayment of the Española Basin: New Mexico Geological Society 50th field conference, Albuquerque Geology, Guidebook, p. 441–448.

Black, B.A., and Hiss, W.L., 1974, Structure and stratigraphy in the vicinity of the Shell Oil Co. Santa Fe Pacific No. 1 test well: New Mexico Geological Society 25th field conference, Ghost Ranch, Guidebook, p. 365–370.

Bredehoeft, J.D., Neuzil, C.E., and Milly, P.C.D., 1983, Regional flow in the Dakota aquifer—A study of the role of confining layers: U.S. Geological Survey Water-Supply Paper 2237, 45 p.

Broadhead, R.F., 1997, Subsurface geology and oil and gas potential of Estancia Basin, New Mexico: New Mexico Bureau of Mines and Mineral Resources Bulletin 157, 54 p.

Bryan, Kirk, 1938, Geology and ground-water conditions of the Rio Grande depression in Colorado and New Mexico: Regional Planning Report, part 6, Upper Rio Grande, p. 197–225.

Bryan, Kirk, and McCann, F.T., 1937, The Ceja del Rio Puerco—A border feature of the Basin and Range Province in New Mexico, part II, Geomorphology: Journal of Geology, v. 46, p. 1–16.

Cather, S.M., 1992, Suggested revisions to the Tertiary tectonic history of north-central New Mexico: New Mexico Geological Society 43d field conference, San Juan Basin IV, Guidebook, p. 109–122.

Cather, S.M., Connell, S.D., and Black, B.A., 2000, Geology of the San Felipe Pueblo NE 7.5 minute quadrangle, Sandoval County, New Mexico, New Mexico Bureau of Mines and Mineral Resources Open-file Geologic Map OF–GM 37, scale 1:24,000.

Cather, S.M., Connell, S.D., Lucas, S., Picha, M.G., and Black, B.A., 2002, Geology of the Hagan 7.5 minute quadrangle, Sandoval County, New Mexico, New Mexico Bureau of Geology and Mineral Resources Open-file Geologic Map OF–GM 50, scale 1:24,000.

Chapin, C.E., 1971, The Rio Grande rift, part 1—Modifications and additions: New Mexico Geological Society 22d field conference, San Luis Basin, Guidebook, p. 191–202.

Chapin, C.E., and Cather, S.M., 1994, Tectonic setting of the axial basins of the northern and central Rio Grande rift, *in* Keller, G.R., and Cather, S.M., eds., Basins of the Rio Grande rift—Structure, stratigraphy, and tectonic setting: Geological Society of America Special Paper 291, p. 5–25.

Condon, S.M., 1989, Revisions of middle Jurassic nomenclature in the southeastern San Juan Basin, New Mexico: U.S. Geological Survey Bulletin 1808–E, 23 p.

Condon, S.M., and Huffman, A.C., Jr., 1988, Revisions in nomenclature of the middle Jurassic Wanakah Formation, northwestern New Mexico and northeastern Arizona: U.S. Geological Survey Bulletin 1633–A, p. 1–12.

Condon, S.M., and Huffman, A.C., Jr., 1994, Northwest-southeast-oriented cross sections of Jurassic through Paleozoic rocks, San Juan Basin and vicinity, Utah Colorado, Arizona, and New Mexico: U.S. Geological Survey Oil and Gas Chart C–142, 3 sheets.

Condon, S.M., and Peterson, Fred, 1986, Stratigraphy of middle and upper Jurassic rocks of the San Juan Basin—Historical perspectives, current ideas, and remaining problems: American Association of Petroleum Geologists Studies in Geology 22, p. 7–26.

Connell, S.D., Cather, S.M., Ilg, Bradley, Karlstrom, K.E., Menne, Barbara, Picha, Mark, Andronicos, Chris, Read, A.S., Bauer, P.W., and Johnson, P.S., 2000, Geology of the Bernalillo and Placitas 7.5 minute quadrangles, Sandoval County, New Mexico: New Mexico Bureau of Mines and Mineral Resources Open-file Geologic Map OF–GM 2 and 16, scale 1:24,000.

Dethier, D.P., 1999, Quaternary evolution of the Rio Grande near Cochiti Lake, northeast Santo Domingo Basin, New Mexico: New Mexico Geological Society 50th field conference, Albuquerque Geology, Guidebook, p. 371–378.

Disbrow, A.E., and Stoll, W.C. 1957, Geology of the Cerrillos area, Santa Fe County, New Mexico: New Mexico Bureau of Mines and Mineral Resources Bulletin 48, 73 p.

Ferguson, J.F., Baldridge, W.S., Braile, L.W., Biehler, S., Gilpin, B., and Jiracek, G.R., 1995, Structure of the Española Basin, Rio Grande rift, from SAGE seismic and gravity data: New Mexico Geological Society 46th field conference, Geology of the Santa Fe Region, Guidebook, p. 105–110.

Goff, Fraser, Gardner, Jamie, and Valentine, Greg, 1990, Geologic map of the St. Peter's Dome area, Jemez Mountains, New Mexico: New Mexico Bureau of Mines and Mineral Resources Geologic Map 69, scale 1:24,000.

Grant, P.R., 1997, Subsurface geology and related hydrologic conditions, Santa Fe embayment and contiguous areas, New Mexico: New Mexico State Engineer Office Technical Report 97–5, 53 p., 3 plates.

Grant, P.R., 1999, Subsurface geology and related hydrologic conditions, Santa Fe embayment and contiguous areas, New Mexico: New Mexico Geological Society 50th field conference, Albuquerque Geology, Guidebook, p. 425–435.

Grauch, V. J. S., and Bankey, Viki, 2003, Aeromagnetic interpretations for understanding the hydrogeologic framework of the southern Española Basin, New Mexico: U. S. Geological Survey Open-file Report 03–124, 44 p., available from http://pubs.usgs.gov/of/2003/ofr–03–124/.

Grauch, V.J.S., Gillespie, C.L., and Keller, G.R., 1999, Discussion of new gravity maps for the Albuquerque Basin: New Mexico Geological Society 50th field conference, Albuquerque Geology, Guidebook, p. 119–124.

Hawley, J.W., and Whitworth, T.M., eds., 1996, Hydrogeology of potential recharge areas for the basin- and valley-fill aquifer systems, and hydrogeochemical modeling of proposed artificial recharge of the upper Santa Fe aquifer, northern Albuquerque Basin: New Mexico Bureau of Mines and Mineral Resources Open-file Report 402d, 575 p., 15 plates, 7 appendices.

Huffman, A.C., Jr., and Condon, S.M., 1993, Stratigraphy, structure, and paleogeography of Pennsylvanian and Permian rocks, San Juan Basin and adjacent areas, Utah, Colorado, Arizona, and New Mexico: U.S. Geological Survey Bulletin 1808–O, 44 p.

Huffman, A.C., Jr., and Condon, S.M., 1994, Southwest-northeast-oriented cross sections of Jurassic through Paleozoic rocks, San Juan Basin and vicinity, Colorado, Arizona, and New Mexico: U.S. Geological Survey Oil and Gas Chart 141, 3 sheets.

Karlstrom, K.E., Amato, J.M., Williams, M.L., Heizler, M., Shaw, C.A., Read, A.S., and Bauer, P., 2004, Proterozoic tectonic evolution of the New Mexico region—A synthesis, *in* Mack, G.H., and Giles, K.A., The Geology of New Mexico, A Geologic History, New Mexico Geological Society, p. 1–34.

Karlstrom, K.E., Cather, S.M., Kelley, S.A., Heizler, M.T., Pazzaglia, F.J., and Roy, M., 1999, Sandia Mountains and Rio Grande rift—Ancestry of structures and history of deformation: New Mexico Geological Society 50th field conference, Albuquerque Geology, Guidebook, p. 155–165.

Kelley, V.C., 1952, Tectonics of the Rio Grande depression of central New Mexico: New Mexico Geological Society 3d field conference, Rio Grande Country, Guidebook, p. 92–105.

Kelley, V.C., 1977, Geology of Albuquerque Basin, New Mexico: New Mexico Bureau of Mines and Mineral Resources Memoir 33, 60 p.

Kelley, V.C., 1978, Geology of the Española Basin, New Mexico: New Mexico Bureau of Mines and Mineral Resources Geologic Map 48, scale 1:125,000.

Kelley, V.C., 1979, Tectonics, middle Rio Grande rift, New Mexico, in Riecker, R.E., ed., Rio Grande rift—Tectonics and magmatism: American Geophysical Union, p. 57–70.

Kelley, V.C., 1982, The right-relayed Rio Grande rift, Taos to Hatch, New Mexico: New Mexico Geological Society 33d field conference, Albuquerque Country II, Guidebook, p. 147–151.

Kelley, V.C., and Northrop, S.A., 1975, Geology of the Sandia Mountains and vicinity: New Mexico Bureau of Mines and Mineral Resources Memoir 29, 136 p.

Kernodle, J.M., McAda, D.P., and Thorn, C.R., 1995, Simulation of ground-water flow in the Albuquerque Basin, central New Mexico, 1901–1994, with projections to 2020: U.S. Geological Survey Water-Resources Investigations Report 94–4251, 114 p.

Kirkland, D.W., Denison, R.E., and Evans, R., 1995, Middle Jurassic Todilto Formation of northern New Mexico and southwestern Colorado—Marine or non-marine: New Mexico Bureau of Mines and Mineral Resources Bulletin 147, 37 p.

Koning, D.J., and Hallett, R.B., 2000, Geology of the Turquoise Hill 7.5 minute quadrangle, Santa Fe County, New Mexico, New Mexico Bureau of Mines and Mineral Resources Open-file Geologic Map OF–GM 41, scale 1:24,000.

Landis, E.R., Dane, C.H., and Cobban, W.A., 1973, Stratigraphic terminology of the Dakota Sandstone and Mancos Shale, west-central New Mexico: U.S. Geological Survey Bulletin 1372–J, 44 p.

Leckie, R.M., Kirkland, J.I., and Elder, W.P., 1997, Stratigraphic framework and correlation of a principal reference section of the Mancos Shale (Upper Cretaceous), Mesa Verde, Colorado: New Mexico Geological Society 48th field conference, Mesozoic Geology and Paleontology of the Four Corners Area, Guidebook, p. 163–216.

Lewis, A.C., and West, Francis, 1995, Conceptual hydrologic systems for Santa Fe County: New Mexico Geological Society 46th field conference, Geology of the Santa Fe Region, Guidebook, p. 299–305.

Lucas, S.G., and Anderson, O.J., 1997, The Jurassic San Rafael Group, Four Corners region: New Mexico Geological Society 48th field conference, Mesozoic Geology and Paleontology of the Four Corners Area, Guidebook, p. 115–132.

Lucas, S.G., Anderson, O.J., and Pigman, C., 1995, Jurassic stratigraphy in the Hagan Basin, north-central New Mexico: New Mexico Geological Society 46th field conference, Geology of the Santa Fe Region, Guidebook, p. 247–256.

Lucas, S.G., Cather, S.M., Abbott, J.C., and Williamson, T.E., 1997, Stratigraphy and tectonic implications of Paleogene strata in the Laramide Galisteo Basin, north-central New Mexico: New Mexico Geology, v. 19, p. 89–95.

Lucas, S.G., Estep, J.W., and Anderson, O.J., 1999, Correlation of Jurassic strata from the Colorado Plateau to the High Plains, across the Rio Grande rift, north-central New Mexico: New Mexico Geological Society 50th field conference, Albuquerque Geology, Guidebook, p. 317–326.

Lucas, S.G., and Heckert, A.B., 1995, Triassic stratigraphy around the Sandia uplift, central New Mexico: New Mexico Geological Society 46th field conference, Geology of the Santa Fe Region, Guidebook, p. 233–241.

Lucas, S.G., Heckert, A.B., and Estep, J.W., 1999, Correlation of Triassic strata across the Rio Grande rift, north-central New Mexico: New Mexico Geological Society 50th field conference, Albuquerque Geology, Guidebook, p. 305–310.

Lucas, S.G., Rowland, J.M., Kues, B.S., Estep, J.W., and Wilde, G.L., 1999, Uppermost Pennsylvanian and Permian stratigraphy and biostratigraphy at Placitas, New Mexico: New Mexico Geological Society 50th field conference, Albuquerque Geology, Guidebook, p. 281–292.

Maynard, S.R., Sawyer, D.A., and Rogers, J., 2001, Preliminary geologic map of the Madrid 7.5 minute quadrangle: New Mexico Bureau of Mines and Geology Open-file Report DM–40, scale 1:24,000.

Menne, Barbara, 1989, Structure and stratigraphy of the northwestern part of the Sandia Mountains, New Mexico: Albuquerque, University of New Mexico, M.S. thesis, 163 p.

Minor, S.A., and Hudson, M.R., 2006, Regional survey of structural properties and cementation patterns of fault zones in the northern part of the Albuquerque Basin, New Mexico—Implications for ground-water flow: U.S. Geological Survey Professional Paper 1719, 28 p.

Molenaar, C.M., 1983, Major depositional cycles and regional correlations of Upper Cretaceous rocks, southern Colorado Plateau and adjacent areas, *in* Reynolds, M.W., and Dolly, E.D., eds., Mesozoic paleogeography of west-central United States: Society of Paleontologists and Mineralogists Rocky Mountain Section, Denver, p. 201–224.

Myers, D.A., 1982, Stratigraphic summary of Pennsylvanian and lower Permian rocks, Manzano Mountains, New Mexico: New Mexico Geological Society 33d field conference, Albuquerque Country II, Guidebook, p. 233–237.

Neuzil, C.E., 1994, How permeable are clays and shales?: Water Resources Research, v. 30, no. 2, p. 145–150.

Peery, R.L., and Pearson, J.W., 1994, Hydrogelogy and water-resource assessment, proposed La Bajada subdivision, Santa Fe County, NM: John Shomaker & Associates consultant report, 33 p. plus maps and tables.

Picha, M.G., 1982, Structure and stratigraphy of the Montezuma salient, Hagan Basin area, Sandoval County, New Mexico: Albuquerque, University of New Mexico, M.S. thesis, 248 p.

Plummer, L.N., Bexfield, L.M., Anderholm, S.K., Sanford, W.E., and Busenberg, E., 2004a, Hydrochemical tracers in the Middle Rio Grande Basin, USA—1. Conceptualization of groundwater flow: Hydrogeology Journal, v. 12, no. 4, p. 359–388.

Plummer, L.N., Bexfield, L.M., Anderholm, S.K., Sanford, W.E., and Busenberg, E., 2004b, Geochemical Characterization of ground-water flow in the Santa Fe Group aquifer system, Middle Rio Grande Basin, New Mexico, U.S. Geological Survey Water-Resources Investigation Report 03–4131, 395 p.

Sanford, W.E., Plummer, L.N., McAda, D.P., Bexfield, L.M., and Anderholm, S.K., 2000, Estimation of hydrologic parameters for the ground-water model of the middle Rio Grande Basin using carbon-14 and water-level data, *in* Cole, J.C., ed., U.S. Geological Survey Middle Rio Grande Basin Study—4th Annual Workshop, Albuquerque, New Mexico, February 15–16, 2000, Proceedings: U.S. Geological Survey Open-File Report 00–488.

Sanford, W.E., Plummer, L.N., McAda, D.P., Bexfield, L.M., and Anderholm, S.K., 2004a, Hydrochemical tracers, in the Middle Rio Grande Basin, USA—2. Calibration of a groundwater-flow model: Hydrogeology Journal, v. 12, no. 4, p. 389–407.

Sanford, W.E., Plummer, L.N., McAda, D.P., Bexfield, L.M., and Anderholm, S.K., 2004b, Use of environmental tracers to estimate parameters for a predevelopment ground-water-flow model of the Middle Rio Grande Basin, New Mexico: U.S. Geological Survey Water-Resources Investigation Report 03–4286, 102 p.

Santos, E.S., 1975, Lithology and uranium potential of Jurassic formations in the San Ysidro–Cuba and Majors Ranch areas, northwestern New Mexico: U.S. Geological Survey Bulletin 1329, 22 p., 1:48,000-scale geologic map.

Sawyer, D.A., Shroba, R.R., Minor, S.A., and Thompson, R.A., 2002, Geologic map of the Tetilla Peak 7.5 minute quadrangle, Santa Fe and Sandoval Counties, New Mexico: U.S. Geological Survey Miscellaneous Field Studies Map MF–2352, scale 1:24,000.

Shomaker, J.W., 1995, Hydrogeology of the Ortiz Mountains and vicinity: New Mexico Geological Society 46th field conference, Geology of the Santa Fe Region, Guidebook, p. 313–318.

Smith, G.A., 2004, Middle to Late Cenozoic development of the Rio Grande rift and adjacent regions in northern New Mexico, *in* Mack, G.H., and Giles, K.A., eds., The geology of New Mexico—A geologic history: New Mexico Geological Society Special Publication 11, p. 331–358.

Smith, G.A., and Kuhle, A.J., 1998a, Geologic map of the Santo Domingo Pueblo 7.5 minute quadrangle, Sandoval County, New Mexico: New Mexico Bureau of Mines and Mineral Resources Open-file Digital Map OFDM 26, scale 1:24,000.

Smith, G.A., and Kuhle, A.J., 1998b, Geologic map of the Santo Domingo Pueblo SW 7.5 minute quadrangle, Sandoval County, New Mexico: New Mexico Bureau of Mines and Mineral Resources Open-file Digital Map OF–DM–26, 1 sheet and text, scale 1:24,000.

Smith, G.A., and Kuhle, A.J., 1998c, Hydrostratigraphic implications of new geologic mapping in the Santo Domingo Basin, New Mexico: New Mexico Geology, v. 20, p. 21–27.

Smith, G.A., McIntosh, William, and Kuhle, A.J., 2001, Sedimentologic and geomorphic evidence for seesaw subsidence of the Santo Domingo accommodation-zone basin, Rio Grande rift, New Mexico: Geological Society of America Bulletin, v. 113, p. 561–574.

Smith, R.L., Bailey, R.A., and Ross, C.S., 1970, Geologic map of the Jemez Mountains, New Mexico: U.S. Geological Survey Miscellaneous Investigations Map I–571, scale 1:125,000.

Spiegel, Zane, and Baldwin, Brewster, 1963, Geology and water resources of the Santa Fe area: U.S. Geological Survey Water-Supply Paper 1525, 258 p.

Stearns, C.E., 1953a, Early Tertiary volcanism in the Galisteo-Tonque area, north-central New Mexico: American Journal of Science, v. 251, p. 415–452.

Stearns, C.E., 1953b, Tertiary geology of the Galisteo-Tonque area, New Mexico: Geological Society of America Bulletin, v. 64, p. 459–508.

Stearns, C.E., 1953c, Upper Cretaceous, Galisteo-Tonque area, New Mexico: American Association of Petroleum Geologists Bulletin, v. 37, p. 961–974.

Sun, Ming-shan, and Baldwin, Brewster, 1958, Volcanic rocks of the Cienega area, Santa Fe County, New Mexico: New Mexico Bureau of Mines and Mineral Resources Bulletin 54, 80 p. and geologic map, scale 1:15,840.

Thorn, C.R., McAda, D.P., and Kernodle, J.M., 1993, Geohydrologic framework and hydrologic conditions in the Albuquerque Basin, central New Mexico: U.S. Geological Survey Water-Resources Investigations Report 93–4149, 106 p., 2 plates.

Titus, F.B., Jr., 1980, Ground water in the Sandia and northern Manzano Mountains, New Mexico, New Mexico Bureau of Mines and Mineral Resources Hydrologic Report 5, 66 p.

Tweto, Ogden, 1978, Tectonic map of the Rio Grande rift system in Colorado: New Mexico Bureau of Mines and Mineral Resources Circular 163, plate 1, scale 1:1,000,000.

Tweto, Ogden, 1979, The Rio Grande rift system in Colorado, in Riecker, R.E., ed., Rio Grande rift—Tectonics and magmatism: American Geophysical Union, p. 33–56.

Woodward, L.A., 1987, Geology and mineral resources of Sierra Nacimiento and vicinity: New Mexico Bureau of Mines and Mineral Resources Memoir 42, 85 p.

Published in the Central Region, Denver, Colo.
Manuscript approved for publication February 10, 2006
Graphics by authors
Photocomposition by Mari L. Kauffmann (Contractor, ATA Services)
Edited by Mary-Margaret Coates (Contractor, ATA Services)

Stratigraphy of Upper Cenozoic Fluvial Deposits of the La Bajada Constriction Area, New Mexico

By David P. Dethier and David A. Sawyer

Chapter B of

The Cerrillos Uplift, the La Bajada Constriction, and Hydrogeologic Framework of the Santo Domingo Basin, Rio Grande Rift, New Mexico

Edited by Scott A. Minor

Professional Paper 1720–B

U.S. Department of the Interior
U.S. Geological Survey

Contents

Abstract 27
Introduction 27
Stratigraphic Nomenclature and Correlations 28
Fluvial Basin-Fill Deposits 28
    Lithologic Characteristics 28
    Isotopic and Amino-Acid-Racemization Ages 29
Stratigraphic Framework 31
    Upper Miocene Through Lower Pleistocene Basin-Fill Deposits 31
    Pleistocene (Post-Bandelier Tuff) Through Holocene Deposits 34
Incisional and Aggradational History of the Ancestral Rio Grande 36
Hydrogeologic Implications 37
References Cited 38

Figures

B1. Sketch map of the Cochiti Pueblo area showing location of axial river gravel deposits, Cerros del Rio lava flows, and selected geologic features 29
B2. Diagram showing relation between amino acid racemization ratio in *Succinea* and deposit age, in thousands of years 31
B3. Stratigraphic sections west of the Rio Grande 33
B4. Stratigraphic sections near the Rio Grande 35
B5. Schematic drawing showing time-position (east-west) distribution of coarse axial river facies deposits and interlayered volcanic rocks in the La Bajada constriction area 36

Table

B1. Age and height relations of upper Cenozoic alluvium, tephra, and volcanic rocks in the Cochiti Pueblo map area 30

Stratigraphy of Upper Cenozoic Fluvial Deposits of the La Bajada Constriction Area, New Mexico

By David P. Dethier and David A. Sawyer

Abstract

Coarse- to medium-grained upper Cenozoic fluvial sediments deposited in the Santo Domingo Basin and adjoining La Bajada constriction record the influence of faulting, volcanism, and climate change on protracted deposition by the ancestral Rio Grande and adjacent piedmont drainages. Axial sand and gravel deposited by the ancestral Rio Grande were derived from uplands to the northeast and northwest of the La Bajada constriction. Interfingering piedmont sand, silt, and local gravel were derived from the Sangre de Cristo Mountains to the east and from the Jemez Mountains to the west. These sediments form part of the Santa Fe Group, a sequence of Miocene and younger sediments deposited in a series of structural basins along the Rio Grande rift in northern New Mexico. Eastern piedmont deposits of arkosic sand, silt, and clay are derived from Precambrian granitic basement rocks and intertongue with coarser axial-river gravel and sand derived from granite and distinctive quartzite. These two mappable sedimentary facies are considered informal units within the Sierra Ladrones Formation, whose type area is to the south in the Albuquerque Basin.

Equivalent upper and middle Miocene piedmont deposits in the Española Basin to the northeast compose the Tesuque Formation. Uppermost eastern piedmont sediments in the Santo Domingo Basin, consisting of sand, silt, clay, and local gravel, may be temporally correlative in part with the Ancha Formation of the Santa Fe area to the east. Upper Miocene and Pliocene western piedmont deposits, which were derived from an active volcanic complex in the adjoining Jemez Mountains, are assigned to the Cochiti Formation. Deposition of the Cochiti volcaniclastic sediments postdates emplacement of the 7–6.2 Ma Peralta Tuff Member of the Bearhead Rhyolite. Western piedmont deposits contain more gravel and coarser sand than the eastern piedmont sediments, and they are dominated by compositionally diverse volcanic clasts derived from the upper Miocene Keres Group of the Jemez volcanic field.

Piedmont and axial Rio Grande sedimentary deposits in the La Bajada constriction area are interlayered with and locally overlie Pliocene and early Pleistocene volcanic rocks. Multiple lava flows and domes that erupted between 2.7 and 1.1 Ma from the Cerros del Rio volcanic field were emplaced onto basin-fill sediments in the La Bajada constriction area. Two large ash-flow tuff sheets of the Bandelier Tuff that erupted at 1.61 and 1.22 Ma buried upland and valley areas in the constriction. Interlayered sediments and volcanic rocks in the northeast part of the Santo Domingo basin are preserved in a complex series of horsts and grabens west of the La Bajada fault zone and are exposed best along the La Bajada fault-zone escarpment and near the village of Cochiti Lake. Coarse-grained alluvium continued to be deposited in the La Bajada constriction area during the Pleistocene by the Rio Grande in the axial part of the basin and by tributary streams on adjacent piedmonts. Faulting, episodes of greatly increased sediment load, and damming by lava flows and sediment provided controls on sediment deposition. The composite thickness of the Santa Fe Group basin-fill stratigraphic section exceeds 300 m in the northeast part of the Santo Domingo basin, and it increases to 3–4 km south of the San Francisco fault in the central part of the basin. Distribution and continuity of late Miocene through late Pliocene alluvial deposits and their inferred subsurface extent imply mainly basin aggradation during their deposition. Pleistocene fluvial incision by the ancestral Rio Grande and its tributaries in White Rock Canyon removed earlier volcanic dams. Several episodes of aggradation and terrace development punctuated erosion during post-Bandelier time in the La Bajada constriction area, suggesting that discharge and sediment load were linked to climatic cycles or to other processes that intensified after early Pleistocene time. Alluvial terrace fills younger than late middle Pleistocene record lateral asymmetry of sediment preservation south of Cochiti Dam; the asymmetry was caused by basinal tilt owing to fault movements or westward growth of the eastern piedmont deposits (or both).

Introduction

Studies by the U.S. Geological Survey were begun in 1996 to improve understanding of the geologic framework of the Albuquerque composite basin and adjoining areas, in order that more accurate hydrogeologic parameters could be applied to new hydrologic models. The ultimate goal of this multidisciplinary effort has been to better quantify estimates of future water supplies for northern New Mexico's growing urban centers, which largely subsist on aquifers in the Rio Grande rift

basin (Bartolino and Cole, 2002). From preexisting hydrologic models it became evident that hydrogeologic uncertainties were large in the Santo Domingo Basin area, immediately upgradient from the greater Albuquerque metropolitan area, and particularly in the northeast part of the basin referred to as the La Bajada constriction (see chapter A, this volume, for a geologic definition of this feature as used in this report). Accordingly, a priority for new geologic and geophysical investigations was to better determine the hydrogeologic framework of the La Bajada constriction area. This chapter along with the other chapters of this report present the results of such investigations as recently conducted by the U.S. Geological Survey.

Exposed coarse-grained upper Cenozoic fluvial deposits in the La Bajada constriction area record protracted deposition by the ancestral Rio Grande and adjacent piedmont drainages that was influenced by faulting, climate change, and lava dams. Axial river gravel and sand are the most abundant subsurface aquifer materials in the Rio Grande valley and La Bajada constriction area (Smith and Kuhle, 1998c, Smith, McIntosh, and Kuhle, 2001) and may increase recharge where hydraulically connected with underlying aquifers. A thorough understanding of the stratigraphic architecture, facies changes, and spatial distribution of fluvial sediments within the La Bajada constriction and adjacent basins is critical to developing a hydrogeologic framework model of the region. In this chapter, we synthesize the results of geologic mapping and limited subsurface information to describe the stratigraphy and distribution of upper Cenozoic fluvial basin-fill sediments in the La Bajada constriction area (pl. 2).

Stratigraphic Nomenclature and Correlations

Fluvial sand and gravel deposited by the ancestral Rio Grande and piedmont sediments derived from uplands to the northeast and northwest of the La Bajada constriction are correlated broadly with the Santa Fe Group ("formation" of Bryan and McCann, 1937, and Bryan, 1938; Santa Fe Group in Spiegel and Baldwin, 1963; Tedford, 1981; and Chapin and Cather, 1994). In this report, we adopt the stratigraphic terminology of Smith, McIntosh, and Kuhle (2001) for the upper Santa Fe Group deposits in the Santo Domingo Basin. They used the name Sierra Ladrones Formation (of the Santa Fe Group) (Machette, 1978) for ancestral Rio Grande axial river gravel and sand deposits rich in granite and quartzite clasts (unit QTsa; unit abbreviations are those of pl. 2 of this report) together with intertonguing eastern piedmont facies derived from granitic basement rocks (unit QTsp). Uppermost Miocene(?) to Pleistocene eastern piedmont sand, mud, and local gravel (unit QTsp) correlate in part with the Ancha Formation and underlying Tesuque Formation in the Española Basin (Spiegel and Baldwin, 1963; Kuhle and Smith, 2001; Koning and others, 2002). In the La Bajada constriction area, the western piedmont facies of the Santa Fe Group is composed of volcaniclastic sediments shed from the Jemez volcanic field. We follow Smith and Lavine (1996) by using Cochiti Formation (unit QTc) for younger western piedmont deposits in the Santo Domingo Basin that overlie the 7–6.2 Ma Peralta Tuff Member of the Bearhead Rhyolite (unit Tbp). Older proximal volcaniclastic deposits of the Jemez volcanic field are informally named Keres Group volcaniclastic deposits (unit Tkvs). Southwest of Peralta Canyon, upper Pliocene piedmont gravel of Lookout Park (unit Tglp) caps Cochiti Formation sediments (Smith, McIntosh, and Kuhle, 2001), which in turn probably overlie unnamed and unexposed older Miocene basin-fill deposits.

The stratigraphic terminology adopted here is consistent with that used by Connell (2001, 2004) for deposits of similar lithology, age, and origin downstream in the Albuquerque Basin. Use of the name Sierra Ladrones Formation in the La Bajada constriction area and adjacent areas of the Rio Grande rift has recent precedents (Tedford and Barghoorn, 1997; Connell, 2001; Smith, McIntosh, and Kuhle, 2001; Connell and others, 2002; Koning and others, 2002; Smith, 2004). Some disagreements persist, however, about the stratigraphic rank, timing, and origin of some Santa Fe Group deposits in the Albuquerque Basin (Connell and others, 1999; Tedford and Barghoorn, 1999; and Williams and Cole, 2005).

Fluvial Basin-Fill Deposits

Lithologic Characteristics

Coarse-grained, mainly gravelly, unconsolidated sediment of the Santa Fe Group exposed in the La Bajada constriction area records the depositional history of the Rio Grande and its tributary piedmont streams during the late Cenozoic. Gravel clasts in these fluvial deposits were derived from three main source areas: (1) quartzites, metavolcanic rocks, chert, and other high-grade Precambrian metamorphic rocks were transported from the northwest by the ancestral Rio Chama and from the north by the ancestral Rio Grande; (2) intermediate, silicic, and minor basaltic rocks were transported from the west and northwest by piedmont streams draining the Jemez Mountains; and (3) granitic rocks, high-grade metamorphic rocks, and minor metasedimentary rocks were transported from the east and northeast by the ancestral Santa Fe River and its tributary piedmont streams.

Ancestral Rio Grande axial-gravel deposits of the Sierra Ladrones Formation (unit QTsa, pl. 2) are coarse grained—generally sand to cobble and boulder gravel—and commonly are well sorted in surface exposures. Matrix of the gravel is generally coarse arkosic sand. Lenses and local lenticular beds of fine sand and silty sand locally are rich in altered pumice.

Piedmont alluvium flanking the axial gravel locally is also coarse grained but commonly contains more sand and silty sand and is more poorly sorted than the axial river alluvium. Some of the poorly sorted piedmont beds are debris-flow deposits. Western piedmont alluvium of

the Cochiti Formation (unit QTc) contains abundant clasts derived from the ~7-Ma Bearhead Rhyolite (unit Trb) and fewer clasts of older Keres Group andesites, rhyolites, and dacites (Smith and Kuhle, 1998c). Pumice-rich intervals and interlayered lavas help to constrain the age of the piedmont alluvium (Smith, McIntosh, and Kuhle, 2001). In exposures near Cochiti Lake, eastern piedmont alluvium of the Sierra Ladrones Formation (unit QTsp) is rich in granitic debris and is interlayered with basalt flows and with lacustrine, eolian, and local basaltic hydromagmatic deposits of the Cerros del Rio volcanic field.

Most piedmont and axial alluvial deposits observed beneath Quaternary fluvial terraces and between volcanic units have exposed thicknesses of 5–30 m. Total exposed thickness of interstratified alluvium of the Rio Grande (unit QTsa) and western piedmont gravel (unit QTc), however, locally exceeds 70 m along Cochiti Canyon and in the southwestern part of the map area (pl. 2). In some areas these fluvial deposits are exposed for distances >1 km. Near Cochiti Dam, the stratigraphic thickness of ancestral Rio Grande deposits (unit QTsa) is interpreted to locally exceed 350 m (Smith, McIntosh, and Kuhle, 2001). The Dome Road well, about 4 km west of Cochiti Lake, penetrated nearly 400 m of Cochiti Formation western piedmont alluvium (Chamberlin, Jackson, and Connell, 1999; chapter G, this volume).

Contact relations and lateral extent of the Santo Domingo Basin alluvial deposits are known mainly from surface exposures. These exposures suggest that upper Santa Fe Group sediments were deposited mostly as a conformable sequence during late Miocene to early Pleistocene (that is, 1.61 Ma) time. Although episodes of downcutting by the Rio Grande during this time period produced intraformational disconformities, large angular unconformities were not recognized in the upper part of the basin-fill sequence by Smith, McIntosh, and Kuhle (2001). The stratigraphy of the Santa Fe Group in the La Bajada constriction is similar to that of the adjoining Albuquerque and Española Basins, in that basin filling continued episodically until early Pleistocene (that is, post-Bandelier Tuff) time. However, Williams and Cole (2005) describe a prominent unconformity beneath Pliocene rocks in the Albuquerque Basin and, in the Española Basin and adjacent White Rock Canyon (pl. 1, fig. B1), prominent disconformities separate upper Miocene rocks from Pliocene units and separate Pliocene strata from the Bandelier Tuff (Reneau and Dethier, 1996).

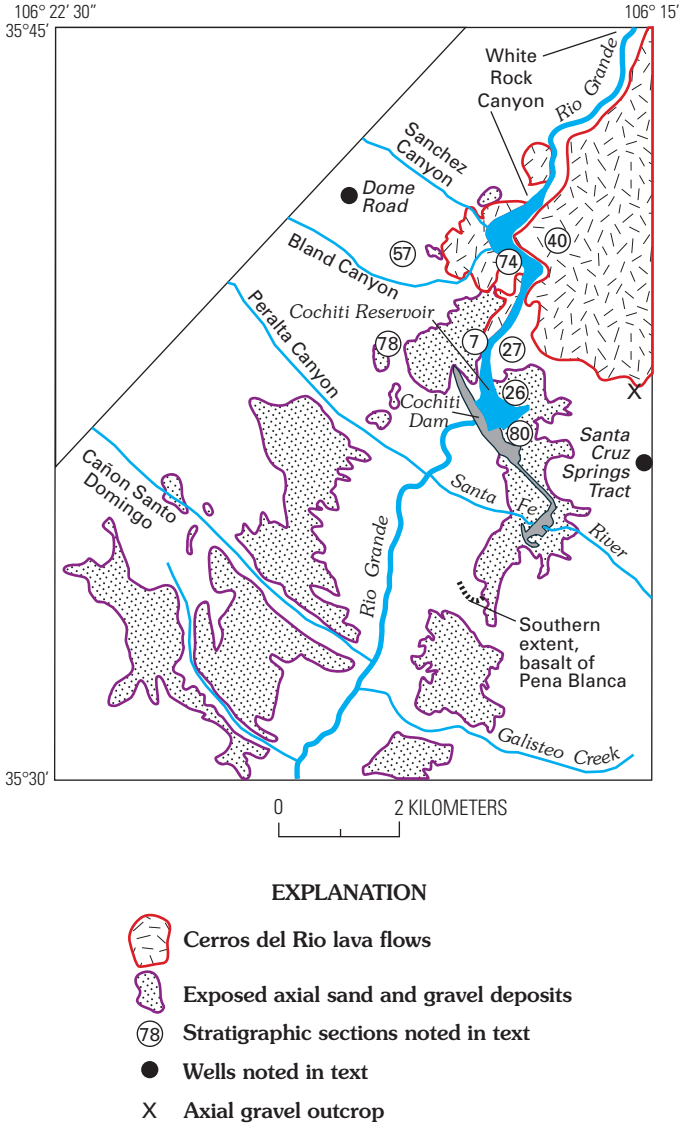

Figure B1. Cochiti Pueblo area and vicinity showing location of axial river gravel deposits, Cerros del Rio lava flows, selected geologic features, and stratigraphic sections noted in text and shown in figures B3 and B4.

Isotopic and Amino-Acid-Racemization Ages

Local stratigraphic relations, $^{40}Ar/^{39}Ar$ dating of basaltic rocks and silicic tuffs, ^{14}C ages of organic material in sediments, and amino-acid-racemization ratios (AAR ratios) for gastropod fossils in Quaternary deposits provide age control (table B1) in the northeast part of the Santo Domingo Basin. The Bearhead Rhyolite (unit Trb, pl. 2) and its Peralta Tuff Member (unit Tbp), dated at 7–6 Ma (Smith, McIntosh, and Kuhle, 2001), provide a minimum limiting age for the oldest river gravels in the study area as well as for the Cochiti Formation (unit QTc), which is derived in part from the Bearhead Rhyolite. A radiometric age of 6.82 Ma for rhyolitic pumice within river gravel (table B1) provides additional local age control for upper Miocene basin-fill deposits in the La Bajada constriction area (Smith and Kuhle, 1998a,b; Smith, McIntosh, and Kuhle, 2001). No radiometric ages exist for alluvium or volcanic rocks deposited between about 6 and 3 Ma in the northeast part of the Santo Domingo Basin.

Table B1. Age and height relations of upper Cenozoic alluvium, tephra, and volcanic rocks in the Cochiti Pueblo map area.

[$^{40}Ar/^{39}Ar$ ages from Smith and others, 2001; W.C. McIntosh, personal commun., 1997; Izett and Obradovich, 1994 (Guaje Pumice Bed); and Sarna-Wojcicki and others, 1987. ^{14}C ages from Reneau and Dethier, 1996; Reneau and others, 1996; and Lanphere and others, 2002. Height above Rio Grande measured from the active channel (or former active channel where inundated by Cochiti Reservoir) to the top of gravel or base of volcanic flow. ND, not determined]

Dating method and surficial or bedrock unit (pl. 2)	Map unit symbol (pl. 2)	Age (k.y.)	Height above Rio Grande (m)	Location and stratigraphic context
$^{40}Ar/^{39}Ar$				
Peralta Tuff Member of Bearhead Rhyolite.	Tbp	6,840–6,810	ND	Interlayered with axial gravel, Tent Rocks area.
Pumiceous alluvium in Rio Grande axial gravel.	QTsa	6,880–6,820	ND	Rhyolite tephra interlayered with Sierra Ladrones Formation axial gravel west of Cochiti Pueblo.
Rhyolite tephra, basal Cochiti Formation	QTc	6,190	ND	Tephra in basal Cochiti Formation, Tent Rocks area.
Basalt of Pena Blanca	Tbpb	2,710	40	Pena Blanca flow overlies axial alluvium.
Basalt of White Rock Canyon	Tb	2,550	30	Overlies axial gravel east and west of Cochiti Reservoir.
Pumiceous alluvium in Cochiti Formation	QTc	1,850	45–55	Pumice from rhyolite of San Diego Canyon; underlies Otowi (lower) Member of Bandelier Tuff.
Rio Grande alluvium	QTsa	1,610	95–100	Beneath Otowi Member of Bandelier Tuff near La Bajada escarpment.
Basalt of Cochiti	QTbc	1,460	75–85	Overlies Guaje pumice bed and pumiceous alluvium east of Cochiti Reservoir.
Dacite of Arroyo Montoso	Qda	1,310	210	Overlies Otowi Member of Bandelier Tuff, north of La Bajada fault zone.
Tshirege (upper) Member of Bandelier Tuff.	Qbt	1,220	90–100	In paleochannel along Rio Grande.
Basaltic andesite of Cochiti Cone	Qcc	1,140	75?	Overlies axial alluvium containing clasts of upper, Tshirege Member of Bandelier Tuff.
Oldest alluvial terrace deposits of Rio Grande.	Qta_1	1,220–639	[1]75	Axial Rio Grande sediments containing Lava Creek B ash, beneath Qta_1, west of Santo Domingo Pueblo area.
Old alluvial terrace deposits of Rio Grande.	Qta_2	550	58	Reworked Valles Rhyolite pumice in Qta_2 fill.
Amino-acid racemization ratios				
Old alluvial terrace deposits of Rio Grande.	Qta_2	[2]250–300	60–70	From gastropods at two sites.
Intermediate alluvial terrace deposits of Rio Grande.	Qta_3	60–300?	38–48	Probably late middle Pleistocene.
^{14}C, thermoluminescence, and electron spin resonance.				
El Cajete tephra	Qec	[3]48–61	15(?)	Near level of Qta_4 terrace.
^{14}C and amino-acid racemization				
Young alluvial terrace deposits of Rio Grande.	Qta_4	[4]>38	15–18	Sediment on Qta_4 terrace; amino-acid racemization analyses suggest age of 70–30 ka.
^{14}C				
Older alluvial deposits of Rio Grande	Qoa	≥43.5	15	Base of overlying lacustrine sediment, northern White Rock Canyon.
Older alluvial deposits of Rio Grande	Qoa	14–12	5–12	Interbedded with lacustrine sediment, White Rock Canyon.
Channel and floodplain deposits of Rio Grande.	Qal	9	5	Central White Rock Canyon.

[1]In Española Basin north of White Rock Canyon, Lava Creek B ash is ~110 m above Rio Grande (Dethier and others, 1990); in lower Jemez River drainage, ash is ~95 m above grade (Rogers and Smartt, 1996).

[2]Based on hydrolysate aIle/Ile ratios (amino-acid racemization) from *Succinea* or *Vallonia* from stratigraphic sections DN–96–26 and DN–96–80 (Dethier and McCoy, 1993).

[3]Carbonized logs in El Cajete tephra yield ^{14}C ages of 50 to >58 ka, and thermoluminescence ages on buried soils give age estimates 48–61 ka (Reneau and others, 1996). Electron-spin-resonance dating of stable Ti centers in quartz provides ages of 53 ka for the El Cajete tephra and 59 ka for the genetically related Battleship Rock ignimbrite (Toyoda and others, 1995).

[4]Shell dates are based on hydrolysate aIle/Ile ratios (amino-acid racemization) from *Succinea* and *Vallonia* from locality DN–96–18 of Dethier and McCoy (1993) and are assumed to be minimum limiting ages.

Age control for Pliocene-Pleistocene alluvial deposits is based mainly on locally derived volcanic rocks. Basaltic hydromagmatic volcanism and deposition of associated deposits (unit Tbm, pl. 2) centered near the modern White Rock Canyon (pl. 1, fig. B1) may have begun as early as 2.9 Ma (Reneau and Dethier, 1996), and basalt flows and basaltic tuff (units Tbj, Tbb, Tbs) erupted soon after at about 2.7 Ma from several vents along the southern and eastern flanks of the Cerros del Rio volcanic field.

Pliocene axial gravels of the Rio Grande (unit QTsa, pl. 2) underlie basalt flows (units Tb, Tbf) dated at about 2.5 Ma (table B1) where exposed at several locations along the margins of Cochiti Reservoir. Early Pleistocene gravelly alluvium (unit Qog) overlies some of these flows (Dethier, 1999). Latest Pliocene and early Pleistocene stratigraphic control of the western piedmont (unit QTc) and axial river sequences is provided by tuff derived from the rhyolite of San Diego Canyon (about 1.85 Ma) and by the widespread Otowi (lower, unit Qbo) Member (1.61 Ma) and Tshirege (upper, unit Qbt) Member (1.22 Ma) of the Bandelier Tuff (table B1) (Izett and Obradovich, 1994). Several dated and a number of undated flows composed of andesite, trachyandesite, and dacite are younger than the Otowi Member, and one andesite flow (unit Qcc) overlies the Tshirege Member; these flows provide local stratigraphic control for early Pleistocene deposits in the eastern part of the La Bajada constriction area. The Lava Creek B ash (639 thousand years old (ka); Lanphere and others, 2002) and layers of reworked pumice from the Valles Rhyolite (550 ka; rhyolite of South Mountain or rhyolite of San Antonio Mountain) are interbedded locally with middle Pleistocene terrace deposits (units Qta_1, Qta_2; Smith, McIntosh, and Kuhle, 2001).

Approximate ages calculated from AAR ratios for gastropod fossils (fig. B2) and ^{14}C ages provide age limits for middle to late Pleistocene deposits (table B1). Several gastropod genera collected at 7 sites from 2 alluvial fill terraces of the Rio Grande (units Qta_2 and Qta_4; pl. 2) were analyzed by using techniques described by Dethier and McCoy (1993). We derived a preliminary AAR age relation using the genus *Succinea* from the La Bajada constriction area; the relation is based primarily on the parabolic racemization curve of Dethier and McCoy (1993), which has been modified for the slightly higher temperatures in the Cochiti Dam area (fig. B2). Values for AAR ratios obtained on samples from the nearby and slightly cooler valley of the Jemez River plot close to the Española Basin curve except for the two oldest samples, which are altered (fig. B2) (Rogers and Smartt, 1996). The AAR data suggest that the Qta_2 terrace fill was deposited about 300–250 ka (table B1). These AAR ages seem inconsistent with a $^{40}Ar/^{39}Ar$ date of 550 ka for reworked Valles Rhyolite pumice in another deposit mapped as unit Qta_2. If the reworked pumice provides a close limiting age for the fill and if the AAR ages are correct, then the Rio Grande may have remained approximately 60 m above present grade for 200 thousand years (k.y). or backfilled to that height after post-550 ka downcutting. AAR ages show that unit Qta_4 terrace fill was deposited between about 70 and 30 ka, which is consistent with minimum limiting ^{14}C ages of >43.5 and >38 ka for terrace fills at approximately the same height above the Rio Grande elsewhere (table B1).

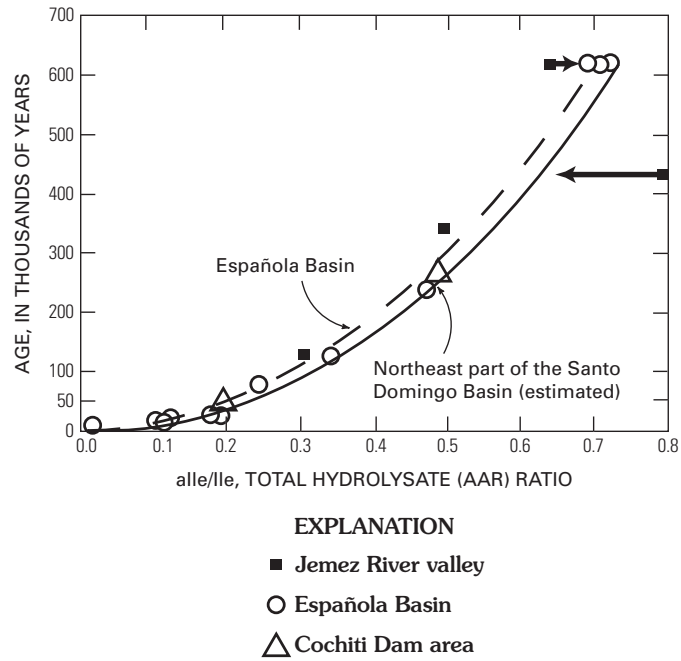

Figure B2. Relation between amino acid racemization (AAR) ratio in *Succinea* and deposit age, in thousands of years. Parabolic curve for northeast part of the Santo Domingo Basin estimated from curve for the Española Basin (Dethier and McCoy, 1993). Analyses from the Jemez River valley are from Rogers and Smartt (1996). Data points with horizontal arrows pointing toward parabolic curve derived from AAR values reported by Rogers and Smartt (1996) for diagenetically altered samples.

Stratigraphic Framework

Upper Miocene Through Lower Pleistocene Basin-Fill Deposits

Alluvial and piedmont-fan sand and gravel basin-fill sediments deposited during the Miocene are exposed in the La Bajada constriction area. Upper Oligocene–lower Miocene(?) ashy siltstones that crop out along the La Bajada escarpment, 10 km east-southeast of Cochiti Reservoir near the village of La Bajada (pl. 1), may correlate with the Abiquiu(?) Formation (pl. 2) (Stearns, 1953; Sawyer and others, 2002). These siltstones and younger basin-fill deposits cannot be traced north and west from the La Bajada exposures because massive landslide deposits and extensive colluvium mantle pre-basalt geologic units along the La Bajada escarpment. To the east of the escarpment, Pliocene to middle Pleistocene piedmont deposits of the Ancha Formation and the Tuerto

Gravel (unit QTt, pl. 2) overlie Oligocene and older rocks that are described in chapter A (this volume). On the western margin of the La Bajada constriction, gravel-rich deposits of the Cochiti Formation are interlayered with and overlie the upper Miocene Bearhead Rhyolite (unit Trb). Miocene Santa Fe Group basin-fill deposits are inferred to lie beneath the central part of the La Bajada constriction but are nowhere exposed. Below we discuss the upper Miocene through Pleistocene basin-fill deposits in more detail.

We divide upper Miocene, Pliocene, and early Pleistocene basin-fill deposits into three stratigraphic units that consist of the sedimentary facies described earlier: (1) Cochiti Formation western piedmont alluvium (unit QTc, pl. 2); (2) Sierra Ladrones Formation axial river gravel (unit QTsa); and (3) Sierra Ladrones Formation eastern piedmont alluvium (unit QTsp). These units include (1) deposits coeval with or older than the approximately 2.7–2.5-Ma Cerros del Rio basalt flows (units Tbb, Tbj, Tbs, Tb); (2) Pliocene and Pleistocene deposits younger than the basalts but older than the 1.22-Ma Tshirege (upper) Member of the Bandelier Tuff (unit Qbt); and (3) deposits that are present principally in the La Majada graben (fig. A4) that are probably younger than Cerros del Rio basalt but older than the <600 ka alluvium of La Majada Mesa (unit Qalm) and its associated erosion surface. Smith and Kuhle (1998a,b) mapped alluvial deposits older than early Pleistocene as Cochiti Formation (western piedmont facies) and Sierra Ladrones Formation (Rio Grande axial river and eastern piedmont facies); they mapped younger Pleistocene deposits as a sequence of alluvial terrace deposits.

Axial river gravel and sand deposits older than middle Pliocene (unit QTsa) have been mapped in many places in the La Bajada constriction area (pl. 2). Peralta Tuff Member of the Bearhead Rhyolite (unit Tbp; 6.88–6.81 Ma) interlayered with coarse axial river gravel and sand deposits in the Tent Rocks area (pl. 2) demonstrate that a river transporting clasts from northern sources flowed through the western part of the map area as early as latest Miocene time (Smith and Kuhle, 1998a,b,c; Smith, McIntosh, and Kuhle, 2001). Along the La Bajada escarpment, at the mouth of Tetilla Arroyo (pl. 1), a >30-m-thick section of axial river gravel crops out beneath basalt flows (unit Tbf) dated at about 2.5 Ma (see “X” in fig. B1). This outcrop, on the upthrown side of the La Bajada fault zone (pl. 2; fig. B1), provides evidence that the ancestral Rio Grande deposited gravel east of the fault zone and at least 5.5 km east of the modern Rio Grande channel before the middle Pliocene. The eastern limit of Rio Grande axial river gravel older than middle Pliocene is poorly constrained beneath lava flows of the Cerros del Rio volcanic field (pl. 2; also see chapter G, this volume).

South of Peralta Canyon, ancestral Rio Grande axial gravel (unit QTsa) is moderately exposed throughout a broad area that extends as far as about 12 km west of the modern Rio Grande (pl. 2; fig. B1). In this area the gravel interfingers with piedmont deposits of the Cochiti Formation (unit QTc). A mantle of younger western piedmont gravel of Lookout Park (unit Tglp; Smith and Kuhle, 1998a,b,c) locally overlies the axial river gravel deposits near the west edge of the map area (pl. 2). The gravel of Lookout Park, in turn, is locally overlain by erosional remnants of early Pleistocene Otowi Member of the Bandelier Tuff (unit Qbo). South of Cochiti Dam, ancestral Rio Grande axial gravel and sand (units QTsa, Tsls) interfinger with eastern piedmont alluvium (unit QTsp) as much as 5 km east of the modern Rio Grande (fig. B1). Farther south, on the north side of Galisteo Creek, axial river sand (unit Tsls) underlies eastern piedmont alluvium, which in turn underlies the Otowi Member of the Bandelier Tuff (pl. 2) (Smith and Kuhle, 1998b).

Ages of capping basalt flows (unit Tb, pl. 2) indicate that Rio Grande axial gravel is older than about 2.5 Ma in lower White Rock Canyon in the northern part of the map area (table B1). In the upper part of this canyon about 15 km north of Cochiti Reservoir, basalt flows as old as 2.9 Ma overlie coarse Rio Grande alluvium (Reneau and Dethier, 1996). To the south in the Santo Domingo Valley (pl. 1) the 2.7-Ma basalt of Peña Blanca (unit Tbpb) overlies >20 m of Rio Grande axial sand (unit Tsls) that interfingers with eastern piedmont alluvium (unit QTsp) (pl. 2). Cuttings from the Santa Cruz Springs Tract well (figs. B1, G1, G3) suggest that at least 30 m of axial river gravel, interbedded with eastern piedmont alluvium, overlies a 2.57–2.55-Ma basalt at depth (Smith and Kuhle, 1998a; Smith, McIntosh, and Kuhle, 2001; G.A. Smith, written commun., 2001). This interpretation is consistent with the evidence described above that the ancestral Rio Grande flowed at least 5 km east of its present course during middle Pliocene time. Along the western shore of Cochiti Reservoir, Rio Grande axial gravel (unit QTsa) is exposed beneath basalt flows (unit Tb) dated at about 2.5 Ma (stratigraphic section DN–96–7, fig. B3*C*).

The thickest and most extensive exposures of western piedmont deposits (Cochiti Formation) and interfingering ancestral Rio Grande alluvium (Sierra Ladrones Formation axial river gravel facies) are near, west, and southwest of Cochiti Dam (pl. 2), along deeply dissected drainages such as those in lower Bland Canyon and near stratigraphic section DN–96–78 (figs. B1, B3*A*). As indicated above and discussed in more detail in chapter G (this volume), the Dome Road well penetrated 400 m of Cochiti Formation western piedmont deposits (fig. G5). The Dome Road well did not encounter axial-gravel-facies alluvium and thus provides a local western limit for the Pliocene ancestral Rio Grande.

Silt and clay-rich lacustrine deposits (units Tsll, Tslm, pl. 2) exposed locally north of Galisteo Creek are intercalated with axial sand deposits (unit Tsls) and underlie 2.7–2.55-Ma basalts (unit Tbpb). The lacustrine deposits are several meters thick and contain laterally extensive diatomite layers. Fossil diatom assemblages suggest that climate at the time of their deposition was cooler than at present and that the lowland landscape was forested, perhaps similar to the modern Jemez Mountains (J.P. Bradbury, U.S. Geological Survey, written commun., 1996). Other clay-rich lacustrine deposits are interpreted on the basis of geophysical and well data to underlie the Otowi Member of the Bandelier Tuff east of the Pajarito fault zone (chapters F and G, this volume).

A. Section DN–96–78

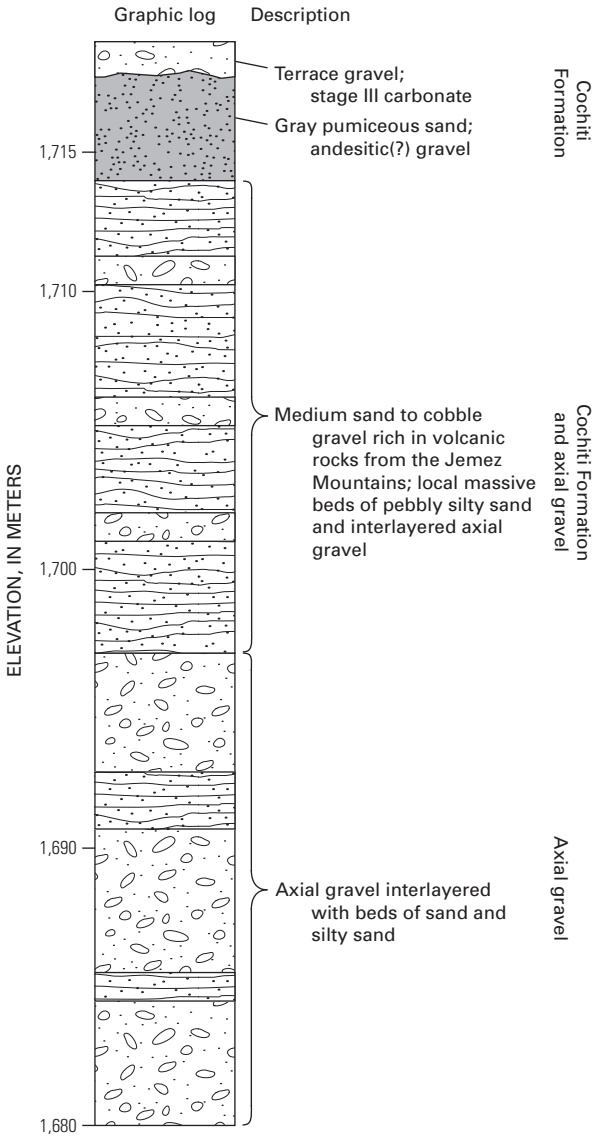

B. Section DN–96–57

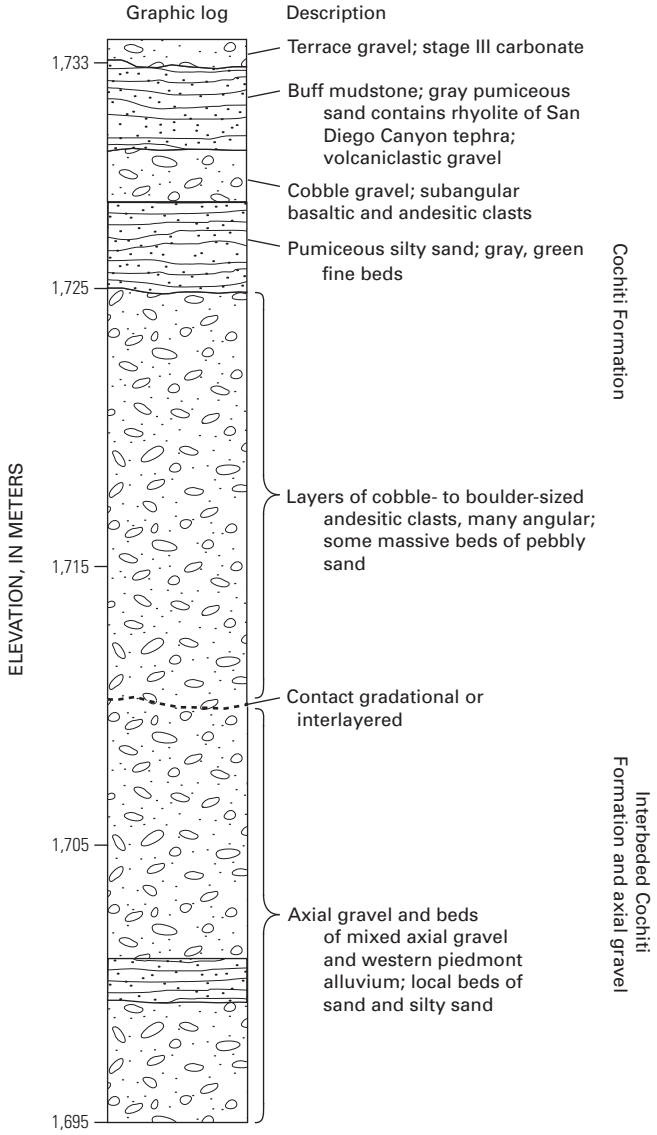

C. Section DN–96–7

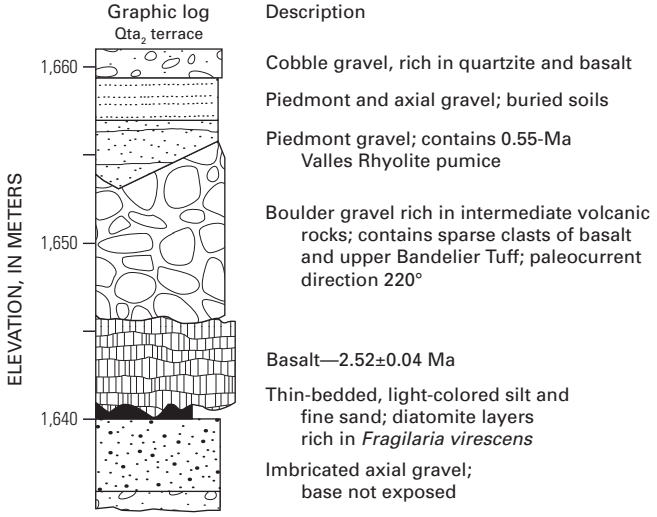

Figure B3. Stratigraphic sections west of the Rio Grande; locations (last number of section designation) shown in fig. B1. *A*, Graphic log and description of stratigraphic section DN–96–78. *B*, Graphic log and description of stratigraphic section DN–96–57. *C*, Graphic log and description of stratigraphic section DN–96–7.

Upper Pliocene–lower Pleistocene deposits and volcanic rocks in the La Bajada constriction area include Rio Grande older gravelly alluvium (unit Qog, pl. 2), western piedmont sediments of the uppermost Cochiti Formation (unit QTc), older alluvium of Cerro Toledo Rhyolite interval (unit Qact), Bandelier Tuff (units Qbo, Qbt), and some younger basaltic flows from the Cerros del Rio volcanic field. North of Galisteo Creek, on the south flank of La Majada Mesa, uppermost (early to middle Pleistocene) Santa Fe Group eastern piedmont deposits (unit QTs) can be identified locally where the 1.61-Ma Otowi Member of the Bandelier Tuff (unit Qbo) separates them from underlying eastern piedmont deposits (unit QTsp). Rio Grande axial gravels (unit QTsa) of Pliocene-Pleistocene age crop out near and east of the modern Rio Grande (pl. 2) (G.A. Smith, written commun., 2001). Northwest and northeast of Cochiti Dam, thin piedmont gravels of the Cochiti Formation (stratigraphic section DN–96–57, fig. B3*B*) contain rhyolite of San Diego Canyon tephra (about 1.85 Ma) and fill southeast-trending paleochannels that underlie remnants of the Otowi Member of the Bandelier Tuff. These stratigraphic relations demonstrate that during latest Pliocene or earliest Pleistocene time, streams depositing western piedmont gravel flowed east of Cochiti Reservoir into an area that later (during middle Pleistocene time) received eastern piedmont gravel and alluvial-fan deposits (Smith, McIntosh, and Kuhle, 2001). Transport and deposition of sediment on piedmont slopes continued after eruption of the Otowi Member of the Bandelier Tuff; the resulting piedmont deposits in the central La Bajada constriction area (unit Qact, for example) are relatively thin and fill channels cut <15 m deep into the underlying tuff.

Pleistocene (Post-Bandelier Tuff) Through Holocene Deposits

Geomorphic and stratigraphic relations suggest that several episodes of aggradation punctuated fluvial incision during post-Bandelier time. After eruption of the Tshirege (upper) Member of the Bandelier Tuff (unit Qbt) at 1.22 Ma, the Rio Grande migrated to near its present position, deposited a complex alluvial terrace fill sequence, and incised to its present elevation (Dethier, 1999). Deposits that form the highest and thickest alluvial terraces (unit Qta_1) may record extremely rapid erosion of the Tshirege Member of the Bandelier Tuff (unit Qbt) in the lower part of White Rock Canyon (pl. 1, fig. B1) and its tributary valleys (stratigraphic section DN–96–40, fig. B4*D*). The outcrop pattern of these early(?) Pleistocene alluvial terrace deposits (unit Qta_1) is fan-shaped (pl. 2) (Dethier, 1999). Thick (10–30 m) alluvial deposits beneath the unit Qta_1 terrace surfaces contain 3–5-m blocks of upper Bandelier Tuff (unit Qbt), coarse boulder gravel from the western piedmont, and subordinate amounts of reworked older axial river gravel (unit QTsa). The outcrop pattern and composition of the unit Qta_1 alluvial terrace deposits suggests that they formed after the Rio Grande had breached a natural dam at the constriction near the northwestern end of the La Bajada fault zone. Sediment fill that dammed the river was derived from eastward-flowing streams south of Capulin Canyon (pl. 1); it is composed of tuff blocks eroded from the lower part of White Rock Canyon by the Rio Grande. Stratigraphic (stratigraphic section DN–96–26, fig. B4*C*) and geomorphic relations north of the Cochiti Pueblo map area suggest that even after the dam failed, post-1.22-Ma resistant basaltic lava flows impeded headward incision by the Rio Grande through White Rock Canyon until middle Pleistocene time (Reneau and Dethier, 1996).

La Majada Mesa is a prominent geomorphic feature bounded on the west by the Rio Grande, on the south by Galisteo Creek, and on the east by the La Bajada fault zone (pl. 2). The mesa is capped east of Cochiti Dam by eolian sand and at least 10–12 m of underlying sandy alluvium with gravelly lenses that is informally called the alluvium of La Majada Mesa (unit Qalm). This alluvium contains numerous buried soils that suggest a history of alternating landscape stability and accretion. The uppermost soil has an eroded Bt horizon above a stage III to IV calcic horizon. Locally the upper soil lacks a Bt horizon and has a stage II to III calcic horizon. The alluvium of La Majada Mesa overlies an extensive, gently west-sloping (about 0.2°–2°), erosion surface formed on upper Santa Fe Group sediments (unit QTs). This surface likely was graded to the Rio Grande when it formed, but it now projects to about 75 m above the present river. The alluvium of La Majada Mesa is similar in age to, or slightly younger than, the "La Bajada pediment" of Kirk Bryan, the intermediate of his three high erosion surfaces graded to the Rio Grande (Bryan and McCann, 1938). The alluvium of La Majada is possibly correlative in part with the "Ridge terrace" of Aby (1997) and with the axial-gravel terrace (unit Qal_1) of Dethier (1999), which has an age of about 650–550 ka (Dethier and McCoy, 1993) but locally includes sediments almost as old as the upper Bandelier Tuff.

Younger alluvial fill–terrace deposits (units Qta_2, Qta_3, Qta_4) are inset within and below the unit Qta_1 terrace deposits near the modern Rio Grande channel (pl. 2) (Dethier, 1999; Smith, McIntosh, and Kuhle, 2001). These alluvial deposits are composed of axial river gravel as thick as 30 m and are overlain by, and locally interfinger with, sandy alluvium derived from both eastern and western piedmonts. Early(?) Pleistocene and younger piedmont terrace alluvial deposits (units Qtp_1, Qtp_2, Qtp_3, and Qtp_4) are preserved from the Cochiti Reservoir area southward to the main part of the Santo Domingo Basin. Local stratigraphic relations of the older Rio Grande alluvial fill-terrace deposits and gravelly alluvium (units Qog, Qta_1) are obscure at many sites because of the similar composition and size of gravel clasts (stratigraphic section DN–96–27, fig. B4*A*). Age estimates (table B1) suggest that unit Qta_2 deposits aggraded between about 550 and 300 ka and that extensive younger fill–terrace deposits (units Qta_3, Qta_4) are middle and late Pleistocene in age. In the vicinity of Cochiti Lake, the Rio Grande cut down tens of meters before aggradation of the unit Qta_2 fill, which in turn was followed by additional substantial downcutting. Extensive deposits of unit Qta_1 and unit Qta_2 crop

A. Section DN–96–27

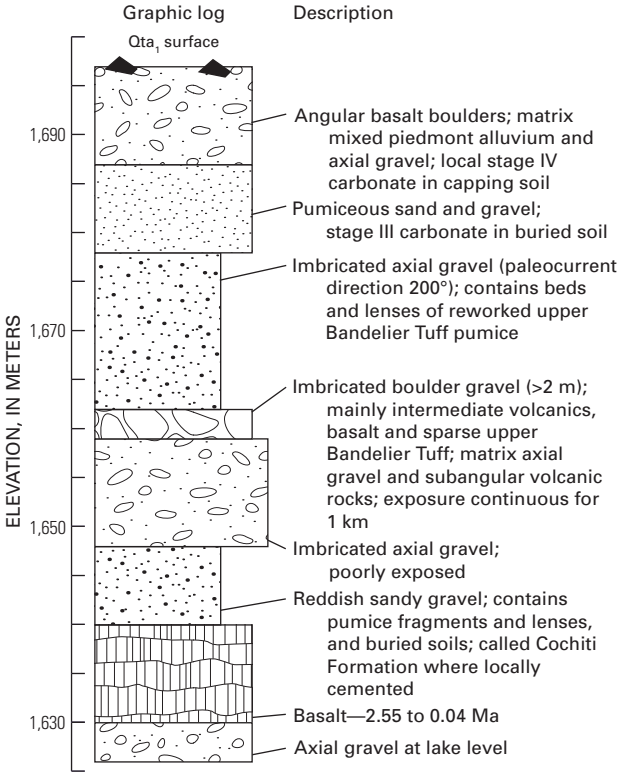

B. Section DN–96–74

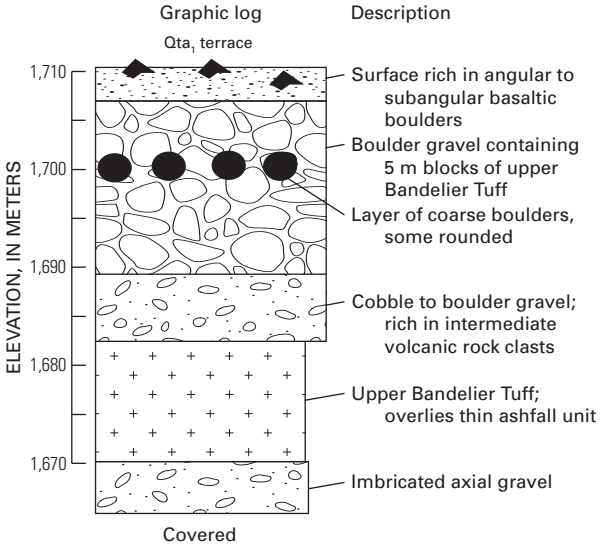

C. Section DN–96–26

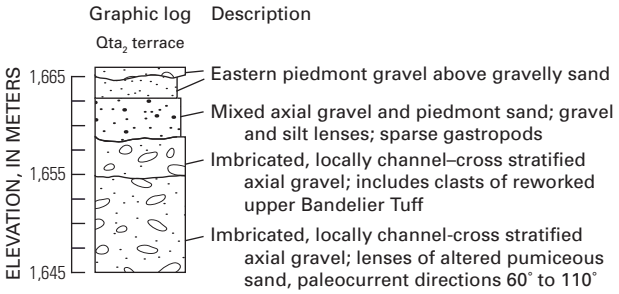

D. Section DN–96–40

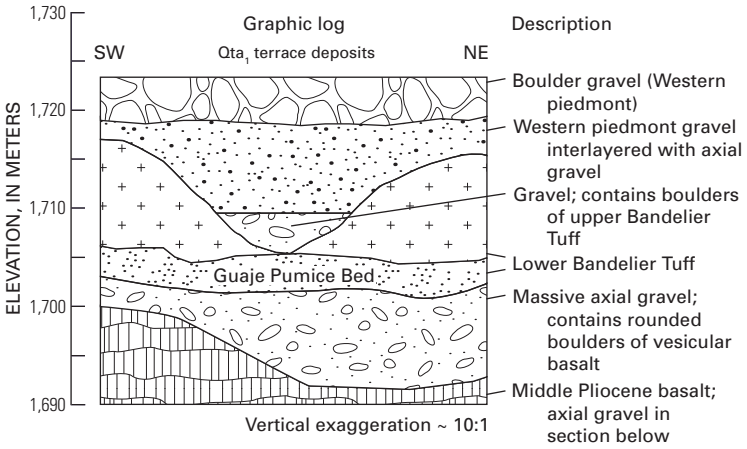

Figure B4. Stratigraphic sections near the Rio Grande; locations (last number of section designation) shown in fig. B1.
A, Graphic log and description of stratigraphic section DN–96–27.
B, Graphic log and description of stratigraphic section DN–96–74.
C, Graphic log and description of stratigraphic section DN–96–26.
D, Graphic log and description of stratigraphic section DN–96–40.

out north of Cochiti Dam, but alluvial deposits of early(?) to middle Pleistocene age are poorly preserved south of the dam (pl. 2). Near and south of Cochiti Dam, middle and late Pleistocene alluvial terrace deposits (units Qta_3, Qta_4) crop out mainly east of the Rio Grande, where they are covered by thin deposits of eastern piedmont alluvium (units Qtp_3, Qtp_4, Qpu) and locally overlie older axial river gravel and sand (units QTsa, Tsls). The youngest extensive fill-terrace deposits (unit Qta_3) are preserved mainly between Cochiti Dam and Galisteo Creek, east of the Rio Grande (pl. 2) (Smith and Kuhle, 1998a). Smith, McIntosh, and Kuhle (2001) attribute the lateral asymmetry (that is, eastern dominance) of younger alluvial fill remnants to middle and late Pleistocene migration of faulting and stream deposition toward the eastern side of the Santo Domingo Basin.

Holocene fluvial deposits (unit Qal, pl. 2) form the floodplain and low terraces along the Rio Grande and its tributaries south of Cochiti Dam. North and east of the dam, undifferentiated late Pleistocene and Holocene gravelly alluvial fan deposits (unit Qfa) flank tributary arroyos, but axial river deposits are covered by Cochiti Reservoir.

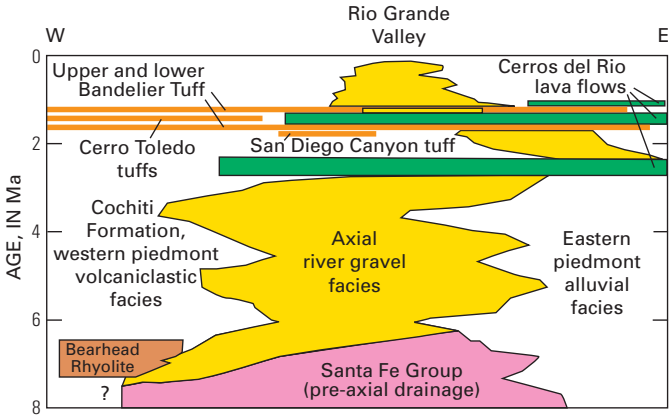

Figure B5. Time-position (east-west) distribution of coarse axial river facies deposits and interlayered volcanic rocks in the La Bajada constriction area. Width of drawing represents lateral (east-west) distance of approximately 20 km.

Incisional and Aggradational History of the Ancestral Rio Grande

Exposures of coarse-grained alluvium in the La Bajada constriction area record deposition by the late Cenozoic Rio Grande in the axial part of the basin and by tributary streams on adjacent piedmonts (fig. B5). These fluvial deposits also provide evidence of depositional control by faulting, episodes of dramatically increased sediment load, and damming by lava flows and sediment. Thickness of the composite basin-fill stratigraphic section exceeds 300 m and locally may approach 1,200 m (Smith, McIntosh, and Kuhle, 2001), particularly in the vicinity of Cochiti Dam. Distribution and continuity of late Miocene through late Pliocene alluvial deposits and their inferred subsurface extent imply mainly basin aggradation during this time in the La Bajada constriction area. To the south in the northern Albuquerque Basin, Lozinsky and others (1991) and Connell and others (2001) interpreted nearly continuous basin filling in the eastern part of the basin from late Miocene through early Pleistocene time, whereas Williams and Cole (2005) hypothesize that the hydraulic regime changed and the western basin margin eroded during latest Miocene, probably in response to climate change.

Despite dominant aggradation in the area, axial and tributary streams may have incised considerably in the area of the La Bajada constriction during intervals in late Miocene and early Pliocene time. The substantial volume of coarse alluvium near Cochiti Dam requires extensive erosion in the upstream drainage basin and bed-load transport by an energetic axial river. Near White Rock Canyon, the ancestral Rio Grande cut down >250 m through slightly lithified sediments of the Santa Fe Group between about 8.4 and 2.9 Ma (Reneau and Dethier, 1996). Downcutting by the Rio Grande and latest Miocene–early Pliocene erosion (Manley, 1979) upstream in the Española Basin may record regional incision driven by climate change or local headward migration of a knick zone driven by fault-controlled subsidence of the La Bajada constriction area. The gravel-transporting ancestral Rio Grande extended at least as far south as the southern end of the Cochiti Pueblo map area (pl. 2) during late Miocene–early Pliocene time.

Geologic relations from adjacent basins help provide a context for interpreting upper Cenozoic deposits of the La Bajada constriction area. North of the area, previous workers (Spiegel and Baldwin, 1963; Griggs, 1964; Galusha and Blick, 1971; Manley, 1979) noted unconformities below and above the upper Miocene Chamita Formation of the Española Basin and interpreted the upper unconformity in terms of tectonic deformation and establishment of an axial drainage. Determination of the timing of the following two important events in the time-stratigraphic evolution of the Rio Grande basins depends on stratigraphic interpretations of upper Cenozoic northern-provenance axial gravel deposits within the basin-fill sequence: cessation of “closed” basin deposition, and integration of the Rio Grande as an axial system (Connell, 2001, 2004). It is difficult to determine, however, when either of these events occurred in the La Bajada constriction. Correlation of deposits within the upper part of the basin fill is hampered by shallow level of exposure, multiple cycles of erosion and deposition that recycled sedimentary rocks of similar type, and difficulty in determining whether changes from aggradation to erosion are local or regional in extent. Distinguishing a change from deposition to long-term incision by the Rio Grande would provide a convenient stratigraphic criterion for separating Santa Fe Group from post-Santa Fe Group deposits. However, in the La Bajada constriction area, even where rift basin-fill sediments are deeply dissected and well exposed, it is difficult to conclude that evidence of post-early Pleistocene, erosion represents the initial change to basin-scale incision.

Axial river gravel deposits yield geochronologic evidence (see earlier discussion) of a through-flowing ancestral Rio Grande in the western part of the La Bajada constriction as early as about 7 Ma (fig. B5). Quartzite-rich sediment of inferred late Miocene(?) age presumably derived from a distant source to the north was described from subsurface drill cuttings along the western margin of the Española Basin (Purtymun, 1995), although this finding has not been corroborated by more recent work. Dacitic tephra interlayered with northern-source axial river gravel deposits that has been dated by $^{40}Ar/^{39}Ar$ techniques at about 5 Ma (WoldeGabriel and others, 2001) is exposed near the base of the Puye Formation in the western part of the Española Basin. Older(?) coarse gravels also are present in the subsurface beneath the Pajarito plateau (Reneau and Dethier, 1996; Rogers and Smartt, 1996), but it is not known if they were deposited by the ancestral Rio Grande (WoldeGabriel and others, 2001). Reneau and Dethier (1996) interpreted subsurface data and exposures near White Rock Canyon as evidence that before the middle Pliocene the Rio Grande flowed west of its present course and that downcutting began during latest Miocene or early Pliocene time.

Demonstrably uppermost Miocene basin-fill deposits are exposed only in the southwest part of the La Bajada constriction area, and no exposures of early Pliocene deposits have been identified in the area. Erosional unconformities resulting from base-level changes are preserved within middle Pliocene alluvial deposits at localities near Cochiti Reservoir. Basalt dated at about 2.9 Ma (unit Tb, pl. 2) disconformably overlies Rio Grande axial gravel alluvium at river level northeast of the reservoir. A separate, undated basalt flow (also unit Tb) also disconformably overlies Rio Grande gravel some 60 m higher and 1,500 m west of the river-level basalt. Also, 2.5-Ma flows are present about 30 m lower than the undated basalt flow around Cochiti Reservoir where they disconformably overlie axial gravel and lacustrine deposits. During the interval 2.5–1.6 Ma, the Rio Grande cut a canyon 170 m deep in basalt at Water Canyon about 15 km north of Cochiti Reservoir (pl. 1) (Reneau and Dethier, 1996). Such episodes of Pliocene and Pleistocene downcutting in White Rock Canyon north of the La Bajada constriction reflect a knickpoint that migrated upstream, driven by faulting or regional downcutting (or both).

In addition to changes in base level, Rio Grande alluvial deposits record considerable lateral migration of the axial drainage from one side of the basin to the other (fig. B5). Smith, McIntosh, and Kuhle (2001) interpreted a late Pliocene eastward shift in river position and alluvial deposition as a fluvial response to eastward tilting of the Santo Domingo Basin. Alternatively, this eastward shift of the river may record one or more of three other events: (1) blockage by lava flows and maar deposits (Self and others, 1996) near the north end of Cochiti Reservoir; (2) upland erosion and expansion of the western piedmont fans; and (3) drainage changes due to headward cutting by the Rio Grande in response to climate change or faulting. At about 1.8 Ma the ancestral Rio Grande flowed several kilometers east of Cochiti Reservoir, at an elevation lower than present river level, before migrating westward to the vicinity of Cochiti Reservoir and aggrading about 75 m before about 1.2 Ma (stratigraphic section DN–96–26, fig. B4*C*; fig. B5).

Erosion by the Rio Grande after 1.22 Ma rapidly removed deposits of the upper (Tshirege) Member of the Bandelier Tuff (unit Qbt, pl. 2) that filled portions of the lower part of White Rock Canyon and its tributary valleys. Resulting tuffaceous debris accumulated in early(?) Pleistocene alluvial terrace-fill deposits (unit Qta_1) that subsequently were incised by the Rio Grande. The next youngest alluvial fill (unit Qta_2) records a separate episode of aggradation and incision during middle Pleistocene time (550–250 ka), and some of the younger basin fill sediments record similar aggradational episodes (Dethier, 1999). Periodic cessation of middle and late Pleistocene incision followed by aggradation and terrace development in the La Bajada constriction area suggests that discharge and sediment load were linked to climatic cycles or to other events that intensified after early Pleistocene time. Alluvial terrace fills younger than late middle Pleistocene (unit Qta_3) also record lateral asymmetry of sediment preservation south of Cochiti Dam (pl. 2), likely reflecting basinal tilt due to fault movements (Smith, McIntosh, and Kuhle, 2001) or westward growth of the eastern piedmont deposits (or both).

Hydrogeologic Implications

Pliocene and younger ancestral Rio Grande axial gravel and sand are the most important aquifer material in the subsurface of the Rio Grande valley (Smith and Kuhle, 1998b) owing to their high porosity and permeability and great subsurface volume. Surface gravels may serve as a recharge zone where they are hydraulically connected with underlying aquifers. Near-surface Holocene coarse alluvium in the La Bajada constriction area is only tens of meters thick and lies above the water table, but Pleistocene and older gravel in the subsurface is locally more than a hundred meters thick and may have considerable lateral extent. Coarse alluvial deposits of similar age form critical portions of the aquifer in the Albuquerque Basin to the south (for example, Kernodle, McAda, and Thorn, 1995). It seems likely that pre-middle Pliocene gravel submerged beneath Cochiti Reservoir for more than two decades promotes recharge of the Rio Grande valley aquifer southward from the Cochiti Pueblo area. Lateral seepage of water into agricultural lands of Cochiti Pueblo and Peña Blanca from Cochiti Dam provides evidence of this process, which has required substantial engineering mitigation (Blanchard and others, 1993). Geophysical data and interpretation (chapters D, F, and G, this volume) provide additional constraints regarding the subsurface extent and configuration of coarse alluvial deposits in the La Bajada constriction area.

References Cited

Aby, S.B., 1997, The terraces of Cochiti Canyon—Soil development and relation to activity in the Pajarito fault zone: Albuquerque, University of New Mexico, M.S. thesis, 159 p.

Bartolino, J.R., and Cole, J.C., 2002, Ground-water resources of the middle Rio Grande Basin, New Mexico: U.S. Geological Survey Circular 1222, 132 p.

Blanchard, P.J., 1993, Ground-water-level fluctuations in the Cochiti Dam–Peña Blanca area, Sandoval County, 1976–89: U.S. Geological Survey Water-Resources Investigations Report 92–4193, 72 p.

Bryan, Kirk, 1938, Geology and ground-water conditions of the Rio Grande depression in Colorado and New Mexico, in U.S. National Resources Planning Board, The Rio Grande joint investigation in the upper Rio Grande Basin: Washington, D.C., U.S. Government Printing Office, v. 1, pt. 2, p. 197–225.

Bryan, Kirk, and McCann, F.T., 1937, The Ceja del Rio Puerco—A border feature of the Basin and Range province in New Mexico, pt. 1, Stratigraphy and structure: Journal of Geology, v. 45, p. 801–828.

Bryan, Kirk, and McCann, F.T., 1938, The Ceja del Rio Puerco—A border feature of the Basin and Range province in New Mexico, pt. 2, Geomorphology: Journal of Geology, v. 46, p. 1–16.

Chamberlin, R.M., Jackson, P.B., and Connell, S.D., 1999, Field logs of borehole drilled for monitoring well at Dome Road site, Cañada de Cochiti Grant, Sandoval County, New Mexico: New Mexico Bureau of Mines and Mineral Resources Open–file Report 444c, 30 p.

Chapin, C.E., and Cather, S.M., 1994, Tectonic setting of the axial basins of the northern and central Rio Grande rift, *in* Keller, G.R., and Cather, S.M., eds., Basins of the Rio Grande rift—Structure, stratigraphy, and tectonic setting: Geological Society of America Special Paper 294, p. 5–25.

Connell, S.D., 2001, Stratigraphy of the Albuquerque Basin, Rio Grande rift, New Mexico—A progress report, A–1, *in* Connell, S.D., Love, D.W., and Lucas, S.G., eds., Stratigraphy and tectonic development of the Albuquerque Basin, central Rio Grande rift—Mini-papers in field trip guidebook for the Geological Society of America Rocky Mountain–South Central section meeting, Albuquerque, New Mexico: New Mexico Bureau of Mines and Mineral Resources Open-file Report 454B, p. A1–A27.

Connell, S.D., 2004, Geology of the Albuquerque Basin and tectonic development of the Rio Grande rift in north-central New Mexico, *in* Mack, G.H., and Giles, K.A., eds., The geology of New Mexico—A geologic history: New Mexico Geological Society Special Publication 11, p. 359–388.

Connell, S.D., Cather, S.M., Dunbar, N.W., McIntosh, W.C., and Peters, L., 2002, Stratigraphy of the Tanos and Blackshare Formations (lower Santa Fe Group), Hagan embayment, Rio Grande rift, New Mexico: New Mexico Geology, v. 24, p. 107–117.

Connell, S.D., Koning, D.J., and Cather, S.M., 1999, Revisions to the stratigraphic nomenclature of the Santa Fe Group, northwestern Albuquerque Basin, New Mexico: New Mexico Geological Society 50th field conference, Albuquerque Geology, Guidebook, p. 337–353.

Connell, S.D., Love, D.W., and Lucas, S.G., eds., 2001, Stratigraphy and tectonic development of the Albuquerque Basin, central Rio Grande rift—Mini-papers in field trip guidebook for the Geological Society of America Rocky Mountain–South Central section meeting, Albuquerque, New Mexico: New Mexico Bureau of Mines and Mineral Resources Open-file Report 454B, 93 p.

Dethier, D.P., 1999, Quaternary evolution of the Rio Grande near Cochiti Lake, northeast Santo Domingo Basin, New Mexico: New Mexico Geological Society 50th field conference, Albuquerque Geology, Guidebook, p. 371–378.

Dethier, D.P., and McCoy, W.D., 1993, Aminostratigraphic relations and age of Quaternary deposits, northern Española Basin, New Mexico: Quaternary Research, v. 39, p. 222–230.

Galusha, Ted, and Blick, J.C., 1971, Stratigraphy of the Santa Fe Group, New Mexico: Bulletin of the American Museum of Natural History, v. 144, 127 p.

Griggs, R.L., 1964, Geology and groundwater resources of the Los Alamos area, New Mexico: U.S. Geological Survey Water-Supply Paper 1735, 107 p.

Izett, G.A., and Obradovich, J.D., 1994, $^{40}Ar/^{39}Ar$ age constraints for the Jaramillo normal subchron and the Matuyama-Brunhes geomagnetic boundary: Journal of Geophysical Research, v. 99 (B2), p. 2925–2934.

Kernodle, J.M., McAda, D.P., and Thorn, C.R., 1995, Simulation of ground-water flow in the Albuquerque Basin, central New Mexico, 1901–1994, with projections to 2020: U.S Geological Survey Water-Resources Investigations Report 94–4251, 114 p.

Koning, D.J., Connell, S.D., Pazzaglia, F.J., and McIntosh, W.C., 2002, Redefinition of the Ancha Formation and Plio-Pleistocene deposition in the Santa Fe embayment, north-central New Mexico: New Mexico Geology, v. 24, p. 75–87.

Kuhle, A.J., and Smith, G.A., 2001, Alluvial-slope deposition of the Skull Ridge Member of the Tesuque Formation, Española Basin, New Mexico: New Mexico Geology, v. 23, p. 30–37.

Lanphere, M.A., Champion, D.E., Christiansen, R.L., Izett, G.A., and Obradovich, J.D., 2002, Revised ages for tuffs of the Yellowstone Plateau volcanic field—Assignment of the Huckleberry Ridge Tuff to a new geomagnetic polarity event: Geological Society of America Bulletin, v. 114, p. 559–568.

Lozinsky, R.P., Hawley, J.W., and Love, D.W., 1991, Geologic overview and Pliocene-Quaternary history of the Albuquerque Basin, central New Mexico: New Mexico Bureau of Mines and Mineral Resources Bulletin 137, p. 157–162.

Machette, M.N., 1978, Geologic map of the San Acacia quadrangle, Socorro County, New Mexico: U.S. Geological Survey Map GQ–1415, scale 1:24,000.

Manley, K., 1979, Stratigraphy and structure of the Española Basin, Rio Grande rift, New Mexico, *in* Riecker, R.E., ed., Rio Grande rift—Tectonics and magmatism: Washington, D.C., American Geophysical Union, p. 71–86.

Purtymun, W.D., 1995, Geologic and hydrologic records of observation wells, test holes, test wells, supply wells, springs and surface water in the Los Alamos area: Los Alamos National Laboratory Report LA–12883–MS, 339 p.

Reneau, S.L., and Dethier, D.P., 1996, Pliocene and Quaternary history of the Rio Grande, White Rock Canyon and vicinity, New Mexico: New Mexico Geological Society 47th field conference, Jemez Mountains Region, Guidebook, p. 317–324.

Reneau, S.L., Gardner, J.N., and Forman, S.L., 1996, New evidence for the age of the youngest eruptions in the Valles caldera, New Mexico: Geology, v. 24, p. 7–10.

Rogers, J.B., and Smartt, R.A., 1996, Climatic influences on Quaternary alluvial stratigraphy and terrace formation in the Jemez River valley, New Mexico: New Mexico Geological Society 47th field conference, Jemez Mountains Region, Guidebook, p. 347–356.

Sarna-Wojcicki, A.M., Morrison, S.D., Meyer, C.E., and Hillhouse, J.W., 1987, Correlation of upper Cenozoic tephra layers between sediments of the western United States and comparison with biostratigraphic age data: Geological Society of America Bulletin, v. 98, p. 207–223.

Sawyer, D.A., Shroba, R.R., Minor, S.A., and Thompson, R.A., 2002, Geologic map of the Tetilla Peak quadrangle, Santa Fe and Sandoval Counties, New Mexico: U.S. Geological Survey Miscellaneous Field Studies Map MF–2352, scale 1:24,000.

Self, Stephen, Heiken, Grant, Sykes, M.L., Wohletz, Kenneth, Fisher, R.V., and Dethier, D.P., 1996, Field excursions to the Jemez Mountains, New Mexico: New Mexico Bureau of Mines and Mineral Resources Bulletin 134, 72 p.

Smith, G.A., 2004, Middle to Late Cenozoic development of the Rio Grande rift and adjacent regions in northern New Mexico, *in* Mack, G. H., and Giles, K.A., eds., The geology of New Mexico—A geologic history: New Mexico Geological Society Special Publication 11, p. 331–358.

Smith, G.A., and Kuhle, A.J., 1998a, Geologic map of the Santo Domingo Pueblo quadrangle, Sandoval County, New Mexico: New Mexico Bureau of Mines and Mineral Resources, Open-file Digital Map OF–DM 26, scale 1:24,000.

Smith, G.A., and Kuhle, A.J., 1998b, Geologic map of the Santo Domingo Pueblo SW quadrangle, Sandoval County, New Mexico: New Mexico Bureau of Mines and Mineral Resources Open-file Digital Map OF–DM 26, 1 sheet and text, scale 1:24,000.

Smith, G.A., and Kuhle, A.J., 1998c, Hydrostratigraphic implications of new geologic mapping in the Santo Domingo Basin, New Mexico: New Mexico Geology, v. 20, p. 21–27.

Smith, G.A., and Lavine, Alex, 1996, What is the Cochiti Formation?: New Mexico Geological Society 47th field conference, Jemez Mountains Region, Guidebook, p. 219–224.

Smith, G.A., McIntosh, William, and Kuhle, A.J., 2001, Sedimentologic and geomorphic evidence for seesaw subsidence of the Santo Domingo accommodation-zone basin, Rio Grande rift, New Mexico: Geological Society of America Bulletin, v.113, p. 561–574.

Spiegel, Zane, and Baldwin, Brewster, 1963, Geology and water resources of the Santa Fe area, New Mexico: U.S. Geological Survey Water-Supply Paper 1525, 258 p.

Stearns, C.E., 1953, Tertiary geology of the Galisteo-Tonque area, New Mexico: Geological Society of America Bulletin, v. 64, p. 459–508.

Tedford, R.H., 1981, Mammalian biochronology of the late Cenozoic basins of New Mexico: Geological Society of America Bulletin, pt. 1, v. 92, p. 1008–1022.

Tedford, R.H., and Barghoorn, E.S., 1997, Miocene mammals of the Espanola and Albuquerque Basins, north-central New Mexico, *in* Lucas, S.G., Estep, J.W., Williamson, T.E., and Morgan, S., eds., New Mexico's fossil record 1: New Mexico Museum of Natural History and Science Bulletin 11, p. 77–95.

Tedford, R.H., and Barghoorn, E.S., 1999, Santa Fe Group (Neogene), Ceja del Rio Puerco, northwestern Albuquerque Basin, Sandoval County, New Mexico: New Mexico Geological Society 50th field conference, Albuquerque Geology, Guidebook, p. 327–335.

Williams, P.L., and Cole, J.C., 2005, Preliminary geologic map of the Albuquerque 30′ × 60′ quadrangle, north-central New Mexico: U.S. Geological Survey Open-File Report 2005–1418, 64 p., scale 1:100,000.

WoldeGabriel, Giday, Warren, R.G., Broxton, D.E., Vaniman, D.T., Heizler, M.T., Kluk, E.C., and Peters, L., 2001, Episodic volcanism, petrology, and lithostratigraphy of the Pajarito Plateau and adjacent areas of the Española Basin and the Jemez Mountains, *in* Crumpler, L.S., and Lucas, S.G., eds., Volcanology in New Mexico: New Mexico Museum of Natural History and Science Bulletin 18, p. 97–129.

Published in the Central Region, Denver, Colo.
Manuscript approved for publication February 10, 2006
Graphics by authors
Photocomposition by Mari L. Kauffmann (Contractor, ATA Services)
Edited by Mary-Margaret Coates (Contractor, ATA Services)

Cenozoic Volcanism of the La Bajada Constriction Area, New Mexico

By Ren A. Thompson, David A. Sawyer, Mark R. Hudson, V.J.S. Grauch, and W.C. McIntosh

Chapter C of

The Cerrillos Uplift, the La Bajada Constriction, and Hydrogeologic Framework of the Santo Domingo Basin, Rio Grande Rift, New Mexico

Edited by Scott A. Minor

Professional Paper 1720–C

U.S. Department of the Interior
U.S. Geological Survey

Contents

Abstract 43
Introduction 43
Overview of Regional Geology 44
    Geologic Structure and Volcanism 44
    Stratigraphic Framework 44
Pre-Rift Tertiary Volcanism 49
Jemez Volcanic Field 49
Santa Ana Mesa Volcanic Field 50
Cerros Del Rio Volcanic Field 50
    Aerial Distribution, Geochronology, and Geochemistry 52
    Magnetic Polarities 54
    Structural Controls on Eruption 57
Summary 58
References Cited 58

Figures

C1. Map showing location and general geology of the Jemez Mountains and adjacent basins of the Rio Grande rift 45
C2. Geologic map of the Cochiti Pueblo (La Bajada constriction) area 46
C3. Stratigraphic column showing generalized stratigraphic relations for the La Bajada constriction region 48
C4. Diagram of total alkali versus silica for select Cerros del Rio volcanic rock samples 51
C5. Diagram of $^{40}Ar/^{39}Ar$ ages of volcanic rocks of Cerros del Rio volcanic field relative to magnetic geochron for 2.96–1.00 Ma 53
C6. Equal-area stereo diagram showing paleomagnetic site mean directions for selected samples from the Cerros del Rio volcanic field 54
C7. Diagram showing interpreted correlations of volcanic units 56

Tables

C1. New $^{40}Ar/^{39}Ar$ age determinations from Cerros del Rio volcanic field 52
C2. Paleomagnetic data from Cerros del Rio volcanic field 55

Cenozoic Volcanism of the La Bajada Constriction Area, New Mexico

By Ren A. Thompson, David A. Sawyer, Mark R. Hudson, V.J.S. Grauch, and W.C. McIntosh

Abstract

Late Tertiary to Quaternary volcanic rocks of the La Bajada constriction region, situated along the Rio Grande rift in northern New Mexico, consist of pre-rift and rift-related volcanic rocks of four discrete volcanic fields. These volcanic rocks include (1) a deeply dissected and incomplete section of pre-rift mafic- to intermediate-composition volcanic and volcaniclastic deposits exposed in the Cieneguilla area southeast of the La Bajada constriction; (2) intermediate- to silicic-composition pre-caldera and caldera-related rocks of the Jemez volcanic field west of the constriction; (3) basaltic volcanic rocks of the Santa Ana Mesa volcanic field in the center of the Santo Domingo basin; and (4) basaltic to intermediate-composition volcanic rocks of the Cerros del Rio volcanic field that overlap the eastern part of the constriction. All four of these volcanic fields are described in this chapter; and a primary focus is on the Cerros del Rio volcanic field because it bears most profoundly on the hydrogeologic framework and tectonic evolution of the La Bajada constriction.

The Plio-Pleistocene Cerros del Rio field is one of the largest (>700 km2) basaltic volcanic fields in the Rio Grande rift and preserves a record of the late-stage, volcano-tectonic evolution of the northeastern Santo Domingo and southwestern Española rift basins. Integrated geologic map, paleomagnetic, and aeromagnetic data were used to establish aerial distributions and stratigraphic relations of major eruptive units within the field. $^{40}Ar/^{39}Ar$ age determinations were used to establish timing of major eruptive episodes and, in conjunction with stratigraphic data, to provide temporal constraints on displacement of exposed or inferred faults within the volcanic field. Mostly flat-lying lava flows and pyroclastic deposits of the Cerro del Rio field erupted from multiple basaltic to dacitic volcanoes in three main phases. First-phase eruptions formed large volcanoes with constructive topography, such as Montoso Peak and Cerro Colorado, between 2.8 and 2.6 Ma during the normal-polarity Gauss magnetic chron and are associated with positive aeromagnetic anomalies. Second-phase eruptions issued from numerous smaller-volume vents; erupted lava flows commonly filled topographic lows between the older, larger volcanoes. These lavas were erupted between 2.5 and 2.2 Ma during the reversed-polarity Matuyama magnetic chron and, where sufficiently thick, are associated with negative aeromagnetic anomalies. A final 1.5- to 1.1-Ma eruptive phase is represented by the 1.46-Ma basaltic andesite of Cochiti Cone and smaller volume, younger volcanic centers in the western third of the Cerro del Rio field.

A series of northerly striking faults traversing the western part of the Cerro del Rio volcanic field down-dropped lava flows of the first- and second-phase eruptions into the actively subsiding northeastern margin of the Santo Domingo basin. Ancient down-to-west scarps along the Cochiti Cone fault and the La Bajada fault zone are locally mantled by volcanic deposits from Cochiti Cone, and similar buried faults likely controlled the emplacement of Cochiti Cone feeder dikes and edifice conduits. Older faults inferred from topographic lineaments are subparallel to these young faults and cut some second-stage volcanic centers. Younger second-stage centers form isolated and aligned zones of volcanic vents on strike with these inferred faults. Feeder dikes for these localized eruptive centers may have been emplaced along northerly striking fault zones within underlying basin-fill sediments of the Santa Fe Group.

Introduction

Studies by the U.S. Geological Survey were begun in 1996 to improve understanding of the geologic framework of the Albuquerque composite basin and adjoining areas, in order that more accurate hydrogeologic parameters could be applied to new hydrologic models. The ultimate goal of this multidisciplinary effort has been to better quantify estimates of future water supplies for northern New Mexico's growing urban centers, which largely subsist on aquifers in the Rio Grande rift basin (Bartolino and Cole, 2002). From preexisting hydrologic models it became evident that hydrogeologic uncertainties were large in the Santo Domingo Basin area, immediately up gradient from the greater Albuquerque metropolitan area, and particularly in the northeast part of the basin referred to as the La Bajada constriction (see chapter A, this volume, for a geologic definition of this feature as used in this report). Accordingly, a priority for new geologic and geophysical investigations was to better determine the hydrogeologic framework of the La Bajada constriction area. This chapter along with the other chapters of this report present the results of such investigations as recently conducted by the U.S. Geological Survey.

Overview of Regional Geology

Geologic Structure and Volcanism

The Rio Grande rift resulted from middle Cenozoic crustal extension in the southern Rocky Mountains. It is characterized by continental-scale rifting, subsidence of discrete basins, and uplift of rift margins. The continental extension was accompanied by lithospheric attenuation, asthenospheric upwelling, and intrarift magmatism. The ensuing volcanism spanned the range of terrestrial magma types and eruption modes, was largely episodic, and commonly reflected emplacement controlled by local structures superimposed on major crustal discontinuities.

In northern New Mexico, the Rio Grande rift is predominantly expressed by a series of north-trending, right-stepping en echelon grabens and half grabens that are structurally linked by northeast-trending accommodation zones. The most notable accommodation zone in the Jemez Mountains region is the Embudo fault zone (EB, fig. C1) that separates the east-dipping half-graben of the San Luis Basin from the west-dipping Española Basin. This accommodation zone coincides with the northeast-trending Jemez lineament (Mayo, 1958), a presumed Precambrian crustal shear zone or suture zone. Cenozoic volcanism marks the trend of the Jemez lineament (Luedke and Smith, 1978), the loci of which may reflect conduits for mantle-derived magmas that dominate post-Miocene volcanism (Baldridge, 1979a, Baldridge and others, 1984). Volcanism of the Jemez region is juxtaposed on the intersection of the Jemez lineament with the Rio Grande rift and is manifest in the long-lived, compositionally diverse Jemez field, which culminated in the spectacular caldera-forming eruption of the Bandelier Tuff rhyolites and shorter lived basaltic centers of the Cerros del Rio and Santa Ana Mesa volcanic fields (fig. C1). Eruption of synextensional mafic lavas is characteristic of magmatism in the Rio Grande rift (Lipman and Mehnert, 1979; Baldridge and others, 1980; Dungan and others, 1989; McMillan, 1998). The smaller mafic fields' proximity to the large-volume silicic field of the Jemez Mountains suggests that the lavas of the Cerros de Rio and Santa Ana Mesa volcanic fields reflect the large volumes of mafic magmas required to sustain the long-lived intermediate to silicic volcanism of the Jemez Mountains. However, it is likely that basaltic rift volcanism of the Cerros del Rio and Santa Ana Mesa fields is using structural weaknesses associated with late Pliocene extension as conduits for eruption of mafic magmas on the margins of the Jemez magmatic system.

A goal of this chapter is to better document the relation between volcanism and extensional faulting in the La Bajada constriction area. Many older structures that form the western boundary of the rift in the Jemez Mountains are largely buried beneath the latest plateau-forming outflow sheets of the Bandelier Tuff that erupted out of the Valles caldera. Likewise, pre-Pleistocene faults east of the Rio Grande are obscured by overlying upper Pliocene basaltic lavas of the Cerros del Rio volcanic field. The relation between major eruptive periods in the La Bajada constriction region and active extensional faulting is based in large part on new detailed geologic mapping and associated geochronologic studies (Smith and Kuhle, 1998a,b; Sawyer and others, 2002; R. Thompson, R. Shroba, and D. Dethier, unpub. data, 2005), fault studies (Minor and Hudson, 2006) (chapter E, this volume), and regional geophysical investigations (chapters D and F, this volume). The results of these efforts bear directly on interpretations of the subsurface configuration of the northeast part of the Santo Domingo Basin, the La Bajada constriction, the Cerrillos uplift, and the southern Española Basin. Consequently, a summary of the volcanic stratigraphy of the La Bajada constriction region (fig. C1), presented in this chapter, forms a basis for geochronologic constraints on the timing of late Cenozoic extension and faulting in the southwestern Española and northern Santo Domingo rift basins.

Figure C1 (following page). Location and general geology of the Jemez Mountains and adjacent basins of the Rio Grande rift. Double-headed arrows indicate approximate trend of the Jemez lineament. CDRVF, Cerros del Rio volcanic field; LBC, La Bajada constriction; SAMVF, Santa Ana Mesa volcanic field; TPVF, Taos Plateau volcanic field. Faults and fault zones: EB, Embudo; JZ, Jemez; LB, La Bajada; PJ, Pajarito. Rectangle shows location of figure C2, and inset map shows location of detailed map along Rio Grande rift in New Mexico.

Stratigraphic Framework

The stratigraphic framework of Cenozoic volcanic deposits in the La Bajada constriction region is complex, because it includes pre-rift and rift-related rocks from no fewer than four discrete volcanic fields. In the following section we describe (1) the pre-rift volcanic sequence and related sedimentary rocks in the southeastern part of the study area, (2) the regional stratigraphic relations of volcanic rocks of the Jemez and Santa Ana Mesa volcanic fields, and (3) rocks of the Cerros del Rio volcanic field. The Cerros del Rio field is the primary focus of this discussion owing to the juxtaposition of volcanic deposits of this field with major pre-rift and rift-related structures defining the La Bajada constriction and because of the temporal constraints on faulting provided by geochronologic and stratigraphic age control of major eruptive events of the Cerros del Rio.

The distribution of Cenozoic volcanic rocks and associated volcaniclastic sediments in the La Bajada constriction region is depicted in plate 2 and figure C2. Generalized volcanic stratigraphic sections, modified from plate 2, are presented in figure C3. Stratigraphic units are described based on historical or established nomenclature where feasible.

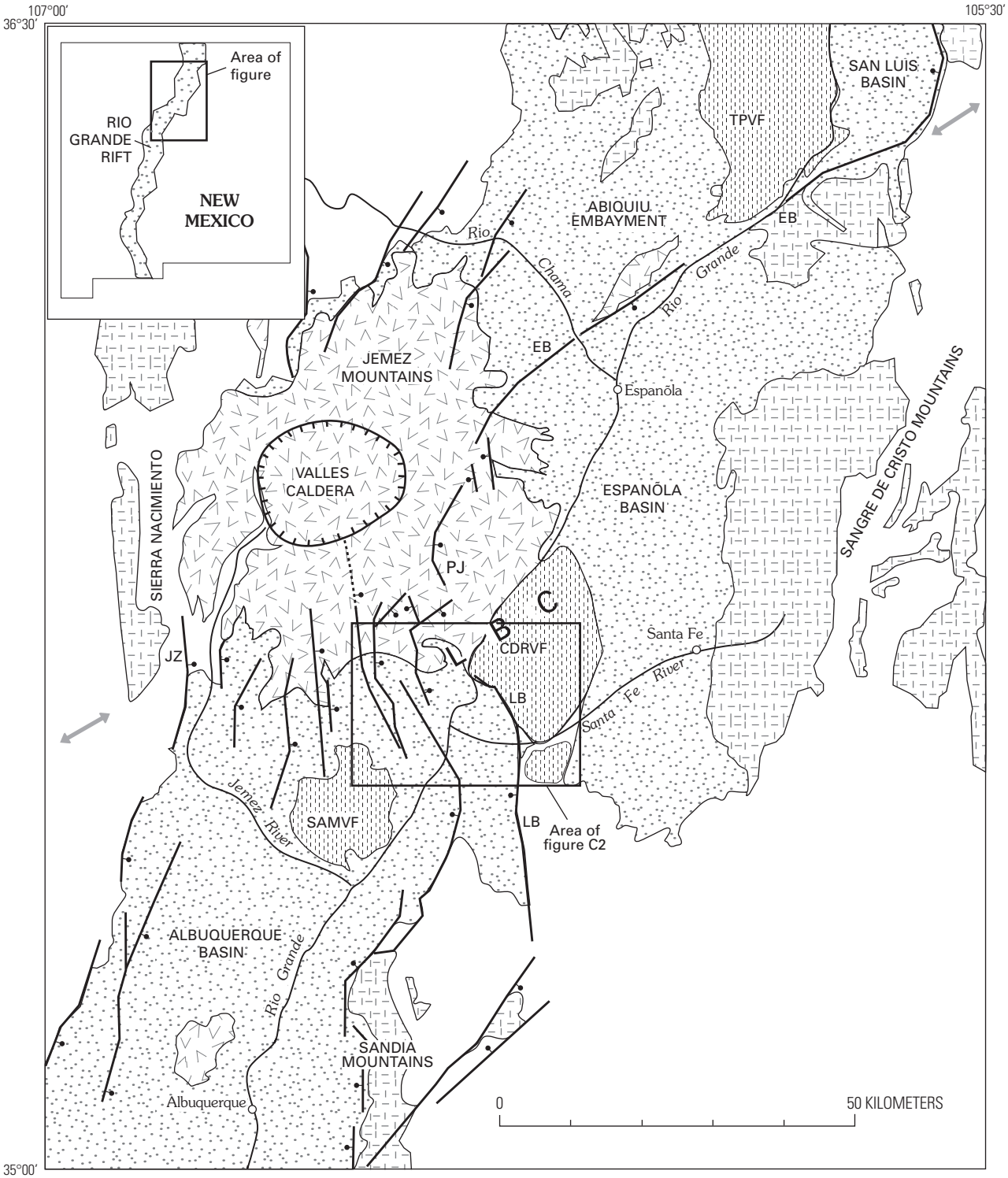

EXPLANATION

- **Pleistocene–Pliocene basaltic volcanic fields**
- **Pleistocene–Miocene volcanic rocks**
- **Pleistocene–Oligocene basin-fill sediment**
- **Lower Oligocene–Paleozoic rocks**
- **Precambrian rocks**
- **Major fault**—Bar and ball on downthrown block; dotted where concealed
- **Boundary of caldera**
- **Trend of Jemez lineament**

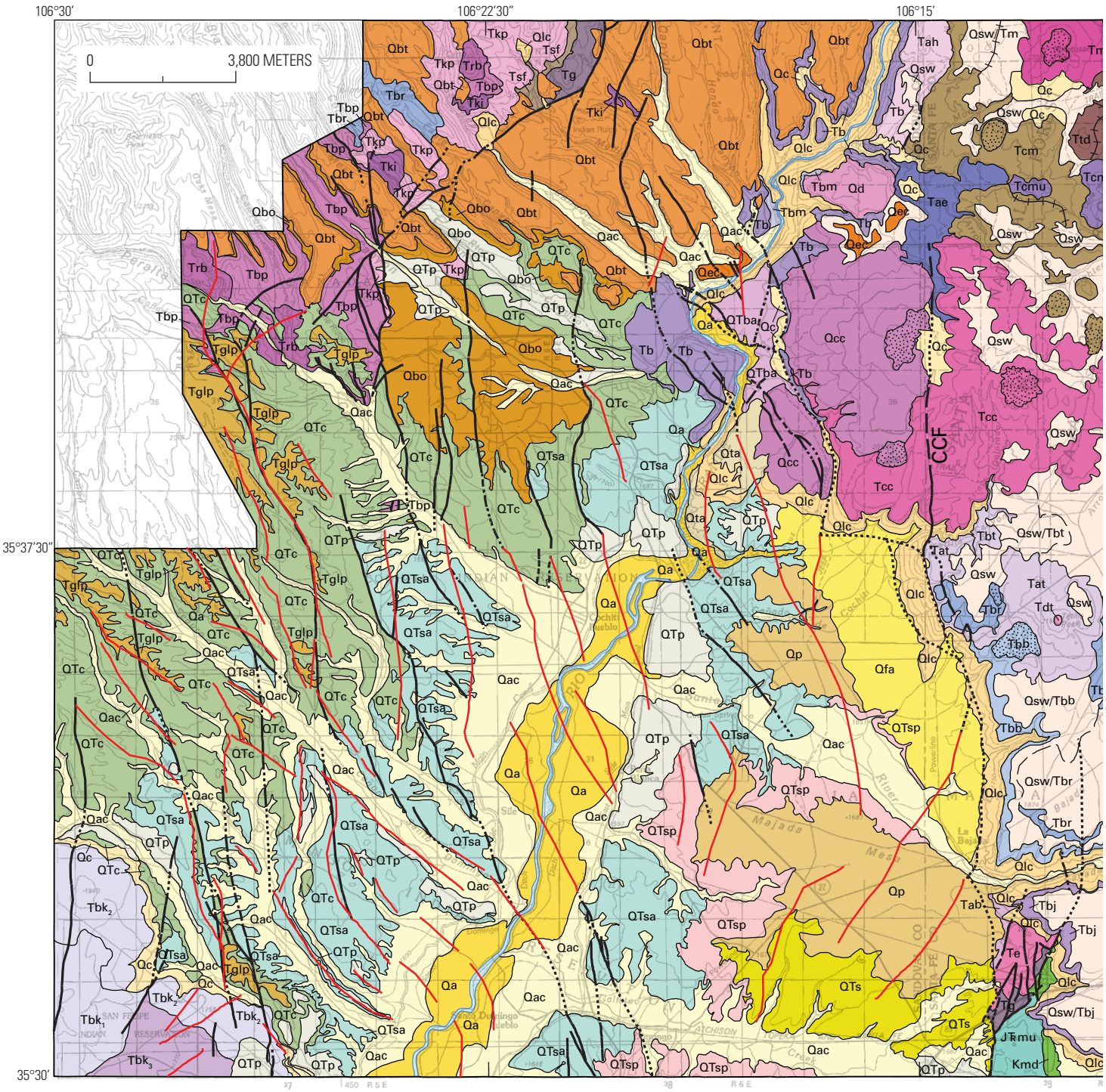

LIST OF MAP UNITS IN LA BAJADA CONSTRICTION REGION

[Units not listed in stratigraphic order within each geologic period]

QUATERNARY

Qc	Colluvium, undivided
Qa	Flood-plain and stream-channel deposits
Qac	Alluvium and colluvium, undivided
Qfa	Fan alluvium
Qlc	Landslide and colluvial deposits, undivided
Qp	Young pediment deposits
Qsw	Sheetwash deposits—Underlying Tertiary basalt unit indicated where mapped
Qsw/Tbb	Sheetwash deposits over basalt of La Bajada
Qsw/Tbj	Sheetwash deposits over basalt of Mesita de Juana Lopez
Qsw/Tbr	Sheetwash deposits over basalt of Caja del Rio
Qsw/Tbs	Sheetwash deposits over basalt of Tsinat Mesa
Qsw/Tbt	Sheetwash deposits over basalt of Tetilla Hole
Qsw/Tm	Sheetwash deposits over basaltic andesite of Cerro Montoso
Qta	Terrace and alluvial deposits
Qec	El Cajete tephra

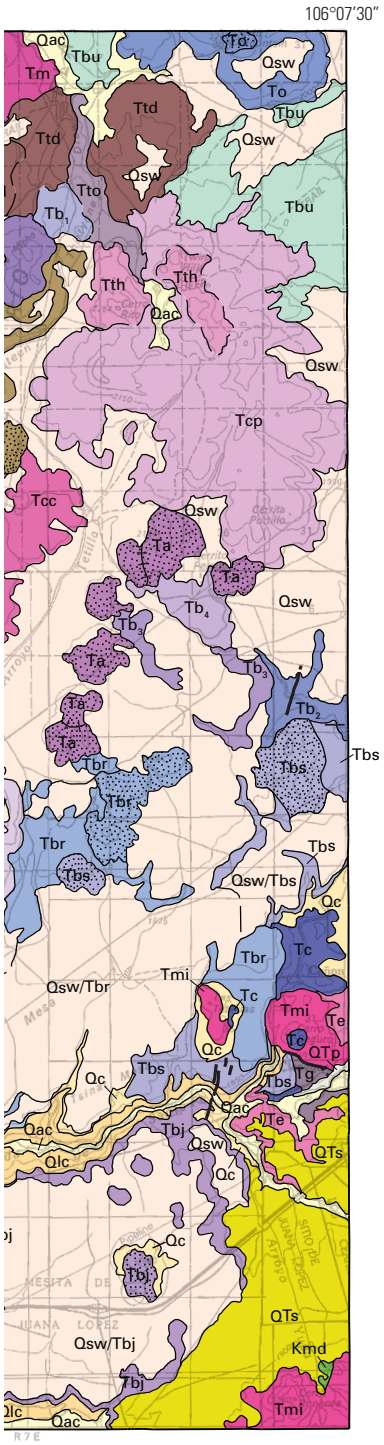

	Bandelier Tuff
Qbt	**Tshirege Member**
Qbo	**Otowi Member**
Qcc	**Basaltic andesite of Cochiti Cone**
Qd	**Dacite of White Rock Canyon**
QTba	**Basalt of Cochiti**
QTp	**Old pediment deposits**
QTs	**Upper part of Santa Fe Group, undivided**
	Sierra Ladrones
QTsa	**Axial river facies**
QTsp	**Eastern piedmont facies**
QTc	**Cochiti Formation**
	TERTIARY
Tglp	**Gravel of Lookout Park**
To	**Andesite of Ortiz Mountain**
Ttd	**Basaltic andesite of Tank 31**
Tth	**Andesite of Twin Hills**
Tto	**Basalt of Thirty One Draw**
Tae	**Andesite of Arroyo Eighteen**
Tah	**Andesite of Hill 6385**
	Flows of Bajada Mesa
Tb_4	**Upper basalt**
Tb_3	**Lower basalt**
Tb_2	**Basaltic andesite of Petroglyph Canyon**
Tb_1	**Basalt of Hill 7071**
	Basalt of Santa Ana Mesa
Tbk_3	**Upper basalt**
Tbk_2	**Middle basalt**
Tbk_1	**Lower basalt**
Ta	**Late andesite of Caja del Rio**
Tbr	**Basalt of Caja del Rio**
Tbt	**Basalt of Tetilla Hole**

Tbu	**Basalt of Canada Ancha**
Tm	**Basaltic andesite of Cerro Montoso**
Tcc	**Andesite of Cerro Colorado**
Tcmu	**Late andesite of Cerro Micho**
Tcm	**Basaltic andesite of Cerro Micho**
Tcp	**Andesite of Cerro Portrillo**
Tb	**Basalt of White Rock Canyon**
Tat	**Andesite of Tetilla Peak**
Tdt	**Dacite of Tetilla Peak**
Tbj	**Basalt of Mesita de Juana Lopez**
Tbb	**Basalt of La Bajada**
Tbs	**Basalt of Tsinat Mesa**
Tbm	**Hydromagnetic deposits of White Rock Canyon**
Trb	**Bearhead Rhyolite**
Tbp	**Peralta Tuff Member of Bearhead Rhyolite**
Tki	**Intrusive dacite of Paliza Canyon Formation**
Tkp	**Paliza Canyon Formation, undivided**
Tsf	**Middle part of Santa Fe Group, undivided**
Tab	**Abiquiu(?) Formation**
Tc	**Cieneguilla Basanite**
Te	**Espinaso Formation**
Tmi	**Monzonite and monzonite porphyry**
Tg	**Galisteo Formation**
	CRETACEOUS
Kmd	**Mancos Shale and Dakota Sandstone, undivided**
	JURASSIC
JTRmu	**Morrison, Wanakah, Entrada, Todilto, and Chinle Formations, undivided**

Cinder deposits—Formed during same eruptive event as underlying flow

Contact—Dashed where approximately located

Magnetic boundary—Abrupt difference in rock-magnetic properties inferred from aeromagnetic data

Fault inferred from aeromagnetic data

Fault—Offset unknown. Dashed where approximately located; dotted where concealed. CCF, Cochiti Cone fault

Figure C2 (above and facing page). Geology of the La Bajada constriction area (scale 1:125,000) emphasizing volcanic deposits; modified from geologic map shown on plate 2. Geologic map data from Spiegel and Baldwin (1963); Smith, Bailey, and Ross (1970); Bachman (1975); Kelly and Kudo (1978); Goff, Gardner, and Valentine (1990); Dethier (1997); Smith and Kuhle (1998a,b); Sawyer and others (2002); and mapping by R.A. Thompson (unpub. data, 2005), R.R. Shroba (unpub. data, 2005), and D.P. Dethier (unpub. data, 2005).

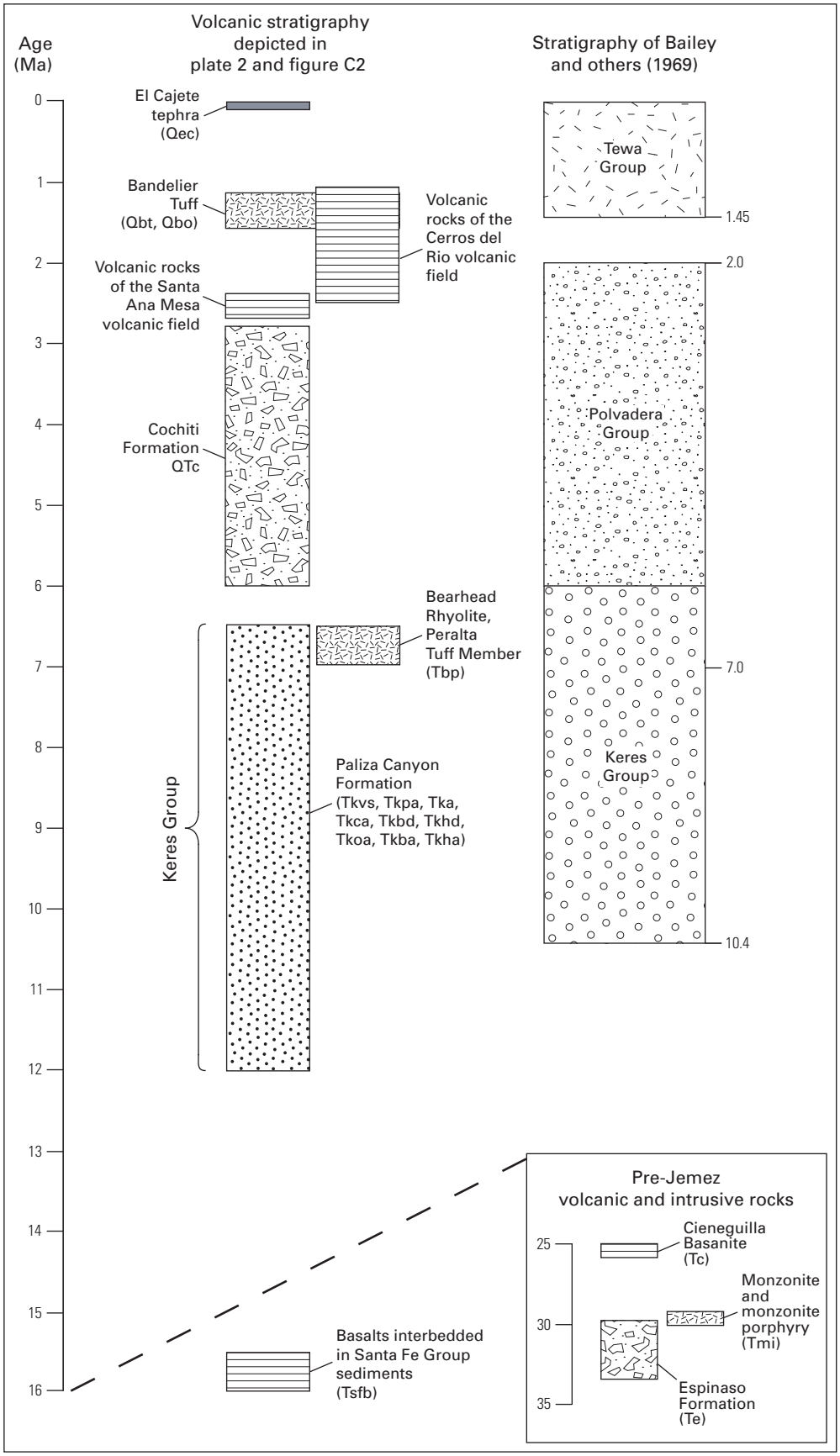

Figure C3. Generalized stratigraphic relations for the La Bajada constriction region. Published data sources include Bailey, Smith, and Ross (1969); Gardner and others (1986); Lavine, Smith, and Goff (1996); WoldeGabriel and others (1996); G.A. Smith (personal commun., 2002); and mapping by R.A. Thompson (unpub. data, 2005), R.R. Shroba (unpub. data, 2005), and D.P. Dethier (unpub. data, 2005).

Pre-Rift Tertiary Volcanism

Exposures of pre-rift middle Tertiary intrusions, volcanic rocks, and volcaniclastic sedimentary deposits are confined to the southeastern part of the map area (pl. 2, fig. C2). They form the bedrock under a broad, irregular paleoerosion surface upon which Pliocene rocks of the Cerros del Rio volcanic field and basin-fill sediments of the Santa Fe Group were deposited. The Espinaso Formation (unit Te, pl. 2, fig. C2), northern Cerrillos Hills intrusions (unit Tmi), and Cieneguilla volcanic complex (unit Tc, Cieneguilla Basanite) are confined to the footwall block of the La Bajada fault zone. Existing radiometric ages for these rocks are poorly constrained and range from late Eocere to early Miocene. These ages suggest that the volcanism likely was associated with the transition from post-Laramide arc volcanism (related to subduction) to early extensional volcanism (related to rifting) as recognized elsewhere in uplifted rift margins in northern New Mexico and southern Colorado (Thompson, Dungan, and Lipman, 1986; Lipman, 1988; Thompson, Johnson, and Mehnert, 1991, Miggins and others, 2002)

The Espinaso Formation is composed of andesite lava flows and volcaniclastic breccias that are unconformably overlain by two separate dacite flow sequences with interbedded volcaniclastic sedimentary rocks. Sun and Baldwin (1958) reported K-Ar age determinations of 19.5±0.5 and 19.6±0.6 Ma on biotite and feldspar, respectively, collected from the upper dacite lava flow. These ages might not be primary because they are younger than ages reported for the overlying Cieneguilla lava flows and because the upper dacite is similar in composition and mineralogy to the youngest of the Cerrillos Hills intrusions (36–31 Ma) to the southeast (Sawyer and others, 2002).

Eocene and Oligocene intrusive rocks of the Cerrillos Hills in the Cochiti Pueblo map area (unit Tmi, pl. 2, fig. C2) consist of fine-grained, subvolcanic stocks and dikes of monzonite and monzonite porphyry. These rocks are exposed at Cerro Bonanza, Cerro Seguro, Las Tetillitas, and within Cañada de Santa Fe (pls. 1, 2). The augite monzonite porphyry of Cerro Seguro is compositionally similar to the stratigraphically highest dacites of the Espinaso Formation. Baldridge and others (1980) reported a K-Ar biotite age of 30.2±0.7 Ma and, more recently, Sauer (1999) obtained a 29.40±0.05-Ma $^{40}Ar/^{39}Ar$ plateau age on biotite for the monzonite of Cerro Seguro. This intrusion domed flanking deposits of the Galisteo Formation (unit Tg) and the lower part of the Espinaso Formation (unit Te) near Cañada de Santa Fe; thus, these deformed deposits must be considerably older than previously reported by Sun and Baldwin (1958). Disbrow and Stoll (1957) tentatively correlated the Cerro Seguro intrusions with late stage Cerrillos Hills intrusive activity.

Rocks of the Cieneguilla volcanic complex (Cieneguila Basanite), which conformably overlie the Espinaso Formation, consist of basanite and nephelenite lava flows and interbedded volcaniclastic and epiclastic sediments (Sterns, 1953; Sun and Baldwin, 1958; Baldridge, 1979b; Baldridge and others, 1980). These deposits overlie the Espinaso Formation in Cañada de Santa Fe and south of the Mesita de Juana Lopez vent (fig. C2). The sequence is as thick as 200 m and contains four discrete packages of lava flows, each containing as many as five discontinuous lava flows, basaltic tephra, and interbedded volcaniclastic sediments. Baldridge and others (1980) reported a whole-rock K-Ar age of 25.1±0.7 Ma on a lava-flow sequence that assumes the same regional northeasterly dip as the underlying Espinaso Formation. North- to northeast-trending dikes of similar composition cut older rocks in the footwall of the La Bajada fault south of Cañada de Santa Fe (Sawyer and others, 2002).

Jemez Volcanic Field

The Jemez Mountains host a spectacular example of a long-lived, large-volume, compositionally varied volcanic field that culminated in caldera-forming eruptions of silicic ignimbrites; this field has been the subject of studies on the nature of caldera-forming process and the emplacement mechanisms of rhyolite ash-flow tuffs (Smith and Bailey, 1966, 1968). Geologic and hydrologic framework investigations also established a regional stratigraphic nomenclature (Griggs, 1964; Bailey, Smith, and Ross, 1969; Smith, Bailey, and Ross, 1970). Subsequent investigations, supported by large-scale mapping and additional radiometric age determinations, have led to revisions of the original nomenclature, particularly as applied to precaldera and postcaldera eruptive units (Gardner and others, 1986; Lavine, Smith, and Goff, 1996; Reneau, Gardner, and Forman, 1996).

In the La Bajada constriction area, within the highlands of the Pajarito Plateau, precaldera deposits are largely concealed beneath the Otowi and Tshirege Members of the Pleistocene Bandelier Tuff, erupted during collapse of the Jemez caldera (pl. 2, fig. C2). Consequently, exposures of precursory basaltic to rhyolitic volcanic rocks are limited to the dissected footwall block of the Pajarito fault zone (that is, the Saint Peters Dome block, fig. A2) and southeastern slopes of the precaldera eruptive surface. With the exception of deposits associated with basaltic volcanism of the Cerros del Rio volcanic field, postcaldera volcanic deposits in the La Bajada constriction area are limited to reworked pumice and ash deposits of the approximately 50-ka El Cajete tephra (unit Qec, pl. 2, figs. C2, C3) (Reneau, Gardner, and Forman, 1996; Reneau, McDonald, and others, 1996; Wolf, Gardner, and Reneau, 1996). This pumice and ash blanket the northeastern slopes of eroded volcanic highlands east of the Rio Grande.

All precaldera volcanic and volcaniclasitic deposits of the Pajarito Plateau (pl. 1) belong to the Keres Group as defined by Bailey, Smith, and Ross (1969) and modified by Gardner and others (1986). The Keres Group rests unconformably on Santa Fe Group sediments (unit Tsf, pl.2) and locally on 16-Ma basaltic lava flows (unit Tsfb) related to rifting (Goff, Gardner, and Valentine, 1990). The Keres Group consists predominantly of andesite to dacite lavas, pyroclastic deposits,

volcanic breccias, and sedimentary deposits (Gardner and others, 1986; Lavine, Smith, and Goff, 1996). Age of the volcanic rocks ranges from approximately 12 Ma near the base of the Paliza Canyon Formation to approximately 6.5 Ma, the youngest age reported for the Bearhead Rhyolite; most volcanism occurred between 10 and 8 Ma (Gardner and others, 1986; McIntosh and Quade, 1995; Lavine, Smith, and Goff, 1996; Justet, 1999).

In the La Bajada constriction area near Saint Peters Dome (pl. 2, fig. A2), Keres Group rocks are dominated by andesite and dacite lava flows, domes, and minor intrusives (units Tkha, Tkba, Tkoa, Tkhd, Tkbd, Tkca, Tka, Tkpa; pl. 2); they extend westward underneath the Pajarito Plateau and crop out in the highlands of the San Miguel Mountains. Local olivine basalt lava flows and cinder deposits are found near the base and top of the section (Goff, Gardner, and Valentine, 1990). Collectively, these deposits compose the Paliza Canyon Formation.

The youngest eruptive products included in the Keres Group are the isolated high-level intrusions of Bearhead Rhyolite (unit Trb, pl. 2) (Smith, Bailey, and Ross, 1970; Goff, Gardner, and Valentine, 1990) and associated Peralta Tuff Member of the Bearhead Rhyolite (unit Tbp) (figs. C2, C3). The sparsely phyric Bearhead Rhyolite occurs as localized lava domes and as flows and their pyroclastic aprons, emplaced during two discrete, short-lived intervals between 7 Ma and 6.5 Ma (G. Smith, personal commun., 2002). The Peralta Tuff Member of the Bearhead Rhyolite comprises pyroclastic flow, fall, and surge deposits related to localized emplacement of lava domes. In the footwall block of the Pajarito fault zone (pl. 2), the Paliza Canyon Formation is locally intercalated with compositionally similar deposits of the Canovas Canyon Formation (units Tkct, Tkrc).

The Cochiti Formation (unit QTc, pl. 2) contains volcaniclastic detritus shed from the volcanic highlands of Keres Group volcanic centers (Smith, Bailey, and Ross, 1970; Goff, Gardner, and Valentine, 1990). Locally, it may instead contain temporally and spatially equivalent primary volcanic deposits. Lavine, Smith, and Goff (1996) proposed a more restrictive use of the term "Cochiti Formation" to include only those sedimentary deposits that postdate emplacement of the Bearhead Rhyolite lavas and pyroclastic deposits of the Peralta Tuff Member. As such, the Cochiti Formation as depicted in plate 2 and figure C2 represents a temporal equivalent to other upper Santa Fe deposits of the Santo Domingo and Española Basins. The Cochiti Formation is discussed in more detail in the context of basin-fill sedimentary deposits in chapter B (this volume).

Santa Ana Mesa Volcanic Field

Bryan (1938) and Kelly and Kudo (1978) used the term "San Felipe volcanic field" to refer to the basaltic lavas that capped Santa Ana Mesa north of the confluence of the Jemez River and the Rio Grande (pl. 1). Subsequently, Baldridge (1979a) and Personius (2002) referred to the same lavas as the Santa Ana Mesa volcanic field (SAMVF, figs. C1, A2). In the northeastern portion of this volcanic field lava flows and associated pyroclastic deposits form a succession of chemically and mineralogically similar olivine tholeiites (Baldridge, 1979a) erupted from low-relief shield volcanoes and small, late-stage cinder cones (units Tbk_1, Tbk_2, Tbk_3; pl. 2, fig. C2). Basal lava flows form a broad plateau erupted onto a low-relief erosional surface cut into sediments of the Santa Fe Group (unit QTsa) and Cochiti Formation (unit QTc). Hydromagmatic deposits and basaltic tuffs lie at the base of the volcanic succession and are similar in character to those observed in the Cerros del Rio volcanic field. K-Ar ages (Kelly and Kudo, 1978; Bachman and Mehnert, 1978) and $^{40}Ar/^{39}Ar$ ages (Smith and Kuhle, 1998a,b) on the lava flows range from 2.6 to 2.4 Ma. North-striking normal faults displace the Santa Ana Mesa flows (fig. E1) by as much as 100 m, and similar faults may have exerted synvolcanic structural control on magma conduits as evidenced by the predominant north-trending alignment of cinder cones delineating late-stage vent areas.

Cerros Del Rio Volcanic Field

The Cerros del Rio volcanic field (CDRVF; pl. 1, figs. C1, A2) is a predominantly basaltic to andesitic volcanic plateau in the La Bajada constriction area. This field is bounded on the southwest by the La Bajada fault zone (pl. 1, fig. A4), forms a topographic high, and is overlain by Española Basin fill deposits to the north and east; Pleistocene ash-flow tuffs of the Jemez volcanic field abut the northwest margin of this high (fig. C2). Pliocene to Quaternary volcanic rocks of the Cerros del Rio field overlie much of the La Bajada constriction, obscuring the stratigraphic and structural link between the Española and Santo Domingo Basins (fig. A2; chapter G, this volume). Lavas and related pyroclastic deposits of this field have a surface expression of 700 km^2 and reflect eruption of at least 120 km^3 of rift-related mafic magma. Most of the lava flows predate large-volume silicic eruptions of the Jemez volcanic field; however, late stage eruptions from the field postdate eruption of the Bandelier Tuff. Eruptive centers in this field are typically central-vent volcanoes ranging from low-relief shields to steep-sided, breached cinder cone remnants. Lavas range from 48 to 65 wt percent SiO_2 (fig. C4); their geomorphic expression strongly correlates with their whole-rock chemistry. Low-silica, subalkaline basaltic lavas are thin (<3–4 m), were erupted from broad shield volcanoes, and traveled long distances, whereas transitional to mildly alkaline basalts and basaltic andesites form thick (as much as 30 m thick), discontinuous lava flows and were erupted from high-relief, steep-sided, dissected vents. Dacitic lavas are related to late-stage dome growth and eruption of thick (as much as 50 m thick) blocky lava flows from one well-defined vent area at Tetilla Peak (TP, pl. 1) and also form lava flows exposed in tributary canyons of White Rock Canyon (pl. 1).

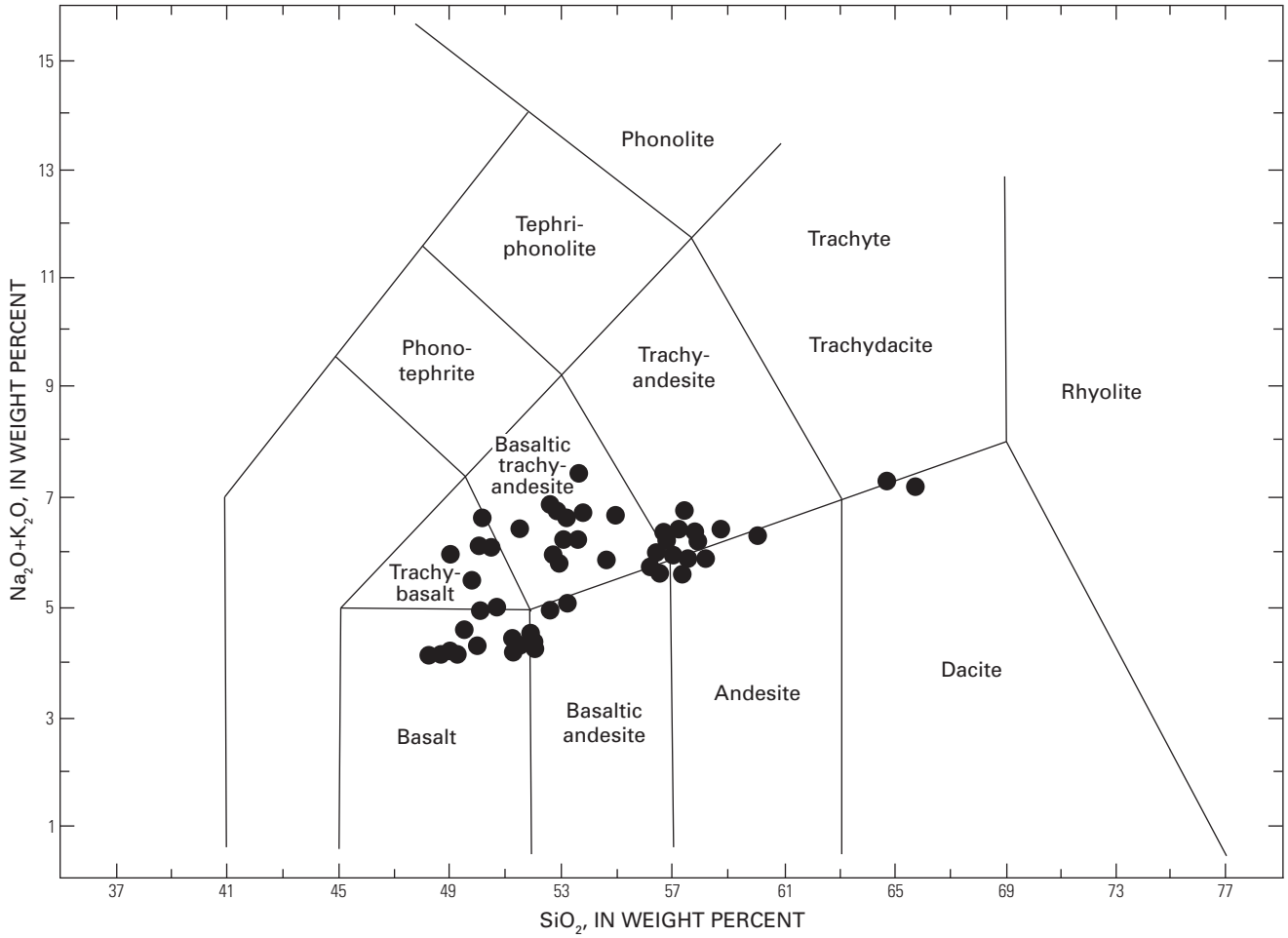

Figure C4. Total alkali versus silica for select Cerros del Rio volcanic rock samples. Diagram illustrates the range of chemical compositions represented by early-, middle-, and late-phase eruptions. Classification and fields based on Le Bas and others (1986).

Previous regional investigations identified the areal extent, stratigraphic position, broad compositional spectrum, and geochronologic constraints of the Cerros del Rio lavas (Spiegel and Baldwin, 1963; Smith and others, 1970; Aubele, 1978; Bachman and Mehnert, 1978; Aubele, 1979; Baldridge, 1979a). More recent stratigraphic and geochronologic control from Cerros del Rio volcanic field lavas exposed on the Pajarito Plateau (pl. 1) and in western White Rock Canyon are summarized in WoldeGabriel and others (1996, 2001), and petrologic constraints on the evolution of limited suites of Cerros del Rio lavas were presented in Zimmerman and Kudo (1979), Dunker and others (1991), and Wolfe, Heikoop, and Ellisor (2000).

The geologic map relations for the Cerros del Rio volcanic field presented in figure C2 and plate 2 are based on mapping investigations by Aubele (1978), Dethier (1997), and Sawyer and others (2002) and on maps by R.A. Thompson and D.P. Dethier (unpub. data, 2005). Volcanic deposits of the central, southern, and western Cerros del Rio were mapped at 1:24,000 scale and simplified for presentation at 1:125,000 scale (fig. C2). All of the volcanic unit names are informal, with the exception of the Otowi and Tshirege Members of the Bandelier Tuff. Volcanic units delineate monogenetic eruptive centers where possible; however, simplification from the original mapping dictates consolidation of map units on the basis of lithologic character, stratigraphic position, age, aeromagnetic and paleomagnetic signature, and aerial extent of similar or related deposits.

Thickness of the volcanic pile ranges considerably from a maximum exposed thickness of approximately 100 m in White Rock Canyon to a few meters along the eastern margin of the field. Along the eastern margin, lava flows and basaltic hydromagmatic deposits dip gently beneath basin-fill deposits of the Ancha Formation (Grauch and Bankey, 2003). Driller's records from the 1200-Foot well in the south central part of the Cerros del Rio volcanic field (pl. 2) indicate approximately 240 m of basaltic lava flows, pyroclastic deposits, and interbedded alluvium (fig. G2). Projected thicknesses for the entire volcanic field are represented in a set of serial cross sections on plate 6.

Aerial Distribution, Geochronology, and Geochemistry

Volcanic deposits of the Cerros del Rio volcanic field are divided into a threefold classification representing early, middle, and late phases of eruption spanning approximately 2.7–1.1 Ma (fig. C5, table C1). These subdivisions are based on 1:24,000-scale geologic mapping, stratigraphic studies, $^{40}Ar/^{39}Ar$ geochronology, and paleomagnetic and aeromagnetic data. Limited geochemical data were used to classify lithologic types within the stratigraphic subdivisions but were not used to infer stratigraphic position. Results of new $^{40}Ar/^{39}Ar$ age determinations are presented in figure C5 and table C1, and a total alkali versus silica geochemical classification diagram using the scheme of Le Bas and others (1986) is presented in figure C4.

Early-phase eruptions produced areally extensive, large-volume, plateau-forming lava flows ranging in age from 2.7 to 2.6 Ma (fig. C5). They form much of the La Bajada escarpment, prominent cliffs of northern White Rock Canyon, and the southeastern margin of the volcanic field (fig. C2). Vents associated with these lava flows characteristically are large composite cinder cones, such as the topographically prominent peaks at Mesita de Juana (unit Tbj), Cerro Montoso (unit Tm), Cerro Colorado (unit Tcc), and unnamed source areas for the basalt of La Bajada (unit Tbb) and basalt of Tsinat Mesa (unit Tbs) (pl. 2, fig. C2). These centers and their associated lava flows are predominantly basalt to basaltic andesite (fig. C4). Evolved dacite compositions for early-phase eruptions were limited to late emplacement of a small lava dome at Tetilla Peak (unit Tdt). This lava dome was emplaced after eruption of pyroxene-plagioclase-hornblende andesites from the same Tetilla Peak vent area (unit Tat).

Middle-phase volcanism was less extensive and was typified by smaller eruptive volumes than early-phase eruptions. However, the eruptive interval for middle-phase activity was at least twice as long as that observed for the early phase as implied by $^{40}Ar/^{39}Ar$ age determinations ranging from 2.5 to 2.2 Ma (fig. C5). Map units depicted in figure C2 illustrate complex stratigraphic relations resulting from three primary factors. First, individual eruptive centers yielded highly variable eruption volumes and not all map units have known vent areas. Second, fluvial erosional topography developed on the surface of early-phase flows before resulting canyons were filled by middle-phase lava flows, and inverted stratigraphy resulted. Third, the morphology of vents and flows is variable and reflects the compositional variation (from basaltic to andesitic) of lava erupted from middle-phase volcanoes. Andesite volcanoes form discrete, high-relief centers (units To, Tcp; fig. C2), whereas smaller volume basalt and basaltic-andesite centers are typified by smaller eruptive volumes, widespread distribution of basaltic to basaltic andesite lava flows, and multiple vent areas likely associated with fissure eruption (units Tcm, Tcmu, Ta, Tb_1, Tb_2, Tb_3, Tb_4, Ttd, Tto). In all cases, flow morphology of individual centers reflects the relative silica content and consequently the viscosity of eruptive products.

Figure C5 (facing page). $^{40}Ar/^{39}Ar$ ages and associated ±2σ analytical errors (vertical bars) of volcanic rocks of the Cerros del Rio volcanic field plotted relative to the magnetic geochron for the time period 2.96–1.00 Ma; inset shows age control and magnetic geochron for late-phase Quaternary volcanic rocks of the time period 1.48–1.00 Ma. Map unit symbols in parentheses defined in Explanation on figure C2. Polarity of unit interpreted from aeromagnetic data listed to right of unit symbol. Sample locations shown on plate 2 and listed in table C1. Map unit symbols: Qcc, basaltic andesite of Cochiti Cone; Qd, dacite of White Rock Canyon; QTba, basalt of Cochiti; Tb, basalt of White Rock Canyon; Tb_2, basaltic andesite of Petroglyph Canyon; Tb_3, lower flow unit of Bajada Mesa; Tbb, basalt of La Bajada; Tbj, basalt of Mesita de Juana Lopez; Tbs, basalt of Tsinat Mesa; Tbt, basalt of Tetilla Hole; Tcc, andesite of Cerro Colorado; Tm, basaltic andesite of Cerro Montoso; To, andesite of Ortiz Mountain.

Eruptive products from late-phase volcanoes are restricted to a narrow corridor west of the Cochiti Cone fault (CCF, fig. C2) and east of the Rio Grande in lower White Rock Canyon (pl. 1). Three primary eruptive centers (units Qcc, Qd, QTba; fig. C2) have been identified and range in age from approximately 1.5 to 1.1 Ma (fig. C5). In White Rock Canyon, all three volcanoes locally overlie erosional remnants of the Tshirege Member of the Bandelier Tuff, and the youngest eruptions from Cochiti Cone (unit Qcc) locally overlie the Otowi Member of the Bandelier Tuff. Lavas from the two oldest of these volcanoes (units QTba, Qd) overlie middle-phase basaltic andesites (unit Tb) in White Rock Canyon, and deposits from multiple vents of the Cochiti Cone volcano overlie both early-phase (unit Tcc) and middle-phase (unit Tb) lava flows in White Rock Canyon and along the La Bajada escarpment (fig. C2). Compositions of late-phase lavas are predominantly basaltic andesite, but evolved dacite compositions were erupted from the northernmost (unit Qd) of the three centers in White Rock Canyon.

Table C1. New $^{40}Ar/^{39}Ar$ age determinations from Cerros del Rio volcanic field.

[Map unit symbols as depicted in fig. C2]

Sample number	Map unit symbol	Latitude (°N)	Longitude (°W)	Age (Ma)	±2σ analytical error (Ma)
96DTP05	Tbr	35.56211	106.21927	2.35	0.06
96DTP12	Tbr	35.61245	106.17496	2.42	0.03
96DTP13	Tbj	35.52126	106.20072	2.66	0.08
96DTP19	Tbb	35.60031	106.23528	2.61	0.14
96DTP24	Tbr	35.60642	106.23145	2.44	0.06
96TCD01	Tbb	35.63425	106.25990	2.67	0.05
DN85113	Qd	35.71800	106.27100	1.31	0.08
DN9628b	QTba	35.63224	106.29850	1.46	0.06
96TCD08	Qcc	35.64658	106.27849	1.14	0.13
96TMP08	Tm	35.73605	106.21491	2.59	0.05
96TMP09	Tb_3	35.64588	106.16958	2.19	0.13
96TMP14	To	35.73797	106.14033	2.32	0.06
96TMP22	Tbt	35.63330	106.22938	2.49	0.05
96TMP38	Tcc	35.66350	106.21941	2.60	0.10
96TMP43	Tb_2	35.62990	106.13520	2.50	0.06

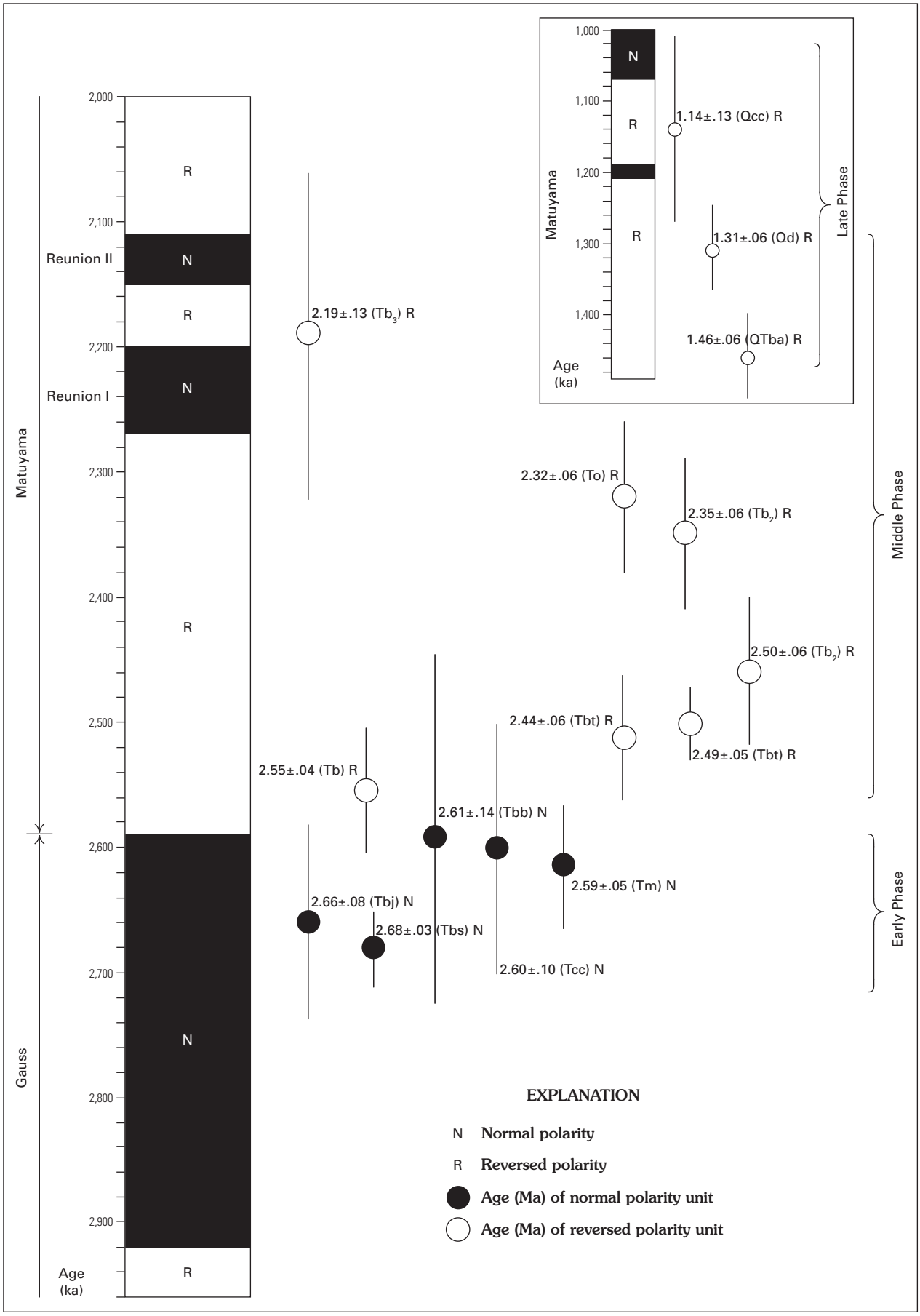
Matuyama
Gauss
Reunion II
Reunion I
Age (ka)
2,000
2,100
2,200
2,300
2,400
2,500
2,600
2,700
2,800
2,900
R
N
2.19±.13 (Tb3) R
2.32±.06 (To) R
2.35±.06 (Tb2) R
2.50±.06 (Tb2) R
2.44±.06 (Tbt) R
2.49±.05 (Tbt) R
2.55±.04 (Tb) R
2.61±.14 (Tbb) N
2.59±.05 (Tm) N
2.66±.08 (Tbj) N
2.68±.03 (Tbs) N
2.60±.10 (Tcc) N
Middle Phase
Early Phase
1,000
1,100
1,200
1,300
1,400
1.14±.13 (Qcc) R
1.31±.06 (Qd) R
1.46±.06 (QTba) R
Late Phase
EXPLANATION
N Normal polarity
R Reversed polarity
Age (Ma) of normal polarity unit
Age (Ma) of reversed polarity unit

Magnetic Polarities

The aeromagnetic expression of volcanic rocks is commonly dominated by remnant magnetization. Volcanic rocks with strong, reverse-polarity, remnant magnetization produce distinctive, high-amplitude negative anomalies, whereas normal-polarity remnant magnetization produces high-amplitude positive anomalies (chapter D, this volume). Recognition of these distinctive anomalies in relation to mapped volcanic rock units, combined with paleomagnetic measurements, can be used to locate flow contacts, determine areal flow extent, and assign ages to undated rock units.

Aeromagnetic data for the Cerros del Rio volcanic field were compiled from two surveys flown with 400-m and 150-m line spacings and observation heights of 73 m and 150 m above ground, respectively. The data were analytically continued to a common observation surface 100 m above ground, merged, and reduced to pole (chapter D, this volume). Aeromagnetic signatures of the Cerros del Rio volcanic field express many small, mostly negative, magnetic anomalies of large amplitude, relating to magnetizations inherited during cooling of individual lava flows and associated pyroclastic deposits. Magnetic anomalies correlate well with preliminary paleomagnetic site means for the volcanic field showing both reversed and normal magnetic polarities corresponding with signatures of both Gauss and Matuyama magnetic chrons. On plate 5, geologic map data derived from figure C2 are overlaid on a shaded-relief version of the reduced-to-pole aeromagnetic data, and paleomagnetic sample sites and polarities are shown. A summary of paleomagnetic site means for selected samples of the Cerros del Rio volcanic field is illustrated in figure C6, and paleomagnetic data for selected samples are presented in table C2. The errors associated with $^{40}Ar/^{39}Ar$ age determinations (fig. C5) preclude assignment of mapped lithologic units to magnetic chrons or subchrons solely on the basis of geochronology. However, magnetic properties in conjunction with age distributions and observed stratigraphic relations have proven useful in delineating map units and assigning them to major eruptive phases.

Early-phase eruptions were confined to the latest Gauss magnetic chron (figs. C5, C7) and are characterized by moderate to strong normal polarity signatures (plate 5) supported by normal paleomagnetic site means for units Tat, Tbs, Tbj, Tm, and Tbb (fig. C6). It is likely that much of the plateau is underlain by younger phases of Cerros del Rio volcanic rocks that produce strong negative magnetic polarities, and it is unclear what effect this polarity signature may have on thinly veneered overlying units of variable age and polarity.

Most middle-phase eruptions occurred during the early Matuyama magnetic chron but appear, on the basis of geochronology and magnetic properties, to extend into the Reunion subchrons (fig. C5). Early eruptive units within this phase, for example Tbt, Tb_2, and To, have $^{40}Ar/^{39}Ar$ ages ranging from 2.49 to 2.32 Ma, and their strong reversed aeromagnetic polarities are corroborated by reversed paleomagnetic site means for units Tbt and To. Units Tto, Tbb, Tb, and Tbr occur

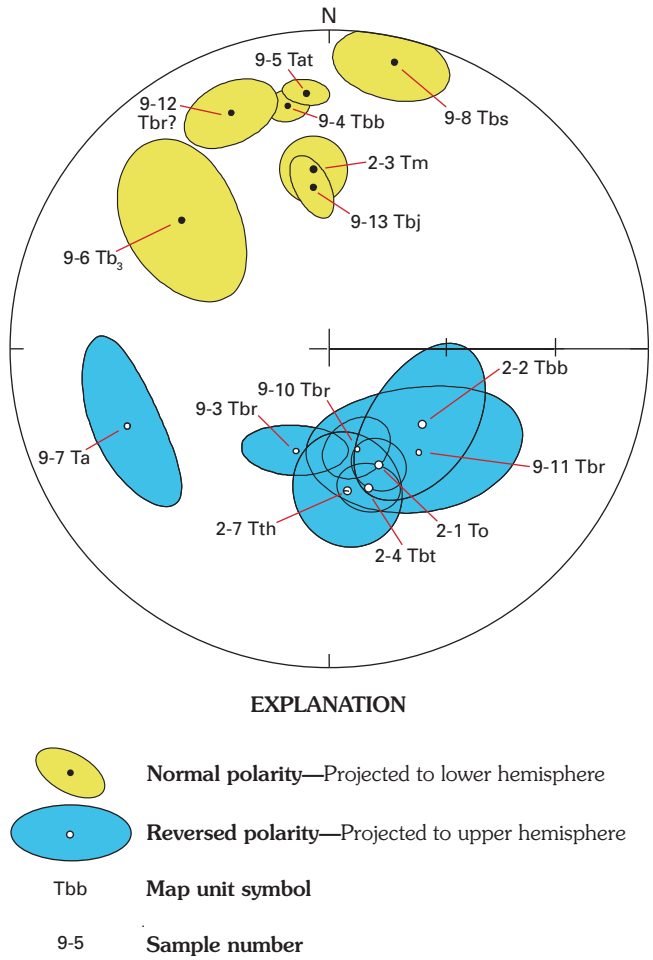

Figure C6. Paleomagnetic site mean directions for selected samples from the Cerros del Rio volcanic field (sample locations shown on pl. 5). Dots are projections onto an equal-area stereo diagram. Colored ovals about site mean directions are cones of 95 percent statistical confidence. Samples for paleomagnetic analysis collected by use of a portable rock drill and oriented by use of magnetic and solar compasses and a clinometer. In the laboratory, natural remanent magnetization of samples was measured using a spinner magnetometer. All samples were subjected to progressive alternating-field demagnetization, typically with nine or more steps, to peak fields of 100–200 nT. Most samples affected to some degree by secondary magnetizations imparted by lightning, and thus data from remagnetization circles (Halls, 1976) commonly were combined with best-fit linear directions (Kirschvink, 1980) to define site mean directions. Site means and dispersion parameters (table C2) calculated using Bingham statistics (Onstott, 1980) or Fisher statistics (Fisher, 1953). Map unit symbols: Ta, late andesite of Caja del Rio; Tat, andesite of Tetilla Peak; Tb_3, lower flow unit of Bajada Mesa; Tbb, basalt of La Bajada; Tbj, basalt of Mesita de Juana Lopez; Tbr, basalt of Caja del Rio; Tbs, basalt of Tsinat Mesa; Tbt, basalt of Tetilla Hole; Tm, basaltic andesite of Cerro Montoso; To, andesite of Ortiz Mountain; Tth, andesite of Twin Hills.

Table C2. Paleomagnetic data from Cerros del Rio volcanic field.

[Latitude and Longitude referenced to 1927 North American datum; Xo, site average magnetic susceptibility (SI volume unit of measure); N/No., ratio of number of samples accepted to number of samples demagnetized; Decl., Incl., declination and inclination of site-mean directions; α95–1, α95–2, minimum and maximum axes of ellipse of 95 percent confidence cone about mean direction (Onstott, 1980); K1, K2, concentration parameters; Oval az., oval azimuth for confidence ellipse. Site means for 9MRG–4, 2MRG–5, and 2MRG–15 calculated using statistics of Fisher (1953) and have single values for confidence cone oval and concentration parameter and no oval azimuth value]

Site	Latitude (°N)	Longitude (°W)	Xo	N/No.	Decl. (°)	Incl. (°)	α_{95-1}	α_{95-2}	K1	K2	Oval az.
9MRG–3	35.5624	106.2193	2.28E–2	8/8	198	–62.3	6.77	13.59	–35.6	–2.8	72.8
9MRG–4	35.5516	106.2220	2.09E–2	6/8	350.5	24.4	5.01		179.8		
9MRG–5	35.6005	106.2028	2.98E–3	8/8	355.1	21.1	4.04	5.53	–117.6	–1.2	58.1
9MRG–6	35.6452	106.1707	3.31E–2	4/8	310.9	39	13.5	24.47	–19.7	–2.2	165.9
9MRG–7	35.6223	106.1818	3.48E–2	6/8	248.8	–32.8	10.01	21.09	–22.1	–2.8	85
9MRG–10	35.6081	106.1965	2.92E–2	8/10	164.3	–63.2	7.51	9.41	–30.4	–0.8	66.1
9MRG–11	35.5682	106.1635	3.22E–2	4/8	139.4	–54.8	16.37	27.75	–14.4	–1.8	129
9MRG–12	35.5661	106.1610	2.13E–2	8/8	337.4	21.6	9.55	10.66	–26	–0.4	103.4
9MRG–13	35.5213	106.2008	2.60E–2	6/8	354.3	48.2	4.37	9.45	–106.2	–3.3	18.1
2MRG–1	35.7392	106.1394	2.34E–2	8/8	156.7	–57.5	6.2	7.5	–37.5	–0.7	159.9
2MRG–2	35.7366	106.1393	3.27E–2	7/8	129.1	–59.2	13.8	21.7	–12.4	–1.5	84.1
2MRG–3	35.7369	106.2045	2.58E–2	9/9	355.0	42.9	7.9	9.4	–22.4	–0.6	2.5
2MRG–4	35.6328	106.2287	3.68E–2	8/8	164.2	–52.6	6.3	7.9	–47.2	–0.9	125.8
2MRG–5	35.6428	106.2267	3.59E–2	8/8	168.1	–59.6	3.9		198.8		
2MRG–6	35.7055	106.1700	1.20E–2	7/8	138.4	–68.6	5.1	6.1	–92.3	–0.7	34.2
2MRG–7	35.7065	106.1660	7.67E–3	8/8	172.7	–53.0	13.0	15.7	–10.7	–0.6	9.5
2MRG–8	35.6926	106.1637	7.02E–3	8/8	352.5	57.9	11.9	16.6	–15.1	–1.1	18.0
2MRG–11	35.6506	106.1732	2.87E–2	8/8	343.5	47.8	9.9	31.2	–15.9	–4.2	91.5
2MRG–12	35.6467	106.1761	1.20E–2	8/8	154.8	–63.2	6.2	11.6	–34.6	–2.4	37.9
2MRG–13	35.6565	106.1715	4.70E–3	8/8	348.6	47.7	4.2	4.9	–108.3	–0.6	8.1
2MRG–14	35.6562	106.1707	3.26E–2	7/8	332.8	57.1	8.7	15.4	–26.4	–2.1	47.2
2MRG–15	35.6397	106.1452	3.22E–2	7/8	160.5	–68.2	9.7		40.0		

in similar stratigraphic position and also possess negative aeromagnetic signatures, but they are undated. Units Tbr and Tbb have reversed paleomagnetic site means. Stratigraphically younger, undated units that possess normal aeromagnetic polarities include units Tcp, Tb_1, and Tcmu (fig. C7). It is stratigraphically permissible that these units were erupted during either the Reunion I or Reunion II normal excursions. This interpretation is supported by the observation that morphologically younger cinder cones (unit Tth, fig. C2) lying stratigraphically above unit Tcp possess strong reversed aeromagnetic signatures. A particularly problematic series of middle-phase deposits are represented by unit Ta. A series of morphologically similar, small, cinder cones belonging to this unit overlie a related lava flow dated by $^{40}Ar/^{39}Ar$ methods at 2.19±13 Ma. The overlying cinder cones have both negative and positive aeromagnetic signatures for short lateral distances unaccompanied by discernable lithologic or temporal variation in the deposits. It is permissible within the errors of existing age determinations that eruption intervals spanned magnetic reversals, perhaps many times, within the Reunion subchrons of the Matuyama and resulted in lithologically similar deposits with both positive and negative aeromagnetic characteristics.

Late-phase deposits were emplaced during a short interval (1.46–1.14 Ma) of the Matuyama magnetic chron but potentially encompass two reversed subchrons (fig. C5). No paleomagnetic data exist for the three volcanic units composing these late-phase eruptions, but existing age data, stratigraphic relations, and aeromagnetic data support the following preliminary interpretations: (1) The oldest eruptive center (unit Qba, fig. C2) produces a moderately strong negative polarity signature consistent with the 1.46 Ma $^{40}Ar/^{39}Ar$ age determination for this unit. (2) Unit Qd also produces a moderately strong negative polarity signature consistent with the 1.31 Ma $^{40}Ar/^{39}Ar$ age determination for this eruptive center. (3) Cochiti Cone (unit Qcc) produces predominantly strong negative aeromagnetic anomalies with the exception of strong positive anomalies observed near the base of the volcano on the west, southwest, and southeast shoulders (pl. 5). The $^{40}Ar/^{39}Ar$ age determination of 1.14±13 Ma for this center encompasses potentially two normal subchrons within the Matuyama,

Pleistocene
Pliocene
Late Phase
Middle Phase
Early Phase
Qec
Qcc
Qbt
Qd
Qbo
QTba
Ta
Tb4?
Tb3?
Tth
Tb1
Tcmu?
Tcp
Ttd
To
Tbr
Tae
Tcm
Tto
Tbu
Tbb
Tb
Tbt
Tb2
Tah
Tdt
Tat
Tcc
Tm
Tbj
Tbb
Tbs
Inferred or determined normal magnetic polarity
Inferred or determined reversed magnetic polarity

Figure C7 (facing page). Correlation of map units interpreted on the basis of known stratigraphic relations, $^{40}Ar/^{39}Ar$ geochronology, aeromagnetic data, and paleomagnetic determinations. Eruptive phases of the Cerros del Rio volcanic field indicated by brackets on right side of figure. Map unit symbols: QTba, basalt of Cochiti; Qbo, Otowi Member of Bandelier Tuff; Qbt, Tshirege Member of Bandelier Tuff; Qcc, basaltic andesite of Cochiti Cone; Qd, dacite of White Rock Canyon; Qec, El Cajete tephra; Ta, late andesite of Caja del Rio; Tae, andesite of Arroyo Eighteen; Tah, andesite of Hill 6385; Tat, andesite of Tetilla Peak; Tb_1, basalt of Hill 7071; Tb_2, basaltic andesite of Petroglyph Canyon; Tb_3, lower flow unit of Bajada Mesa; Tb_4, upper flow unit of Bajada Mesa; Tb, basalt of White Rock Canyon; Tbb, basalt of La Bajada; Tbj, basalt of Mesita de Juana Lopez; Tbr, basalt of Caja del Rio; Tbs, basalt of Tsinat Mesa; Tbt, basalt of Tetilla Hole; Tbu, basalt of Canada Ancha; Tcc, andesite of Cerro Colorado; Tcm, basaltic andesite of Cerro Micho; Tcmu, late andesite of Cerro Micho; Tcp, andesite of Cerro Portrillo; Tdt, dacite of Tetilla Peak; Tm, basaltic andesite of Cerro Montoso; To, andesite of Ortiz Mountain; Ttd, basaltic andesite of Tank 31; Tth, andesite of Twin Hills; Tto, basalt of Thirty One Draw.

both younger and older than the preferred age of 1.14 Ma. A reasonable interpretation is that early lavas of Cochiti Cone erupted during the short normal subchron of the Matuyama between 1.19 Ma and 1.21 Ma and that the main eruptive phase followed during a reversed magnetic subchron between 1.19 and 1.07 Ma. However, the relatively thin cover of Cochiti Cone lava flows may simply reflect the predominant aeromagnetic signature of underlying lava flows of normal magnetic affinity.

Structural Controls on Eruption

Most structures defining the boundaries of the La Bajada constriction are largely buried beneath Pliocene volcanic cover of the Cerros del Rio volcanic field (chapter G, this volume). Possible rift-related, northwest-trending faults and aeromagnetic lineaments similar to those in the northeast part of the Santo Domingo Basin are also obscured by volcanic cover east of the La Bajada fault zone. However, the timing of basaltic volcanism, its feeder mechanisms, and vent locations can be used to infer potential structural control on magma emplacement, providing constraints on subsurface fault geometries.

Early-phase volcanism appears to have been broadly distributed across the volcanic highlands and surrounding plateau that overlaps basin-fill deposits of the northeastern Santo Domingo and southern Española Basins. Vent locations at Mesita de Juana (unit Tbj), Tetilla Peak (unit Tat), Cerro Colorado (unit Tcc), and Cerro Montoso (unit Tm) exhibit a broad north-trending alignment (fig. C2). It is likely that these aligned large vents formed in response to broad, regional, east-west directed extension that was roughly perpendicular to the strikes of the younger La Bajada and Cochiti Cone faults farther west in the Cerros del Rio field.

Structural control on eruption mechanisms during the middle-phase eruptive episode is generally more difficult to discern, because lavas erupted from small systems with locally migrating vent areas characteristic of fissure-controlled basaltic eruptions. Numerous overlapping vents and local stratigraphic complexities obscure what was likely vent alignments based on evidence for comagmatic extensional faulting. Alignments of remnant cinder cones on La Bajada Mesa (pl. 1) (units Ta, Tbr; fig. C2) have northeast trends that broadly parallel locally exposed feeder dikes for these systems. These northeast trends are similar to the trend of a nearby geophysically inferred fault or fault zone buried beneath the Cerros del Rio volcanic field (pl. 2) that may form a structural boundary of the La Bajada constriction (chapters F and G, this volume). Thus, it is possible that the vent alignments are controlled by buried, preexisting faults.

Westward migration of active faulting (chapter E, this volume) after eruption of early- and middle-phase lavas is documented along the prominent escarpment of the La Bajada fault zone and in subtle surface expressions of faulting along the Cochiti Cone fault (CCF, fig. C2) and northern extensions of this system that form offset terraces in lava flows east of the Rio Grande in the northernmost part of the map area (pl. 2, fig. C2). These down-to-the-west normal faults, in conjunction with numerous subsidiary faults of similar orientation but lesser displacement, are at least partly responsible for maintaining the substantial topographic relief of the Cerros del Rio volcanic field east of the Rio Grande relative to middle-phase stratigraphic counterparts to the west.

Late-phase volcanism is restricted to centers west of the Cochiti Cone fault. Two primary vent areas for Cochiti Cone (unit Qcc, fig. C2), which are in the hanging-wall block of this fault and whose alignment parallels the presumed trace of the fault, were likely controlled by it. Units produced by all three late eruptive centers (units Qcc, Qd, QTba) are confined to a narrow corridor structurally bordered by the youngest faulting events (chapter E, this volume). Smith, Bailey, and Ross (1970) have depicted several vent areas for Cochiti Cone, including isolated vents west of the easternmost La Bajada fault strand in the area of the Solar T windmill of Cochiti Pueblo (plate 2 and marked Solar TW on fig. G1). Recent mapping suggests that Cochiti Cone eruptions may be in part coeval with displacement along the northernmost part of the La Bajada fault zone and in places postdate major offset. Lava flows from Cochiti Cone vent areas east of the northern La Bajada escarpment cascaded westward over the eastern La Bajada fault scarp to form much of the lower plateau surface containing the solar windmill. This history accounts for the lack of near-vent deposits on the lower surface and negates the requirement of separate vent areas for Cochiti Cone deposits west of the eastern La Bajada fault strand.

Summary

1. Stratigraphic and geochronologic data for Cenozoic volcanic rocks of the La Bajada constriction region are used to constrain the spatial and temporal evolution of rift-related faulting and basin formation in the zone of structural overlap between the Santo Domingo and Espanola Basins of the Rio Grande rift.

2. Pliocene volcanic deposits of the Cerros del Rio largely obscure pre-rift and early rift structures that control local deposition of basin-fill sediments in the La Bajada constriction area. Structural control of volcanism is also obscured by limited exposure and is complicated by a history of many phases of eruption from many centers of variable age, composition, and volume. However, Pliocene volcanism of the Cerros del Rio can be divided into early, middle, and late eruptive phases that reflect generally decreasing areal extent and eruptive volume with time.

3. Vent areas were predominantly single-vent, low-angle, shield volcanoes, multivent cinder-cone complexes, orcinder-cone clusters related to structurally controlled fissure eruptions. A general northeast alignment of middle-phase vent areas may reflect structural control of subsurface plumbing systems. All volcanoes were dike fed; dikes are variably oriented, but preliminary evidence suggests that larger vent complexes trend predominantly northeast.

4. Vents and vent alignments of late-phase eruptive centers step to the west as compared with early- and middle-phase eruptive centers. Vent locations appear to migrate in response to westward migration of active major down-to-west normal faults. The topographic high which Pleistocene Bandelier Tuff abuts is related to constructive topography associated with Cerros del Rio vent areas in addition to structural relief related to throw along the La Bajada fault zone, Cochiti Cone fault, and subsidiary faults.

References Cited

Aubele, J.C., 1978, Geology of the Cerros del Rio volcanic field, Santa Fe, Sandoval, and Los Alamos Counties, New Mexico: Albuquerque, University of New Mexico, M.S. thesis, 136 p.

Aubele, J.C., 1979, The Cerros del Rio volcanic field: New Mexico Geological Society 30th field conference, Santa Fe Country, Guidebook, p. 243–252.

Bachman, G.O., and Mehnert, H.H., 1978, New K-Ar dates and the late Pliocene to Holocene geomorphic history of the central Rio Grande region, New Mexico: Geological Society of America Bulletin, v. 89, no. 2, p. 283–292.

Bailey, R.A., Smith, R.L., and Ross, C.S., 1969, Stratigraphic nomenclature of volcanic rocks in the Jemez Mountains, New Mexico: U.S. Geological Survey Bulletin 1274–P, p. 1–19.

Baldridge, W.S., 1979a, Petrology and petrogenesis of Plio-Pleistocene basaltic rocks from the central Rio Grande rift, New Mexico, and their relation to rift structure, *in* Riecker, R.E., ed., Rio Grande rift—Tectonics and magmatism: American Geophysical Union, Washington, D.C., p. 323–353.

Baldridge, W.S., 1979b, Mafic and ultramafic inclusion suites from the Rio Grande rift (New Mexico) and their bearing on the composition and thermal state of the lithosphere: Journal of Volcanology and Geothermal Research, v. 6, p. 319–351.

Baldridge, W.S., Damon, P.E., Shafiqullah, M., and Bridwell, R.J., 1980, Evolution of the central Rio Grande rift, New Mexico—New potassium-argon ages: Earth and Planetary Science Letters, v. 51, p. 309–321.

Baldridge, W.S., Olsen, K.H., and Callender, J.F., 1984, Rio Grande rift, problems and perspectives: New Mexico Geological Society 35th field conference, Rio Grande Rift—Northern New Mexico, Guidebook, p. 1–12.

Bartolino, J.R., and Cole, J.C., 2002, Ground-water resources of the Middle Rio Grande Basin, New Mexico: U.S. Geological Survey Circular 1222, 132 p.

Bryan, Kirk, 1938, Geology and ground-water conditions of the Rio Grande depression in Colorado and New Mexico: National Resource Commission, Washington, Regional Planning, pt. 6, Rio Grande joint investigations in the upper Rio Grande Basin, v. 1, pt. 2, sec. 1, p. 197–225.

Dethier, D.P., 1997, Geology of the White Rock quadrangle, Los Alamos and Santa Fe Counties, New Mexico: New Mexico Bureau of Mines and Mineral Resources Geologic Map GM–73, scale 1:24,000.

Disbrow, A.E., and Stoll, W.C., 1957, Geology of the Cerrillos area, Santa Fe County, New Mexico: New Mexico Bureau of Mines and Mineral Resources Bulletin 48, 73 p.

Dungan, M.A., Thompson, R.A., Stormer, J.S., and O'Neill, J.M., 1989, Rio Grande rift volcanism—Northeastern Jemez zone, New Mexico: New Mexico Bureau of Mines and Mineral Resources Memoir 46, p. 435–486.

Dunker, K.E., Wolfe, J.A., Harmon, R.S., Leat, P.T., Dickin, A.P., and Thompson, R.N., 1991, Diverse mantle and crustal components in lavas of the NW Cerros del Rio volcanic field, New Mexico: Contributions to Mineralogy and Petrology, v. 108, p. 331–345.

Fisher, R.A., 1953, Dispersion on a sphere: Proceedings of the Royal Society [London], Series A217, v. 295–305.

Gardner, J.N., Goff, Fraser, Garcia, S., and Hagan, R.C., 1986, Stratigraphic relations and lithologic variations in the Jemez volcanic field, New Mexico: Journal of Geophysical Research, v. 91, p. 1763–1778.

Goff, Fraser, Gardner, Jamie, and Valentine, Greg, 1990, Geologic map of the St. Peters Dome area, Jemez Mountains, New Mexico: New Mexico Bureau of Mines and Mineral Resources Geologic Map 69, scale 1:24,000.

Grauch, V.J.S., and Bankey, Viki, 2003, Aeromagnetic interpretations for understanding the hydrogeologic framework of the southern Española Basin, New Mexico: U.S. Geological Survey Open-File Report 03–124, available from http://pubs.usgs.gov/of/2003/ofr–03–124/.

Griggs, R.L., 1964, Geology and groundwater resources of the Los Alamos area, New Mexico: U.S. Geological Survey Water-Supply Paper 1753, 107 p.

Halls, H.C., 1976, A least-squares method to find remanence directions from converging remagnetization circles: Geophysical Journal of the Royal Astronomical Society, v. 45, p. 297–304.

Justet, Leigh, 1999, The geochronology and geochemistry of the Bearhead Rhyolite, Jemez volcanic field, New Mexico: Las Vegas, University of Nevada, M.S. thesis, 152 p.

Kelley, V.C., and Kudo, A.M., 1978, Volcanoes and related basalts of Albuquerque Basin, New Mexico: New Mexico Bureau of Mines and Mineral Resources Circular 156, 30 p.

Kirschvink, J.L., 1980, The least-squares line and plane and the analysis of paleomagnetic data: Geophysical Journal of the Royal Astronomical Society, v. 62, p. 699–718.

Lavine, Alex, Smith, G.A., and Goff, Fraser, 1996, Volcaniclastic rocks of the Keres Group—Insights into mid-Miocene volcanism and sedimentation in the southeastern Jemez Mountains: New Mexico Geological Society 47th field conference, Jemez Mountains Region, Guidebook, p. 211–218.

Le Bas, M.J., Le Maitre, R.W., Streckeisen, A., and Zanettin, B., 1986, A chemical classification of volcanic rocks based on the total alkali-silica diagram: Journal of Petrology, v. 27, p. 745–750.

Lipman, P.W., 1988, Evolution of silicic magma in the upper crust—The mid-Tertiary Latir volcanic field and its cogenetic granitic batholith, northern New Mexico, USA: Royal Society of Edinburgh—Earth Science, Transactions, 79, p. 265–288.

Lipman, P.W., and Mehnert, H.H., 1979, The Taos Plateau volcanic field, northern Rio Grande rift, New Mexico, *in* Riecker, R.E., ed., Rio Grande rift—Tectonics and magmatism: Washington, D.C., American Geophysical Union, p. 289–309.

Luedke, R.G., and Smith, R.L., 1978, Map showing the distribution, composition, and age of the late Cenozoic volcanic centers in Arizona and New Mexico: U.S. Geological Survey Miscellaneous Investigations Series Map I–1091A, scale 1:1,000,000.

Mayo, E.B., 1958, Lineament tectonics and some ore districts of the southwest: Mining Engineering, v. 10, p. 1169–1175.

McIntosh, W.C., and Quade, Jay, 1995, $^{40}Ar/^{39}Ar$ geochronology of tephra layers in the Santa Fe Group, Española Basin, New Mexico: New Mexico Geological Society 46th field conference, Santa Fe Region, Guidebook, p. 279–287.

McMillan, N.J., 1998, Temporal and spatial magmatic evolution of the Rio Grande rift: New Mexico Geological Society 49th field conference, Las Cruces Country II, Guidebook, p. 107–116.

Miggins, D.P., Thompson, R.A., Pillmore, C.L., Snee, L.W., and Stern, C.R., 2002, Extension and uplift of the northern Rio Grande rift—Evidence from $^{40}Ar/^{39}Ar$ geochronology from the Sangre de Cristo Mountains, south-central Colorado and northern New Mexico, *in* Menzies, M.A., Klemperer, S.L., Ebinger, C.J., and Baker, J., eds., Volcanic rifted margins: Geological Society of America Special Paper 362, p. 47–74.

Minor, S.A., and Hudson, M.R., 2006, Regional survey of structural properties and cementation patterns of fault zones in the northern part of the Albuquerque Basin, New Mexico—Implications for ground-water flow: U.S. Geological Survey Professional Paper 1719, 28 p.

Onstott, T.C., 1980, Application of the Bingham distribution function in paleomagnetism studies: Journal of Geophysical Research, v. 85, p. 1500–1510.

Personius, S.F., 2002, Geologic map of the Santa Ana Pueblo quadrangle, Sandoval County, New Mexico: U.S. Geological Survey Miscellaneous Field Studies Map MF–2405, scale 1:24000.

Reneau, S.L., Gardner, J.N., and Forman, S.L., 1996, New evidence for the age of the youngest eruption in the Valles caldera, New Mexico: Geology, v. 24, p. 7–10.

Reneau, S.L., McDonald, E.V., Gardner, J.N., Kolbe, T.R., Carney, J.S., Watt, P.M., and Longmire, P.A., 1996, Erosion and deposition on the Pajarito Plateau, New Mexico, and implications for geomorphic responses to late Quaternary climatic change: New Mexico Geological Society 47th field conference, Jemez Mountains Region, Guidebook, p. 391–397.

Sauer, R.R.,1999, Petrochemistry and geochronology of plutons relative to tectonics in the San Pedro–Ortiz porphyry belt, New Mexico: Boulder, University of Colorado, M.S. thesis, 115 p.

Sawyer, D.A., Shroba, R.R., Minor, S.A., and Thompson, R.A., 2002, Geologic map of the Tetilla Peak quadrangle, Santa Fe and Sandoval Counties, New Mexico: U.S. Geological Survey Miscellaneous Field Studies Map MF–2352, scale 1:24,000.

Smith, G.A., and Kuhle, A.J., 1998a, Geology of the Santo Domingo Pueblo quadrangle, Sandoval County, New Mexico: New Mexico Bureau of Mines and Mineral Resources Open-file Geologic Map OF–GM 15, scale 1:24,000.

Smith, G.A., and Kuhle, A.J., 1998b, Geology of the Santo Domingo SW quadrangle, Sandoval County, New Mexico: New Mexico Bureau of Mines and Mineral Resources Open-file Geologic Map OF–GM 26, scale 1:24,000.

Smith, R.L., and Bailey, R.A., 1966, The Bandelier Tuff—A study of ash-flow eruption cycles from zoned magma chambers: Bulletin of Volcanology, v. 29, p. 83–104.

Smith, R.L., and Bailey, R.A., 1968, Resurgent cauldrons, *in* Coats, R.R., Hay, R.L., and Anderson, C.A., eds., Studies in volcanology: Geological Society of America Memoir 116, p. 613–662.

Smith, R.L., Bailey, R.A., and Ross, C.S., 1970, Geologic map of the Jemez Mountains, New Mexico: U.S. Geological Survey Miscellaneous Investigations Map I–571, scale 1:125,000.

Spiegel, Zane, and Baldwin, Brewster, 1963, Geology and water resources of the Santa Fe area, New Mexico: U.S. Geological Survey Water-Supply Paper 1525, 258 pp.

Stearns, C.E., 1953, Tertiary geology of the Galisteo-Tonque area, New Mexico: Geological Society of America Bulletin, v. 64, p. 459–508.

Sun, Ming-shan, and Baldwin, Brewster, 1958, Volcanic rocks of the Cienega area, Santa Fe County, New Mexico: New Mexico Bureau of Mines and Mineral Resources Bulletin 54, 80 p.

Thompson, R.A., Dungan, M.A., and Lipman, P.W., 1986, Multiple differentiation processes in early rift calc-alkaline volcanics, northern Rio Grande rift, New Mexico: Journal of Geophysical Research, v. 91, p. 6046–6058.

Thompson, R.A., Johnson, C.M., and Mehnert, H.H., 1991, Oligocene basaltic volcanism of the northern Rio Grande rift–San Luis Hills, Colorado: Journal of Geophysical Research, v. 96, p. 13,577–13,592.

WoldeGabriel, Giday, Laughlin, A.W., Dethier, D.P., and Heizler, M., 1996, Temporal and geochemical trends of lavas in White Rock Canyon and the Pajarito Plateau, Jemez volcanic field, New Mexico, USA: New Mexico Geological Society 47th field conference, Jemez Mountains Region, Guidebook, p. 251–261.

WoldeGabriel, Giday, Warren, R.G., Broxton, D.E., Vaniman, D.T., Heizler, M.T., Kluk, E.C., and Peters, L., 2001, Episodic volcanism, petrology, and lithostratigraphy of the Pajarito Plateau and adjacent areas of the Española Basin and the Jemez Mountains: New Mexico Museum of Natural History and Science Bulletin, vol. 18, p. 97–129.

Wolf, J.A., Gardner, J.N., and Reneau, S.L., 1996, Field characteristics of the El Cajete pumice deposit and associated southwestern moat rhyolites of the Valles caldera: New Mexico Geological Society 47th field conference, Jemez Mountains Region, Guidebook, p. 311–316.

Wolf, J.A., Heikoop, C.E., and Ellisor, R., 2000, Hybrid origin of Rio Grande rift hawaiites: Geology, v. 28, no. 3, p. 203–206.

Zimmerman, C., and Kudo, A.M., 1979, Geology and petrology of Tetilla Peak: New Mexico Geological Society 30th field conference, Santa Fe Country, Guidebook, p. 253–256.

Published in the Central Region, Denver, Colo.
Manuscript approved for publication February 10, 2006
Graphics by authors
Photocomposition by Mari L. Kauffmann (Contractor, ATA Services)
Edited by Mary-Margaret Coates (Contractor, ATA Services)

Gravity and Aeromagnetic Studies of the Santo Domingo Basin Area, New Mexico

By V.J.S. Grauch, David A. Sawyer, Scott A. Minor, Mark R. Hudson, and Ren A. Thompson

Chapter D of

The Cerrillos Uplift, the La Bajada Constriction, and Hydrogeologic Framework of the Santo Domingo Basin, Rio Grande Rift, New Mexico

Edited by Scott A. Minor

Professional Paper 1720–D

U.S. Department of the Interior
U.S. Geological Survey

Contents

Abstract 63
Introduction 63
Gravity Data and Methods 64
    Data Compilation 64
    Estimating Thickness of Basin Fill 64
    Locating Faults From Gravity Data 66
Aeromagnetic Data and Methods 69
    Data Compilation 69
    Locating Faults From Aeromagnetic Data 71
    Estimating Depth 71
Regional Gravity Features 72
    Santo Domingo Basin 72
    Cerros del Rio Volcanic Field and Cerrillos Uplift 72
    Jemez Volcanic Field and Saint Peters Dome 73
    Northeast Santo Domingo Basin and La Bajada Constriction 73
Regional Aeromagnetic Features 73
Profile Model Across the La Bajada Constriction 75
Aeromagnetic Investigations of the Cochiti Pueblo Area 75
    Cerros del Rio Volcanic Field 77
    Cochiti Graben 81
    Central Reservoir Horst 81
    La Majada Graben 82
Summary 82
References Cited 83

Figures

D1. Map of isostatic residual gravity for Santo Domingo Basin and surrounding areas 65
D2. Diagram of density-depth step functions generalized from drill-hole density logs 66
D3–D5. Maps showing:
    D3. Estimated thickness of upper Cenozoic basin fill in Santo Domingo Basin area 67
    D4. Estimated elevation of bedrock at base of upper Cenozoic basin fill in Santo Domingo Basin area 68
    D5. Reduced-to-pole aeromagnetic data for Santo Domingo Basin area 70
D6. Geophysical model of regional profile oriented northwest-southeast across the La Bajada constriction 76
D7. Map of reduced-to-pole aeromagnetic data for Cochiti Pueblo area 79
D8. Diagram showing correspondence between age, magnetic-polarity epoch, aeromagnetic signature, and paleomagnetic polarities of some upper Cenozoic volcanic units of the Cerros del Rio volcanic field 80

Table

D1. Explanatory notes keyed to figure D6, Geophysical model of regional profile oriented northwest-southeast across the La Bajada constriction 78

Gravity and Aeromagnetic Studies of the Santo Domingo Basin Area, New Mexico

By V.J.S. Grauch, David A. Sawyer, Scott A. Minor, Mark R. Hudson, and Ren A. Thompson

Abstract

Investigations of gravity and aeromagnetic data at both regional and local scales contribute to an overall understanding of the subsurface geologic and hydrogeologic framework of the Santo Domingo Basin area. Gravity data indicate that the Santo Domingo Basin is bounded on the southeastern side by steeply dipping faults of large vertical displacement and on the northwestern side by a homocline or series of down-to-basin faults. The Cerrillos uplift is reflected in a north-south gravity high that includes and is much larger than the area of Oligocene intrusions of the Ortiz Mountains and Cerrillos Hills, as indicated by the regional magnetic data. Within the La Bajada constriction, the gravity data and associated models indicate a northeast-trending trough 10–14-km wide that projects under the Cerros del Rio volcanic field; the trough likely contains Santa Fe Group sediments about 1 km thick. Moderate- to high-amplitude, positive aeromagnetic anomalies in the Cerros del Rio volcanic field are associated with basalts that formed during the Gauss normal magnetic-polarity epoch (2.70–2.59 Ma), whereas negative anomalies of similar amplitude are associated with basalts that formed during the Matuyama reversed magnetic-polarity epoch (2.59 Ma–776 ka). In the western half of the Cochiti Pueblo study area, magnetic piedmont basin-fill sediments of the Cochiti Formation and axial river gravels are expressed as subtle aeromagnetic anomalies that correlate with topography. Numerous faults that offset these magnetic sediments have aeromagnetic expressions that help delineate faults where they are concealed or inferred. An extensive northeast-elongated negative anomaly in the southern part of the intrabasin La Majada graben is interpreted as a post-2.59-Ma buried flow that dips to the east and ranges in depth from about 300 to 450 m. This interpretation implies that 525–725 m of displacement has occurred along the La Bajada fault zone during the last 2.4 m.y.

Introduction

Studies by the U.S. Geological Survey were begun in 1996 to improve understanding of the geologic framework of the Albuquerque composite basin and adjoining areas, in order that more accurate hydrogeologic parameters could be applied to new hydrologic models. The ultimate goal of this multidisciplinary effort has been to better quantify estimates of future water supplies for northern New Mexico's growing urban centers, which largely subsist on aquifers in the Rio Grande rift basin (Bartolino and Cole, 2002). From preexisting hydrologic models it became evident that hydrogeologic uncertainties were large in the Santo Domingo Basin area, immediately upgradient from the greater Albuquerque metropolitan area, and particularly in the northeast part of the basin referred to as the La Bajada constriction (see chapter A, this volume, for a geologic definition of this feature as used in this report). Accordingly, a priority for new geologic and geophysical investigations was to better determine the hydrogeologic framework of the La Bajada constriction area. This chapter along with the other chapters of this report present the results of such investigations conducted since 1996 by the U.S. Geological Survey.

Gravity and aeromagnetic methods are geophysical techniques that can be used to investigate the subsurface geology that influences groundwater flow and storage in the Santo Domingo Basin and adjoining parts of the Albuquerque and Española Basins. Gravity methods rely on measurements of the Earth's gravitational field at the surface to determine changes in bulk density of the crust, whereas aeromagnetic methods measure variations in the strength of the Earth's magnetic field from the air to determine variations in magnetization. From these measurements, geophysicists deduce the spatial distribution of the physical properties in the earth and interpret these distributions in terms of lithologic properties and subsurface structure.

Gravity studies can place constraints on basin geometry, the nature and orientation of basement structures, and regional variations in the thickness of basin fill. Aeromagnetic data help determine the lateral limits of intrusions, delineate buried faults and igneous rocks and, in some places, clearly distinguish between basalts extruded during different magnetic-polarity epochs. This chapter focuses on the methods and results of interpreting these kinds of features from gravity and aeromagnetic data at both regional scale for the Santo Domingo Basin and surrounding region (fig. A2) and at detailed scale for the Cochiti Pueblo area (fig. A4). We relied heavily on information and results from geophysical and geologic studies presented in other chapters of this

report. In the final chapter (chapter G), results from all studies described in this volume are brought together to construct a three-dimensional geologic framework and discuss its hydrogeologic implications. We first present background information on the data, methods, and types of approaches that we used to interpret the data. Next, we discuss regional interpretations from the gravity and aeromagnetic data, present a two-dimensional profile model that illustrates and integrates these interpretations, and discuss interpretations of high-resolution aeromagnetic data in more detail for the Cochiti Pueblo area. Finally, we summarize the salient results that were used to construct the three-dimensional geologic framework described in chapter G (this volume).

Gravity Data and Methods

Regional gravity studies have been critical in the definition of the basins and boundaries of the central Rio Grande rift from mid-1970s onward (Cordell, 1976, 1979; Birch, 1982; Ferguson and others, 1995; Grauch, Gillespie, and Keller, 1999). Gravity data are particularly effective in determining the subsurface configuration of basins within the Rio Grande rift, owing to the generally large contrast in density between the low-density basin fill (Santa Fe Group sediments) and the moderate- to high-density bedrock composing the basin floor and sides (pre-Miocene sedimentary and volcanic rocks and Precambrian basement). In addition, gravity data can be used to determine the location of basement uplifts and other major structures and the depths to which the Santa Fe Group sediments are linked between basins.

Data Compilation

Gravity data are typically collected in the field at individual stations and processed into Bouguer gravity anomaly data or Bouguer gravity data. These reductions include subtraction of theoretical or predicted values of the Earth's gravitational attraction at the elevation of the measurement point and removal of the effects of homogeneous masses underneath and adjacent to the measurement point (such as a neighboring hill). In this process, one must assume a certain density for the earth, typically 2,670 kg/m^3, so that the resulting variations shown on anomaly maps represent masses that deviate from that density.

In order to focus on density variations within the upper crust, a regional field is commonly removed from Bouguer gravity data. The regional field can be determined in a number of ways, such as trend fitting, modeling, or wavelength filtering. A regional field that is based on an Airy isostatic model is advantageous because it is understandable in physical terms and easily repeated between studies. Subtraction of the regional isostatic field from Bouguer gravity data gives isostatic residual gravity data, which can be used to examine density variations in the upper crust (Simpson and others, 1986). The exact parameters of the isostatic model need not be accurate nor does the Airy mechanism of isostasy need be completely satisfied for construction of a useful regional field (Simpson and others, 1986).

Isostatic residual gravity data for this study (pl. 3, fig. D1) were extracted from a recent compilation for the Albuquerque Basin area (Grauch, Gillespie, and Keller, 1999; Gillespie and others, 2000), which builds on data collected by previous workers since the 1970s. Data for the Santo Domingo Basin area originate primarily from the statewide compilation of Heywood (1992) and secondarily from a database of the Rio Grande rift maintained at the University of Texas at El Paso. In most of the Santo Domingo Basin area, the data provide adequate coverage (average station spacing of about 5 km, pl. 3) to represent regional gravity features (fig. D1).

Estimating Thickness of Basin Fill

The isostatic residual gravity map (pl. 3, fig. D1) primarily expresses variations in the thickness of the basin sediments. As a first-order approximation, lower values correspond with thicker fill. To estimate the thickness of basin fill from gravity data requires that one know the densities of sediments and rock units (or their average density differences) at various depths, measurements of thickness in many locations, or both. Because this information is limited in the Santo Domingo Basin region, we relied on a model developed as part of a study of the middle Rio Grande Basin (Grauch, Rodriguez, and Deszcz-Pan, 2002). This model covers a large region surrounding the Albuquerque Basin and includes the Santo Domingo and southern Española Basins.

In the regional model, basin-fill thickness was estimated by using an iterative three-dimensional modeling method that incorporates density versus depth functions for different geologic units (Jachens and Moring, 1990; Blakely and Jachens, 1991). Generalized density-depth functions for the modeling (fig. D2) were determined by use of density logs from wells in the Albuquerque Basin (Birch, 1982) and from a few additional wells located east of and outside the Santo Domingo Basin

Figure D1 (facing page). Isostatic residual gravity for the Santo Domingo Basin and surrounding areas, shown in color contours. Data extracted from Heywood (1992) and Gillespie and others (2000). Gray gradient lines that locate the steepest portions of gravity gradients were determined from regional horizontal-gradient magnitudes; line thickness corresponds with value of magnitude (see text). Thin magenta lines in the Cerrillos uplift outline aeromagnetic highs related to Eocene and Oligocene monzonite intrusions (pl. 4, fig. D5). Selected audiomagnetotelluric stations (chapter F, this volume) are represented by white triangles. Three deep wells near Valles caldera (PC–1, VC–1, AET–4) are discussed in the text. AE, Abiquiu embayment; CH, Cerrillos Hills; EA, El Alto graben of Cordell (1979); HB, Hagan bench; HEB, Hagan embayment; OM, Ortiz Mountains; SE, Santa Fe embayment; VG, Velarde graben of Cordell (1970); ZH, Ziana horst. Small black box outlines area of figure D7.

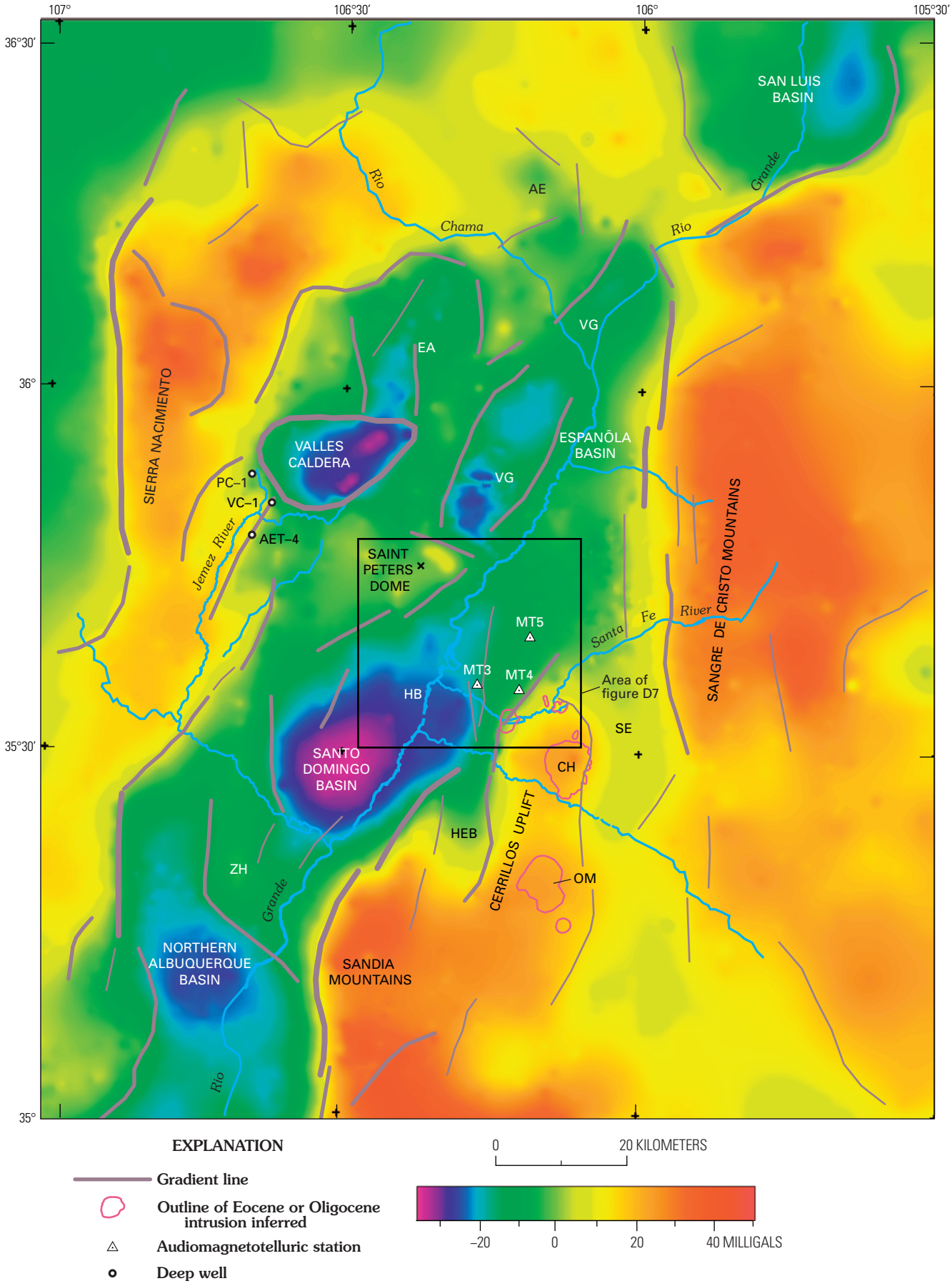
107°
106°30′
106°
105°30′
36°30′
36°
35°30′
35°
SAN LUIS BASIN
Rio Grande
Rio Chama
AE
VG
EA
SIERRA NACIMIENTO
VALLES CALDERA
ESPAÑOLA BASIN
VG
PC–1
VC–1
AET–4
Jemez River
SAINT PETERS DOME
MT5
MT3
MT4
HB
Santa Fe River
Area of figure D7
SANGRE DE CRISTO MOUNTAINS
SE
SANTO DOMINGO BASIN
CH
HEB
CERRILLOS UPLIFT
OM
ZH
Rio Grande
NORTHERN ALBUQUERQUE BASIN
SANDIA MOUNTAINS
EXPLANATION
Gradient line
Outline of Eocene or Oligocene intrusion inferred
Audiomagnetotelluric station
Deep well
0
20 KILOMETERS
–20
0
20
40 MILLIGALS

(located on figs. D3, D4). We assumed that the Santa Fe Group is substantially less dense than older units at comparable depths (fig. D2), an assumption that generally allows the modeling procedure to separate the gravity effects of the Santa Fe Group from those of older units. Volcanic fields having great depth extent, such as the Jemez volcanic field, were given a separate density function (assumed to be 2,350 kg/m^3 on the basis of modeling of Nowell, 1996). Other volcanic areas consisting primarily of basalts no more than about 250 m thick, such as the Santa Ana and Cerros del Rio volcanic fields (SAMVF and CDRVF, fig. C1), were considered volumetrically unimportant compared with the mass of sediments contained in the basins (Cordell, 1976; Birch, 1982). As a consequence, the model represents the collective thickness of the volcanic units and the Santa Fe Group sediments in volcanic areas.

Because the model was constructed from limited information on thickness and density of sediments and rock units near the Santo Domingo Basin, the estimates of fill thickness should be viewed in a regional sense. If assumed densities are too high, estimated thicknesses will be too large; if assumed densities are too low, estimated thickness will be too small. For this report, we have subtracted the values of a subset of the regional thickness model (fig. D3) from smoothed topographic elevations to give an elevation model of the top of bedrock (fig. D4). The thickness model shows variations that may relate to potential aquifer thickness. The bedrock elevation model illustrates basin geometry.

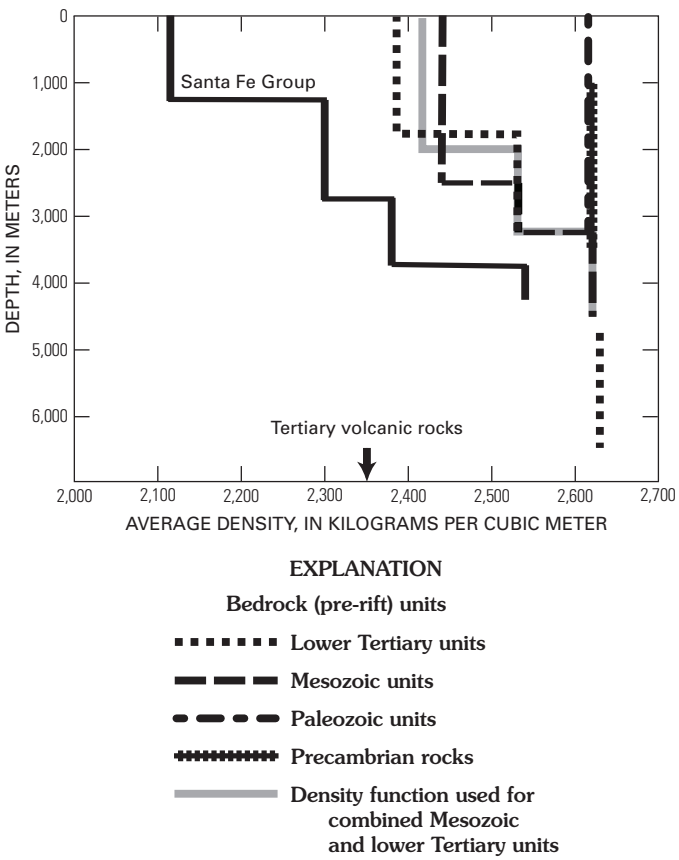

Figure D2. Density-depth step functions generalized from drill-hole density logs and used to construct the basin-fill thickness and bedrock elevation models (figs. D3 and D4, respectively). Densities of the high volume of Tertiary volcanic units in the vicinity of the Valles caldera could not be adequately characterized by drill-hole information. Instead, a constant density of 2,350 kg/m^3 was assumed (value marked by arrow at the bottom of the graph), on the basis of results of gravity modeling by Nowell (1996).

Locating Faults From Gravity Data

Steep gradients in the gravity field are commonly associated with abrupt lateral density contrasts, for example across faults or other steeply dipping surfaces such as homoclines. The horizontal-gradient method is commonly used to locate steep gradients, because the steepest parts of gradients are not necessarily obvious from inspection of gravity maps. Analogous to taking a derivative to find the inflection point of a curve, the method uses the local maxima of the magnitudes of the horizontal gradient to locate steep gradients (Cordell, 1979).

Gravity gradient lines (gray lines, fig. D1) mark the locations of steep gradients in the isostatic residual gravity field of the Santo Domingo Basin area. These lines were derived by using a modification to the horizontal-gradient method that focuses on regional gradients (Grauch and Johnston, 2002) and are generally similar to those computed by Cordell (1979) north of lat 35°30′N. These gradients are likely associated with major faults or homoclines. The gradients having the greatest magnitude, represented by the thickest lines (fig. D1), indicate that materials with contrasting densities are juxtaposed at steeply dipping faults (or fault systems) that extend to considerable depth, implying large throw on the fault (or faults). The gradients having the smallest magnitudes, represented by thin lines, indicate either smaller throw, less contrast in density, or structures that dip more shallowly, such as multiple, small, synthetic faults or a homocline. The locations of the lines may be shifted down-dip over nonvertical structures (Grauch and Cordell, 1987).

Figure D3 (facing page). Contours of estimated thickness of upper Cenozoic basin fill in Santo Domingo Basin area derived from a gravity model covering a much larger area (Grauch, Rodriguez, and Deszcz-Pan, 2002). Basin fill composed primarily of Santa Fe Group sediments, but it also contains basalts erupted from the Cerros del Rio (CDRVF) and Santa Ana Mesa (SAMVF) volcanic fields (figs. A2, C1). The model should be used only to define general geometry, owing to limitations of density assumptions, regional data coverage, and lack of deep drill-hole constraints in the Santa Domingo Basin area. Wells used to constrain the model are shown. Magnetotelluric stations described in chapter F (this volume). HEB, Hagan embayment; NAB, northern Albuquerque Basin. The geophysical model shown in figure D6 located along line of cross section, which is coincident with geologic cross section F-F′ (pl. 6F) or F-F″ (chapter G, this volume).

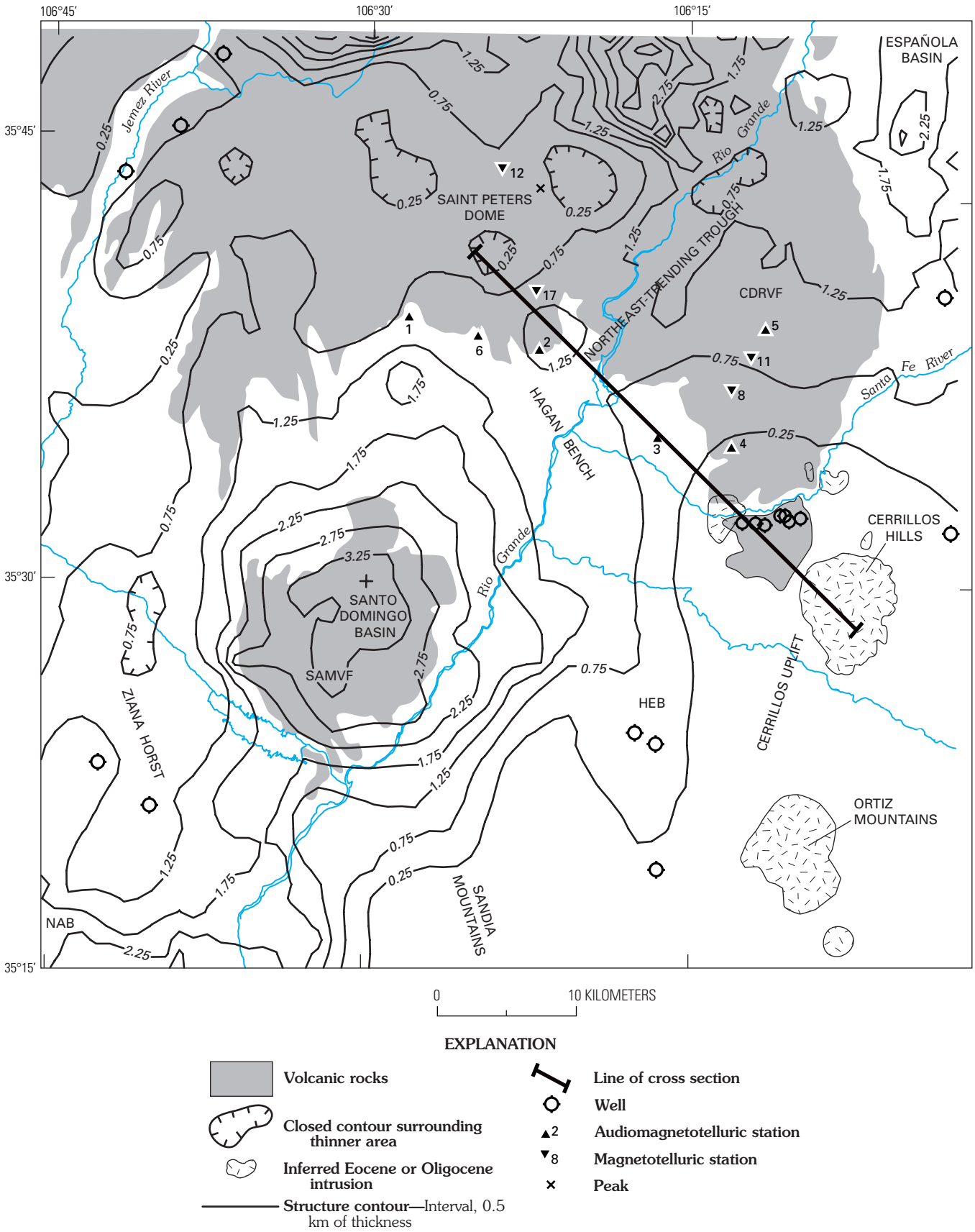

EXPLANATION

- Volcanic rocks
- Closed contour surrounding thinner area
- Inferred Eocene or Oligocene intrusion
- Structure contour—Interval, 0.5 km of thickness
- Line of cross section
- Well
- ▲2 Audiomagnetotelluric station
- ▼8 Magnetotelluric station
- × Peak

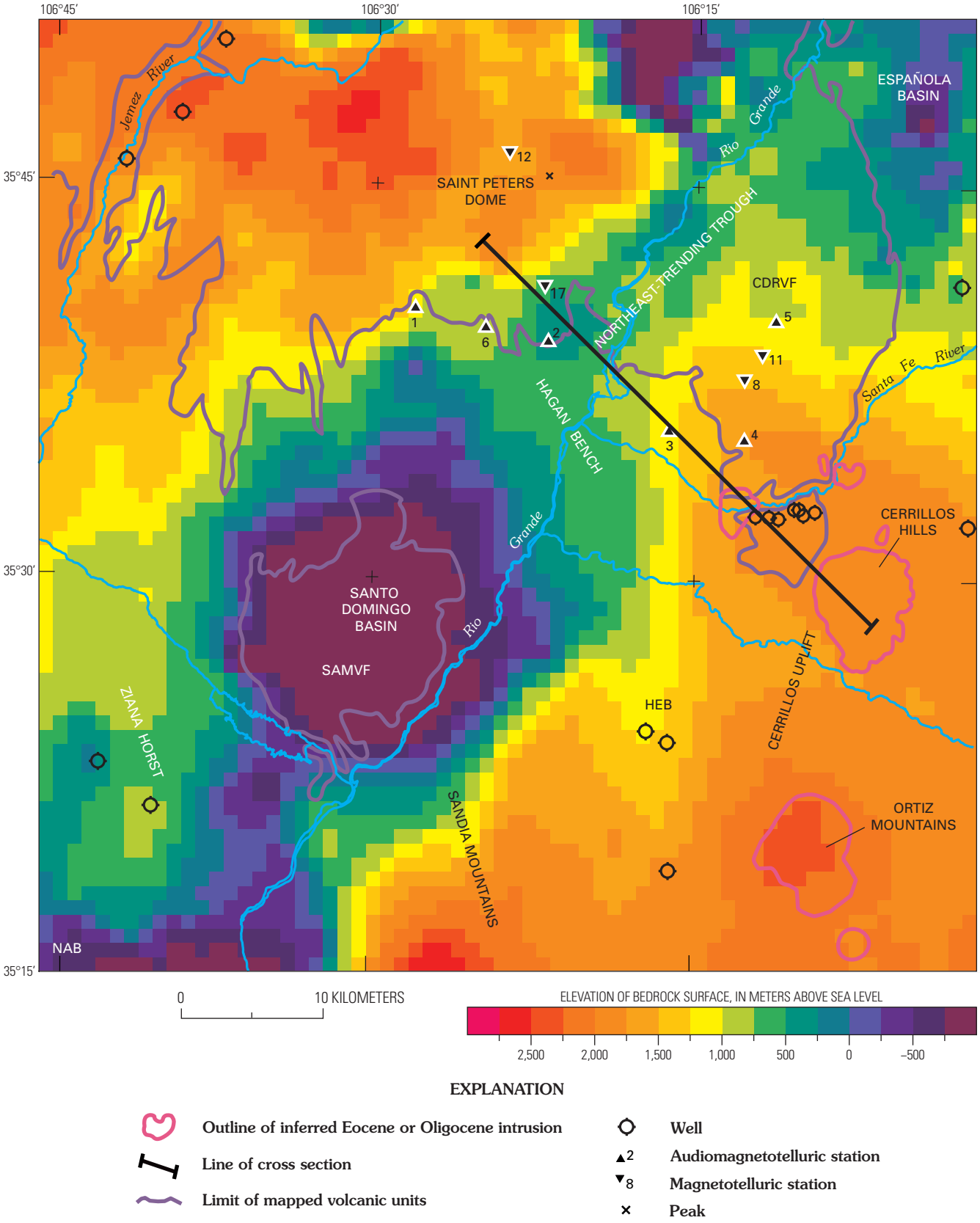

EXPLANATION

Outline of inferred Eocene or Oligocene intrusion

Line of cross section

Limit of mapped volcanic units

Well

▲2 Audiomagnetotelluric station

▼8 Magnetotelluric station

× Peak

Figure D4 (facing page). Estimated elevation of bedrock at base of upper Cenozoic basin fill in the Santo Domingo Basin area; map provides general guides for basin geometry. Bedrock elevation model was constructed by subtracting values of the thickness model (fig. D3) from corresponding values of a digital elevation model that was first smoothed by use of a running- average technique. CDRVF, Cerro del Rio volcanic field; HEB, Hagan embayment; NAB, northern Albuquerque Basin; SAMVF, Santa Ana Mesa volcanic field. The geophysical model shown in figure D6 located along line of cross section, which is coincident with geologic cross section F-F′ (pl. 6*F*) or F-F″ (chapter G, this volume).

An example of the advantages of the horizontal-gradient method is shown by the gradient that surrounds the gravity low associated with the Valles caldera (fig. D1). The gradient varies in steepness around the gravity low, so the steepest part (gradient line) is not necessarily obvious from the color contours. Another example is at the northern tip of the Sandia Mountains (fig. D1), where the gradient line is oriented more southerly than the obvious trend of the color contours, creating an en echelon configuration with the gradient line to the south.

Aeromagnetic Data and Methods

Aeromagnetic methods traditionally have been used to map solely crystalline basement and igneous rocks at depth. Recent work in the Albuquerque Basin has demonstrated that these methods are also useful for mapping faults that offset basin fill and for delineating buried igneous bodies in the near surface (Grauch, 2001a). Aeromagnetic data represent variations in the strength of the Earth's magnetic field that are produced by changes in magnetization of the crust. Magnetization of rocks is determined by the quantity of magnetic minerals (commonly titanomagnetites) and by the strength and direction of remanent magnetization carried by those magnetic minerals. The quantity of magnetic minerals is measured as magnetic susceptibility and produces an induced magnetization. The remanent magnetization is based on the permanent alignment of magnetic domains within the rock and is measured using paleomagnetic methods (Butler, 1992; chapter C, this volume).

Aeromagnetic surveys respond to the total magnetization of rocks, which is the vector sum of the induced and remanent magnetizations. Igneous and crystalline metamorphic rocks commonly have high total magnetizations compared with other rock types, whereas sedimentary rocks and poorly consolidated sediments have much lower magnetizations (Reynolds and others, 1990; Hudson and others, 1999). The induced component is dominant in Santa Fe Group units, although total magnetization is fairly low. Moreover, higher magnetic susceptibilities generally correspond with coarser grained units (Hudson and others, 1999). In contrast, the remanent component is commonly dominant in volcanic units, which have high total magnetizations (Bath, 1968; Reynolds and others, 1990). Volcanic rocks with reverse-polarity remanent components that dominate total magnetization produce distinctive, high-amplitude negative aeromagnetic anomalies, such as the ones corresponding with the basalt at Santa Ana Mesa (fig. D5). Strong, positive aeromagnetic anomalies related to volcanic units can be inferred to indicate a normal-polarity magnetization, although these anomalies may be caused by dominant induced components as well.

Data Compilation

The aeromagnetic data for this study were assembled from a regional data compilation and two detailed airborne geophysical surveys: the Cochiti survey, generally flown over Cochiti Pueblo lands, and the Sandoval–Santa Fe survey, which covers the rest of the study area and overlaps with the Cochiti survey (U.S. Geological Survey, Sander Geophysics, Ltd., and Geoterrex-Dighem, 1999). The Cochiti survey, which was designed primarily to collect electromagnetic data (chapter F, this volume), was flown with 400-m line spacing; the magnetometer was nominally 73 m above ground. The Sandoval–Santa Fe survey, which was designed to gather high-resolution magnetic information, was flown with 150-m line spacing; the magnetometer was nominally 150 m above ground. Data from the surveys were analytically continued to a common observation surface 100 m above ground, digitally merged onto a grid with 50-m intervals, and then transformed by a standard reduction-to-pole operation (Sweeney, Grauch, and Phillips, 2002). This last operation, resulting in reduced-to-pole (RTP) data (Blakely, 1995), corrects for shifts of the main anomaly from the center of the magnetic source that occur at most latitudes owing to the oblique orientation of the measured magnetic field with respect to the Earth's surface (the field is vertical only at the magnetic poles). A similar operation, called the pseudogravity transformation or computation of the magnetic potential (Blakely, 1995), also minimizes these shifts, but at the same time considerably reduces the resolution of the data. This operation is commonly an interim step in methods that locate faults or estimate source depths (discussed below). The RTP and pseudogravity transformations require an assumption about the directions of magnetization of the magnetic sources. Generally, it is assumed that the total magnetizations of most rocks in the study area align parallel or anti-parallel to the Earth's main field (in the study area, declination is 11°, inclination is 63°). This collinearity assumption probably works well in most of the survey area, because the primarily Tertiary rock units have been rotated large amounts only in isolated areas (chapter E, this volume).

The final aeromagnetic compilation is displayed in color shaded relief (color plus illumination) on plate 4 and figure D5. The colors primarily reflect the broad variations in the data, whereas the illumination emphasizes detailed variations, especially those that are somewhat linear. The regional data were extracted from a state compilation in which the data were

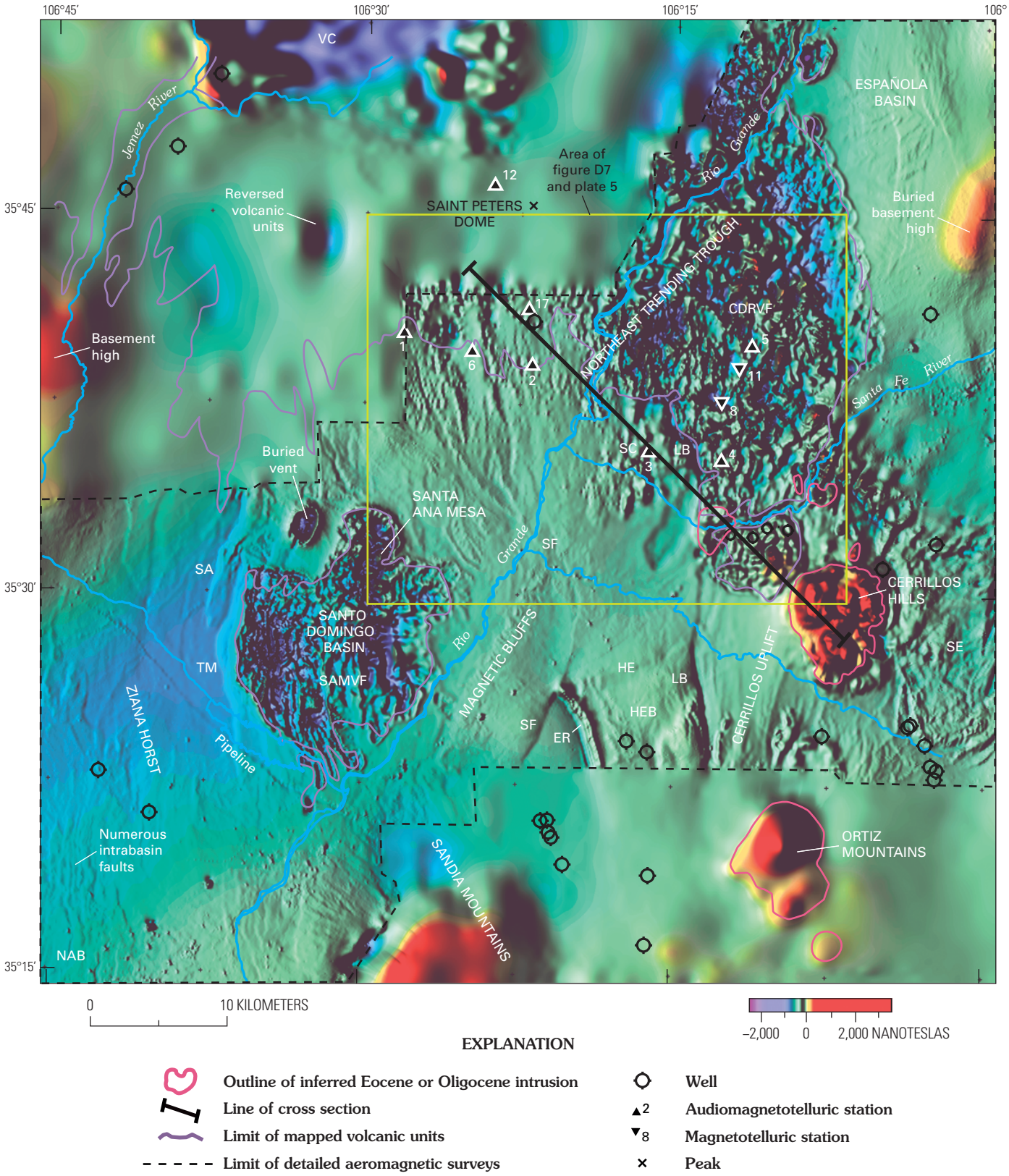

EXPLANATION

- Outline of inferred Eocene or Oligocene intrusion
- Line of cross section
- Limit of mapped volcanic units
- Limit of detailed aeromagnetic surveys
- Well
- ▲2 Audiomagnetotelluric station
- ▼8 Magnetotelluric station
- × Peak

Figure D5 (facing page). Reduced-to-pole aeromagnetic data for the Santo Domingo Basin area shown in color shaded relief, illuminated from the west. Detailed data combined with regional data are from Sweeney, Grauch, and Phillips (2002). Outlines of Oligocene intrusions determined from aeromagnetic data. CDRVF, Cerro del Rio volcanic field; ER, Espinaso Ridge; HE, Hagan Embayment fault zone; HEB, Hagan embayment; LB, La Bajada fault zone; NAB, northern Albuquerque Basin; SA, Santa Ana fault; SAMVF, Santa Ana Mesa volcanic field; SC, Sanchez fault; SE, Santa Fe embayment; SF, San Francisco fault; TM, Tamaya fault; VC, Valles caldera. The geophysical model of figure D6 is located along the line of cross section.

continued to a surface 300 m above ground (Kucks, Hill, and Heywood, 2001). The lower resolution of the Cochiti survey compared with the Santa Fe–Sandoval survey is evident by the discontinuous appearance of linear anomalies, such as those surrounding magnetotelluric station 17 near the northern boundary of the survey (pl. 4, fig. D5), which is caused by inadequate information between flight lines.

Locating Faults From Aeromagnetic Data

High-resolution aeromagnetic data allow discrimination of many subtle linear to arcuate features in areas where magnetic relief is fairly low (pl. 4, fig. D5); these features are enhanced by shading in the image display. These linear to arcuate patterns commonly correspond with geologically mapped faults and are produced by the juxtaposition of variably magnetic sediments (Grauch, Hudson, and Minor, 2001). The aeromagnetic expression of known faults can then be used to extend faults beyond their mapped surface exposure or to infer previously unknown faults where they are covered by thin surficial deposits (Grauch, 2001b).

Analogous to its use with gravity data, the horizontal-gradient method can be applied to RTP aeromagnetic or pseudogravity data to derive gradient lines that locate steep gradients associated with faults (Cordell and Grauch, 1985; Grauch, Hudson, and Minor, 2001). However, interpretation of the gradients is more ambiguous because of the high resolution of the aeromagnetic data, the effects of magnetic terrain (Grauch and Cordell, 1987), and the greater variability of magnetic properties compared with those of density. The locations of maxima from the horizontal-gradient method (using RTP data or pseudogravity data) can represent the locations of (1) faults, where a magnetic contrast is produced by structural juxtaposition of units; (2) contacts, where the magnetic contrast is produced by the limit of deposition of a magnetic unit against a less magnetic one; (3) steep topographic slopes, where the magnetic contrast is produced by the interface between rock and air; or (4) abrupt changes in magnetization within one rock unit, produced by primary differences in magnetization or by secondary destruction or growth of magnetic minerals. In addition, multiple gradients can occur where thin, horizontal sheet-like sources are vertically offset from thicker sources at depth, a distribution of rock units called a thin-thick layers model (Grauch, Hudson, and Minor, 2001).

Faults were interpreted for the Cochiti Pueblo area (pl. 2) from RTP magnetic data and maps of the horizontal-gradient magnitude of RTP magnetic data and pseudogravity (not shown), based on the following criteria. First, only linear or extensive semilinear gradients were considered; this criterion eliminates gradients produced by abrupt changes in magnetization within one rock unit. Second, gradients judged as due solely to topographic slopes were eliminated. Finally, multiple gradients were inspected in relation to topography and geology to determine if they were produced by a fault that fits the thin-thick layers model or by multiple faults. High-magnitude gradients corresponding with moderate to low topographic relief indicate that a magnetization contrast in addition to the topographic slope must be present. These gradients were interpreted as faults because topography commonly correlates with faults. High-magnitude gradients at high-relief topographic slopes required geologic examination to determine if the slope was caused by an erosional edge, a contact, or a fault. A particular origin could not be definitively determined for many gradients, so that many of them are not shown on the geologic map (pl. 2).

Estimating Depth

Depths to the tops of rock bodies were estimated from aeromagnetic data for the Cochiti Pueblo area in two ways—one based on horizontal gradients that operates on the entire grid of data and one that applies multiple algorithms along a profile of data in order to determine a consensus of solutions pertaining to individual anomalies. The method based on horizontal gradients uses the premise that anomalies with broad gradients are produced by deeper sources than those with steep gradients (Blakely, 1995). By measuring the width of the horizontal gradient curve, an estimated depth to the source can be computed (Roest and Pilkington, 1993; Phillips, 1997). Phillips (2000) determined that depth estimates are accurate for contacts that extend to great depth where the method is applied to RTP data and for contacts that extend only to shallower depths (such as those of a sheet) where the method is applied to pseudogravity data. Because the depths to which the contacts extend are unknown, solutions from RTP and pseudogravity data can be viewed as minimum and maximum estimates of the true depth (Phillips, 2000). The advantage of this method is its comprehensive coverage of the area and its ability to examine gradients that have various orientations. Its disadvantage is the dependence on the shape of the source body and problems with interference from neighboring sources (Phillips, 2000). Selected depth estimates derived from the RTP and pseudogravity data for the Cochiti Pueblo area are shown on plate 5.

The approach using profile data applies multiple depth-estimation algorithms (computer program PDEPTH; Phillips, 1997) to compute many depth solutions (locations

in three-dimensional space) for different source shapes. A single depth estimate for an anomaly is determined where solutions with small errors (determined by the individual algorithms) are clustered. The advantage of this method is the use of multiple algorithms, which increases the confidence of the result. The disadvantages arise from its application to profiles, which limit the data coverage and require that the profiles be orthogonal to the anomaly gradients for accuracy (Blakely, 1995).

Depths estimated by use of aeromagnetic data commonly contain appreciable error that is hard to quantify, because assumptions must be made about the shapes of buried sources (Blakely, 1995). Neither approach used in this study can resolve depths closer than one grid interval (50 m), which was chosen to represent the resolution of the overall survey (Reid, 1980).

Regional Gravity Features

Isostatic residual gravity data indicate that the Española Basin, the northern Albuquerque Basin, and the intervening Santo Domingo Basin form discrete depressions within the central Rio Grande rift (fig. D1). The Santo Domingo Basin is discussed below. The Española Basin is expressed by two northeast-southwest elongated lows contained within a wider, moderate, gravity low (fig. D1). Geophysical models indicate that the eastern elongated low (Velarde graben (VG) and the northern half of the western low (El Alto graben, EA) represent a series of aligned depressions or axial troughs contained within a generally shallow basin (Cordell, 1979; Biehler and others, 1991; Ferguson and others, 1995). The deepest part of the basin (>3 km) is located within the Velarde graben just north of Saint Peters Dome (Cordell, 1979), where it is buried beneath Jemez volcanic rocks that make up the Pajarito plateau (fig. D3). The Velarde graben appears disconnected from the deepest parts of the Santo Domingo Basin, as expressed by gravity lows (fig. D1) and the bedrock elevation model (fig. D4).

The northern Albuquerque Basin is generally bounded by north- and northwest-striking fault systems (Grauch, Gillespie, and Keller, 1999), orientations that differ markedly from the northeast elongations of the Española and Santo Domingo Basins (fig. D1). It is separated from the Santo Domingo Basin by a north-trending gravity high that corresponds with the Ziana horst (ZH, fig. D1), a basement high evident in drill-hole and seismic data (Russell and Snelson, 1994). A 10-km-wide connection between Santa Fe Group sediments of the Santo Domingo Basin and the northern Albuquerque Basin is evident within a northeast-trending trough about 1.5 km deep at the southwestern side of the Santo Domingo Basin (figs. D3, D4).

Santo Domingo Basin

The Santo Domingo Basin corresponds with a large, northeast-elongated gravity low that ranges from 20 to 35 km wide (fig. D1). Basalts of the Santa Ana Mesa volcanic field are located over the deepest part of the gravity low (fig. D1) and the area of thickest (>3 km) basin fill (SAMVF, fig. D3). Major faults are also symmetrically arranged about this area (chapter E, this volume; fig. A3).

The gravity low is bounded on the west by the north-trending gravity high corresponding with the Ziana horst (ZH, fig. D1). The east side of the horst is delineated by the traces of the exposed Tamaya (TM) and Santa Ana (SA) faults (pl. 3, fig. A3). A strong gradient generally follows the Santa Ana fault on the north but diverges from the Tamaya fault on the south.

The northern side of the gravity low consists of a broad gradient that trends northeast from the northern end of the Ziana horst to the southeast corner of Saint Peters Dome (fig. D1). The broadness suggests that this side of the basin is a southeast-dipping homocline or that it is composed of many small faulted steps rather than a few faults with large throw. Mapped faults with good exposure cross the gravity gradient obliquely (MC, BR, CA, SI, and CC, fig. A3). This side of the basin may have originated as an earlier, now inactive and buried, northeast-striking fault system associated with an early, late Miocene to early Pliocene, episode of subsidence in the Santo Domingo Basin (chapter E, this volume).

The southern side of the gravity low trends northeast, following U.S. Interstate 25 from the northwest shoulder of the Sandia Mountains to about 6 km southeast of the La Bajada fault (LB, pl. 3 and fig. A3). Northeast-trending gradient lines along this side of the basin (fig. D1) indicate steeply dipping faults that parallel mapped faults (pl. 3, fig. A3) (Connell and Wells, 1999; Connell, 2002; chapter E, this volume). The steepness of the gravity gradient along most of the southern margin of the basin indicates that, regionally, the faults produce a large, nearly vertical offset. In contrast, the gentler gravity gradients surrounding the Hagan embayment (HEB, fig. D1), especially on the southwest side, suggest a homocline or series of down-to-basin faults.

The eastern side of the Santo Domingo gravity low trends north-northeast from the Hagan embayment to the Santa Fe River (pl. 3, fig. D1). North of the river, the gravity gradient broadens appreciably and gravity gradient lines are oriented in three directions (pl. 3, fig. D1): one that trends northeast-southwest and passes just south of audiomagnetotelluric station 4, one that trends north-south near long 106°15′N., and one that trends north-northwest for a short distance near audiomagnetotelluric station 3. According to the bedrock elevation model (fig. D4), the north-south gradient line is associated with a relatively abrupt, 750-m westward increase in the thickness of basin fill, which marks the eastern margin of the Hagan bench and the western boundary of the Cerrillos uplift.

Cerros del Rio Volcanic Field and Cerrillos Uplift

The gravity high associated with the Cerrillos uplift (Kelley, 1952) is a north-south-elongated high located between the Hagan and Santa Fe embayments (HEB and SE, fig. D1). It includes Eocene and Oligocene intrusions in the Ortiz Mountains and Cerrillos Hills, the lateral extent of which is defined by their magnetic expression (magenta outlines near CH and

OM, fig. D1). The gravity expression and geologic relations (chapter A, this volume) suggest that the uplift is a basement-cored structural uplift rather than a dome caused by intrusion of a laccolith (Stearns, 1953; Disbrow and Stoll, 1957; Grant, 1999). Both the geometry and magnitude of the gravity high are analogous to those associated with other north-south-trending rift-flank uplifts along the margin of the Rio Grande rift, such as the Sangre de Cristo and Sandia Mountains on the eastern sides of the Española and Albuquerque Basins, respectively (fig. D1). The Cerrillos gravity high is arranged en echelon with respect to the similarly oriented gravity high associated with the Sandia Mountains (fig. D1), suggesting a tectonic relation.

The northern termination of the Cerrillos uplift is not well resolved. Basin fill thickens gradually to the north and northeast on this side under cover of the Cerros del Rio volcanic field (CDRVF, fig. D3). Ground-based audiomagnetotelluric soundings suggest that the apparent northward dip of the uplift is accommodated at least in part by a fault between stations 4 and 5 (fig. D1), which offsets the Mancos Shale 600 m down to the north (chapter F, this volume). A northeast-trending gravity gradient line passing just south of audiomagnetotelluric station 4 (fig. D1) is south of the fault inferred from the audiomagnetotelluric data, is not represented by a difference in thickness of basin fill (fig. D3), and does not correspond with any obvious magnetic lineament (fig. D5). These relations suggest that the gravity gradient line represents a pre-rift fault, such as one that juxtaposes basement against pre-Tertiary sedimentary rocks as depicted on cross section E-E′ of plate 6.

Jemez Volcanic Field and Saint Peters Dome

A ridge of moderately high gravity values (3–13 mgal) between the Santo Domingo Basin and the Valles caldera trends westerly from Saint Peters Dome almost to the Jemez River (fig. D1). The gravity ridge probably represents a structural ridge on the Precambrian basement. The area is mostly covered by volcanic rocks of the Jemez field (fig. A1), which are unlikely to produce moderate gravity values because of the relatively low densities indicated by models of the Valles caldera (2,350 kg/m^3; Nowell, 1996). On the west side of the gravity ridge, several en echelon northeast-trending gravity gradient lines mark step-like increases in gravity values to the northwest toward the Nacimiento Mountains (fig. D1), where Precambrian rocks are exposed. The step-wise increases in gravity toward exposed Precambrian rocks suggest that the basement steps up toward the Nacimiento Mountains. A step-faulted basement is evident locally near the Jemez fault zone (JZ, figs. A2, A3), which is near the middle of the three gravity gradient lines (fig. D1). The Jemez fault zone consists of multiple east-northeast- and northeast-striking normal faults, which mostly displace Precambrian and younger rocks down to the east (Goff and others, 1988; Kelley and others, 2003). Cross sections constructed from drill holes show multiple normal faults with cumulative displacements on the Precambrian surface of 470 m down to the south between PC–1 and AET–4 and 254 m down to the southeast between PC–1 and VC–1 (fig. D1; Goff and others, 1988). By inference, basement likely steps down from the Jemez fault area to produce the Saint Peters Dome gravity ridge. Profile modeling, discussed in the section Profile Model Across the La Bajada Constriction, suggests that the Precambrian surface south of Saint Peters Dome is nearly at sea level (~2 km depth). This basement elevation, which is ~1,400 m lower than the Precambrian surface at deep well AET–4 (fig. D1; Goff and others, 1988), may represent a high point of the basement ridge because gravity values are highest in the eastern part of the gravity ridge.

Northeast Santo Domingo Basin and La Bajada Constriction

The northern parts of the San Francisco and Sile faults (SF and SI, figs. A2, A3) divides the Santo Domingo Basin into two principal parts: the deep Santo Domingo Basin beneath Santa Ana Mesa and a shallower bench between the San Francisco and La Bajada fault systems (fig. D4). The area of the bench, where the basin fill averages about 1 km thick (fig. D3), generally corresponds with the Hagan bench of Kelley (1977).

The bedrock elevation model shows a trough that is 10- to 14-km wide and trends northeast where the Rio Grande traverses the Cerros del Rio volcanic field (fig. D4). Santa Fe Group sediments and basalts of the Cerros del Rio field collectively are about 1.25 km thick in the trough (fig. D3). Given that time-domain electromagnetic (TDEM) data indicate the Cerros del Rio basalts are 200–300 m thick (fig. F14*A*), we estimate that sediments within the trough are generally 1 km thick. The relative uniformity of the trough between the Española and Santo Domingo Basins in the thickness and bedrock elevation models (figs. D3, D4) suggests that there may be substantial continuity of basin-fill sediments and facies between the two basins.

Regional Aeromagnetic Features

The principal features of the regional aeromagnetic map (pl. 4, fig. D5) are related to igneous rocks, crystalline basement rocks, magnetic sediments, faults, and anthropogenic structures. We discuss these features in order of prominence on the aeromagnetic map.

A strong negative anomaly that corresponds with the Valles caldera along the northern part of the study area (fig. D5) is likely caused by intracaldera Bandelier Tuff. Ash-flow tuffs erupted during two episodes of caldera collapse (1.61 and 1.22 Ma) are recognized as members of the Bandelier Tuff (Gardner and Goff, 1996). They both likely acquired reversed polarities because they cooled during the latter part of the Matuyama magnetic polarity epoch, when the Earth's field was reversed (fig. C5) (Berggren and others, 1995). Paleomagnetic measurements confirm the reversed polarity (Doell and others,

1968). Although the strong negative anomaly corresponding with the Valles caldera indicates high remanence, outflow sheets of Bandelier Tuff produce very weak magnetic anomalies in the Española Basin (Grauch and Bankey, 2003). Thus, Bandelier Tuff is unlikely to be the cause of the strong negative anomalies located outside the caldera west of Saint Peters Dome and adjacent to the northern part of the Cerros del Rio volcanic field. The anomalies are too poorly resolved in the present data set to identify an alternative possibility.

Basalts of the Santa Ana Mesa volcanic field correspond with many small, mostly negative, high-amplitude anomalies that indicate rocks with strong, reversed-polarity remanence (pl. 4, fig. D5). The 2.5-Ma age of the basalts (Kelley and Kudo, 1978; Smith and Kuhle, 1998b) indicates that they erupted during the early part of the Matuyama epoch (fig. C5). Two strongly negative, north-trending, magnetic anomalies on the east and west sides of the field are associated with two principal chains of volcanic vents (Kelley and Kudo, 1978). A strong negative ellipsoidal anomaly occurs just northwest of the exposed field (fig. D5) in an area mostly covered by young piedmont gravels (Chamberlain and others, 1999). The steep gradients of the anomaly, its similarity to the anomalies associated with vents on Santa Ana Mesa, and limited exposures of basalts (Chamberlain and others, 1999) imply that the source of the anomaly is an isolated, buried volcano that is related to the field.

A distinctive pattern of small anomalies, similar to the pattern over Santa Ana Mesa, is associated with the Cerros del Rio volcanic field (pl. 4, fig. D5). This pattern is composed of positive anomalies as well as mostly negative anomalies. The area is discussed in more detail in the section on the Cochiti Pueblo area.

The broad, high-amplitude, positive elliptical anomaly associated with the Cerrillos Hills (fig. D5) encompasses several outcrops of Eocene and Oligocene monzonite intrusions (unit Tmi, pl. 2), indicating that these intrusions form a composite stock. On the basis of the laccolithic characteristics of these intrusions (Disbrow and Stoll, 1957; Giles, 1995), the stock is likely composed of several overlapping cupola intrusions. The Ortiz Mountains are associated with a similar-looking magnetic high, which also delineates the main lateral extent of a stock. Both of the magnetically defined Cerrillos Hills and Ortiz Mountains stocks (CH and OM, fig. D1) have a more limited areal extent than the gravity high of the Cerrillos uplift that encompasses them. The limited extents of the magnetic anomalies and their clear separation from each other are further evidence that the gravity high is caused by a structural uplift that is more extensive than the two separate stocks.

Prominent, broad, high-amplitude anomalies are associated with the Sandia and Nacimiento Mountains in the south-central and northwestern parts of the study area, respectively (fig. D5). These anomalies reflect uplifted Precambrian crystalline basement that has high total magnetization. A similar, but more subdued, magnetic high lies east of the Cerros del Rio volcanic field, within an area of mapped deposits of the Santa Fe Group in the Española Basin (fig. D5). The source of this anomaly has been interpreted as Precambrian basement buried about 1–2 km below the surface (Grauch and Bankey, 2003).

Sharp linear or curvilinear anomalies are apparent in the high-resolution aeromagnetic data where magnetic relief is low (pl. 4, fig. D5). Many of these anomalies correspond with mapped faults (Grauch, Hudson, and Minor, 2001; Grauch and Bankey, 2003). The aeromagnetic data reveal the full extent of the faults where they are concealed beneath surficial deposits and allow a more comprehensive view of the fault patterns. Many of the major faults have prominent expression in the aeromagnetic data. Examples are the Tamaya (TM) and Santa Ana (SA) faults along the northwestern and western sides of the Santa Ana Mesa volcanic field, the San Francisco fault (SF) in the central part of the study area, and the La Bajada fault zone (LB) (pl. 4, fig. D5). The San Francisco fault, which in the gravity data marks the division between the deep Santo Domingo Basin and the Hagan bench, truncates a strong positive linear anomaly that is associated with the volcaniclastic Espinaso Formation exposed at Espinaso Ridge (pl. 4; ER, fig. D5). The linear anomaly is truncated on the north by faults recognized by Kelley (1977), which we call the Hagan Embayment fault zone (HE, fig. D5). The Espinaso Formation also produces mottled aeromagnetic patterns where it is exposed along the west side of La Bajada fault zone and throughout the Santa Fe embayment (pl. 4; SE, fig. D5) (Grauch and Bankey, 2003).

Not all curvilinear or linear anomalies are related to faults. Linear anomalies between Cerros del Rio volcanic field and Santa Ana Mesa are due to topographic ridges composed of basin-fill deposits of the Cochiti Formation (unit QTc, pls. 2, 5). The common correlation of aeromagnetic data with topography in this area indicates that the Cochiti Formation is fairly magnetic, possibly owing to abundant coarse volcanic clasts derived from the Jemez Mountains (Bailey, Smith, and Ross, 1969; Smith and Lavine, 1996; Smith, McIntosh, and Kuhle, 2001). Coarse-grained facies of the Santa Fe Group correspond with higher magnetization in the northern Albuquerque Basin (Hudson and others, 1999). Similarly, correlation of aeromagnetic anomalies with a series of low bluffs along the east side of the Rio Grande, east of Santa Ana Mesa, indicates that Pleistocene ancient Rio Grande gravel deposits composing the bluffs are fairly magnetic (included in unit QTsa, pl. 5; “magnetic bluffs,” fig. D5).

The linear anomaly that trends northwest, subparallel to the Jemez River, from the southern tip of Santa Ana Mesa to the western border of the study area is produced by a cathodically protected pipeline. Very small, isolated, moderate-amplitude positive anomalies, which commonly look like pock marks, are scattered across the aeromagnetic map (pl. 4, fig. D5). These anomalies correspond with anthropogenic features such as landfills, commercial buildings, water tanks, and bridges.

Profile Model Across the La Bajada Constriction

We constructed a two-dimensional model (fig. D6) to fit gravity and magnetic data along a regional profile across the La Bajada constriction (shown on figs. D3–D5 and labeled F-F′ on pl. 2). The profile model provides a general concept of the deep geometry of the La Bajada constriction and neighboring border terranes, which was used to construct the base of the geologic cross section F-F″ (pl. 6). The profile was chosen to cross perpendicular to the northeast-trending trough in the La Bajada constriction (figs. D3, D4), while optimizing its proximity to sources of data, such as gravity stations, wells, and magnetotelluric or audiomagnetotelluric stations (pl. 2). As a consequence, the model cannot fully address many other important features, such as the La Bajada fault zone, because the profile crosses such features obliquely. Gravity data along the profile primarily address the configuration of the basin, whereas magnetic data provide general information on the contacts of the Cerrillos intrusion. In addition, the regional extent of the profile can lead only to general conclusions about the La Bajada constriction, such as major structural blocks and thickness of basin fill.

Knowledge of the physical properties of geologic units involved in the modeling, independent information on their thicknesses and depths, and guides from geologic concepts all are critical for constraining the ambiguities inherent in gravity and magnetic models. The density-depth functions that were developed for the basin-fill thickness and bedrock elevation models (fig. D2) provide reasonable assumptions for densities of the units in the model. Magnetic susceptibilities of the igneous rocks were assigned values that seemed reasonable on the basis of geophysical models for the Española Basin (Grauch and Bankey, 2003). Independent depth constraints come from wells discussed in chapter G (this volume), audiomagnetotelluric and magnetotelluric models described in chapter F (this volume), and concepts developed from geologic studies that are reported elsewhere in this report (primarily chapters A, C, E, and G, this volume) and those by others (Goff, Gardner, and Valentine, 1990; Cather, 1992, 2004; Smith, McIntosh, and Kuhle, 2001; Maynard and Lisenbee, 2002). In addition, a preliminary view of proprietary seismic reflection data (Baldridge and others, 2001) provided conceptual guides just west of the La Bajada fault zone. Note that depth information from the wells and audiomagnetotelluric stations is limited to the top 0.5–1 km, or less than 25 percent of the vertical extent of the model (fig. D6). Individual units that are 100–200 m thick have negligible effect on the fit of the model; for simplicity they are not included in the model. Some geologic units could not be distinguished by physical property (notably the Mesozoic and lower Tertiary rocks); they were modeled as one unit. More detailed discussion of how the independent information was applied and which parts of the model are well or poorly constrained are keyed by number on the profile model (fig. D6) to explanatory notes in table D1.

As in the models of basin-fill thickness and corresponding bedrock elevation (figs. D3, D4), the profile model shows the La Bajada constriction as an asymmetric rift-basin filled with 500 to 1,500 m of Santa Fe Group sediments and Miocene and younger volcanic and volcaniclastic rocks (fig. D6). The deepest part of the basin lies adjacent to the western border terrane, the Saint Peters Dome block. Underlying the rift basin, the profile model is thought to accommodate 1,000–1,300 m of combined thickness of Mesozoic and lower Tertiary rocks, primarily on the basis of geologic considerations (chapter G, this volume).

The western border terrane at Saint Peters Dome consists of structurally elevated Precambrian basement, consistent with interpretations of the regional gravity map discussed in the section Regional Gravity Features. Geologic relations are the primary constraint on the depiction of the sedimentary units overlying the Precambrian basement, where the model shows a poor fit to the gravity data (note 1, fig. D6 and table D1). The gravity data suggest that these units are thinner than expected, that some of the rock units or the basement have a greater density than expected, or a combination of these possibilities.

Over the Cerrillos uplift, the model is consistent with a basement uplift containing the Cerrillos intrusions (fig. D6). The shallow portion of the model is primarily determined from geologic relations (chapter G, this volume; pl. 6*F*). An intrusion of probable Oligocene age beneath Cañada de Santa Fe is indicated in local areas by aeromagnetic and geologic evidence, although it appears to have physical properties that differ from those of the other Cerrillos intrusions (note 6, table D1). Differences in magnetic susceptibilities are required for a model fit of Cerrillos intrusions farther southeast to the observed data (note 9, table D1), which is consistent with a composite stock complex. The nearly vertical boundaries between the differing magnetic susceptibilities on the eastern side of the intrusive complex, which are also required by the model, suggest that laccolithic sills in this area (Stearns, 1953; Disbrow and Stoll, 1957; Grant, 1999) are volumetrically minor compared with the total volume of intrusive material. Grauch and Bankey (2003) reached a similar conclusion from a study of aeromagnetic and gravity data that included the eastern portion of the Cerrillos intrusive complex.

Aeromagnetic Investigations of the Cochiti Pueblo Area

High-resolution aeromagnetic data over the Cochiti Pueblo area (fig. A4) allow us to develop more local aeromagnetic interpretations that are compatible with interpretations of the airborne TDEM data (chapter F, this volume) and the new geologic map compilation (chapters A–E, this volume; pl. 2). Figure D7 displays a color image of the aeromagnetic data within the same geographic area as plate 5 (box on fig. D5). On plate 5, the same aeromagnetic color image is overlain by geologic contacts from the generalized geologic map shown in

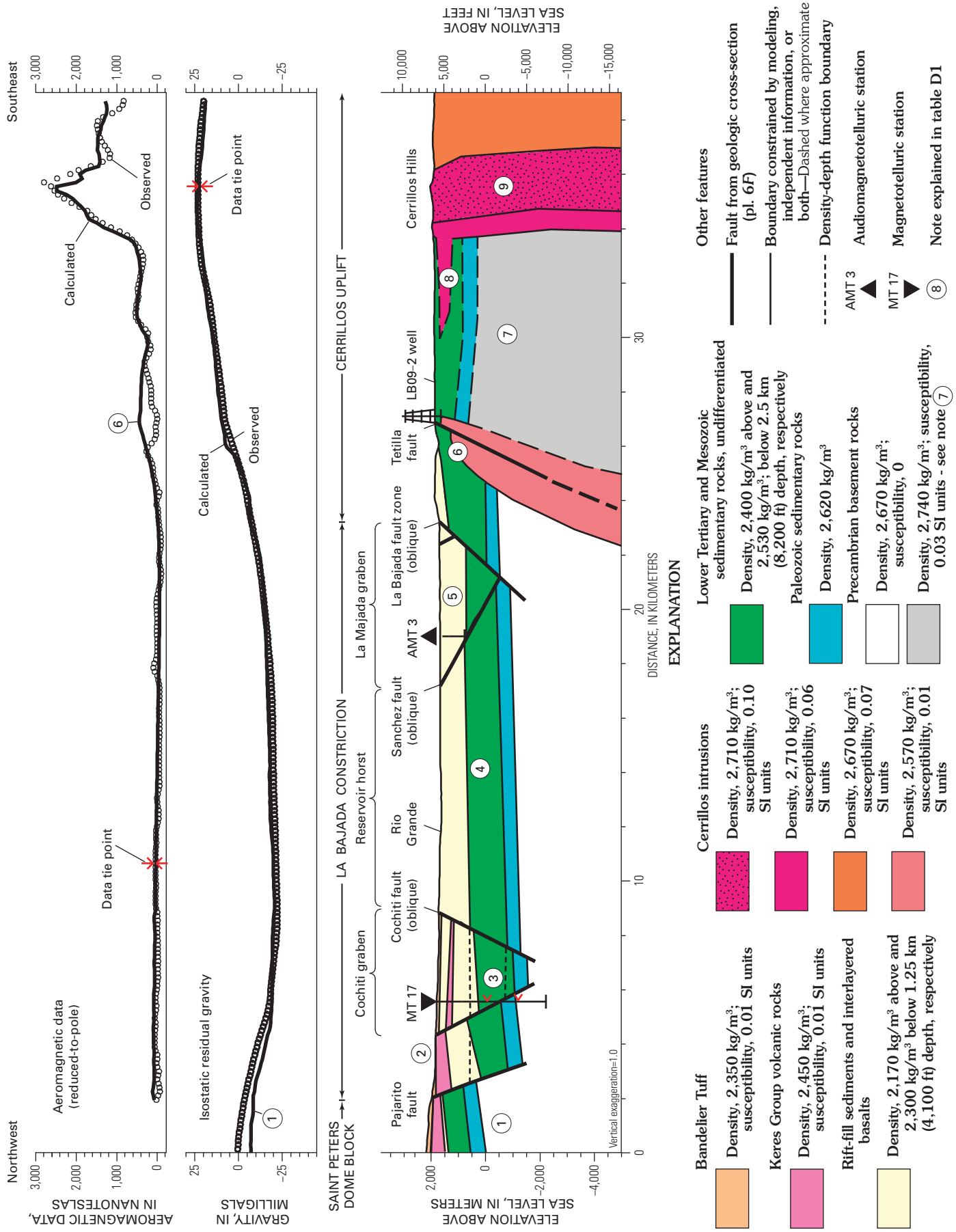
Northwest
Southeast
AEROMAGNETIC DATA, IN NANOTESLAS
Aeromagnetic data (reduced-to-pole)
Calculated
Observed
Data tie point
GRAVITY, IN MILLIGALS
Isostatic residual gravity
Calculated
Observed
Data tie point
SAINT PETERS DOME BLOCK
LA BAJADA CONSTRICTION
CERRILLOS UPLIFT
Cochiti graben
Reservoir horst
La Majada graben
Pajarito fault
MT 17
Cochiti fault (oblique)
Rio Grande
Sanchez fault (oblique)
AMT 3
La Bajada fault zone (oblique)
Tetilla fault
LB09–2 well
Cerrillos Hills
ELEVATION ABOVE SEA LEVEL, IN METERS
ELEVATION ABOVE SEA LEVEL, IN FEET
Vertical exaggeration=1.0
DISTANCE, IN KILOMETERS
EXPLANATION
Bandelier Tuff
Density, 2,350 kg/m3; susceptibility, 0.01 SI units
Keres Group volcanic rocks
Density, 2,450 kg/m3; susceptibility, 0.01 SI units
Rift-fill sediments and interlayered basalts
Density, 2,170 kg/m3 above and 2,300 kg/m3 below 1.25 km (4,100 ft) depth, respectively
Cerrillos intrusions
Density, 2,710 kg/m3; susceptibility, 0.10 SI units
Density, 2,710 kg/m3; susceptibility, 0.06 SI units
Density, 2,670 kg/m3; susceptibility, 0.07 SI units
Density, 2,570 kg/m3; susceptibility, 0.01 SI units
Lower Tertiary and Mesozoic sedimentary rocks, undifferentiated
Density, 2,400 kg/m3 above and 2,530 kg/m3; below 2.5 km (8,200 ft) depth, respectively
Paleozoic sedimentary rocks
Density, 2,620 kg/m3
Precambrian basement rocks
Density, 2,670 kg/m3; susceptibility, 0
Density, 2,740 kg/m3; susceptibility, 0.03 SI units - see note 7
Other features
Fault from geologic cross-section (pl. 6F)
Boundary constrained by modeling, independent information, or both—Dashed where approximate
Density-depth function boundary
AMT 3
Audiomagnetotelluric station
MT 17
Magnetotelluric station
Note explained in table D1

Figure D6 (facing page). Geophysical model of the regional profile oriented northwest-southeast across the La Bajada constriction, coincident with geologic cross section F-F′ (pl. 6*F*; see pl. 2 for line of cross section) or F-F″ (chapter G, this volume). Calculated gravity and magnetic values from model are compared to the corresponding observed isostatic residual gravity and reduced-to-pole aeromagnetic data (pls. 3, 4, respectively). Modeled geologic units and their assigned density in kilograms per cubic meter (kg/m^3) and magnetic susceptibility in SI units are coded by color in explanation. See table D1 for discussion of numbered notes. Magnetic data adjusted by a constant value of 400 nT.

figure C2 and underlain by a shaded digital elevation model. Aeromagnetic anomalies labeled on figure D7 are discussed in the text and provide a key for looking at the same anomalies on plate 5 in comparison with the geology and topography.

Faults were interpreted from the aeromagnetic data following the criteria outlined in the section Locating Faults From Aeromagnetic Data. All interpreted faults are marked on figure D7, but only those that were verified from geologic considerations are incorporated onto plate 2 and discussed in chapter E (this volume). Faults are difficult to detect in the color image of aeromagnetic data (pl. 5, fig. D7). They are best viewed using a shaded-relief display, as in figure D5.

Determining the aeromagnetic expression of exposed igneous rocks in the Cerros del Rio volcanic field places constraints on the nature and age of the buried volcanic rocks elsewhere. Aeromagnetic expression of exposed volcanic units is determined through comparisons of aeromagnetic data, topography, and geology (pls. 2, 5). Many aeromagnetic anomalies have shapes that correspond with topographic features (pl. 5). Examination of these correlations can provide information on the magnetic properties of the rocks composing the terrain (Grauch, 1987). Positive aeromagnetic anomalies that increase in value with increasing relief (positive terrain correlation) indicate a strong induced component, strong normal-polarity remanent component, or both. Negative aeromagnetic anomalies that decrease in value with increasing relief (negative terrain correlation) indicate a strong reversed-polarity remanent magnetization for the rocks that compose the terrain. Preliminary interpretations of polarities from aeromagnetic data for the Tetilla Peak 7.5 minute quadrangle (Sawyer and others, 2001) used magnetic terrain correlations. The interpretations were later generally confirmed by the reconnaissance paleomagnetic study of this report (chapter C, this volume) and are presented in the next section.

Cerros del Rio Volcanic Field

Basalts and andesites of the Cerros del Rio volcanic field possess both reversed and normal remanent magnetic polarities, which are supported by paleomagnetic measurements (chapter C, this volume) and strong positive and negative aeromagnetic anomalies (pl. 5, fig. D7). On the basis of $^{40}Ar/^{39}Ar$ ages, the dual polarities primarily arise from magmatic activity that spanned the transition from the Gauss normal to the Matuyama reversed magnetic polarity epochs at 2.59 Ma (figs. C5, D8). Expression of these polarities in the aeromagnetic data are demonstrated for several mapped volcanic units by comparing the mapped contacts, age data, magnetic terrain correlations, and paleomagnetic measurements (fig. D8). In particular, the relation between positive aeromagnetic anomalies and evidence for normal polarity suggests that moderate- to high-amplitude positive anomalies arise from a dominant normal-polarity remanent magnetization, rather than from a dominant induced magnetization. Negative terrain correlation with Quaternary units likely reflect formation during the latter part of the Matuyama magnetic polarity epoch, coinciding with reverse polarity intervals between 1770 and 1211 ka or 1201 and 1070 ka (fig. C5) (Berggren and others, 1995). An example is the andesite at Cochiti Cone (feature E10, fig. D7; corresponds with unit Qcc, pl. 5).

The relations depicted in figure D8 suggest that the aeromagnetic character of mapped units can be used to help resolve stratigraphic and age relations in the absence of absolute age data (chapter C, this volume), but so doing is beyond the scope of this report. The following general conclusions aid our understanding of buried magnetic sources in the Cochiti Pueblo area.

1. The oldest volcanic units in the field (2.70–2.59 Ma) formed during the Gauss normal magnetic polarity epoch, generally have normal polarity, and are commonly associated with positive aeromagnetic anomalies.

2. Younger volcanic units, Pliocene to Pleistocene in age (2.59 Ma–780 ka), formed during the Matuyama reversed magnetic polarity epoch, generally have reversed polarity, and commonly are associated with negative aeromagnetic anomalies.

Using these relations, we infer that buried basalt of Matuyama age is located in several areas of the volcanic field where strong negative anomalies have no obvious geologic or topographic correlation. One area is north of Tetilla Peak (TP, pl. 1) in the west-central part of the Cerros del Rio field (feature E9, pl. 5 and fig. D7), which is covered by thin Quaternary sheetwash deposits (unit Qsw/Tbt, pl. 5). The source of the negative anomalies is probably buried basalt of Tetilla Hole (unit Tbt), on the basis of samples of this unit in the nearby canyon that give an age of 2.49 Ma (pl. 2) and show reversed polarity (paleomagnetic sample 2MRG–4, pl. 5). An area of negative anomalies in the southwestern part of the field has an elongate shape that is reminiscent of a channel, roughly parallel to the present Cañada de Santa Fe (feature E4, fig. D7). Quaternary sheetwash deposits overlie relatively flat terrain across the area (unit Qsw/Tbr, pl. 5). It may be an old channel, filled with a thickened sequence of reversed-polarity basalt of Caja del Rio (unit Tbr), which is mapped nearby and possesses reversed-polarity remanence (paleomagnetic samples 9MRG–3, 9MRG–10, and 9MRG–11, pl. 5; chapter C, this volume).

Table D1. Explanatory notes keyed to figure D6, Geophysical model of regional profile oriented northwest-southeast across the La Bajada constriction.

Note on figure D6	Explanation
1	Thicknesses of geologic units above the basement derived from geologic constraints (chapter G; pls. 2, 6*F*). The density of the Keres Group volcanic rocks is roughly estimated to be 2,450 kg/m^3, on the basis of expected densities for a mixture of ashflow tuff and volcaniclastic rocks (Telford and others, 1990). The poor fit to the gravity curve could be rectified by a local increase in density of the Keres Group volcanic rocks or Precambrian basement, but geologic considerations discourage further elevation of the Precambrian basement block.
2	Gravity data indicate that the vertical displacement associated with the Pajarito fault zone is distributed over a wide zone, as suggested by the location of the gravity gradient line just southeast of Saint Peters Dome (pl. 3, fig. D1). Therefore, an intermediate block between Saint Peters Dome and the Cochiti graben is required to fit the gravity curve.
3	Cochiti Formation (upper Santa Fe Group) near station MT–17 extends at least 400 m (1,312 ft) deep within the Dome Road well (fig. G5). Depth of penetration of the model for station MT–17 (chapter F) is shown by the line below the inverted solid triangle. Red arrowheads point to the minimum and maximum range of depths (1,900–3,000 m or 6,234–9,843 ft) for the top of the Paleozoic section, which is interpreted as the boundary between low and moderate resistivities as shown on fig. D6. The interface between the Santa Fe Group and underlying lower Tertiary–Mesozoic section is approximately determined by the gravity modeling (fig. D6; bedrock elevation model, fig. D4).
4	The thickness of the Santa Fe Group generally follows the bedrock elevation model (fig. D4). Thickness of underlying section is based on geologic considerations (chapter G, pl. 6*F*) combined with gravity modeling.
5	The oblique angle of the profile model to the strikes of the La Bajada and Sanchez faults inhibits proper modeling of the configuration of the La Majada graben in two dimensions. More comprehensive geologic and geophysical interpretations for the area depict a graben that is filled with sediments, basalt layers, and landslide material to an unknown depth (section Aeromagnetic Investigations of the Cochiti Pueblo Area, chapter D; chapters E and F; pl. 6*F*).
6	A small magnetic stock is indicated below the Cañada de Santa Fe by a lack of correspondence between aeromagnetic patterns and topography in map view (chapter D; anomaly E3 on fig. D7). East of the fault zone, monzonite found at 200 m (656 ft) depth in the LB09–2 well (pl. 6*D*) and exposed in outcrop nearby (pl. 2) argues for a related intrusion at shallower depths, as shown. However, the model requires lower magnetic susceptibility (0.01 SI) and lower density (2,570 kg/m^3) than those for the other Cerrillos intrusions (0.06–0.10 SI and 2,670–2,710 kg/m^3) to fit the gravity and magnetic curves. Altered minerals in the outcrop suggest that the physical properties of the intrusion were modified after emplacement. In addition, the mismatch between the computed magnetic anomaly and the observed data (note 6 along the aeromagnetic curve) coinciding with the eastern half of the intrusion could arise from interference by negative anomalies produced by near-surface reversed-polarity volcanic rocks (fig. D7).
7, 8	Geologic relations at the surface (chapter E; pl. 2) indicate that Upper Cretaceous and older sedimentary units overlying the basement are dipping eastward from the Tetilla fault zone under the volcanic cover of the Cerros del Rio volcanic field. These rocks were intruded to an unknown extent by laccolithic sills related to one of the Cerrillos intrusions (Maynard and Lisenbee, 2002) and by feeder dikes related to the Cerros del Rio basalts (chapter C). The geophysical model cannot adequately represent this geologic complexity. To compensate, we assume a higher magnetic susceptibility (0.03 SI) and density (2,740 kg/m^3) for the underlying basement rocks (note 7) and an arbitrary thickness of material intended to represent the laccolithic character of the Cerrillos intrusion (note 8). In addition, Cerros del Rio basalts are thin in comparison with the scale of the model (pl. 6*F*). They have little influence on the gravity data but contribute in a major way to the observed aeromagnetic data (section Aeromagnetic Investigations of the Cochiti Pueblo Area, chapter D). Because of their minor contribution to the gravity data and their uncertain magnetic properties, we do not attempt to represent them in the model.
9	Composite stocks of the Cerrillos intrusive complex (Maynard and Lisenbee, 2002) are reflected by variations in modeled density (2,670–2,710 kg/m^3) and magnetic susceptibility (0.06–0.10 SI) that are required for a model fit. Even greater variability in the physical properties of the Cerrillos intrusions is likely, which is reflected by the variable match of the computed and observed curves. Although measured values are not available for comparison, the high susceptibilities required by the magnetic modeling indicate that remanence is a major contributor to the total magnetization. Fits to the magnetic curve also indicate that the intrusive contacts are steep at depth.

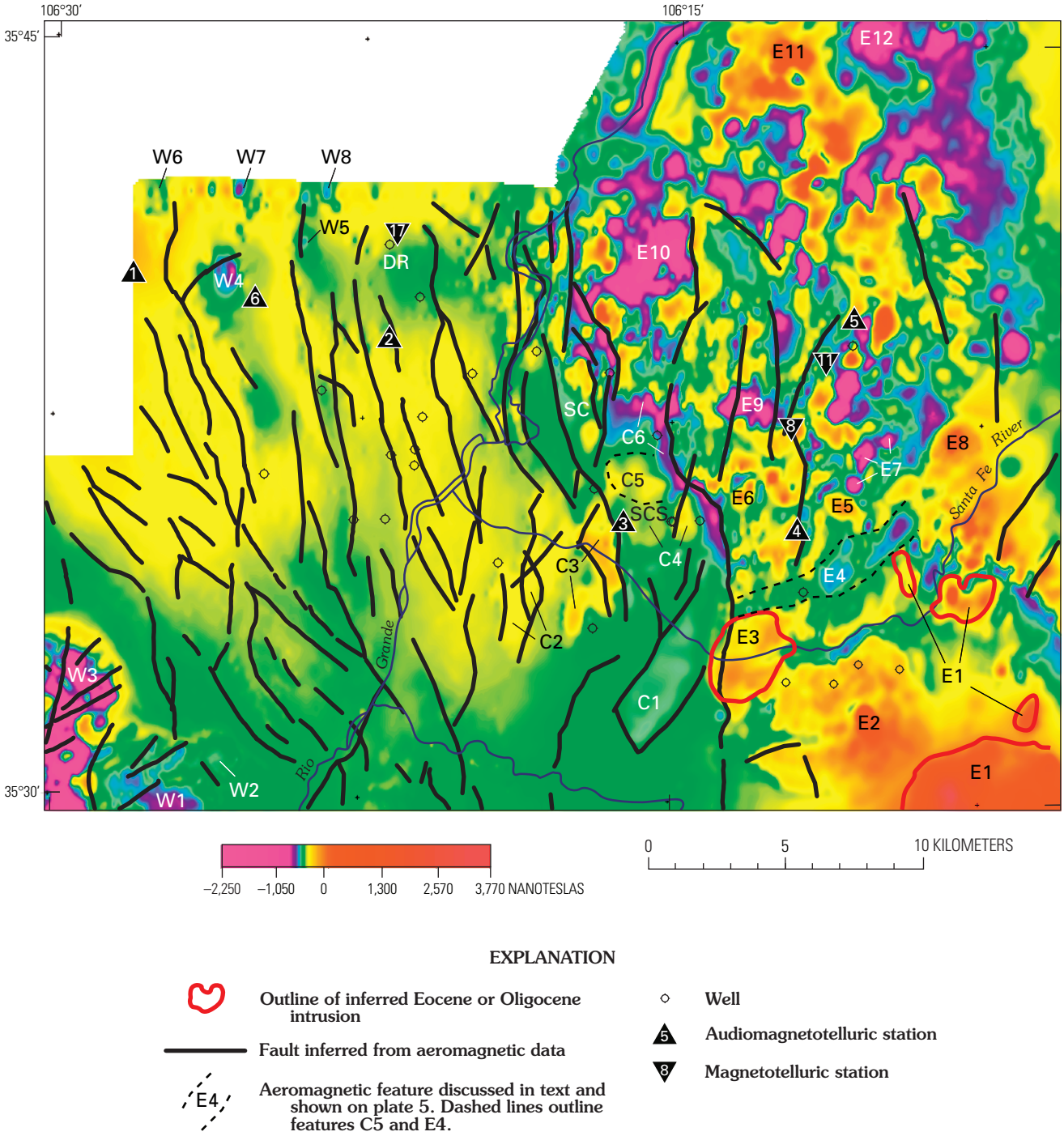

Figure D7. Reduced-to-pole detailed aeromagnetic survey data of Cochiti Pueblo area, shown with color. Interpreted features labeled as discussed in text and referenced in figure D8. Aeromagnetic data are from Sweeney, Grauch, and Phillips (2002). DR, Dome Road well; SC, Sanchez fault; SCS, Santa Cruz Springs Tract well.

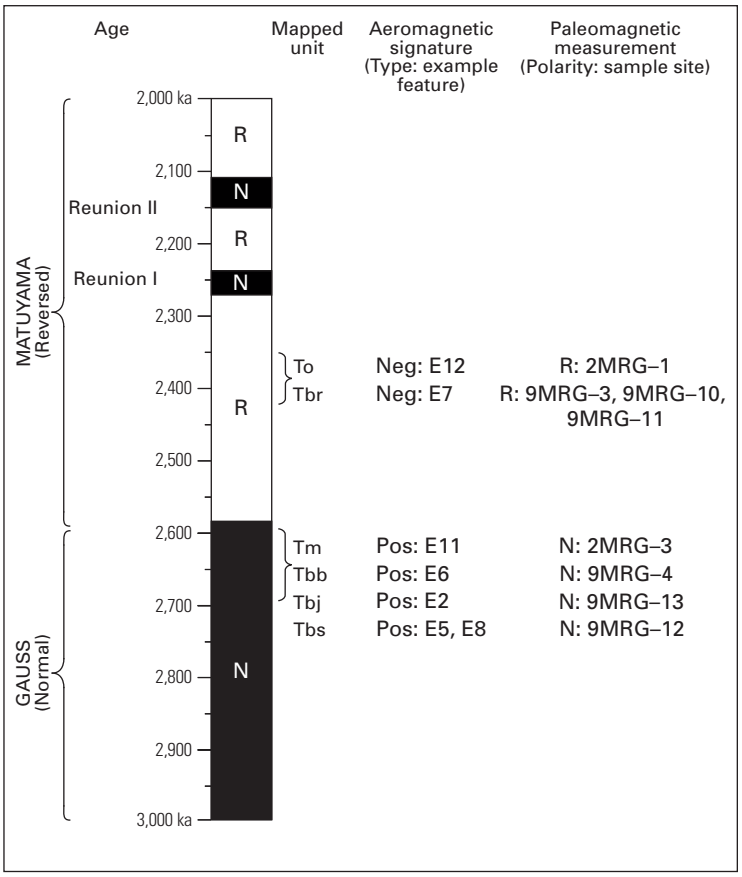

EXPLANATION

Map units (pls. 2, 5)

To **Andesite of Ortiz Mountain**
Tbr **Basalt of Caja del Rio**
Tm **Basaltic andesite of Cerro Montoso**
Tbb **Basalt of La Bajada**
Tbj **Basalt of Mesita de Juana**
Tbs **Basalt of Tsinat Mesa**

Aeromagnetic signature

Pos: **Positive correlation with terrain**
Neg: **Negative correlation with terrain**
Letter-number codes refer to anomalies on figure D7

Paleomagnetic measurement

R: **measured reverse-polarity remanence**
N: **measured normal-polarity remanence**
Numbers refer to sample sites (pls. 2, 5)

Figure D8. Correspondence between age, magnetic-polarity epoch, aeromagnetic signature, and measured paleomagnetic polarities of some mapped upper Cenozoic volcanic units of the Cerros del Rio volcanic field. Aeromagnetic signature based on correlation of anomalies with terrain in the area of a mapped geologic unit. A positive aeromagnetic signature refers to positive anomalies that correlate in shape and value with the shape and relief of topography. A negative aeromagnetic signature refers to negative anomalies that correlate in shape but inversely in value with relief. Shaded and unshaded columns to right of age scale refer to normal- and reverse-polarity epochs, respectively. Magnetic polarity time scale from Berggren and others (1995) and Honey, Hudson, and Obradovich (1998).

The large, high-amplitude, positive magnetic anomaly associated with the monzonite at the Cerrillos Hills stock complex (fig. D5) and several outlying anomalies related to outcrops of monzonite (unit Tmi and feature E1, pl. 5; feature E1, fig. D7) are evident in the southeastern corner of the aeromagnetic map. A positive anomaly in the western part of Cañada de Santa Fe (feature E3, fig. D7) corresponds poorly with terrain even though a deep canyon crosses its northern extent. The lack of correspondence with terrain suggests that the source lies buried below the depth of the canyon bottom. It may be an Oligocene intrusion related to the Cerrillos Hills intrusive rocks (chapter C, this volume). On the other hand, no anomalies are associated with two occurrences of monzonite nearby. One is a small outcrop located about 2 km up-canyon from the feature E3 anomaly (unit Tmi, pl. 2; not shown on pl. 5). The other was found at 200 m depth in well LB09–2 (pl. 6*D*, fig. D6, and discussion in chapter G, this volume), located on the south rim of Cañada de Santa Fe (fig. G1).

Cochiti Graben

Throughout most of the Cochiti graben (figs. A4, E9), the relatively magnetic Cochiti Formation (unit QTc, pl. 5) and axial river gravels (unit QTsa) produce aeromagnetic anomalies with amplitudes of about 20–30 nT (pl. 4, fig. D5). Many of these linear anomalies correlate with terrain (compare pls. 4 and 5), but others have steep gradients that cannot be due solely to terrain. They have been interpreted as faults by following the criteria outlined in the section Locating Faults From Aeromagnetic Data. These and other faults interpreted from the aeromagnetic data (fig. D7) contributed to the overall understanding of faults in the study area (chapter E, this volume).

Several areas in the northwestern part of the study area have negative anomalies that indicate reversed-polarity sources (features W4–W8, pl. 5 and fig. D7.). Although Bandelier Tuff is exposed in the area of two of these anomalies (units Qbt, Qbo, pl. 5; features W7, W8, pl. 5 and fig. D7), its expected low magnetization (discussed previously) suggests that the source is buried underneath the tuff. For two reasons, rocks related to the Bearhead Rhyolite (unit Trb, pl. 2) are the likely source. First, a separate high-amplitude negative anomaly in the area (feature W4) is centered on an exposed lava dome of Bearhead Rhyolite (pl. 5). Second, moderately high resistivities (>200 ohm-m) at depths of 50–200 m (feature W4, fig. F7*B*–*E*) encompass all the negative anomalies except feature W5. The source under feature W5 is not apparent.

Variations in the amplitude and extent of negative anomalies (features W1–W3, pl. 5 and fig. D7) are evident over reversed-polarity basalts on Santa Ana Mesa (unit $Tbk_{1–3}$, pl. 5). The variations in amplitude cannot be directly correlated with the extent of mapped units. For example, the most negative values (less than –500 nT at feature W3) generally follow the oldest mapped basalt (unit Tbk_1, pl. 5), but they only partially correspond with a younger basalt (unit Tbk_2, pl. 5) at the northern mesa edge. Anomalies with moderately negative values (–100 to –500 nT at features W1 and W2) extend over mapped basalt to the mesa edge, but they do not differ in character across a mapped contact between two of the units (Tbk_2 and Tbk_3, pl. 5). These relations suggest that the sources lie mostly beneath the surface, consistent with the interpretation that the high-amplitude negative anomalies are related to intrusive material underlying the vents.

Central Reservoir Horst

The central Reservoir horst lies between the Cochiti and Sanchez faults (figs. A4, E9). The Sanchez fault can be traced by using aeromagnetic data from where it is mapped at the Rio Grande to the south along the sides of elongated anomalies or between breaks in anomalies for about 10 km (SC, fig. D7). This magnetic boundary is most apparent in the color shaded-relief display (SC, fig. D5). The fault is also apparent in resistivity cross sections from the TDEM data (chapter F, this volume). The Sanchez fault also bounds the west side of the La Majada graben (figs. A4, E9).

Two adjacent areas of high magnetic values (amplitudes 150–200 nT) appear related (feature C3, pl. 5 and fig. D7). The areas of high magnetic values correspond with an area of moderate (about 100 ohm-m) resistivities apparent in the TDEM depth slices from 100–200 m (fig. F7*D*–*F*) and in the TDEM cross section for line 630 below 100 m depth at easting 384 km (fig. F11*D*). Magnetotelluric station 3 requires a resistor (100 ohm-m) in this location as well (fig. F5). The correlation of aeromagnetic data and resistivity models and the large vertical extent of the moderate-resistivity values suggest that the source of the aeromagnetic anomalies is a volcanic vent or shallow intrusion. The 2.71-Ma basalt of Peña Blanca (unit Tbpb, pl. 2; not distinguished on pl. 5) may have flowed from the inferred vent. It is exposed about 3 km to the west and dips gently to the east underneath Santa Fe Group sediments toward the inferred vent. Its correspondence with positive aeromagnetic values (feature C2, fig. D7), which suggests a normal-polarity remanence, is compatible with its formation during the normal-polarity Gauss epoch (fig. C5). Another vent and possible source of the Peña Blanca basalt inferred from geologic relations near Cochiti Dam (G.A. Smith, University of New Mexico, oral commun., 1998) is located on the northwest edge of the area of high aeromagnetic values. Its proximity suggests that the vents inferred from geophysical and geological data may be genetically related.

The estimates of minimum depth to the source of anomaly C3, as derived from the gridded RTP data, fall within the range 50–100 m (open circles, pl. 5), which is comparable to the 100-m minimum depth obtained from resistivity models (line 630, fig. F11*D*). In contrast, maximum depth estimates from the pseudogravity grid (× symbols, pl. 5) give values of 100 m on the west compared with 200–250 m on the east. The variation in estimates of minimum and maximum depth implies that the source is thin (sheet-like) on the west and thicker to the east, a configuration that is suggested, but not well resolved, by TDEM data (fig. F11*D*).

La Majada Graben

Within the La Majada graben (figs. A4, E9), two areas of positive magnetic anomalies (features C4 and C5, pl. 5 and fig. D7) have amplitudes on the order of 100 nT. These anomalies correspond with the lateral extents of moderately high resistors in the TDEM inversions: 50–300 ohm-m in feature C4 from 50–100 m depth (fig. F7*B–D*) and 50–125 ohm-m for feature C5 from 70–200 m depth (figs. F7*C–F* and F11*G*, line 626 at easting 385–386 km). Minimum depth estimates from the gridded RTP data (50–100 m, open circles, pl. 5) agree with the resistivity inversions, whereas the maximum depth estimates from the gridded pseudogravity data (250–500 m, H symbols, pl. 5) do not. The large estimates of maximum depth suggest that the magnetic sources are continuous to 250–500 m depth, rather than to more shallow depths as indicated by the TDEM results.

The Santa Cruz Springs Tract well (SCS, fig. D7; fig. G3) may provide an explanation for this discrepancy in the vicinity of feature C4, despite its location within an anomalous area of low magnetic values near an inferred fault (pl. 5, fig. D7). Santa Fe Group sediments in the well are medium to coarse grained and, as compared with deposits higher in the well, contain more volcanic clasts between about 40–100 m depth (fig. G3). Grain size is finer from 100 to 165 m depth. The thickness and depths of coarse material overlying finer material are compatible with the TDEM results down to at least 200 m depth in the vicinity of the well (fig. F7*A–F*). The magnetic properties of the coarse-grained sediments are probably comparable to those of the Cochiti Formation, suggesting that they may be an important contributor to the magnetic anomalies but are not their sole source. Basalt encountered at depths of 165–256 m in the well are dated at 2.59 Ma or older (fig. G3). This age suggests that the rocks have normal-polarity remanence and would produce positive aeromagnetic anomalies (fig. D8). Thus, we suggest that the aeromagnetic anomalies of features C4 and possibly C5 are caused by two separate sources that are considered as one by the depth estimation algorithm. The two sources are coarse-grained Santa Fe Group at a moderate level and basalt of probable Gauss age at deeper levels. The TDEM inversions, which did not penetrate deep enough to detect the basalt, reflect only the variations in the Santa Fe Group.

The strong negative anomaly beside the La Bajada fault (feature C6, pl. 5 and fig. D7) has several possible explanations: (1) Large slump blocks (unit Qlc, pl. 5) that are composed of reversed-polarity basalts and have experienced minor reorientation, (2) reversed-polarity Quaternary flows from Cochiti Cone (chapter C, this volume; feature E10, pl. 5 and fig. D7), (3) effects of the geometry of the magnetic sources at the fault (Grauch, Hudson, and Minor, 2001), (4) magnetic-terrain effects related to the escarpment and the position of the airplane that collected the data, or (5) some combination of these possibilities. The first two possibilities are supported by evidence in the TDEM depth-slice maps of moderately high resistivities that do not extend below 150 m depth (fig. F7). However, the TDEM data in this area are influenced by the large differences in flight elevation across the La Bajada escarpment (chapter F, this volume).

An elongated negative anomaly in the southern part of the La Majada graben (feature C1, pl. 5 and fig. D7) measures about 6–7 km long and 2 km wide, is oriented northeast-southwest, and shows most prominently in the color shaded-relief display (fig. D5). The negative anomaly and shape of the source indicate a reversed-polarity volcanic flow, likely related to one of the volcanic units exposed in the Cerros del Rio volcanic field that erupted after 2.59 Ma (figs. C5, D8). The anomaly edges are fairly linear and abrupt (fig. D5), suggesting that the flow has been faulted or is fault controlled (fig. D7). North of the Santa Fe River, the eastern edge of the anomaly curves into the La Bajada fault zone; to the south it parallels the trace of the southern Tetilla fault zone (pl. 5). Profile-based estimates of depth and source type (described in the section Estimating Depth) were determined for two profiles across the anomaly (red lines, pl. 5). The results indicate the source is thin compared with its width (that is, sheet-like), dips to the east, and lies at 270–340 m depth on the northwestern side and 410–490 m depth on the southeastern side (red ticks along the profiles, pl. 5). For comparison, the range of maximum depths determined from gridded RTP and pseudogravity data is 200–250 m on the northwestern side and 500–700 m on the southeastern side (H symbols, pl. 5). The negative anomaly also has little relation to areas of high resistivity on the TDEM depth slice maps (fig. F7), which is consistent with a source at depths greater than 200–250 m, below the expected detection limit of the TDEM survey in this area (chapter F, this volume).

The buried flow producing the negative anomaly in the southern part of the graben (feature C1, pl. 5 and fig. D7) may be related to the ~2.4 Ma basalt of Caja del Rio (unit Tbr, pl. 5), because this unit has reversed polarity remanence and is exposed nearby, east of the La Bajada fault zone (chapter C, this volume; paleomagnetic sample 9MRG–3, pl. 5). The difference between the estimated 1,150–1,350 m elevation of the buried flow and the ~1,875 m elevation of the exposures of basalt of Caja del Rio on the mesa east of the fault zone is 525–725 m, which gives a rough estimate on the amount of cumulative throw that may have been accommodated by the La Bajada fault zone in the last 2.4 m.y.

Summary

Gravity data for the study area contribute to an overall understanding of basin geometry, the nature and orientation of basement structures, and regional variations in thickness of basin fill. Aeromagnetic data help determine the lateral limits of intrusions, delineate buried faults and igneous rocks and, in some places, clearly distinguish between basalts extruded during different magnetic polarity epochs. Combined with geologic and geophysical constraints provided by the other chapters in this report, gravity and magnetic interpretations contribute directly and indirectly to the subsurface geologic

and hydrogeologic framework model that is presented in chapter G (this volume). The salient interpretations are enumerated as follows.

1. The Santo Domingo Basin is expressed as a large rhombic gravity low, elongated on northeast-trending structures on its northwestern and southeastern sides (fig. D1). The gravity gradients surrounding the low indicate that the basin is bounded by steeply dipping faults of large vertical displacement on the southeastern side and by a homocline or series of down-to-basin faults on the northwestern side. The Hagan bench and the La Bajada constriction occupy the northeastern part of the basin. The Ziana horst and an unnamed trough connecting the Santo Domingo and Albuquerque Basins lie on the southwestern side. Many well-exposed faults along the northwestern side strike north-northwest oblique to the northeast trend of the basin margins (chapter E, this volume; fig. A3).

2. The Cerrillos uplift is reflected in a north-south gravity high that includes and is much larger than the area of Oligocene intrusions of the Ortiz Mountains and Cerrillos Hills, as indicated by the regional magnetic data. This gravity expression is consistent with a basement-cored rift-flank uplift, analogous to the Sandia Mountains. The western boundary follows the southern portion of the La Bajada fault zone, and the eastern boundary corresponds with the western, synclinal limb of the Santa Fe embayment. The northern termination of the Cerrillos uplift is located under the Cerros del Rio volcanic field. A gravity gradient line trending northeast from the mouth of Cañada de Santa Fe is probably due primarily to thickening of pre-Tertiary rocks. Santa Fe Group sediments also thicken farther to the north and northeast.

3. A moderate gravity high that trends westerly from Saint Peters Dome is primarily due to elevated Precambrian basement (approximately 2 km deep) that gradually steps up toward the Nacimiento Mountains, where it is exposed.

4. Within the La Bajada constriction, the gravity data and associated models indicate a northeast-trending trough, 10–14 km wide, that likely contains Santa Fe Group sediments about 1 km thick. The trough projects from the northeastern part of the Santo Domingo Basin just northwest of Cochiti Dam to the southwestern part of the Española Basin about 10 km east of Saint Peters Dome. It is buried under 200–300 m of basalt in the Cerros del Rio volcanic field for most of its extent. A profile model across the constriction emphasizes that the rift basin is somewhat asymmetric in that the deepest part lies adjacent to the Saint Peters Dome block on the west.

5. Comparison of high-resolution aeromagnetic data for the Cerros del Rio volcanic field with topography, age dating, geologic mapping, and paleomagnetic measurements indicates that mapped volcanic units formed during the Gauss normal magnetic-polarity epoch (2.70–2.59 Ma) are associated with moderate- to high-amplitude positive anomalies, whereas those units formed during the Matuyama reversed magnetic-polarity epoch (2.59 Ma–776 ka) are associated with moderate- to high-amplitude negative anomalies. These relations can be used to aid geologic mapping of basalts within the volcanic field and to interpret aeromagnetic anomalies related to buried igneous rocks west of the field.

6. Throughout much of the western half of the Cochiti Pueblo study area, sediments at the surface are magnetic enough to produce aeromagnetic anomalies that correlate with topography. These anomalies are especially apparent over exposures of volcaniclastic deposits of the Cochiti Formation and interfingering axial river gravels. Numerous offsets of these magnetic sediments along faults produce aeromagnetic gradients that appear linear in shaded-relief displays of the data. These aeromagnetic expressions help delineate faults where they are concealed or inferred.

7. The aeromagnetic data help define the southern part of the Sanchez fault, which divides the Reservoir horst on the west from the La Majada graben on the east.

8. An extensive northeast-elongated negative anomaly in the southern part of the La Majada graben is interpreted as a buried, possibly fault-bounded flow that dips to the east and ranges in depth from about 300 to 450 m. The buried flow was probably erupted after 2.59 Ma, possibly related to the ~2.4-Ma basalt of Caja del Rio. These basalts are exposed 525–725 m higher east of the La Bajada fault zone on top of the Caja del Rio Plateau. This elevation difference gives a rough estimate of the amount of throw that may have occurred along the La Bajada fault zone in the last 2.4 m.y.

References Cited

Bailey, R.A., Smith, R.L., and Ross, C.S., 1969, Stratigraphic nomenclature of volcanic rocks in the Jemez Mountains, New Mexico: U.S. Geological Survey Bulletin 1274–P, 19 p.

Baldridge, W.S., Ferguson, J.F., Braile, L.W., Biehler, S., Jiracek, G.R., Gilpin, B.E., Alumbaugh, D.L., Gratwick, D.S., Richards, T.L., and Hasterok, D.P., 2001, Architecture of the southern Espanola Basin (Rio Grande rift) and flank uplift adjacent to the La Bajada fault [abs.]: Geological Society of America Abstracts with Programs, v. 33, no. 5, p. 61.

Bartolino, J.R., and Cole, J.C., 2002, Ground-water resources of the Middle Rio Grande Basin, New Mexico: U.S. Geological Survey Circular 1222, 132 p.

Bath, G.D., 1968, Aeromagnetic anomalies related to remanent magnetism in volcanic rock, Nevada Test Site: Geological Society of America Memoir 110, p. 135–146.

Berggren, W.A., Kent, D.V., Swisher, C.C., III, and Aubry, M.P., 1995, A revised Cenozoic geochronology and chronostratigraphy, *in* Berggren, W.A., Kent, D.V., Aubry, M.P., and Hardenbol, J., eds., Geochronology, time scales and global stratigraphic correlation: SEPM (Society of Sedimentary Geologists) Special Publication 54, p. 129–212.

Biehler, Shawn, Ferguson, J.F., Baldridge, W.S., Jiracek, G.R., Aldern, J.L., Martinez-Garcia, M., Fernandez, R., Romo, J., Gilpin, B., Braile, L.W., Hersey, D.R., Luyendyk, B.P., and Aiken, C.L.V., 1991, A geophysical model of the Española Basin, Rio Grande rift, New Mexico: Geophysics, v. 56, p. 340–353.

Birch, F.S., 1982, Gravity models of the Albuquerque Basin, Rio Grande rift: Geophysics, v. 47, p. 1185–1197.

Blakely, R.J., 1995, Potential theory in gravity and magnetic applications: Cambridge, U.K., Cambridge University Press, 441 p.

Blakely, R.J., and Jachens, R.W., 1991, Regional study of mineral resources in Nevada—Insights from three-dimensional analysis of gravity and magnetic anomalies: Geological Society of America Bulletin, v. 103, p. 795–803.

Butler, R.F., 1992, Paleomagnetism—Magnetic domains to geologic terranes: Boston, Blackwell, 319 p.

Cather, S.M., 1992, Suggested revisions to the Tertiary tectonic history of north-central New Mexico: New Mexico Geological Society 43d field conference, San Juan Basin IV, Guidebook, p. 109–122.

Cather, S.M., 2004, Laramide orogeny in central and northern New Mexico and southern Colorado, *in* Mack, G.H., and Giles, K.A., eds., The geology of New Mexico: New Mexico Geological Society Special Publication 11, p. 203–248.

Chamberlin, R.M., Pazzaglia, F.J., Wegmann, K.W., and Smith, G.A., 1999, Preliminary geologic map of the Loma Creston 7.5 minute quadrangle, Sandoval County, New Mexico, New Mexico Bureau of Mines and Mineral Resources Open-file Geologic Map OF–GM 25, scale 1:24,000.

Connell, S.D., 2002, Geology of the northern Sandia Mountains and Albuquerque Basin, Placitas, and Bernalillo area, Sandoval Country, New Mexico: New Mexico Bureau of Mines and Mineral Resources New Mexico Decision-Makers Field Guide 1, p. 140–143.

Connell, S.D., and Wells, S.G., 1999, Pliocene and Quaternary stratigraphy, soils, and tectonic geomorphology of the northern flank of the Sandia Mountains, New Mexico—Implications for the tectonic evolution of the Albuquerque Basin: New Mexico Geological Society 50th field conference, Albuquerque Basin, Guidebook, p. 379–391.

Cordell, Lindrith, 1976, Aeromagnetic and gravity studies of the Rio Grande graben in New Mexico between Belen and Pilar: New Mexico Geological Society Special Publication 6, p. 62–70.

Cordell, Lindrith, 1979, Gravimetric expression of graben faulting in Santa Fe country and the Española Basin, New Mexico: New Mexico Geological Society 30th field conference, Santa Fe Country, Guidebook, p. 59–64.

Cordell, Lindrith, and Grauch, V.J.S., 1985, Mapping basement magnetization zones from aeromagnetic data in the San Juan Basin, New Mexico, *in* Hinze, William J., ed., The utility of regional gravity and magnetic anomaly maps: Society of Exploration Geophysicists, p. 181–197.

Disbrow, A.E., and Stoll, W.C., 1957, Geology of the Cerrillos area, Santa Fe County, New Mexico: New Mexico Bureau of Mines and Mineral Resources Bulletin 48, 73 p.

Doell, R.R., Dalrymple, G.B., Smith, R.L., and Bailey, R.A., 1968, Paleomagnetism, potassium-argon ages, and geology of rhyolites and associated rocks of the Valles caldera, New Mexico: Geological Society of America Memoir 116, p. 211–248.

Ferguson, J.F., Baldridge, W.S., Braile, L.W., Biehler, S., Gilpin, B., and Jiracek, G.R., 1995, Structure of the Española Basin, Rio Grande rift, from SAGE seismic and gravity data: New Mexico Geological Society 46th field conference, Santa Fe Region, Guidebook, p. 105–110.

Gardner, J.N., and Goff, Fraser, 1996, Geology of the northern Valles caldera and Toledo embayment, New Mexico: New Mexico Geological Society 47th field conference, Jemez Mountains Region, Guidebook, p. 225–230.

Giles, D.L., 1995, Cerrillos mining district: New Mexico Geological Society 46th field conference, Santa Fe Region, Guidebook, p. 61–62.

Gillespie, C.L., Grauch, V.J.S., Oshetski, Kim, and Keller, G.R., 2000, Principal facts for gravity data collected in the southern Albuquerque Basin and a regional compilation, central New Mexico: U.S. Geological Survey Open-File Report 00–490; digital data available from http://pubs.usgs.gov/of/2000/ofr-00-0490/.

Goff, Fraser, Gardner, Jamie, and Valentine, Greg, 1990, Geologic map of the St. Peters Dome area, Jemez Mountains, New Mexico: New Mexico Bureau of Mines and Mineral Resources Geologic Map 69, scale 1:24,000.

Goff, Fraser, Shevenell, Lisa, Gardner, J.N., Vuataz, F.-D., and Grigsby, C.O., 1988, The hydrothermal outflow plume of Valles caldera, New Mexico, and a comparison with other outflow plumes: Journal of Geophysical Research, v. 93, p. 6041–6058.

Grant, P.R., 1999, Subsurface geology and related hydrologic conditions, Santa Fe embayment and contiguous areas, New

Mexico: New Mexico Geological Society 50th field conference, Albuquerque Geology, Guidebook, p. 425–435.

Grauch, V.J.S., 1987, A new variable-magnetization terrain correction method for aeromagnetic data: Geophysics, v. 52, no. 1, p. 94–107.

Grauch, V.J.S., 2001a, Using high-resolution aeromagnetic surveys to map subsurface hydrogeology in sediment-filled basins—A case study over the Rio Grande rift, central New Mexico, USA: Exploration Geophysics, v. 32, p. 209–213.

Grauch, V.J.S., 2001b, High-resolution aeromagnetic data, a new tool for mapping intrabasinal faults—An example from the Albuquerque Basin, New Mexico: Geology, v. 29, p. 367–370.

Grauch, V.J.S., and Bankey, Viki, 2003, Aeromagnetic interpretations for understanding the hydrogeologic framework of the southern Española Basin, New Mexico: U.S. Geological Survey Open-File Report 03–124, available at http://pubs.usgs.gov/of/2003/ofr-03-124/.

Grauch, V.J.S., and Cordell, Lindrith, 1987, Limitations of determining density or magnetic boundaries from the horizontal gradient of gravity or pseudogravity data: Geophysics, v. 52, no. 1, p. 118–121.

Grauch, V.J.S., Gillespie, C.L., and Keller, G.R., 1999, Discussion of new gravity maps for the Albuquerque Basin area: New Mexico Geological Society 50th field conference, Albuquerque Geology, Guidebook, p. 119–124, plates C and D, p. 136–137.

Grauch, V.J.S., Hudson, M.R., and Minor, S.A., 2001, Aeromagnetic expression of faults that offset basin fill, Albuquerque Basin, New Mexico: Geophysics, v. 66, p. 707–720.

Grauch, V.J.S., and Johnston, C.S., 2002, Gradient window method—A simple way to separate regional from local horizontal gradients in gridded potential-field data [abs.]: 2002 Technical Program Expanded Abstracts, 72d Annual Meeting, Society of Exploration Geophysicists, p. 762–765.

Grauch, V.J.S., Rodriguez, B.D., and Deszcz-Pan, Maria, 2002, How geophysical methods have been used to understand the subsurface, *in* Bartolino, J.R., and Cole, J.C., Ground-water resources of the middle Rio Grande Basin, New Mexico: U.S. Geological Survey Circular 1222, p. 36–37.

Hester, D.J., 1998, USGS Middle Rio Grande Basin Study develops terrain data: New Mexico Geographic Information Council, The Map Legend newsletter, spring/summer 1998, v. 9, no. 2, p. 3.

Heywood, C.E., 1992, Isostatic residual gravity anomalies of New Mexico: U.S. Geological Survey Water-Resources Investigations Report 91–4065, 27 p.

Honey, J.G., Hudson, M.R., and Obradovich, J.D., 1998, The occurrence of the Reunion II subchron in lacustrine beds in the Beaver Basin, Utah, *in* Tomida, Y., Flynn, L.J., and Jacobs, L.L., eds., Advances in vertebrate paleontology and geochronology, Tokyo National Science Museum Monograph 14, p. 17–38.

Hudson, M.R., Mikolas, Marlo, Geissman, J.W., and Allen, B.D., 1999, Paleomagnetic and rock magnetic properties of Santa Fe Group sediments in the 98th Street core hole and correlative surface exposures, Albuquerque Basin, New Mexico: New Mexico Geological Society 50th field conference, Albuquerque Basin, Guidebook, p. 355–361.

Jachens, R.C., and Moring, B.C., 1990, Maps of the thickness of Cenozoic deposits and the isostatic residual gravity over basement for Nevada: U.S. Geological Survey Open-File Report 90–404, 15 p.

Kelley, Shari, Kempter, K.A., Goff, Fraser, Rampey, M., Osburn, G.R., and Ferguson, C.A., 2003, Geology of the Jemez Springs 7.5 minute quadrangle, Sandoval County, New Mexico: New Mexico Bureau of Geology and Mineral Resources Open-file Geologic Map OF–GM 73, scale 1:24,000

Kelley, V.C., 1952, Tectonics of the Rio Grande depression of central New Mexico: New Mexico Geological Society 3d field conference, Rio Grande Country, Guidebook, p. 92–105.

Kelley, V.C., 1977, Geology of Albuquerque Basin, New Mexico: New Mexico Bureau of Mines and Mineral Resources Memoir 33, 60 p.

Kelley, V.C., and Kudo, A.M., 1978, Volcanoes and related basalts of Albuquerque Basin, New Mexico: New Mexico Bureau of Mines and Mineral Resources Circular 156, 30 p., 2 plates.

Kucks, R.P., Hill, P.L., and Heywood, C.E., 2001, New Mexico aeromagnetic and gravity maps and data—A web site for distribution of data, version 1.0: U.S. Geological Survey Open-File Report 01–0061, available at http://pubs.usgs.gov/of/2001/ofr-01-0061/.

Maynard, S.R., and Lisenbee, A.L., 2002, Geology of the Picture Rock 7.5 minute quadrangle, Santa Fe County, New Mexico, New Mexico Bureau of Geology and Mineral Resources Open-file Geologic Map OF–GM 51, scale 1:12,000.

Nowell, D.A.G., 1996, Gravity modelling of the Valles caldera: New Mexico Geological Society 47th field conference, Jemez Mountains Region, Guidebook, p. 121–128.

Phillips, J.D., 1997, Potential-field geophysical software for the PC, version 2.2: U.S. Geological Survey Open-File Report 97–725. Available at http://pubs.usgs.gov/of/1997/ofr-97-0725/.

Phillips, J.D., 2000, Locating magnetic contacts—A comparison of the horizontal gradient, analytic signal, and local wavenumber methods [abs.]: 2000 Technical Program Expanded Abstracts, 70th Annual Meeting, Society of Exploration Geophysicists, p. 402–405.

Reid, A.B., 1980, Aeromagnetic survey design: Geophysics, v. 45, no. 5, p. 973–976.

Reynolds, R.L., Rosenbaum, J.G., Hudson, M.R., and Fishman, N.S., 1990, Rock magnetism, the distribution of magnetic minerals in the Earth's crust, and aeromagnetic anomalies: U.S. Geological Survey Bulletin 1924, p. 24–45.

Roest, W.R., and Pilkington, Mark, 1993, Identifying remanent magnetization effects in magnetic data: Geophysics, 58, 653–659.

Russell, L.R., and Snelson, S., 1994, Structure and tectonics of the Albuquerque Basin segment of the Rio Grande rift—Insights from reflection seismic data, *in* Keller, G.R., and Cather, S.M., eds., Basins of the Rio Grande rift—Structure, stratigraphy, and tectonic setting: Geological Society of America Special Paper 291, p. 83–112.

Sawyer, D.A., Shroba, R.R., Minor, S.A., and Thompson, R.A., 2001, Geologic map of the Tetilla Peak quadrangle, Santa Fe and Sandoval Counties, New Mexico: U.S. Geological Survey Miscellaneous Field Studies Map MF–2352, scale 1:24,000.

Simpson, R.W., Jachens, R.C., Blakely, R.J., and Saltus, R.W., 1986, A new isostatic map of the conterminous U.S. with a discussion on the significance of isostatic residual anomalies: Journal of Geophysical Research, v. 91, p. 8348–8372.

Smith, G.A., and Kuhle, A.J., 1998b, Geologic map of the Santo Domingo Pueblo SW 7.5 minute quadrangle, Sandoval County, New Mexico: New Mexico Bureau of Mines and Mineral Resources Open-file Digital Map OF–DM–26, 1 sheet and text, scale 1:24,000.

Smith, G.A., and Lavine, Alex, 1996, What is the Cochiti Formation?: New Mexico Geological Society 47th field conference, Jemez Mountains Region, Guidebook, p. 219–224.

Smith, G.A., McIntosh, W., and Kuhle, A.J., 2001, Sedimentologic and geomorphic evidence for seesaw subsidence of the Santo Domingo accommodation-zone basin, Rio Grande rift, New Mexico: Geological Society of America Bulletin, v. 113, p. 561–574.

Stearns, C.E., 1953, Tertiary geology of the Galisteo-Tonque area, New Mexico: Geological Society of America Bulletin, v. 64, p. 459–508.

Sweeney, R.E., Grauch, V J.S., and Phillips, J.D., 2002, Merged digital aeromagnetic data for the Albuquerque and southern Española Basins, New Mexico: U.S. Geological Survey Open-File Report 02–205, available at http://pubs.usgs.gov/of/2002/ofr-02-0205/.

Telford, W.M., Geldart, L.P., and Sheriff, R.E., 1990, Applied geophysics (2d ed.): Cambridge, U.K., Cambridge University Press, 770 p.

U.S. Geological Survey, Sander Geophysics, Ltd., and Geoterrex-Dighem, 1999, Digital aeromagnetic data from the Sandoval–Santa Fe, Belen, and Cochiti airborne surveys, covering areas in Rio Arriba, Sandoval, Santa Fe, Socorro, and Valencia Counties, New Mexico: U.S. Geological Survey Open-File Report 99-404, 1 CD–ROM

Published in the Central Region, Denver, Colo.
Manuscript approved for publication February 10, 2006
Graphics by authors
Photocomposition by Mari L. Kauffmann (Contractor, ATA Services)
Edited by Mary-Margaret Coates (Contractor, ATA Services)

Structure of the Santo Domingo Basin and La Bajada Constriction Area, New Mexico

By Scott A. Minor, Mark R. Hudson, V.J.S. Grauch, and David A. Sawyer

Chapter E of

The Cerrillos Uplift, the La Bajada Constriction, and Hydrogeologic Framework of the Santo Domingo Basin, Rio Grande Rift, New Mexico

Edited by Scott A. Minor

Professional Paper 1720–E

U.S. Department of the Interior
U.S. Geological Survey

Contents

Abstract 91
Introduction 91
Santo Domingo Basin Structural Framework 92
Regional Tectonic Setting 92
Structural Geometry 92
Faults and Faulting 95
Kinematics 95
Structure of Tetilla and La Bajada Fault Zones 96
Deformational Style of the Tetilla Fault Zone 99
Basinward Shift of Rift Border Faulting 103
Structural Development of Santo Domingo Basin 105
Structural Geology of La Bajada Constriction 106
Structural Symmetry 106
Sanchez and Northern La Bajada Fault Zones 108
Hydrogeologic Character of Santo Domingo Basin Faults 108
Fault Zone Structure and Hydrogeology 108
Fault Zone Cement Patterns 111
Hydrogeologic Summary 113
References Cited 113

Figures

E1. Map of the northern Albuquerque and Santo Domingo Basins showing major intrabasin and basin-bounding faults 93
E2. Rose diagrams showing frequency of orientation and slip geometry of faults in the Santo Domingo and northern Albuquerque Basins 95
E3. Map of major faults in Santo Domingo Basin region highlighting fault-plane exposures with lower angle slickenline rakes or overprinted slickenlines (or both) 97
E4. Geologic map of the southwestern part of Tetilla Peak quadrangle showing structural geometry of the Tetilla fault zone where it is truncated by the younger La Bajada fault zone 98
E5. Rose diagrams showing orientation and kinematic attributes of fault-slip data collected within the La Bajada and Tetilla fault zones 100
E6. Sketch maps showing two structural interpretations of the La Bajada and branching Tetilla fault zones based on structural and paleomagnetic data 101
E7. Equal-area projections of rock magnetic data from samples of Eocene Galisteo Formation 102
E8–10. Maps of:
E8. Northern Albuquerque, Santo Domingo, and Española Basins, showing migration patterns and timing of active rift-border faulting 104
E9. La Bajada constriction area showing structural configuration of intrabasin area and basin borders 107

E10. Northernmost La Bajada fault zone showing inward hooking and scalloped traces where it overlaps with opposite-displacement Sanchez fault 109
E11. Diagram of generalized fault zone showing various architectural components and damage zone fracture types observed in faults exposed in studied basins.....110
E12. Map of Santo Domingo Basin region showing asymmetrically distributed carbonate and silica fault zone cements.....112

Table

E1. Rock magnetic data from Eocene Galisteo Formation, New Mexico.....103

Structure of the Santo Domingo Basin and La Bajada Constriction Area, New Mexico

By Scott A. Minor, Mark R. Hudson, V.J.S. Grauch, and David A. Sawyer

Abstract

The Santo Domingo Basin, located within the Rio Grande rift in northern New Mexico, is topographically subdued and structurally distinct compared with the adjacent Española and northern Albuquerque rift basins, yet it contains structural elements in common with both neighboring basins. A northeast elongation of the Santo Domingo Basin is expressed along its northwestern and southeastern margins by partly buried, relatively large displacement, northeast-striking faults and fault segments that merge with large north-striking fault zones bordering the adjacent basins. Internally, the Santo Domingo Basin exhibits a symmetric, semiconcentric, inward-dipping fault pattern that is centered on the deepest part of the basin as defined by a gravity low. Geologic age relations on the margins of the Española, Santo Domingo, and northern Albuquerque Basins suggest that active border faulting progressively migrated basinward during the Neogene. This relation is clearly demonstrated on the east shoulder of the Santo Domingo Basin by the Tetilla fault zone, an early rift-border and extensional-transfer structure that was abandoned sometime before about 2.5 Ma as basin-margin subsidence was taken up on the La Bajada fault zone farther west. Owing to basinward migration of faulting in the Santo Domingo Basin, intrabasin faults may have longer growth-fault histories and larger dip-slip displacements in the subsurface compared with the border faults, an interpretation supported by the presence of pronounced gravity gradients well basinward of the outer border faults. Fault slickenline observations indicate that most basinal faults formed with nearly pure normal slip and that many of these faults were reactivated with greater components of strike-slip motion. Oblique- and strike-slip reactivated normal faults, concentrated near the northwestern and southeastern basin margins, may be related to the lateral transfer of extensional strain to adjoining basins. Paleomagnetic results from the Tetilla fault zone suggest that such strain transfer is at least locally accommodated by inclined-axis rotation of fault blocks.

In the northeastern part of the Santo Domingo Basin in the area of the La Bajada constriction, northwest-striking overlapping faults of opposing dip project into the basin from opposite sides but die out along strike. These faults include young scalloped splays of the northern La Bajada fault zone and the opposite-dipping, newly defined Sanchez fault. Although these faults do not provide complete structural closure of the northeast end of the basin, they may locally redirect and retard southerly, down-gradient flow of ground water through the constriction area. A series of segmented, right-stepping, faulted antiforms and grabens within the La Bajada constriction track the northeastward migration of the local rift axis.

Fault zones in the Santo Domingo Basin area are characterized by outer damage zones, which typically contain strike-parallel minor fractures that may either enhance or impede groundwater flow along the faults, and by centrally located, low permeability, clay-rich fault cores that likely impede cross-fault flow. Host-rock lithologies strongly influence the width of fault-zone components and control variations in fracturing and other brittle-strain features. An abundance of asymmetrically distributed fault-zone cements indicates that fault-parallel and fault-compartmentalized groundwater flow was, and may continue to be, common in the basin aquifers. The Santo Domingo Basin contains many faults of varied geometry, internal structure, and cement distribution that impart significant heterogeneity of permeability within the basin aquifer.

Introduction

Studies by the U.S. Geological Survey were begun in 1996 to improve understanding of the geologic framework of the Albuquerque composite basin and adjoining areas, in order that more accurate hydrogeologic parameters could be applied to new hydrologic models. The ultimate goal of this multidisciplinary effort has been to provide better quantify estimates of future water supplies for northern New Mexico's growing urban centers, which largely subsist on aquifers in the Rio Grande rift basin (Bartolino and Cole, 2002). From preexisting hydrologic models it became evident that hydrogeologic uncertainties were large in the Santo Domingo Basin area, immediately upgradient from the greater Albuquerque metropolitan area, and particularly in the northeast part of the basin referred to as the La Bajada constriction (see chapter A, this volume, for a geologic definition of this feature as used in this report). Accordingly, a priority for new geologic and geophysical investigations was to better determine the hydrogeologic framework of the La Bajada constriction area. This chapter, along with the other chapters of this report, presents the results of such investigations as recently conducted by the U.S. Geological Survey.

In this chapter we describe and interpret the salient structural features of the Santo Domingo rift basin and overlapping La Bajada constriction and the geometry and kinematics of intrabasin faults. (The reader is referred to chapter A of this report for preliminary geographic and geologic definitions and descriptions of the Santo Domingo Basin, La Bajada constriction, intrabasin structural blocks, and rift-flank uplifted blocks.) An understanding of the structural configuration and structure-induced anisotropy and heterogeneity of the basin and constriction helps elucidate the geologic controls on ground-water flow within and between basins. Below we describe and interpret the fault architecture of the overall Santo Domingo Basin to provide geologic and tectonic context for more detailed discussions that follow of the La Bajada constriction and adjacent uplifted structural blocks. Spatial-temporal patterns of faulting throughout the basin are also discussed. The structural geometry of the La Bajada constriction area is addressed in detail, including the configuration and significance of major, partly concealed, bordering fault zones. Finally, the structural characteristics and cement patterns of fault zones surveyed within the Santo Domingo Basin are summarized, and we then assess the influence that they may have on ancient and modern ground-water flow.

Santo Domingo Basin Structural Framework

Regional Tectonic Setting

The late Cenozoic Rio Grande rift (fig. A1) is an extensional tectonic feature of the Basin and Range structural province (Wernicke, 1992). Temporal changes in the geometry and kinematics of rift faults are commonly related to Neogene clockwise rotation of the regional direction of tectonic extension or the horizontal least principal stress axis (Aldrich, Chapin, and Laughlin, 1986; Chapin and Cather, 1994), which is widely recognized throughout the Basin and Range province (Zoback, Anderson, and Thompson, 1981). Some workers have linked the tectonic history of the rift to northward translation and clockwise rotation of the Colorado Plateau (Hamilton and Myers, 1966; Cather, 1997; Wawrzyniec and others, 2002) (fig. A1). In this interpretation, the rift is a localized transtensional tectonic feature that has accommodated both extension and dextral transcurrent movement along the eastern margin of the plateau block (Wawrzyniec and others, 2002).

The middle part of the Rio Grande rift that is the focus of the present study consists of three structurally linked, north-trending, right-stepping, en echelon extensional basins that formed mainly during the Neogene (Kelley, 1982; Chapin and Cather, 1994). From south to north, they are the northern Albuquerque Basin, Santo Domingo Basin; and Española Basin (figs. A1, A2). Growth faults are common in these basins, implying that faulting and sedimentation were broadly coeval during basin formation (May and Russell, 1994; Connell, Koning, and Cather, 1999). Most basins of the Rio Grande rift in northern New Mexico and southern Colorado form an en echelon chain of half grabens that alternately face east and west (Chapin and Cather, 1994; Russell and Snelson, 1994). The northern Albuquerque Basin is a poorly defined half graben in which basin-fill sediments are mostly tilted gently to the east and are cut on the east side by west-dipping normal faults, including the large-displacement Rincon fault (RC) whose footwall block is expressed by the precipitous front of the Sandia Mountains (Kelley, 1977) (figs. A2, E1). The half-graben structural geometry of the Española Basin is better developed than that of the northern Albuquerque Basin and the graben is tilted in the opposite direction (west) (Kelley, 1982; Chapin and Cather, 1994). The large down-to-east Pajarito fault (PJ) forms the recent western boundary of the Española Basin and marks the eastern limit of the Jemez Mountains within its footwall block (fig. A2).

Structural Geometry

The topographically subdued Santo Domingo Basin is structurally distinct from the adjoining Española and northern Albuquerque Basins, and yet it contains structural elements that appear to be inherited from both. North of the Santa Ana Mesa volcanic field (SAMVF, fig. A2) the Santo Domingo Basin possesses an antiformal fault-block geometry, in which down-to-west normal faults and gentle (<15°) eastward stratal dips prevail in the eastern part of the basin and opposing fault displacements and stratal dips dominate in the northwestern part (figs. A2, E1) (Smith, McIntosh, and Kuhle, 2001). The same pattern of opposing (that is, down-to-basin) fault displacements continue into the southern part of the basin (fig. E1), but strata in this part of the basin form a gently eastward-dipping homocline tilted towards the basin-bounding San Francisco fault (SF, fig. E1) regardless of the dip directions of local intrabasinal faults (Kelly, 1977). The eastward dips of strata in the southernmost part of the basin are similar to dips of strata

Figure E1 (facing page). Northern Albuquerque and Santo Domingo Basins showing major intrabasin and basin-bounding faults. Faults based on an unpublished regional fault compilation by M.R Hudson, S.A. Minor, and V.J.S. Grauch; see Hudson and others (1999) for sources of data. Basin boundaries are based largely on isostatic residual gravity data of Grauch, Gillespie, and Keller (1999). Geophysical data used to infer concealed faults are discussed in text and in chapters D and F, this volume. Faults and fault zones: AD, Algodones; BR, Borrego; CA, Camada; CC, Cañada de Cochiti; CO, Cochiti; EC, Escala; EH, East Heights; EZ, East Ziana; HE, Hagan Embayment; JZ, Jemez; LB, La Bajada; PB, Pico Butte; PJ, Pajarito; PL, Placitas; RC, Rincon; SA, Santa Ana; SC, Sanchez; SH, Sand Hill; SI, Sile; SF, San Francisco; SL, South Luce; SP, South Pajarito; SY, San Ysidro; TJ, Tijeras; TM, Tamaya; TT, Tetilla; VV, Valley View; WZ, West Ziana; ZC, Zia County Dump.

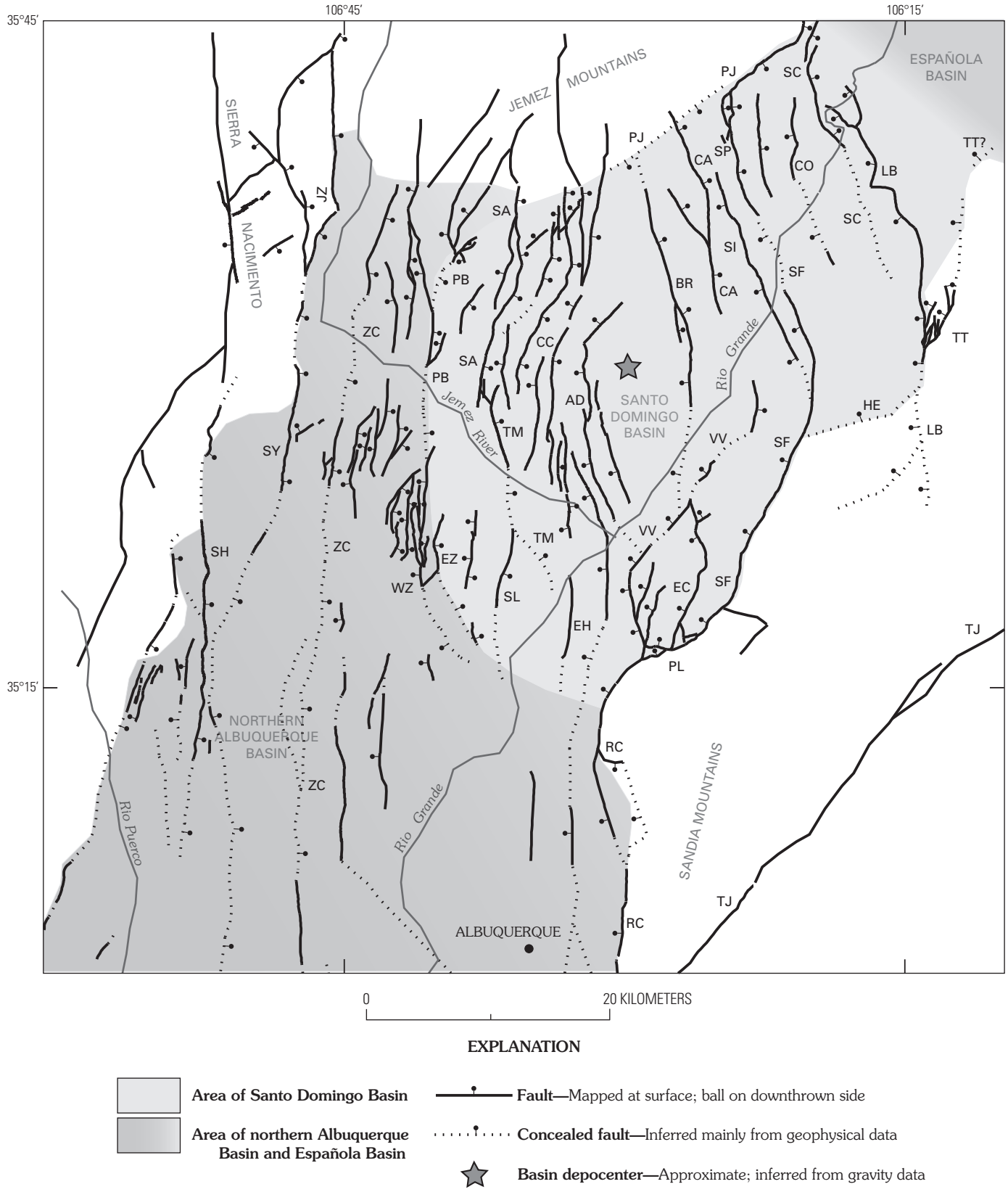

EXPLANATION

Area of Santo Domingo Basin

Area of northern Albuquerque Basin and Española Basin

Fault—Mapped at surface; ball on downthrown side

Concealed fault—Inferred mainly from geophysical data

Basin depocenter—Approximate; inferred from gravity data

in adjoining parts of the northern Albuquerque Basin. Down-to-west faults are more common and have longer traces and greater throws near the southeast and east borders of the Santo Domingo Basin, compared with down-to-east faults, which are more abundant and have longer traces and greater throws near the northwest and west basin borders (fig. E1). Toward the basin center the dominance of one direction of fault dip is diminished and replaced by overlapping or interleaved faults that may dip in either direction (Smith, McIntosh, Kuhle, 2001). The San Francisco (SF) fault bounding the southeast side of the basin connects by means of the Placitas fault (PL) into the Rincon fault (RC), which is the master fault that bounds the Albuquerque Basin half graben (fig. A2, E1). In similar fashion, the Pajarito fault (PJ) bordering the northwest side of the Santo Domingo Basin becomes the master bounding fault of the Española half-graben basin to the north. Thus, fundamental bounding structures of all three basins are structurally linked.

The regional fault compilation shown in figure E1, partly based on high-resolution aeromagnetic data (fig. D5) (Grauch, 1999; chapter D, this volume), reveals within the Santo Domingo Basin a symmetric, semiconcentric fault pattern that is centered on the east-central part of the late Pliocene Santa Ana Mesa volcanic field (SAMVF, fig. A2). The center of this semicircular fault pattern also coincides with the deepest part of the basin, or depocenter (star symbol, fig. E1), defined by isostatic residual gravity (pl. 3, fig. A3) (Grauch, Gillespie, and Keller, 1999). Furthermore, some of the larger semicircular down-to-east faults (Pico Butte (PB)–East Ziana (EZ), Santa Ana (SA)–Tamaya (TM), and Cañada de Cochiti (CC) faults) and down-to-west faults (San Francisco (SF), Sile (SI) and La Bajada (LB) faults) form a crude, opposing, inward-hooking pattern in map view (figs. A2, A3, E1).

Regional gravity data and topography indicate that the Santo Domingo Basin is elongate in a northeast-southwest direction despite the northerly strike of many intrabasin faults (figs. A2, A3, E1) (see also gravity discussion in chapter D, this volume). The southeast and northwest margins of the Santo Domingo Basin are marked by moderate- to large-displacement faults that curve, bend, or splay into northeasterly strikes, parallel to the direction of basin elongation, and collectively define the structural borders of those sides of the basin. Examples include the Placitas (PL), southern San Francisco (SF), Valley View (VV), and Hagan Bench (HB) faults (southeast margin) and the northern Pico Butte (PB), Santa Ana (SA), southern Cañada de Cochiti (CC), and Pajarito (PJ) faults (northwest margin) (figs. A2, A3, E1). A concealed southwest extension of the Pajarito fault inferred from a coincident strong linear gravity gradient (fig. A3) (see chapter D, this volume) forms part of the northwest border of the Santo Domingo basin and may structurally link with a northeast-striking segment of the Santa Ana fault (figs. A2, E1). Thus, the northeast-elongated nature of the basin appears to be structurally expressed along its northwest and southeast margins by partly buried, relatively large displacement, northeast-striking faults and fault segments. Crosscutting and overlapping relations of faults and young basin-fill sediments and volcanic rocks, particularly on the northwest side of the basin, indicate that movement along many of the semicircular, northerly striking faults within the Santo Domingo Basin continued after movement ceased on northeast-striking basin-margin faults.

In contrast to its northeast-trending elongated sides, the Santo Domingo Basin is not completely bounded by faults along its narrower southern and northeast margins. The southwest part of the Santo Domingo Basin is separated from the northern Albuquerque Basin by the Ziana horst (Ziana anticline of Kelly, 1977), a relatively uplifted, fault-bounded, north-trending structural culmination or ridge that has negligible topographic expression (fig. A2) but forms a moderate linear gravity high (fig. A3). The Ziana structural ridge can be projected continuously northward on the basis of gravity data into the footwall block of the basin-bordering Pico Butte (PB) fault (figs. A2, A3). To the south the West Ziana (WZ) and East Ziana (EZ) faults, which bound the Ziana horst, and the nearby Tamaya (TM) fault curve in a concentric manner and project southeastward as inferred from subtle linear aeromagnetic anomalies nearly to the Rio Grande (pl. 4, fig. A2), but the faults do not appear to extend all the way to the southeastern basin-bounding Rincon fault (RC). Thus, the southern end of the Santo Domingo Basin does not appear to be entirely fault bounded even though a broad, weak gravity high separates this part of the basin from the northern Albuquerque Basin (fig. D1; chapter D, this volume). In the northeast Santo Domingo Basin the northwest-striking Sile (SI) and northern San Francisco (SF) faults (figs. A2, A3, E1) separate a deep, main part of the basin from the shallower Hagan bench (fig. D4). The Sile and San Francisco faults do not project across the entire width of the basin, and northeast of them, within the area of the La Bajada constriction, northwest-striking and complexly interleaved faults with opposing dips similarly extend only part way across the basin (fig. E1). Therefore, the aggregate fault network in the constriction area, which is discussed in more detail below, does not form a complete structural barrier between the Santo Domingo Basin and adjacent Española Basin.

Strike and dip were measured on principal slip planes in the cores of numerous fault zones exposed in the Santo Domingo and northern Albuquerque Basins to further characterize the geometry and configuration of intrabasin faults and, along with slip measurements, to investigate fault kinematics (see following section). Most fault planes dip between 55° and 77° (66° mean) (fig. E2). Within the Santo Domingo Basin, faults mostly dip towards the basin center, consistent with the relatively symmetrical fault geometry of the basin. Most fault surfaces are planar at outcrop scale, but several, mainly larger displacement (that is, >100 m), fault surfaces possess large mullions that trend subparallel to the principal slip direction and create curvilinear fault traces.

Dip-slip displacement on individual faults within and bordering the Santo Domingo Basin ranges from less than 10 m to more than 4,000 m at surface exposures, although most faults have dip displacements of less than 100 m. Displacement diminishes along strike towards fault terminations as

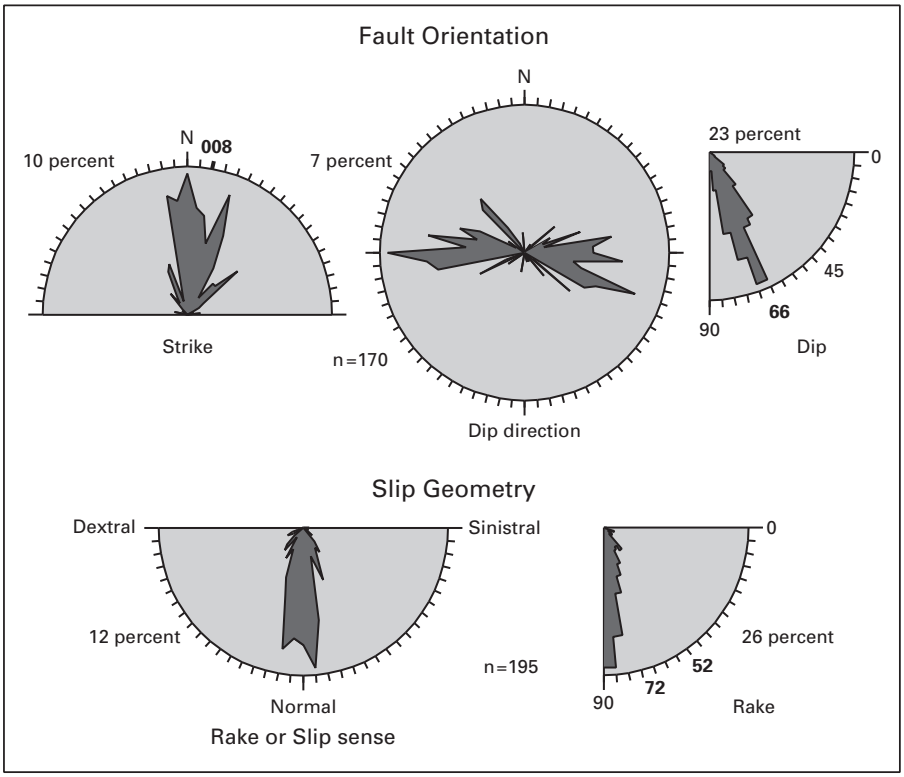

Figure E2. Frequency of orientation and slip geometry of faults in Santo Domingo and northern Albuquerque Basins. Percentage next to each diagram indicates relative maximum radius; numbers in bold indicate mean strike, dip, and rake values. Faults dominantly strike north (008° mean), dip moderately (66° mean) east or west, and have normal slip sense (72° mean rake). Overprinted, generally lower rake slickenlines (52° mean) indicate reactivation of many faults by normal-oblique slip.

increasing amounts of extensional strain are accommodated by adjacent overlapping or en echelon faults of opposing or same dip direction. As a result of growth faulting, the footwall blocks of many, and perhaps most, basin faults have experienced greater cumulative dip displacements than indicated by stratigraphic offsets observed at the surface. Faults with the largest surface displacements (>250 m) and longest traces (>25 km) are concentrated along or near the margins of the basin (figs. A2, E1). Surface traces of several large basin-border faults (La Bajada (LB), Hagan Bench (HB), San Francisco (SF), and East Ziana (EZ)–Pico Butte (PB) faults) are positioned 3–7 km outward of the strong gradients defining the perimeter of the northeast-trending main-basin gravity low (fig. A3). This configuration suggests that the greatest dip slip and basin subsidence occurred along faults such as the Santa Ana (SA), Tamaya (TM), and Valley View (VV) that are concentric with, but located a short distance basinward of, the outer border faults (fig. A3). These inner basin margin faults have smaller surface displacements than the >1.5 km of throw that must be accommodated along them at depth, as is implied by large coincident gravity gradients (chapter D, this volume). Such differential vertical displacement is consistent with growth-fault geometries that have been observed throughout the middle Rio Grande rift (May and Russell, 1994).

Faults and Faulting

Kinematics

Determination of the kinematic history (that is, changes in slip sense and slip geometry) of faults in the Santo Domingo Basin provides clues about the evolving roles of faults within the tectonic framework of the Rio Grande rift. Rake angles of slickenlines (striations) observed on faults in the Santo Domingo Basin have a mean of about 75°, and their mode is 85°–90° (fig. E2) (Minor and Hudson, 2006).

These data, together with the senses of slip revealed by offset stratigraphic units, indicate that most of the faults underwent nearly pure normal slip (fig. E2). Nevertheless, a considerable number of fault surfaces contain younger (crosscutting) normal-oblique slickenlines (rake=30°–60°) or even strike-slip slickenlines (rake ≤30°), indicating that many normal faults were reactivated with greater components of strike-slip motion (Minor and Hudson, 2006). Preliminary analysis of the fault-slip data indicates that the overprinted strike-slip patterns in the Santo Domingo Basin are not mainly the result of an Neogene clockwise rotation of the regional stress field (Zoback, Anderson, and Thompson, 1981), which would have resulted in a basin-wide progressive overprinting of northerly striking sinistral-slip faults and slickenlines by dextral-slip faults and slickenlines. No basin-wide statistical correlation of strike-slip sense with fault strike has been found, although components of dextral slip were observed over a broader range of fault strikes (northwest to northeast) than components of sinistral slip (north to northeast). In local structural domains, either dextral slip components (such as north of Santa Ana Mesa volcanic field) or sinistral slip components (such as southeastern border faults of Santo Domingo Basin) are dominant on faults within a certain strike range. Primary and overprinted oblique-slip and strike-slip slickenlines are concentrated in two fault belts near the northwestern and southeastern margins of the Santo Domingo Basin (fig. E3). The northwestern belt is on trend with a cluster of moderate-rake faults along the western margin of the northern Albuquerque Basin. Oblique slip and strike slip presumably facilitated lateral transfer of extensional strain between structurally linked en echelon basins such as those along the middle Rio Grande rift (Faulds and Varga, 1998; Minor and Sawyer, 1999; Chamberlin, 1999). In the Santo Domingo Basin, the existence of oblique- and strike-slip reactivated normal faults near the northwest and southeast basin margins may also be related to another factor: local rotation of fault blocks or principal stress trajectories (or both). Such rotation may have been produced by concentrated lateral shear owing to large extensional strain gradients along the basin margins. Our Santo Domingo fault-slip observations, in particular the evidence for interspersed dextral and sinistral slip components, do not clearly support regional synrift dextral transtension as proposed by Wawrzyniec and others (2002).

Structure of Tetilla and La Bajada Fault Zones

Excellent exposures in the footwall escarpment of the La Bajada fault zone south of Cañada de Santa Fe (pls. 1, 2; fig. A4) allow detailed structural characterization of the Tetilla fault zone, which may have a structural history and geometry similar to those of other early northeast-striking faults bordering the Santo Domingo and northern Albuquerque rift basins. The Tetilla fault zone is inferred to have formed the eastern border of the Santo Domingo basin in Miocene and Pliocene(?) time before basin-border fault subsidence was transferred to the north-striking La Bajada fault zone (Minor and Sawyer, 1999; Sawyer and others, 2002). The 1.2-km-wide Tetilla fault zone consists of north-northeast- to northeast-striking, mainly down-to-basin faults that cut north- to northwest-dipping Eocene to Miocene sedimentary and volcanic rocks (Galisteo (unit Tg), Espinaso (unit Te), and Abiquiu (unit Tab) Formations) (fig. E4). Faults of the Tetilla zone project northeastward beneath, but do not cut, the younger capping 2.7–2.4-Ma basalt flows of the Cerros del Rio volcanic field. The easternmost down-to-basin fault juxtaposes Eocene to Miocene rocks and synrift basin fill against Mesozoic rocks, and it projects northeastward beneath the basalt flows to a northerly strike in Cañada de Santa Fe (fig. E4). Several smaller north-northeast-striking faults, in turn, branch northward from this eastern border fault (fig. E4). North of Cañada de Santa Fe, the north-striking border fault of the Tetilla fault zone can be projected under Cerros del Rio basalt flows on the basis of surface geologic constraints, aeromagnetic lineaments, and subsurface electromagnetic data indicating abrupt westward thickening of buried Santa Fe Group sediments (pl. 2, fig. D7) (see also cross section C-C′, pl. 6; chapter G, this volume). Electromagnetic data (chapter F, this volume) also suggest that this north-striking boundary fault may extend north of Tetilla Peak under the basalt flows and curve eastward into, and structurally link with, a northeast-striking fault or fault zone that accommodates about 650 m of down-to-north displacement of the basal Santa Fe Group contact with underlying Mancos Shale (pl. 2, fig. F4*A*) (cross sections B-B′ and E-E′, pl. 6). Although this inferred buried fault zone can not be confidently projected farther northeast without additional subsurface data, it plausibly may connect with one or more major structures in the southwestern part of the Española Basin. Thus, the Tetilla fault zone represents an older (earlier than 2.7 Ma) rift-border fault system that may have transferred extensional strain between the Santo Domingo and adjacent Española Basins.

Figure E3 (facing page). Major faults in Santo Domingo Basin region; fault-plane exposures with lower angle slickenline rakes or overprinted slickenlines (or both) are marked. Such faults are concentrated along northwest and southeast margins of Santo Domingo Basin. Faults based on an unpublished regional fault compilation by M.R Hudson, S.A. Minor, and V.J.S. Grauch; see Hudson and others (1999) for sources of data. Basin boundaries are based largely on isostatic residual gravity data of Grauch, Gillespie, and Keller (1999). Geophysical data used to infer concealed faults are discussed in text and in chapters D and F, this volume. Faults and fault zones: AD, Algodones; BR, Borrego; CA, Camada; CC, Cañada de Cochiti; CO, Cochiti; EC, Escala; EH, East Heights; EZ, East Ziana; HE, Hagan Embayment; JZ, Jemez; LB, La Bajada; PB, Pico Butte; PJ, Pajarito; PL, Placitas; RC, Rincon; SA, Santa Ana; SC, Sanchez; SH, Sand Hill; SI, Sile; SF, San Francisco; SL, South Luce; SP, South Pajarito; SY, San Ysidro; TJ, Tijeras; TM, Tamaya; TT, Tetilla; VV, Valley View; WZ, West Ziana; ZC, Zia County Dump.

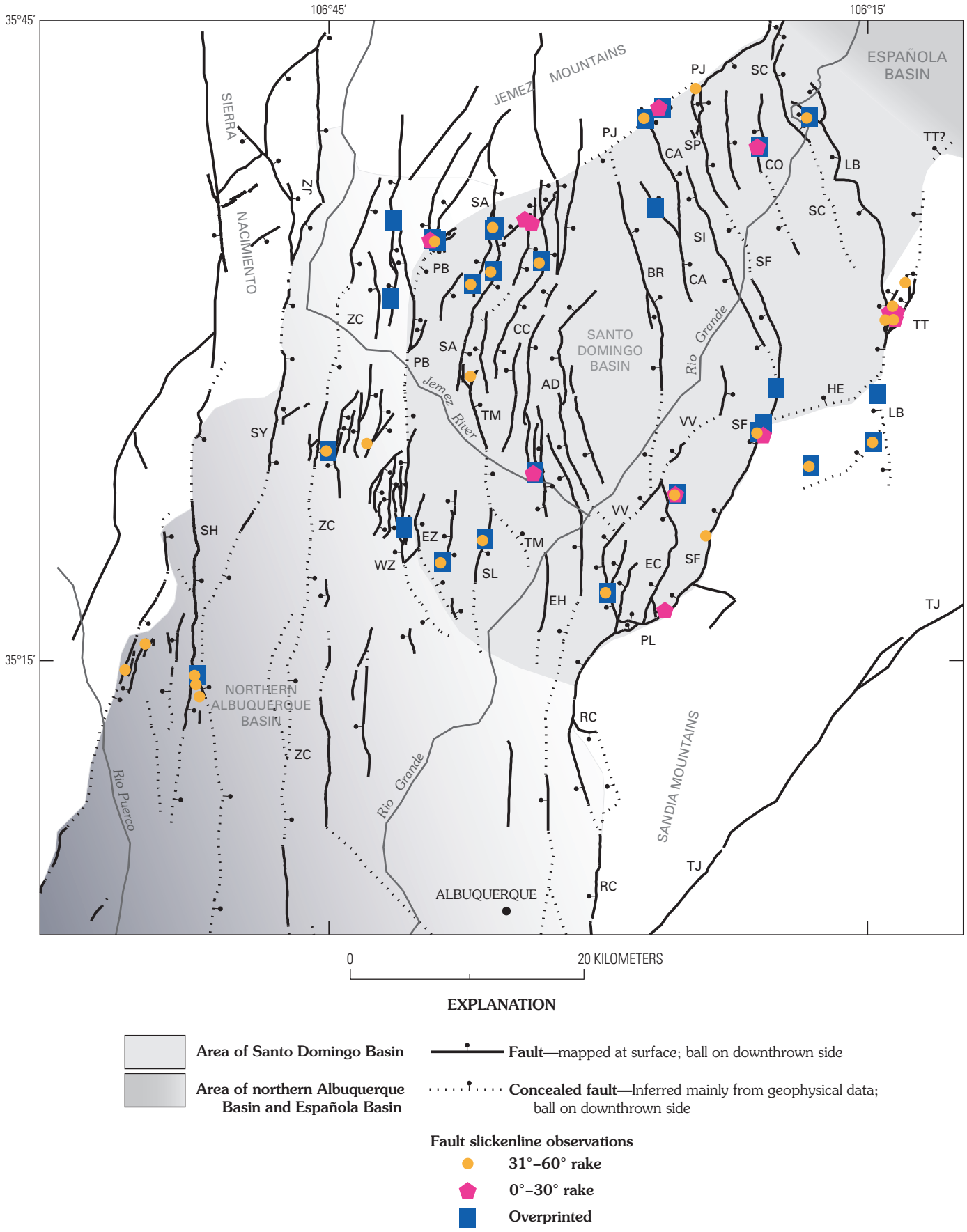

EXPLANATION

Area of Santo Domingo Basin

Area of northern Albuquerque Basin and Española Basin

Fault—mapped at surface; ball on downthrown side

Concealed fault—Inferred mainly from geophysical data; ball on downthrown side

Fault slickenline observations

- **31°–60° rake**
- **0°–30° rake**
- **Overprinted**

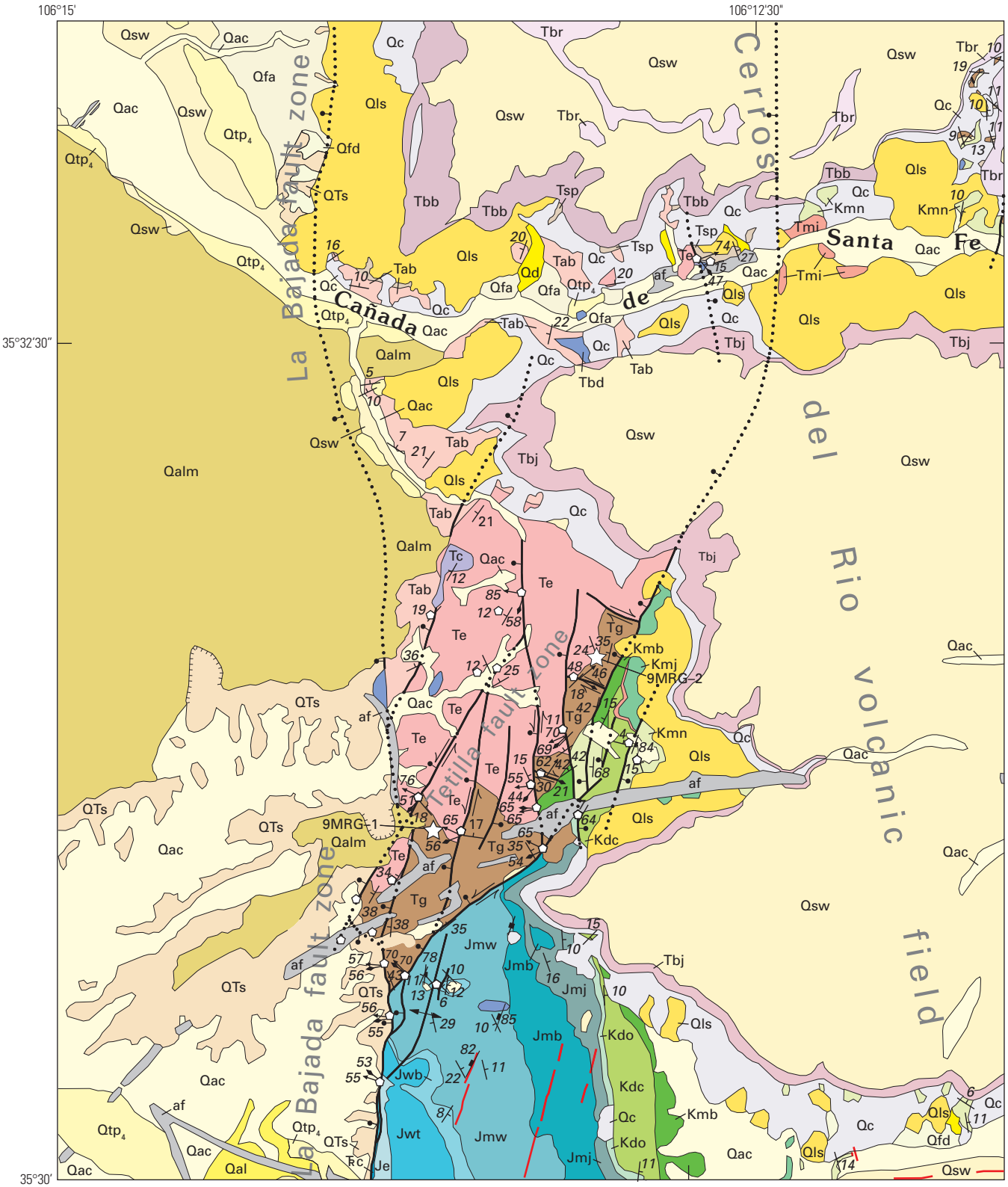

EXPLANATION

Fault—Dotted where concealed; ball and bar on downthrown side; opposing arrows show sense of strike-slip component of movement; single barbed arrow shows direction and angle of dip; diamond arrow shows trend and rake of slickenlines

Anticline

Basalt (Tbj?) dike

0 1 KILOMETER

Bedding—Strike and dip

Joint—Strike and dip

Fault-slip measurement site

Paleomagnetic sample site

Figure E4 (facing page). Southwestern part of Tetilla Peak 7.5 minute quadrangle (from Sawyer and others, 2002) showing structural geometry of Tetilla fault zone where it is truncated by the younger La Bajada fault zone. Refer to plate 2 for explanation of map unit labels. Tetilla fault zone is constrained to be older than 2.7-Ma basaltic flows of the Cerros del Rio volcanic field (units Tbj, Tbb, Tbr) that overlap the northeast projection of the zone, whereas the younger La Bajada zone displaces similar 2.3-Ma flows about 500 m north of map area. Most faults within the Tetilla zone strike north-northeast; have down-to-west, normal-sinistral, oblique-slip displacement; and splay northward off a large-displacement fault bordering the east side of zone. Note small dextral-slip cross faults within exposed Tetilla zone.

Rift-border faulting migrated basinward to the north-striking, normal-slip La Bajada fault zone after 2.7 Ma. The prominent La Bajada fault zone extends along the base of the north-trending La Bajada escarpment; along it, 2.7-Ma early basalt flows of the Cerros del Rio volcanic field were dropped as much as 600 m basinward (pl. 6; fig. E4). Slip surfaces within this fault zone dip 50°–60° W. and possess normal-slip slickenlines (78°–86° S. rake) (fig. E5).

Geologic relations (chapter C, this volume) and electromagnetic data (chapter F, this volume) (fig. F12*A*–*C*) indicate that another northerly striking, possibly early rift-border fault (Cochiti Cone fault, pl. 2 (see also fig. E9)) is truncated by the La Bajada fault zone about 12 km north of the Tetilla fault zone. Small-displacement antithetic faults are also apparent just west of the Cochiti Cone fault as indicated by electromagnetic data (cross section A-A′, pl. 6). Geologic and geochronologic relations indicate that this down-to-basin fault was active during Cerros del Rio basaltic eruptions between 2.6 and 1.1 Ma, so it remained active somewhat later than the Tetilla zone before rift faulting in the area became restricted to the La Bajada and intrabasinal faults farther west.

Deformational Style of the Tetilla Fault Zone

Kinematic, magnetic, and paleomagnetic data from the Tetilla fault zone constrain the deformational style and history of this extensional transfer fault zone. Faults of the Tetilla zone possess normal-oblique–slip slickenlines (50°–75° S. rake); the larger displacement west-dipping faults have sinistral slip components, whereas the smaller east-dipping faults have dextral slip components (fig. E5). The Tetilla faults are generally steeply dipping (60°–90°), consistent with their strike slip components. The sinistral and dextral oblique slip on faults of opposing dip in the Tetilla zone is difficult to explain kinematically. One possible mechanism is opposing-sense rotation of fault blocks about moderately inclined axes owing to bulk sinistral transtension that accompanied lateral transfer of extension along the Tetilla paleorift boundary (fig. E6*A*) (Minor and Sawyer, 1999). Alternatively, northerly ramping that accompanied rift-flank uplift of rocks south of the Tetilla rift-border fault may have tilted original normal-slip faults northward, resulting in apparent sinistral and dextral oblique-slip slickenline orientations (fig. E6*B*). A third possibility is that the observed structural patterns resulted from a combination of the above two mechanisms.

To test for possible inclined-axis rotation associated with the strike-slip components of faulting in the Tetilla fault zone, magnetic fabrics and paleomagnetism of the Galisteo Formation were investigated at two sites. At site 9MRG–1 (see fig. E4 for location), 20 samples were collected from north-northeast-dipping sandstone and siltstone beds distributed through about 24 m of section. At site 9MRG–2, 18 samples were collected from 3 west-dipping sandstone intervals spaced at more or less equal intervals through about 50 m of section. Results of the magnetic and paleomagnetic investigations are summarized in table E1 and fig. E7.

Magnetic fabrics within the Galisteo Formation were investigated by using anisotropy of magnetic susceptibility (Hrouda, 1982). The principal axes of the minimum susceptibility (K3) for all samples are nearly perpendicular to bedding, as is typical for sedimentary rocks (fig. E7*A*). Axes of maximum susceptibility (K1) also cluster at each site; they trend north-northeast at site 9MRG–1 and northwest at site 9MRG–2. These axes lie at high angles to directions of Laramide shortening, and tentatively they are interpreted as intersection lineations between sedimentary and tectonic fabrics developed perpendicular to shortening (Housen and van der Pluijm, 1991).

Paleomagnetic analysis of Galisteo samples employed progressive thermal demagnetization to isolate characteristic remanent magnetization components. Remanent magnetization was unblocked at temperatures as high as 685°C, indicating that hematite was the principal carrier of the remanent magnetization in these red beds. For site 9MRG–1, remanent magnetization components mostly have south declinations and negative inclinations, indicating a reversed polarity (fig. E7*B*). One sample from the middle part of the section carries a normal-polarity remanent magnetization that is roughly antipodal to the reversed-polarity samples; the remanent magnetization direction for this sample was inverted to calculate the site mean direction. Analysis of five samples either did not isolate a single remanent magnetization component during demagnetization or isolated components that had directions that were intermediate between those of the reversed- and normal-polarity samples; these results were omitted from the site mean calculation. For site 9MRG–2, thermal demagnetization isolated well-defined, normal-polarity remanent magnetization in nearly all the samples (fig. E7*B*). Data from one sample that probably unblocked a mixture of normal- and reversed-polarity magnetization were omitted from the calculation of site mean direction.

The mean directions for the two sites became less similar after they were corrected for tilt, which suggests a negative fold test; the inclinations for the sites became more similar after they were corrected for tilt, and the difference between

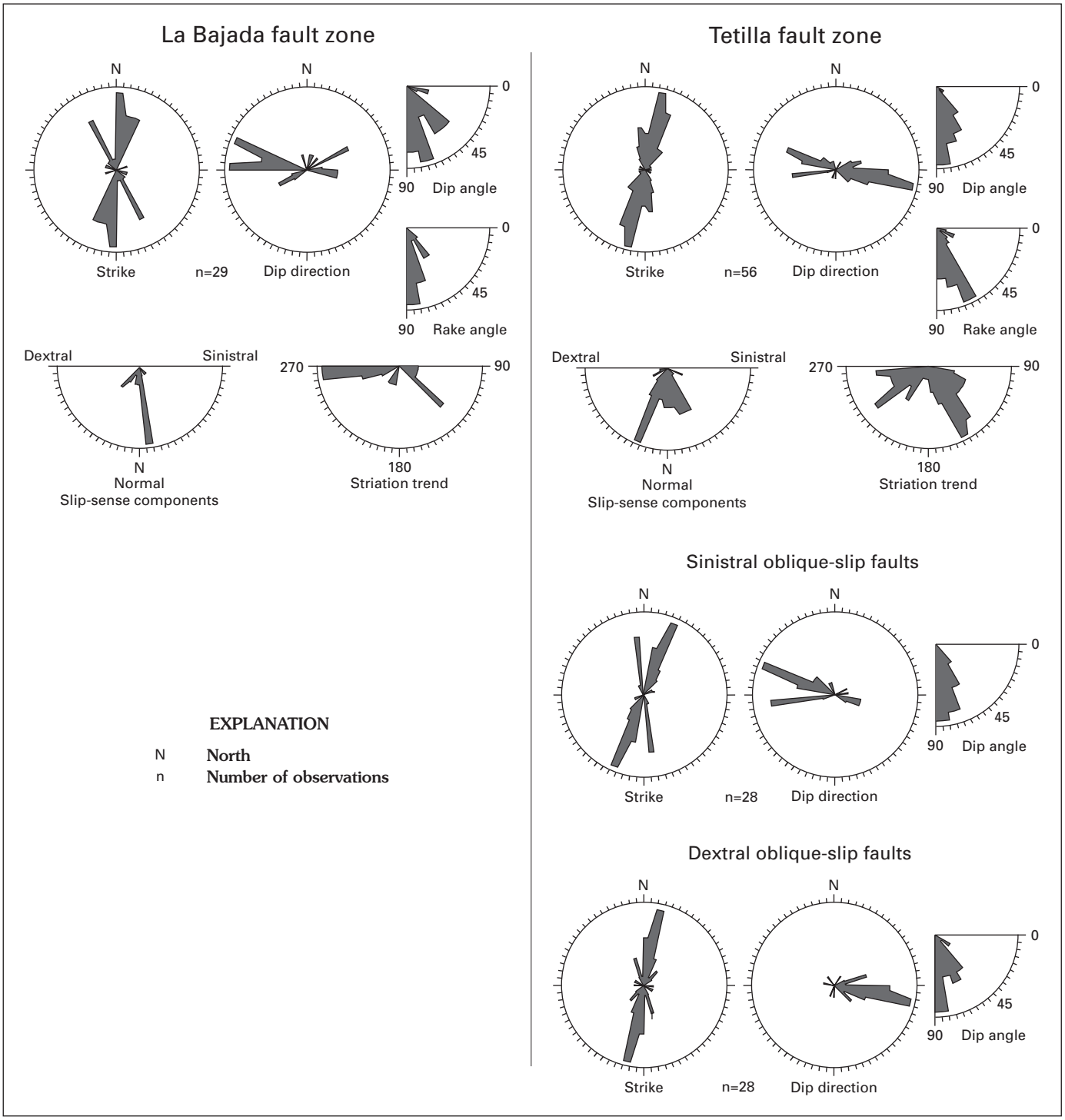

Figure E5. Orientation and kinematic attributes of fault-slip data collected within La Bajada and Tetilla fault zones. On slip-sense components diagrams, Dextral refers to pure dextral slip, Normal to pure normal slip, and Sinistral to pure sinistral slip. Most La Bajada faults dip 45°–80° W. and possess normal-slip slickenside striae (rake, 75°–90° S.). In comparison, Tetilla faults generally dip more steeply (60°–90°) and possess normal-oblique slip striae (rake, 60°–75° S.); west-dipping faults possess sinistral slip components whereas east-dipping faults possess dextral slip components.

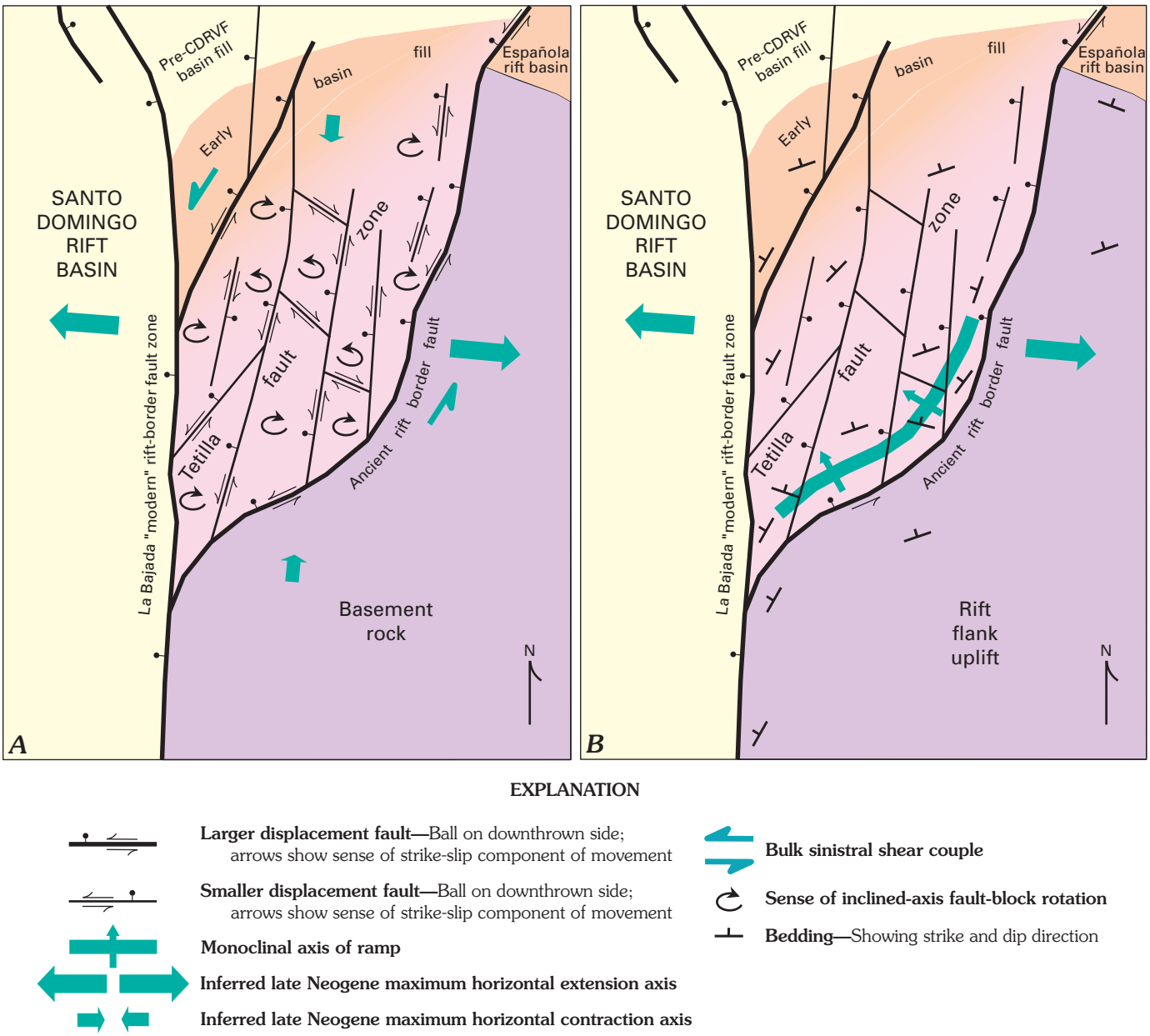

Figure E6. Two structural interpretations (A and B) of La Bajada and branching Tetilla fault zones based on structural and paleomagnetic data. See text for description of interpretations. The two interpretations differ in structural mechanisms invoked for Tetilla fault zone but not in interpreted temporal shift of rift-border faulting and structural role of the La Bajada zone. CDRVF, Cerros del Rio volcanic field.

the tilt-corrected directions is mostly in declination (fig. E7*B*). The difference in declinations of the remanent magnetizations is of the same sense and magnitude as for the declinations of the K1 axes. We interpret these declination differences to reflect differential vertical-axis rotation at the two sites (compare with fig. E7*A*, *B*).

By assuming that the remanent magnetizations carried by hematite were acquired as a chemical remanent magnetization soon after deposition of the Eocene Galisteo Formation, their declinations can be compared with expected directions calculated from magnetic poles of appropriate age from the North American apparent polar wander path (Besse and Courtillot, 1991) to quantify the absolute amount and sense of vertical-axis rotation. Compared with the declination of a 40-Ma expected direction, the vertical-axis rotation estimate at site 9MRG–1 is 19.1°±8.7° (clockwise) and at site 9MRG–2 is –36.6°±7.9° (counterclockwise) (fig. E7*B*). Compared with the expected direction, the inclinations of each site's mean direction after correction for tilt are shallow and statistically distinct at both sites (flattening at site 9MRG–1 is 33.3°±7.4° and at site 9MRG–2 is 17.0°±7.9°). At reversed-polarity site 9MRG–1, this flattening could reflect incomplete removal of a

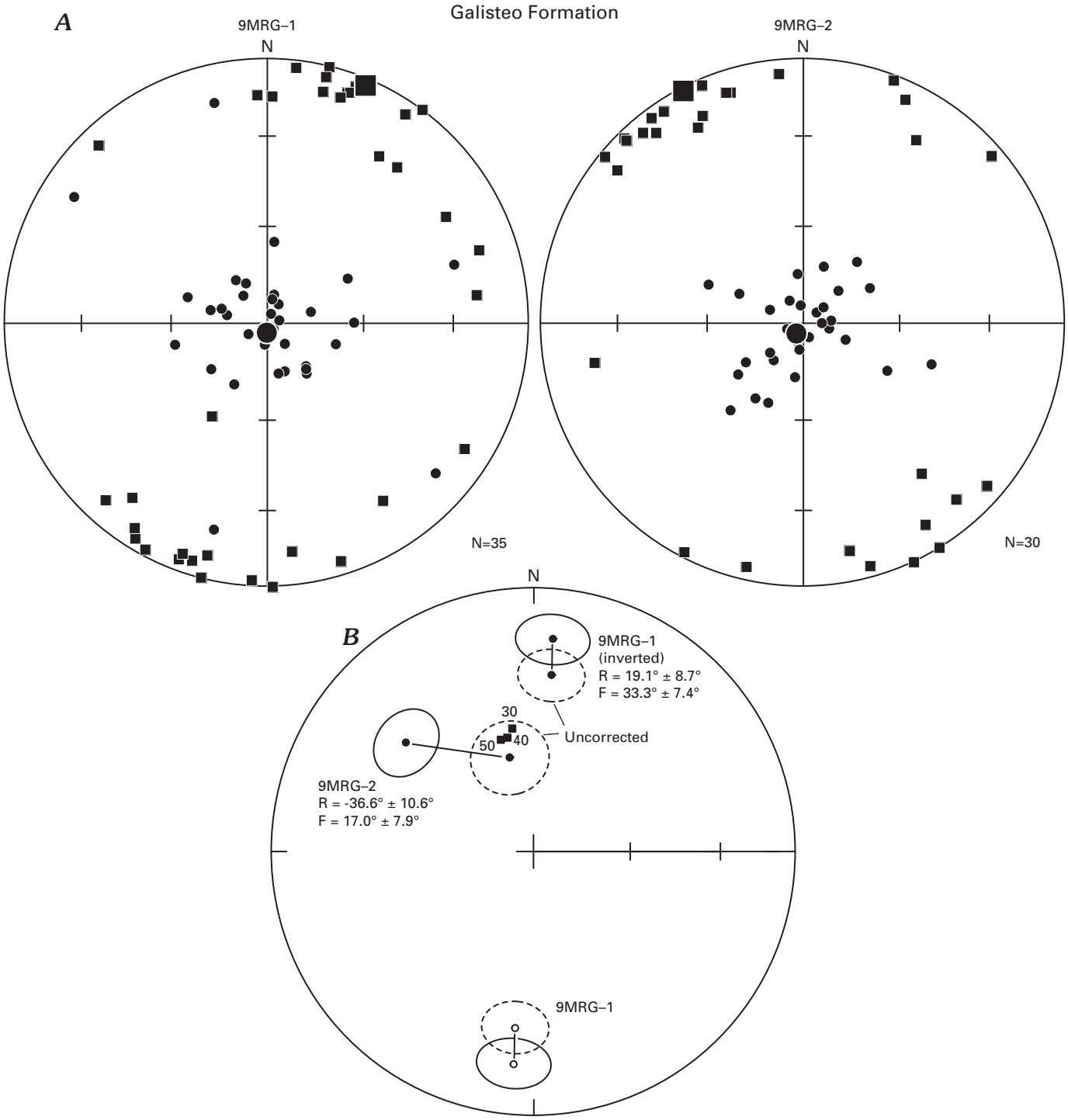

Figure E7. Rock magnetic data from samples of Eocene Galisteo Formation collected at sites 9MRG–1 and 9MRG–2 (see fig. E4 for locations) within Tetilla fault zone. Filled symbols are projections onto lower hemisphere and open symbols are projections onto upper hemisphere. *A*, Anisotropy of magnetic susceptibility data; squares and circles represent maximum and minimum principal axes of magnetic susceptibility ellipsoids, respectively. All directions are corrected for bedding dip. Small symbols are sample directions and large symbols are site-mean directions. *B*, Paleomagnetic site-mean directions before and after correction for bedding dip. Reversed-polarity site mean for 9MRG–1 is inverted through the origin for comparison with normal-polarity expected directions (squares) for the interval 50–30 Ma. For tilt-corrected site mean directions, rotation (R) and inclination flattening (F) parameters were calculated using methods of Demarest (1983) with reference to the 40-Ma expected direction.

Table E1. Rock magnetic data from Eocene Galisteo Formation, New Mexico.

[Latitude and Longitude referenced to 1927 North American datum; N/No, ratio of samples used in calculating the paleomagnetic site-mean directions to number of samples measured; Strike and Dip, tilt corrections in which dip direction 90° clockwise from strike direction; $Decl_0$, $Incl_0$, and $Decl_1$, $Incl_1$ are declination and inclination of the site-mean direction in uncorrected and tilt-corrected coordinates, respectively; R is the resultant vector; *k* is precision parameter (Fisher, 1953); and α_{95} is the radius of the cone of 95 percent confidence about the site-mean direction; $Decl_{K1}$, $Incl_{K1}$ and $Decl_{K3}$, $Incl_{K3}$ are declination and inclination of site-mean principle axes of maximum and minimum magnetic susceptibility, respectively, after tilt correction]

Site	Latitude (°N)	Longitude (°W)	N/No.	Strike (°)	Dip (°)	Dec_{I0} (°)	Inc_{I0} (°)	R	*k*	α95 (°)	$Decl_1$ (°)	$Incl_1$ (°)	$Decl_{K1}$ (°)	$Incl_{K1}$ (°)	$Decl_{K3}$ (°)	$Incl_{K3}$ (°)
9MRG–1	35.5181	106.2234	13/18	282	12	185.8	–33.3	12.4444	22	9.1	186.4	–21.0	22.6	3.1	183.1	87.1
9MRG–2	35.5279	106.2144	16/18	184	38	345.8	59.9	14.9447	14	10.1	310.5	36.6	332.5	1.3	214.8	86.2

normal polarity overprint, but incomplete removal would not explain the anomaly at site 9MRG–2. Most likely the inclination anomalies reflect deflection of the remanent magnetization during sedimentary compaction (Deamer and Kodama, 1990).

These results indicate local block rotations about steeply inclined axes, although the sense and amount of rotation was not uniform. Clockwise rotation (site 9MRG–1) is consistent with the sinistral components of slip recorded on down-to-basin faults (Freund, 1970). Counterclockwise rotation detected at site 9MRG–2 is unexpected given the preponderance of sinistral slip components within the Tetilla fault zone. However, the site is located within a local domain containing several dextral strike-slip cross faults that abut northerly striking sinistral-oblique faults (fig. E4). These and other dextral faults within the Tetilla fault zone may have accommodated local counterclockwise rotation (Freund, 1970).

The opposing-sense, inclined-axis rotations detected within the Tetilla fault zone are consistent with the proposed model that invokes transtension along the Tetilla paleorift boundary (fig. E6*A*). The opposing rotations suggest that bulk strain in the zone was more closely allied with pure shear than simple shear, perhaps owing to concurrent north-south contraction and east-west extension across the zone (fig. E6*A*). The existing data do not permit us to determine if rift-flank uplift and ramping (fig. E6*B*) also contributed to the Tetilla fault zone deformation.

Basinward Shift of Rift-Border Faulting

The geometry and evolution of rift-border faults along other parts of the Santo Domingo Basin margin resemble the Tetilla–La Bajada fault zone system, and we infer similar progressive spatial shifts of rift faulting on both sides of the basin. The east-northeast-striking Placitas fault zone (PL, figs. A2, E1), which forms part of the southeast border of the Santo Domingo Basin, is an oblique-slip transfer fault zone that links the Rincon (RC) and San Francisco (SF) border faults (Connell and others, 1995; Karlstrom and others, 1999). The Placitas zone is similar to the Tetilla fault zone in that north-striking, mainly down-to-basin, normal and oblique-normal faults abut its north side (fig. E3) and northward stratal dips exist within and adjacent to the zone (Connell and others, 1995). Karlstrom and others (1999) inferred that northward stratal tilting in the area mostly resulted from Neogene extensional uplift of the Sandia Mountains, and they invoked Laramide and younger changes in the principal strain axes to explain the complex oblique-slip and strike-slip slickenlines on individual faults in the Placitas zone. They also inferred that the Placitas fault zone and southern San Francisco fault are inactive, and they viewed northern extensions of the Rincon fault—including the Valley View (VV) fault—as the more recently active basin-bounding structures (see also the northern La Bajada fault zone (LB)) (figs. A2, E1).

The Hagan Embagment fault (HE), northeast of the Placitas area (figs. A2, E1), is probably an analogous extinct transfer fault zone that relayed extensional strain to the southern La Bajada fault zone (LB) before activity became restricted to the northern San Francisco fault (SF). Young displacement along the San Francisco fault north of the Hagan Embagment fault intersection is indicated by its offset of the 1.61-Ma lower part of the Bandelier Tuff (Smith and Kuhle, 1998; Smith, McIntosh, and Kuhle, 2001). Kelley (1977) similarly inferred that both the northern San Francisco fault and the Rincon fault south of Placitas are relatively young “bench” faults that had moved more recently than the Tijeras (TJ)–southern La Bajada (LB) “back-bench” fault zones to the east. The youthful geomorphology of the Sandia Mountains block was cited by Kelley (1977) as evidence of recent uplift along the Rincon fault.

Thus, structural and geomorphic evidence indicates that the active eastern borders of both the Santo Domingo and northern Albuquerque Basins shifted west-northwest, towards the rift axis, as the basins developed in the Neogene (fig. E8). The most recently active border faults, such as the northern La Bajada and northern San Francisco faults, are probably long-lived growth faults that were active within the basin interiors early in their histories. Evidence of growth-fault relations along faults within the Albuquerque and Santo Domingo Basins is provided by gravity, seismic, and drill-hole data indicating abrupt stratigraphic thickening on the downthrown sides of faults (Russell and Snelson, 1994). Also, the nature of aeromagnetic anomalies along intrabasinal faults (fig. D5) are consistent with growth-fault structural and stratigraphic geometries (Grauch, Hudson, and Minor, 2001; chapter D, this volume).

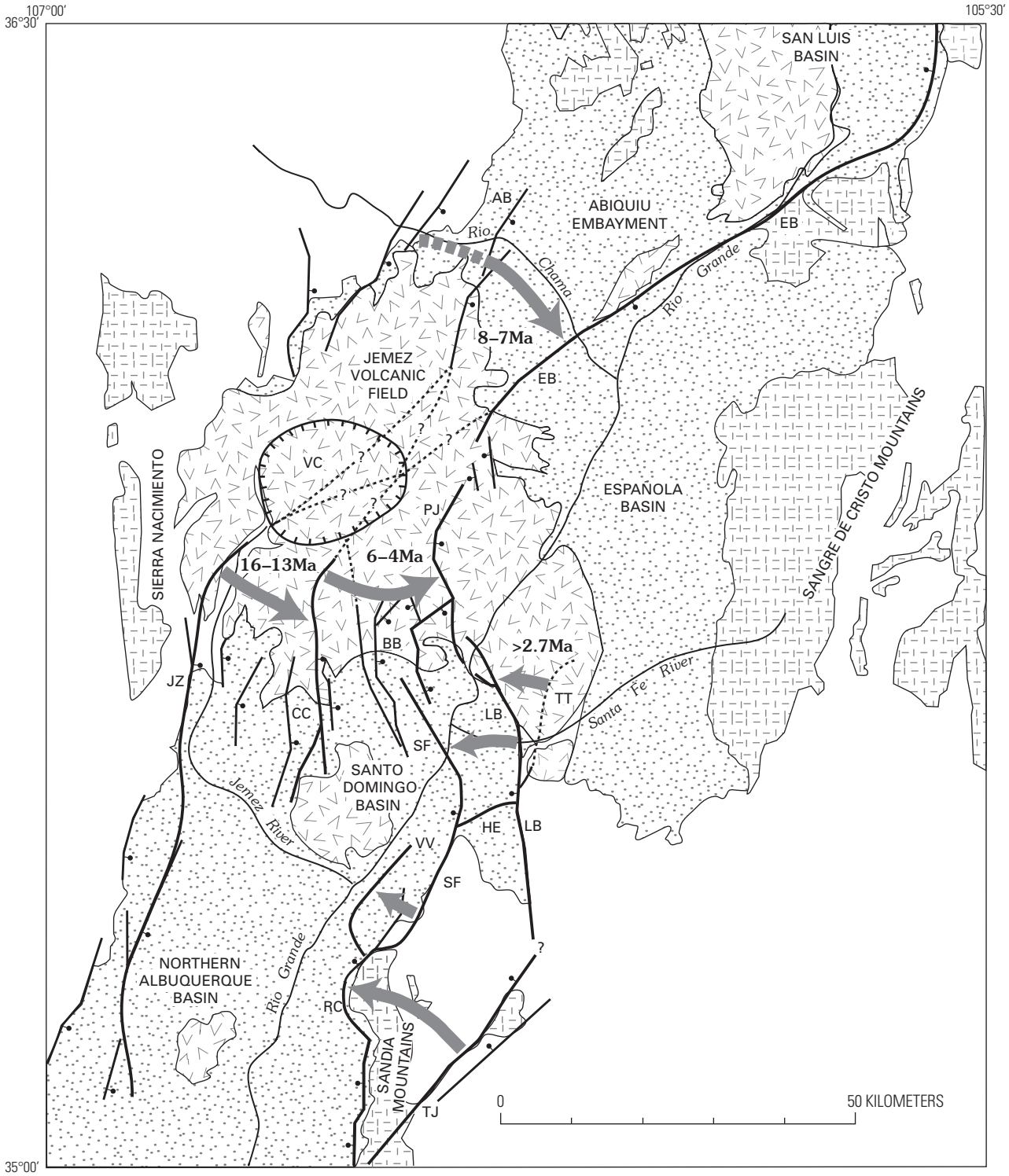

EXPLANATION

- **Pleistocene–Miocene volcanic rocks**
- **Pleistocene–Oligocene basin-fill sediment**
- **Lower Oligocene–Paleozoic rocks**
- **Precambrian rocks**
- **Active or once-active rift border fault—**Bar and ball on downthrown side; dotted where concealed; queried where uncertain
- **Other fault—**Bar and ball on downthrown side
- **Caldera boundry**
- **Migration direction of active rift border faulting—**Dashed where uncertain

Figure E8 (facing page). Northern Albuquerque, Santo Domingo, and Española Basins, showing migration patterns (curved gray arrows) and timing of active rift-border faulting. See text for discussion. Border faults delineated by thick black lines. Modified from Smith, McIntosh, and Kuhle (2001). VC, Valles caldera. Faults and fault zones: AB, Abiquiu, BB, Bearhead Basin; CC, Cañada de Cochiti; EB, Embudo; HE, Hagan Embayment; JZ, Jemez; LB, La Bajada; PJ, Pajarito; RC, Rincon; SF, San Francisco; TJ, Tijeras; TT, Tetilla; VV, Valley View.

Evidence of basinward shifts of rift-border faults on the northwest side of the Santo Domingo Basin and on the west side of the Española Basin was reported by several workers (Gardner and Goff, 1984; Aldrich, 1986; Baldridge and others, 1994). Gardner and Goff (1984) and Aldrich (1986) suggested that the Neogene active structural margin of the rift migrated progressively eastward from the northern Jemez fault (JZ, figs. A2, E1, E8) to the Cañada de Cochiti fault (CC), and finally (about 5 Ma) to the Pajarito fault (PJ) along the edge of the modern Española Basin. The first two fault zones are inferred to have projected to the northeast and linked with northwestern border faults of the Española Basin (Embudo fault zone (EB)) prior to burial by Neogene deposits of the Jemez volcanic field and subsequent collapse of the Valles caldera (VC, fig. E8). The Pajarito fault astride the Saint Peters Dome block (fig. A2) may have formed as early as the late Oligocene and probably remained active while the Española Basin was subsiding (Cather, 1992), whereas down-to-east fault zones farther west, such as the Cañada de Cochiti zone, probably became extinct late in the Miocene.

On the north side of the Jemez volcanic field in the lower Rio Chama area, Baldridge and others (1994) inferred similar abandonment and eastward shift of border faulting toward the axis of the Española Basin. They determined that border faulting in the Abiquiu embayment ended between 8 and 7 Ma and migrated basinward to the Embudo fault zone (EB, fig. E8) (Baldridge and others, 1994). The northeast-striking older Abiquiu border faults (AB) are roughly aligned with the older border faults just south of the Valles caldera (JZ, CC), suggesting that both sets of faults may have once been part of a continuous border fault zone before Jemez volcanism (dotted queried faults, fig. E8).

The inward migration of active border faulting on both sides of the basins suggests that the zone of active rifting progressively narrowed during the Neogene (fig. E8). Faults in the axial parts of the rift basins may have been active for the greatest period of time and may have the most continuous and complete growth-fault histories, whereas toward the margins faults may have gone extinct at progressively earlier times. A similar pattern of faults younging toward the rift axis could alternatively be explained by a fixed-width axial zone of active faulting coupled with rift-normal extension that resulted in outward movement of fault blocks. In such a scenario faults would have become extinct once they moved outside the zone of active rift faulting. However, the cumulative amount of Miocene and younger crustal extension owed to rifting in the region is too small, only about 14 percent across the northern Albuquerque Basin (Woodward, 1977), to fully explain the abandonment of outer rift-border faults. Thus, we view rift narrowing as the chief cause of the observed faulting patterns. Baldridge and others (1994) came to a similar conclusion on the basis of their fault-timing observations on the northwest side of the Española Basin. We suggest that rift narrowing may be due to localization of strain within the crust. In this process rift-related extension occurs in a progressively narrower zone of faults in response to increasingly localized lithospheric necking (Buck, Lavier, and Poliakov, 1999) or to cooling along the rift axis.

Our interpretation differs from that of Kelley (1977), who inferred that a series of narrow central grabens formed first and that the basins got wider with time as rift faulting expanded outward. Kelley's model was based on inferred uplift and erosional stripping of pre-rift Cretaceous and Eocene deposits on the flanks of the early rift and coeval preservation of these deposits within narrow central troughs owing to early trough subsidence. However, this irregular distribution of pre-rift deposits can instead be attributed to localized Laramide structural and depositional patterns (Cather, 1992).

Structural Development of Santo Domingo Basin

To summarize, the salient structural attributes of the Santo Domingo Basin are (1) a northeast basin elongation defined by a large, gravity-expressed, oval, deep (>3 km) inner basin that is flanked along its longer margins by northeast-striking, partly buried, down-to-basin faults; (2) crudely semicircular, concentrically arranged, mostly down-to-basin, normal-slip faults that commonly curve into or offset the northeast-striking border faults on the northwest and southeast sides of the basin; (3) the common presence of late dextral and sinistral oblique-slip and strike-slip fault slickenlines that are interspersed in the longer, northeast-trending, margins of the basin; (4) at the southern and northeastern ends of the basin, interleaved or overlapping faults of opposing dip that project into the basin from opposite sides but which die out along strike and thus do not provide complete structural closure of the basin; and (5) outer limits of active border faulting that appear to have migrated basinward during rifting and abandoned faults on the flanks of the rift whereas inner basin-margin faults remained active throughout longer time spans and acquired more pronounced growth-fault geometries.

Given these observations, we infer that early structural development of the Santo Domingo Basin was dominated by oblique-normal rifting along northeast-striking faults. These early fault trends may have been inherited from northeast-striking Proterozoic shear zones that have been recognized in basement rocks regionally (Karlstrom and others, 1999). Along the rift margins large northeast-striking faults (such as the San Francisco (SF) and Pajarito (PJ) faults, fig. A2)

likely propagated northeastward and southwestward from the northern Albuquerque and southwestern Española Basins, respectively. An intrabasinal network of semicircular faults began to develop soon after establishment of northeast-striking basin-margin faults, presumably to accommodate intrarift, roughly east-west, extension concentrated in the area of the eventual basin depocenter. Many of these concentric faults merged with, curved into, or otherwise used the northeast fault trends, suggesting that the two fault systems eventually evolved into a single kinematically coordinated system. As rifting, basin subsidence, and deposition proceeded, displacement continued or increased on intrabasin, northerly striking, faults and fault segments and on inner-margin, northeast-striking faults, whereas fault movement diminished on the outer flanks of the basin. Thus, rift-related faulting became increasingly centered and spatially confined near the Santo Domingo Basin depocenter (shaded star on fig. E1).

The northeast-striking faults flanking the Santo Domingo Basin likely served as oblique transfer faults (Faulds and Varga, 1998) that accommodated and transferred rift-related extensional strain between the Española and northern Albuquerque Basins (figs. A2, E1) (Kelly, 1977, 1982; Chamberlin, 1999; Karlstrom and others, 1999; Minor and Sawyer, 1999). Early sinistral-oblique slip indicators are expected on most of these faults, if one assumes that the regional maximum extension and minimum horizontal stress directions were east-west to west-northwest–east-southeast (Woodward, 1977; Aldrich, Chapin, and Laughlin, 1986) during the early tectonic history of the Santo Domingo Basin. However, slip data from basin-margin faults indicate that strain was complex, involving normal slip and younger sinistral as well as dextral slip on faults having a variety of orientations. Although poorly understood, such fault-related strain probably reflects localized rotation of fault blocks or principal stress trajectories caused by concentrated lateral shear, which was itself caused by large extensional strain gradients along the basin margins. The dominantly normal-slip character of northerly striking semicircular faults in the central part of the basin suggests that away from the basin margins, faults formed in more favorable orientations with respect to the regional stress field, extensional strain was relatively uniform, and thus lateral shear was diminished.

Given the unique symmetrical structural geometry of the Santo Domingo Basin and its apparent structural linkages to the adjacent rift basins, Smith, McIntosh, and Kuhle (2001), following Faulds and Varga (1998), viewed the entire basin as a broad antithetic, anticlinal, strike-parallel accommodation zone linking the opposing northern Albuquerque and Española half-graben basins. We adopt this structural interpretation of the Santo Domingo Basin and, furthermore, suggest that the overall semicircular fault pattern partly resulted from the mechanical interaction and interference of overlapping, oppositely dipping faults that propagated and splayed northward and southward into the basin from as far as the margins of the adjoining basins.

Structural Geology of La Bajada Constriction

Structural Symmetry

The La Bajada constriction area in the northeast part of the Santo Domingo Basin possesses a structural symmetry that reflects overlapping structural elements inherited from the Española Basin and northern Albuquerque Basin (fig. A2) (Smith, McIntosh, and Kuhle, 2001). This area has a north-northwest-trending structural grain that is imparted by interleaved down-to-east and down-to-west faults (pl. 2, fig. E9). Down-to-west faults (La Bajada and San Francisco fault zones) are most common east of the Rio Grande and increase in throw towards the south, whereas faults with opposite throw and displacement gradients prevail west of the Rio Grande (such as South Pajarito and Camada faults) (fig. E9). Along the northwest side of the La Bajada constriction, surface traces of several of the larger intrabasin faults abut, curve into, or end just south of the northeast-striking Pajarito border fault zone. In the southeast part of the constriction, concealed but aeromagnetically expressed intrabasin faults apparently terminate well short of the La Bajada fault zone (pl. 2, fig. E9). Thus, basin-fill deposits in the northeast part of the constriction may have some structural connection with similar deposits to the southwest, which may facilitate downgradient flow of ground water through the constriction (see chapter G, this volume, for further discussion of this topic).

Smith, McIntosh, and Kuhle (2001) described antiformal (opposing) stratal dips in the northeast part of the Santo Domingo Basin, which is expressed by gentle (≤15°) east dips east of the Cochiti graben and gentle west dips west of the graben (cross sections A-A′, B-B′, and F-F″, pl. 6; fig. E9). The axial Cochiti graben is bounded by the opposite-dipping South Pajarito and Cochiti faults and contains gently dipping beds cut by a graben-parallel, small-displacement fault. South of the graben the antiform axis steps westward and is expressed by relatively abrupt reversals in stratal dip across the Camada fault (sections C-C′ and D-D′, pl. 6; fig. E9) (Smith, McIntosh, and Kuhle, 2001). In general, stratal dips are greatest in fault blocks directly adjacent to the antiform axis (or Cochiti graben) and gradually decrease towards the east and west margins of the basin (pl. 6; fig. E9).

Figure E9 (facing page). La Bajada constriction area showing structural configuration of intrabasin areas and basin borders. Gray background shading shows topography of area. North-northwest structural grain of basin interior is oblique to northeast trend of La Bajada constriction and basin-border faults (such as the Pajarito fault). Interleaved intrabasin faults displace sediments down both to southwest and northeast.

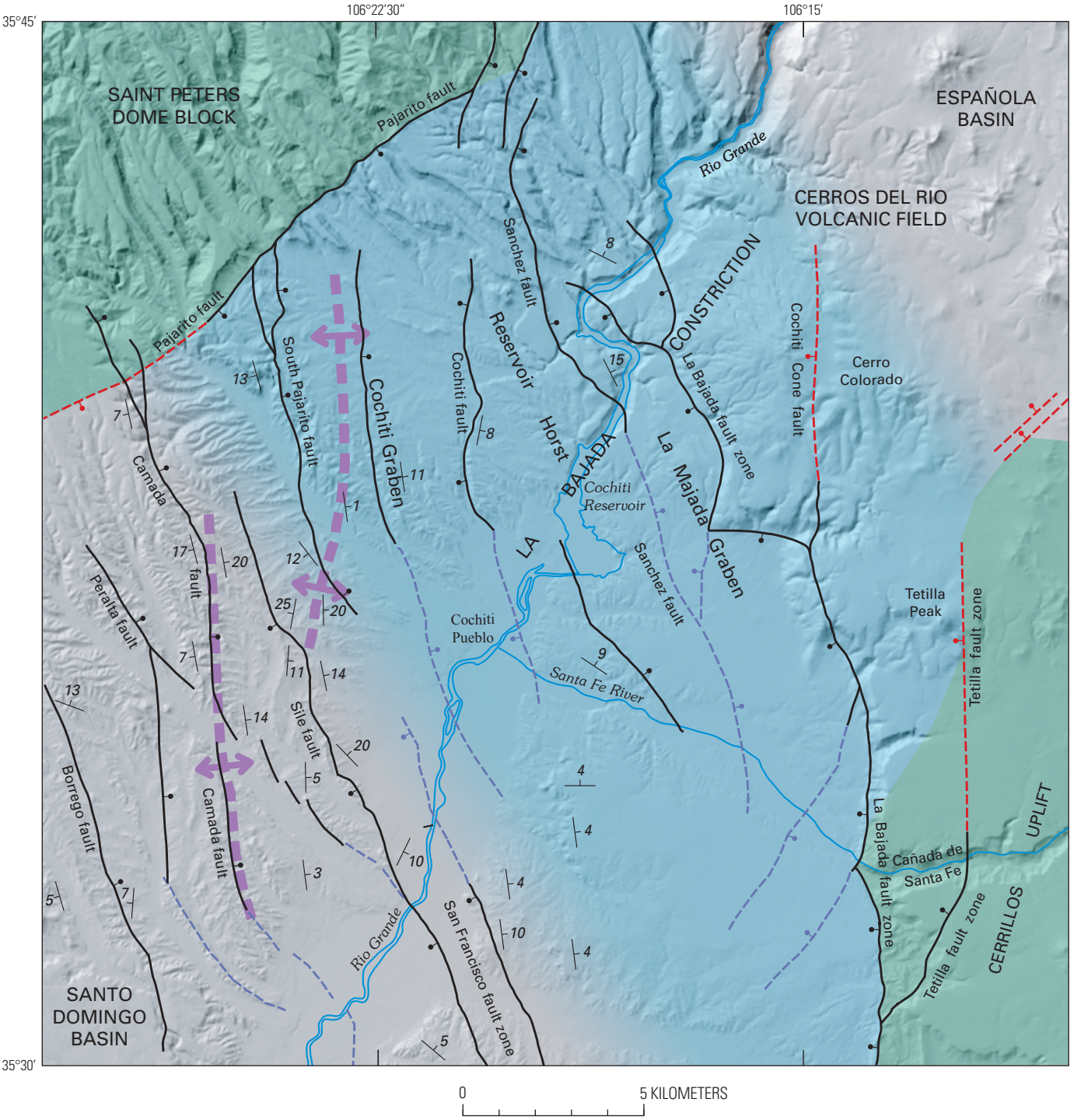

EXPLANATION

Area of La Bajada constriction

Areas of rift-flank uplift

Exposed fault or fault zone—Ball on downthrown side

Concealed fault—Inferred from aeromagnetic lineament

Concealed fault—Inferred from gravity gradient or magnetotelluric soundings

Antiform axis—Approximately located

14 **Bedding**—Strike and dip direction

East of the Cochiti graben and adjacent Reservoir horst is the narrower and possibly younger La Majada graben, which is bounded by basinward-hooking strands of the La Bajada fault zone and the opposite-dipping Sanchez fault (figs. E9, E10). Although not antiformal, the northern part of this graben, where the La Bajada fault zone converges and dies out toward the adjacent Sanchez fault, may represent the youngest in a series of segmented, right-stepping, faulted antiforms or grabens that track northeastward migration of the rift axis (see discussion in next section). Latest movement on the northern La Majada graben faults (that is, northern La Bajada and Sanchez faults, fig. E9) postdates eruption of the 1.14-Ma basaltic andesite of Cochiti Cone (unit Qcc, pl. 2) and possibly follows deposition of the 55-ka El Cajete tephra (unit Qec, pl. 2) (chapter G, this volume).

The structural symmetry and rift history described above generally support the tectonic model of Smith, McIntosh, and Kuhle (2001). They inferred a complex pattern of back-and-forth, "seesaw" subsidence and tilting in the northeast part of the Santo Domingo Basin, including the La Bajada constriction area, in which the locus of normal-fault activity alternated between sides of the basin. As a refinement to the "seesaw" model, we suggest that subsidence within the Santo Domingo Basin was accommodated by faults propagating simultaneously southward and northward from, respectively, the Española and northern Albuquerque Basins. We infer that basin-margin faulting also shifted towards the basin axis as rifting proceeded, resulting in a narrowing zone of active rifting. Within the La Bajada constriction area, basin-axis faulting apparently stepped progressively right, or northeast, toward the narrowest part of the constriction and the young northern La Majada graben (fig. E9).

Sanchez and Northern La Bajada Fault Zones

The northern La Bajada fault zone and nearby Sanchez fault are discussed in detail in this section to elucidate the structural evolution and configuration of this important narrow part of the La Bajada constriction. The La Bajada fault zone strikes northward from where it crosses the older Tetilla fault zone for about 10 km and then curves to the northwest and terminates near the opposite-dipping Sanchez fault (pl. 2, figs. E9, E10). The Sanchez fault is here defined as the south-southeast-striking, down-to-east fault that approaches and nearly merges with the Pajarito fault zone where it bends prominently near Saint Peters Dome (pl. 2, fig. E9). On the basis of aeromagnetic data, the Sanchez fault (SC) appears to project southward beyond the Rio Grande for at least 10 km parallel to the La Bajada fault zone (pl. 2, fig. D7). The northern La Bajada fault zone along its overlap with the Sanchez fault is characterized by scalloped traces and oblique slip (fig. E10). The La Bajada fault zone bifurcates near the Rio Grande into splays that hook towards the Sanchez fault (fig. E10). Both splays terminate short of the Sanchez fault, but because the two fault systems dip toward each other they may intersect at shallow depth. The scalloped and hooked geometry of the northern La Bajada fault zone suggests that this part of the fault zone evolved by mechanical interaction and linkage of originally left-stepping en echelon fault segments (Olson and Pollard, 1989; Childs, Watterson, and Walsh, 1995; Acocella, Gudmundsson, and Funiciello, 2000). The hooking of the La Bajada fault zone splays towards the nearby Sanchez fault (fig. E10) suggests that there also has been mechanical interaction between these two fault zones. The scalloped, segmented geometry of the La Bajada fault zone traces and the fact that this part of the fault zone offsets units as young as the 1.14-Ma basaltic andesite of Cochiti Cone (unit Qcc, pl. 2) suggest that the northern part of the fault zone is relatively youthful and structurally immature (Acocella, Gudmundsson, and Funiciello, 2000).

Fault kinematic indicators reveal that most intrabasin faults in the La Bajada constriction area have undergone normal slip (rakes >60°). Similar to indicators in the rest of the basin, oblique-slip and, rarely, strike-slip indicators are observed only locally on faults on the northwest and southeast margins of the constriction (Tetilla (TT) and Pajarito (PJ) fault zones, fig. E3). The left-stepping en echelon traces of the intrabasin Sile fault (fig. E9) and the discontinuous, poorly exposed fault on the northeast side of Cañon Santo Domingo (pls. 1, 2) suggest that oblique slip occurred along those faults. However, only normal-slip indicators are observed on the Sile fault, and most intrabasin faults in the La Bajada constriction area have relatively straight traces that lack direct evidence of pronounced oblique slip. The normal-slip nature of faults within the La Bajada constriction implies that during faulting the horizontal maximum extension direction in this part of the basin was oriented approximately southwest, towards the Santo Domingo Basin depocenter (shaded star, fig. E1).

Hydrogeologic Character of Santo Domingo Basin Faults

Structural properties and cement patterns of fault zones within the Santo Domingo Basin and northern Albuquerque Basin have been investigated by two of the authors (Minor and Hudson, 2006) to facilitate hydrogeologic characterization and modeling of faults in the Albuquerque Basin aquifer. Results of that study that bear on the hydrogeologic properties of faults in the Santo Domingo Basin and, in particular, the La Bajada constriction are summarized below. Implications of the constriction fault geometry on ground-water flow are discussed in chapter G of this volume.

Fault Zone Structure and Hydrogeology

A typical fault zone in the Santo Domingo Basin area has three structural components: (1) a central fault core consisting of a narrow zone of concentrated shear strain, attenuation, and local grain-size reduction; (2) adjacent mixed zones composed of transitional domains of bedding disruption, entrainment, and localized particulate flow; and

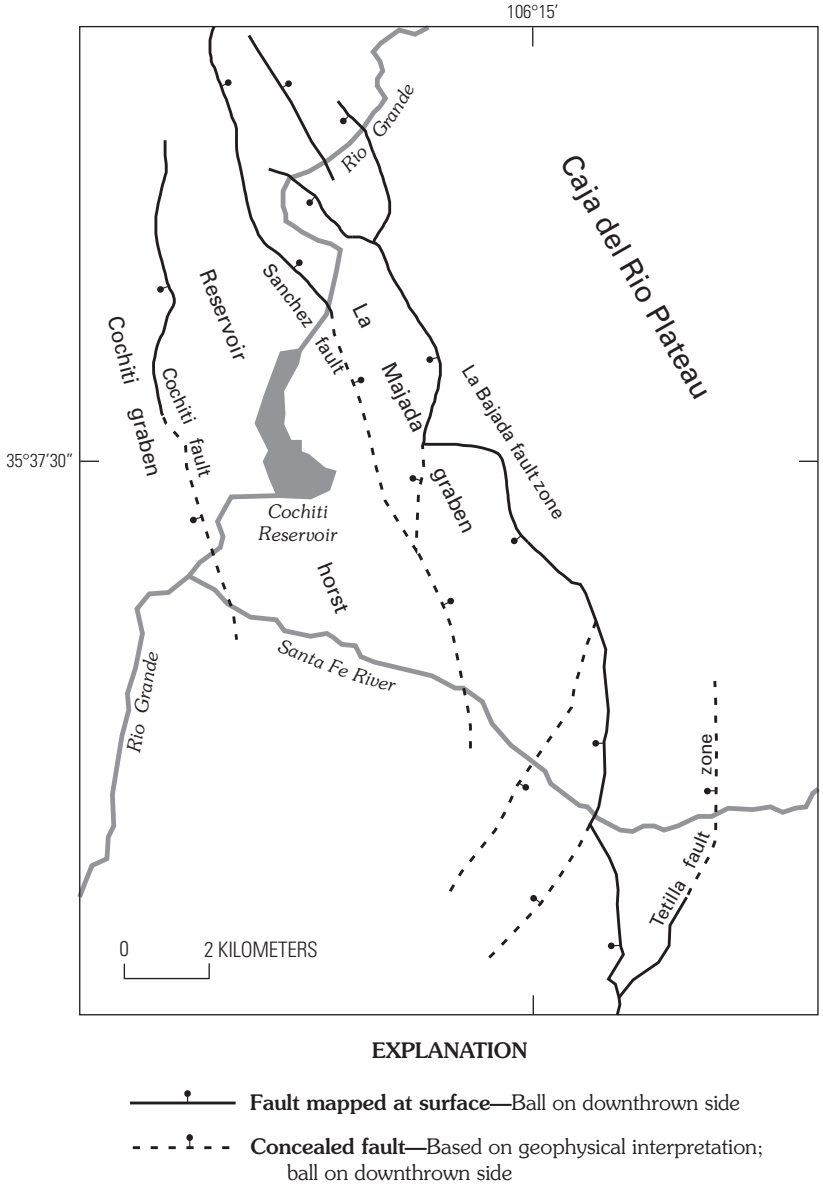

EXPLANATION

Fault mapped at surface—Ball on downthrown side

Concealed fault—Based on geophysical interpretation; ball on downthrown side

Figure E10. Inward hooking and scalloped traces of northernmost La Bajada fault zone where it overlaps with opposite-displacement Sanchez fault. Peculiar La Bajada fault zone geometry is attributed to mechanical interaction and linkage of en echelon fault segments as well as interaction of La Bajada fault with Sanchez fault. See text for further discussion. Faults shown as mapped at surface based on plate 2 and Sawyer and others (2002); concealed fault segments based on geophysical interpretations presented in chapter D (this volume).

(3) outer damage zones consisting of tabular rock volumes containing subsidiary faults, fractures, deformation bands, veins, and drag folds that decrease in intensity outwards (fig. E11). This structural architecture is consistent with fault zone observations in the Albuquerque Basin (Heynekamp and others, 1999; Rawling, Goodwin, and Wilson, 2001). Sheared and foliated clay-rich cores are common in nearly all faulted protoliths within the northeastern part of the Santo Domingo Basin. Clays within the cores appear to be derived from fault-entrained clay-bearing clastic protoliths (Caine, Evans, and Forster, 2004). Fault cores also contain variable amounts of silt, sand, and more rarely pebbles where faults cut coarser grained facies of the Sierra Ladrones (units QTsa, QTsp, pl. 2) and Cochiti (unit QTc) Formations. Sheared, brecciated, and comminuted volcanic rock cores are concentrated along the northern and northeastern margins of the basin where tuffs and lavas of the Jemez and Cerros del Rio volcanic fields are prevalent. Given the fine-grained clay-rich nature of a large majority of fault cores in a variety of protoliths, it is likely that most of the cores have very low permeability, especially in directions normal to the fault core (Knipe, 1993; Caine, Evans, and Forster, 1996; Caine and Forster, 1999; Heynekamp and others, 1999; Rawling, Goodwin, and Wilson, 2001; Caine, Evans, and Forster, 2002). Thus, despite their relatively narrow widths (mean of 0.1 m compared with ~10 m for damage zones), continuous undisturbed cores should act as important seals to across-fault fluid flow and contribute to anisotropic permeability within intrabasin fault zones (Knipe, 1993; Caine and Forster, 1999; Rawling, Goodwin, and Wilson, 2001; Caine, Evans, and Forster, 2002).

Variations in the protolith, especially grain size, affect observed fault zone properties. The width of a fault zone generally increases with decreasing grain size in sedimentary protoliths, but a large proportion of the narrowest fault zone components is in or adjacent to protoliths rich in clay (or mudstone) and silt (or siltstone). Most of the widest fault zones are in well-lithified volcanic rocks and other similar, well-indurated protoliths, whereas relatively narrow fault zone components tend to be hosted by protoliths rich in gravel, such as those within axial-river facies of the Sierra Ladrones Formation (unit QTsa, pl. 2; chapter B, this volume). These preliminary correlations of fault-zone properties and protolith suggest that knowledge of major subsurface lithostratigraphic changes in the basin can be used to help predict downdip variations in fault zone widths and width-dependant hydrologic properties.

Four main categories of fractures are recognized in fault damage zones in the study area: (1) opening-mode, or extension, fractures, (2) synthetic mesoscale shear fractures (that is, faults) and deformation bands, (3) antithetic mesoscale shear fractures and deformation bands, and (4) cross, or oblique, fractures (fig. E11). Zones of breccia are also present locally. Fault zones in relatively lithified and indurated volcanic and sedimentary protoliths, which are concentrated along the northern and eastern margins of the Santo Domingo Basin, are most likely to have open, hydraulically conductive shear and extension fractures within their damage zones (Caine, Evans, and Forster, 1996). In contrast, intrabasin fault damage zones in poorly to moderately consolidated sediments of the Santa Fe Group commonly contain low-permeability deformation bands (Heynekamp and others, 1999; Rawling,

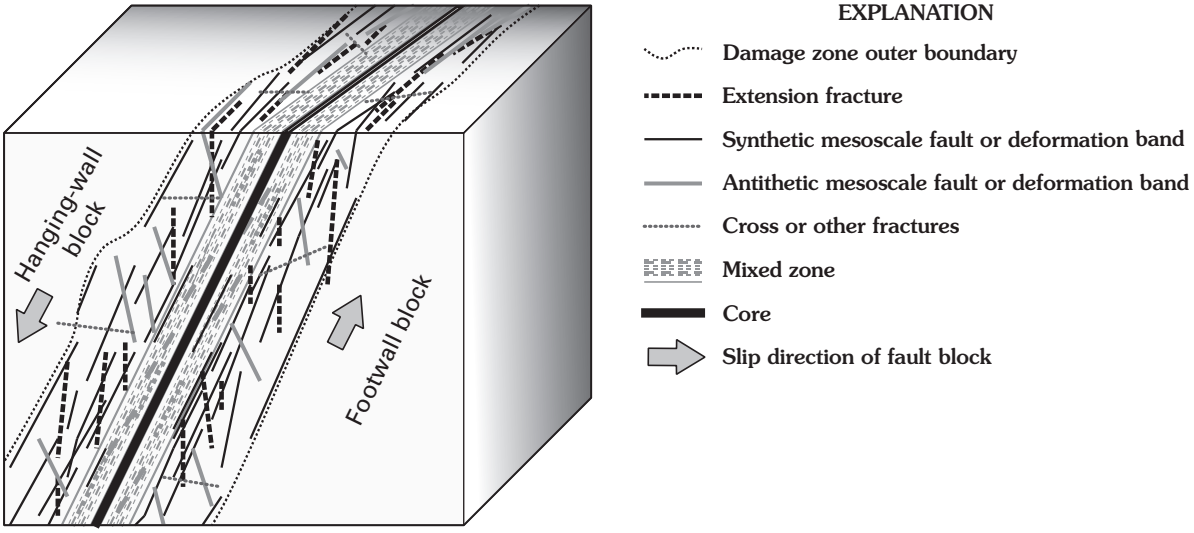

Figure E11. Various architectural components and damage zone fracture types observed in faults exposed in studied basins. See discussion in text.

Goodwin, and Wilson, 2001) as well as variable-permeability open-to-closed shear fractures and rare extension fractures. Damage zones dominated by uncemented extension fractures and synthetic and antithetic shear fractures have enhanced permeability in directions approximately parallel to the principal fault plane or core (Sibson, 1996; Caine and Forster, 1999). As the density of deformation bands in damage zones increases, as is commonly the case in faults cutting basin-fill sediments, bulk fault-zone permeability and especially fault-normal permeability typically decrease (Rawling, Goodwin, and Wilson, 2001). Regardless of the structural composition of the damage zones, most fault zones in the Santo Domingo Basin should retard or restrict across-fault ground-water flow owing to the combined effect of low-permeability damage-zone structures and very low permeability clay-rich cores.

Fault Zone Cement Patterns

The permeability of fault zones is substantially reduced where they are cemented and, thus, faults can evolve from zones of high permeability to zones of low permeability (Knipe, 1993; Mozley and Goodwin, 1995; Caine and Forster, 1999). If we assume that fault zone cements are indicators of focused flow of ancient fluid (Knipe, 1993; Mozley and Goodwin, 1995; Caine and Forster, 1999), then the spatial distribution of fault zone cements across a faulted aquifer basin can be used to identify areas of concentrated flow of ancient ground water.

Fault-zone cement is common in the Santo Domingo Basin, particularly where fault zones are rich in gravel or sand. Intrabasin faults are cemented principally by silica or carbonate minerals. Silica cements are limited to fault zones in the northwestern part of the Santo Domingo Basin mainly north of the Jemez River and west of the Rio Grande (fig. E12), where they become more concentrated northward towards the Jemez volcanic field. In the La Bajada constriction area silica cement is present along the northern San Francisco (SF), Sile (SI), and South Pajarito (SP) faults (fig. E12). Silica-cemented portions of fault zones commonly form prominent topographic ribs or ridges. Silica cements include microcrystalline cristobalite (or tridymite) and opaline and chalcedonic silica. On the basis of the mineralogy and spatial restriction of the silica cements, we infer that the cements precipitated from hydrothermal fluids flowing southward, downgradient, and possibly upwards along faults emanating from magmatic centers within the Jemez volcanic field.

Carbonate cements, mostly micritic and less common sparry calcite, are widely distributed in the Santo Domingo Basin (fig. E12) (see also Mozley and Goodwin, 1995; Heynekamp and others, 1999). Fault-zone sandstones that are strongly cemented with calcite commonly stand out in positive topographic relief. Concentrated calcite cements are also expressed as spherical to spherulitic concretions that weather into balls as much as several centimeters in diameter, but elongate carbonate cement concretions such as those used by Mozley and Goodwin (1995) to infer the orientation of ancient ground-water flow are rarely observed. Both carbonate and silica cements occupy some fault zones in the northern part of the study area, and contact and crosscutting relations indicate that the carbonate mostly precipitated later than the silica. The most strongly carbonate-cemented fault zones are located south of the area of silica cement in the southern Santo Domingo and northern Albuquerque Basins (fig. E12). In the La Bajada constriction area the Borrego (BR), Sile (SI), South Pajarito (SP), San Francisco (SF), and La Bajada (LB) fault zones are locally well cemented with carbonate (fig. E12).

Most fault zones are asymmetrically cemented; the cements are localized on one side of the fault in the mixed zone and in sand-rich portions of the adjacent fault core (fig. E12). Some cements extend into the inner part of the hanging-wall or footwall damage zone, but they rarely continue beyond the outer edge of the damage zone. The restriction of strongly cemented zones to one side of fault zones for considerable distance along strike (as much as 15 km) suggests that the faults localized or channeled the flow of fluids rather than fortuitously juxtaposing cemented and uncemented stratigraphic intervals. However, where protoliths have been cemented during diagenesis, fault-controlled cement is difficult to distinguish from previously existing cement in beds that were entrained in the fault zone.

In some parts of the basin, cement asymmetry locally alternates across a series of adjacent fault blocks. For example, opposing silica cement asymmetries are observed along the Sile (SI) and San Francisco (SF) faults in the La Bajada constriction area (fig. E12). The northern San Francisco fault and the aligned end of the oppositely dipping South Pajarito fault (SP) to the north are both silica cemented on their west sides, whereas the neighboring Sile fault is cemented on its east side (fig. E12). Such closely spaced reversals in cement asymmetry strongly suggest local fault-baffled or -compartmentalized ancient flow, and a regional hydrologic gradient was locally modified owing to fault permeability structures that acted as both conduits and barriers. The Sile (SI) and South Pajarito (SP) faults contain separate zones of silica and carbonate cement on opposite sides of their respective fault zones (fig. E12), suggesting that earlier cemented (silica?) zones acted as seals to later (carbonate-bearing?) ground-water flow.

Evidence of recurring fault cementation and fracturing is provided by numerous observations of one or more generations of cemented veins and fractures that cut earlier cemented sediments within the mixed zone, presumably owing to the effects of episodic fault deformation concentrated near the fault cores. Parts of fault zones that once focused fluid flow eventually became cemented and are now zones of lower permeability, unless the cements themselves developed opening-mode fractures during renewed fault movements. Strong cementation of fault zones that have not experienced refracturing has shifted the regions of highest relative permeability away from the cemented zones and low-permeability fault core, presumably laterally toward the outer damage zone, and in some cases to the other side of the fault zone.

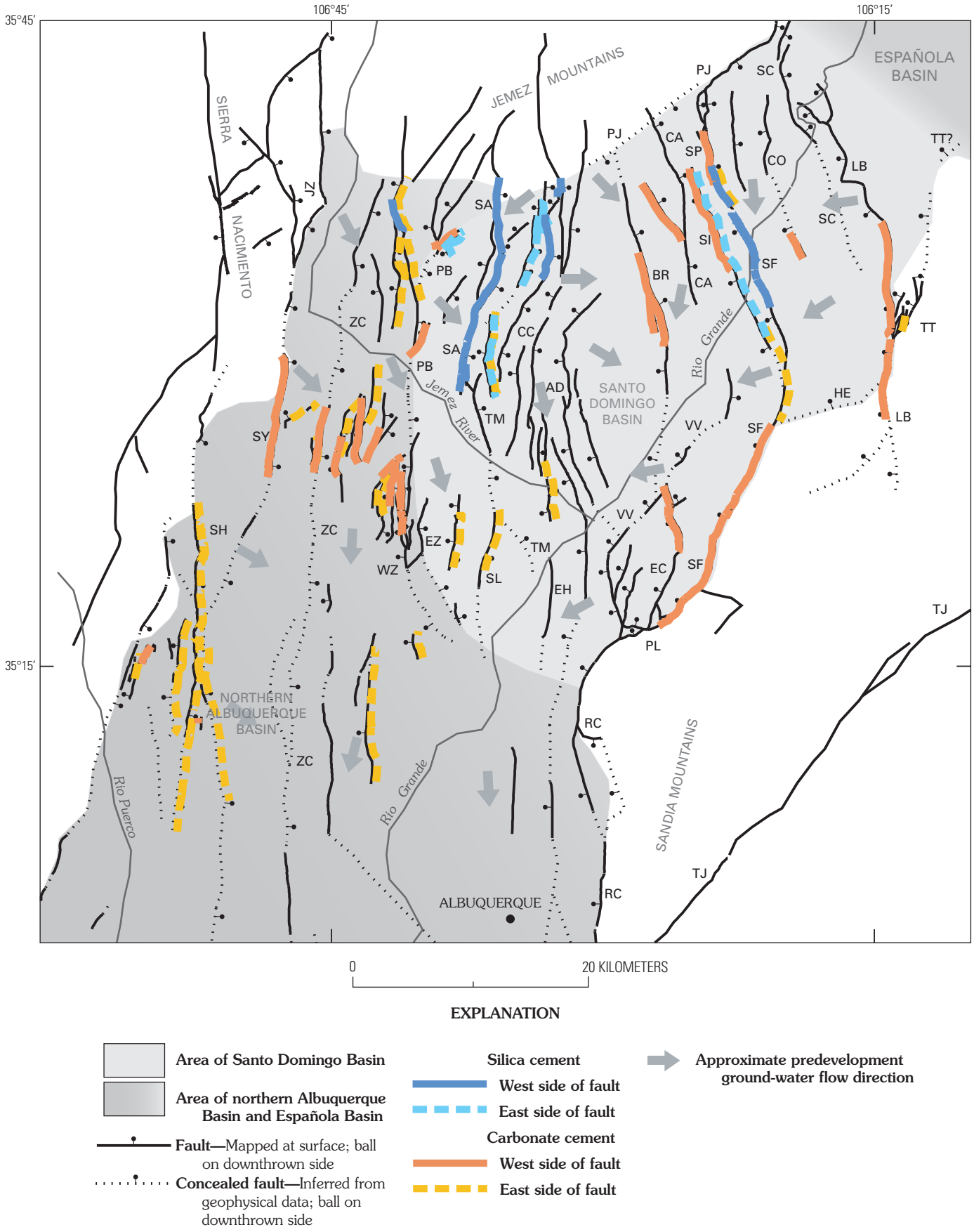
35°45′
106°45′
106°15′
35°15′
ESPAÑOLA BASIN
SIERRA NACIMIENTO
JEMEZ MOUNTAINS
SANTO DOMINGO BASIN
NORTHERN ALBUQUERQUE BASIN
SANDIA MOUNTAINS
ALBUQUERQUE
Rio Grande
Jemez River
Rio Puerco
PJ
SC
CA
SP
CO
LB
TT?
TT
SI
SF
BR
JZ
SA
PB
ZC
CC
AD
TM
HE
VV
SY
SH
EZ
WZ
SL
EH
EC
PL
RC
TJ
0
20 KILOMETERS
EXPLANATION
Area of Santo Domingo Basin
Area of northern Albuquerque Basin and Española Basin
Fault—Mapped at surface; ball on downthrown side
Concealed fault—Inferred from geophysical data; ball on downthrown side
Silica cement
West side of fault
East side of fault
Carbonate cement
West side of fault
East side of fault
Approximate predevelopment ground-water flow direction

Figure E12 (facing page). Santo Domingo Basin region showing asymmetrically distributed carbonate and silica fault zone cements. Silica cement is restricted to northern Santa Domingo Basin along faults near Jemez volcanic field, whereas carbonate cement is distributed throughout basin. Fault cement asymmetries show no systematic pattern relative to basin positions and modern ground-water flow directions (thick gray arrows). Flow directions based on water-elevation map of Bexfield and Anderholm (2000). Faults and fault zones: AD, Algodones; BR, Borrego; CA, Camada; CC, Cañada de Cochiti; CO, Cochiti; EC, Escala; EH, East Heights; EZ, East Ziana; HE, Hagan Embayment; JZ, Jemez; LB, La Bajada; PB, Pico Butte; PJ, Pajarito; PL, Placitas; RC, Rincon; SA, Santa Ana; SC, Sanchez; SH, Sand Hill; SI, Sile; SF, San Francisco; SL, South Luce; SP, South Pajarito; SY, San Ysidro; TJ, Tijeras; TM, Tamaya; TT, Tetilla; VV, Valley View; WZ, West Ziana; ZC, Zia County Dump.

Hydrogeologic Summary

Fault zones observed in the Santo Domingo Basin area are characterized by (1) outer damage zones that typically contain strike-parallel deformation bands and open extensional and shear fractures that may enhance or impede ground-water flow along the faults; (2) mixed zones composed of entrained and partly dismembered blocks of protolith rock or sediment; and (3) centrally positioned, low permeability, clay-rich fault cores that likely impede cross-fault flow. Protolith lithology strongly influences fault-zone architecture and component widths and controls variations in fracturing and other brittle-strain features.

Cements, recognized as a proxy for concentrated flow of ancient ground water, are common along fault zones in the basin. Silica cements are limited to faults that emanate from the Jemez volcanic field north of the basin, whereas carbonate fault cements are widely distributed. Coarse sediments (gravel and sand) host the greatest cement concentrations within fault zones; cements are also concentrated along open fractures and, to a lesser degree, along shear fractures and deformation bands within inner damage zones. Cements are commonly concentrated on one side of a fault and thus cement the fault zone asymmetrically. From observed spatial patterns of asymmetrically distributed fault zone cements, we infer that fault-parallel and -compartmentalized ground-water flow was, and may continue to be, common in the basin aquifers.

Our study indicates that the Santo Domingo Basin is densely populated with faults of various geometry, internal structure, and cement distribution. These aspects of the faults impart considerable heterogeneity of permeability within the basin aquifer. The types and statistical range of fault zone features appear to be consistent throughout the basin, a fact that is useful in creating simulations of ground-water flow that incorporate the influence of faults.

References Cited

Acocella, Valerio, Gudmundsson, Agust, and Funiciello, Renato, 2000, Interaction and linkage of extension fractures and normal faults—Examples from the rift zone of Iceland: Journal of Structural Geology, v. 22, p. 1233–1246.

Aldrich, M.J., Jr., 1986, Tectonics of the Jemez lineament in the Jemez Mountains and Rio Grande rift: Journal of Geophysical Research, v. 91, no. B2, p. 1753–1762.

Aldrich, M.J., Jr., Chapin, C.E., and Laughlin, A.W., 1986, Stress history and tectonic development of the Rio Grande rift, New Mexico: Journal of Geophysical Research, v. 91, no. B6, p. 6199–6211.

Baldridge, W.S., Ferguson J.F., Braile, L.W., Wang, Bin, Eckhardt, Kristine, Evans, David, Schultz, Craig, Gilpin, Bernard, Jiracek, G.R., and Biehler, Shawn, 1994, The western margin of the Rio Grande rift in northern New Mexico—An aborted boundary?: Geological Society of America Bulletin, v. 105, p. 1538–1551.

Bartolino, J.R., and Cole, J.C., 2002, Ground-water resources of the Middle Rio Grande Basin, New Mexico: U.S. Geological Survey Circular 1222, 132 p.

Besse, Jean, and Courtillot, Vincent, 1991, Revised and synthetic apparent polar wander paths for the African, Eurasian, North American and Indian plates, and true polar wander since 200 Ma: Journal of Geophysical Research, v. 96, p. 4029–4050.

Bexfield, L.M., and Anderholm, S.K., 2000, Predevelopment water-level map of the Santa Fe Group aquifer system in the middle Rio Grande Basin between Cochiti Lake and San Acacia, New Mexico: U.S. Geological Survey Water-Resources Investigations Report 00–4249, 1 sheet.

Buck, W.R., Lavier, L.L., and Poliakov, A.N., 1999, How to make a rift wide: Philosophical Transactions of the Royal Society [London], v. 357, p. 671–693.

Caine, J.S., Evans, J.P., and Forster, C.B., 1996, Fault zone architecture and permeability structure: Geology, v. 24, p. 1025–1028.

Caine, J.S., and Forster, C.B., 1999, Fault zone architecture and fluid flow—Insights from field data and numerical modeling, *in* Haneberg, W.C., Mozley, P.S., Moore, J.C., and Goodwin, L.B., eds., Faults and subsurface fluid flow in the shallow crust: American Geophysical Union Geophysical Monograph 113, p. 101–127.

Caine, J.S., Minor, S.A., Grauch, V.J.S., and Hudson, M.R., 2002, Potential for fault zone compartmentalization of groundwater aquifers in poorly lithified, Rio Grande rift-related sediments, New Mexico [abs.]: Geological Society of America Abstracts with Programs, v. 34, no. 4, p. 59.

Caine, J.S., Minor, S.A., and Hudson, M.R., 2004, On the lack of geochemical anomalies associated with faulting in poorly lithified, siliciclastic Santa Fe Group sediments, NM [abs.], *in* Hudson, M.R., ed., Geologic and Hydrogeologic Framework of the Española Basin—3d Annual Española Basin Workshop, Santa Fe, New Mexico, March 2–3, 2004, Proceedings: U.S. Geological Survey Open-File Report, OF–2004–1093, p. 26.

Cather, S.M., 1992, Suggested revisions to the Tertiary tectonic history of north-central New Mexico: New Mexico Geological Society 43d field conference, San Juan Basin IV, Guidebook, p. 109–122.

Cather, S.M., 1997, Constraints of Mesozoic piercing points on magnitude of northward Laramide translation of Colorado Plateau in north-central New Mexico: New Mexico Geology, v. 19, p. 50.

Chamberlin, R.M., 1999, Partitioning of dextral slip in an incipient transverse shear zone of Neogene age, northwestern Albuquerque Basin, Rio Grande rift, New Mexico [abs.]: Geological Society of America Abstracts with Programs, v. 31, no. 7, p. 113.

Chapin, C.E., and Cather, S.M., 1994, Tectonic setting of the axial basins of the northern and central Rio Grande rift, *in* Keller, G.R., and Cather, S.M., eds., Basins of the Rio Grande rift—Structure, stratigraphy, and tectonic setting: Geological Society of America Special Paper 291, p. 5–25.

Childs, Conrad, Watterson, Juan, and Walsh, J.J., 1995, Fault overlap zones within developing normal fault systems: Journal of the Geological Society [London], v. 152, p. 535–549.

Connell, S.D., Cather, S.M., Karlstrom, K.E., Read, A., Ilg, B., Menne, B., Picha, M.G., Andronicus, C., Bauer, P.W., and Anderson, O.J., 1995, Geology of the Placitas 7.5 minute quadrangle, Sandoval County, New Mexico: New Mexico Bureau of Mines and Mineral Resources Open-file Digital Map 2, scale 1:12,000.

Connell, S.D., Koning, D.J., and Cather, S.M., 1999, Revisions to the stratigraphic nomenclature of the Santa Fe Group, northwestern Albuquerque Basin, New Mexico: New Mexico Geological Society 50th field conference, Albuquerque Geology, Guidebook, p. 337–353.

Deamer, G.A., and Kodama, K.P., 1990, Compaction-induced inclination shallowing in synthetic and natural clay-rich sediments: Journal of Geophysical Research, v. 95, p. 4511–4529.

Demarest, H.H., 1983, Error analysis of the determination of tectonic rotation from paleomagnetic data: Journal of Geophysical Research, v. 88, p. 4321–4328.

Faulds, J.E., and Varga, R.J., 1998, The role of accommodation zones and transfer zones in the regional segmentation of extended terranes, *in* Faulds, J.E., and Stewart, J.H., eds., Accommodation zones and transfer zones—The regional segmentation of the Basin and Range Province: Geological Society of America Special Paper 323, p. 1–45.

Fisher, R.A., 1953, Dispersion on a sphere: Proceedings of the Royal Society [London], Series A217, v. 295–305.

Freund, Raphael, 1970, Rotation of strike-slip faults in Sistan, southeast Iran: Journal of Geology, v. 78, p. 188–200.

Gardner, J.N., and Goff, Fraser, 1984, Potassium-argon dates from the Jemez volcanic field— Implications for tectonic activity in the north-central Rio Grande rift: New Mexico Geological Society 35th field conference, Rio Grande Rift, Northern New Mexico, Guidebook, p. 75–81.

Grauch, V.J.S., 1999, Principal features of high-resolution aeromagnetic data collected near Albuquerque, New Mexico: New Mexico Geological Society 50th field conference, Albuquerque Geology, Guidebook, p. 115–118.

Grauch, V.J.S., Gillespie, C.L., and Keller, G.R., 1999, Discussion of new gravity maps for the Albuquerque Basin area: New Mexico Geological Society 50th field conference, Albuquerque Geology, Guidebook, p. 119–124, plates C and D, p. 136–137.

Grauch, V.J.S., Hudson, M.R., and Minor, S.A., 2001, Aeromagnetic expression of faults that offset basin fill, Albuquerque Basin, New Mexico: Geophysics, v. 66, no. 3, p. 707–720.

Hamilton, W.B., and Myers, W.B., 1966, Cenozoic tectonics of the western United States: Reviews of Geophysics, v. 4, p. 509–549.

Heynekamp, M.R., Goodwin, L.B., Mozley, P.S., and Haneberg, W.C., 1999, Controls on fault-zone architecture in poorly lithified sediments, Rio Grande rift, New Mexico—Implications for fault-zone permeability and fluid flow, *in* Haneberg, W.C., Mozley, P.S., Moore, J.C., and Goodwin, L.B., eds., Faults and subsurface fluid flow in the shallow crust: American Geophysical Union Geophysical Monograph 113, p. 27–49.

Housen, B.A., and van der Pluijm, B.A., 1991, Slaty cleavage development and magnetic anisotropy fabrics: Journal of Geophysical Research, v. 96, p. 9937–9946.

Hrouda, František, 1982, Magnetic anisotropy of rocks and its application in geology and geophysics: Geophysical Surveys, v. 5, p. 37–82.

Hudson, M.R., Minor, S.A., Grauch, V.J.S., and Personius, S.F., 1999, Preliminary characterization of faults in the middle Rio Grande Basin [abs.], *in* Bartolino, J.R., ed., U.S. Geological Survey Middle Rio Grande Basin Study: U.S. Geological Survey Open-File Report 99–203, p. 40–41.

Karlstrom, K.E., Cather, S.M., Kelley, S.A., Heizler, M.T., Pazzaglia, F.J., and Roy, M., 1999, Sandia Mountains and

Rio Grande rift—Ancestry of structures and history of deformation: New Mexico Geological Society 50th field conference, Albuquerque Geology, Guidebook, p. 155–165.

Kelley, V.C., 1977, Geology of Albuquerque Basin, New Mexico: New Mexico Bureau of Mines and Mineral Resources Memoir 33, 60 p.

Kelley, V.C., 1982, The right-relayed Rio Grande rift, Taos to Hatch, New Mexico: New Mexico Geological Society 33d field conference, Albuquerque Country II, Guidebook, p. 147–151.

Knipe, R.J., 1993, The influence of fault zone processes and diagenesis on fluid flow, *in* Horbury, A.D., and Robinson, A.G., eds., Diagenesis and basin development: American Association of Petroleum Geologists Studies in Geology 36, p. 135–148.

May, S.J., and Russell, L.R., 1994, Thickness of the syn-rift Santa Fe Group in the Albuquerque Basin and its relation to structural style, *in* Keller, G.R., and Cather, S.M., eds., Basins of the Rio Grande rift—Structure, stratigraphy, and tectonic setting: Geological Society of America Special Paper 291, p. 113–124.

Minor, S.A., and Hudson, M.R., 2006, Regional survey of structural properties and cementation patterns of fault zones in the northern part of the Albuquerque Basin, New Mexico: Implications for ground-water flow: U.S. Geological Survey Professional Paper 1719, 28 p.

Minor, S.A., and Sawyer, D.A., 1999, Structural evolution of a rift border fault zone—La Bajada fault zone, Rio Grande rift, northern New Mexico [abs.]: Geological Society of America Abstracts with Programs, v. 31, no. 7, p. 112.

Mozley, P.S., and Goodwin, L.B., 1995, Patterns of cementation along a Cenozoic normal fault—A record of paleoflow orientations: Geology, v. 23, p. 539–542.

Olson, J.E., and Pollard, D.D., 1989, Inferring paleostresses from natural fracture patterns—A new method: Geology, v. 17, p. 345–348.

Rawling, G.C., Goodwin, L.B., and Wilson, J.L., 2001, Internal architecture, permeability structure, and hydrologic significance of contrasting fault-zone types: Geological Society of America Bulletin, v. 29, no. 1, p. 43–46.

Russell, L.R., and Snelson, S., 1994, Structure and tectonics of the Albuquerque Basin segment of the Rio Grande rift—Insights from reflection seismic data, *in* Keller, G.R., and Cather, S.M., eds., Basins of the Rio Grande rift—Structure, stratigraphy, and tectonic setting: Geological Society of America Special Paper 291, p. 83–112.

Sawyer, D.A., Shroba, R.R., Minor, S.A., and Thompson, R.A., 2002, Geologic map of the Tetilla Peak 7.5 minute quadrangle, Santa Fe and Sandoval Counties, New Mexico: U.S. Geological Survey Miscellaneous Field Studies Map MF–2352, scale 1:24,000.

Sibson, R.H., 1996, Structural permeability of fluid-driven fault-fracture meshes: Journal of Structural Geology, v. 18, p. 1031–1042.

Smith, G.A., and Kuhle, A.J., 1998, Hydrostratigraphic implications of new geologic mapping in the Santo Domingo Basin, New Mexico: New Mexico Geology, v. 20, p. 21–27.

Smith, G.A., McIntosh, William, and Kuhle, A.J., 2001, Sedimentologic and geomorphic evidence for seesaw subsidence of the Santo Domingo accommodation-zone basin, Rio Grande rift, New Mexico: Geological Society of America Bulletin, v. 113, p. 561–574.

Wawrzyniec, T.F., Geissman, J.W., Melker, M.D., and Hubbard, Mary, 2002, Dextral shear along the eastern margin of the Colorado Plateau—A kinematic link between Laramide contraction and Rio Grande rifting (ca. 75–13 Ma): Journal of Geology, v. 110, p. 305–324.

Wernicke, Brian, 1992, Cenozoic extensional tectonics of the U.S. Cordillera, *in* Burchfiel, B.C., Lipman, P.W., and Zoback, M.L., eds., The Cordilleran orogen—Conterminous U.S.: Geological Society of America, The geology of North America, v. G-3, p. 553–581.

Woodward, L.A., 1977, Rate of crustal extension across the Rio Grande rift near Albuquerque, New Mexico: Geology, v. 5, p. 269–272.

Zoback, M.L., Anderson, R.E., and Thompson, G.A., 1981, Cainozoic evolution of the state of stress and style of tectonism of the Basin and Range Province of the western United States: Philosophical Transactions of the Royal Society [London], v. 300, p. 407–434.

Published in the Central Region, Denver, Colo.
Manuscript approved for publication February 10, 2006
Graphics by authors
Photocomposition by Mari L. Kauffmann (Contractor, ATA Services)
Edited by Mary-Margaret Coates (Contractor, ATA Services)

Electromagnetic Studies and Subsurface Mapping of Electrical Resistivity in the La Bajada Constriction Area, New Mexico

By Brian D. Rodriguez, Maria Deszcz-Pan, and David A. Sawyer

Chapter F of

The Cerrillos Uplift, the La Bajada Constriction, and Hydrogeologic Framework of the Santo Domingo Basin, Rio Grande Rift, New Mexico

Edited by Scott A. Minor

Professional Paper 1720–F

U.S. Department of the Interior
U.S. Geological Survey

Contents

Abstract 121
Introduction to Electromagnetic Methods 121
Electrical Rock Properties 121
Ground-based Electromagnetic Surveys 123
    Magnetotelluric Survey 123
    Resistivity Models Based on Magnetotelluric Survey 126
    Geologic Interpretation of Surface Electromagnetic Models 131
Airborne Electromagnetic Surveys 142
    Time-Domain Electromagnetic Survey 143
    Resistivity Models Based on Time-Domain Electromagnetic Survey 144
    Geologic Interpretation of Airborne Electromagnetic Models 148
Summary 159
References Cited 162

Figures

F1. Index map of airborne time-domain electromagnetic survey areas in middle Rio Grande Basin, New Mexico 122
F2. Maps showing Cochiti Pueblo airborne time-domain electromagnetic survey area and magnetotelluric survey stations northeast of Albuquerque, New Mexico 124
F3. Diagrams showing data used to construct two-dimensional finite-element resistivity models of the Cochiti Pueblo time-domain electromagnetic survey area 127
F4. Resistivity models with lithologic interpretation constructed from audiomagnetotelluric data from Cerros del Rio volcanic field 130
F5. Two-dimensional finite-element resistivity model with lithologic interpretation constructed from high-frequency magnetotelluric data for Cochiti Pueblo area 132
F6. Two-dimensional finite-element resistivity model constructed from low-frequency magnetotelluric data 133
F7. Maps showing time-domain electromagnetic depth slices from 20 m to 200 m depth in the Cochiti Pueblo survey area 135
F8–F11. Cross sections showing:
    F8. Resistivity under flight line 620 in the Cochiti Pueblo time-domain electromagnetic survey area and induction-resistivity log for well CEPO 2 in Cochiti Pueblo 142
    F9. Resistivity under flight line 630 in the Cochiti Pueblo time-domain electromagnetic survey area; resistivity-depth image 145
    F10. Resistivity under flight line 630 in the Cochiti Pueblo time-domain electromagnetic survey area; least-squares inversion 145
    F11. Cross sections showing east-west time-domain electromagnetic resistivity profiles in the Cochiti Pueblo survey area 146

F12. Maps showing time-domain electromagnetic elevation slices from 1,750 to 1,400 m elevation in the Cochiti Pueblo survey area 149
F13. Cross sections showing north-south profiles in the Cochiti Pueblo time-domain electromagnetic survey area....156
F14. Maps showing depth to surface of >100 ohm-m resistive layer and elevation of >100 ohm-m resistive layer in the Cochiti Pueblo time-domain electromagnetic survey area....160

Tables

F1. Audiomagnetotelluric and magnetotelluric station coordinates and elevations in the Cochiti Pueblo area, New Mexico 126
F2. Range of average resistivity values in regional induction logs for stratigraphic units encountered in wells in study region 134
F3. Location of wells referred to in table F2 134

Electromagnetic Studies and Subsurface Mapping of Electrical Resistivity in the La Bajada Constriction Area, New Mexico

By Brian D. Rodriguez, Maria Deszcz-Pan, and David A. Sawyer

Abstract

Airborne and surface electromagnetic surveys were used to map changes in electrical resistivity with depth in the La Bajada constriction and Cochiti Pueblo area; these changes in resistivity are related to variations in rock or deposit types that, in turn, influence aquifers in the study area. In the eastern Cerros del Rio volcanic field, the location and geometry of the northern boundary of the Cerrillos uplift are constrained by our electromagnetic survey results. This boundary defines the southeastern extent of the La Bajada constriction through which groundwater hydraulically connected with the Rio Grande flows as it passes from the Española Basin into the Santo Domingo Basin. The largely concealed Tetilla fault zone is also detected by the electromagnetic surveys in this area; it appears to form the western boundary of an east-dipping block of electrically conductive Mancos Shale. In the north-central part of the La Bajada constriction, a large area of lower resistivity coincides with a silt or clay lacustrine unit in upper Santa Fe Group basin-fill deposits. In the central part of the constriction, higher resistivities correspond in part with ancestral Rio Grande axial gravel deposits. On the western flank of the La Bajada constriction, our electromagnetic survey results provide constraints on the relative position of basement and on the thicknesses of Paleozoic, Mesozoic, and Tertiary sedimentary rocks on either side of the constriction-bounding Pajarito fault zone.

Introduction to Electromagnetic Methods

Studies by the U.S. Geological Survey were begun in 1996 to improve understanding of the geologic framework of the Albuquerque composite basin and adjoining areas, in order that more accurate hydrogeologic parameters could be applied to new hydrologic models. The ultimate goal of this multidisciplinary effort has been to better quantify estimates of future water supplies for northern New Mexico's growing urban centers, which largely subsist on aquifers in the Rio Grande rift basin (Bartolino and Cole, 2002). From preexisting hydrologic models it became evident that hydrogeologic uncertainties were large in the Santo Domingo Basin area, immediately upgradient from the greater Albuquerque metropolitan area, and particularly in the northeast part of the basin referred to as the La Bajada constriction (see chapter A, this volume, for a geologic definition of this feature as used in this report). Accordingly, a priority for new geologic and geophysical investigations was to better determine the hydrogeologic framework of the La Bajada constriction area. This chapter along with the other chapters of this report present the results of such investigations recently conducted by the U.S. Geological Survey.

Airborne and surface electromagnetic (EM) surveys are described here as part of U.S. Geological Survey investigations of the subsurface distribution of sedimentary and volcanic rocks in the Cochiti Pueblo and La Bajada constriction areas (survey area D, fig. F1). An airborne time-domain electromagnetic (TDEM) survey was used to map changes in electrical resistivity with depth that are related to differences in rock type; these various rock types, in turn, affect the hydrologic properties of aquifers in the region. A ground-based magnetotelluric (MT) survey was used to calibrate TDEM results and to obtain electrical resistivity information from depths greater than the limits of the TDEM survey. In this chapter we discuss the electrical rock property called resistivity, the surface (MT) and airborne (TDEM) electromagnetic methods used in our study, and our approach to modeling and interpreting MT and TDEM data. We present subsurface maps and cross sections of resistivity and interpret the basic geologic framework of the study area on the basis of these data.

Electrical Rock Properties

Electromagnetic geophysical methods detect variations in the electrical properties of rocks—in particular electrical resistivity (or its inverse, electrical conductivity). Electrical resistivity can be correlated with geologic units on the surface and at depth by using lithologic logs to provide a three-dimensional picture of subsurface geology. The resistivity of geologic units largely depends on their fluid content,

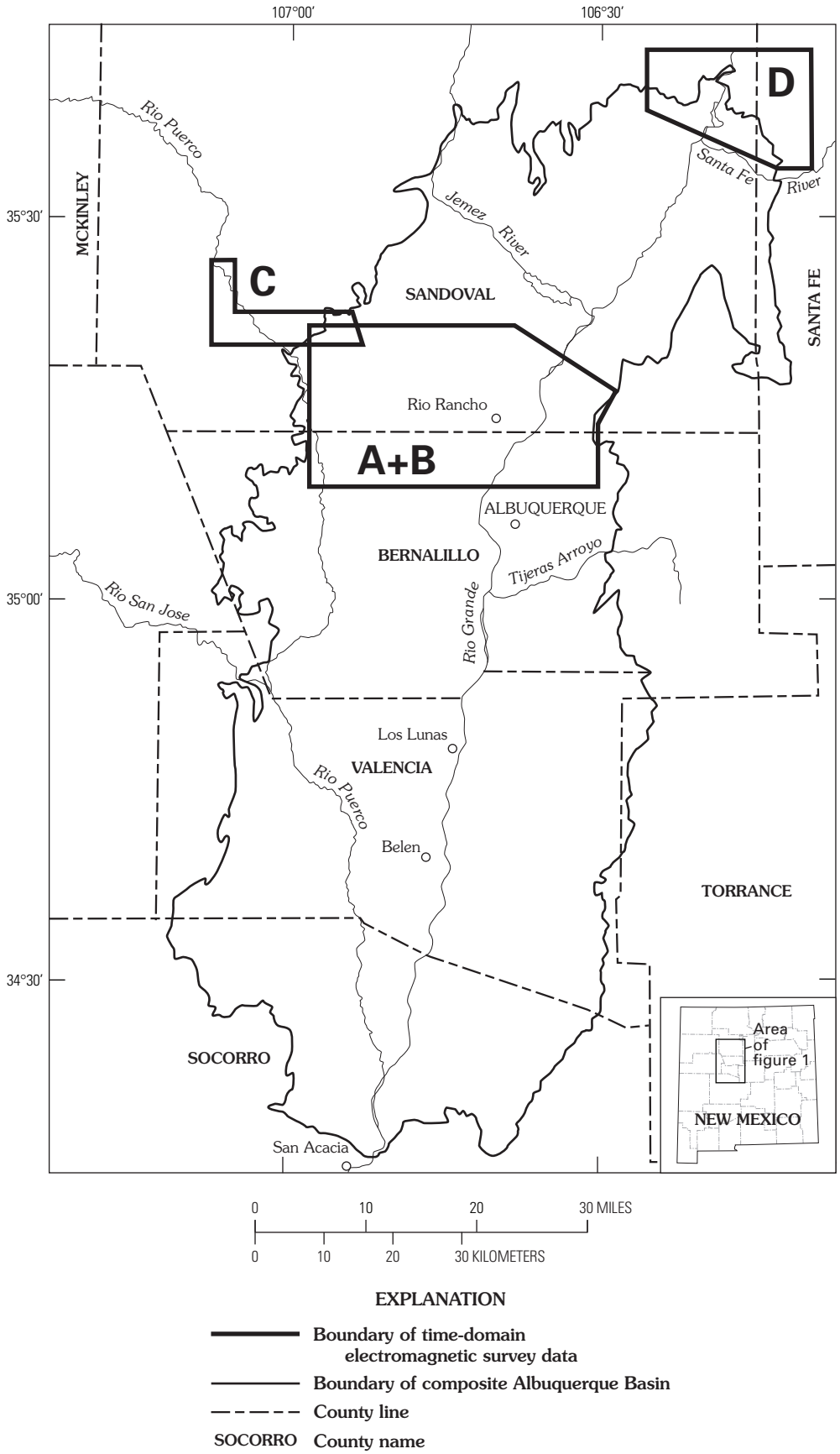

Figure F1. Airborne time-domain electromagnetic survey areas in the middle Rio Grande Basin north of Albuquerque, New Mexico, modified from Bartolino (1999). A+B, Rio Rancho survey area. C, Rio Puerco survey area, both described in Deszcz-Pan and others (2000). D, Cochiti Pueblo survey area discussed in this chapter.

porosity, fracture density, temperature, and content of conductive minerals (Keller and Frischknecht, 1966). Fluids in the pore spaces and fracture openings, especially saline fluids, can reduce resistivities in what would otherwise be a resistive rock matrix. Resistivity can also be lowered by electrically conductive clay minerals, graphitic carbon, and deposits of metallic minerals. Altered volcanic rocks commonly contain replacement minerals that have resistivities that are only a tenth of the resistivities of minerals in unaltered surrounding rocks (Nelson and Anderson, 1992). Water-saturated clay-rich alluvium, marine shale, and other mudstones are normally very conductive—a few (1–3) ohms per meter to a few tens (10–20) of ohms per meter. Water-saturated, unconsolidated, terrestrial alluvial sediments are commonly moderately conductive (10–70 ohm-m). Sediments containing conglomerate and coarse, clean sand possess resistivities at the higher end of the range, and impure sand and siltstone lie at the lower end. The resistivity of water-saturated unconsolidated sediment, at low temperature and measured at low frequencies, is controlled by the relative proportion of clay minerals, porosity, interconnected pore structures, and dissolved minerals (Keller, 1987; Palacky, 1987).

Unaltered, unfractured igneous rocks are normally very resistive (typically a few hundred to thousands of ohm-m). Carbonate rocks are moderately to highly resistive (hundreds to thousands of ohms per meter) depending upon their fluid content, porosity, fracture characteristics, and impurities. Metamorphic rocks (that do not contain graphite) are moderately to highly resistive (hundreds to thousands of ohms per meter). Resistivity may be low (less than 100 ohm-m) along fault zones that were fractured enough to have once hosted fluids (generally water or brine) from which conductive minerals were deposited. Higher subsurface temperatures cause greater mobility of ions in the fluids and increase the energy level above the activation energy for electrons or ions, factors that considerably reduce rock resistivity (Keller and Frischknecht, 1966). Tables of electrical resistivity for a variety of rocks, minerals, and geologic environments may be found in Keller (1987) and Palacky (1987).

Ground-Based Electromagnetic Surveys

The MT method is a passive ground-based electromagnetic geophysical technique that investigates the distribution of electrical resistivity (or its inverse, electrical conductivity) below the surface at depths of tens of meters to tens of kilometers (Vozoff, 1991). It does so by measuring the Earth's natural electric and magnetic fields. Worldwide lightning activity at frequencies of 10,000 to 1 hertz (Hz) and geomagnetic micropulsations at frequencies of 1 to 0.001 Hz provide the main frequency bands used by the MT method. The natural electromagnetic waves propagate vertically in the Earth because the very large contrast in the resistivity of the air and the Earth causes a vertical refraction of the electromagnetic wave at the Earth's surface (Vozoff, 1972).

The natural electric and magnetic fields are recorded in two orthogonal, horizontal directions (the vertical magnetic field is also recorded). The resulting time-series signals are used to derive Earth-tensor apparent resistivities and phases after first converting them to complex cross-spectra using fast Fourier transform techniques and least-squares, cross-spectral analysis (Bendat and Piersol, 1971) to solve for a tensor transfer function. If one assumes that the Earth consists of a two-input, two-output, linear system in which the orthogonal magnetic fields are input and the orthogonal electric fields are output, then the calculated function relates the observed electric fields to the magnetic fields. Before it is converted to apparent resistivity and phase, the tensor is normally rotated into principal directions that usually correspond with the direction of maximum and minimum apparent resistivity. For a two-dimensional Earth, the MT fields can be decoupled into transverse electric and transverse magnetic modes. Two-dimensional resistivity modeling is generally computed to fit both modes. When the geology satisfies the two-dimensional assumption, the MT data for the transverse electric mode are assumed to represent the electric field along geologic strike, and the data for the transverse magnetic mode are assumed to represent the electric field across strike. The MT method is well suited for studying complicated geologic environments because the electric and magnetic relations are sensitive to vertical and horizontal variations in resistivity. The method is capable of establishing whether the electromagnetic fields are responding to subsurface rock bodies of effectively one, two, or three dimensions. An introduction to the MT method and references for a more advanced understanding are contained in Dobrin and Savit (1988) and Vozoff (1991).

Magnetotelluric Survey

Six high-frequency MT soundings (stations 1–6, table F1) were acquired in 1997 in the Cochiti Pueblo survey area (figure F2*A*). Spacing between soundings ranged from 4.5 to 11 km. Some stations were used to calibrate the inversion of the airborne TDEM data. These stations were located in areas that had a locally one-dimensional TDEM response and were close to roads but distant from sources of electrical noise, such as power lines. Horizontal electric fields were sensed using titanium electrodes placed in an L-shaped, three-electrode array with dipole lengths of 30 m. The orthogonal, horizontal magnetic fields in the direction of the electric-field measurement array were sensed using high magnetic permeability, mu-metal-cored (80 percent nickel, 15 percent iron, 5 percent molybdenum) induction coils. Frequencies sampled ranged from 20,000 to 4 Hz by use of single-station recordings of both orthogonal horizontal components of the electric and magnetic fields and of the vertical magnetic field. These frequencies lie at the high end of the MT spectrum and are commonly referred to as audiomagnetotelluric (AMT) frequencies. Sampling these frequencies in the Cochiti Pueblo allowed us to probe the subsurface from depths of tens of meters to about one kilometer (Williams, Rodriguez, and Sampson,

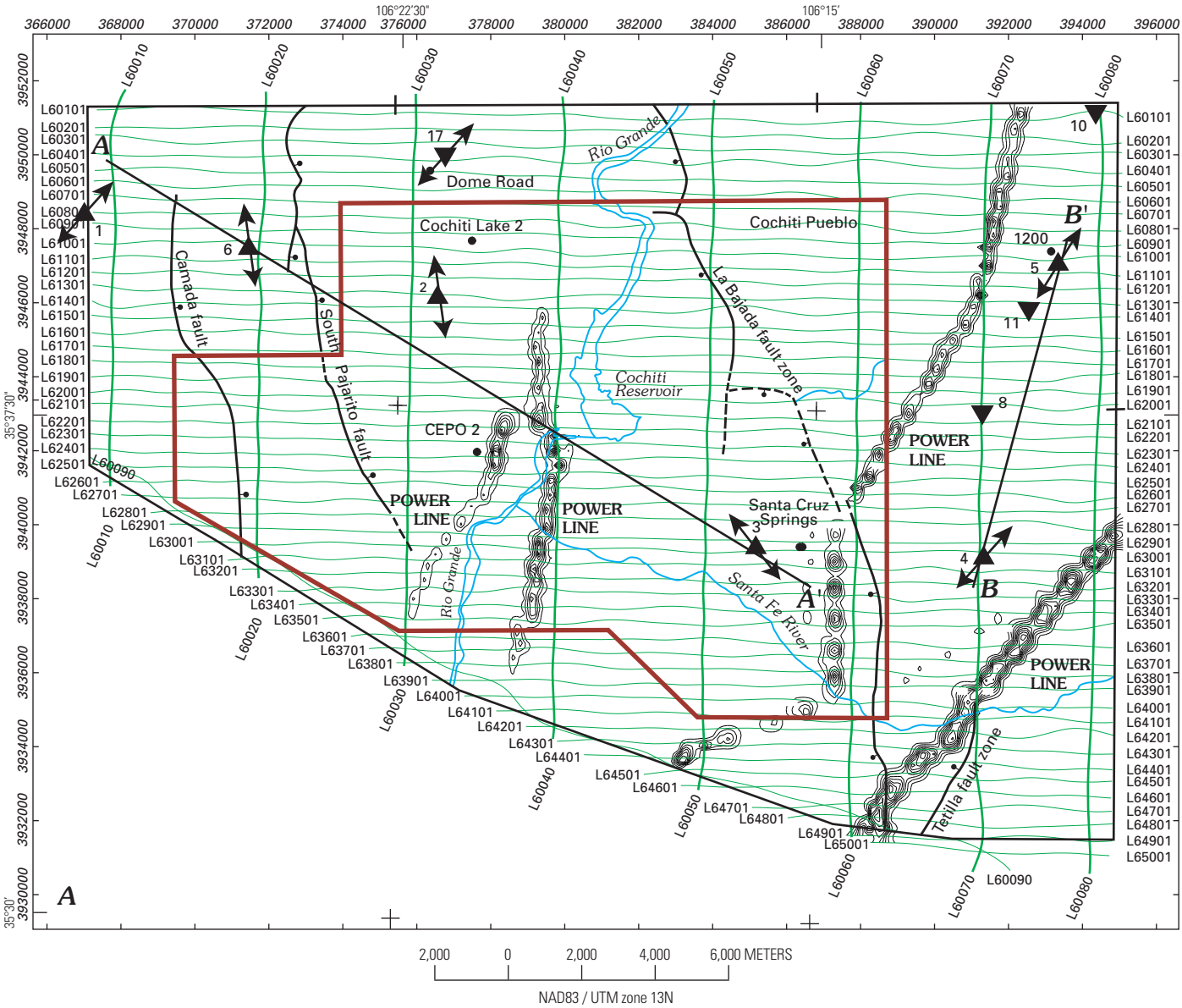

EXPLANATION

- Power line noise (10 mV contour interval)
- Cochiti Pueblo boundary
- Fault—Dashed where uncertain; ball on downthrown side
- Strike of resistivity
- Flight line
- Audiomagnetotelluric station
- Magnetotelluric station
- Water well

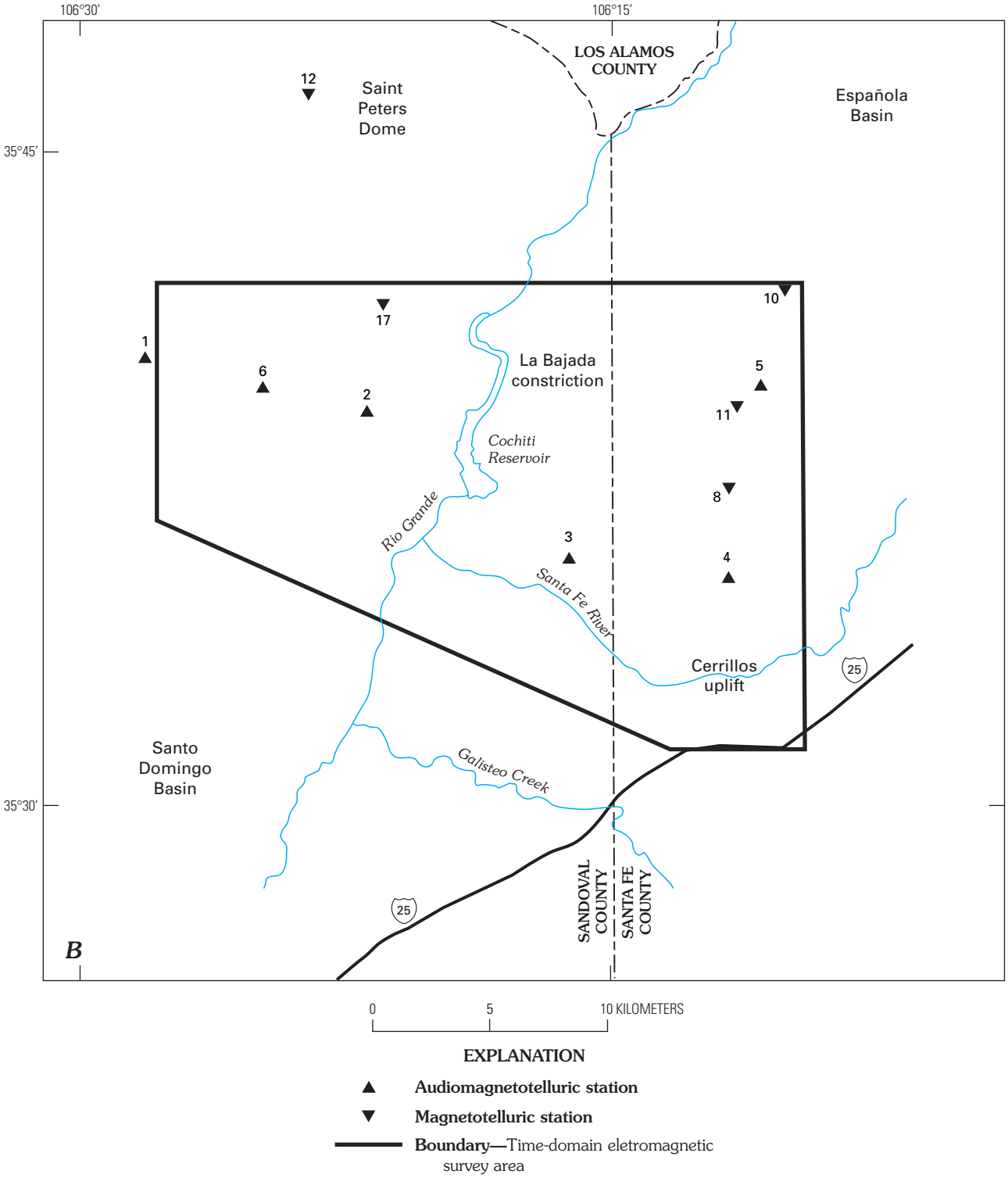

Figure F2 (above and facing page). Cochiti Pueblo time-domain electromagnetic survey area (survey area D, fig. F1) northeast of Albuquerque, New Mexico. High-frequency magnetotelluric (AMT) sounding stations 1–6 acquired in 1997; low-frequency magnetotelluric (MT) sounding stations 8, 10, 11, 12, and 17 acquired in 2002. *A*, Flight lines flown in airborne time-domain electromagnetic survey. *B*, Location of AMT and MT stations. The La Bajada constriction contains Santa Fe Group basin-fill sedimentary aquifers linking the Española and Santo Domingo Basins. Cerrillos uplift constrained by gravity data (chapter D, this volume) and by AMT stations 4 and 5 and MT stations 8, 10, and 11.

2001). Five low-frequency MT soundings (table F1) were also acquired in 2002 in the survey area (sites 8, 10, 11, 12 and 17), fig. F2*B*.

The recorded time-series data were transformed to the frequency domain using Fourier analysis to determine a two-dimensional apparent resistivity and phase tensor at each site. The data were rotated to maximum and minimum apparent resistivity directions so that propagation modes for the signals were decoupled into transverse electric and transverse magnetic modes. This treatment supplies the local strike of electrical sources (illustrated by double-headed arrows in fig. F2*A)*. Local reference sensors were used to help reduce bias in the determinations of impedance that otherwise would be caused by noise in the instruments or the environment (Gamble, Goubau, and Clarke, 1979; Clarke and others, 1983). We also sorted cross-power files to select optimal signal-to-noise data sets. Figure F3*A*, *B* shows observed data represented by digitized values of the transverse electric and transverse magnetic modes from the AMT soundings after the raw data curves were smoothed (Williams, Rodriguez, and Sampson, 2001).

The effects of near-surface resistivity anomalies can cause "static shifts" (Sternberg, Washburne, and Pellerin, 1988) in the data. Such shifts are minor in most of this data set. Only at station 4 was a static shift larger than one-third of a log decade. At the remaining stations very minor static shifts ranged from 0.0 to less than 0.3 of a log decade. Only the large static shifts were accounted for in subsequent two-dimensional modeling of the data.

Resistivity Models Based on Magnetotelluric Survey

The AMT data were modeled by use of a two-dimensional finite-element resistivity algorithm (Wannamaker, Stodt, and Rijo, 1985) called PW2D. The two-dimensional resistivity model is constructed by adjusting the resistivity values beneath the profile of AMT stations, so that for all stations the calculated two-dimensional response agrees with the measured data. From our six AMT stations, we constructed two profiles. Profile A-A′ (fig. F2*A*), at a bearing of N. 70° W., passes directly through AMT stations 6 and 3. AMT stations 1 and 2 are projected more than 1 km north and south, respectively, onto the line A-A′. The profile B-B′ (fig. F2*A*) lies between AMT stations 4 and 5 at a bearing of N. 15° E. The finite-element grid used in these models consisted of 51×26 variable-dimension cells that extended 10 km horizontally beyond the profile end points and 2 km

Figure F3 (facing and following 2 pages). Observed and computed data used to generate two-dimensional finite-element resistivity models (figs. F4*A*, F5, F6) in the Cochiti Pueblo time-domain electromagnetic survey area (area D, fig. F2). *A*, High-frequency magnetotelluric (AMT) observed apparent resistivity data. *B*, AMT observed apparent phase data. *C*, Low-frequency magnetotelluric (MT) observed apparent resistivity data. *D*, MT observed apparent phase data.

Table F1. Audiomagnetotelluric and magnetotelluric station coordinates and elevations in the Cochiti Pueblo area, New Mexico.

[Coordinates are referenced to the 1866 Clarke spheroid and North American 1927 Western United States datum; stations listed in order from west to east; locations determined by use of a global positioning system; longitude and latitude format is in decimal degrees. AMT, audiomagnetotelluric; MT, magnetotelluric; UTM, Universal Transverse Mercator]

Station	Type of sounding	Longitude	Latitude	UTM (m)		Elevation	
				North	East	(m)	(ft)
1	AMT	–106.46612	35.67263	3,948,430	13,367,310	2,063	6,768
6	AMT	–106.41874	35.66382	3,947,390	13,371,585	1,760	5,774
12	MT	–106.38889	35.76750	3,958,861	13,374,449	2,380	7,808
2	AMT	–106.36313	35.65193	3,946,000	13,376,600	1,740	5,709
17	MT	–106.36167	35.68583	3,949,770	13,376,785	1,750	5,741
3	AMT	–106.26918	35.59192	3,939,230	13,385,020	1,657	5,436
4	AMT	–106.20242	35.58593	3,938,490	13,391,060	1,903	6,243
8	MT	–106.20222	35.62361	3,942,655	13,391,127	2,020	6627
5	AMT	–106.17803	35.66128	3,946,820	13,393,370	2,045	6,709
11	MT	–106.18861	35.64639	3,945,184	13,392,391	2,025	6,644
10	MT	–106.16806	35.69806	3,950,901	13,394,319	2,170	7,119

A

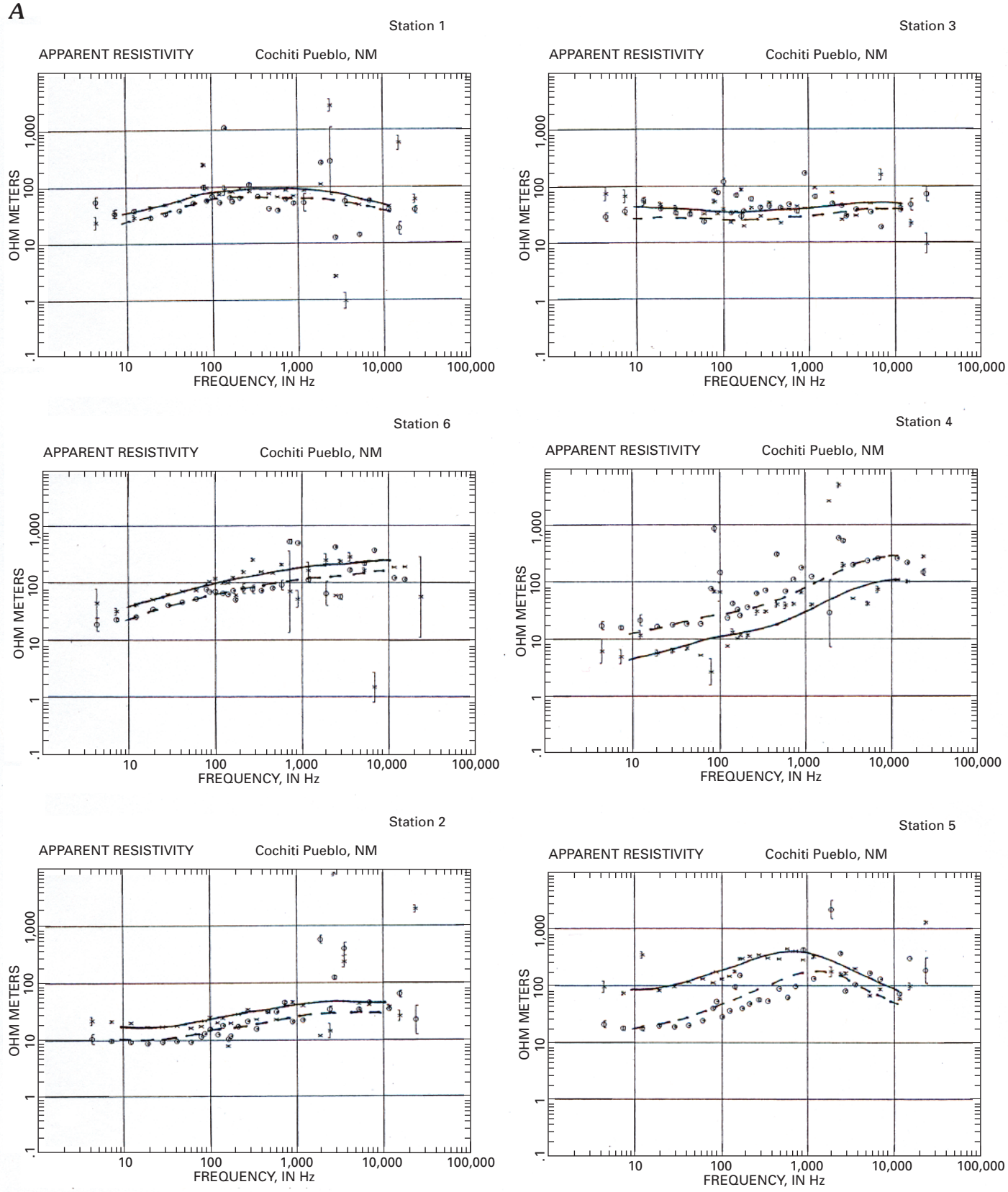

EXPLANATION

x	Observed transverse electric data	[	Observed transverse magnetic error
o	Observed transverse magnetic data	———	Computed transverse electric data
]	Observed transverse electric error	— — —	Computed transverse magnetic data

B

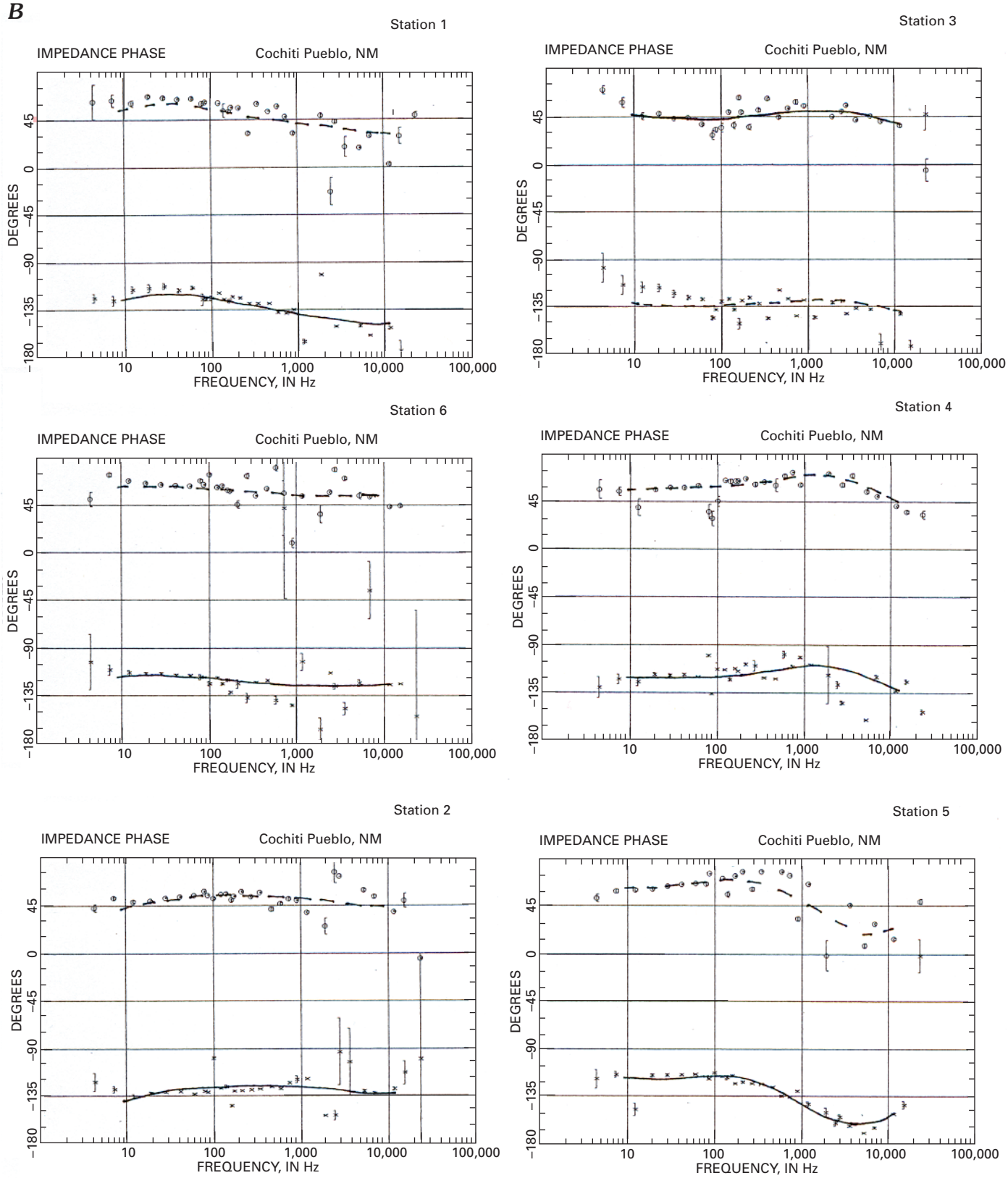

EXPLANATION

x	Observed transverse electric data	[	Observed transverse magnetic error
o	Observed transverse magnetic data	———	Computed transverse electric data
]	Observed transverse electric error	— — —	Computed transverse magnetic data

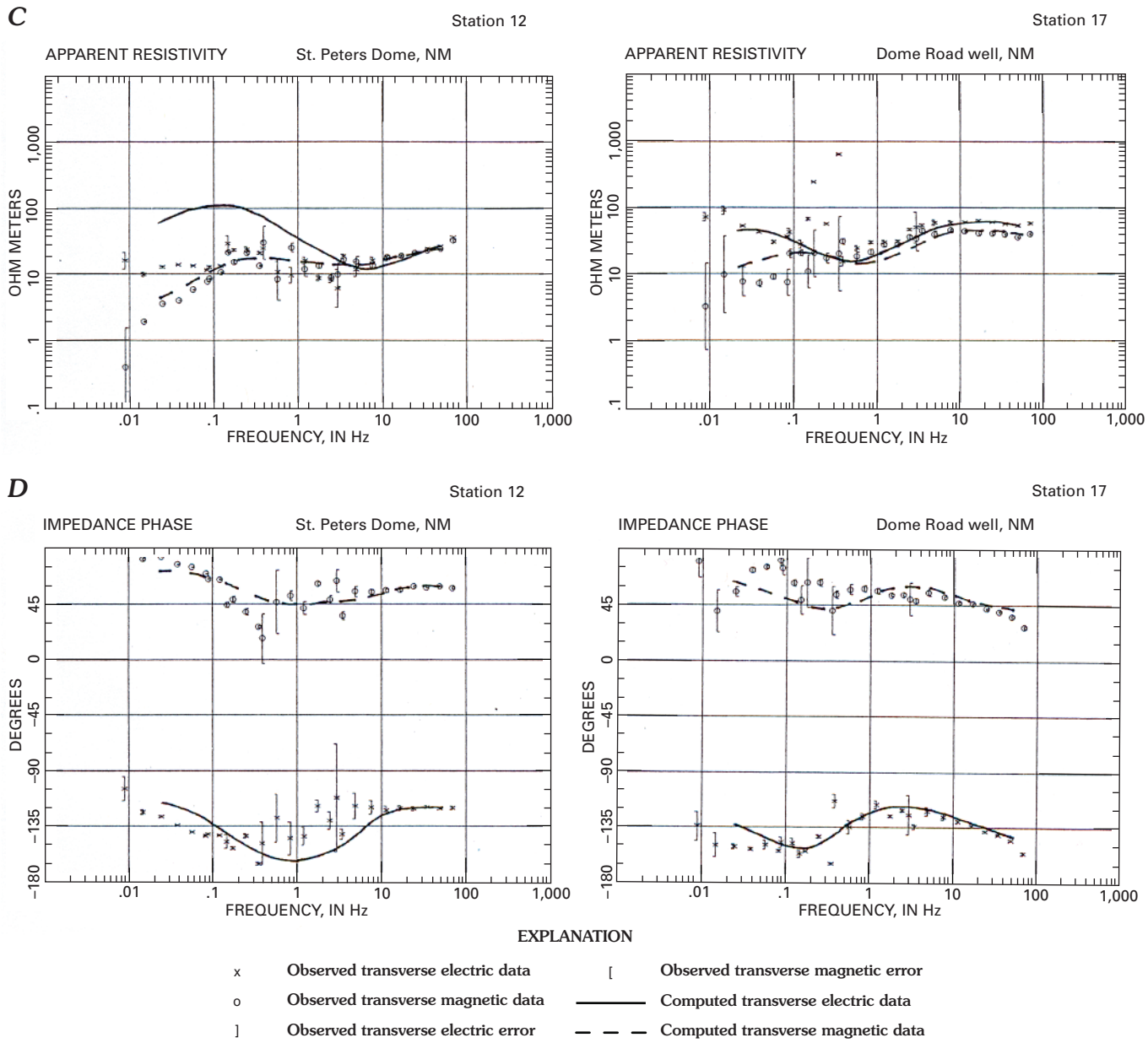

vertically to minimize edge effects. In the finer part of the mesh, the size of the horizontal element ranged between 500 and 1,000 m. The size of the vertical element ranged from 5 m near the surface to 300 m below 1 km depth. We forward modeled by perturbing each two-dimensional model (figs. F4*A*, F5) in an attempt to derive the best-fitting calculated response to the transverse electric and transverse magnetic observed responses. Most of the vertical boundaries in the resistivity model represent the minimum widths of a resistive body needed by the AMT data beneath the AMT station. These vertical boundaries generally could be moved 500 m or more in the direction indicated by horizontal arrows in figures F4*A* and F5. The deepest horizontal layer beneath each station in the resistivity model represents the minimum thickness that the layer must have to fit the lowest frequencies of the AMT data.

The MT data were also modeled with program PW2D. The finite-element grid used in these models consisted of 108×70 variable dimension cells that extend 3,000 km horizontally beyond the profile end points and 350 km vertically to minimize edge effects. In the finer part of the mesh, the horizontal element size was 140 m. The vertical element size ranged from 2.5 m near the surface to 1 km below 5 km depth. We forward modeled each two-dimensional model (fig. F6) in an attempt to fit the calculated response to the transverse electric- and transverse magnetic-mode observed responses. Two stations were exceptions: we did not attempt to fit the transverse electric mode below 0.1 Hz at station 12 or below 0.03 Hz at station 17, because the observed data indicated a three-dimensional response (Williams and Rodriguez, 2003). At these frequencies, we primarily attempted to fit the transverse magnetic mode data (Wannamaker, Hohmann, and Ward, 1984).

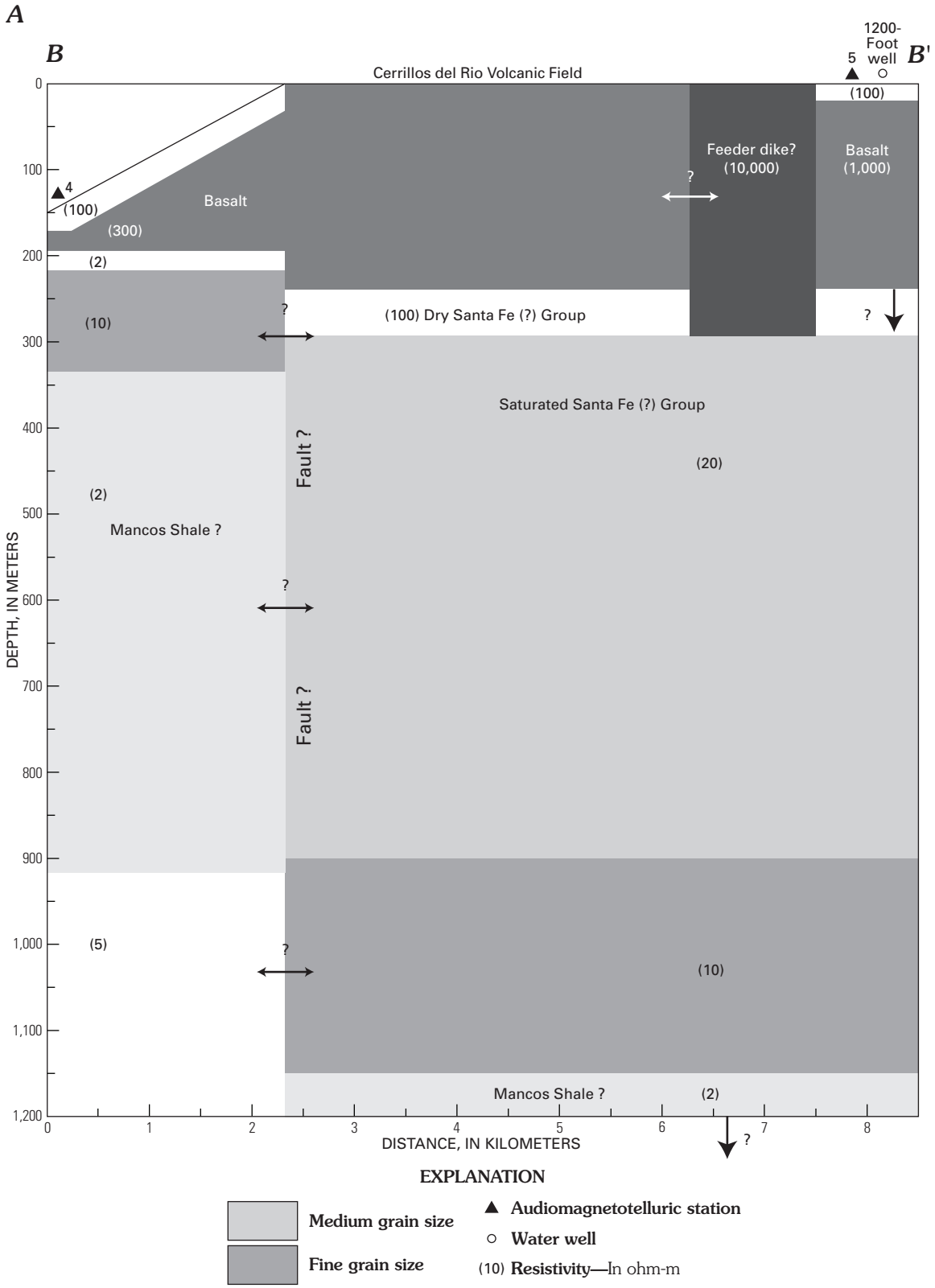
A
B
B'
1200-Foot well
5
Cerrillos del Rio Volcanic Field
(100)
Feeder dike? (10,000)
Basalt (1,000)
4
(100)
Basalt
(300)
(2)
(10)
(100) Dry Santa Fe (?) Group
Saturated Santa Fe (?) Group
(20)
Fault ?
(2)
Mancos Shale ?
Fault ?
(5)
(10)
Mancos Shale ?
(2)
DEPTH, IN METERS
DISTANCE, IN KILOMETERS
EXPLANATION
Medium grain size
Fine grain size
Audiomagnetotelluric station
Water well
(10) Resistivity—In ohm-m

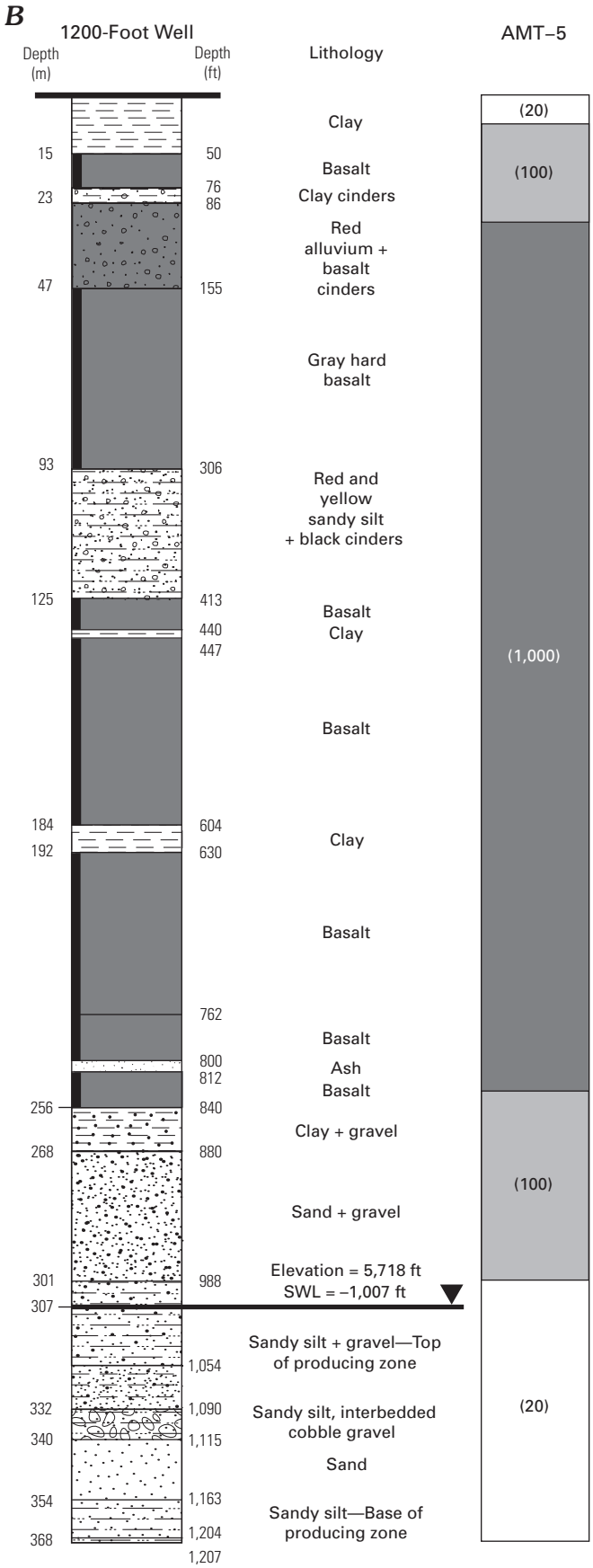

Figure F4 (left and facing page). *A*, Two-dimensional finite-element resistivity model (with lithologic interpretation) constructed from high-frequency magnetotelluric (AMT) data for the Cerros del Rio volcanic field profile B-B′ (fig. F2*A*) in the Cochiti Pueblo time-domain electromagnetic survey area. Arrows within the model indicate uncertainty in the placement of boundaries. Vertical exaggeration is 10. *B*, Comparison of the resistivity model of AMT data at station 5 (fig. F4*A*) and lithology of the 1200-Foot well. Locations of AMT station 5 and 1200-Foot well shown on figure F2*A*.

The calculated fits of our two-dimensional resistivity models (figs. F4*A*, F5, F6) are shown in figure F3. Resistivity boundaries in the model are only approximate because all of the AMT stations are separated by more than 1 km, and the MT stations are separated by more than 8 km. Because of the wide spacing of stations, undetected rock units or structures may exist between stations that are not identified in the resistivity model.

Geologic Interpretation of Surface Electromagnetic Models

Geologic interpretations are based on the resistivity structures revealed in the modeled AMT and MT data (figs. F4*A*, F5, F6) and on regional induction log resistivities of saturated geologic units in seven wells (tables F2, F3): Dome Road (fig. F2*A*), CEPO 2 (fig. F2*A*), Pelto Ortiz 1 (fig. A3), Pelto Blackshare 1 (fig. A3), Black Oil Ferrill 5 (fig. A3), Transocean McKee 1 (fig. A3), and Shell Laguna Wilson Trust 1 (south of our survey area). The northerly electrical strike directions in figure F2*A* can be considered a function of the prominent structural grain of those geologic units, the approximate trend of the shallow geologic structure near the AMT stations (figs. F4*A*, F5), and the approximate structural trend in the upper few kilometers of crust near the MT stations (fig. F6).

As described in chapter A (this volume), the Cochiti Pueblo study area is subdivided into three principal geologic terranes: the western Saint Peters Dome uplifted block, the central subsided La Bajada constriction, and the eastern Cerrillos uplift (fig. A4). AMT and MT stations 1 and 12 are in the western part of the Saint Peters Dome block, in volcanic rocks of the southeastern Jemez volcanic field; stations 2, 3, 6, and 17 are in the northeast part of the Santo Domingo Basin in the central part of the La Bajada constriction; and stations 4 and 5 lie along the northern border of the Cerrillos uplift (figs. F2*B*, A4).

The south-north profile, B-B′ (fig. F2*A*), in the eastern Cerros del Rio volcanic field terrane, shows a moderately resistive basalt (100–300 ohm-m) exposed at the surface that has a thickness of 60±10 m beneath station 4 (fig. F4*A*). Beneath the basalt, a very conductive interval (3 ohm-m) that is 20±10 m thick may be a lacustrine mudstone sequence in

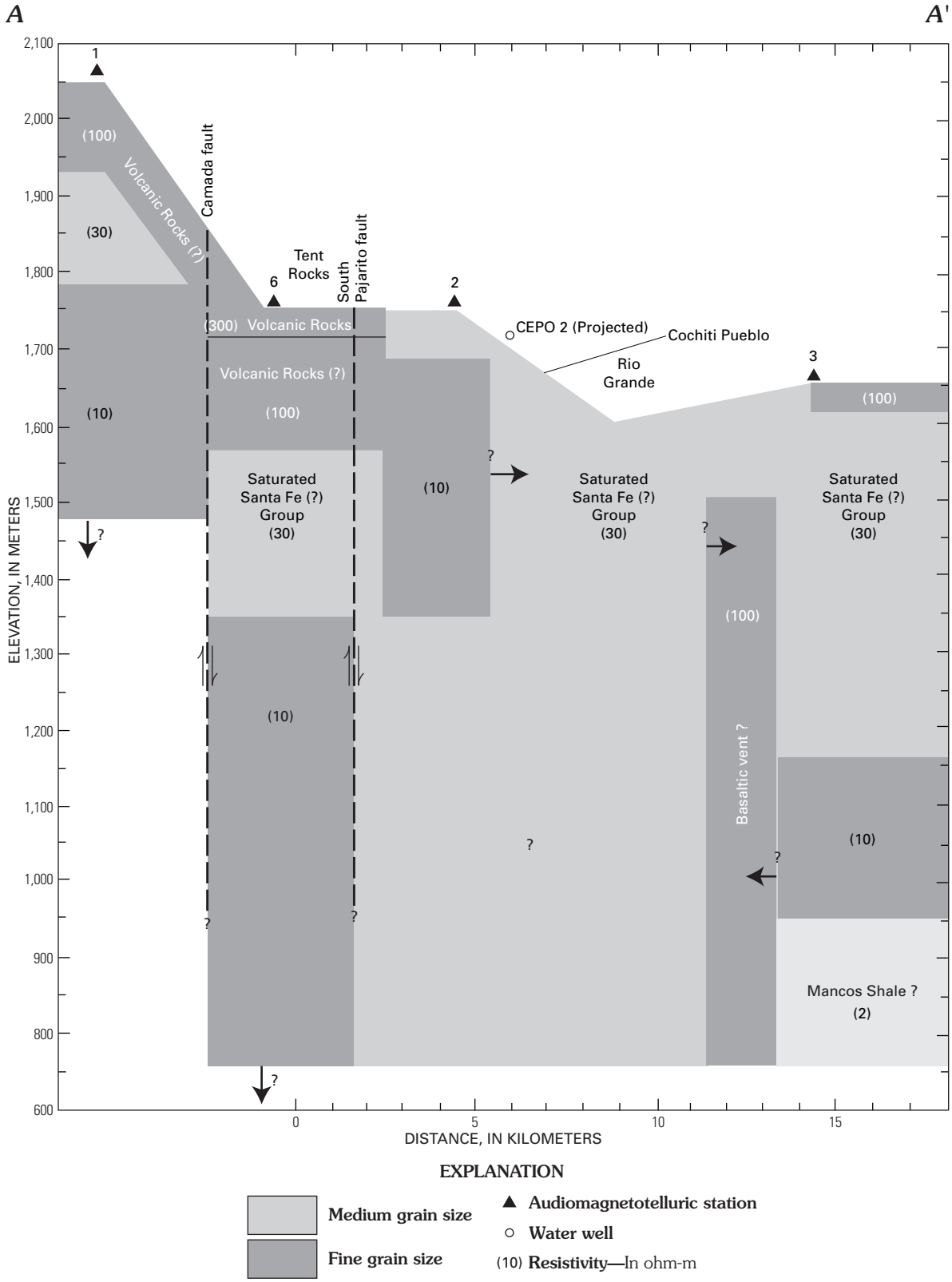

Figure F5. Two-dimensional finite-element resistivity model (with lithologic interpretation) from high-frequency magnetotelluric (AMT) data for the Cochiti Pueblo profile (A-A′, fig. F2*A*) in the Cochiti Pueblo time-domain electromagnetic survey area. Arrow near question mark within the model indicates uncertainty in placement of boundary. Vertical exaggeration is 20.

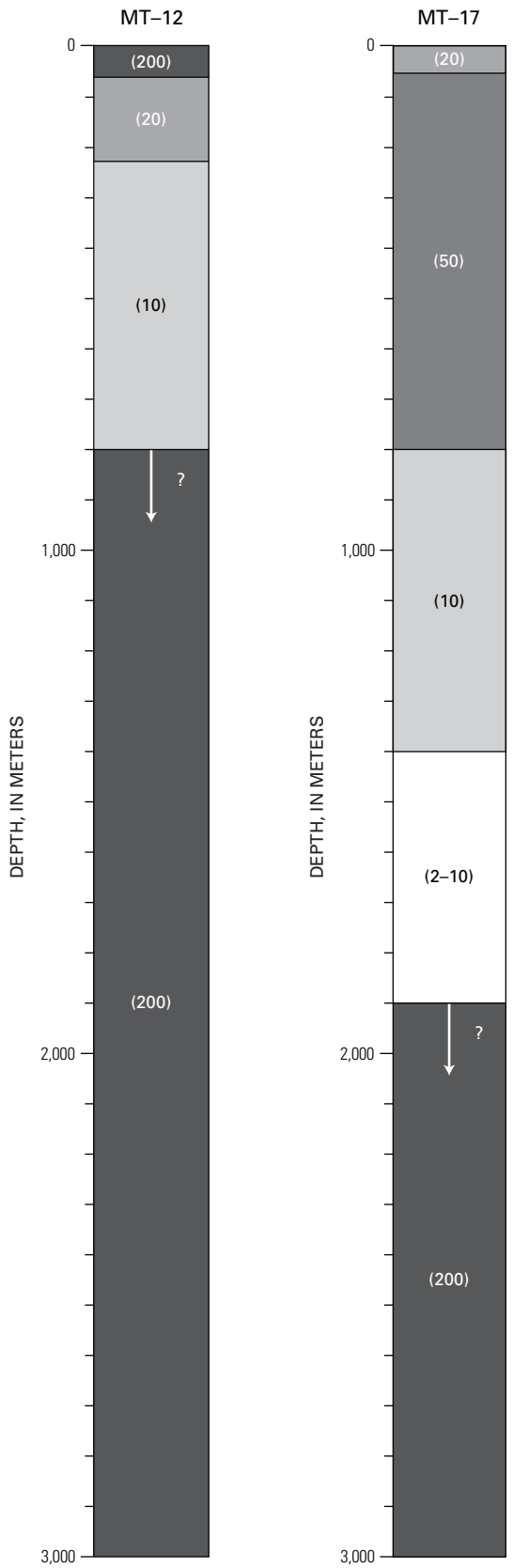

Figure F6. Two-dimensional finite-element resistivity model from low-frequency magnetotelluric (MT) data for MT sounding stations 12 and 17 (see fig. F2*B* for locations). Arrow near question mark within the model indicates uncertainty in placement of boundary.

the upper part of the Santa Fe Group. This conductive interval is underlain by moderately conductive rocks (10 ohm-m); those rocks, which probably include a saturated, fine-grained Santa Fe interval, volcaniclastic Oligocene Espinaso Formation, and possibly the Eocene Galisteo Formation sedimentary rocks, have a composite thickness of 100±20 m. Some part of the weathered Mancos Shale could be included within this 10-ohm-m zone below the basalt. However, the very conductive horizon (2 ohm-m) beginning at a depth of 180±20 m below the AMT station is likely clay-rich Cretaceous marine deposits of the Mancos Shale. Preliminary MT models of this sounding show that the conductive interval is 620±80 m thick. Beneath this very conductive interval, less conductive rocks (5 ohm-m) probably include units of Permian, Triassic, and Jurassic sedimentary rocks.

A resistive interval of basalts (1,000 ohm-m) of the Cerros del Rio at station 5 (fig. F4*A*) are 250±25 m thick. This basalt interval ranges from 60 to 250 m thick between stations 4 and 5. Approximately 140 m of the 250 m basalt thickness at station 5 reflects constructional topography resulting from the growth of basaltic volcanoes. A remarkably detailed driller's log (fig. F4*B*) exists for a water well (the 1200-Foot well) 200 m northwest of AMT station 5. The thickness of the basalt (256 m) measured on a lithology log constructed from the driller's record corresponds closely with the thickness of basalt determined in the AMT model (250±25 m). As recorded in the driller's log, the static water elevation lay at 307 m depth, so our forward modeling used a value of 100 ohm-m for the unsaturated Santa Fe Group sand and gravel above the water table. Saturated sand and silty sand of the Santa Fe Group typically have resistivities in the 20–70 ohm-m range. The modeled electrical sounding shows that 20 ohm-m material extends to a depth of 900±100 m. Beneath the 20 ohm-m material is a 10 ohm-m interval with a thickness of 250±100 m. The 10 ohm-m material may include early Tertiary Galisteo and Espinaso Formations that cannot be separated from Santa Fe Group solely on the basis of their electrical signatures. Espinaso Formation is found in the Yates La Mesa petroleum test well 2 (10 km to the northeast, north of the Santa Fe River, pl. 2), but deposits of the Galisteo may have been eroded or never deposited to the north. Very conductive (2 ohm-m) inferred Mancos Shale occurs at a depth of 1,150±100 m and has lower electrical resistivity than other units in the region. Between station 4, where the top of the Mancos is 1,700 m above sea level, and station 5, where it is 900 m, the top of the Mancos apparently drops 800 m. Thus, these MT results provide evidence for 800 m of Tertiary structural relief at the north end of the Cerrillos uplift. The shallow Mancos Shale located at AMT station 4, immediately south of Tetilla Peak, provides the

Table F2. Range of average resistivity values in regional induction logs for stratigraphic units intersected in wells in study region.

[Well abbreviations: B, Black Oil Ferrill 5; C, CEPO 2; D, Dome Road; PB, Pelto Blackshare 1; PO, Pelto Ortiz 1; T, Transocean McKee 1; S, Shell Laguna Wilson Trust 1]

Epoch or Period	Stratigraphic unit or level	Ohm-m	Thickness (m)	Well
Pliocene–Miocene	Santa Fe Group	8–70	400–451	D, PB, C
Oligocene	Espinaso Formation	10–20	533	PB
Eocene	Galisteo Formation	5–20	526–1,376	PB, PO, B
Cretaceous	Upper	2–40	420–1,526	PB, PO, B, S, T
Jurassic	Upper/Middle	2–20	223–453	PB, S, T
Triassic	Upper	2–15	482–933	S, T
Permian	Upper/Lower	6–200	262–659	S, T
Pennsylvanian	Upper/Middle/Lower	7–200	585–766	S, T

Table F3. Location of wells referred to in table F2.

[Coordinates listed below are referenced to the 1866 Clarke spheroid and North American 1927 datum; stations listed in order from west to east; locations determined using a global positioning system; longitude and latitude format is decimal degrees; UTM, Universal Transverse Mercator]

Well	Longitude	Latitude	UTM (m)		Elevation	
			North	East	(m)	(ft)
B	–106.041	35.386	3,916,149	13,405,451	1,787	5,889
C	–106.351	35.627	3,943,183	13,377,650	1,632	5,379
D	–106.365	35.683	3,949,468	13,376,462	1,765	5,818
PB	–106.269	35.397	3,917,611	13,384,758	1,831	6,034
PO	–106.058	35.412	3,919,049	13,403,938	1,761	5,804
T	–105.990	35.390	3,916,545	13,410,088	1,801	5,935
S	–106.968	35.024	3,877,277	13,320,453	1,643	5,415

farthest northwest constraint for the edge of the Cerrillos uplift. This AMT-defined northwest edge is consistent with the subsurface extent of the uplift on the basis of gravity data (chapter D, this volume). The feeder dike shown in figure F4*A* may be oriented in any one of several azimuthal directions with respect to station 5. It could correspond with dikes associated with the Cerro Colorado vent to the west (fig. F7*A*), the Cerrito Portrillo andesite volcano to the northeast (pl. 2), or a N. 20° E.–trending linear chain of younger basalts and andesites to the southeast (pl. 2). The high accuracy of the thickness of resistive basalt determined by the sounding at AMT station 5, as compared with the driller's log for the 1200-Foot well, suggests that electrical soundings of this type may be an accurate method of determining the thickness of volcanic deposits in the Cerros del Rio volcanic field and in similar settings underlain by shallow volcanic rocks of variable thickness. The advantage of the ground AMT soundings is the much greater depth of investigation, as much as 1,200 m in the AMT station 5 example, as opposed to a maximum depth of about 300 m depth for the airborne TDEM data in a favorable situation (for example, no thick, shallow conductors). Detailed comparison of the AMT data from station 5 with the lithologic log from the 1200-Foot well (fig. F4*B*) also provides some insight into the degree of resolution of the AMT soundings and plan-mapping techniques: Modeling of the AMT data was able to resolve the thickness of resistive basalt only to within 10 percent. Also, in the upper 47 m, we were not able to distinguish the 24-m interval of dry basalt cinders from

Figure F7 (facing and following 5 pages). Depth slices in the Cochiti Pueblo time-domain electromagnetic survey area (*A*–*F*), drawn on the basis of least-squares inversions. Solid numbered triangles represent high-frequency magnetotelluric sounding stations. C3, C4, C5, W4, magnetic anomalies discussed in chapter D (this volume); F, inferred fine grain size sediments; V, inferred volcanic rock. *A*, 20-m-depth slice. *B*, 50-m-depth slice. *C*, 70-m-depth slice. *D*, 100-m-depth slice. *E*, 150-m-depth slice. *F*, 200-m-depth slice.

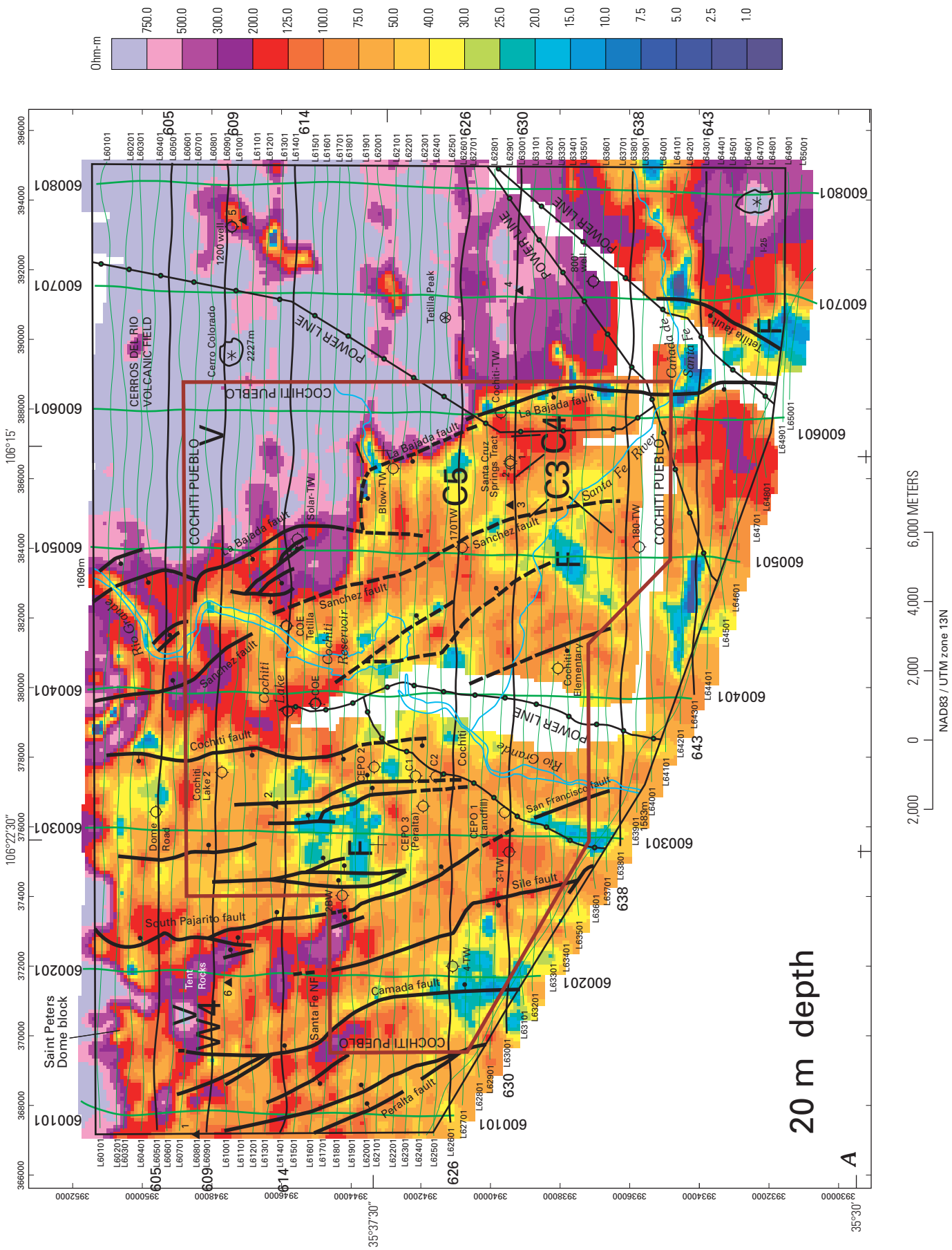
Ohm-m
750.0
500.0
300.0
200.0
125.0
100.0
75.0
50.0
40.0
30.0
25.0
20.0
15.0
10.0
7.5
5.0
2.5
1.0
20 m depth
A
NAD83 / UTM zone 13N
6,000 METERS
4,000
2,000
0
2,000
CERROS DEL RIO VOLCANIC FIELD
COCHITI PUEBLO
Saint Peters Dome block
Cerro Colorado
Tetilla Peak
POWER LINE
Rio Grande
Santa Fe River
Cochiti Lake
Cochiti Reservoir
Santa Fe NF
Cochiti Elementary
Santa Cruz Springs Tract
Canada de Santa Fe
Tetilla fault
La Bajada fault
Sanchez fault
Cochiti fault
South Pajarito fault
Camada fault
Peralta fault
Sile fault
San Francisco fault
Dome Road
Tent Rocks
Cochiti-TW
Blow-TW
Solar-TW
170TW
180-TW
3-TW
4-TW
CEPO 1 (Landfill)
CEPO 2
CEPO 3 (Peralta)
COE Tetilla
COE
1200 well
800 well
1583m
1609m
2227m
35°37'30"
35°30'
106°22'30"
106°15'

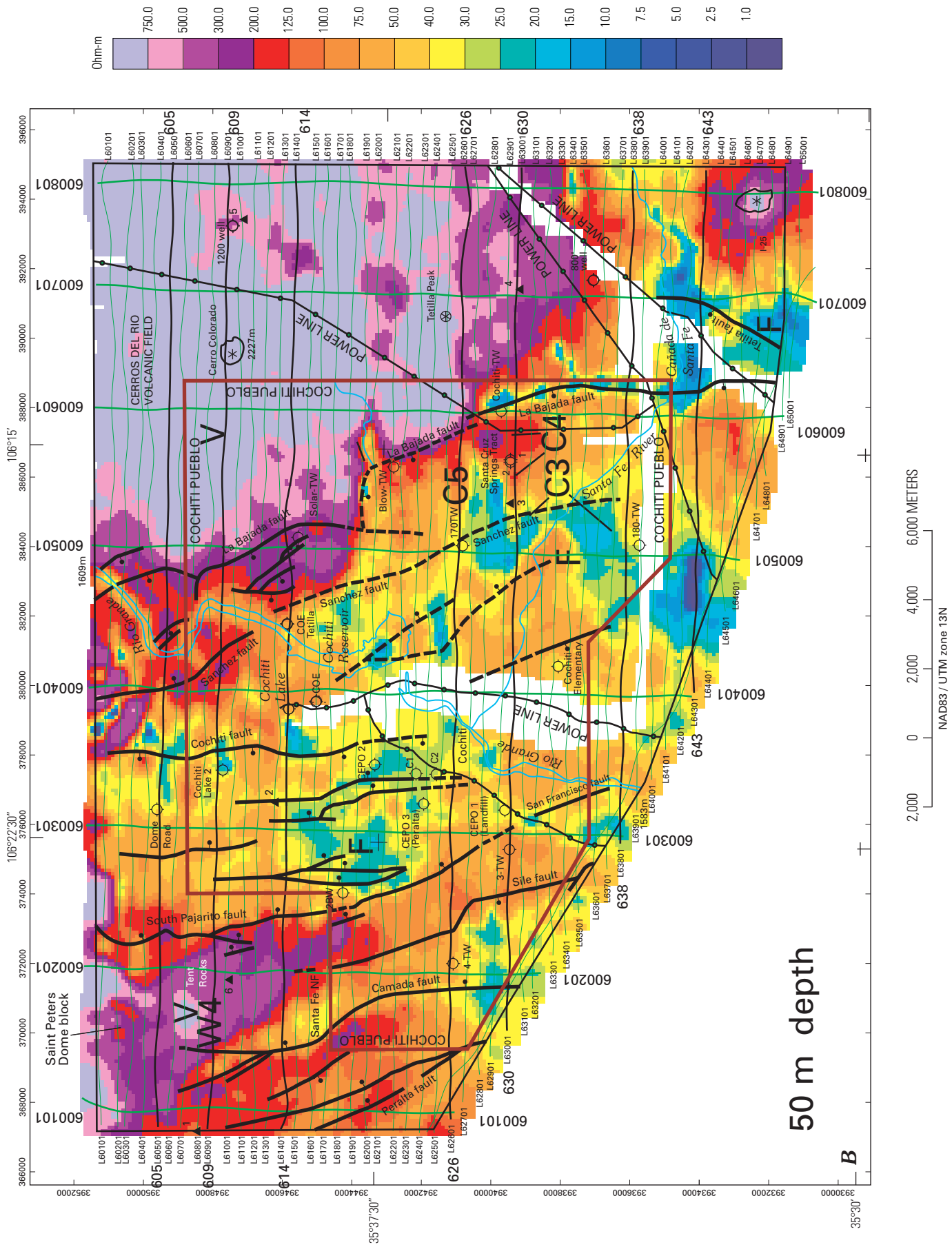
Ohm-m
750.0
500.0
300.0
200.0
125.0
100.0
75.0
50.0
40.0
30.0
25.0
20.0
15.0
10.0
7.5
5.0
2.5
1.0
50 m depth
B
CERROS DEL RIO VOLCANIC FIELD
COCHITI PUEBLO
Cerro Colorado
2227m
1200 well
Tetilla Peak
POWER LINE
La Bajada fault
Sanchez fault
Cochiti fault
Cochiti Lake
Cochiti Reservoir
Rio Grande
Santa Fe River
Canada de Santa Fe
Tetilla fault
San Francisco fault
Sile fault
Camada fault
Peralta fault
South Pajarito fault
Saint Peters Dome block
Dome Road
Tent Rocks
Santa Fe NF
Cochiti Elementary
Santa Cruz Springs Tract
Solar-TW
Blow-TW
170TW
180-TW
3-TW
4-TW
CEPO 1 (Landfill)
CEPO 2
CEPO 3 (Peralta)
COE
Tetilla
1583m
1609m
806' well
I-25
C1
C2
C3
C4
C5
F
V
W4
605
609
614
626
630
638
643
6008001
6007001
6006001
6005001
6004001
6003001
6002001
6001001
366000
368000
370000
372000
374000
376000
378000
380000
382000
384000
386000
388000
390000
392000
394000
396000
3952000
3948000
3944000
3942000
3940000
3938000
3936000
3934000
3932000
3930000
106°22'30"
106°15'
35°37'30"
35°30'
2,000
0
2,000
4,000
6,000 METERS
NAD83 / UTM zone 13N

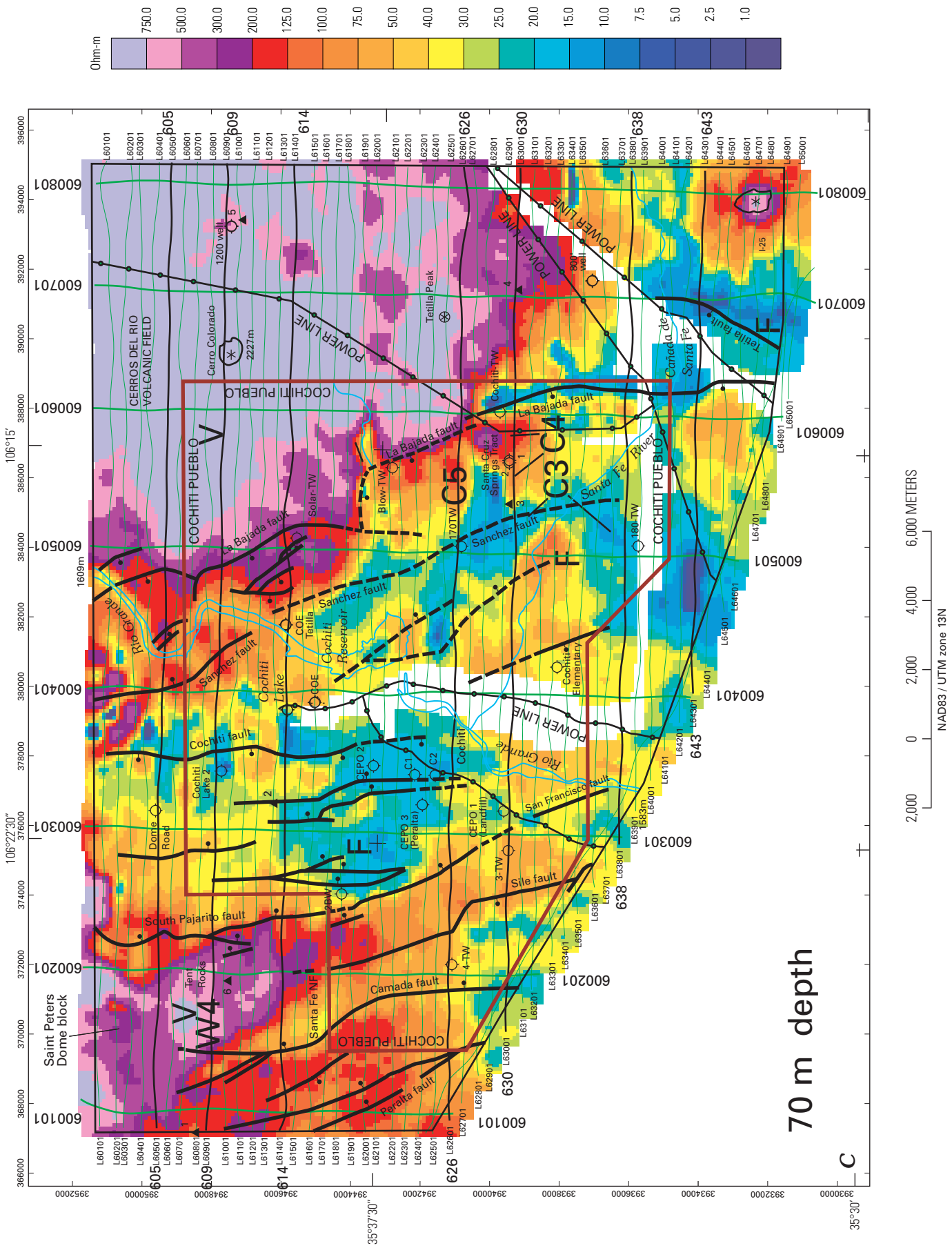
Ohm-m
750.0
500.0
300.0
200.0
125.0
100.0
75.0
50.0
40.0
30.0
25.0
20.0
15.0
10.0
7.5
5.0
2.5
1.0
70 m depth
CERROS DEL RIO VOLCANIC FIELD
COCHITI PUEBLO
Cerro Colorado
Tetilla Peak
POWER LINE
La Bajada fault
Sanchez fault
Cochiti fault
Cochiti Lake
Cochiti Reservoir
Santa Fe River
Rio Grande
Camada fault
Peralta fault
Sile fault
San Francisco fault
South Pajarito fault
Saint Peters Dome block
Santa Fe NF
Cochiti Elementary
Santa Cruz Springs Tract
Tent Rocks
Dome Road
Tetilla fault
NAD83 / UTM zone 13N
6,000 METERS

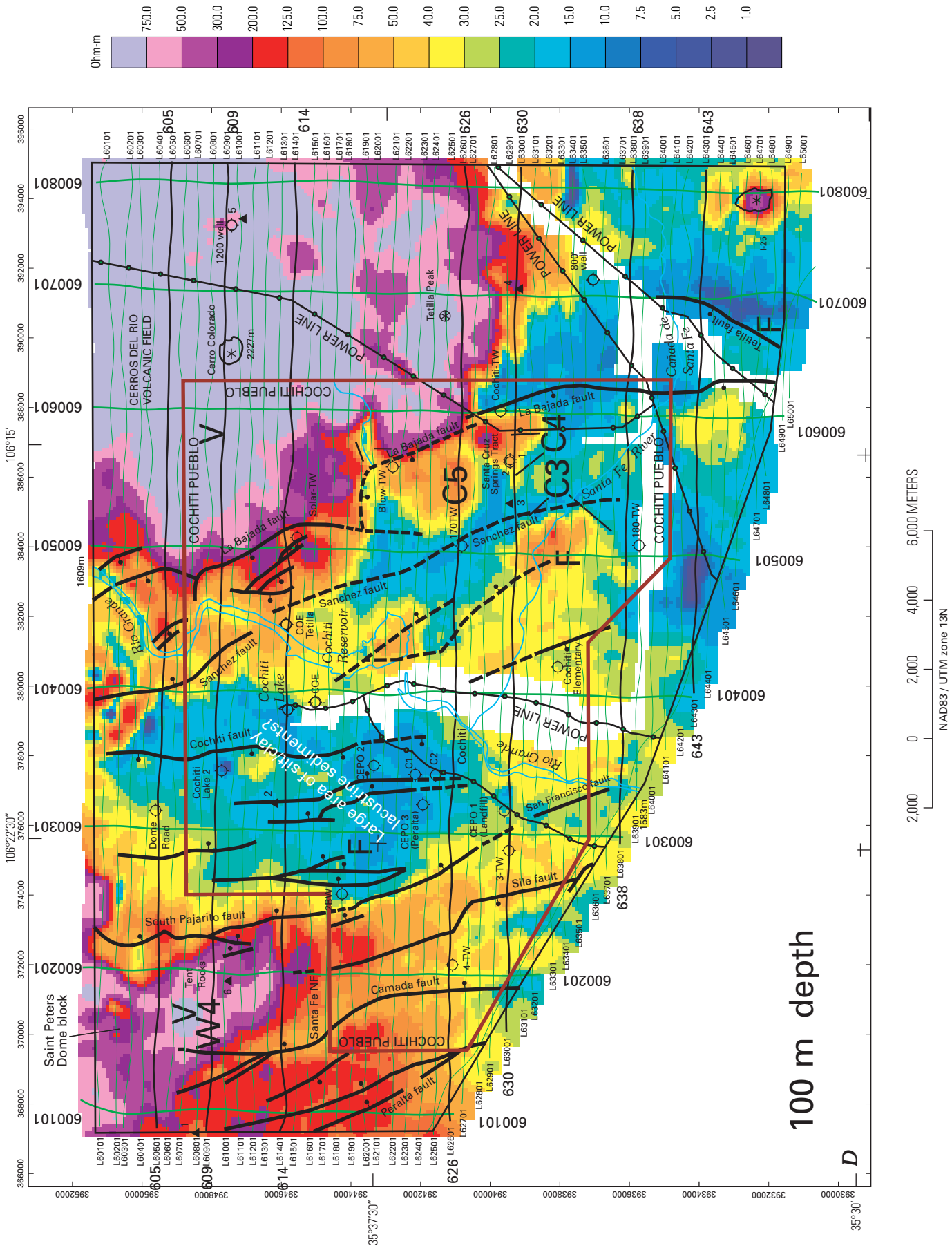
Ohm-m
750.0
500.0
300.0
200.0
125.0
100.0
75.0
50.0
40.0
30.0
25.0
20.0
15.0
10.0
7.5
5.0
2.5
1.0
100 m depth
D
CERROS DEL RIO VOLCANIC FIELD
Carro Colorado
2227m
1200 well
Tetilla Peak
POWER LINE
COCHITI PUEBLO
La Bajada fault
Santa Cruz Springs Tract
Cochiti-TW
Solar-TW
Blow-TW
170TW
180-TW
Sanchez fault
Santa Fe River
Tetilla fault
Cañada de Santa Fe
Cochiti Reservoir
Cochiti Lake
COE Tetilla
Cochiti Elementary
Cochiti fault
Cochiti Lake 2
Dome Road
Rio Grande
Large area of siliciclay lacustrine sediments?
CEPO 1 (Landfill)
CEPO 2
CEPO 3 (Peralta)
San Francisco fault
Sile fault
3-TW
4-TW
South Pajarito fault
Camada fault
Peralta fault
Saint Peters Dome block
Santa Fe NF
Tent Rocks
1583m
1609m
C1
C2
C3
C4
C5
F
I-25
605
609
614
626
630
638
643
106°15'
106°22'30"
35°37'30"
35°30'
NAD83 / UTM zone 13N
6,000 METERS
4,000
2,000
0
2,000

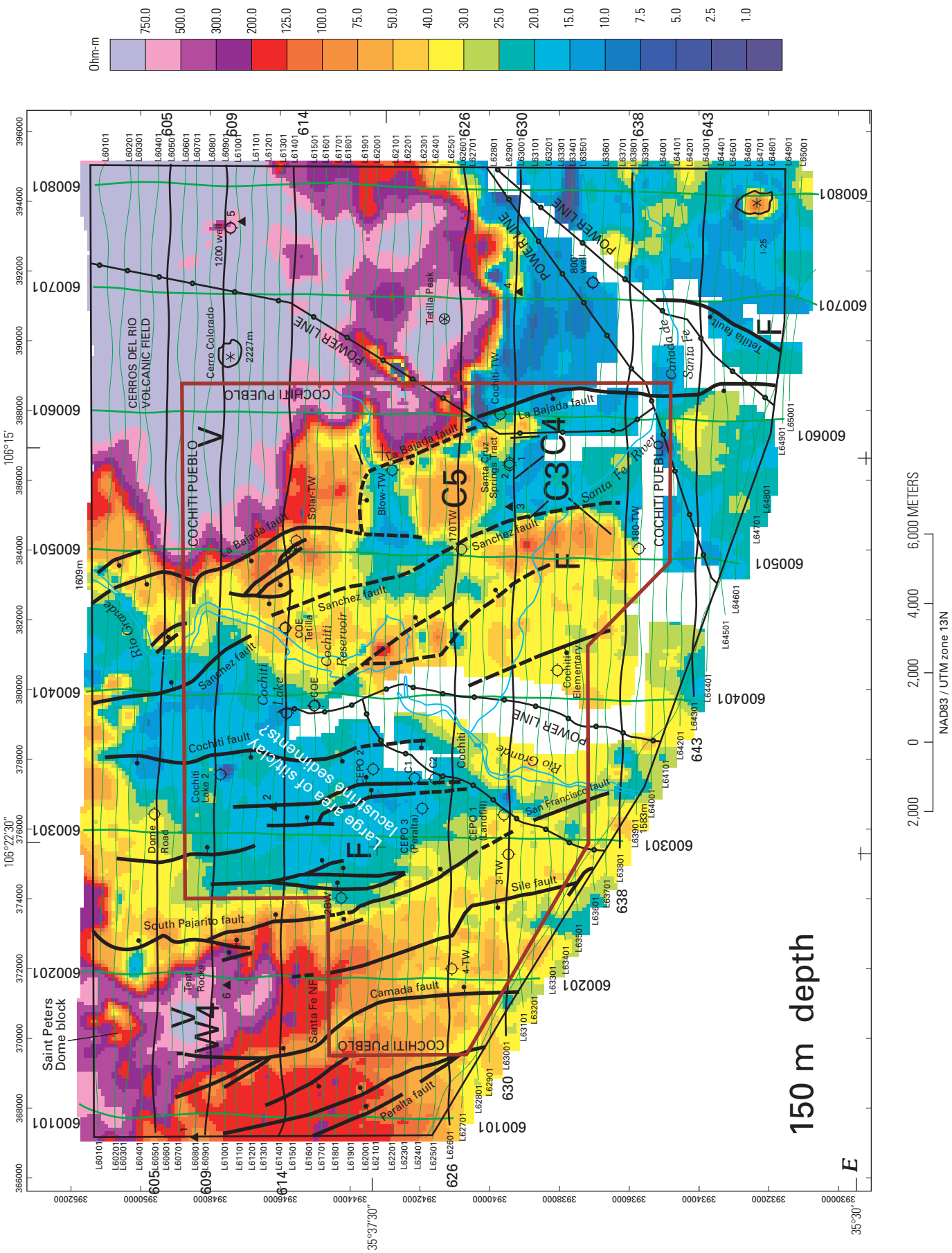
Ohm-m
750.0
500.0
300.0
200.0
125.0
100.0
75.0
50.0
40.0
30.0
25.0
20.0
15.0
10.0
7.5
5.0
2.5
1.0
150 m depth
CERROS DEL RIO VOLCANIC FIELD
COCHITI PUEBLO
Saint Peters Dome block
Large area of stylolaty tectonite sediments?
Cochiti Lake
Cochiti Reservoir
Santa Fe River
Rio Grande
Canada de Santa Fe
POWER LINE
La Bajada fault
Sanchez fault
Cochiti fault
South Pajarito fault
Camada fault
Peralta fault
Sile fault
San Francisco fault
Santa Fe NF
Tetilla Peak
Cerro Colorado
Dome Road
Cochiti Elementary
Santa Cruz Springs Tract
Cochiti-TW
Blow-TW
Solar-TW
170TW
180 TW
3-TW
4-TW
1200 well
800 well
2227m
1609m
1583m
I-25
C1
C2
C3
C4
C5
CEPO 1 (Landfill)
CEPO 2
CEPO 3 (Peralta)
COE Tetilla
COE
NAD83 / UTM zone 13N
6,000 METERS
4,000
2,000
0
2,000
106°15'
106°22'30"
35°37'30"
35°30'

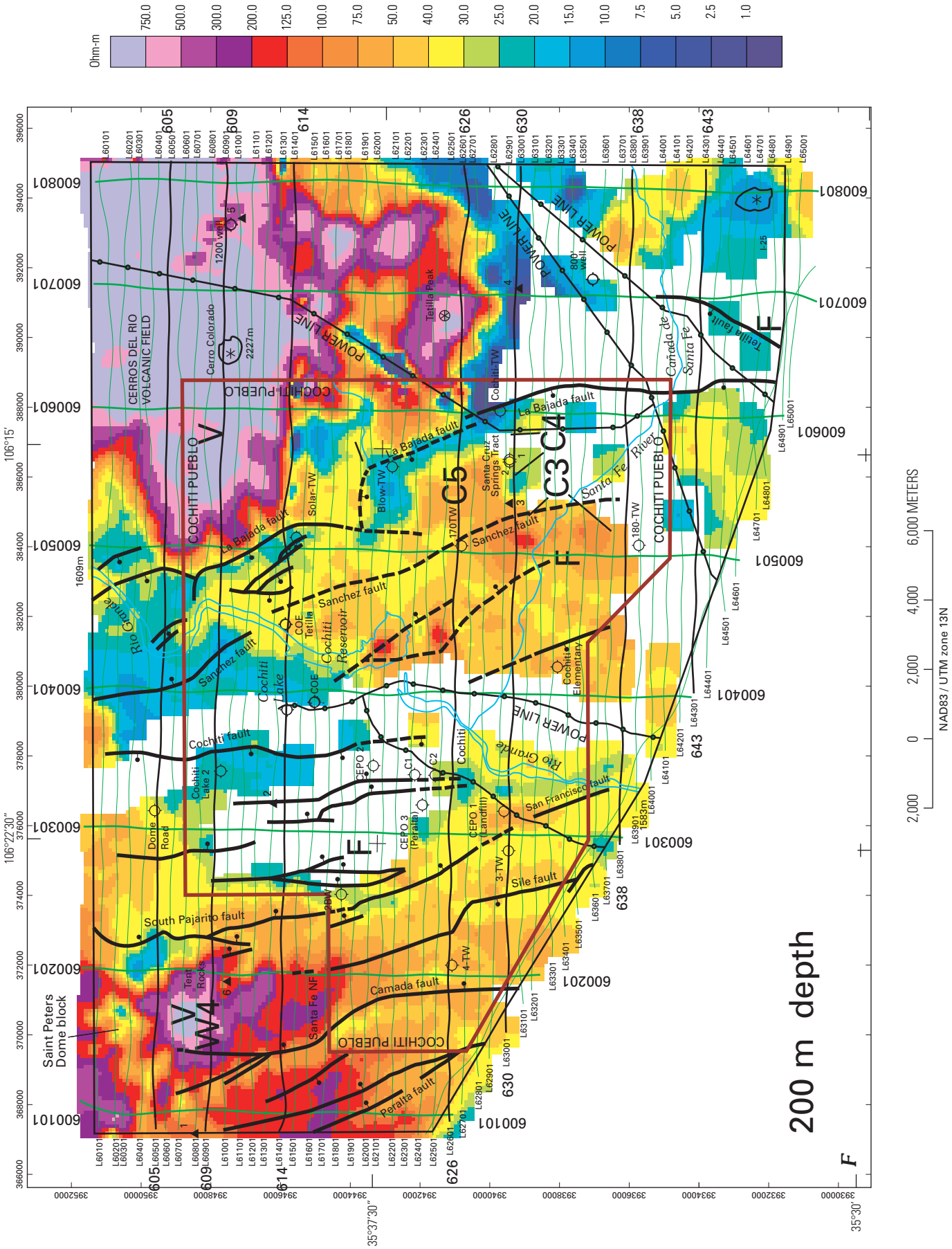
Ohm-m
750.0
500.0
300.0
200.0
125.0
100.0
75.0
50.0
40.0
30.0
25.0
20.0
15.0
10.0
7.5
5.0
2.5
1.0
200 m depth
CERROS DEL RIO VOLCANIC FIELD
COCHITI PUEBLO
Cerro Colorado
2227m
Tetilla Peak
POWER LINE
La Bajada fault
Sanchez fault
Cochiti fault
South Pajarito fault
Camada fault
Peralta fault
Sile fault
San Francisco fault
Santa Fe River
Rio Grande
Cochiti Lake
Cochiti Reservoir
Santa Cruz Springs Tract
Saint Peters Dome block
Santa Fe NF
Dome Road
Tent Rocks
Cochiti Elementary
Tetilla fault
Camada de
Solar-TW
Blow-TW
170TW
180-TW
Cochiti-TW
3-TW
4-TW
CEPO 1 (Landfill)
CEPO 2
CEPO 3 (Peralta)
COE Tetilla
1200 well
800 well
1583m
1609m
C5
C4
C3
C2
C1
W4
W5
F
605
609
614
626
630
638
643
6000101
6000201
6000301
6000401
6000501
6000601
6000701
6000801
L25
L65001
L64901
L64801
L64701
L64601
L64501
L64401
L64301
L64201
L64101
L64001
L63901
L63801
L63701
L63601
L63501
L63401
L63301
L63201
L63101
L63001
L62901
L62801
L62701
L62601
L62501
L62401
L62301
L62201
L62101
L62001
L61901
L61801
L61701
L61601
L61501
L61401
L61301
L61201
L61101
L61001
L60901
L60801
L60701
L60601
L60501
L60401
L60301
L60201
L60101
L60050
L60040
L60301
L60201
L60101
106°15'
106°22'30"
35°37'30"
35°30'
396000
394000
392000
390000
388000
386000
384000
382000
380000
378000
376000
374000
372000
370000
368000
395200
395000
394800
394600
394400
394200
394000
393800
393600
393400
393200
393000
2,000
0
2,000
4,000
6,000 METERS
NAD83 / UTM zone 13N

hard basalt beneath, because the resistivity of the cinders was intermediate between the resistivities of the dry clay and the hard basalt.

The northwest-southeast profile, A-A′ (fig. F2*A*) in the Cochiti Pueblo area is based on four AMT stations. The profile extends across the South Pajarito fault (fig. F5). The westernmost sounding (station 1) was made in the Saint Peters Dome block; the three eastern soundings on the profile (stations 6, 2, and 3) were made in the northeast part of the Santo Domingo Basin. At stations 1 and 6, volcanic rocks and interstratified volcaniclastic deposits are at the surface and in the upper part of the profile. Station 1 is just outside (to the west) of the area of the geologic map compilation of the Cochiti Pueblo area shown in plate 2. The geology under station 1 consists of thin Pliocene gravel of Lookout Park overlying Cochiti Formation in the footwall block of the Camada fault. On the basis of aeromagnetic and TDEM data, it appears that station 1 is just outside the area of Miocene Bearhead Rhyolite lava domes and intrusions and the shallow deposits consist of very proximal coarse, high-resistivity volcaniclastic Cochiti Formation (100 ohm-m) from 2,060 m to about 1,940 m elevation. This material is underlain by a 150±30-m-thick interval of moderate resistivity (30 ohm-m) that probably correlates with medium-grained sand and gravel of the Cochiti Formation. The bottom of the profile has low resistivity (10 ohm-m) and probably is silt and silty fine sand within the Cochiti Formation or possibly even middle Miocene deposits of the Santa Fe Group that are locally present in the Saint Peters Dome block beneath upper Miocene Keres Group basalt, andesite, and rhyolite volcanic rocks. The base of the 10 ohm-m material is not resolved by the AMT sounding, but it has a minimum thickness of 310±60 m.

AMT station 6 is located in Peralta Canyon within the Kashe-Katuwe Tent Rocks National Monument (pl. 1) in thin Quaternary alluvium directly adjoining large cliff exposures of Peralta Tuff Member of the Bearhead Rhyolite and overlying basal Cochiti Formation (pl. 2). The upper 30 m of AMT sounding 6 consists of high-resistivity (300 ohm-m) (fig. F5) rhyolite lava and coarse proximal breccia or sediments derived from the extrusive dome of Bearhead Rhyolite exposed in lower Peralta Canyon (Smith, 2001). The underlying 150 m of moderately resistive material (100 ohm-m) may be coarse-grained sedimentary material derived from the Bearhead Rhyolite, or it may be similar near-vent breccias and pyroclastic deposits partially to wholly saturated by a perched water table. These volcanic or volcaniclastic materials are underlain by moderately conductive saturated, coarse-grained deposits (30 ohm-m) of the Santa Fe Group (Cochiti Formation) that have a thickness of 220±40 m. Beneath it is a more conductive saturated fine-grained sedimentary interval (10 ohm-m), probably in the middle part of the Santa Fe Group, whose base was not resolved but which has a minimum thickness of 600±100 m. The similar sequences of resistivities between stations 1 and 6 argue for considerable eastward thickening of the more resistive 100 ohm-m and 30 ohm-m intervals across the Camada fault and for similar thickening of fine-grained Santa Fe Group(?) sediments (10 ohm-m) beneath them.

AMT stations 2 and 3, in the northeast part of the Santo Domingo Basin, reflect electrical responses of basin-fill sediments of the Santa Fe Group. A moderately conductive, unsaturated, fine-grained Santa Fe interval (30 ohm-m), and the lower part of the Bandelier Tuff (Otowi Member) immediately beneath station 2 (fig. F5) have a combined thickness of 60±10 m. A conductive fine-grained Santa Fe sedimentary interval (10 ohm-m) beneath has a minimum thickness of 360±40 m. Although relatively coarse grained Cochiti Formation is widespread on the west side of the Rio Grande, at AMT sounding 2 we did not resolve a moderate- to high-resistivity unit below the water table. We cannot determine from the AMT data the electrical characteristics beneath this thick conductive interval. Such are the limitations of sparse data sampled more than a kilometer apart. Nevertheless, nearby subsurface deposits of the ancient Rio Grande should be widespread. The shallow part of the conductor at AMT station 2, at depths of 60–200 m or more, may be a different fine-grained Santa Fe facies. The well log from CEPO 2 (fig. F8*B*) shows a prominent conductor of less than 10 ohm-m at 160–260 ft (49–79 m) depth.

At AMT station 3 (fig. F5), east of the Rio Grande, a resistive, unsaturated, medium-grained Santa Fe interval (100 ohm-m) is 45±5 m thick. A resistive inferred basaltic vent (100 ohm-m) at 140±20 m depth has a minimum thickness of 860±100 m and is offset relative to the vertical sounding. Underlying, moderately conductive, saturated Santa Fe Group sediments (30 ohm-m) are likely medium to coarse (axial) sand and lesser gravel with a minimum thickness of 550±60 m. A more conductive fine-grained Santa Fe interval (10 ohm-m) beneath has a minimum thickness of 100±50 m. An underlying very conductive interval (2 ohm-m), at an elevation of 960 m, may be Mancos Shale. If so, the elevation of the top of the Mancos Shale drops 760 m between station 3 (fig. F5) and station 4 (fig. F4*A*) across the La Bajada fault zone (fig. F2*A*).

MT station 12 is located west of Saint Peters Dome to the north of the area of the geologic map of the Cochiti Pueblo area (pl. 2, fig. F2*B*). Upper resistive material (200 ohm-m) directly beneath station 12 (fig. F6) has a thickness of 60±10 m. Bandelier Tuff is exposed nearby at the surface. Moderately conductive material (20 ohm-m) beneath, which has a minimum thickness of 165±20 m, is probably a medium-grained sedimentary facies of the Santa Fe Group. A more conductive interval (10 ohm-m) below probably includes fine-grained Santa Fe Group sediments, Espinaso Formation volcaniclastic rocks, and Galisteo Formation sedimentary rocks that have a composite minimum thickness of 575±100 m. Poor data quality prevented us from solving for its maximum thickness. We modeled resistive material (200 ohm-m) at a minimum depth of 800±100 m that may be Paleozoic limestones. The top of this resistive interval is about 1,580 m above sea level. Because of poor data quality and the three-dimensional MT response at low frequencies, we are less certain of its true elevation and resistivity.

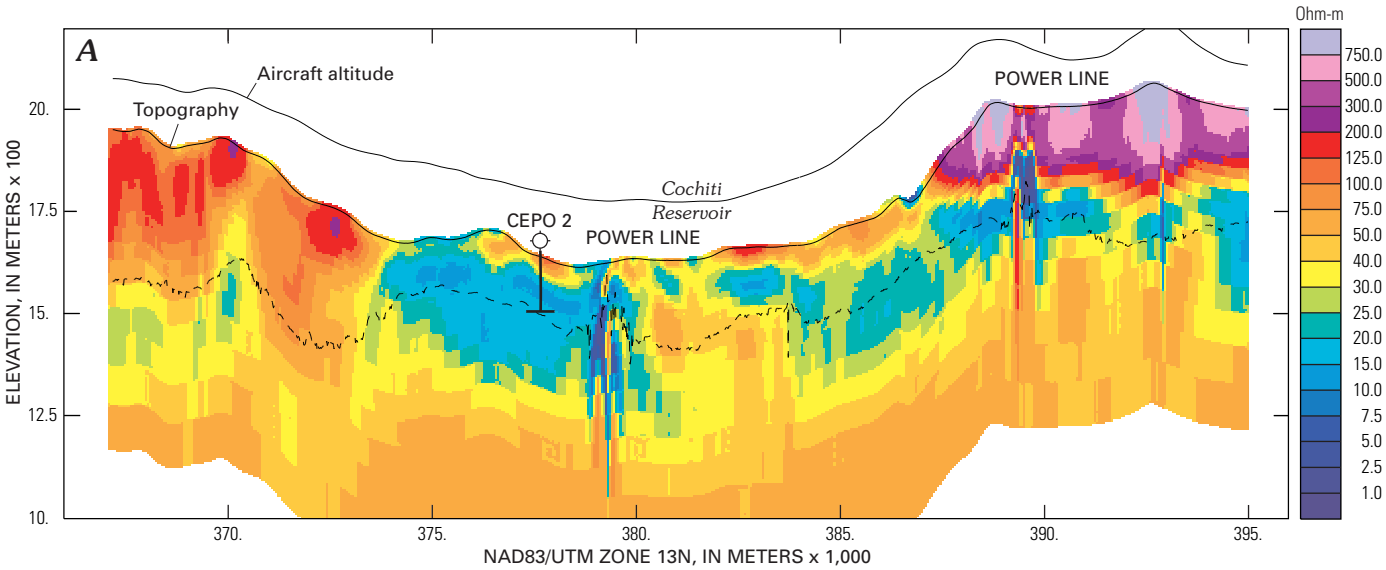

Figure F8 (above and facing page). *A*, Resistivity under flight line 620 in the Cochiti Pueblo time-domain electromagnetic survey area, drawn on the basis of least-squares inversion and showing location of CEPO 2 induction-resistivity well. Line floating above cross section represents aircraft altitude; faint dashed line represents maximum valid depth limit used for geologic interpretations. Vertical exaggeration is 10. *B*, Induction-resistivity log for well CEPO 2 in Cochiti Pueblo. Solid line is long-normal (induction) resistivity; faint dashed line is 30-ft moving average of long-normal resistivity; open circles connected with black dashed line indicate depths of resistivity contours (15, 20, 25, 30, 40, 50, 75, 100, and 125 ohm-m values) obtained from resistivity inversion shown in figure F8*A*; SWL is static water level. Grain size labels (Coarse, Medium, Fine) refer to bulk average lithology of the middle Rio Grande Basin Santa Fe Group sediments (Cole and others, 1999). Lithologic descriptions to left of grain-size labels from figure G4.

MT station 17 is located near the Dome Road well (fig. F2*A*) in the La Bajada constriction. The 400 m of section within the Dome Road well consists almost entirely of Cochiti Formation sand and gravel (Chamberlin, Jackson, and Connell, 1999). An induction-resistivity log (fig. G5) shows average resistivities that range from about 20 ohm-m to 60 ohm-m and a median resistivity of about 40 ohm-m. An uppermost, moderately conductive (20 ohm-m), 50±10-m-thick interval at MT station 17 (fig. F6) correlates with the 30 ohm-m average resistivity logged in the upper 70 m of the Dome Road well. An underlying, moderately resistive (50 ohm-m) interval, 750±80 m thick, correlates with the induction log resistivities that averaged 30 ohm-m between depths of 70–250 m and with average resistivities that ranged from 30 to 60 ohm-m at depths of 250–400 m (the base of the log). Moderately conductive material (10 ohm-m) below probably includes fine-grained sediments of the Cochiti Formation, volcaniclastic sedimentary rocks of the Espinaso Formation, and Galisteo Formation sedimentary rocks that have a composite thickness of 600±100 m. Beneath this interval is a conductive section (2–10 ohm-m) that may contain carbonaceous shale of the Cretaceous Menefee Formation and Mancos Shale, Jurassic sandstones, and mudstones of the Triassic Chinle Formation. The elevation of the top of this interval is about 350 m above sea level, which represents a drop in elevation of 610 m relative to a similar interval at station 3. If the conductive intervals beneath stations 17 and 3 represent the same geologic horizons, then the resistivity structure beneath station 17 reveals a deepening of the Rio Grande rift. We modeled resistive material (200 ohm-m) at a minimum depth of 1,900±150 m (–150 m elevation) at station 17 that may be Paleozoic limestone. As we stated at the beginning of this section, these geologic interpretations were guided by induction log resistivities from several wells in the region (tables F2, F3). If these inferred geologic horizons are correct, then the boundary between the 2–10 ohm-m and the 200 ohm-m layers represents the boundary between Mesozoic and Paleozoic rocks. Thus, these MT results have provided additional constraints on the relative positions of basement rocks and the thicknesses of Paleozoic, Mesozoic, and Tertiary sedimentary rocks on either side of the Pajarito fault zone.

Airborne Electromagnetic Surveys

The airborne time-domain electromagnetic (TDEM) method is an active geophysical technique that uses artificially generated electromagnetic fields to investigate the electrical resistivity of the subsurface. The TDEM method probes the electrical properties of the Earth from depths of a few meters to depths of several hundred meters depending on the geology and the TDEM system specifications. The depth of investigation can reach hundreds of meters in cases of very resistive, dry, low-porosity rocks such as unweathered volcanic rocks but only about 100 m in water-saturated clay-rich sediments that are markedly less resistive than unweathered volcanic rocks.

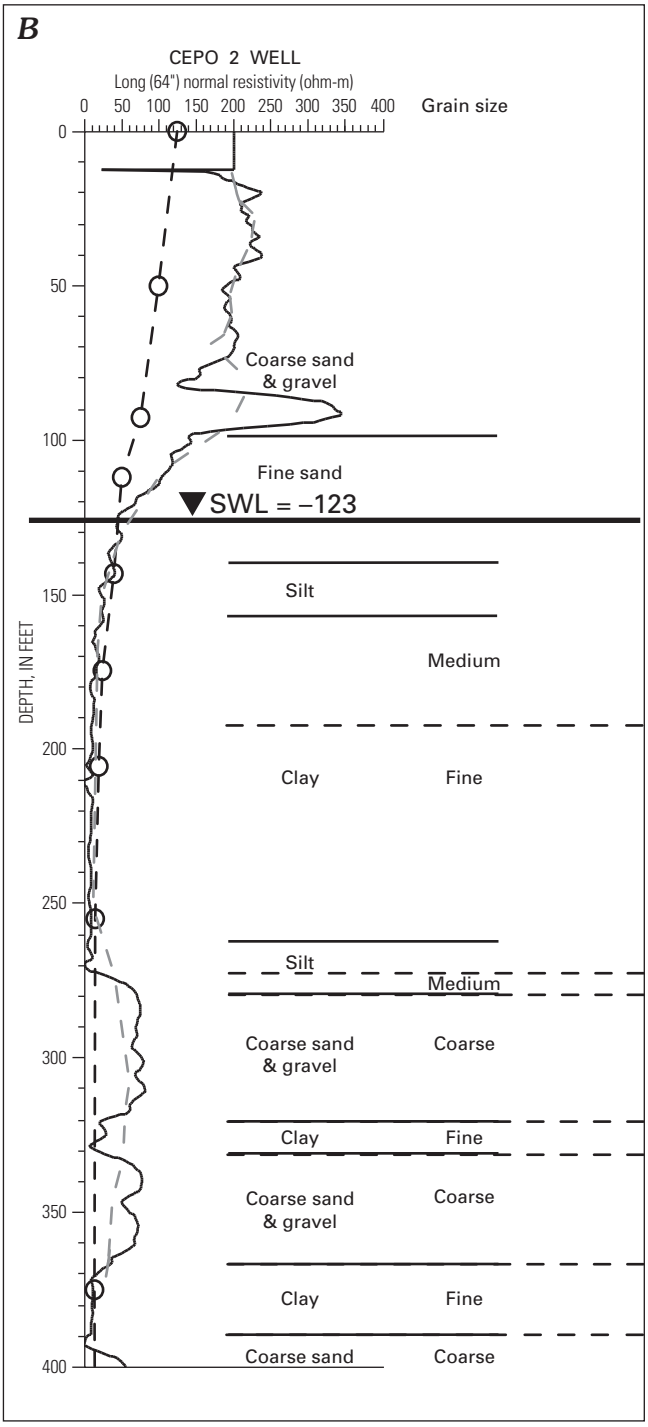

Furthermore, the resistivity of the upper few meters may not be well resolved in the case of conductive near-surface rocks, and the upper tens of meters may not be well resolved in the case of resistive rocks. The depth of penetration and the resolution of the model can be modified by the choice of TDEM system and by incorporating survey parameters designed to target a particular geologic problem.

In a typical TDEM system, a loop of current-carrying wire (the transmitter) is mounted on an aircraft and sends pulses of electromagnetic energy (usually 30–90 times per second) at fixed time intervals. A receiver is mounted in a cigar-shaped unit, commonly called a bird, that is towed on a cable below and behind the aircraft. The receiver measures the electromagnetic impulses as a function of time. The shape of the impulses measured by the receiver and their decay rates after the cessation of the transmitter current are affected by the presence of the Earth. In general (assuming that all system and survey parameters remain constant), a stronger signal and slower rate of decay indicate lower resistivity in the subsurface, whereas a weaker signal and faster rate of decay indicate higher resistivity. Signals recorded at earlier times (microseconds after current turnoff) provide information on shallower depths, whereas signals recorded at later times (milliseconds after current turnoff) provide information on deeper depths (Palacky and West, 1991). Lower rates at which transmitted pulses are repeated allow longer measurements of signal decay between pulses; resistivity information is thus obtained from deeper subsurface regions. The tradeoff for deeper penetration is lower horizontal resolution along the flight lines. The horizontal resolution also depends on the TDEM system dimensions and the survey parameters such as flight elevation and flight-line spacing. The signal received is affected by many factors, but ideally the strength of the signal recorded at a given time reflects the resistivity distribution in the subsurface. The measured voltages can be modeled as electrical resistivity distribution with depth.

Several factors dictated the decision to use the airborne TDEM method for this investigation. First, airborne methods efficiently collect large amounts of information over a wide area. Spatial sampling of the subsurface is determined by the line spacing and by the sampling rate along the flight lines. Second, airborne TDEM can be used to infer the general distribution of electrical resistivity to depths greater than is typically possible in frequency-domain airborne electromagnetic surveys. Third, the method can be applied in difficult terrain that is not readily accessible by road for ground-based electromagnetic methods. Access was a controlling factor for much of the survey area, because of sparse roads in and around Cochiti Pueblo.

One drawback of the method is that cultural features, because of their wide bandwidth, strongly affect the responses of the TDEM system. Fences, pipelines, communication lines, railways, and other man-made conductors can contaminate the responses. The areas affected by such cultural noise cannot be used for interpretation. The majority of cultural anomalies can be easily identified, but sometimes the cultural noise response is subtle and can be mistaken for the Earth's response. Cultural noise in this survey severely affected only a very limited part of the TDEM data, mainly near a few large power lines (fig. F2*A*).

Time-Domain Electromagnetic Survey

Airborne TDEM data were collected on March 3–7, 1997, by Geoterrex, Inc., which used a GEOTEM system (Deszcz-Pan and others, 2000). The survey area is in the vicinity of Cochiti

Pueblo (pl. 1; survey area D, fig. F1). The purpose of the survey was to delineate facies changes within the basin fill that may control local and regional ground-water flow and to help define the three-dimensional extent of the principal axial-river gravel aquifer in the subsurface of the Santa Fe Group basin fill. In the GEOTEM system, a transmitter mounted on an airplane pulses an electromagnetic signal 30 times per second. In the receiver, towed about 50 m below and 125 m behind the airplane, the electromagnetic signal is recorded as a voltage at specific times during and after each pulse.

The receiver measures three spatial components of the transmitter signal: x, y, and z. Our interpretations are based primarily on the z-component (vertical) of the received signal. The x-component (in-line) was processed but was used only to check consistency between the x- and z-components. The y-component (transverse) was ignored because this component should be zero in the one-dimensional geometry that was assumed for the processing of the data.

The Cochiti Pueblo survey covered approximately a 15×20 km area. The aircraft was flown at 120 m above ground level using a 400-m flight-line spacing (fig. F2*A*). Above the small urban area in the Cochiti Pueblo, the flight height reached about 250 m above ground level. During the five days of the Cochiti survey, about 100,000 soundings were recorded. The sounding spacing along the flight lines was about 13 m. At each of the sounding points, 60 channels of time-domain data were recorded, 20 in each of the x, y, and z spatial directions. Of the 20 channels, 4 channels recorded a signal when the transmitter pulse was on, and 16 channels were designated to record the signal received after the transmitter signal ended. The transmitter signal was a half-sinusoidal wave that was on for 4.166 ms and off for 13.371 ms.

Resistivity Models Based on Time-Domain Electromagnetic Survey

Inversion of recorded signal to resistivities does not produce a single, unique result; the result depends on the algorithms used. All algorithms are based on the assumption that the calculated response from a given Earth model must match the measured fields within some specified error. All models are approximations and not a true resistivity distribution in the Earth. In the inversion of this TDEM data we assumed a one-dimensional model such that under each survey point the resistivity changes only in one dimension: depth. By stitching together the resistivity models for each point along the flight lines we obtained a resistivity cross section along each flight line. Maps of resistivity at given depths below the surface, or at given elevations above sea level, were obtained by combining resistivity cross sections from the flight lines.

Inversion results for the survey were provided courtesy of BHP World Minerals. Two proprietary one-dimensional Earth resistivity algorithms were used in inverting the TDEM data: one based on a layered Earth model and a second based on a thin-sheet Earth model. In the first model the subsurface is approximated by a stack of horizontal layers, each having a certain resistivity and thickness. In this algorithm (Ellis, 1998), for each survey point, the fields measured at 16 time-channels after the transmitter current turnoff were simultaneously compared with calculated responses. The least-squares error between measured and calculated data was minimized by iteratively adjusting the resistivity model until the error diminished to a specified value. The inversion model consists of 24 layers of fixed thickness over a half-space (thick homogeneous bottom model layer). The layer thicknesses are initially specified and remain constant along the flight line. The layer thicknesses increase from 5 m on the surface to 110 m for the deepest layer in proportion to the decrease in resolution with depth of electromagnetic methods. The basement resistivity was fixed at 50 ohm-m. The depth of this artificial basement (780 m) is well below the signal-penetration depth, but experience shows that the presence of a deep basement of fixed resistivity stabilizes the inversion algorithm. The model calculations are quite complicated and time consuming.

The second model assumes that measured responses at two measurement times can be modeled by a thin, conductive sheet floating in free space. An assembly of sheets whose calculated responses matches the responses measured at two subsequent times, moving from the earliest to the latest, represent subsurface resistivity as a function of increasing depth. In this algorithm (Liu and Asten, 1993) a conductive, horizontal, thin sheet in free space is used to approximate Earth resistivity distribution with depth. The measured responses at the two earliest times after the transmitter current is turned off are used to uniquely determine conductance and the distance between the thin sheet and the receiver. Then the position and conductance of the sheet matching the responses at the next pair of later times is found. The process is continued for all later pairs. The model resulting from this transformation is called a resistivity depth image (Deszcz-Pan and others, 2000). The calculated response for the thin sheet is analytic so the algebraic transformation calculations are very fast and simple.

Both model algorithms have their merits; however, we found that the layered model resistivities better matched induction log resistivities and MT models. When we compared results obtained by three geophysical methods—resistivity models calculated from AMT soundings, bulk average resistivities calculated from induction logs, and resistivity cross sections calculated by least-squares inversion—we found that the maximum depth provided by the resistivity-depth-image cross sections (for example, fig. F9) could be used as the maximum valid depth limit for the least-squares resistivity inversion. We plotted this maximum depth on each least-squares resistivity inversion cross section at any given point along the flight line. This maximum resistivity-depth-image depth is shown as a dashed line on the inversion cross section (for example, fig. F10). AMT and TDEM models correlate well, as shown by a comparison of AMT soundings and one of the least-squares inversion cross sections (fig. F11*D*). Some exceptions occurred near the maximum resistivity-depth-image depth limit (especially when a conductor at

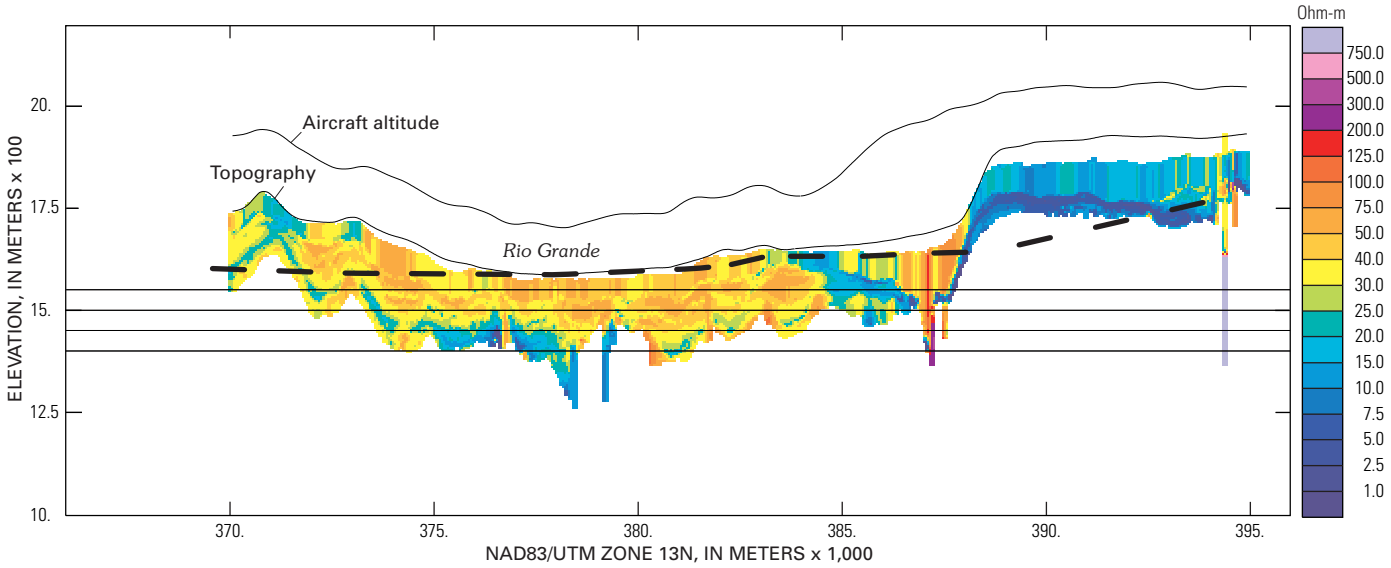

Figure F9. Resistivity under flight line 630 in the Cochiti Pueblo time-domain electromagnetic survey area, drawn on the basis of resistivity-depth image algorithm. Solid horizontal lines represent subsurface elevations 1,400, 1,450, 1,500, and 1,550 m. Line floating above cross section represents aircraft altitude. Vertical exaggeration is 10.

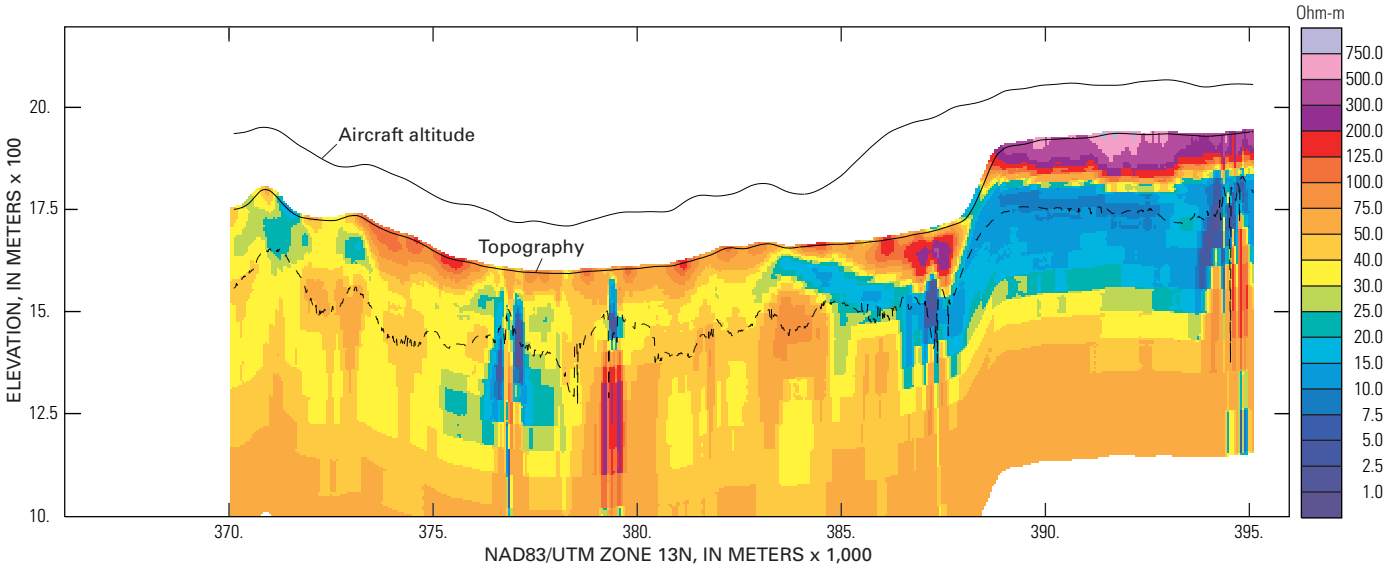

Figure F10. Resistivity under flight line 630 in the Cochiti Pueblo time-domain electromagnetic survey area, drawn on the basis of least-squares inversion. Line floating above cross section represents aircraft altitude; faint dashed line represents maximum depth estimated from resistivity-depth image (fig. F9). Vertical exaggeration is 10.

Figure F11 (following 3 pages). East-west resistivity profiles in the Cochiti Pueblo time-domain electromagnetic survey area (cross sections F14*A*–*G*), drawn on the basis of least-squares inversions. Faint dashed line in each section represents maximum depth estimated from resistivity-depth image; numbers below magnetotelluric (MT) or audiomagnetotellurid (AMT) stations refer to modeled resistivities. Vertical exaggeration is 10. *A*, Flight line 605 showing Dome Road well and MT station 17. *B*, Flight line 609 showing AMT stations 1, 6, and 5 and Cochiti Lake 2 and 1200-Foot wells. *C*, Flight line 614 showing AMT station 2. *D*, Flight line 630 showing AMT stations 3 and 4, magnetic anomalies C3 and C4, and Santa Cruz Springs well. *E*, Flight line 638 showing Mancos Shale in footwall block of La Bajada fault zone. *F*, Flight line 643 showing Cerrillos uplift in footwall block of La Bajada fault zone. *G*, Flight line 626 showing magnetic anomaly C5.

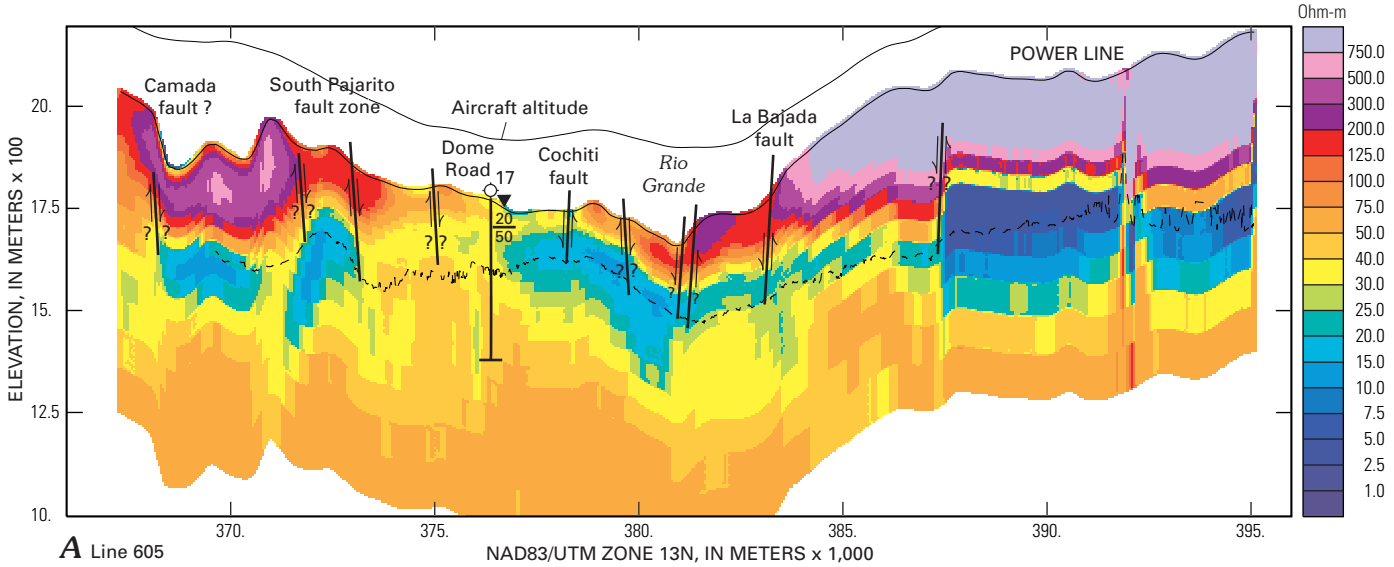

A Line 605

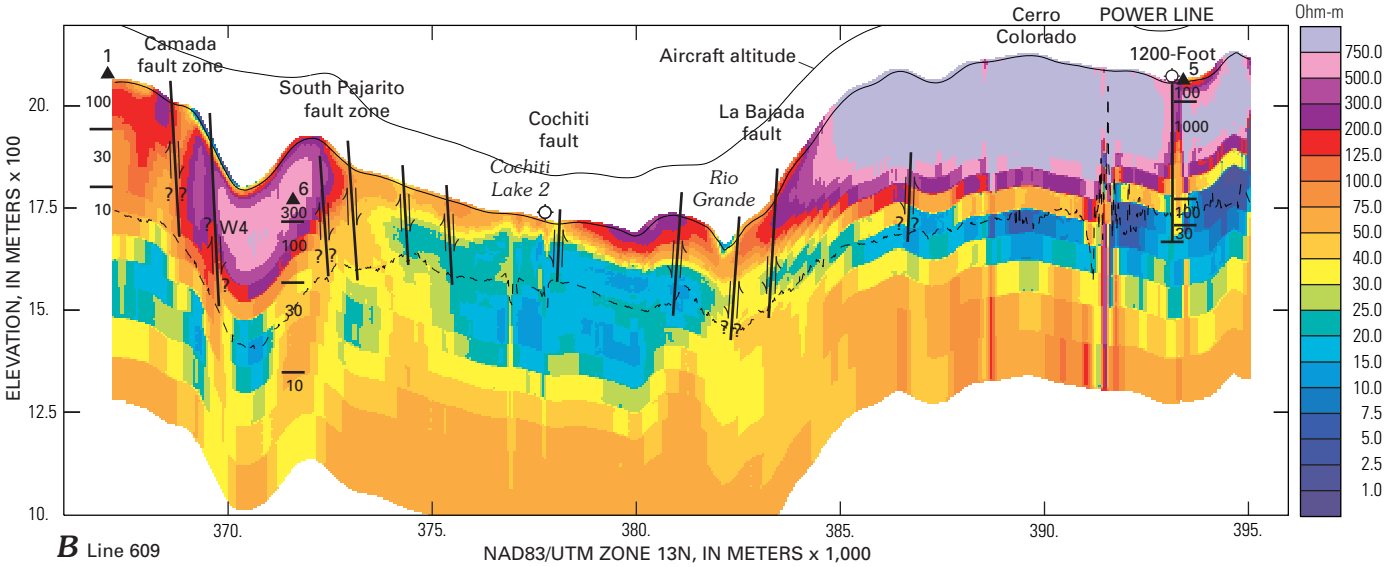

B Line 609

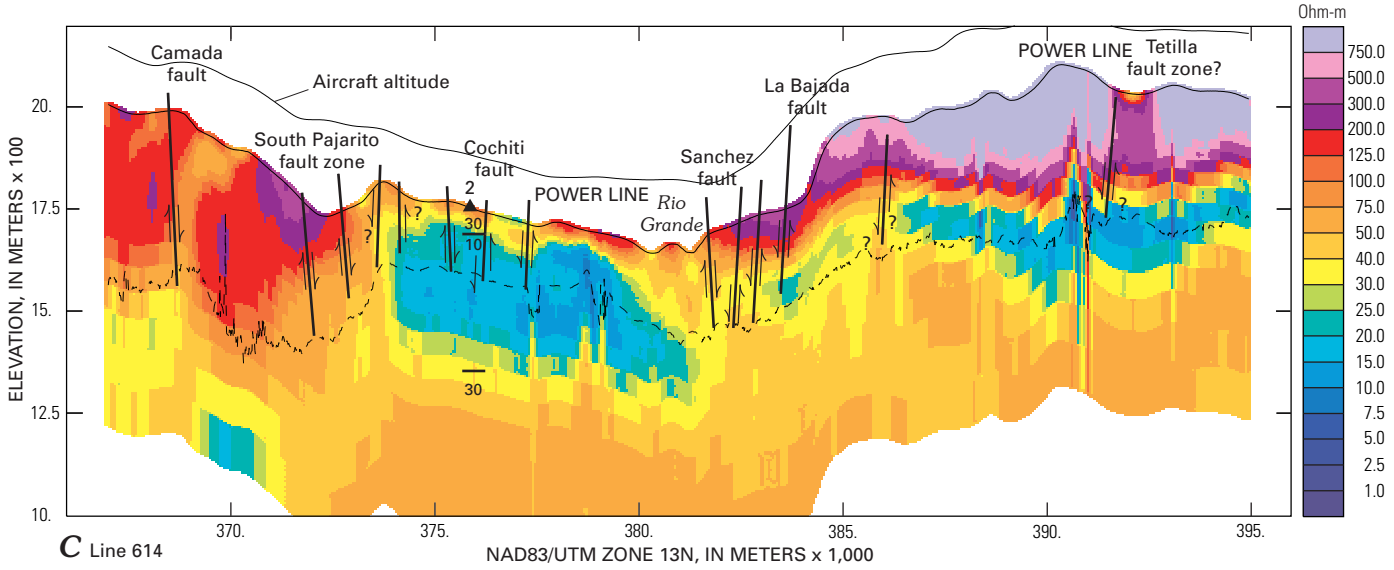

C Line 614

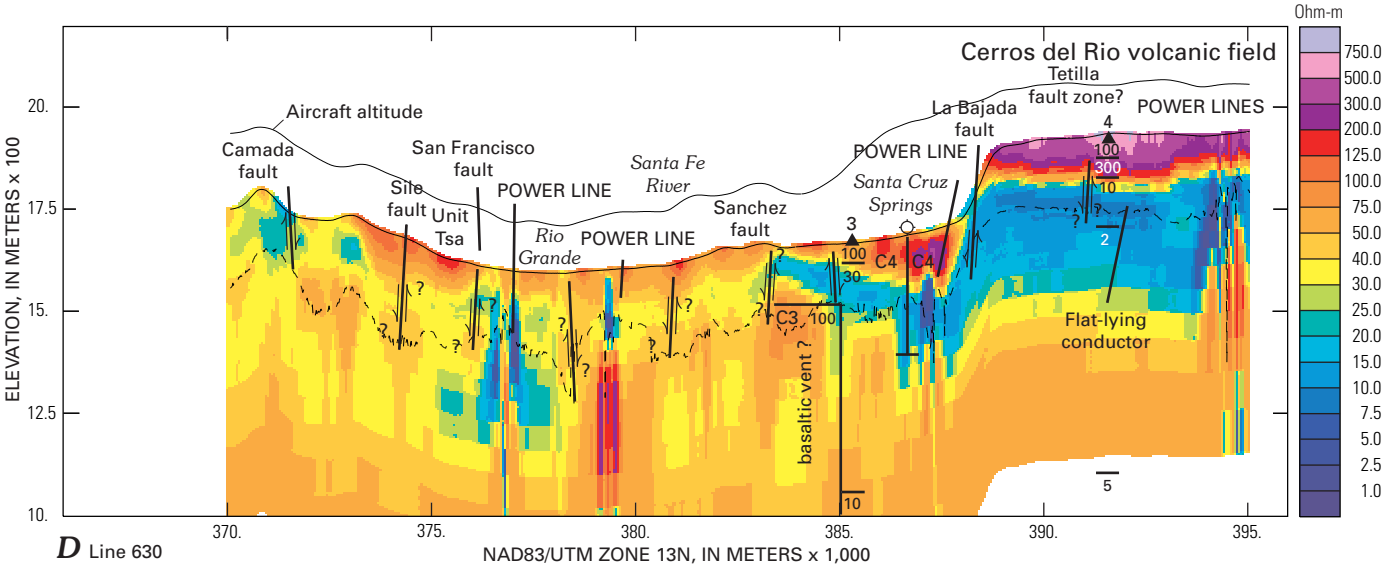

D Line 630

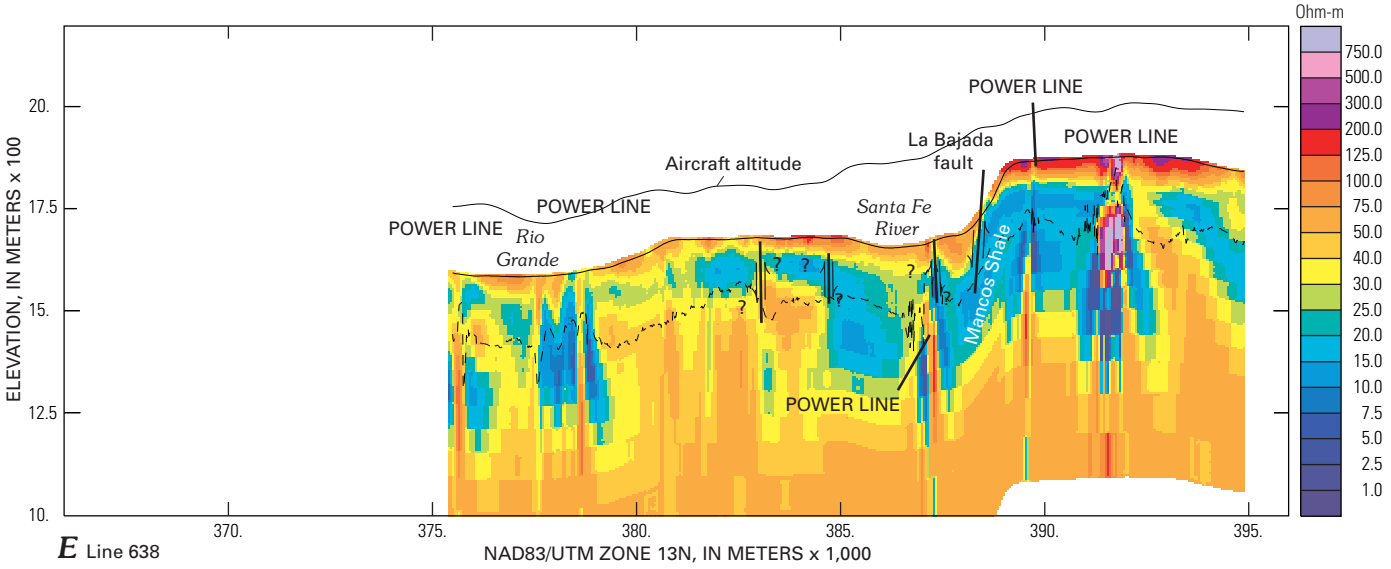

E Line 638

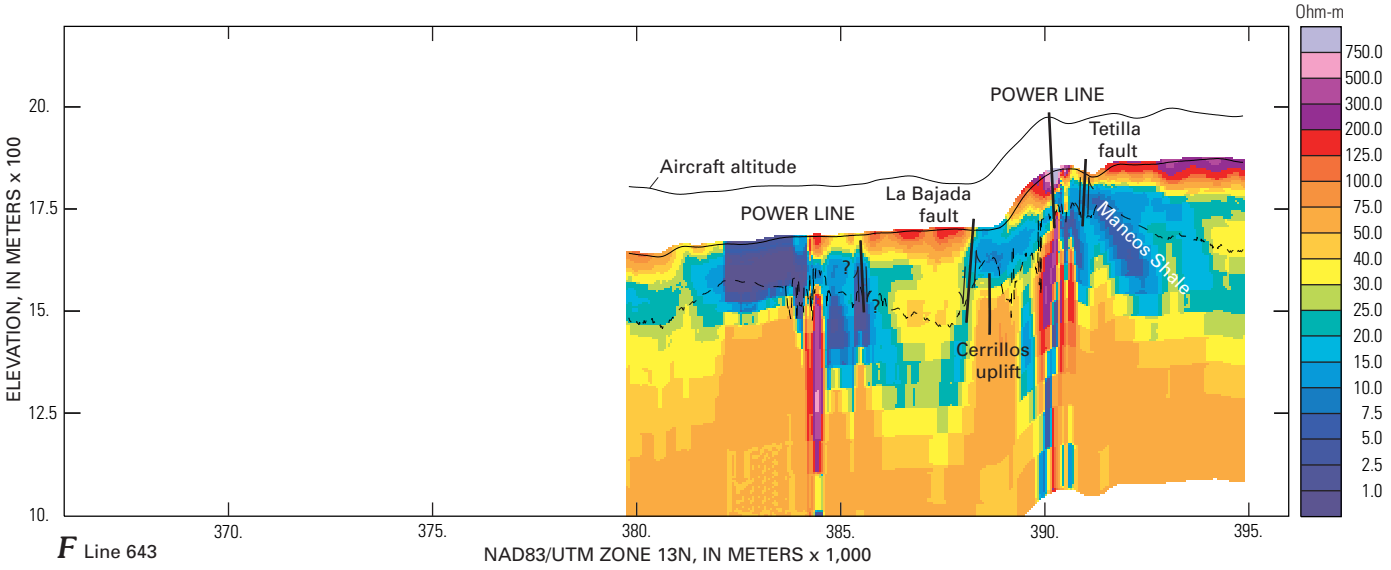

F Line 643

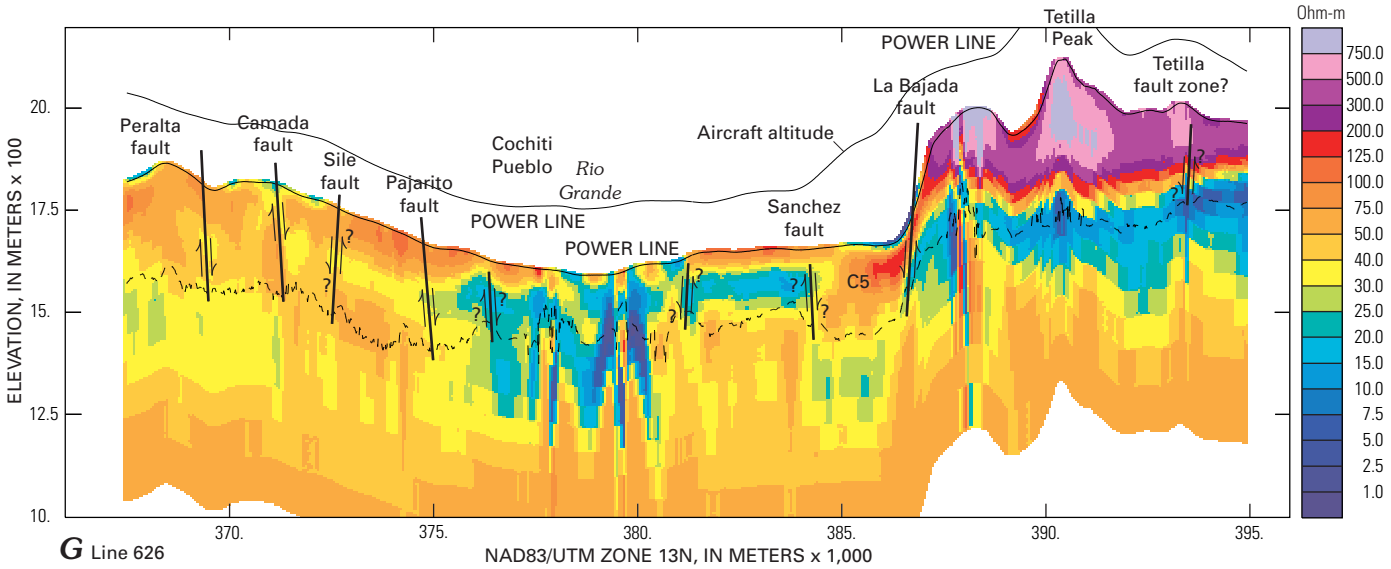

least 100 m thick lay above the resistivity-depth-image limit) and also in the upper 50 m (where the least-squares inversion close to the surface generally yields resistivities higher than the shallowest AMT resistivities). AMT data suggest that some inversion resistivities below the resistivity-depth-image limit are still valid (especially when a thick section of resistive material lies above the resistivity-depth-image depth limit). Rather than plotting as a blank area the resistivity values below the resistivity-depth-image depth limit on the resistivity cross sections, we included all values of the inversion. So doing allowed us to view those cases where a conductor exists beneath a thick section of resistive materials but below the resistivity-depth image-depth limit (for example, below the magnetic anomaly labeled C5 in fig. F11*G*; refer to fig. D7). We are of the opinion that in these cases the TDEM response is sensitive to the conductor at depth below the thick resistor, even though that conductor is below the resistivity-depth-image depth limit. However, the basement resistivity was fixed at 50 ohm-m, so interpretations should not use the last resistivity gradient between the basement resistivity of 50 ohm-m and the shallower resistivity feature in question.

By using the line-by-line least-squares inversions found by the above procedures, plan maps of resistivity were generated for the survey area by combining the least-squares inversion cross sections into a three-dimensional grid of resistivity. Resistivities below the maximum resistivity-depth-image depth limit were set to plot a blank area. Areas that were either outside the survey region or were at elevations above the ground surface were also plotted as blank areas. Horizontal depth-slice maps of resistivity (fig. F12*A*–*F*) at 50 m elevation intervals were generated from the least-squares inversion results along each of the flight lines. Elevations mapped were 1,750, 1,700, 1,550, 1,500, 1,450 and 1,400 m above sea level (elevations 1,550, 1,500, 1,450, and 1,400 m are marked by thin, horizontal lines on fig. F9). Figure F7*A*–*F* shows resistivity maps (also generated from the same least-squares inversion results) at constant depths below the surface (20, 50, 70, 100, 150 and 200 m) draped on topography. We did not use the resistivity-depth image results to produce the depth-slice maps because the resistivities derived from the resistivity-depth image algorithm generally did not extend to the surface and did not correlate very well with the AMT soundings in the upper 50 to 100 m (for example, fig. F11*D*). Vertical cross sections from the least-squares inversions were generated along each of the 50 east-west flight lines and for 8 north-south flight lines. Selected profiles are depicted in figures F11 and F13.

Geologic Interpretation of Airborne Electromagnetic Models

The TDEM survey objectives, defined in the preceding Time-Domain Electromagnetic Survey section, were based on the assumption that the axial-river gravel deposits, which are the

Figure F12 (followin 6 pages). Elevation slices in the Cochiti Pueblo time-domain electromagnetic survey area (*A*–*F*), drawn on the basis of least-squares inversions. Solid numbered triangles are high-frequency magnetotelluric (AMT) sounding stations. Labels C, M, and F are inferred sedimentary grain size: coarse, medium, and fine, respectively. V marks inferred volcanic rock. Inferred grain size labels appear only on elevation slices below the water table (*C*–*F*); approximate boundaries are shown by lighter dashed lines. *A*, 1,750-m elevation slice. *B*, 1,700-m elevation slice. *C*, 1,550-m elevation slice. *D*, 1,500-m elevation slice. *E*, 1,450-m elevation slice. *F*, 1,400-m elevation slice.

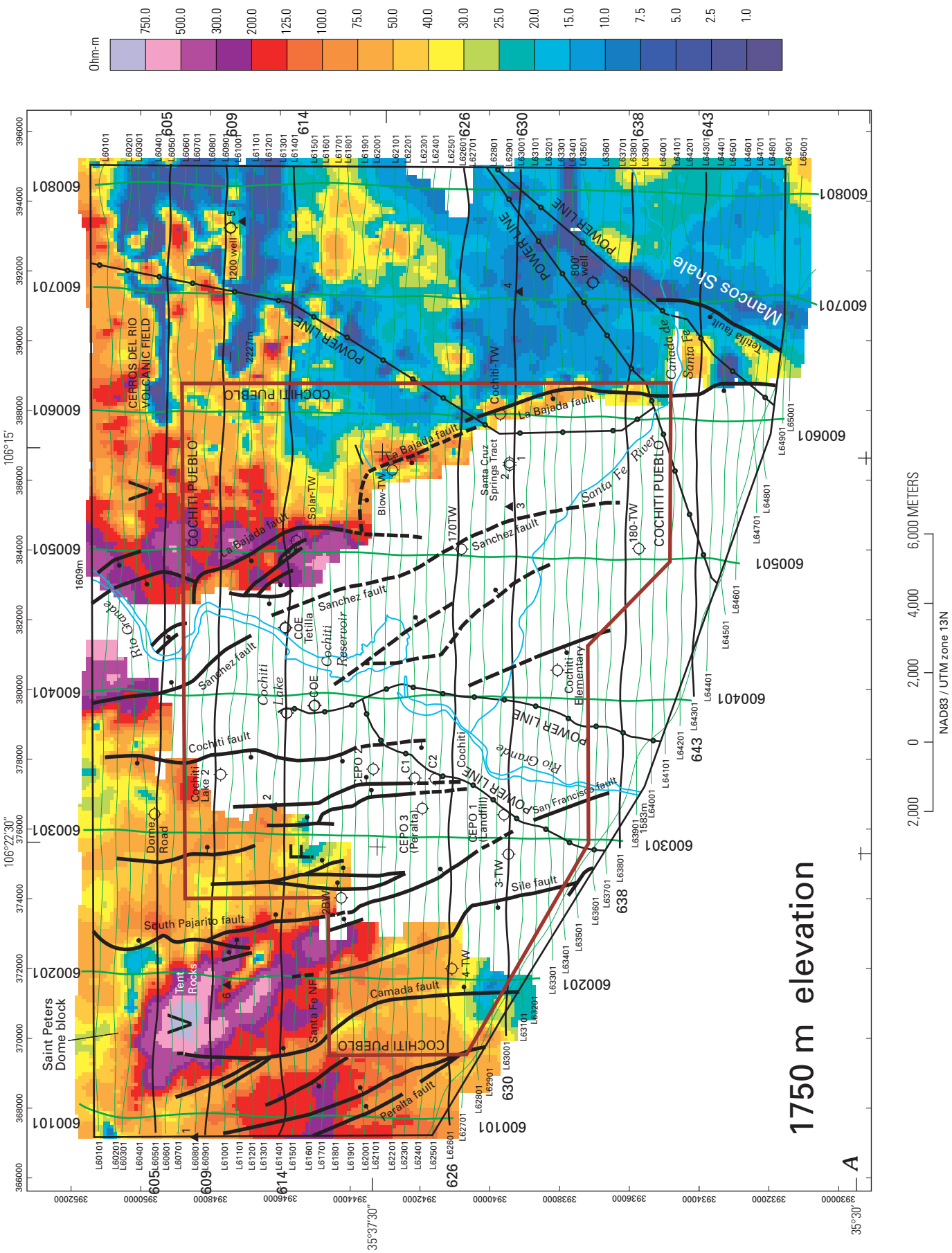
Ohm-m
750.0
500.0
300.0
200.0
125.0
100.0
75.0
50.0
40.0
30.0
25.0
20.0
15.0
10.0
7.5
5.0
2.5
1.0
1750 m elevation
A
Manzanos Shale
CERROS DEL RIO VOLCANIC FIELD
COCHITI PUEBLO
POWER LINE
Santa Fe River
Rio Grande
Cochiti Lake
Cochiti Reservoir
Cochiti Elementary
Saint Peters Dome block
Tent Rocks
Dome Road
Cochiti Lake 2
Cochiti fault
South Pajarito fault
Camada fault
Peralta fault
Sile fault
San Francisco fault
Sanchez fault
La Bajada fault
Tetilla fault
Camada de
Santa Fe
Santa Cruz Springs Tract
Cochiti-TW
Solar-TW
Blow-TW
170TW
180-TW
3-TW
4-FW
COE Tetilla
COE
CEPO 1 (Landfill)
CEPO 2
CEPO 3 (Peralta)
C1
C2
Santa Fe NF
1200 well
800' well
2227m
1609m
1583m
605
609
614
626
630
638
643
NAD83 / UTM zone 13N
6,000 METERS
4,000
2,000
0
2,000
106°15'
106°22'30"
35°37'30"
35°30'

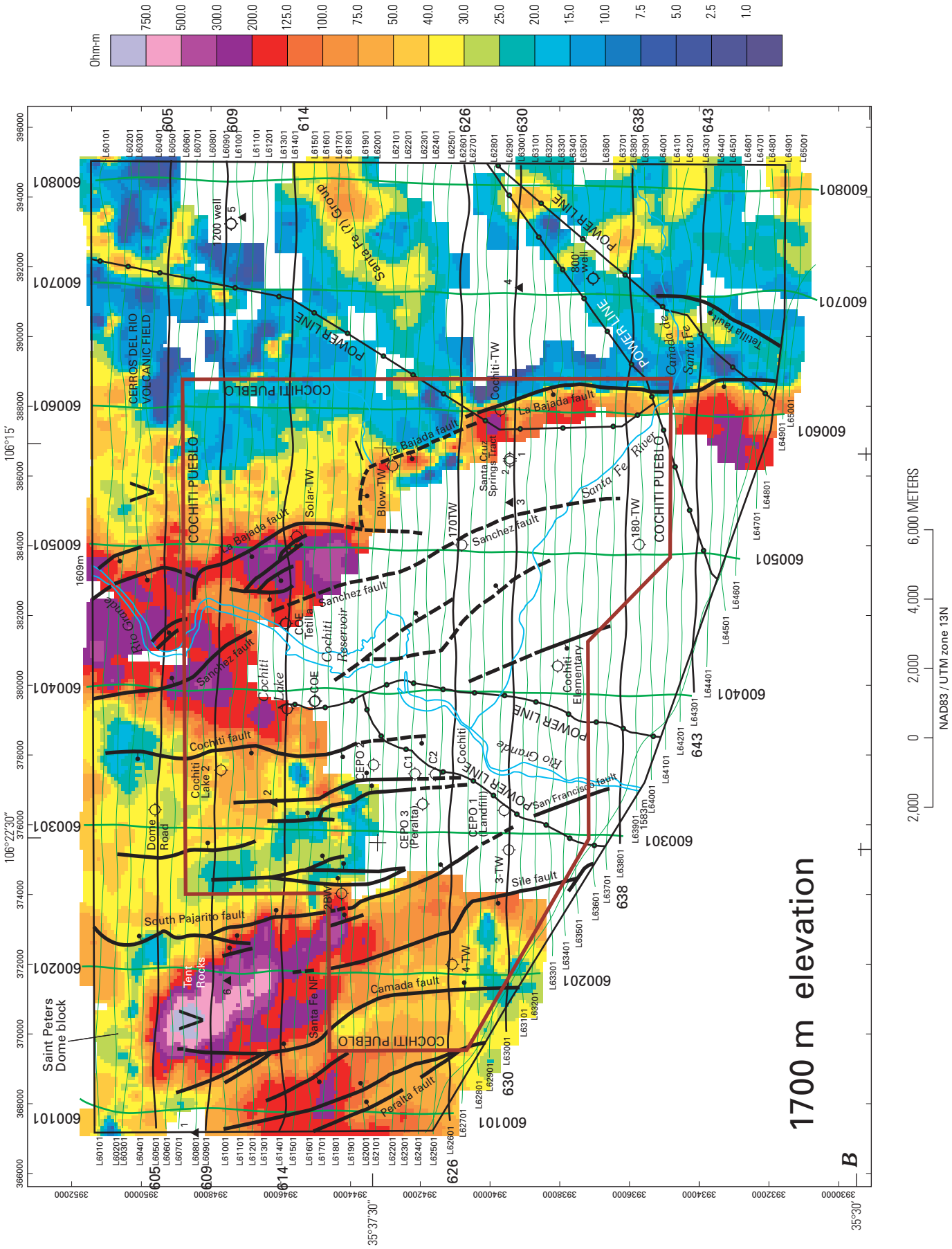
Ohm-m
750.0
500.0
300.0
200.0
125.0
100.0
75.0
50.0
40.0
30.0
25.0
20.0
15.0
10.0
7.5
5.0
2.5
1.0
1700 m elevation
B
CERROS DEL RIO VOLCANIC FIELD
COCHITI PUEBLO
Santa Fe (?) Group
POWER LINE
Santa Cruz Springs Tract
La Bajada fault
Sanchez fault
Cochiti fault
South Pajarito fault
Camada fault
Peralta fault
Sile fault
San Francisco fault
Santa Fe River
Rio Grande
Cochiti Reservoir
Cochiti Lake
Cochiti Lake 2
Cochiti Elementary
Dome Road
Saint Peters Dome block
Tent Rocks
Santa Fe NF
Tetilla fault
Camada de Santa Fe
1200 well
800 well
Solar-TW
Blow-TW
170TW
180-TW
Cochiti-TW
3-TW
4-TW
CEPO 1 (Landfill)
CEPO 3 (Peralta)
CEPO 4
GOE
C1
C2
1609m
1583m
2,000 0 2,000 4,000 6,000 METERS
NAD83 / UTM zone 13N
106°22'30"
106°15'
35°37'30"
35°30'

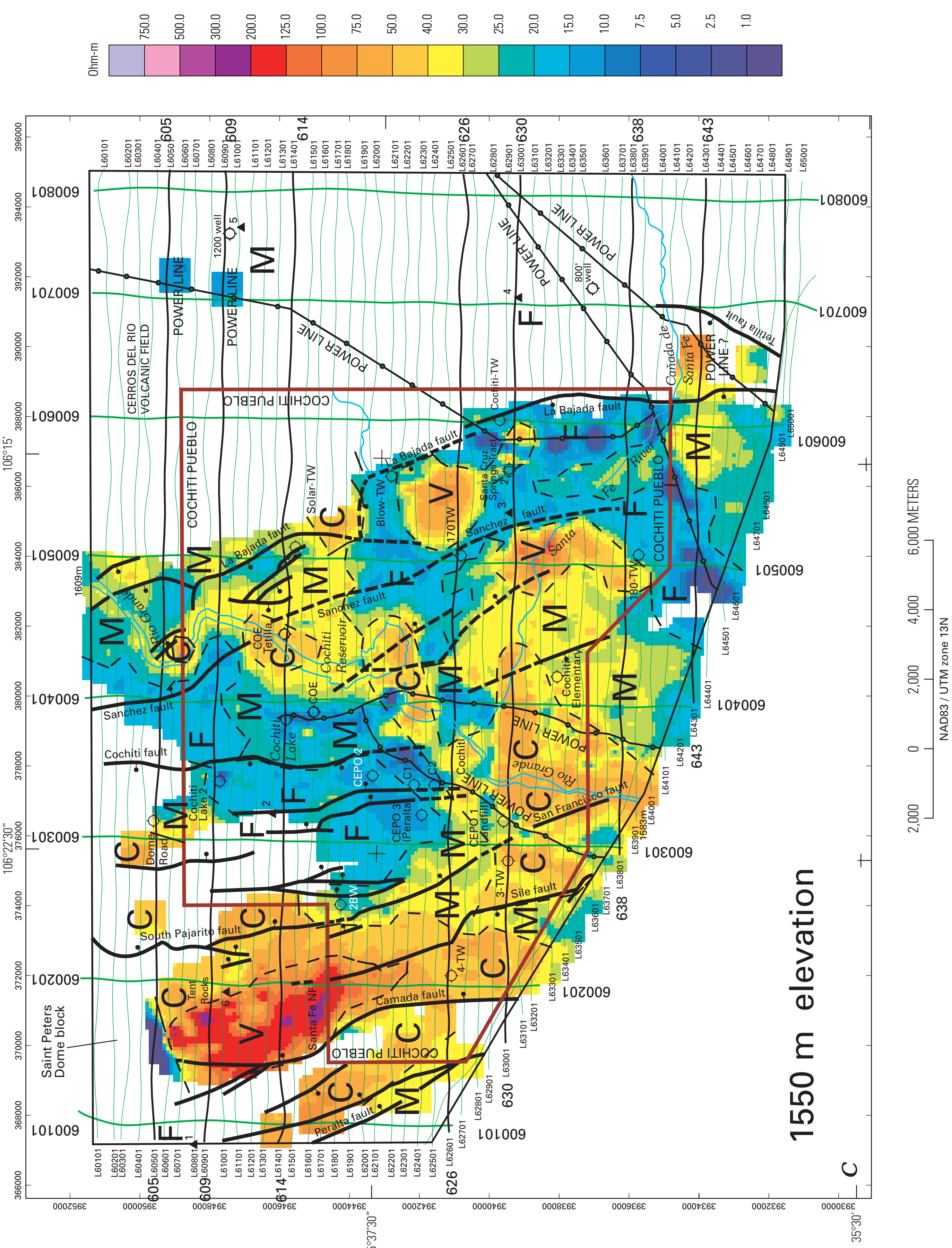
Ohm-m
750.0
500.0
300.0
200.0
125.0
100.0
75.0
50.0
40.0
30.0
25.0
20.0
15.0
10.0
7.5
5.0
2.5
1.0
1550 m elevation
C
CERROS DEL RIO VOLCANIC FIELD
COCHITI PUEBLO
POWER LINE
POWER LINE ?
1200 well
800' well
Saint Peters Dome block
La Bajada fault
Sanchez fault
Cochiti fault
South Pajarito fault
Camada fault
Peralta fault
Sile fault
San Francisco fault
Tetilla fault
Rio Grande
Cochiti Lake
Cochiti Reservoir
Santa Fe River
Cañada de Santa Fe
Tent Rocks
Santa Fe NF
Dome Road
Cochiti Lake 2
Cochiti Elementary
Santa Cruz Springs Tract
COE Tetilla
Solar-TW
Blow-TW
170TW
180-TW
Cochiti-TW
3-TW
4-TW
2BW
CEPO 1 (Landfill)
CEPO 2
CEPO 3 (Peralta)
1609m
1583m
106°15′
106°22′30″
35°37′30″
35°30′
2,000
0
2,000
4,000
6,000 METERS
NAD83 / UTM zone 13N

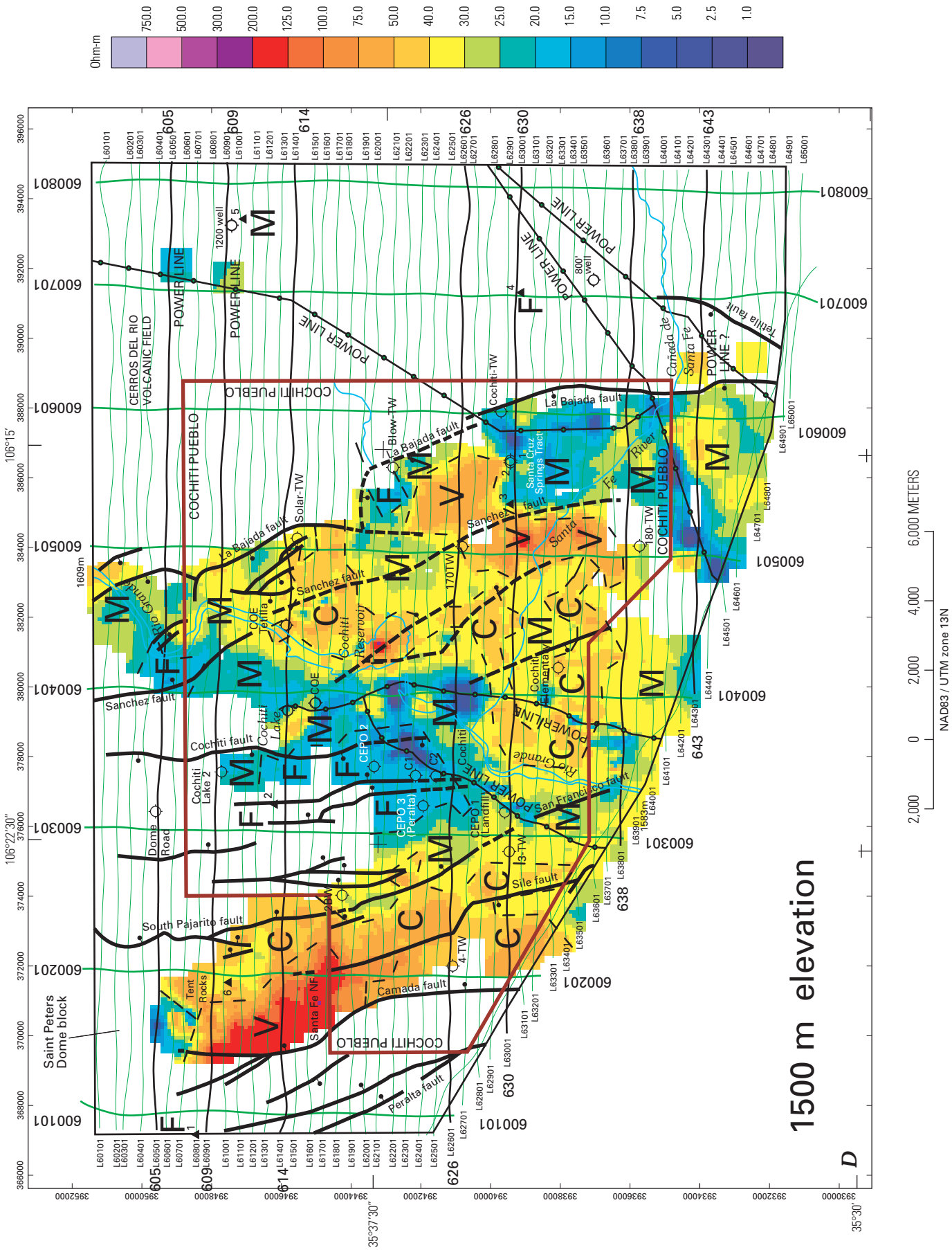
Ohm-m
750.0
500.0
300.0
200.0
125.0
100.0
75.0
50.0
40.0
30.0
25.0
20.0
15.0
10.0
7.5
5.0
2.5
1.0
1500 m elevation
D
CERROS DEL RIO VOLCANIC FIELD
POWER LINE
COCHITI PUEBLO
La Bajada fault
Sanchez fault
Cochiti fault
South Pajarito fault
Camada fault
Peralta fault
Sile fault
San Francisco fault
Santa Cruz Springs Tract
Cochiti Reservoir
Cochiti Lake
Cochiti Lake 2
Cochiti Elementary
Santa Fe River
Rio Grande
Saint Peters Dome block
Tent Rocks
Dome Road
Santa Fe NF
Solar-TW
Blow-TW
Cochiti-TW
170TW
180-TW
4-TW
13-TW
CEPO 1 (Landfill)
CEPO 2
CEPO 3 (Peralta)
COE
1200 well
800' well
Tetilla fault
Canada de Santa Fe
POWER LINE 2
1609m
1683m
2600m
2200m
106°15'
106°22'30"
35°37'30"
35°30'
2,000 0 2,000 4,000 6,000 METERS
NAD83 / UTM zone 13N

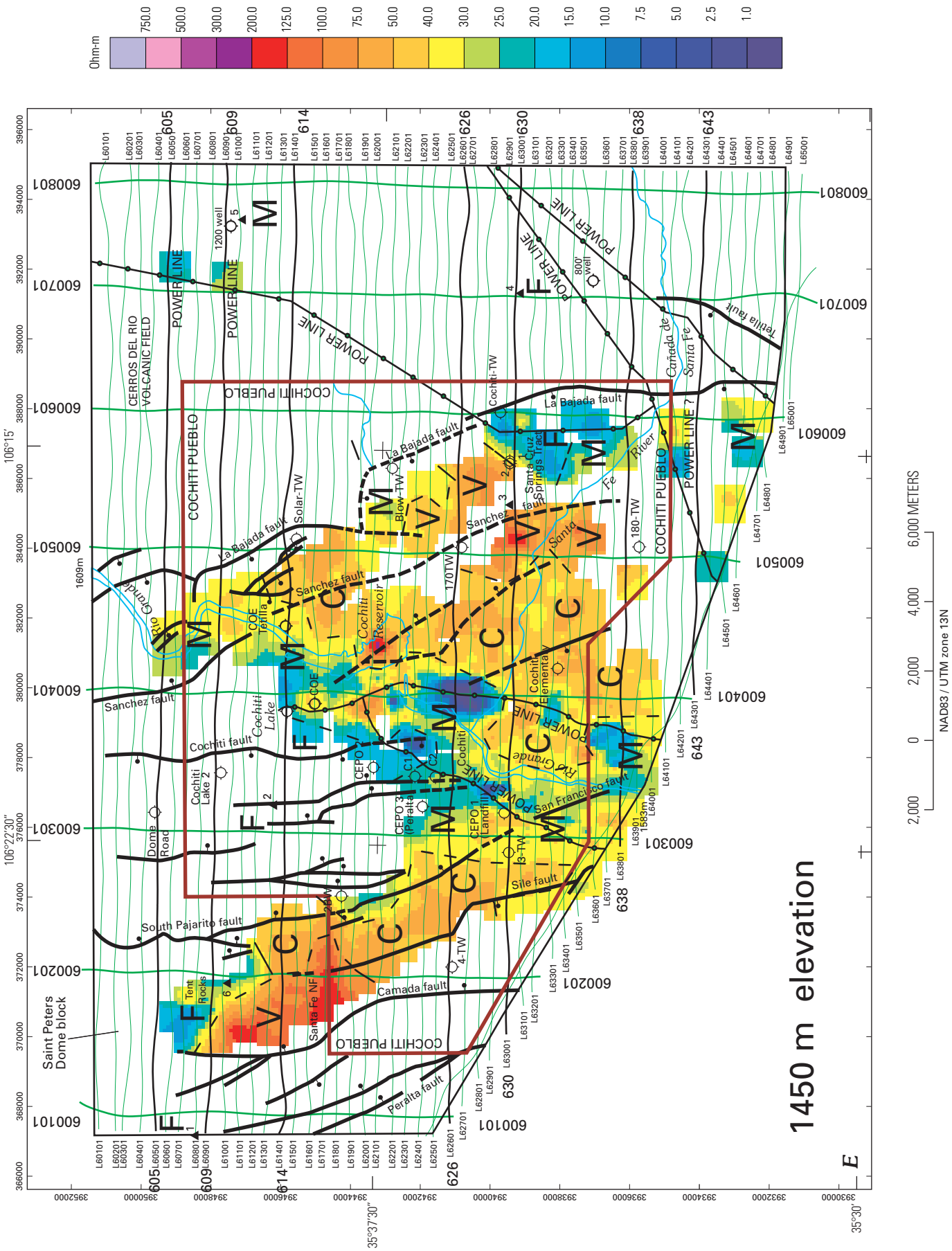
Ohm-m
750.0
500.0
300.0
200.0
125.0
100.0
75.0
50.0
40.0
30.0
25.0
20.0
15.0
10.0
7.5
5.0
2.5
1.0
1450 m elevation
COCHITI PUEBLO
CERROS DEL RIO VOLCANIC FIELD
POWER LINE
Saint Peters Dome block
Tent Rocks
Santa Fe NF
Cochiti Lake
Cochiti Reservoir
Sanchez fault
La Bajada fault
Cochiti fault
South Pajarito fault
Camada fault
Peralta fault
Sile fault
San Francisco fault
Santa Cruz Springs fault
Tetuna fault
Canada de Santa Fe
Rio Grande
Santa Fe River
Dome Road
Cochiti Lake 2
Cochiti Elementary
CEPO 1 (Landfill)
CEPO 3 (Peralta)
1200 well
800' well
Solar-TW
Blow-TW
170TW
180-TW
13-TW
4-TW
Cochiti-TW
1583m
1609m
NAD83 / UTM zone 13N
6,000 METERS
4,000
2,000
0
2,000
106°22'30"
106°15'
35°37'30"
35°30'

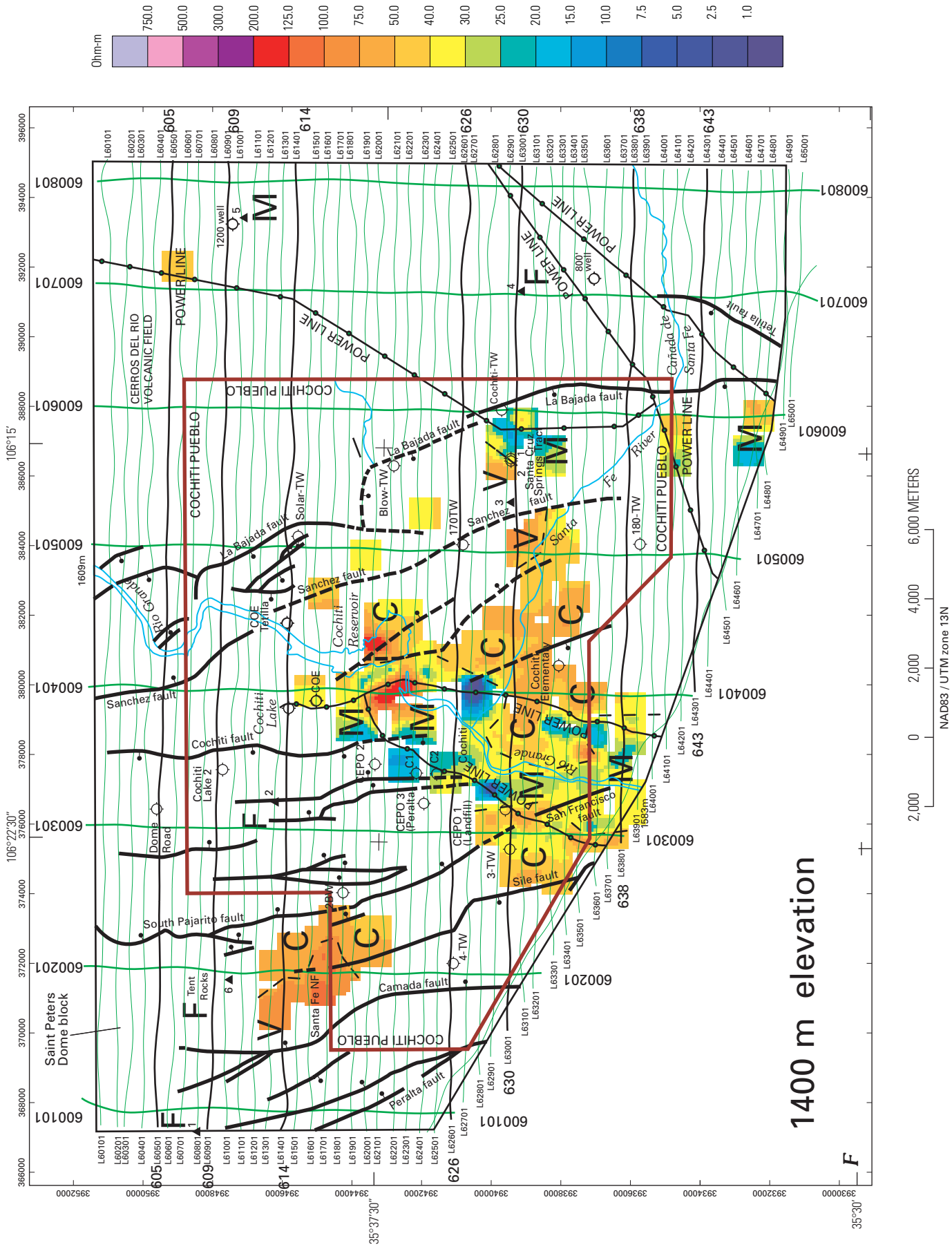
Ohm-m
750.0
500.0
300.0
200.0
125.0
100.0
75.0
50.0
40.0
30.0
25.0
20.0
15.0
10.0
7.5
5.0
2.5
1.0
1400 m elevation
CERROS DEL RIO VOLCANIC FIELD
COCHITI PUEBLO
POWER LINE
La Bajada fault
Sanchez fault
Cochiti fault
South Pajarito fault
Camada fault
Peralta fault
Sile fault
San Francisco fault
Santa Cruz Springs Trace fault
Tetilla fault
Cochiti Reservoir
Cochiti Lake
Cochiti Lake 2
Cochiti Elementary
Saint Peters Dome block
Santa Fe NF
Tent Rocks
Dome Road
Rio Grande
Santa Fe
Ritter
Canada de
1200 well
800' well
Blow-TW
Solar-TW
170TW
180-TW
Cochiti-TW
3-TW
4-TW
CEPO 1 (Landfill)
CEPO 2
CEPO 3 (Peralta)
COE
1609m
1583m
106°15'
106°22'30"
35°37'30"
35°30'
NAD83 / UTM zone 13N
2,000 0 2,000 4,000 6,000 METERS

main aquifers in the middle Rio Grande Basin (Bartolino, 1999), will have a higher electrical resistivity than surrounding finer grained materials (Hearst, Nelson, and Paillet, 2000). However, the resistivities obtained from TDEM are only indirectly related to the water content and the sediment grain size at depth, and they must be correlated with other geologic information.

The correlation of TDEM inversion resistivities with grain size within the Santa Fe Group sediments was possible with the help of induction and lithologic logs from wells in the survey area. To make the correlation reliable, the well had to meet three criteria: be within 200 m of the nearest flight line, have both induction and lithologic logs in the same depth range as the TDEM survey, and be at least 200 m away from cultural noise (using a cutoff value of 10,000 microvolts) owing to power lines, pipelines, or other man-made electrical power sources. Only four logged wells lay within areas covered by airborne surveys (Deszcz-Pan and others, 2000) met criteria for reliability. Three wells are in Rio Rancho (survey area A+B, fig. F1); one well (CEPO 2, fig. F2*A*; induction log, fig. F8*B*) was in Cochiti Pueblo (survey area D, fig. F1). Deszcz-Pan and others (2000) showed that one-dimensional inversion algorithms, developed and owned by BHP World Minerals, provided resistivity cross sections that closely correlate with the Rio Rancho well logs. The resistivity inversion also closely correlates with the one Cochiti Pueblo well log (CEPO 2, fig. F2*A*) below the static water level (SWL, fig. F8*B*). Above the static water level (upper 37 m (120 ft)), the inversion resistivity underestimated the induction log resistivity. The underestimation probably reflects the influence of an adjacent shallow conductor (20 ohm-m) just south of CEPO 2 (fig. F7*A*) that dips underneath CEPO 2 at 50 m (165 ft) depth (fig. F7*B*). Also, at 84–102 m (275–335 ft) depth, the inversion did not resolve the interval, 9–12 m (30–40 ft) thick, of moderately resistive coarse-grained sediments (60 ohm-m) (fig. F8*B*). This failure indicates that TDEM inversion for this survey was able to resolve only those resistive units whose thickness is greater than about 15 percent of their burial depth. Except for this resolution limitation and the underestimated resistivity in the upper 37 m (120 ft), the inversion correlates well with lithologic grain size below the water table.

Resistivities were correlated with grain size only in the saturated zone (Deszcz-Pan and others, 2000), owing to the lack of information about partial saturation in the vadose zone. Deszcz-Pan and others (2000) correlated resistivity and grain size in the saturated zone as follows: coarse grain size (40–70 ohm-m), medium grain size (20–40 ohm-m), and fine grain size (10–20 ohm-m). We also observed changes in TDEM response at several faults mapped at the surface (figs. F7, F12) and at faults inferred from a high-resolution airborne magnetic survey (Grauch, 1999; chapter D, this volume), delineating pronounced changes in lithology in Santa Fe Group sediments owing to fault juxtapositions. Variations in the pattern of resistivity can thus be linked to hydrostratigraphic changes across faults, including growth-fault-related facies variations in sediments of the Santa Fe Group and contemporaneous volcanic deposits.

The resistivity models obtained by the airborne TDEM survey correlate with the three principal geologic terranes in the La Bajada constriction area depicted in figure A4. Basaltic rocks of the Cerros del Rio volcanic field, in the footwall of the La Bajada fault zone (fig. F7), are characterized by very high resistivities (>500–750 ohm-m). Higher resistivity areas generally correspond with vent areas of individual volcanoes. The tapering edges of unsaturated thin basalts generally have resistivities of 30–100 ohm-m. The southern boundary of the resistive basalts dips north and is bounded by conductive sedimentary rocks. However, the increase in thickness of the >100 ohm-m resistive section (fig. F14*A*) correlates with higher elevation cones and vents within the Cerros del Rio volcanic field. Comparison of the thickness diagram with a map of the calculated base of the resistive section (fig. F14*B*) clearly shows that most of the thickening pattern is due to increasing constructional topography of the Cerros del Rio volcanoes. As determined by results from AMT station 5 and the 1200-Foot well (fig. F4*B*), both the volcanic lavas and the Santa Fe Group sediments thicken to the north (see also geologic cross sections, pl. 6). The east-dipping Mancos Shale is distinctive in the depth slices at 70 and 100 ohm-m (fig. F7*C*, *D*) just east of the Tetilla fault zone, where resistivity for this very conductive marine shale is below 7.5 ohm-m. The east-dipping Mancos Shale can also be seen in cross section in the 643 TDEM resistivity profile (fig. F11*F*) east of the Tetilla fault zone. On the TDEM 1,750-m elevation-slice map (fig. F12*A*), south of the northeast-trending power line and south of flight line 638, the Tetilla fault zone appears to form the western boundary of the east-dipping conductive Mancos Shale. The resistivity character of the Cerros del Rio area north of the two northeast-trending power lines, near AMT station 4, appears to differ from that south of the power lines. North of the power lines, the east-dipping conductive material on the 630 TDEM resistivity profile (fig. F11*D*) is gone, and minor breaks disrupt what otherwise appear to be fairly flat-lying conductive layers. The 1,700-m-elevation TDEM slice map (fig. F12*B*) depicts moderately resistive material surrounded by moderately conductive material, which suggests a structural block between AMT stations 4 and 5 at a bearing of about N. 60° E. The structure of this block can also be seen north of AMT station 4 in the north-south 600701 TDEM resistivity profile (fig. F13*G*) and south of AMT station 5 in the north-south 600801 TDEM resistivity profile (fig. F13*H*). The moderately resistive character of this section is similar to that of sediments in the Santa Fe Group.

The western terrane, Saint Peters Dome block (figs. F12, F7), also displays high resistivity values in the footwall block of the Pajarito fault zone, and those higher resistivities continue south into the Santo Domingo Basin between the Pajarito and Sile faults. In the west, an exposed rhyolite dome and related pyroclastic deposits near Tent Rocks (V, figs. F12, F7) have high resistivities. The dome and pyroclastic deposits have peak resistivities greater than 500–750 ohm-m in the depth range of 100–150 m below the surface, so their highest values are more limited here than in the basaltic rocks of the Cerros

Figure F13 (below and following 2 pages). North-south profiles in the Cochiti Pueblo time-domain electromagnetic survey area (cross sections *A*–*H*), drawn on the basis of least-squares inversions. Dashed line in each section is maximum depth estimated from resistivity-depth image; numbers below wells or stations represent modeled resistivities. Vertical exaggeration is 10. *A,* Flight line 600101 showing audiomagnetotelluric (AMT) station 1. *B*, Flight line 600201 showing AMT station 6. *C,* Flight line 600301 showing Dome Road well. *D*, Flight line 600401 showing Sanchez fault. *E*, Flight line 600501 showing La Bajada fault zone. *F*, Flight line 600601 showing La Bajada fault zone. *G*, Flight line 600701 showing AMT station 4. *H*, Flight line 600801 showing AMT station 5 and 1200-Foot well.

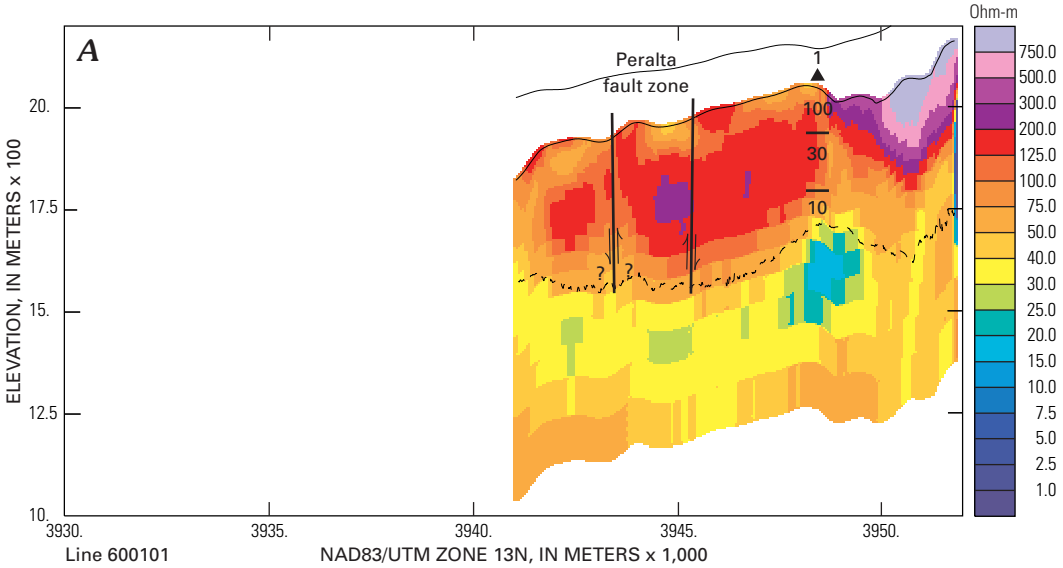

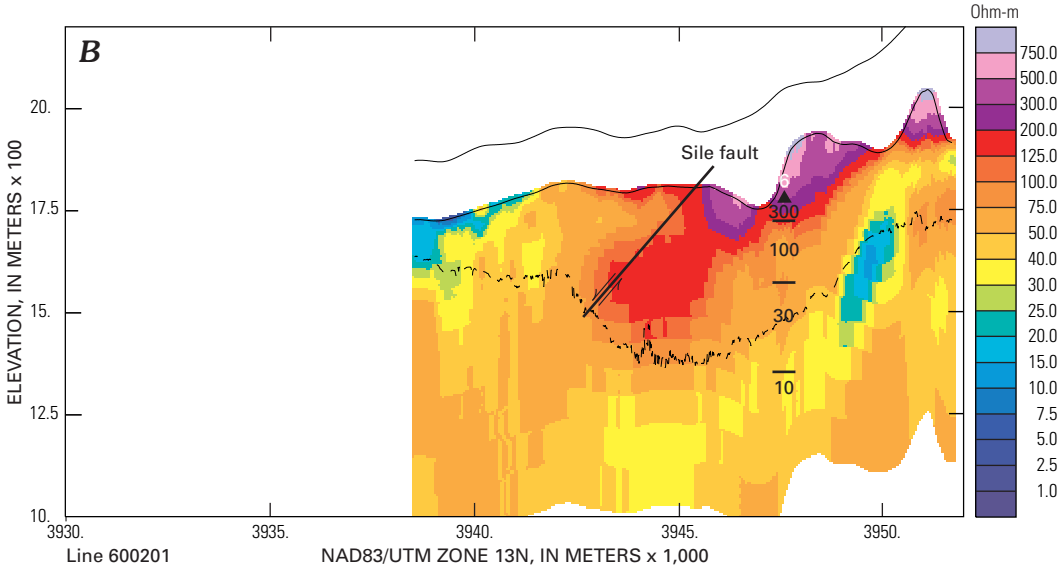

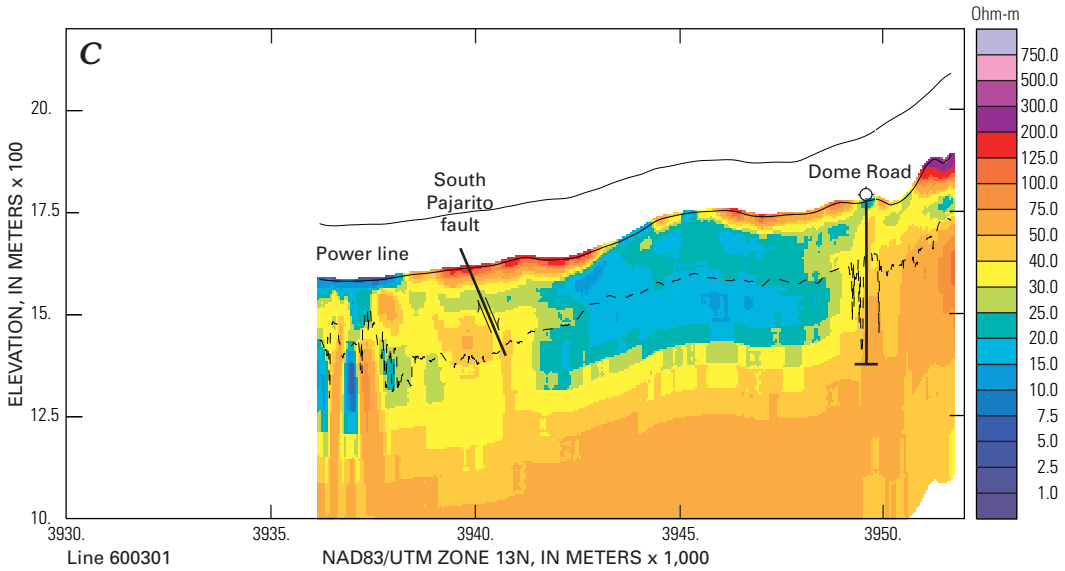
C
Ohm-m
750.0
500.0
300.0
200.0
125.0
100.0
75.0
50.0
40.0
30.0
25.0
20.0
15.0
10.0
7.5
5.0
2.5
1.0
South Pajarito fault
Dome Road
Power line
ELEVATION, IN METERS x 100
20.
17.5
15.
12.5
10.
3930.
3935.
3940.
3945.
3950.
Line 600301
NAD83/UTM ZONE 13N, IN METERS x 1,000

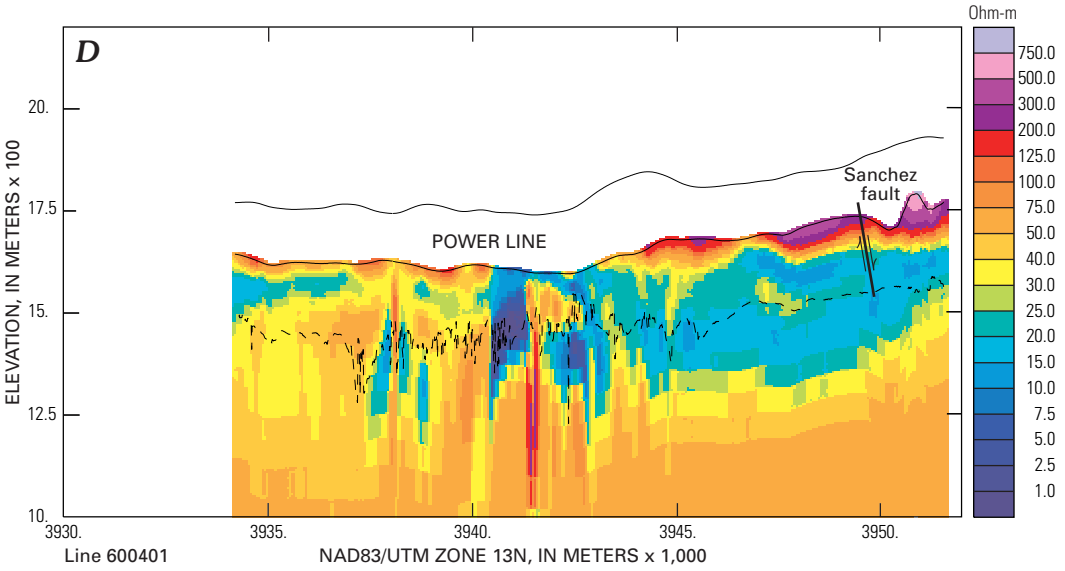
D
Ohm-m
750.0
500.0
300.0
200.0
125.0
100.0
75.0
50.0
40.0
30.0
25.0
20.0
15.0
10.0
7.5
5.0
2.5
1.0
Sanchez fault
POWER LINE
ELEVATION, IN METERS x 100
20.
17.5
15.
12.5
10.
3930.
3935.
3940.
3945.
3950.
Line 600401
NAD83/UTM ZONE 13N, IN METERS x 1,000

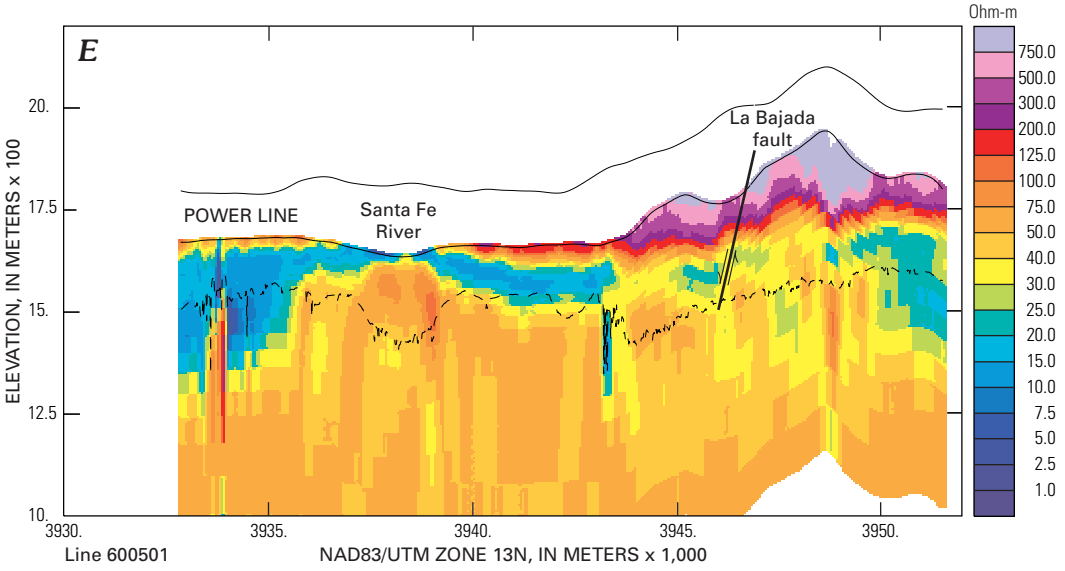
E
Ohm-m
750.0
500.0
300.0
200.0
125.0
100.0
75.0
50.0
40.0
30.0
25.0
20.0
15.0
10.0
7.5
5.0
2.5
1.0
La Bajada fault
POWER LINE
Santa Fe River
ELEVATION, IN METERS x 100
20.
17.5
15.
12.5
10.
3930.
3935.
3940.
3945.
3950.
Line 600501
NAD83/UTM ZONE 13N, IN METERS x 1,000

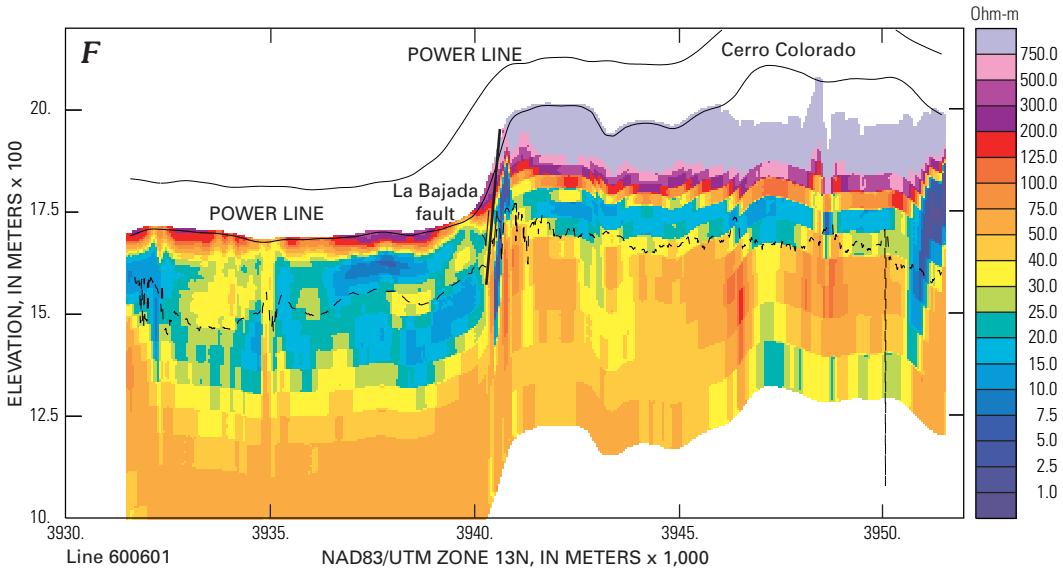
F
POWER LINE
Cerro Colorado
POWER LINE
La Bajada fault
ELEVATION, IN METERS x 100
20.
17.5
15.
12.5
10.
3930.
3935.
3940.
3945.
3950.
Line 600601
NAD83/UTM ZONE 13N, IN METERS x 1,000
Ohm-m
750.0
500.0
300.0
200.0
125.0
100.0
75.0
50.0
40.0
30.0
25.0
20.0
15.0
10.0
7.5
5.0
2.5
1.0

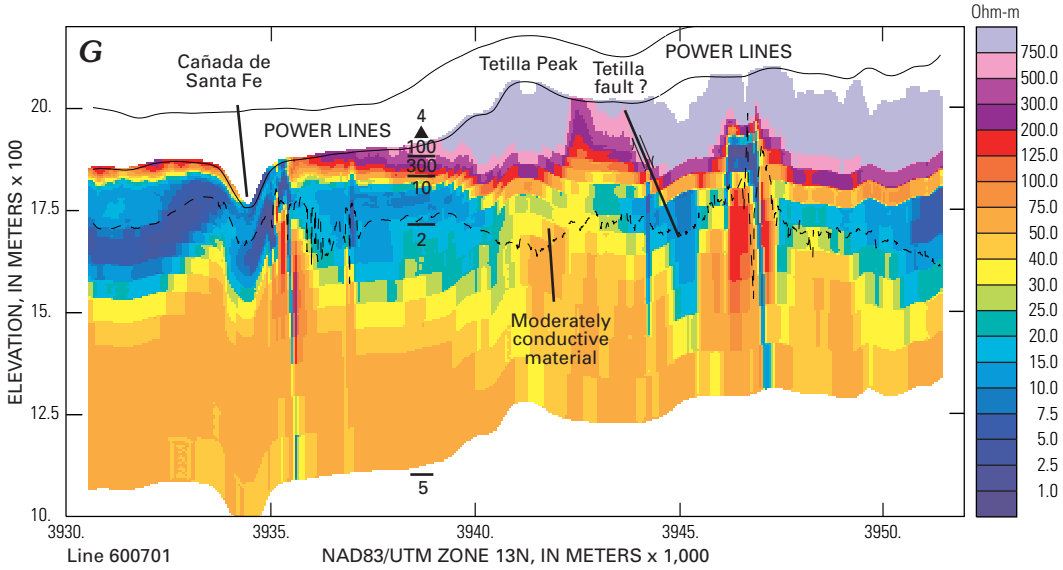
G
Cañada de Santa Fe
Tetilla Peak
Tetilla fault ?
POWER LINES
POWER LINES
4
100
300
10
2
Moderately conductive material
5
ELEVATION, IN METERS x 100
20.
17.5
15.
12.5
10.
3930.
3935.
3940.
3945.
3950.
Line 600701
NAD83/UTM ZONE 13N, IN METERS x 1,000
Ohm-m
750.0
500.0
300.0
200.0
125.0
100.0
75.0
50.0
40.0
30.0
25.0
20.0
15.0
10.0
7.5
5.0
2.5
1.0

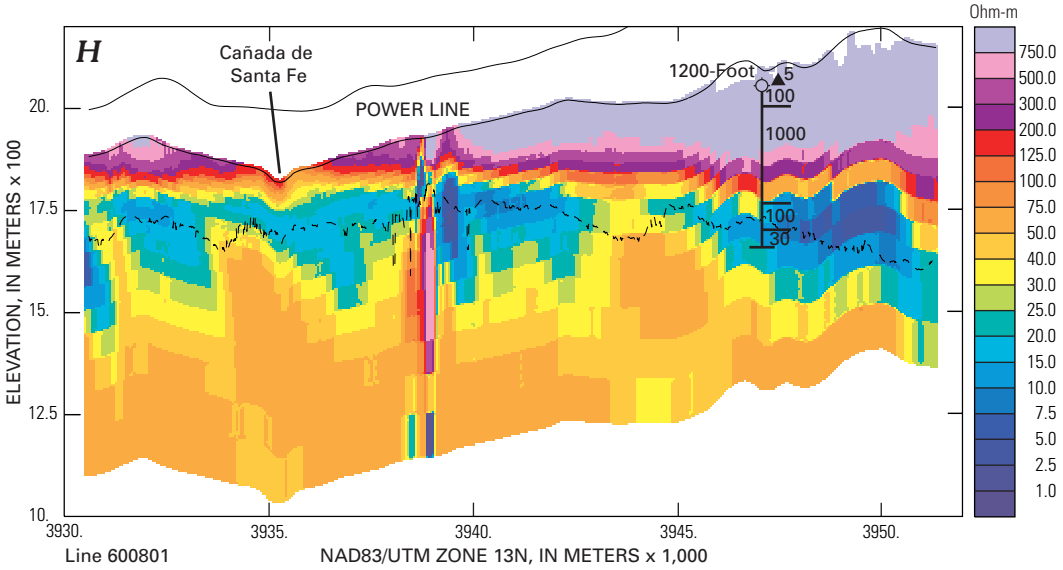
H
Cañada de Santa Fe
POWER LINE
1200-Foot
5
100
1000
100
30
ELEVATION, IN METERS x 100
20.
17.5
15.
12.5
10.
3930.
3935.
3940.
3945.
3950.
Line 600801
NAD83/UTM ZONE 13N, IN METERS x 1,000
Ohm-m
750.0
500.0
300.0
200.0
125.0
100.0
75.0
50.0
40.0
30.0
25.0
20.0
15.0
10.0
7.5
5.0
2.5
1.0

del Rio volcanic field. Resistivity values in the adjoining Cochiti Formation volcaniclastic sediments and axial gravels are also moderately high, in the range of 40–200 ohm-m.

The central La Bajada constriction area (that is, within the Santo Domingo Valley, fig. A4) has the lowest resistivities overall, and deposits in this area are generally less than 50 ohm-m resistivity. In the northern part of this area, a large area of lower resistivity coincides with a silt or clay lacustrine unit (F, near station AMT–2, figs. F12, F7) concealed within deposits of the upper Santa Fe Group. In the central part of the map area, higher resistivities correspond in part with ancestral Rio Grande axial-gravel deposits (C, M, fig. F12*C–F*). In areas lacking other subsurface information, boundaries within these deposits were inferred on the basis of grain size (fig. F12*C–F*); grain size, in turn, was established primarily on the basis of resistivity calibration (as previously described), but it was also constrained by local AMT soundings and lithologic well logs (Deszcz-Pan and others, 2000). The AMT soundings also helped us interpret the northern part of the survey area where thin (30–50 m) but strongly conductive, clay-rich sediments (<10 ohm-m) or rocks effectively blocked out those portions of the elevation-slice maps (fig. F12*C–F*) derived from the TDEM resistivity inversions. The TDEM data west of the La Bajada fault zone show that relatively lower resistivity values correspond with Santa Fe Group piedmont alluvium deposits, whereas relatively higher resistivity values correspond with axial gravel deposits of the ancestral Rio Grande. A large region of buried volcanic rock (V, fig. F12) in the subsurface of the Santo Domingo Basin is imaged by the modeled TDEM data. For example, aeromagnetic data (chapter D, this volume) indicate that a basaltic vent is buried just to the west of the Sanchez fault (magnetic anomaly C3, figs. F7, F11*D*), that abundant volcanic clasts contribute to the moderate resistivities just west of the Santa Cruz Springs well (magnetic anomaly C4, figs. F7, F11*D*), and that the rhyolite at the core of the W4 magnetic high (figs. F7, F11*B*) is at least 250 m thick and has resistivities well above 200 ohm-m. The apparent reduction in spatial size of the displayed resistivities for the deeper elevation slices (fig. F12*D–F*) is in part due to the depth-of-penetration limits of the TDEM survey. More detailed geologic interpretation and comparison of features seen in the TDEM models with geology and other geophysical data sets are discussed in chapter G (this volume).

Summary

Time-domain electromagnetic and magnetotelluric data were used to map changes in electrical resistivity with depth; these changes in resistivity are related to variations in rock types at depth; these variations in turn influence aquifers in the study area. These aquifers are part of the groundwater system hydraulically connected with the Rio Grande as it passes from the Española Basin into the Santo Domingo Basin.

1. In the area of the eastern Cerros del Rio volcanic field, the northern boundary of the Cerrillos uplift is constrained by magnetotelluric data reported in this chapter. Magnetotelluric soundings (figs. F4, F5) indicate that along a north-south line between audio-magnetotelluric stations 4 and 5, a 2 ohm-m conductor inferred to be the Cretaceous Mancos Shale is downdropped from a depth of 180 m at audio-magnetotelluric station 4 to a depth of 1,150 m beneath the surface at audio-magnetotelluric station This offset is evidence for 800 m of Tertiary structural relief at the north end of the Cerrillos uplift. The shallow Mancos Shale located at audio-magnetotelluric station 4, immediately south of Tetilla Peak, provides the farthest northwest constraint for the edge of the Cerrillos uplift and is consistent with the subsurface extent of the uplift based on gravity data.

2. Also in the area of the eastern Cerros del Rio volcanic field, the partly concealed Tetilla fault zone appears to form the western boundary of the east-dipping conductive Mancos Shale, based on time-domain electromagnetic results south of two northeast-trending power lines (fig. F11*F*). We do not see the same east-dipping conductive material in the terrane north of the power lines, near audio-magnetotelluric station 4 (fig. F11*D*), but rather we see minor breaks in what otherwise look like fairly flat-lying conductive layers. Moderately resistive material surrounded by moderately conductive material suggests some kind of structural block between audiomagnetotelluric stations 4 and 5 at a bearing of about N. 60° E. (fig. F12*B*). The structure of this block can also be seen north of audiomagnetotelluric station 4 (fig. F13*G*) and south of audiomagnetotelluric station 5 (fig. F13*H*). This moderately resistive block has resistivities similar to those of Santa Fe Group sediments.

3. In the northern part of the central La Bajada constriction, a large area of lower resistivity, defined by the time-domain electromagnetic survey results, coincides with a silt or clay lacustrine unit (region F, near audiomagnetotelluric station 2, figs. F12, F7) in the upper Santa Fe Group deposits. In the central part of the map, higher resistivities correspond in part with ancestral Rio Grande axial-gravel deposits (regions C and M, fig. F12).

4. The Saint Peters Dome block, in the footwall of the Pajarito fault zone, has a more complex stratigraphy than expected on the basis of the magnetotelluric results. Magnetotelluric soundings (fig. F6, magnetotelluric stations 12 and 17) provide additional constraints on the relative position of basement and thickness of Paleozoic, Mesozoic, and Tertiary sedimentary rocks across the Pajarito fault zone.

Figure F14 (following 2 pages). *A*, Depth to surface of resistive layer (>100 ohm-m) in the Cochiti Pueblo time-domain electromagnetic survey area, drawn on the basis of least-squares inversion. *B*, Elevation to base of surface resistive layer (>100 ohm-m) in the Cochiti Pueblo time-domain electromagnetic survey area, drawn on the basis of least-squares inversion.

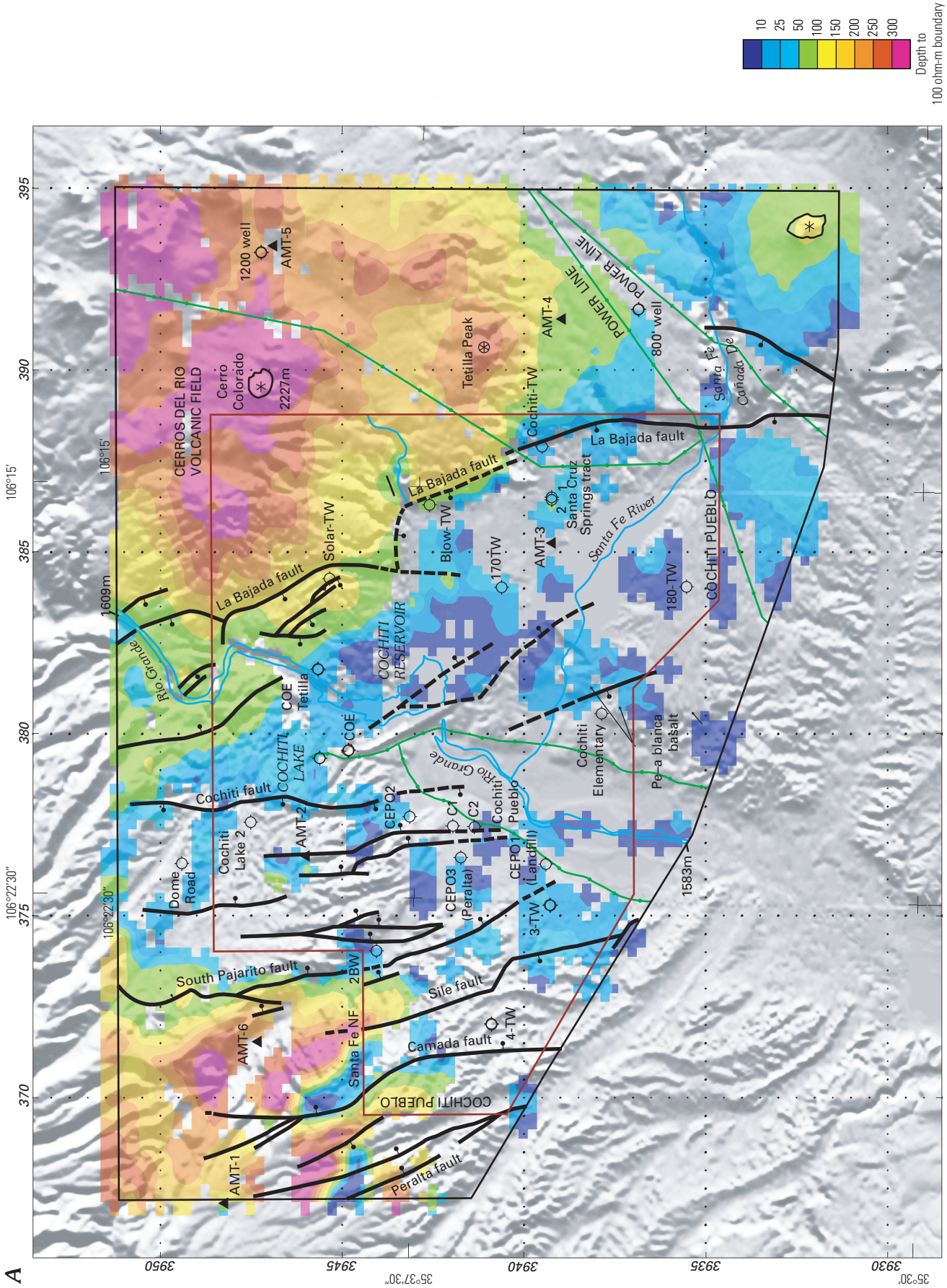
A
Depth to 100 ohm-m boundary
10
25
50
100
150
200
250
300
CERROS DEL RIO VOLCANIC FIELD
Cerro Colorado
2227m
1200 well
AMT-5
Tetilla Peak
AMT-4
POWER LINE
POWER LINE
800' well
Santa Fe
Cañada De
Cochiti-TW
La Bajada fault
La Bajada fault
Santa Cruz Springs tract
Santa Fe River
COCHITI PUEBLO
180-TW
170TW
AMT-3
Blow-TW
COCHITI RESERVOIR
Solar-TW
La Bajada fault
1609m
Rio Grande
COE Tetilla
COE
COCHITI LAKE
Cochiti fault
Cochiti Lake 2
AMT-2
Dome Road
CEPO2
C1
C2
Cochiti Pueblo
Rio Grande
Cochiti Elementary
Pe-a blanca basalt
CEPO1 (Landfill)
CEPO3 (Peralta)
3-TW
1583m
South Pajarito fault
2BW
Sile fault
Camada fault
4-TW
Santa Fe NF
AMT-6
COCHITI PUEBLO
AMT-1
Peralta fault
106°15'
106°22'30"
35°37'30"
35°30'
3950
3945
3940
3935
3930
395
390
385
380
375
370
0
3
6 KILOMETERS
NAD27/UTM ZONE 13N

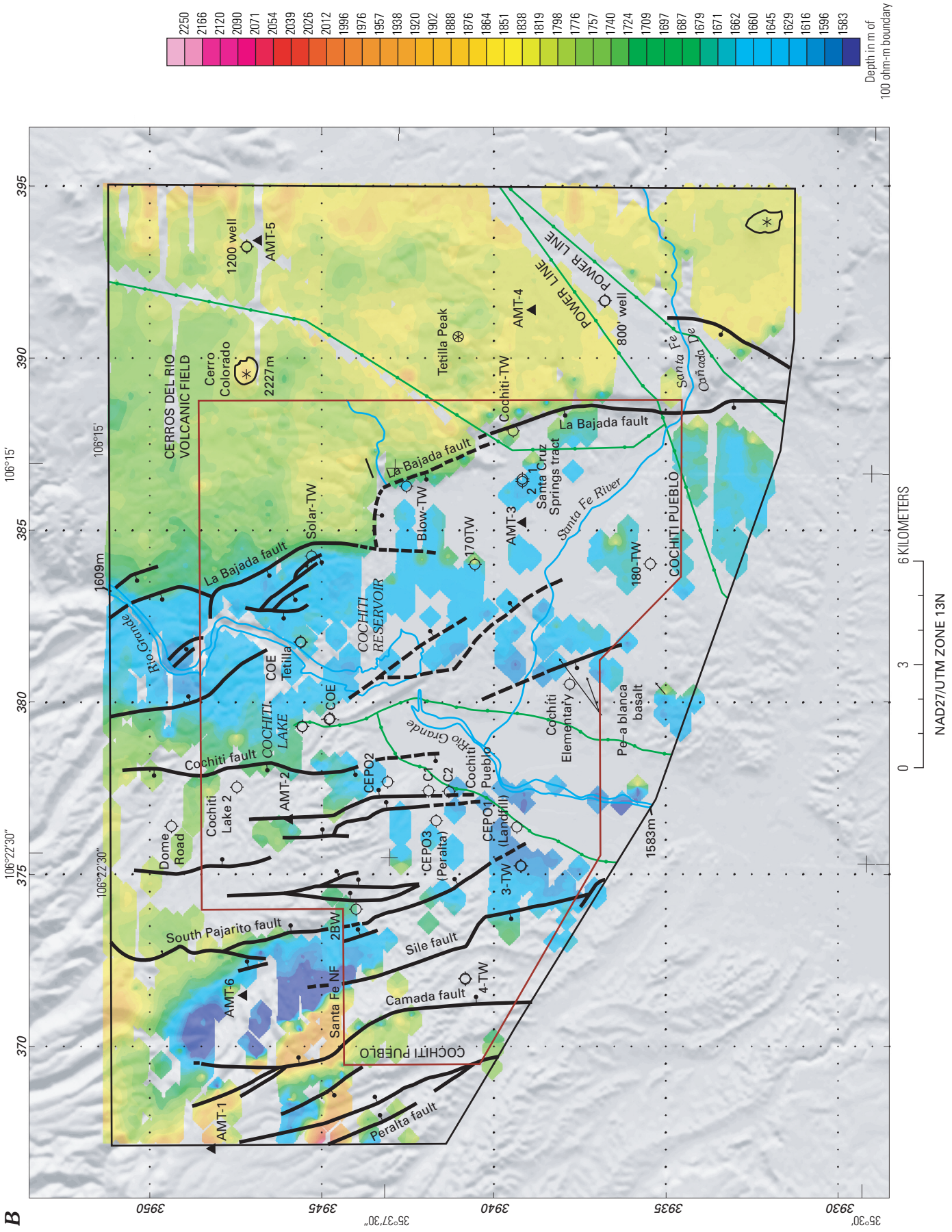
2250
2166
2120
2090
2071
2054
2039
2026
2012
1996
1976
1957
1938
1920
1902
1888
1876
1864
1851
1838
1819
1798
1776
1757
1740
1724
1709
1697
1687
1679
1671
1662
1660
1645
1629
1616
1596
1583
Depth in m of 100 ohm-m boundary
B
CERROS DEL RIO VOLCANIC FIELD
Cerro Colorado
2227m
1200 well
AMT-5
Tetilla Peak
AMT-4
POWER LINE
POWER LINE
800' well
Cochiti-TW
La Bajada fault
La Bajada fault
Santa Cruz Springs tract
Santa Fe River
Santa Fe
Cañada De
COCHITI PUEBLO
Solar-TW
Blow-TW
170TW
AMT-3
180-TW
1609m
La Bajada fault
Rio Grande
COE
Tetilla
COCHITI RESERVOIR
COCHITI LAKE
COE
Cochiti Elementary
Pe-a blanca basalt
Cochiti fault
AMT-2
CEPO2
C1
C2
Cochiti Pueblo
Rio Grande
Cochiti Lake 2
Dome Road
CEPO3 (Peralta)
CEPO1 (Landfill)
3-TW
1583m
South Pajarito fault
2BW
Sile fault
AMT-6
Santa Fe NF
Camada fault
4-TW
COCHITI PUEBLO
AMT-1
Peralta fault
106°15'
106°15'
106°22'30"
106°22'30"
395
390
385
380
375
370
3950
3945
3940
3935
3930
35°37'30"
35°30'
0
3
6 KILOMETERS
NAD27/UTM ZONE 13N

References Cited

Bartolino, J.R., 1999, Introduction, *in* U.S. Geological Survey Middle Rio Grande Basin Study— 3d Annual Workshop, Albuquerque, New Mexico, February 24–25, 1999, Proceedings: U.S. Geological Survey Open-File Report 99–203, p. 2.

Bartolino, J.R., and Cole, J.C., 2002, Ground-water resources of the Middle Rio Grande Basin, New Mexico: U.S. Geological Survey Circular 1222, 132 p.

Bendat, J.S., and Piersol, A.G., 1971, Random data—Analysis and measurement procedures: New York, Wiley Interscience, 407 p.

Chamberlin, R.M., Jackson, P., and Connell, S.D., 1999, Field logs of borehole drilled for monitoring well at Dome Road site, Canada de Cochiti Grant, Sandoval County, New Mexico: New Mexico Bureau of Mines and Mineral Resources Open-file Report 444c, 30 p.

Clarke, J., Gamble, T.D., Goubau, W.M., Koch, R.H., and Miracky, R.F., 1983, Remote-reference magnetotellurics—Equipment and procedures: Geophysical Prospecting, v. 31, p. 149–170.

Cole, J.C., Grauch, V.J.S., Hudson, M.R., Maldonado, F., Minor, S.A., Sawyer, D.A., and Stone, B.D., 1999, Three-dimensional geologic modeling of the middle Rio Grande Basin, *in* Bartolino, J.R., ed., U.S. Geological Survey Middle Rio Grande Basin Study—3d Annual Workshop, Albuquerque, New Mexico, February 24–25, 1999, Proceedings: U.S. Geological Survey Open-File Report 99–203, p. 25–26.

Deszcz-Pan, M., Rodriguez, B.D., Doucette, J.P., Godbout, M., Williams, J.M., Sawyer, D.A., Stone, B.D., and Grauch, V.J.S., 2000, Digital airborne time domain electromagnetic data from surveys over Cochiti Pueblo, Rio Puerco, and Rio Rancho, New Mexico: U.S. Geological Survey Open-File Report 00–502 (CD-ROM).

Dobrin, M.D., and Savit, C.H., 1988, Introduction to geophysical prospecting (4th ed.): New York, McGraw-Hill, 867 p.

Ellis, R.G., 1998, Inversion of airborne electromagnetic data: Exploration Geophysics, v. 29, no. 1–2, p. 121–127.

Gamble, T.D., Goubau, W.M., and Clarke, J., 1979, Magnetotellurics with a remote magnetic reference: Geophysics, v. 44, no. 1, p. 53–68.

Grauch, V.J.S., 1999, Principal features of high-resolution aeromagnetic data collected near Albuquerque, New Mexico: New Mexico Geological Society 50th field conference, Albuquerque Geology, Guidebook, p. 115–118, 133–135.

Hearst, J.R., Nelson, P.H., and Paillet, F.L., 2000, Well logging for physical properties, 2d ed.: New York, John Wiley, 483 p.

Keller, G.V., 1987, Rock and mineral properties, *in* Nabighian, M.N., ed., Electromagnetic methods in applied geophysics, v. 1, Theory: Society of Exploration Geophysicists, p. 13–51.

Keller, G.V., and Frischknecht, F.C., 1966, Electrical methods in geophysical prospecting: New York, Pergamon Press, 517 p.

Liu, G., and Asten, M.A., 1993, Conductance-depth imaging of airborne TEM data: Exploration Geophysics, v. 24, no. 3–4, p. 655–662.

Nelson, P.H., and Anderson, L.A., 1992, Physical properties of ash flow tuff from Yucca Mountain, Nevada: Journal of Geophysical Research, v. 97, no. B5, p. 6823–6841.

Palacky, G.J., 1987, Resistivity characteristics of geologic targets, *in* Nabighian, M.N., ed., Electromagnetic methods in applied geophysics, v. 1, Theory: Society of Exploration Geophysicists, p. 53–129.

Palacky, G.J., and West, G.F., 1991, Airborne electromagnetic methods, *in* Nabighian, M.N., ed., Electromagnetic methods in applied geophysics, v. 2, Application: Society of Exploration Geophysicists, p. 811–879.

Smith, G.A., 2001, Development of a pyroclastic apron adjacent to rhyolite domes in a subsiding basin, upper Miocene Peralta Tuff, Jemez Mountains, New Mexico: New Mexico Museum of Natural History and Science, v. 18, p. 85–96.

Sternberg, B.K., Washburne, J.C., and Pellerin, L., 1988, Correction for the static shift in magnetotellurics using transient electromagnetic soundings: Geophysics, v. 53, p. 1459–1468.

Vozoff, K., 1972, The magnetotelluric method in the exploration of sedimentary basins: Geophysics, v. 37, p. 98–141.

Vozoff, K., 1991, The magnetotelluric method, *in* Nabighian, M.N., ed., Electromagnetic methods in applied geophysics, v. 2, Application, part B: Society of Exploration Geophysicists, Tulsa, Oklahoma, p. 641–711.

Wannamaker, P.E., Hohmann, G.W., and Ward, S.H., 1984, Magnetotelluric responses of three-dimensional bodies in layered earths: Geophysics, v. 49, no. 9, p. 1517–1533.

Wannamaker, P.E., Stodt, J.A., and Rijo, L., 1985, PW2D—Finite element program for solution of magnetotelluric responses of two-dimensional earth resistivity structure (user documentation): Salt Lake City, Utah, Earth Science Laboratory, University of Utah Research Institute, 40 p.

Williams, J.M., and Rodriguez, B.D., 2003, Magnetotelluric data in the southwest Española Basin, northern New Mexico: U.S. Geological Survey Open-File Report 03–199, 128 p.

Williams, J.M., Rodriguez, B.D., and Sampson, J.A., 2001, Magnetotelluric data in the Cochiti Pueblo area, New Mexico: U.S. Geological Survey Open-File Report 01–442, 66 p.

Published in the Central Region, Denver, Colo.
Manuscript approved for publication February 10, 2006
Graphics by authors
Photocomposition by Mari L. Kauffmann (Contractor, ATA Services)
Edited by Mary-Margaret Coates (Contractor, ATA Services)

Hydrogeologic Framework of the La Bajada Constriction Area, New Mexico—Integration of Subsurface and Surface Geology

By David A. Sawyer and Scott A. Minor

Chapter G of

The Cerrillos Uplift, the La Bajada Constriction, and Hydrogeologic Framework of the Santo Domingo Basin, Rio Grande Rift, New Mexico

Edited by Scott A. Minor

Professional Paper 1720–G

U.S. Department of the Interior
U.S. Geological Survey

Contents

Abstract 167
Introduction 167
Subsurface Hydrologic and Geologic Data 168
Water Elevations in the La Bajada Constriction Area 168
Subsurface Geologic Constraints From Wells 172
Cerros del Rio Volcanic Field and Cerrillos Uplift 172
La Bajada Constriction 174
Saint Peters Dome Block 178
Subsurface Hydrogeologic Framework of the La Bajada Constriction Area 178
Introduction 178
Cerrillos Uplift: Southeastern Boundary of the La Bajada Constriction 180
La Bajada Constriction 182
Northwestern Cerros del Rio Volcanic Field 183
La Majada Graben 183
Reservoir Horst 183
Cochiti Graben 184
Saint Peters Dome Block: Northwestern Boundary of the La Bajada Constriction 184
Implications for Ground-water Flow Between Española and Santo Domingo Basins 185
References Cited 186

Figures

G1. Map showing contoured regional water table, water wells, and major faults in La Bajada constriction area 169
G2. Lithologic column of the 1200-Foot well, northeastern La Bajada constriction 173
G3. Lithologic column of the Santa Cruz Springs Tract well, eastern Cochiti Pueblo 175
G4. Gamma ray and long-normal resistivity logs and lithologic interpretation of the CEPO 2 well, Cochiti Pueblo 177
G5. Geophysical and lithologic logs of Dome Road well, northwestern La Bajada constriction 179
G6. Map of La Bajada constriction area showing its boundaries and structure contours on base of Neogene basin-fill deposits 181

Table

G1. Water table elevations in the Cochiti Pueblo and La Bajada constriction areas 170

Hydrogeologic Framework of the La Bajada Constriction Area, New Mexico—Integration of Subsurface and Surface Geology

By David A. Sawyer and Scott A. Minor

Abstract

Summary results of multidisciplinary investigations of the La Bajada constriction presented in this report are synthesized in this chapter. In the area of the constriction, where only sparse information exists regarding the subsurface hydrogeology, an integrated geologic and geophysical approach allows development of a geologic framework model that can provide input for regional ground-water flow models. The combination of surface geology based on new geologic mapping (chapters A, B, C, and E, this volume), airborne geophysics (aeromagnetic and time-domain electromagnetic surveys; chapters D and F, this volume), ground geophysical measurements (gravity and magnetotelluric surveys; chapters D and F, this volume), and data from the few wells in the area (this chapter) provides new constraints on the hydrogeologic framework of the La Bajada constriction area.

Data of differing quality from more than 60 water wells were used to generate a water-level contour map of the La Bajada constriction area, but only a few of these wells provided subsurface geologic constraints. The subsurface geology of the constriction area is depicted in a series of interpretative cross sections that allow three-dimensional visualization of the geologic framework. The northern flank of the Cerrillos uplift, bordering the east side of the La Bajada constriction, consists of north- to northeast-dipping Oligocene and Eocene volcanic and sedimentary deposits underlain by thick Cretaceous and older sedimentary rocks. These rocks form a northeast-facing monoclinal ramp beneath the Cerros del Rio volcanic field that drops into the southwestern Española Basin. The northern tip of the Cerrillos uplift is probably truncated by a northeast-striking fault or fault zone that is structurally linked with the Tetilla fault zone to the southwest. In the structurally low La Bajada constriction and overlapping northeastern Santo Domingo Basin, rift-basin sediments of the Santa Fe Group are interlayered with volcanic deposits from the Jemez and Cerros del Rio volcanic fields. These basin-fill deposits are cut by numerous, mostly north-northwest-striking, normal faults that are inferred to have growth-fault histories that produce increased amounts of dip-slip displacement with increasing depth. The southwest part of the La Bajada constriction is subdivided into three structural blocks separated from one another by prominent intrabasin faults of Miocene and younger age: (1) the eastern La Majada graben, between the La Bajada fault zone and Sanchez fault; (2) the central Reservoir horst, between the Sanchez and Cochiti faults; and (3) the western Cochiti graben, between the Cochiti and South Pajarito faults. The northwest border of the La Bajada constriction consists of the northeast-striking Pajarito fault zone and its uplifted footwall Saint Peters Dome block, composed chiefly of Jemez volcanic rocks and underlying pre-rift sedimentary rocks.

We conclude that through-going aquifers consisting of ancestral Rio Grande axial-river sand and gravel and coarse western-piedmont gravel form the predominant ground-water pathways through the La Bajada constriction between Española and Santo Domingo Basins. Eastern-piedmont sand and silty sand deposits that probably form fair to moderately good aquifers likely extend through the constriction beneath the entire northern Cerros del Rio volcanic field. On the southeast side of the La Bajada constriction within the Cerrillos uplift, thick, clay-rich Cretaceous marine shales of low hydraulic conductivity form a pervasive regional confining unit. Numerous, dominantly north-northwest-striking, intrabasin faults that project part way across the La Bajada constriction may locally partition or compartmentalize and deflect ground-water flow into fault-parallel directions. Complex interfingering of the sedimentary fill and volcanic rocks within the La Bajada constriction and Santo Domingo Basin, together with intrabasin faults that commonly juxtapose hydrologically contrasting geologic layers, result in a matrix of laterally and vertically variable hydrogeologic compartments.

Introduction

Studies by the U.S. Geological Survey were begun in 1996 to improve understanding of the geologic framework of the Albuquerque composite basin and adjoining areas, in order that more accurate hydrogeologic parameters could be applied

to new hydrologic models. The ultimate goal of this multidisciplinary effort has been to better quantify estimates of future water supplies for northern New Mexico's growing urban centers, which largely subsist on aquifers in the Rio Grande rift basin (Bartolino and Cole, 2002). From preexisting hydrologic models it became evident that hydrogeologic uncertainties were large in the Santo Domingo Basin area, immediately up gradient from the greater Albuquerque metropolitan area, and particularly in the northeast part of the basin referred to as the La Bajada constriction (see chapter A, this volume, for a geologic definition of this feature as used in this report). Accordingly, a priority for new geologic and geophysical investigations was to better determine the hydrogeologic framework of the La Bajada constriction area. This chapter and the other chapters of this report present the results of such investigations as recently conducted by the U.S. Geological Survey.

The combination of surface geology based on new geologic mapping (chapters A, B, C, and E, this volume), airborne geophysics (aeromagnetic and time-domain electromagnetic surveys) (chapters D and F, this volume), ground geophysical measurements (gravity and magnetotelluric surveys) (chapters D and F, this volume), and data from a few critical wells (this chapter) provide new constraints on the hydrogeologic framework of the La Bajada constriction area. These lines of evidence can be used to help determine the subsurface distribution of aquifers and confining units of the Rio Grande ground-water flow system, which hydraulically connects the Española and Santo Domingo Basins. In the La Bajada constriction area, where only sparse information exists regarding the subsurface hydrogeology, this integrated geologic and geophysical approach provides the best geologic input available for regional ground-water flow models.

Direct subsurface geologic observations in the area of the La Bajada constriction are restricted to a relatively small number of water wells. No petroleum exploration wells have been drilled in the Santo Domingo Basin or the La Bajada constriction area. This situation contrasts with the considerable quantitative physical-property information available from a modest number of petroleum exploration wells drilled in the adjacent northern Albuquerque Basin and in the Hagan and Santa Fe embayments. The La Bajada constriction represents a critical hydrologic link in the regional Rio Grande aquifer system between the poorly constrained Santo Domingo Basin and the better studied Española Basin. Although sparse subsurface information from the northeast part of the Santo Domingo Basin suggests pronounced changes in regional water elevations across the La Bajada constriction, the large distances between wells and the lack of adequate quantitative geologic and geophysical data preclude accurate characterization of these changes.

In this chapter we first describe the limited subsurface water elevation and geologic information that is available from wells in the area of the La Bajada constriction. We then integrate these well data with regional surface geologic data and geophysical data described in the preceding chapters of this report to construct geologic cross sections and derive a more complete hydrogeologic framework model of the constriction area.

Subsurface Hydrologic and Geologic Data

Water Elevations in the La Bajada Constriction Area

The distribution of wells in the La Bajada constriction area and water-elevation contours based on those wells are displayed in figure G1. Those wells shown in figure G1 for which geologic information is available are keyed to table G1*A*, *B*. Well information for the Cochiti Pueblo area (table G1*A*) includes data derived from L.M. Bexfield (U.S. Geological Survey (USGS), written commun., 1999) and from the water level compilation of Bexfield and Anderholm (2000). Well data presented in table G1*B* were obtained from a variety of sources; some of the wells listed in this table are less accurately located than those listed in table G1*A*. Water elevations south of Cochiti Dam on the east side of the Rio Grande (fig. G1) were measured during a reservoir seepage study conducted after the dam was completed in 1973 (Blanchard, 1993). The wells south of Cañada de Santa Fe and east of the La Bajada fault (fig. G1) were drilled or compiled for a hydrogeologic study of the proposed La Bajada Ranch subdivision (Peery and Pearson, 1994). A few water levels were obtained from well permits on file at the New Mexico Office of State Engineer in Albuquerque. Water levels in the southern and southwestern parts of the area shown in figure G1 were provided by the New Mexico District, Albuquerque Office of the USGS Water Resources Division (J.M. Kernodle, USGS, written commun., 1995; L.M. Bexfield, USGS, written commun., 1999; Bexfield and Anderholm, 2000).

Although they are drawn on the basis of data derived from a variety of sources, the water-elevation contours in the La Bajada constriction area indicate a fairly uniform water-table configuration that generally slopes down to the west and south (fig. G1). Water elevations decrease toward the Rio Grande from the east, north, and northwest, conforming to the overall drop in elevation and natural stream-flow gradient within the Santo Domingo valley. Within the southern Cochiti Pueblo area the water table forms a trough that is centered on the Rio Grande and opens southward into the Santo Domingo Basin (figs. A2, G1). Local deviations from this overall pattern can be detected in areas where more closely spaced

Figure G1. Regional water table (contoured at 50 ft intervals), water wells, and major faults in the La Bajada constriction area. Water table generally consistent with compilations of Titus (1961), Shomaker (1995), and Bexfield and Anderholm (2000). Water elevations not necessarily measured within the same aquifer or confining unit. Data from water wells shown on map summarized in table G1*A*, *B*. In table G1*B* and in text, the prefix "LB" precedes the number assigned to La Bajada Ranch wells southeast of Cañada de Santa Fe in the southeast part of map.

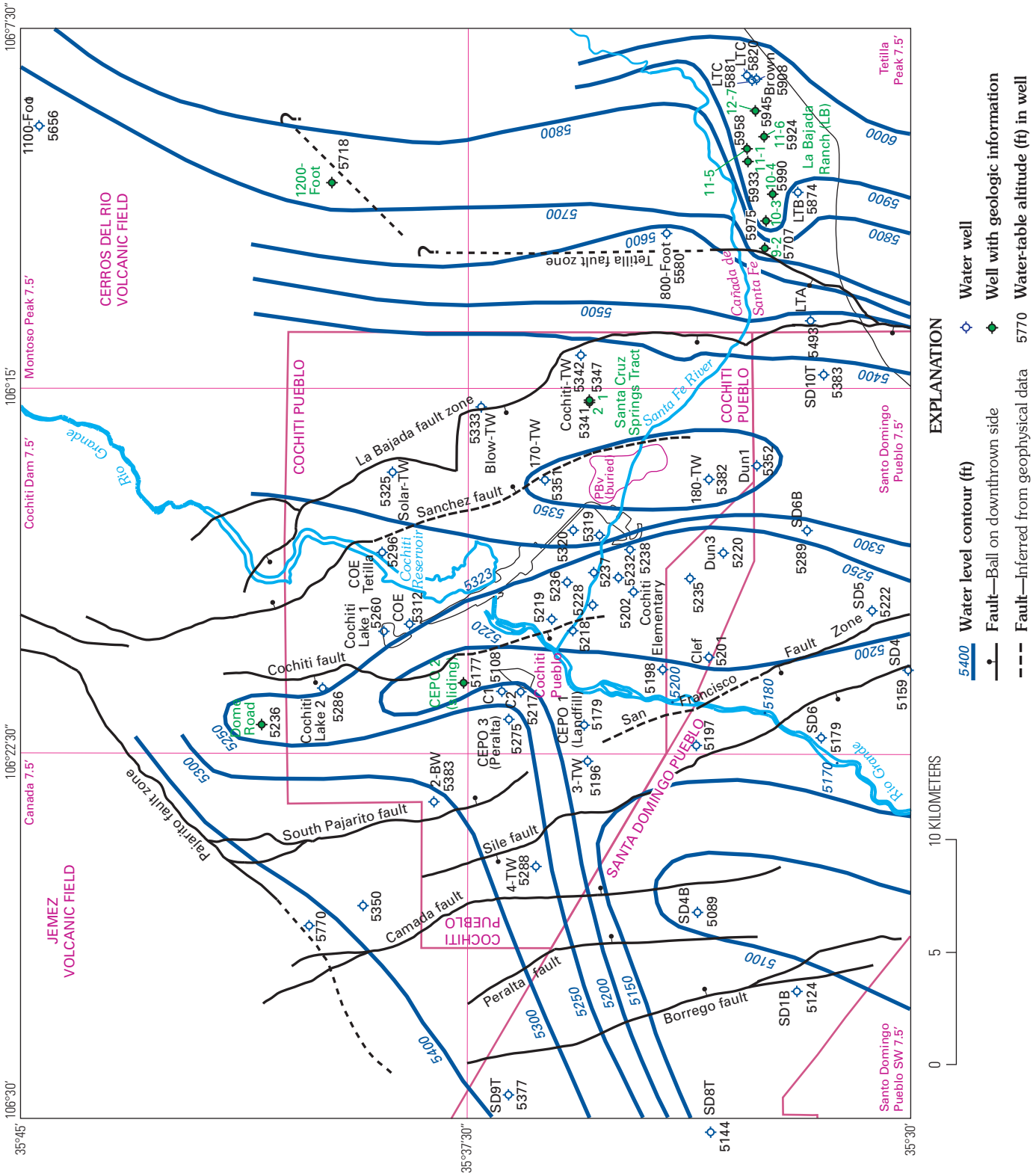
106°30′
106°22′30″
106°15′
106°7′30″
35°45′
35°37′30″
35°30′
Canada 7.5′
Cochiti Dam 7.5′
Montoso Peak 7.5′
Santo Domingo Pueblo 7.5′
Santo Domingo Pueblo SW 7.5′
Tetilla Peak 7.5′
JEMEZ VOLCANIC FIELD
CERROS DEL RIO VOLCANIC FIELD
COCHITI PUEBLO
SANTA DOMINGO PUEBLO
Rio Grande
Cochiti Reservoir
Santa Fe River
Cañada de Santa Fe
La Bajada fault zone
Sanchez fault
Cochiti fault
Palario fault zone
South Pajarito fault
Sile fault
Camada fault
Peralta fault
Borrego fault
Tetilla fault zone
San Francisco Fault Zone
Santa Cruz Springs Tract
La Bajada Ranch (LB)
Dome Road
Cochiti Lake 1
Cochiti Lake 2
COE Tetilla
COE
Solar-TW
Blow-TW
170-TW
Cochiti-TW
180-TW
Dun1
Dun3
Cochiti Elementary
Clef
CEPO 2 (Gliding)
CEPO 3 (Peralta)
CEPO 1 (Landfill)
2-BW
3-TW
4-TW
SD1B
SD4
SD4B
SD6
SD6B
SD8T
SD9T
SD10T
LTA
LTB
LTC
Brown
PBv (buried)
1100-Foot
1200-Foot
800-Foot
10 KILOMETERS
EXPLANATION
5400 Water level contour (ft)
Fault—Ball on downthrown side
Fault—Inferred from geophysical data
Water well
Well with geologic information
5770 Water-table altitude (ft) in well

Table G1*A*. Water table elevations in the Cochiti Pueblo area.

[UTM, Universal Transverse Mercator; total depth, as reported by driller. Sources of data: L.M. Bexfield, U.S. Geological Survey (unpublished data, 1999); Chamberlin and others (1999); Michael Quintana, Cochiti Environmental Protection Office (written commun., 1996); John Sorrell, Bureau of Indian Affairs (written commun., 1996); Spiegel and Baldwin (1963); and unpublished records of the New Mexico Office of State Engineer. Data source abbreviations: CEPO, Cochiti Environmental Protection Office; DAS, D.A. Sawyer; NMBGMR, New Mexico Bureau of Geology and Mineral Resources; OSE, New Mexico Office of State Engineer; USGSWSP, U.S. Geological Survey Water-Supply Paper]

Quad-rangle	SWL (ft)	UTM east (m)	UTM north (m)	Well name	Collar elevation (ft)	Total depth (ft)	Depth to water (ft)	Data source	Local well number
Santo Domingo Pueblo									
	5,347	386347	3939102	Santa Cruz Springs 1	5,501	875	154	DAS, 1998 Mar 13	
	5,341	386312	3939096	Santa Cruz Springs 2	5,494	545	153	DAS, 1998 Mar 13	
	5,202	380370	3937815	Cochiti Elementary	5,362	300	160	Bexfield, 1999 Feb 03	16N.06E.32.224
	5,179	376306	3939370	Landfill well CEPO 1	5,239	130	60	CEPO	
	5,177	377650	3943183	Sliding well CEPO 2	5,379	400	123	Bexfield, 1999 Feb 03	16N.06E.07
	5,351	383867	3940508	170–T Windmill	5,458	170	110	CEPO	
	5,382	383849	3935366	180–T Windmill	5,527	180	145	CEPO	
	5,217	377369	3941337	Cochiti 2 (C2)	5,284		67	CEPO	
Santo Domingo Pueblo SW									
	5,275	376523	3941720	Peralta well CEPO 3	5,335	401	60	CEPO	
	5,383	374004	3944135	Cochiti 2B Windmill	5,533	290	150	Bexfield, 1999 Feb 03	16N.05E.10.2
	5,196	375165	3939312	3–T Windmill	5,330	170	134	CEPO	
	5,288	371913	3940981	4–T Windmill	5,877	630	589	CEPO	
Cochiti Dam									
	5,108	377356	3941984	Cochiti 1 (C1)	5,298	250	190	Bexfield, 1999 Feb 03	16N.06E.18.311
	5,260	379293	3945594	Cochiti Lake 1	5,525	805	265	Bexfield, 1999 Feb 03	16N.06E.05.132
	5,286	377567	3947556	Cochiti Lake 2	5,639	1,142	353	CEPO	
	5,312	379500	3944807	Corps of Engineers	5,579	400	267	CEPO	
	5,296	381761	3945607	Corps of Engineers Tetilla	5,556	400	260	CEPO	
	5,333	386168	3942517	Blow–T Windmill	5,591	350	258	CEPO	
	5,325	384240	3945245	Solar–T Windmill	5,858	650	533	CEPO	
	5,236	376462	3949468	Dome Road	5,818	1,312	582	Chamberlin; NMBGMR	17N.05E.24.344
Tetilla Peak									
	5,342	387721	3939328	Cochiti–T Windmill	5,628	360	286	CEPO	
	5,580	391515	3936625	800-Foot well	6,175	795	595	USGSWSP 1525	16N.07E.33.444
Montoso Peak									
	5,718	393235	3946980	1200-Foot well	6,725	1,207	1,007	OSE	

Table G1*B*. Water table elevations in the La Bajada constriction area.

[All quadrangles are 7.5 minute quadrangles. SWL, elevation of static water level as reported by driller. Primary sources of well data: L.M. Bexfield, U.S. Geological Survey (written commun., 1999 and 2001); P.J. Blanchard, U.S. Geological Survey (Blanchard, 1993); J.M. Kernodle, U.S. Geological Survey (written commun., 1996); John Shomaker and Associates, La Bajada Ranch subdivision report (Shomaker, LBR; Peery and Pearson, 1994); and well-permit records of the New Mexico Office of the State Engineer (OSE)]

Quad-rangle	SWL (ft)	Well name	Collar elevation (ft)	Total depth (ft)	Depth to water (ft)	Aquifer unit	Data source	Local well number	Owner	Date measured
Tetilla Peak										
	5,707	LB09–2	6,110	700	403	Km	Shomaker, LBR	15N.07E.09.4312	W. Thompson	1994 Jul 07
	5,975	LB10–3	6,135	640	160	Km	Shomaker, LBR	15N.07E.10.3143	W. Thompson	1994 Aug 09
	5,990	LB10–4	6,145	640	155	Km	Shomaker, LBR	15N.07E.10.4314	W. Thompson	1994 Aug 09
	5,932	LB11–1	6,125	360	193	Tg/QTa	Shomaker, LBR	15N.07E.11.1431	W. Thompson	1994 Aug 09
	5,958	LB11–5	6,122	475	164	Tg/QTa	Shomaker, LBR	15N.07E.11.1442	W. Thompson	1994 Aug 09
	5,924	LB11–6	6,133	470	209	Tg/QTa	Shomaker, LBR	15N.07E.11.4141	W. Thompson	1994 Aug 09
	5,945	LB12–7	6,085	460	140	Tg	Shomaker, LBR	15N.07E.12.3121	W. Thompson	1994 Aug 09
	5,908	Brown	5,940	54	32		Shomaker, LBR	15N.07E.12.421	Brown	1962 Dec 02
	5,493	LTA	5,668	440	175	QTa	Shomaker, LBR	15N.07E.17.310	L. Thompson	1983 Apr 25
	5,874	LTB					Shomaker, LBR	15N.07E.15.23242	L. Thompson	1994 Jul 15
	5,881	LTC	5,913	55	32	QTa	Shomaker, LBR	5314001653400	L. Thompson	1975 Apr 29
	5,820	LTD	5,900	405	80		Shomaker, LBR	15N.07E.12.24	L. Thompson	1990 Apr 02
Montoso Peak										
	5,656	1100-Foot	6,636		980		Spiegel and Baldwin, 1963			
Canada										
	5,770		5,920		150		OSE			
	5,350		5,970		620		OSE			
Santo Domingo Pueblo SW										
	5,377	SD9T	6,375		998		J.M. Kernodle, 1996			
	5,144	SD8T	5,855		711		J.M. Kernodle, 1996			
	5,089	SD4B	5,635		546		L.M. Bexfield, 1999, 2001	15N.05E.05.243		
	5,124	SD1B	5,124				J.M. Kernodle, 1996			
	5,179	SD6	5,185		6		J.M. Kernodle, 1996; L.M. Bexfield, 2001.			
Santo Domingo Pueblo										
	5,159	SD4	5,360		201		J.M. Kernodle, 1996; L.M. Bexfield, 2001.			
	5,222	SD5	5,275		53		J.M. Kernodle, 1996			
	5,289	SD6B	5,440		151		J.M. Kernodle, 1996			
	5,383	SD10T	5,600		217		J.M. Kernodle, 1996			
	5,219	4–4					Blanchard, 1993			
	5,218	3–2					Blanchard, 1993			
	5,236	18–7					Blanchard, 1993			
	5,228	13–6					Blanchard, 1993			
	5,237						Blanchard, 1993			
	5,320	18–4					Blanchard, 1993			
	5,319	13–8					Blanchard, 1993			
	5,238	13–9					Blanchard, 1993			
	5,232	13–10					Blanchard, 1993			
	5,201	Clef			24		Blanchard, 1993			
	5,235				250		OSE			
	5,220	Dun3			271		OSE			
	5,352	Dun1			138		OSE			
	5,198				72		OSE			

water-elevation data exist. For example, a narrow north-northwest-trending water-table trough is identified in an area west of the Rio Grande extending from the Cochiti Pueblo settlement northwest through the town of Cochiti Lake (fig. G1, area of Cochiti Lake wells 1 and 2 and Dome Road well). This trough may be due to increased water usage in the area, although no water was pumped near the Dome Road well before it was drilled in 1998. Relatively high water levels west of the river at the CEPO 3 Peralta well and Cochiti 2–BW and 4–TW windmills (fig. G1, table G1*A*), provide evidence that the water-table trough west of the Rio Grande bends into a southwest trend beneath Santo Domingo Pueblo lands. The westward shift of the trough relative to the Rio Grande has been noted in previous studies of the regional hydrology and hydrogeology of the area (Titus, 1961; Smith and Kuhle, 1998c; Bexfield and Anderholm, 2000; Smith, McIntosh, and Kuhle, 2001). These studies postulated that the shift is due to higher hydraulic conductivity in sediments west of the Rio Grande than directly beneath it. An anomalously high water-table level (5,770 ft) in the northwesternmost well in the Cochiti Pueblo area (fig. G1), northwest of Tent Rocks National Monument (fig. A4), may be due to a perched water table in the volcanic-rock aquifer (or aquifers) flanking the Jemez Mountains.

East of the Rio Grande the water table generally slopes to the west (fig. G1, Bexfield and Anderholm, 2000), although this part of the basin is not tightly constrained by wells that penetrate the unconfined aquifer system in basin fill. However, data from windmills on the La Majada Mesa surface (pl. 1) suggest a small area of slightly higher water-table elevations southeast of Cochiti Dam. These higher elevations appear to define a water-table mound 10–35 ft above the surrounding water table. Wells surrounding this mound include the 180–TW windmill, 170–TW well, and Dun1 well (fig. G1, table G1*A, B*). Wells that have lower water elevations east and north of the 180–TW well include the Cochiti–TW windmill, the Santa Cruz Springs Tract wells, the Blow–TW windmill, and the farther north and topographically higher Solar–TW windmill. The water-table mound is bounded to the east by a small but persistent water-table trough along the base of the La Bajada fault-zone escarpment (fig. G1). We discuss possible geologic controls of the water-table mound later in this chapter.

Water table measurements in the easternmost La Bajada constriction come from a few deep wells that penetrate rocks of the Cerros del Rio volcanic field and intersect the water table in underlying basin-filling sediments of the Santa Fe Group. North of Cañada de Santa Fe, only three wells have been measured: the 1100-Foot, the 1200-Foot , and 800-Foot wells. On the basis of water elevations in these three wells of 5,656 ft, 5,718 ft, and 5,580 ft, respectively (Spiegel and Baldwin, 1963), the water table can be projected with a relatively smooth gradient down to the 5,400 ft water elevation contour at the base of the La Bajada escarpment (fig. G1). The configuration of the water table in the eastern area is consistent with the configuration shown on previous water-table maps of the surrounding region (Titus, 1961; Spiegel and Baldwin, 1963; Shomaker, 1995; Grant, 1997, 1999; and Bexfield and Anderholm, 2000). At present, no hydrologic evidence suggests any discontinuities in the water-table surface beneath the Cerros del Rio volcanic field (Titus, 1961; Spiegel and Baldwin, 1963) that could be attributed to hydrologic barriers such as basaltic feeder dikes. Numerous intrusive feeder systems likely are associated with the dozens of individual vent areas in the Cerros del Rio volcanic field. However, existing water-elevation data are so sparse in the area of the Cerros del Rio that we are unable to resolve the effect of any specific structures (for example, dikes or faults) on the regional water table.

South of Cañada de Santa Fe and east of the La Bajada fault zone, a number of water table measurements are summarized in a report on the proposed La Bajada Ranch subdivision (Peery and Pearson, 1994). In that study seven new wells were drilled through the Mesita de Juana volcano, the southernmost volcanic vent of the Cerros del Rio volcanic field (pl. 2, fig. A4), and existing well records at the New Mexico Office of State Engineer were compiled (summarized in fig. G1, table G1*B*). The water-elevation and exploratory hydrogeologic information produced by this investigation markedly improved upon that available to Spiegel and Baldwin (1963) in this area. A local higher altitude water-table plateau between 5,900 and 6,000 ft elevation is defined by these well data, suggesting that the associated aquifer may not be connected with the regional hydrologic flow system. The middle and eastern La Bajada Ranch wells penetrate saturated Tuerto Gravel (Koning and others, 2002), which forms the uppermost part of the regional Santa Fe Group aquifer system in the Española Basin. The Tuerto is unsaturated in the westernmost drill holes, and water elevations measured in rocks of subjacent Espinaso Formation, Galisteo Formation, and Mancos Shale provide no clear evidence of ground-water connection with the regional Santa Fe Group aquifer system (Peery and Pearson, 1994).

Subsurface Geologic Constraints From Wells

Despite the existence of more than 20 wells in the Cochiti Pueblo area (fig. G1, table G1*A*) and more than 10 additional wells to the east (table G1*B*; summarized by Peery and Pearson, 1994), only a few of these wells provide subsurface geologic constraints that supplement the surface geologic and geophysical data used in the development of regional hydrogeologic models. Below we discuss these few important wells in the context of Santo Domingo Basin architecture and La Bajada constriction terranes outlined in this report. Geologic well data are discussed from east to west, first for the Cerros del Rio and Cerrillos uplift area, next for the northeast part of the Santo Domingo Basin, and finally for the Saint Peters Dome block.

Cerros del Rio Volcanic Field and Cerrillos Uplift

The eastern boundary of the La Bajada constriction is concealed beneath the Cerros del Rio volcanic plateau (CDRVF) in the footwall block of the La Bajada fault zone

(LB) (fig. A2). In the downthrown block of the Tetilla fault zone (TT, fig. A2), east of the La Bajada fault zone, 2.5–2.7-Ma basalts of the Cerros del Rio volcanic field basalts overlie Santa Fe Group basin-fill sedimentary rocks. The 800-Foot well is located just east of the buried north-striking projection of the Tetilla fault zone (discussed in chapter E of this volume and later in this chapter) which forms part of the eastern border of the constriction (pl. 2, fig. G1). Unfortunately, there is no geologic information available for this well, which was drilled by the Soil Conservation Service before 1938 (Spiegel and Baldwin, 1963). Nonetheless, magnetotelluric station MT–4 (chapter F, this volume; Williams and Rodriguez, 2003; pl. 2; section C-C′, pl. 6) is located just north of this well, and it was used to determine a depth of 240 m to a regional electrical conductor (the Mancos Shale). This result provides evidence to interpret the northernmost extent of the Cerrillos uplift where it is located at shallow depth beneath relatively thin (80 m) thick basalts of the Cerros del Rio volcanic field.

The 1200-Foot well, located north of the 800-Foot well in the central part of the Cerros del Rio volcanic field (pl. 2, fig. G1), was originally drilled by the Soil Conservation Service in the early 1900s and redrilled by the U.S. Forest Service in 1961. A detailed driller's lithologic log was obtained from the well-permit files of the Office of State Engineer in Albuquerque; it is summarized in figure G2. It indicates that the hole penetrated a sequence of basalt flows, each ranging from 26 to 157 ft thick, interbedded with sediments down to a depth of 840 ft. The interflow sediments are clay rich or silt rich, range from 26 to 107 ft thick, and include variable amounts of basaltic cinders. The uppermost basalt is overlain by 50 ft of clay of variable hardness. The strong lithologic contrast in drilling characteristics between the hard basalt flows and softer interbedded sediments increases the likelihood that the driller's log is accurate. The base of the basaltic interval (256 m or 840 ft depth) corresponds closely with the 270±30 m (886±96 ft) thickness of basalt determined at nearby magnetotelluric station MT–5 (sections B-B′ and E-E′; pls. 2, 6; fig. F2*B*). Below the basalt is interbedded clay and gravel from 840 to 880 ft depth and 108 ft of dry sand and gravel. The water table lies at a depth of 1,007 ft in a sandy silt and gravel zone, and the main water-producing zone extends from 1,054 ft depth to the bottom of the hole at 1,207 ft (fig. G2). The most hydrologically conductive interval is a sand zone extending from 1,115 to 1,163 ft depth, bounded above and below by moderately productive sandy silt and interbedded gravel.

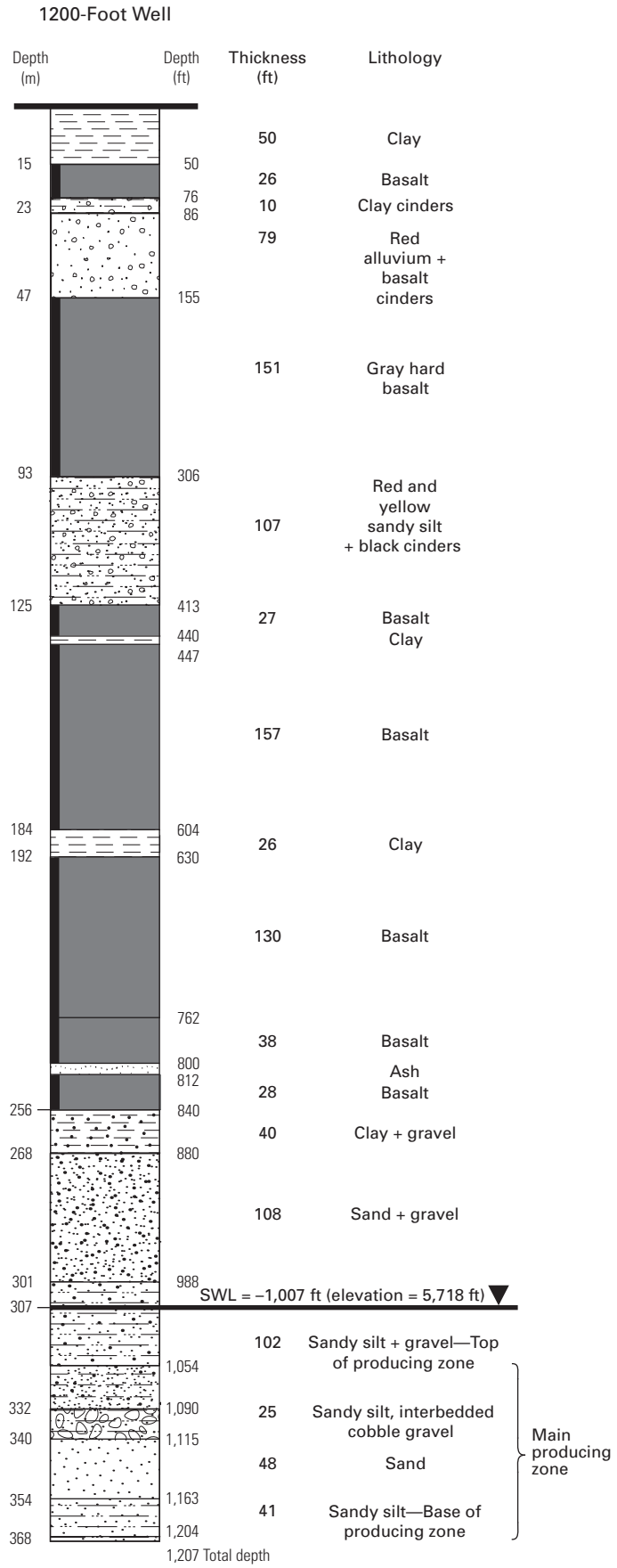

Figure G2. Lithologic column of 1200-Foot well, northeastern La Bajada construction; column based on driller's log obtained from New Mexico Office of State Engineer, Albuquerque. Well cuts at least six basalt flows (gray shading) interbedded with clastic sediments that overlie Santa Fe Group sediments; top of Santa Fe Group is 256 m deep. SWL, static water level.

Subsurface geologic constraints from the Cerrillos uplift area south of Cañada de Santa Fe include data from the seven wells drilled in the proposed La Bajada Ranch subdivision (fig. G1) (Peery and Pearson, 1994) beneath the northern flank of the Mesita de Juana volcano (pl. 2, fig. A4). Lithologic descriptions of cuttings from these wells are briefly summarized here and the water elevations measured in the wells are summarized in table G1*B*. The eastern part of section D-D′ of plate 6 shows our interpretation of the rock units and structures intersected by the La Bajada Ranch wells; it is simpler than the complex stratigraphy and structure interpreted by Peery and Pearson (1994) beneath the surface basalt. The stacked flows of basalt of Mesita de Juana (unit Tbj, pl. 2) range from 60 to 182 ft in total thickness and are largely unsaturated, on the basis of the well cuttings and measured water elevations. Unconsolidated sand and gravel of the Tuerto Gravel (unit QTt) (Koning, Pazzaglia, and McIntosh, 2002; called Ancha Formation in Peery and Pearson, 1994) form the most productive aquifer and compose the upper 40 to 60 ft of the saturated zone in these wells. These sediments were reassigned to the Tuerto based on the dominantly monzonitic provenance of their clasts (Koning, Pazzaglia, and McIntosh, 2002). Beneath the Tuerto, the Eocene Galisteo Formation (unit Tg), consisting of interbedded sandstone and siltstone, forms the major aquifer in the three eastern wells (LB12–7, LB11–5, and LB11–6 (table G1*B*)). Peery and Pearson (1994) interpreted complex stratigraphic juxtapositions within the three central wells (LB11–1, LB10–4, and LB10–3 (table G1*B*)) as owing to faulting. Alternatively, we explain the complexity as owing to unconformities and abrupt stratigraphic thickening and pinch-outs of sedimentary and volcanic or intrusive units (section D-D′, pl. 6). For example, sediments of the Tuerto Gravel have a saturated thickness of almost 165 ft in LB11–1 and overlie the Galisteo Formation. In contrast, Tuerto sand and gravel in the two wells immediately west of LB11–1 (wells LB10–4 and LB10–3) are markedly thinner (<50 ft thick) and overlie 100–150 ft of Espinaso Formation (unit Te) volcaniclastic sediments that contain a vesicular basaltic lava flow and, in turn, overlie the Cretaceous Mancos Shale (unit Km). The westernmost La Bajada Ranch well, LB09–2, penetrates less than 100 ft of the basalt of Mesita de Juana and 40 ft of Tuerto Gravel that rests directly on Mancos Shale. In this well, the water table was penetrated at depth of 403 ft, much deeper than in the other wells (table G1*B*). Tuerto sand and gravel pinches out toward the west before reaching the La Bajada escarpment. Thus, it appears likely that there is little or no hydrologic connection between the shallow Tuerto aquifer in the eastern and central wells and the deeper water level found in the Mancos in the westernmost hole (section D-D′, pl. 6).

La Bajada Constriction

The north-northwest-trending La Majada graben, located between the newly defined southern extension of the Sanchez fault and the La Bajada fault zone, obliquely transects the La Bajada constriction in the northeast part of the Santo Domingo Basin (SC, LB, figs. A4, E9). The Santa Cruz Springs Tract well provides the only subsurface geologic constraints within the La Majada graben (section C-C′, pl. 6; fig. G1). Basalt, basaltic andesite, and andesite lava flows of the Cerros del Rio volcanic field were measured in this well from 540 ft to the bottom of the hole at a depth of 875 ft (fig. G3). The upper 160 ft (540–700 ft depth) of the lava is lighter colored, contains flow bands, and ranges in composition from basaltic andesite to andesite (G.A. Smith, University of New Mexico, written comm., 2001). An age determined for the upper lava, sampled from homogeneous cuttings at a depth of 630 ft, is 2.67±0.06 Ma (Smith, McIntosh, and Kuhle, 2001). Cuttings of the lower basalt lava (700–875 ft depth) consist of darker olivine basalt mixed with lesser amounts of lighter-colored basalt to basaltic andesite. Two argon ages were determined for this interval, 2.57±0.03 Ma (730 ft depth) and 2.57±0.02 Ma (860 ft depth) (Smith, McIntosh, and Kuhle, 2001). These latter two, very precise, ages are indistinguishable. The older age obtained above concordant younger ages is stratigraphically problematic, but it may be that the upper lavas in the hole are derived from landsliding of basaltic rock off the nearby La Bajada fault scarp. This process is pervasive along the modern La Bajada escarpment (Sawyer and others, 2001).

Santa Fe Group basin-fill sediments above the basalts of the Cerros del Rio volcanic field in the Santa Cruz Springs Tract well record distinctive changes in geologic environment in the past 2.5 million years. From 540 to 430 ft depth, generally unconsolidated Santa Fe Group sediments consist of dominantly silty fine sand, interbedded with medium-coarse sand of the eastern piedmont facies of the Sierra Ladrones Formation; from 430 to 340 ft depth, these sediments are overlain by a dominantly fine grained cemented silt facies (fig. G3; (G.A. Smith, University of New Mexico, written comm., 2001). The upper silt facies appears in the time-domain electromagnetic survey (chapter F, this volume) as a low-resistivity zone (section C-C′, pl. 6; figs. F7*E*; F10; F11*D;* F12*C*, *D*), extending undisturbed from the La Majada graben westward across the Sanchez fault zone and into the central Reservoir horst (fig. A4). Overlying these fine-grained deposits are ancestral Rio Grande axial river gravels of the Sierra Ladrones Formation at depths of 240–340 ft. These hydrogeologically important deposits contain abundant coarse sand and gravel; cuttings are derived from a diverse suite of gravel clasts that include quartzite, many types of volcanic rock, and hornblende-bearing pumice (G.A. Smith, University of New Mexico, written commun., 2001). Hydraulically conductive quartzofeldspathic sand is also abundant in this interval. Eastern piedmont facies deposits overlie the axial gravels from depths of 130–240 ft. From depths of 170–210 ft, these sediments include pumice interpreted as the 1.61-Ma Otowi (lower) Member of the Bandelier Tuff. This pumice correlates with outcrops of the Otowi Member exposed at the surface south of the well on the north side of Galisteo Creek (unit Qbo, pl. 2; fig. A4). These upper eastern piedmont facies sediments are pink to buff in color and contain many potassium-feldspar grains as well as basalt clasts derived from basalts of the Cerros del Rio volcanic field in the

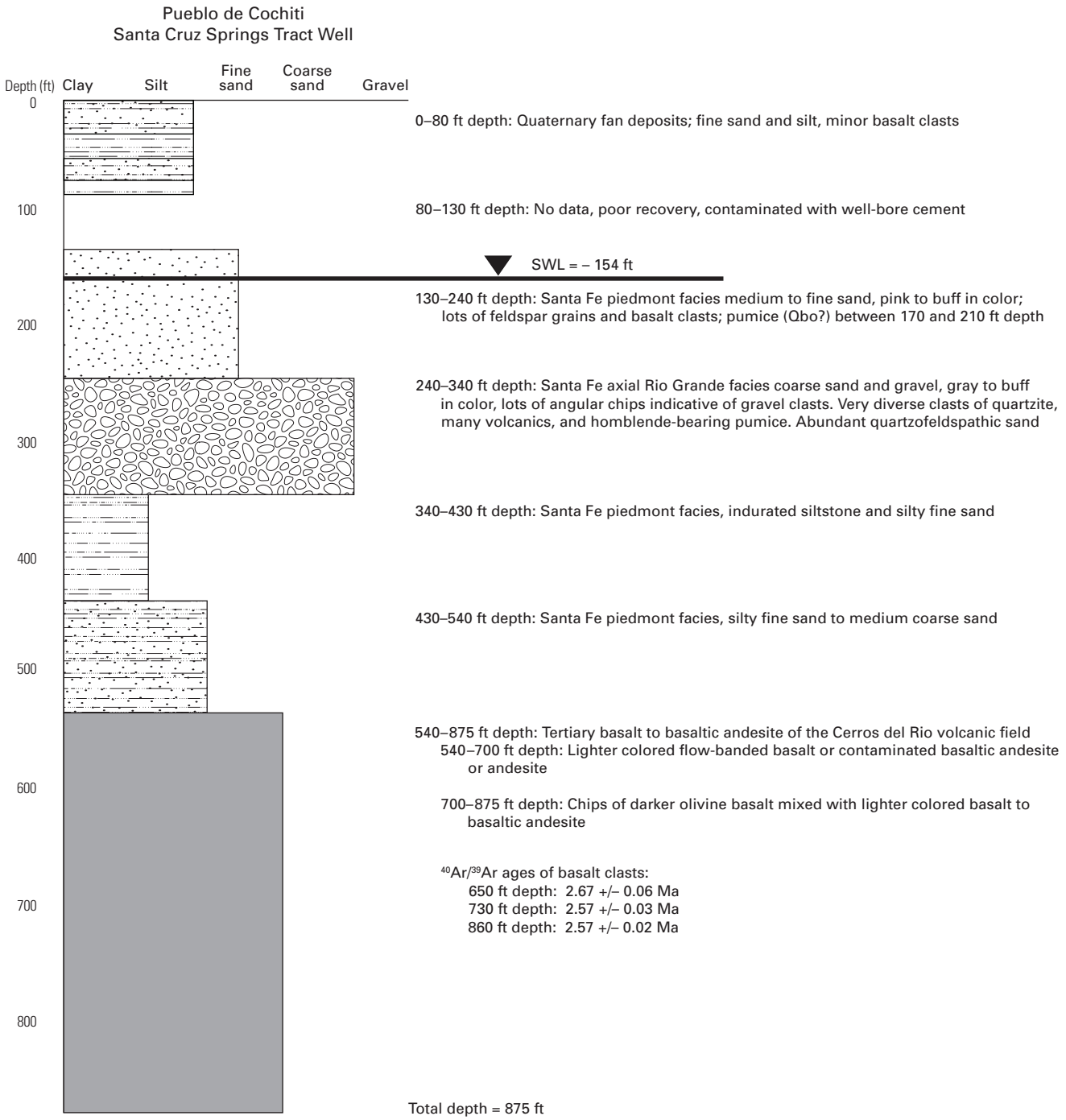

Figure G3. Lithologic column of Santa Cruz Springs Tract well, eastern Cochiti Pueblo. Lithologic descriptions are based on description of cuttings by G.A. Smith (University of New Mexico, written commun., 2001; Smith, McIntosh, and Kuhle, 2001) and on well data provided by John Sorrell (Bureau of Indian Affairs, written commun., 1996). Axial gravels in the well (240–340 ft depth) provide evidence of eastward lateral migration of the Rio Grande nearly to the La Bajada fault zone between 2.5 and 0.5 Ma. Beneath the axial gravel, a silt-rich interval (340–430 ft depth) probably corresponds with a high-electrical-conductivity unit above basalt in magnetotelluric section 630 (chapter F, this volume). $^{40}Ar/^{39}Ar$ ages of basalt clasts from the 650–860 ft depth interval reported in Smith, McIntosh, and Kuhle (2001). The well was drilled for Cochiti Pueblo by the Bureau of Indian Affairs before 1996. SWL, static water level.

footwall block of the La Bajada fault zone. The water table was intersected at a depth of 154 ft within sediments having a mixed arkosic and basaltic provenance characteristic of the eastern piedmont facies. No cuttings were recovered from the 80–130 ft depth interval, and Quaternary surficial deposits consisting of fines form the uppermost interval from 80 ft depth to the surface.

The Santa Cruz Springs Tract well provides evidence for the subsidence history of the southern part of the La Majada graben after deposition of the Cerros del Rio basalts (that is, after 2.5 Ma). More than 540 ft of sediment was deposited in the southern La Majada graben during its development. No evidence has been found to indicate fault offset on middle and upper Pleistocene surficial terrace deposits. Thus, most movement along the Sanchez and La Bajada fault zones bordering the southern La Majada graben occurred before 0.5 Ma (Machette and others, 1998; Smith, McIntosh, and Kuhle, 2001; Sawyer and others, 2001). Fault movement in the northern part of the graben may have continued after deposition of the 55-ka El Cajete tephra that appear to be cut by the Sanchez fault just west of the Rio Grande (D.P. Dethier, oral commun., 1999) (chapter E, this volume). The 2.5–0.5 Ma main episode of graben subsidence coincides with the time of major rhyolite eruptions that formed the Valles caldera. The 1.61-Ma Bandelier Tuff pumice at 210–170 ft depth in the Santa Cruz Springs Tract well (fig. G3) indicates that nearly 60 percent of the sediment was deposited in the first million years after the main volume of basalts of the Cerros del Rio volcanic field had erupted. Lateral migration of the ancestral Rio Grande to the eastern margin of the northeast part of the Santo Domingo Basin during this time was likely coeval with peak tectonic activity along the central part of the La Bajada fault zone (Smith, McIntosh, and Kuhle, 2001). This activity was followed by westward migration of the Rio Grande to a more central position within the northeast part of the Santo Domingo Basin as movement along the central La Bajada fault zone waned during the past 0.5 million years.

The near-surface geology west of the Sanchez fault in the Reservoir horst (pl. 2, fig. A4) is characterized by relatively thin, shallow basalts (units Tb, Tbpb, pl. 2) that form the western edge of the Cerros del Rio volcanic field (sections A-A′, B-B′, C-C′, pl. 6). The axial gravel facies of the Sierra Ladrones Formation (unit QTsa) is widespread beneath the basalts. None of the wells located in this structural block have geophysical logs or geologic descriptions of cuttings. Many of the shallow volcanic rocks underlying the horst, however, have distinctive magnetic and electrical resistivity signatures that are discussed in more detail in chapters D and F (this volume), respectively, and later in this chapter.

The geology of the western La Bajada constriction is made up of volcanic rocks from the proximal Jemez volcanic field to the northwest that interfinger with basin-fill sediments of the Santa Fe Group (sections A-A′, B-B′, C-C′, pl. 6). The Santa Fe Group basin-fill sediments include the western piedmont Cochiti Formation (unit QTc) volcaniclastic facies, and the axial-river (unit QTsa) and eastern piedmont (unit QTsp) facies of the Sierra Ladrones Formation (pl. 2). The main structural feature in this part of the constriction is the Cochiti graben, located between the east-dipping South Pajarito and west-dipping Cochiti faults (pl. 6; fig. A4). Wells drilled in the Cochiti graben include the Cochiti 2–BW and 3–TW windmills, several production wells that supply the Cochiti Pueblo settlement (Cochiti wells 1 and 2; C1 and C2, fig. G1), the monitoring CEPO 1 (Landfill) and CEPO 3 (Peralta) wells, and the Cochiti Golf Course (Cochiti Lake 2) production well (fig. G1, table G1*A*). No subsurface geologic or borehole geophysical data are available for these seven wells, and subsurface geology in the area can only be interpreted from surface geology and geophysical imaging of the subsurface (chapters D and F, this volume). Within the Cochiti graben, geophysical logs and geologic data are available only for the Dome Road and the CEPO 2 (Sliding) wells (fig. G1); they are summarized below.

In the CEPO 2 (Sliding) well, geophysical logs were run down to the completion depth of 400 ft (fig. G4, table G1*A*). This monitoring well was drilled just north of the Cochiti Pueblo town site, where it was collared in Quaternary alluvium at the surface. No geologic descriptions of cuttings or samples were obtained at the time of drilling. Volcaniclastic sediments of the Cochiti Formation interfinger with ancestral Rio Grande axial gravel deposits in outcrops near the well (pl. 2). Resistivity, gamma-ray, neutron, spontaneous potential, and caliper logs were obtained from the well. The gamma-ray and long-normal (64-in.) resistivity logs for the hole are shown in figure G4, against which is plotted our interpretation of sediment grain size. Relatively low gamma-ray values and very high resistivities (generally 150–250 ohm-m) that were recorded above the static water table (123 ft depth) probably correlate with sand and perhaps with some gravel. A very high resistivity zone (200–365 ohm-m) at 80–98 ft depth is probably gravel.

Below the water table, gamma-ray values increase in many discrete thin beds to more than 90 GR API and correspond with a pronounced decrease in resistivity to less than 25 ohm-m (fig. G4). These petrophysical characteristics are most consistent with clay-rich sediments. At 140–269 ft depth, geophysical logs indicate a thick sequence of clay-rich sediments comprising as many as 40 separate clay horizons. These clay-rich beds, most greater than 105 GR API, are interspersed with siltstone and only very minor sandy silt lenses, which are inferred on the basis of the coupled response of gamma-ray and resistivity values, the latter of which are mostly less than 10 ohm-m. This sequence of clay-rich beds was likely deposited in a lacustrine setting, although lake beds have not yet been identified at the surface within the Cochiti Formation.

The lower 130 ft of the well consists of two packages of very high resistivity sediments, probably gravel, interfingering with sand and thinner, low-resistivity and high-gamma-ray, clay-rich intervals (fig. G4). The resistivity of the thicker gravel intervals (40–45 ft) ranges from 50 to 75 ohm-m, very high values compared with resistivities measured for saturated Santa Fe Group sediments by magnetotelluric and time-domain

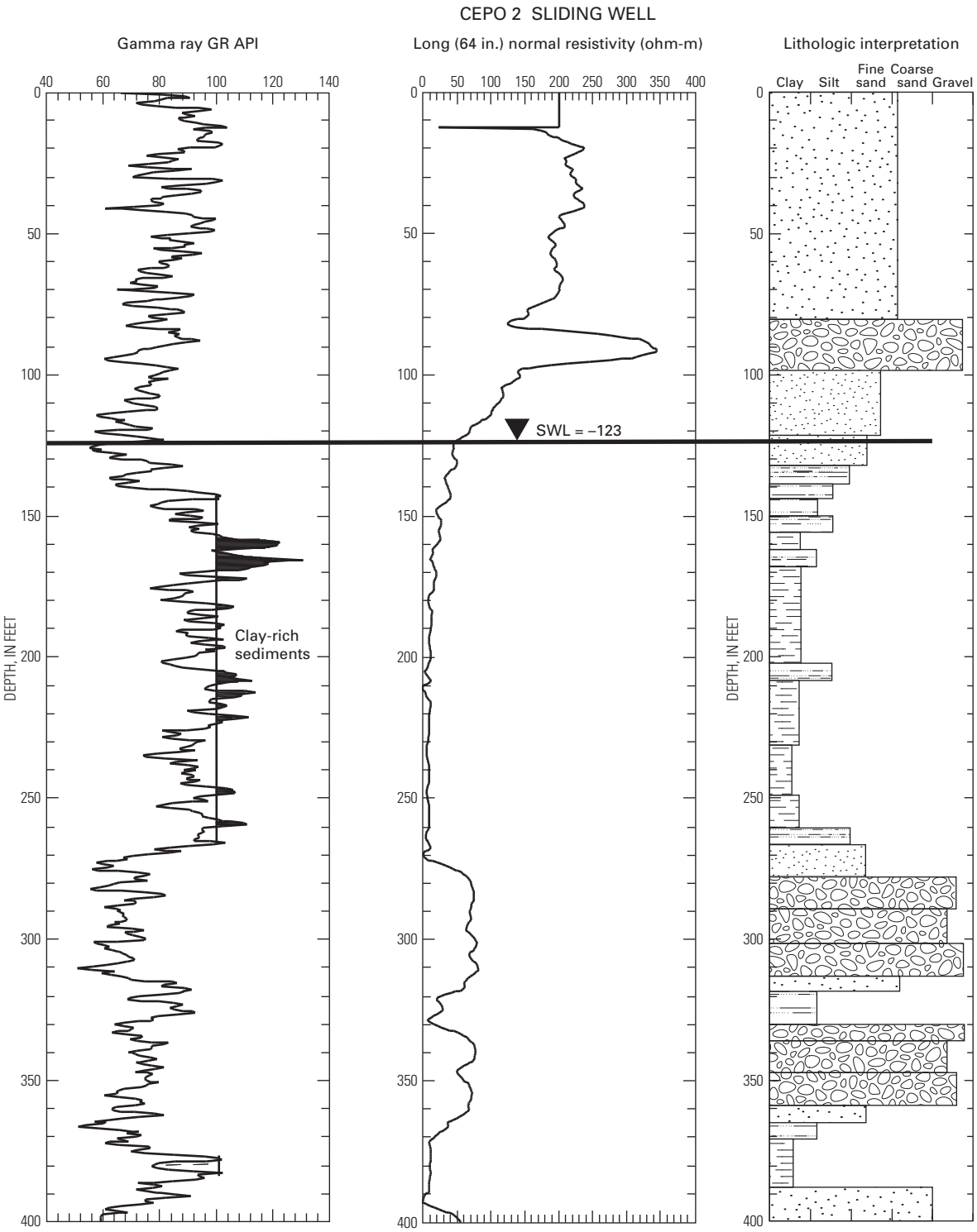

Figure G4. Gamma ray and long-normal resistivity logs and lithologic interpretation of CEPO 2 (Sliding) well in Cochiti Pueblo. The thick, low-resistivity sequence and corresponding high gamma-ray values at depths of 140–269 ft interpreted to represent a thick, clay-rich, probably lacustrine deposit. The well was drilled for Cochiti Environmental Protection Office (CEPO) in September 1996 by Rodgers Drilling and logged by Southwest Geophysical Services. Well data were provided by Jacob Pecos, Gary Valdo, and Michael Quintana of the Cochiti Environmental Protection Office and were digitized by Center Line Data as part of this investigation. SWL, static water level.

electromagnetic surveys (chapter F, this volume). A likely depositional setting of this lower well sequence is a river environment, where the thinner clay-rich zones represent thin overbank muds. As described in chapter F (this volume), the thick, low-resistivity lacustrine(?) zone is widespread west of the Rio Grande in the shallower parts of the saturated zone. Interestingly, it is enough of an electrical conductor in the time-domain electromagnetic survey (chapter F, this volume) to mask the high-resistivity gravels that lie below it in the CEPO 2 well.

The Dome Road well in the northern part of the Cochiti graben was drilled in August and September 1998 by the USGS Water Resources Division, in cooperation with the New Mexico Office of State Engineer. The New Mexico Bureau of Mines and Mineral Resources (Chamberlin, Jackson, and Connell, 1999) provided a geologic description and summary of the geophysical logs of the well. The well was sited on the Cañada de Cochiti Grant, north of Cochiti Pueblo in the west-central part of the Cochiti Dam quadrangle (fig. G1). The well was collared in the basal part of the Otowi Member of the Bandelier Tuff. The base of the tuff was visible in the mud pit only 2 ft below the ground surface. Below the tuff, the entire well was in volcaniclastic gravel and sand of the Cochiti Formation (fig. G5, modified from Chamberlin, Jackson, and Connell, 1999). Chamberlin, Jackson, and Connell (1999) interpreted sediments in the upper part of the hole as equivalent to the gravel of Lookout Park. However, D.P. Dethier (unpub. maps, 2000) did not find this unit as he mapped, and according to G.A. Smith (University of New Mexico, written commun., 2004) it is not present.

The lithologic log from the Dome Road well (fig. G5) indicates at a depth of 545 ft a change in grain size from volcaniclastic pebble gravel above to volcaniclastic sand and gravelly sand below that continues to the completion depth of 1,312 ft (400 m). Geophysical logs (resistivity, gamma-ray, density, density porosity, or neutron porosity) coupled with geologic samples for the Dome Road well (fig. G5, modified from Chamberlin, Jackson, and Connell, 1999) indicate homogeneous deposits of coarse-grained gravel and sand, with little vertical distinction in the interpreted lithology. The grain-size break interpreted from cuttings in the lithologic log is not evident in the borehole geophysical logs. High gamma-ray values (100–150 GR API) are probably related to high U, Th, and K associated with the dominantly rhyolitic clast composition of the Cochiti Formation. Induction resistivity ranged from 30–60 ohm-m throughout the Cochiti Formation without distinctive intervals. Chamberlin, Jackson, and Connell (1999) interpreted the water table in this well to be at a depth of 583 ft, on the basis of the abrupt decrease in sonic log travel time (fig. G5). The volcanic sand, gravelly to silty sand, and minor gravel lenses intersected in the hole below 545 ft are interpreted to have high hydraulic conductivity. Correlation of this well with surface geologic exposures of Cochiti Formation (pl. 2) mapped and described by Smith and Kuhle (1998c) and Smith, McIntosh, and Kuhle (2001) indicates that the Cochiti Formation in this area consists of fairly homogeneous coarse sand and gravel.

Figure G5 (facing page). Geophysical and lithologic logs of Dome Road well, northwest part of La Bajada constriction, based on Chamberlin, Jackson, and Connell (1999). The entire well is in gravel and sand of the western piedmont facies of the Santa Fe Group (Cochiti Formation). Although logs indicate high lithologic variability on a small scale (10–30 ft), resistivity and especially gamma-ray geophysical log responses are broadly similar throughout the entire well. Gamma-ray and neutron logs probably are affected by chemical composition of rhyolite volcanic material and thus deviate from typical simple log responses of mixtures of nonvolcanic clastic sand and clay. Geophysical log abbreviations: Av C Den, average compensated density; Delta-T, travel time; Den Por, density porosity; Ind Res, induction resistivity; Neut Por, neutron porosity; SP, spontaneous potential. SWL, static water level.

Saint Peters Dome Block

Subsurface constraints on geology derived from the Saint Peters Dome block adjacent to the La Bajada constriction are quite limited. No wells with geologic or geophysical logs are drilled in the block west of the northeast-striking segment of the Pajarito fault zone north of Tent Rocks National Monument (pl. 2; figs. A4, G1), and no subsurface geologic information is available from nearby wells east of the southwest projection of the fault zone, including the 5,350 ft water-elevation well and the Cochiti 2–BW windmill (fig. G1).

Subsurface Hydrogeologic Framework of the La Bajada Constriction Area

Introduction

In this section the subsurface geologic framework of the La Bajada constriction and bounding uplifts is described to identify principal geologic factors that may influence groundwater flow between the Española and Santo Domingo Basins. Serial cross sections were constructed to depict subsurface geologic interpretations of the La Bajada constriction area and to facilitate three-dimensional visualization of the hydrogeologic framework of the area. The sections were constructed principally by using the following sources of information: the map compilation of surface geology shown in plate 2; subsurface constraints from the aeromagnetic, gravity, and electromagnetic survey data presented in chapters D and F (this volume); and subsurface hydrologic and geologic data from wells described earlier in this chapter. Below approximately 300 m depth, most geologic relations shown, in particular the interfingering relations of the various facies of the Santa Fe Group (that is, unit QTsp, eastern piedmont deposits of the Sierra Ladrones Formation; unit QTsa, axial gravel deposits of the Sierra

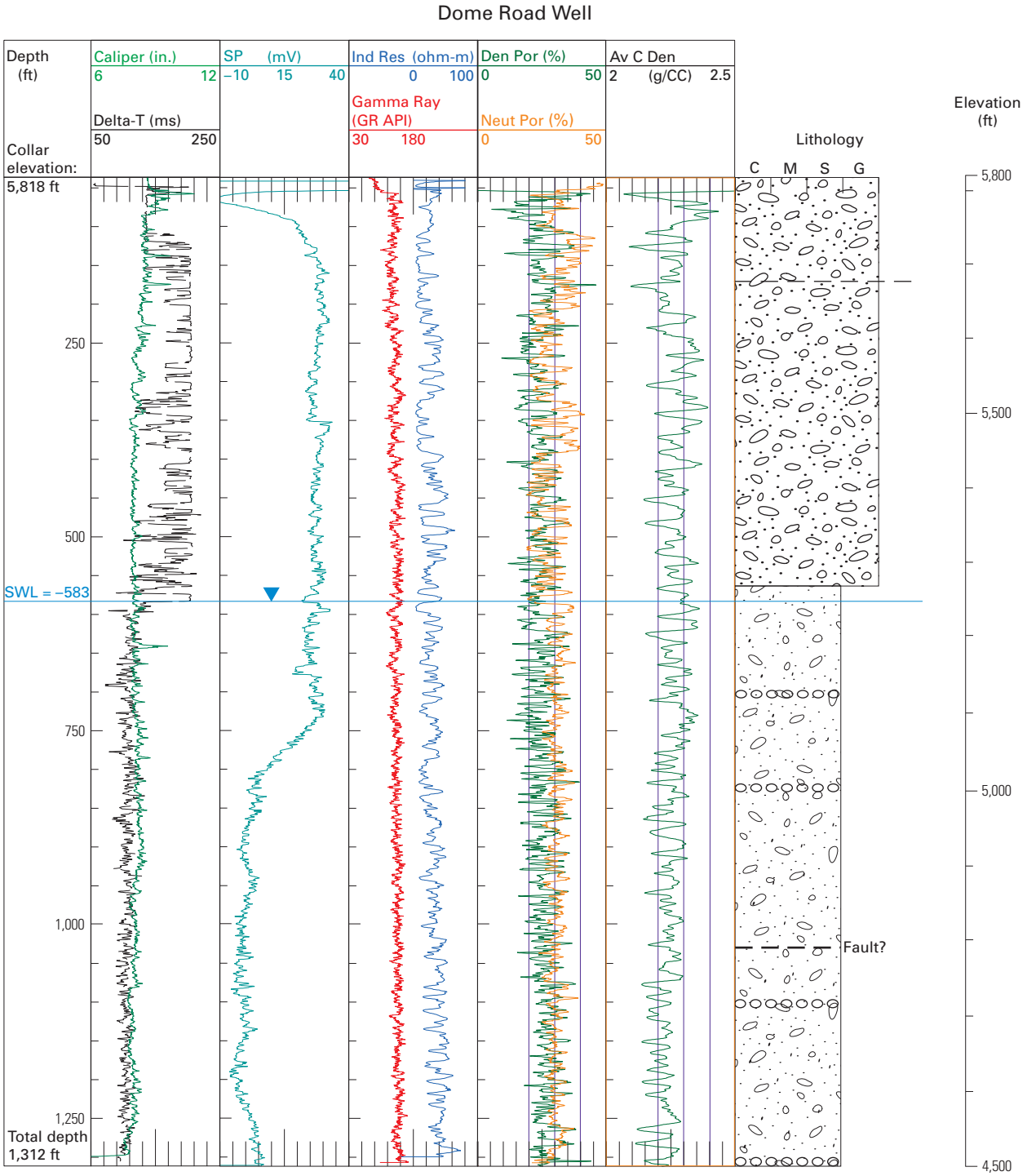
Dome Road Well
Depth (ft)
Caliper (in.)
6 12
Delta-T (ms)
50 250
SP (mV)
−10 15 40
Ind Res (ohm-m)
0 100
Gamma Ray (GR API)
30 180
Den Por (%)
0 50
Neut Por (%)
0 50
Av C Den
2 (g/CC) 2.5
Lithology
C M S G
Elevation (ft)
Collar elevation:
5,818 ft
250
500
SWL = −583
750
1,000
1,250
Total depth 1,312 ft
5,800
5,500
5,000
4,500
Fault?
EXPLANATION
Pebble to boulder gravel
Sand
Sandstone to pebble sandstone
C Clay
M Mud
S Sand
G Gravel

Ladrones Formation; and unit QTc, Cochiti Formation, western piedmont deposits; discussed in Chapter B, this volume), are schematic and conceptual. The cross sections, shown in plate 6 (here referred to as sections A-A′, B-B′, and so forth), follow the profile lines shown on plate 2 and figure G6. Figure G6 summarizes our synthesis of the geologic configuration of the La Bajada constriction as discussed throughout the remainder of the chapter.

Cerrillos Uplift: Southeastern Boundary of the La Bajada Constriction

The La Bajada constriction is bounded on the southeast by the Cerrillos uplift (Kelley, 1952, 1977, 1978, 1979; Baltz, 1978), a bedrock structural high that is largely covered by rocks of the Cerros del Rio volcanic field. Surface geologic evidence for the uplift is largely limited to the gently east-tilted (10°–14°) hogback of Jurassic and Cretaceous sedimentary rocks in the footwall block of the La Bajada fault zone in the southeast part of the study area (pl. 2) (Maynard, Sawyer, and Rogers, 2001). The uplift projects eastward and northward below rocks of the Cerros del Rio volcanic field (sections B-B′, C-C′, D-D′, pl. 6). The Cerrillos uplift is viewed as a rift-flank uplift (Roy and others, 1999) bordering the Santo Domingo Basin of the Rio Grande rift. It is structurally analogous to the paired Sandia Mountains uplift–Hagan embayment bounding the northeast side of the Albuquerque composite basin (fig. A1). However, unlike the Sandia uplift, it was not uplifted as high and remains largely buried beneath younger Pliocene and Pleistocene volcanic and sedimentary rocks.

The Cerrillos uplift limited the depositional thickness and areal extent of Santa Fe Group basin-fill sediments in the area of the eastern La Bajada constriction. Along the northernmost cross section (A-A′, pl. 6), the constriction extends from the northeast part of the Santo Domingo Basin eastward beneath rocks of the Cerros del Rio volcanic field and includes Santa Fe Group basin-fill sediments that are probably continuous, and hydraulically connected, with correlative strata in the adjacent Española Basin. The true nature of interfingering between Cochiti Formation western piedmont sediments (unit QTc in cross section) and Sierra Ladrones Formation eastern piedmont (unit QTsp) and axial gravel (unit QTsa) sediments likely differs from that depicted on the section, but no subsurface data exists in this area to constrain the depositional geometry of these coeval sedimentary facies.

The cross-sectional structural geometry of the buried Cerrillos uplift is depicted in east-west sections B-B′, C-C′, and D-D′ (pl. 6). The northeast flank of the Cerrillos uplift consists of north- to northeast-dipping Cretaceous Mancos Shale (unit Km in sections) and underlying undivided Pennsylvanian, Permian, Triassic, and Jurassic sedimentary rocks (unit JTRP). These dipping strata likely form part of a northeast-verging monoclinal flexure (see east part of section B-B′) that ramps down into the southwestern part of the Española Basin (that is, the Santa Fe embayment) beneath cover rocks of the Cerros del Rio volcanic field (CDRVF, fig. A2). The existence of such a flexure at depth is supported by gravity-defined east-southeast-trending structure contours on the base of the Tertiary basin-fill sedimentary rocks along the northeast flank of the Cerrillos uplift (figs. D4, G6; pl. 2 of Grauch and Bankey, 2003). Spiegel and Baldwin (1963) postulated a down-to-east Cienega fault zone near the inferred flexure, but surface geologic studies have not confirmed its existence despite permissive geophysical evidence (Grauch and Bankey, 2003). Along the northeast flank of the uplift from section B-B′ south through C-C′ to D-D′ (pl. 6), the Mancos Shale is overlain by an increasing thickness of pre-rift Tertiary sedimentary and volcanic rocks that consist of Eocene Galisteo Formation (unit Tg) and Eocene and Oligocene Espinaso Formation (unit Te) and Cieneguilla Basanite (unit Tc). These strata strike northwest and dip 15°–20° NE. beneath Miocene-Pliocene basin-fill sediments of the Santa Fe Group where exposed at the east end of Cañada de Santa Fe (pl. 2) (Sun and Baldwin, 1958; Sawyer and others, 2001). A westward change to a more westerly strike and northerly dip is clearly indicated by the gravity gradient expressed by structure contours at the base of the basin fill (figs. D4, G6; pl. 2 of Grauch and Bankey, 2003).

The pre-Tertiary sedimentary sequence thins markedly from south to north along the axis of the Cerrillos uplift (section E-E′, pl. 6), on the basis of magnetotelluric and audiomagnetotelluric soundings discussed in chapter F (this volume). Pre-Tertiary sedimentary rocks in the core of the Cerrillos uplift at magnetotelluric station MT–4 are interpreted to consist of about 700 m of Cretaceous marine Mancos Shale (unit Km) underlain by 1,700 m of Permian, Triassic, and Jurassic continental sedimentary rocks (unit JTRP) (fig. F11*F*, *D*), consistent with regional stratigraphic thicknesses for these units (table A1). This pre-Tertiary sequence thins owing to an erosional unconformity at the base of Eocene Galisteo Formation that cuts downsection northward (section E-E′, pl. 6). The unconformity gradually cuts downsection through the Mancos Shale sequence so that it is 500–600 m thick in MT–4 and MT–8, only 200 m thick in MT–11, and absent in MT–5 and MT–10 (section E-E′, pl. 6; fig. F11*B*, *D*). Only the thinned subjacent Permian-Jurassic section is present at the north end of the Cerrillos uplift in MT–5 and MT–10. The unconformity likely represents a buried post-Laramide erosional surface on the southern flank of the Laramide Brazos–Pajarito–Sangre de Cristo uplift (Cather, 1992, 2004), an interpretation supported by petroleum-industry seismic data (Black, 1984; Baldridge and others, 2001).

Cretaceous and older strata are upwarped from Cañada de Santa Fe southward (southern part of section E-E′, pl. 6). Such local uplift was probably caused by emplacement of Oligocene monzonite intrusions that deformed their cover rocks, similar to intrusion-related deformation exposed to the south and east in the Cerrillos Hills and at Cerro Seguro and the adjoining Las Tetillitas (pl. 1). The strong magnetic signature of the overlying Cerros del Rio volcanic field masks the subsurface extent of the monzonite intrusions. A northeast-trending gravity gradient

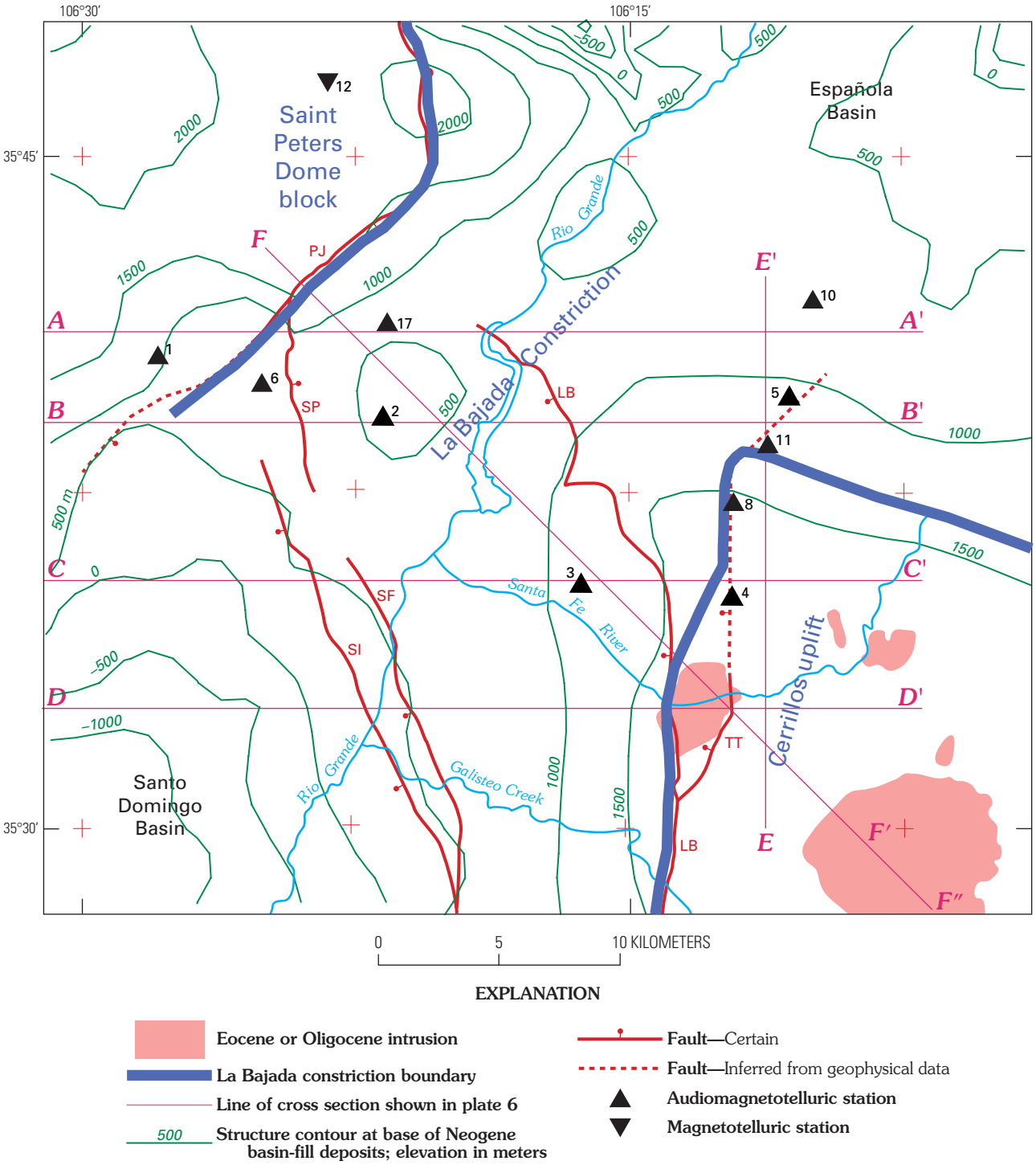

Figure G6. La Bajada constriction area showing its boundaries and gravity-derived structure contours on base of Neogene basin-fill deposits, as described in the text. The boundary of the Cerillos uplift, buried beneath cover rocks of the Cerros del Rio volcanic field, is based on the gravity model cited in chapter D (this volume), magnetotelluric and audiomagnetotelluric data at MT and AMT stations 4, 5, 8, and 11; surface geology; and interpretation of aeromagnetic data. The La Bajada constriction is the locus of downgradient flow of ground water in Santa Fe Group basin-fill aquifers as it passes from the Española Basin into the Santo Domingo Basin. Fault and fault zone abbreviations: LB, La Bajada; PJ, Pajarito; SF, San Francisco; SI, Sile; SP, South Pajarito; TT, Tetilla.

maximum (chapter D, this volume) is located near Cañada de Santa Fe (between station MT–4 and the Santa Fe River; fig. D1) and south of where basin fill abruptly thickens near MT–5 (that is, between MT–11 and MT–8 in section E-E′, pl. 6). This southward shift of the gravity gradient relative to the zone of thickened basin fill probably results from the considerable decrease in structural elevation of the pre-Tertiary rocks between the Cerrillos Hills and the north end of the Cerrillos uplift.

The north flank of the Cerrillos uplift is truncated by an inferred northeast-striking fault or zone of faults that, to the southwest, may structurally link with the Tetilla fault zone (pl. 2; sections B-B′, E-E′, pl. 6; TT, figs. A2 and G6). The existence of this fault zone is most clearly displayed by magnetotelluric soundings (chapter F, this volume). The data indicate a shallow depth (<250 m) to pre-Tertiary rocks at MT stations 4 and 8, a moderate depth (300 m) to these rocks at MT–11, and much greater depth (1,200 m) to them at MT stations 5 and 10. These changing depths require that strata are offset by about 650 m of fault throw in the narrow zone between MT stations 11 and 5 (pl. 2; section E-E′, pl. 6). The local N. 45° E. "electromagnetic" strike direction reported in chapter F (this volume) in the area of these stations (fig. F2*A, B*) suggests that the inferred fault or fault zone strikes northeast (pl. 2; figs. A2, G6). This structure may be analogous to the northeast-striking portion of the Tetilla fault zone exposed south of Cañada de Santa Fe (fig. E4) and may transfer extensional strain between the Santo Domingo and Española Basins (chapter E, this volume).

The Cerrillos uplift is bounded on its northwest edge by the inferred northeast-striking fault or fault zone described above (section B-B′, pl. 6), on the west by the north-striking projection of the Tetilla fault zone (section C-C′), and farther south by the north-striking La Bajada fault zone (section D-D′, pl. 6; figs. A2, A4). These fault structures together represent the southeast boundary of the La Bajada constriction as defined in this report (fig. G6), across which the thickness of Santa Fe Group basin-fill deposits increases to greater than 250 m. North of Cañada de Santa Fe, where the La Bajada fault zone (LB) bends northwest, the boundary of the La Bajada constriction as defined by thick basin fill curves northeastward into the footwall block of the La Bajada fault zone (pl. 2; figs. A2, A4, G6). It resumes a northward trend where it intersects the northern projection of the Tetilla fault zone (TT, figs. A2, A4, G6). The uplift and constriction boundary is inferred to continue northward along the projected Tetilla fault zone and curve into the geophysically defined northeast-striking fault or zone of faults described above.

Comparison of the aeromagnetic signature of the Eocene and Oligocene Cerrillos intrusions (pl. 4) with the area of the Cerrillos uplift based on gravity (pl. 3, fig. A3) indicates that the area of the uplift is much larger than the area of the intrusions. The overall geometry of the Cerrillos uplift reflects a basement-cored uplift (Roy and others, 1999) rather than local deformation around individual stocks of the Cerrillos intrusive center (Maynard, Sawyer, and Rogers, 2001; Maynard, 2005). Uplift of the Cerrillos block tilted and arched rocks as young as the Eocene and Oligocene Espinaso Formation and, on the east flank, the lower Miocene Tesuque Formation (Koning and others, 2006). Two dates have been obtained from pre-Tertiary sediments in the footwall block of the La Bajada fault zone that further constrain the timing of uplift of the block: an apatite fission track cooling age of approximately 31 Ma and an apatite (U-Th)/He age of 20 Ma (S.A. Kelley, New Mexico Institute of Mining and Technology, oral commun., 2001; House, Kelley, and Roy, 2003). The fission track age is indistinguishable from the 28–31 Ma Ar isotopic ages of the nearby Cerrillos intrusions (chapter C, this volume; Maynard, 2005). The younger apatite (U-Th)/He age is similar to Miocene ages obtained for uplift of the Sandia Mountains block about 40 km to the south (House, Kelley, and Roy, 2003). Apatite fission-track ages from the Sandia Mountains reported by Kelley and others (1992), Kelley and Chapin (1995), and House, Kelley, and Roy (2003) indicate that uplift continued in the Sandia block into the middle Miocene (as young as 10–12.5 Ma). Presumably the Cerrillos uplift also continued to rise during the middle Miocene owing to rift-flank uplift accompanying extensional faulting.

La Bajada Constriction

The La Bajada constriction in the northeast part of the Santo Domingo Basin is underlain in the shallow subsurface by rift-basin sediments of the Santa Fe Group that are interlayered with volcanic deposits from the Jemez and Cerros del Rio volcanic fields. Pre-Miocene units are not exposed within the basin, and their lithologic characteristics and structural configuration can be inferred only from geophysical data and limited exposures on the uplifted flanks of the rift. The basin-fill deposits are cut by numerous, mostly north-northwest-striking, normal faults that are inferred to have growth-fault histories, resulting in increased amounts of dip-slip displacement with increasing depth (pl. 6). As described in chapters A and E (this volume), the central La Bajada constriction is subdivided into three structural blocks or domains that are separated from one another by prominent intrabasin and basin-border faults of Miocene and younger age: the eastern La Majada graben, between the Sanchez fault and La Bajada fault zone; the central Reservoir horst, between the Cochiti and Sanchez faults; and the western Cochiti graben, between the South Pajarito fault zone and Cochiti fault (figs. A4, E9). Late Miocene and younger temporal patterns of sedimentation in response to growth faulting, fault-related "seesaw" subsidence (Smith, McIntosh, and Kuhle, 2001), possible inward migration of active rift faulting (chapter E, this volume), and areally restricted volcanism have generated different stratigraphic packages in each of these and surrounding structural blocks. Below we describe, from east to west, the salient geologic features of the following parts of the La Bajada constriction: the northwest Cerros del Rio volcanic field (that is, the area northeast of the La Bajada fault zone and west of the Cerrillos uplift), and each of the three intrabasin structural blocks (that is, La Majada graben, Reservoir horst, and Cochiti graben) (fig. A4).

Northwestern Cerros del Rio Volcanic Field

Tongues of Sierra Ladrones Formation axial river gravels (unit QTsa, pl. 2) likely extend eastward into the footwall block of the La Bajada fault zone beneath cover rocks of the northwestern Cerros del Rio volcanic field, on the basis of limited exposures of such gravels along the La Bajada escarpment (chapter B, this volume; sections A-A′ and B-B′, pl. 6). Assuming that the down-to-west Cochiti Cone fault was an active basin-bounding fault between 2.6 and 1.1 Ma (chapter E, this volume), axial river gravels and eastern piedmont facies sediments (unit QTsp) probably interfinger at least as far east as this fault. Northward, toward the Española Basin, axial river gravels are predicted to extend progressively farther east under the Cerros del Rio volcanic rocks such that lenses or tongues of axial gravel may project well into the footwall block of the Cochiti Cone fault. More certain is the presence of basin-fill piedmont facies sediments beneath the entire northern part of the volcanic field (unit QTsp in sections A-A′ and B-B′, pl. 6). Such buried deposits are predicted north of the Cerrillos uplift where the La Bajada constriction widens and merges with the southwest part of the Española Basin (figs. A2, G6). A network of faults and feeder dikes associated with the Cerros del Rio volcanic units likely cut or intrude basin-fill sediments underlying the volcanic plateau (chapter C, this volume), but the geometry and spatial distribution of such features are unconstrained.

La Majada Graben

The north-northwest trend of the La Majada graben, situated between the northern La Bajada fault zone and the Reservoir horst (figs. A4, E9), is oblique to and cuts across the overall north-northeast trend of sedimentary facies boundaries within the northeast part of the Santo Domingo Basin (pl. 2). As a result, the dominant facies of basin-fill sediments within the graben gradually changes from axial river gravels in the northern part of the block to eastern piedmont sediments in the southern part (compare sections A-A′, C-C′, and F-F″, pl. 6). Given the growth-fault history of the bounding faults, it is likely the ancestral Rio Grande intermittently occupied and flowed along the La Majada graben.

The La Majada graben formed primarily between about 2.5 and 0.5 Ma, during and following eruption of the Pliocene basalts of the Cerros del Rio volcanic field and eruption of andesites during the second phase of the Santo Domingo Basin subsidence, as described by Smith McIntosh, and Kuhle (2001). This period of peak subsidence of the La Majada graben and movement along the La Bajada fault zone coincided with the main caldera-forming eruptions in the Valles caldera within the Jemez volcanic field (Nielson and Hulen, 1984).

Erosion and mass wasting of the La Bajada fault-zone escarpment provided abundant piedmont sediment that was deposited in the graben, which includes Cerros del Rio basalt-derived sedimentary breccias and landslide deposits (Smith, Bailey, and Ross, 1970). Arkosic piedmont facies sediments are also common in the graben, which were derived from the Sangre de Cristo Range east of the Santa Fe embayment. Basaltic lavas of the Cerros del Rio volcanic field are displaced down into the La Majada graben along the La Bajada fault zone and, in the southern part of the graben, basalt flows are overlain by younger basin-fill sediments (sections A-A′, B-B′, and C-C′, pl. 6).

Relatively small displacement, north-northwest-striking, synthetic and antithetic normal faults are common in the northern part of the La Majada graben, whereas larger displacement, more widely spaced faults associated with the scalloped La Bajada fault zone cut obliquely across the southern part of the graben (pl. 2; east-west sections A-A′, B-B′, C-C′, F-F″, pl. 6). The latter faults may serve structurally to compartmentalize and close off the southern end of the graben, which may inhibit the southerly flow of ground water within the block. Stratal dips within the La Majada graben are gentle, generally just a few degrees to the east. However, eastward dips appear to increase southward where they locally exceed 10°.

Reservoir Horst

The north-northwest-trending Reservoir horst is a relatively uplifted structural block located between the Cochiti graben on the west and the La Majada graben on the east (figs. A4, E9). Santa Fe Group basin-fill sediments underlying the horst consist primarily of ancestral Rio Grande axial gravels (unit QTsa, pl. 6), although subordinate amounts of interfingering eastern piedmont facies (unit QTsp) are also present. The lack of geologic data from wells in the horst prevents determination of the subsurface distribution of axial gravels at depth. Similar to the La Majada graben, the Reservoir horst trends obliquely across basin-fill facies boundaries such that, in the north, western piedmont sediments of the Cochiti Formation (unit QTc) are present in the west part of the horst and in the south part of the horst eastern piedmont sediments encroach on the river gravels from the east (compare sections A-A′, B-B′, C-C′, pl. 6). The axial gravel facies becomes more sand rich (unit Tsls) beneath the basalt of Peña Blanca (unit Tbpb), along the east bank of the Rio Grande, at the south end of the horst (chapter B, this volume; pl. 2; section D-D′, pl. 6) (Smith and Kuhle, 1998a, b). In the same area local lacustrine deposits of clay-rich sediment and limestone (units Tslm, Tsll) interfinger with the axial sand and gravel deposits (Smith and Kuhle, 1998b).

Faulted basaltic flows along the western edge of the Cerros del Rio volcanic field (unit Tb, pls. 2, 6) are locally present at the surface or at relatively shallow depth within the northern part of the Reservoir horst (sections A-A′, B-B′, pl. 6). The horst also contains aeromagnetically expressed buried basalt related to the basalt of Peña Blanca (unit Tbpb, pl. 6; feature C4, fig. D7). Distal layers of Otowi Member of the Bandelier Tuff (unit Qbo) are also preserved at the surface within the horst. Only basin-fill sediments (mainly axial gravel, unit QTsa) are predicted in the horst below about 100 m within the depth range of sections A-A′ and B-B′ (pl. 6). Further south,

however, the basalt of Peña Blanca is present down to depths of nearly 300 m, which reflects the southward increase in throw of the La Bajada fault zone (sections C-C′ and F-F″, pl. 6).

Internally, the Reservoir horst is a relatively undeformed block containing only minor faults that strike subparallel to its overall trend. Gentle (<10°) eastward stratal dips are typical throughout the length of the horst (see east-west sections A-A′, B-B′, C-C′, D-D′, pl. 6), in contrast to the moderate northwestward dip of underlying pre-Tertiary sedimentary rocks indicated in the gravity-constrained regional section F-F″ of plate 6 (see also chapter D, this volume). The westward stratigraphic thickening of older, pre-rift Tertiary sedimentary rocks at depth within the horst (unit Tg(?), section F-F″, pl. 6) presumably reflects deformation related to the Laramide Brazos–Pajarito–Sangre de Cristo uplift (Cather, 1992, 2004) and Cerrillos uplift.

Cochiti Graben

The north-northwest-trending Cochiti graben is bounded on the east by the Reservoir horst and on the west by the Saint Peters Dome block and, farther south, by a contiguous unnamed domain of small fault blocks (sections A-A′, B-B′, C-C′, and F-F″, pl. 6; figs. A4, E9). As in the structural blocks to the east, the type and relative volume of basin-fill sedimentary facies gradually change along the length of the graben owing to the oblique trend of the graben relative to the facies boundaries. Basin-fill sediments in the northern part of the graben consist dominantly of western piedmont deposits of the Cochiti Formation (unit QTc, section A-A′; see also description of Dome Road well, fig. G5), whereas at the southern end gravelly axial-river deposits of the Sierra Ladrones Formation prevail (unit QTsa, section C-C′). Western piedmont sediments interfinger with axial-river deposits in gradually shifting proportions along the entire length of the graben (compare east-west sections A-A′, B-B′, C-C′, D-D′). The Cochiti Formation (Smith and Lavine, 1996) is characterized by gravel and coarse sand in the northern part of the Cochiti graben, but the percentage of gravel and the average size of sand grains decrease southward away from the volcanic field (Smith and Kuhle, 1998c).

Rocks of the Jemez volcanic field zone are downdropped into the northern and central parts of the Cochiti graben along faults of the Pajarito and South Pajarito fault zones (pl. 2; sections A-A′, B-B′, and F-F″, pl. 6). These volcanic units are present at several depth intervals, reflecting the broad age range of the east flank of the Jemez volcanic field (Miocene to 1.22 Ma; chapter C, this volume); volcanic deposits and flows include the 1.61- and 1.22-Ma members of the Bandelier Tuff (units Qbt, Qbo, pl. 2), the 7- to 6-Ma units of the Bearhead Rhyolite (units Tbr, Tbp), and older (~10–7 Ma) Keres Group rocks (units Tkpa, Tkct, Tkvs).

Lacustrine sediments are inferred to be present in the shallow subsurface (between about 50 and 150 m depth) in the northern part of the Cochiti graben (unit QTcl, section B-B′, pl. 6) largely on the basis of a localized, electrically conductive interval detected by the time-domain electromagnetic surveys (chapter F, this volume; fig. F7*C–E*). This conductive body is as much as 5 km wide and 10 km long in plan view and extends from Peralta Canyon on the southwest to at least the Sanchez fault on the northeast. At present no samples of lacustrine rocks have been recovered from any wells in the area of the conductive body, so information about texture, mineralogy, and grain size are based on indirect geophysical downhole logging methods. Borehole geophysical data from the CEPO 2 (Sliding) well suggest that as much as 130 ft (40 m) of clay-rich lacustrine sediment was penetrated by the well (fig. G4). Given the large areal dimensions of this body (fig. F7*C–E*) and a thickness of as great as 100 m, the lacustrine sediments may act as a local subhorizontal barrier to ground-water flow. Development of a lake system in this area was likely due to damming by one or more of three mechanisms: basaltic maar volcanism on the floodplain of the Rio Grande (Self and others, 1996), scarp formation along one or more nearby faults, or landsliding off high-relief volcanic landforms or fault escarpments. It is not certain whether the east boundary of the inferred clay-rich body near section B-B′ (pl. 6) is at the Cochiti fault, as depicted in the section, or slightly farther east.

The Cochiti graben dies out just south of lower Peralta Canyon and the village of Cochiti Pueblo (pl. 1), where the bordering South Pajarito and Cochiti faults end near the overlapping Sile and San Francisco faults (figs. A4, E9). The graben also dies out to the north where the Cochiti fault ends south of the northeast-striking segment of the Pajarito fault zone and Saint Peters Dome. Thus, the Cochiti graben is structurally open on both ends. The graben contains several internal north-striking faults that have shorter trace lengths and smaller throws in surface exposures (tens of meters) than the bounding faults (pl. 2; sections A-A′, B-B′, and F-F″, pl. 6). In contrast to the La Majada graben, the Cochiti graben does not appear to be segmented by any large cross faults.

Saint Peters Dome Block: Northwestern Boundary of the La Bajada Constriction

The northwestern border of the La Bajada constriction is formed by the Saint Peters Dome structural block, a basement-cored uplift composing the footwall block of the northeast-striking Pajarito fault zone (PJ, fig. A2) (Kelley, 1952; Goff, Gardner, and Valentine, 1990; Cather, 1992; Abbott, Cather, and Goodwin, 1995). The uplift is evident in gravity data and required by gravity modeling (figs. A3, D1, D6). The surface trace of the block-bounding Pajarito fault zone dies out where the north-striking South Pajarito fault zone merges with it (figs. A2, G6); there is no evidence that the fault offsets sediments of the Cochiti Formation (unit QTc, pl. 2) or the overlying gravel of Lookout Park (unit Tglp) to the southwest. The northeast-striking Pajarito fault zone is aligned, however, with a prominent northeast-trending gravity gradient extending southwest from Saint Peters Dome block that is coincident with the northwest side of Santo Domingo Basin (pl. 4; fig. D1). These observations suggest that a buried older Miocene

(pre-7-Ma Peralta Tuff Member), basin-bounding Pajarito fault segment may continue in the subsurface to the southwest (fig. A2). To the north, the Pajarito fault zone and adjacent Saint Peters Dome block continue northward where they form the western boundary of the deep Pajarito (or southern Velarde) subbasin or graben (Ferguson and others, 1995) of the Española Basin (figs. A2, D1, G6).

The stratigraphic history of the Saint Peters Dome block is complex owing to Miocene and younger rift-flank uplift and proximity to source vents of the Jemez volcanic field. Upper Miocene through Quaternary volcanic rocks, pyroclastic deposits, and associated sediments of the southeastern Jemez volcanic field dominate the upper 1 km of the block (pl. 2; sections A-A′, B-B′, F-F″, pl. 6). Unconformably underlying the Bandelier Tuff cap rock (units Qbt, Qbo, pl. 2) are the Cochiti Formation (unit QTc), the Bearhead Rhyolite (unit Trb) and associated Peralta Tuff Member (unit Tbp), and older Miocene Keres Group volcaniclastic sediments (units Tkvs, Tku of pl. 6 only) intercalated with varied volcanic domes, tuffs and lava flows (units Tkpa, Tku). In the subsurface one or more fingers of axial-river gravels extend westward into the footwall block of the Pajarito fault zone in the southeastern part of the Saint Peters Dome block (Smith, McIntosh, and Kuhle, 2001). The synvolcanic Bearhead Basin, which accumulated at least 500 m of interlayered Peralta Tuff Member pyroclastic and sedimentary deposits between 7 and 6 Ma, may greatly affect the volcanic hydrogeology and structural framework in the southwest part of the Saint Peters Dome block (Smith, 2001). The west edge of this basin is bounded by northern projections of the down-to-east Peralta and Camada faults (pl. 2). As much as 100 m of middle Santa Fe Group basin-fill sedimentary rocks are exposed in the footwall block of the Pajarito fault zone near Saint Peters Dome (unit Tsf, section F-F″), and similar rocks may underlie the Jemez volcanic sequence elsewhere in the Saint Peters Dome block as well as at deeper levels in the northwest part of the La Bajada constriction (Goff and others, 1990).

The Pajarito fault zone bounding the Saint Peters Dome block accommodates greater than 100 m of down-to-the-east offset of the 1.22-Ma upper Bandelier Tuff (unit Qbt) (Goff, Gardner, and Valentine, 1990). Unconstrained fault offsets of older rocks present at depth in the Pajarito hanging-wall block are likely much greater (200–1,000 m), assuming a growth-fault history (sections A-A′, B-B′, F-F″, pl. 6). Large angular unconformities in the footwall between strata of the Eocene Galisteo Formation (dip, 45° W.), the Miocene Santa Fe Group (dip, 10° SW.), and Pliocene and Pleistocene Cochiti Formation and Bandelier Tuff (3°–5° NW. to SE.) reflect episodic uplift and back tilting of the Saint Peters Dome block in Tertiary and Quaternary time. This and other lines of evidence indicate that the Pajarito was an active zone of major normal faulting along the western border of the Española and Santo Domingo Basins from the late Miocene through the Pleistocene. Internally, the Saint Peters Dome block is generally little deformed, although some smaller displacement faults (<25 m) cut pre-Bandelier Tuff rocks (pl. 2).

Implications for Ground-water Flow Between Española and Santo Domingo Basins

Ancestral Rio Grande axial gravel and sand deposits of the upper Miocene to Pleistocene Sierra Ladrones Formation are the most productive aquifers in northern New Mexico (Kernodle and others, 1995). Evidence of high transmissivity of Miocene gravels is provided by deep production wells on the Pajarito Plateau in the western Española Basin northwest of the study area (Purtymun, 1995; Reneau and Dethier, 1996). Similar Miocene and Pliocene deposits are widely distributed in the central part of the La Bajada constriction between the Española and Santo Domingo Basins (Dethier, 1999; Chapter B, this volume), although existing subsurface data do not constrain the eastern extent of axial Rio Grande gravels beneath rocks of the Cerros del Rio volcanic field north and northwest of the Cerrillos uplift. Also, the deepest extent of these highly conductive sediments has not been characterized by any deep water wells in the northeastern or main parts of the Santo Domingo Basin. Nevertheless, ancestral Rio Grande fluvial gravel and sand extend at least from Española on the north southward through the entire Santo Domingo Basin and into the Albuquerque Basin (fig. A1) such that it probably conveys the largest amounts of ground water by underflow from the Española Basin through the Santo Domingo Basin. We conclude that through-going axial river sand and gravel and coarse western piedmont gravel aquifers form the predominant ground-water pathways through the La Bajada constriction.

Western piedmont facies gravel and sand deposits of the Cochiti Formation probably form a substantial aquifer unit in the northwest part of the La Bajada constriction south of Saint Peters Dome, owing to their coarse grain size and inferred moderately high permeability (Smith and Kuhle, 1998c). However, the permeability of these deposits may gradually decrease southward on account of the reduction of their average grain size from gravel to sand away from their Jemez volcanic field source rocks. Eastern piedmont facies sand and silty sand deposits probably form a fair to moderately good aquifer, depending locally on the amount of interbedded silt and clay. The City of Santa Fe's Buckman well field, immediately east of the Rio Grande at the north tip of the Cerros del Rio volcanic field (pl. 1), is perhaps typical of the water supply available from this aquifer unit (Black and Veatch, 1978; Lewis and West, 1995). Other than information gathered in this well field, little is known of the hydrologic characteristics of Santa Fe Group eastern piedmont deposits concealed beneath rocks of the volcanic field.

Cerros del Rio basalt lava flows probably form good fracture-flow aquifers in the subsurface of the La Majada graben and Reservoir horst, given the common presence of cooling joints within such rocks and their tendency to deform by distributed extensional fracturing (Minor and Hudson, 2006). Hydrologic results from the Santa Cruz Springs Tract

well (John Sorrell, U.S. Bureau of Indian Affairs, unpub. data, reported in Smith and Kuhle, 1998c) support this inference. Little is known of the hydrostratigraphy of Santa Fe Group sediments beneath the basalts of the Cerros del Rio volcanic field in the La Majada graben, but it probably includes hydraulically conductive axial Rio Grande gravels that form good aquifers similar to those exposed in the footwall of the La Bajada fault zone. The slight water table trough just west of and parallel to the La Bajada fault zone at the south end of the graben (fig. G1) may reflect a zone of increased hydraulic conductivity in the La Majada graben-fill section, perhaps owing to the combined effects of concentrated axial gravel and enhanced permeability near and parallel to the fault zone.

Poorly consolidated sediments of the Santa Fe Group that are deposited in the late Cenozoic Rio Grande rift basins have high to very high hydraulic conductivity compared with most of the older rocks forming the uplifted blocks that bound the basins. On the southeast side of the La Bajada constriction, low-conductivity clay-rich Cretaceous marine shales form a regional confining unit within the Cerrillos uplift. These shales are at least 600 m thick and are tilted gently to moderately eastward (unit Km, section C-C′, pl. 6), opposite to the regional water table that slopes west toward the modern Rio Grande (fig. G1). These Cretaceous rocks have not completely exchanged their saline marine pore fluids with ground water in the past 80 million years, as implied by the poor water quality recorded in several wells (Lewis and West, 1995). In addition to poor water quality, these clay-rich rocks contain only meager amounts of water. The bulk hydraulic conductivity of the Cretaceous sedimentary rocks is probably further reduced where Eocene and Oligocene stocks and plugs have intruded (units Tmi, Tmh, section F-F″, pl. 6) and contact metamorphosed them. Overlying lower Tertiary sedimentary and volcaniclastic rocks of the Galisteo and Espinaso Formations in the Cerrillos uplift probably have somewhat greater hydraulic conductivity than the Cretaceous shales, but their conductivity is still markedly lower than most of the basin-fill sediments owing to their much greater degree of compaction and induration.

In the Saint Peters Dome block on the opposite, northwest, side of the constriction, flows, domes, and pyroclastic rocks of the Jemez volcanic field have not been studied to determine their hydrologic properties. Local aquifer units may exist where competent volcanic rocks have been intensely fractured during cooling or later deformation. Compared with the Cerrillos uplift, discrete volcaniclastic sedimentary aquifer units are more likely in the Saint Peters Dome block, particularly within volcanic rocks that intertongue with the Cochiti Formation and Keres Group volcaniclastic sediments (units QTc, Tkvs, sections A-A′, B-B′, and F-F″, pl. 6).

The abundant, dominantly north-northwest-striking, intrabasin faults in the La Bajada constriction (pl. 2, fig. E9) may locally partition or compartmentalize ground-water flow (chapter E, this volume) and deflect it into a mainly south-southeast fault-parallel direction. Given the common along-strike persistence of clay cores and cemented damage zones and mixed zones with the intrabasin fault zones, most faults probably impede across-fault flow of ground water (Minor and Hudson, 2006; chapter E, this volume). In contrast, along-fault flow may be enhanced in the tens-of-meters-wide damage zones surrounding the fault cores in protoliths where fracturing, rather than cataclasis (that is, grain-size reduction), was the dominant mode of deformation and where those fractures were not later cemented. Another important consequence of faulting on the regional ground-water flow system is the structural juxtaposition of units with differing bulk hydraulic conductivity within the rift basin-fill sequence. Given the complex interfingering lithostratigraphy of the sedimentary fill of the La Bajada constriction and Santo Domingo Basin, intrabasin faults commonly juxtapose hydrologically contrasting lithologic layers, resulting in laterally and vertically variable fault-zone hydrologic properties. This juxtaposition of dissimilar lithologies is especially pronounced toward the margins of the basin where the lithologically more diverse piedmont facies prevail and interfinger with distal axial river gravels (east-west sections A-A′, B-B′, C-C′, D-D′, pl. 6). In addition, cross faults and fault-zone reactivation can locally alter the permeability along and across intrabasin fault zones and, in some cases, result in fault holes and leakage (for example, Caine and others, 2002). However, other than in the La Majada graben, cross faults striking obliquely with respect to the overall north-northwest structural grain do not appear to be common in the La Bajada constriction area, and most intrabasin faults appear to have been relatively inactive since the middle Pleistocene (Machette and others, 1998).

References Cited

Abbott, J.C., Cather, S.M., and Goodwin, L.B., 1995, Paleogene synorogenic sedimentation in the Galisteo Basin related to the Tijeras-Canoncito fault system: New Mexico Geological Society 46th field conference, Geology of the Santa Fe Region, Guidebook, p. 271–278.

Baldridge, W.S., Ferguson, J.F., Braile, L.W., Biehler, S., Jiracek, G.R., Gilpin, B.E., Alumbaugh, D.L., Gratwick, D.S., Richards, T.L., and Hasterok, D.P., 2001, Architecture of the southern Espanola Basin (Rio Grande rift) and flank uplift adjacent to the La Bajada fault [abs]: Geological Society of America Abstracts with Programs, v. 33, no. 5, p. 61.

Baltz, Elmer, 1978, Resume of the Rio Grande depression in north-central New Mexico: New Mexico Bureau of Mines and Mineral Resources Circular 163, p. 210–228.

Bartolino, J.R., and Cole, J.C., 2002, Ground-water resources of the Middle Rio Grande Basin, New Mexico: U.S. Geological Survey Circular 1222, 132 p.

Bexfield, L.M., and Anderholm, S.K., 2000, Predevelopment water-level map of the Santa Fe Group aquifer system in the Middle Rio Grande Basin between Cochiti Lake and San Acacia, New Mexico: U.S. Geological Survey

Water-Resources Investigations Report 00–4249, 1 map sheet with text, scale approximately 1:400,000.

Black, B.A., 1984, Hydrocarbon potential of the Española Basin—A progress report: New Mexico Geological Society 35th field conference, Rio Grande Rift—Northern New Mexico, Guidebook, p. 223–226.

Black and Veatch, 1978, Construction and testing report, Buckman well no. 2 (New Mexico RG 20516–5–6): Denver, Black and Veatch Consulting Engineers project 6607.002, prepared for Public Service Company of New Mexico, Santa Fe, 36 p.

Blanchard, P.J., 1993, Ground-water-level fluctuations in the Cochiti Dam–Peña Blanca area, Sandoval County, New Mexico, 1976–89: U.S. Geological Survey Water-Resources Investigations Report 92–4193, 72 p.

Caine, J.S., Minor, S.A., Grauch, V.J.S., and Hudson, M.R., 2002, Potential for fault zone compartmentalization of ground-water aquifers in poorly lithified, Rio Grande rift-related sediments, New Mexico [abs.]: Geological Society of America Abstracts with Programs, v. 34, no. 4, p. 59.

Cather, S.M., 1992, Suggested revisions to the Tertiary tectonic history of north-central New Mexico: New Mexico Geological Society 43d field conference, San Juan Basin IV, Guidebook, p. 109–122.

Cather, S.M., 2004, Laramide orogeny in central and northern New Mexico and southern Colorado, in Mack, G.H., and Giles, K.A., eds., The geology of New Mexico, A geologic history: New Mexico Geological Society Special Publication 11, p. 203–248.

Chamberlin, R.M., Jackson, Patricia, and Connell, S.D., 1999, Field logs of borehole drilled for monitoring well at Dome Road site, Cañada de Cochiti Grant, Sandoval County, New Mexico: New Mexico Bureau of Geology and Mineral Resources Open-file Report 444c, 30 p.

Dethier, D.P., 1999, Quaternary evolution of the Rio Grande near Cochiti Lake, northeast part of the Santo Domingo Basin, New Mexico: New Mexico Geological Society 50th field conference, Albuquerque Geology, Guidebook, p. 371–378.

Ferguson, J.F., Baldridge, W.S., Braile, L.W., Biehler, S., Gilpin, B., and Jiracek, G.R., 1995, Structure of the Española Basin, Rio Grande rift, from SAGE seismic and gravity data: New Mexico Geological Society 46th field conference, Geology of the Santa Fe Region, Guidebook, p. 105–110.

Goff, Fraser, Gardner, Jamie, and Valentine, Greg, 1990, Geologic map of the St. Peters Dome area, Jemez Mountains, New Mexico: New Mexico Bureau of Mines and Mineral Resources Geologic Map 69, scale 1:24,000.

Grant, P.R., 1997, Subsurface geology and related hydrologic conditions, Santa Fe embayment and contiguous areas, New Mexico: New Mexico State Engineer Office Technical Report 97–5, 53 p., 3 plates.

Grant, P.R., 1999, Subsurface geology and related hydrologic conditions, Santa Fe embayment and contiguous areas, New Mexico: New Mexico Geological Society 50th field conference, Albuquerque Geology, Guidebook, p. 425–435.

Grauch, V.J.S., and Bankey, Viki, 2003, Aeromagnetic interpretations for understanding the hydrogeologic framework of the southern Española Basin, New Mexico: U.S. Geological Survey Open-File Report 03–124, 44 p.

House, M.A., Kelley, S.A., and Roy, Mousumi, 2003, Refining the footwall cooling history of a rift flank uplift, Rio Grande rift, New Mexico: Tectonics, v. 22, no. 5, p. 1060, doi:101029/2002TC001418 [internal pagination: p. 14–1 to 14–18].

Kelley, V.C., 1952, Tectonics of the Rio Grande depression of central New Mexico: New Mexico Geological Society 3d field conference, Rio Grande Country, Guidebook, p. 92–105.

Kelley, V.C., 1977, Geology of Albuquerque Basin, New Mexico: New Mexico Bureau of Mines and Mineral Resources Memoir 33, 60 p.

Kelley, V.C., 1978, Geology of the Española Basin, New Mexico: New Mexico Bureau of Mines and Mineral Resources Geologic Map 48, scale 1:125,000.

Kelley, V.C., 1979, Tectonics, Middle Rio Grande rift, New Mexico, in Riecker, R.E., ed., Rio Grande rift—Tectonics and magmatism: American Geophysical Union, p. 57–70.

Kelley, S.A., and Chapin, C.E., 1995, Apatite fission-track thermochronology of Southern Rocky Mountain–Rio Grande rift–Western High Plains provinces: New Mexico Geological Society 46th field conference, Geology of the Santa Fe Region, Guidebook, p. 87–96.

Kelley, S.A., Chapin, C.E., and Corrigan, J., 1992, Late Mesozoic to Cenozoic cooling histories of the flanks of the northern and central Rio Grande rift, Colorado and New Mexico: New Mexico Bureau of Mines and Mineral Resources Bulletin 145, 39 p.

Kernodle, J.M., McAda, D.P., and Thorn, C.R., 1995, Simulation of ground-water flow in the Albuquerque Basin, central New Mexico, 1901–1994, with projections to 2020: U.S. Geological Survey Water-Resources Investigations Report 94–4251, 114 p.

Koning, D.J., Pazzaglia, F.J., and McIntosh, W.C., 2002, Redefinition of the Ancha Formation and Plio-Pleistocene deposition in the Santa Fe embayment, north-central New Mexico: New Mexico Geology, v. 24, p. 75–87.

Koning, D.J., Read, A.S., Grauch, V.J.S., and Minor, S.A., 2006, Late Oligocene-Miocene structures in and near the Santa Fe embayment, N.M., and inferences regarding tectonism and paleo-topography [abs.], *in* McKinney, K.C., ed., Geologic and hydrogeologic framework of the Española Basin, Española Basin Workshop, 5th, Santa Fe, New Mexico, March 7–8, 2006, Proceedings: U.S. Geological Survey Open-File Report 2006–1134, p. 36.

Lewis, A.C., and West, Francis, 1995, Conceptual hydrologic systems for Santa Fe County: New Mexico Geological Society 46th field conference, Geology of the Santa Fe Region, Guidebook, p. 299–305.

Machette, M.N., Personius, S.F., Kelson, K.I., Haller, K.M., and Dart, R.L., 1998, Map of Quaternary faults and folds in New Mexico and adjacent areas: U.S. Geological Survey Open-File Report 98–0521, 1 sheet, scale 1:750,000, text 367 p.

Maynard, S.R., 2005, Laccoliths of the Ortiz porphyry belt, Santa Fe County, New Mexico: New Mexico Geology, v. 27, no. 1, p. 3–21.

Maynard, S.R., Sawyer, D.A., and Rogers, J., 2001, Preliminary geologic map of the Madrid 7.5' quadrangle: New Mexico Bureau of Mines and Geology Open-file Report DM–40, scale 1:24,000, 26 p. text.

Minor, S.A., and Hudson, M.R., 2006, Regional survey of structural properties and cementation patterns of fault zones in the northern part of the Albuquerque Basin, New Mexico—Implications for ground-water flow: U.S. Geological Survey Professional Paper 1719, 000 p.

Nielson, D.L., and Hulen, J.B., 1984, Internal geology and evolution of the Redondo dome, Valles caldera, New Mexico: Journal of Geophysical Research, v. 89, p. 8695–8711.

Peery, R.L., and Pearson, J.W., 1994, Hydrogelogy and water-resource assessment, proposed La Bajada subdivision, Santa Fe County, NM: John Shomaker & Associates consultant report, 33 p.

Purtymun, W.D., 1995, Geologic and hydrologic records of observation wells, test holes, test wells, supply wells, springs and surface water in the Los Alamos area: Los Alamos National Laboratory Report LA–12883–MS, 339 p.

Reneau, S.L., and Dethier, D.P., 1996, Pliocene and Quaternary history of the Rio Grande, White Rock Canyon and vicinity, New Mexico: New Mexico Geological Society 47th field conference, Jemez Mountains Region, Guidebook, p. 317–324.

Roy, Mousumi, Karlstrom, K.E., Kelley, S.A., Pazzaglia, F.J., and Cather, S.M., 1999, Topographic setting of the Rio Grande rift, New Mexico—Assessing the role of "rift-flank" uplift in the Sandia Mountains: New Mexico Geological Society 50th field conference, Albuquerque Geology, Guidebook, p. 167–174.

Sawyer, D.A., Shroba, R.R., Minor, S.A., and Thompson, R.A., 2001, Geologic map of the Tetilla Peak quadrangle, Santa Fe and Sandoval Counties, New Mexico: U.S. Geological Survey Miscellaneous Field Studies Map MF–2352, scale 1:24,000.

Self, Stephen, Heiken, Grant, Sykes, M.L., Wohletz, Kenneth, Fisher, R.V., and Dethier, D.P., 1996, Field excursions to the Jemez Mountains, New Mexico: New Mexico Bureau of Mines and Mineral Resources Bulletin 134, 72 p.

Shomaker, J.W., 1995, Hydrogeology of the Ortiz Mountains and vicinity: New Mexico Geological Society 46th field conference, Geology of the Santa Fe Region, Guidebook, p. 313–318.

Smith, G.A., 2001, Development of a pyroclastic apron adjacent to rhyolite domes in a subsiding basin—Upper Miocene Peralta Tuff, Jemez Mountains, New Mexico, *in* Crumpler, L.S., and Lucas, S.G., eds., Volcanology in New Mexico: New Mexico Museum of Natural History and Science Bulletin 18, p. 85–96.

Smith, G.A., and Kuhle, A.J., 1998a, Geologic map of the Santo Domingo Pueblo quadrangle, Sandoval County, New Mexico: New Mexico Bureau of Mines and Mineral Resources Open-file Digital Map OFDM 26, scale 1:24,000.

Smith, G.A., and Kuhle, A.J., 1998b, Geologic map of the Santo Domingo Pueblo SW quadrangle, Sandoval County, New Mexico: New Mexico Bureau of Mines and Mineral Resources Open-file Digital Map OF–DM–26, scale 1:24,000.

Smith, G.A., and Kuhle, A.J., 1998c, Hydrostratigraphic implications of new geologic mapping in the Santo Domingo Basin, New Mexico: New Mexico Geology, v. 20, p. 21–27.

Smith, G.A., and Lavine, Alex, 1996, What is the Cochiti Formation?: New Mexico Geological Society 47th field conference, Jemez Mountains Region, Guidebook, p. 219–224.

Smith, G.A., McIntosh, William, and Kuhle, A.J., 2001, Sedimentologic and geomorphic evidence for seesaw subsidence of the Santo Domingo accommodation-zone basin, Rio Grande rift, New Mexico: Geological Society of America Bulletin, v. 113, p. 561–574.

Smith, R.L., Bailey, R.A., and Ross, C.S., 1970, Geologic map of the Jemez Mountains, New Mexico: U.S. Geological Survey Miscellaneous Investigations Map I–571, scale 1:125,000.

Spiegel, Zane, and Baldwin, Brewster, 1963, Geology and water resources of the Santa Fe area: U.S. Geological Survey Water-Supply Paper 1525, 258 p.

Sun, Ming-Shan, and Baldwin, Brewster, 1958, Volcanic rocks of the Cienega area, Santa Fe County, New Mexico: New Mexico Bureau of Mines and Mineral Resources Bulletin 54, 80 p.

Titus, Frank, Jr., 1961, Ground-water geology of the Rio Grande trough in north-central New Mexico, with sections on the Jemez caldera and the Lucero uplift: New Mexico Geological Society 12th field conference, Albuquerque Country, Guidebook p. 186–192.

Williams, J.M., and Rodriguez, B.D., 2003, Magnetotelluric data in the southwest Española Basin, northern New Mexico: U.S. Geological Survey Open-File Report 03–199, 128 p.

Published in the Central Region, Denver, Colo.
Manuscript approved for publication February 10, 2006
Graphics by authors
Photocomposition by Mari L. Kauffmann (Contractor, ATA Services)
Edited by Mary-Margaret Coates (Contractor, ATA Services)

USGS
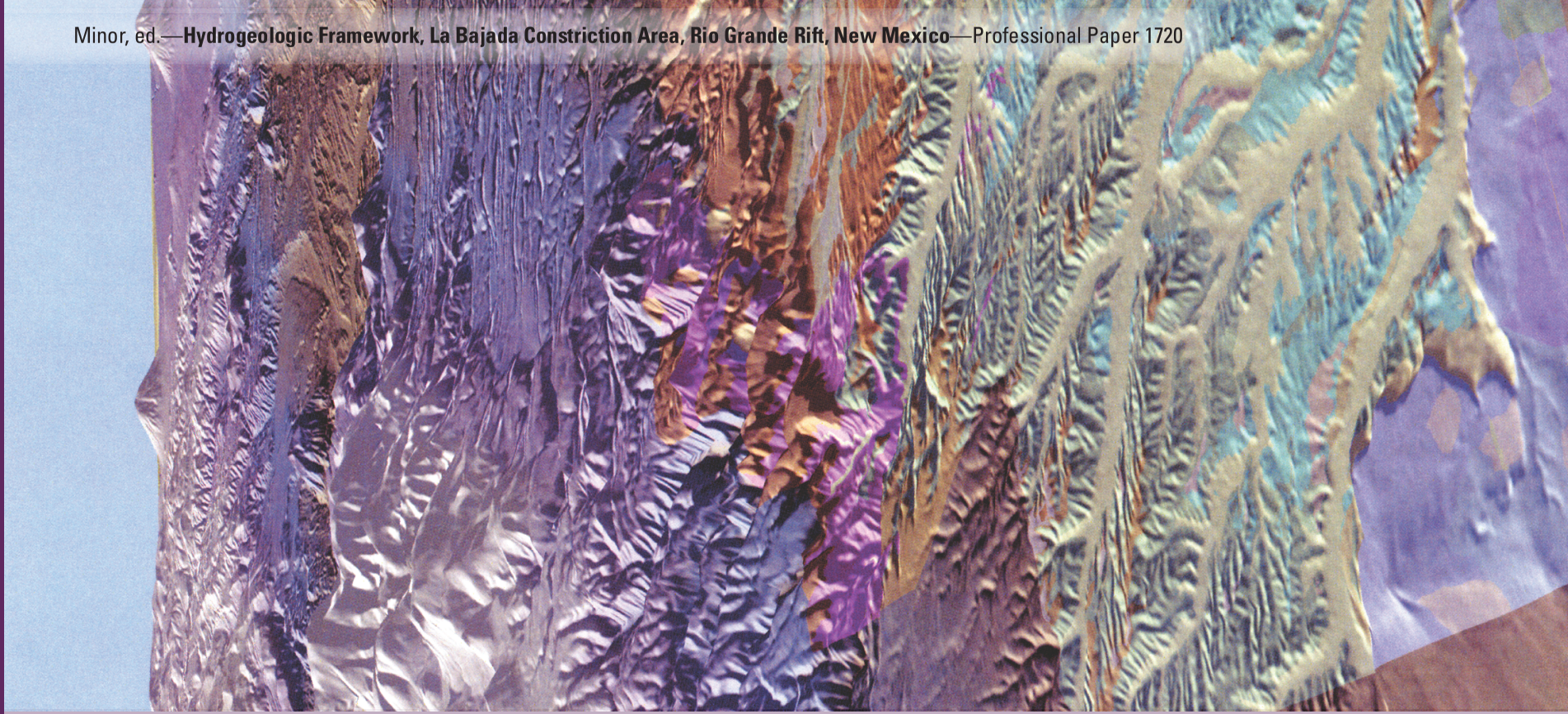
Minor, ed.—**Hydrogeologic Framework, La Bajada Constriction Area, Rio Grande Rift, New Mexico**—Professional Paper 1720